BIOGEOCHEMISTRY OF ANTHROPOGENIC PARTICLES

EDITED BY: Denise M. Mitrano, Antonia Praetorius, Gaetane Lespes and Vera I. Slaveykova

PUBLISHED IN: Frontiers in Environmental Science

frontiers Research Topics

frontiers

ISSN 1664-8714
ISBN 978-2-88966-771-0
DOI 10.3389/978-2-88966-771-0

About Frontiers

Frontiers is more than just an open-access publisher of scholarly articles: it is a pioneering approach to the world of academia, radically improving the way scholarly research is managed. The grand vision of Frontiers is a world where all people have an equal opportunity to seek, share and generate knowledge. Frontiers provides immediate and permanent online open access to all its publications, but this alone is not enough to realize our grand goals.

Frontiers Journal Series

The Frontiers Journal Series is a multi-tier and interdisciplinary set of open-access, online journals, promising a paradigm shift from the current review, selection and dissemination processes in academic publishing. All Frontiers journals are driven by researchers for researchers; therefore, they constitute a service to the scholarly community. At the same time, the Frontiers Journal Series operates on a revolutionary invention, the tiered publishing system, initially addressing specific communities of scholars, and gradually climbing up to broader public understanding, thus serving the interests of the lay society, too.

Dedication to Quality

Each Frontiers article is a landmark of the highest quality, thanks to genuinely collaborative interactions between authors and review editors, who include some of the world's best academicians. Research must be certified by peers before entering a stream of knowledge that may eventually reach the public - and shape society; therefore, Frontiers only applies the most rigorous and unbiased reviews.
Frontiers revolutionizes research publishing by freely delivering the most outstanding research, evaluated with no bias from both the academic and social point of view. By applying the most advanced information technologies, Frontiers is catapulting scholarly publishing into a new generation.

What are Frontiers Research Topics?

Frontiers Research Topics are very popular trademarks of the Frontiers Journals Series: they are collections of at least ten articles, all centered on a particular subject. With their unique mix of varied contributions from Original Research to Review Articles, Frontiers Research Topics unify the most influential researchers, the latest key findings and historical advances in a hot research area! Find out more on how to host your own Frontiers Research Topic or contribute to one as an author by contacting the Frontiers Editorial Office: frontiersin.org/about/contact

BIOGEOCHEMISTRY OF ANTHROPOGENIC PARTICLES

Topic Editors:
Denise M. Mitrano, ETH Zürich, Switzerland
Antonia Praetorius, University of Amsterdam, Netherlands
Gaetane Lespes, Université de Pau et des Pays de l'Adour, France
Vera I. Slaveykova, Université de Genève, Switzerland

Citation: Mitrano, D. M., Praetorius, A., Lespes, G., Slaveykova, V. I., eds. (2021). Biogeochemistry of Anthropogenic Particles. Lausanne: Frontiers Media SA.
doi: 10.3389/978-2-88966-771-0

Table of Contents

frontiers in Environmental Science

EDITORIAL
published: 23 March 2021
doi: 10.3389/fenvs.2021.667140

Editorial: Biogeochemistry of Anthropogenic Particles

Denise M. Mitrano[1]*, *Antonia Praetorius*[2], *Gaëtane Lespes*[3] and *Vera I. Slaveykova*[4]

[1] Department of Environmental Systems Science, ETH Zurich, Zurich, Switzerland, [2] Department of Ecosystem & Landscape Dynamics, Institute for Biodiversity and Ecosystem Dynamics, University of Amsterdam, Amsterdam, Netherlands, [3] Universite de Pau et des Pays de l'Adour, E2S UPPA, CNRS, IPREM, UMR 5254, Helioparc, Pau, France, [4] Environmental Biogeochemistry and Ecotoxicology, Department F.-A. Forel for Environmental and Aquatic Sciences, School of Earth and Environmental Sciences, Faculty of Science, University of Geneva, Genève, Switzerland

Keywords: nanoplastic, microplastic, nanoparticle, water, fate, transport, anthropogenic, ECOTOX

Editorial on the Research Topic

Biogeochemistry of Anthropogenic Particles

INTRODUCTION

The collection of articles published in the Research Topic Biogeochemistry of Anthropogenic Particles in Frontiers in Environmental Science has provided a comprehensive perspective on the biogeochemical cycle of anthropogenic particles in the environment with an emphasis on nano- and microscale materials. The term anthropogenic particles covers a wide range of materials, including those which are manufactured or generated incidentally, or from the degradation of synthetic materials, and subsequently disseminated in(to) the environment. The aims of this Research Topic were thus to explore the state of knowledge, including major advances and challenges, with regards to the sources, occurrence, transformations, and transport of particles, as well as the interactive effects between particles and their environment including living systems. Therefore, we have brought together research papers and reviews on anthropogenic particles, regardless of their origin and nature. This integrative approach has helped to draw parallels between the knowledge already acquired in the field of anthropogenic colloids, not limited to specific chemistry or source of particles, and thus to bridge these different investigation axes to fertilize the research area dedicated to particulate contaminants. Our summary groups the articles published in the Research Topic on four levels; (1) analytical methodologies to assess particles in complex matrices, (2) connecting research across particle chemistries and sources, (3) connecting fate and transport pathways across environmental compartments and (4) connecting research across ecological impacts.

The increased usage and unprecedented release rates of anthropogenic particles into the environment, made from a plethora of materials and originating from various sources, is a specific feature of the Anthropocene. Both the short- and long-term behavior and fate of these particles will depend on their interplay with different environmental matrices over time. Here the particulate nature results in unique properties and behaviors, often not directly comparable to that of other synthetic chemicals and materials. Therefore, understanding the biogeochemistry of man-made particles remains one of the major challenges of modern environmental sciences, even after decades of study. Additionally, it is important to put these anthropogenic materials in context with natural particles,

OPEN ACCESS

Edited by:
Fereidoun Rezanezhad, University of Waterloo, Canada

Reviewed by:
Adrian Mellage, University of Tubingen, Germany

***Correspondence:**
Denise M. Mitrano
denise.mitrano@usys.ethz.ch

Specialty section:
This article was submitted to Biogeochemical Dynamics, a section of the journal Frontiers in Environmental Science

Received: *12 February 2021*
Accepted: *25 February 2021*
Published: *23 March 2021*

Citation:
Mitrano DM, Praetorius A, Lespes G and Slaveykova VI (2021) Editorial: Biogeochemistry of Anthropogenic Particles. Front. Environ. Sci. 9:667140. doi: 10.3389/fenvs.2021.667140

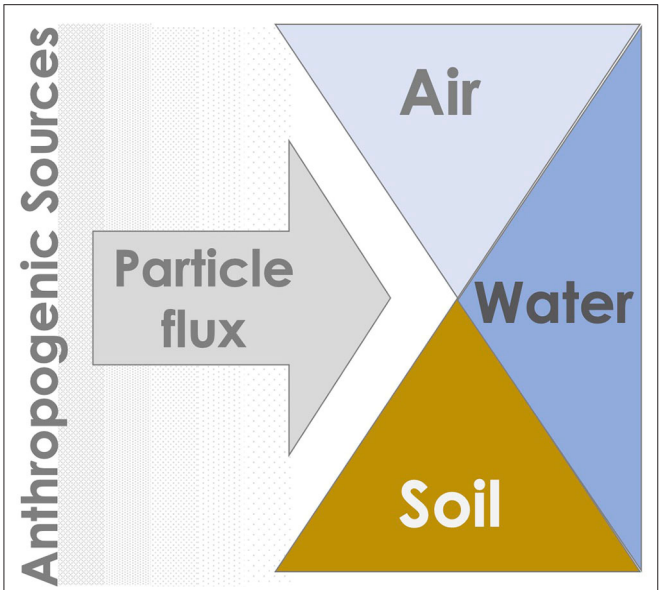

FIGURE 1 | Schematic representation of the emissions of anthropogenic particles, which can be emitted to various environmental compartments.

whose presence is often dominant in many environmental systems (Lespes et al.). Frequently, natural particles and anthropogenic particles of different origins are considered separately despite many overlapping tools, techniques, and processes, which is useful to understand behavior and interactions across different particle types. In this Research Topic, we have brought together an integrated, broad, and cross-sectoral perspective to assess particles of different origins to shed light on common underlying factors to assess the biogeochemistry of anthropogenic particles (**Figure 1**).

Accelerated industrialization and advances in technology have had wide reaching effects, producing particles which can range from incidental by-products of production and combustion processes (e.g., soot, street dust), to those which are intentionally produced in specific sizes and shapes for targeted applications (e.g., TiO_2 in cosmetics, nano-fertilizers) or generated by the breakdown of larger products over time (e.g., microplastics). Released either intentionally or unintentionally, their occurrence in the environment is continuous, although assessing the risks of this diverse group of materials is often cumbersome as scientists grapple with (i) differentiating natural proxies from engineered counterparts, (ii) balancing positive benefits with potential environmental harm (including safer-by-design principles), and (iii) assessing which, if any, mitigation strategies would prove useful and effective. Regardless of their origin, particles can play a special role in environmental systems and behave fundamentally different in terms of fate, transport, and biological interactions than dissolved chemicals or bulk materials. Therefore, understanding the biogeochemistry of these smallest of man-made materials is crucial in assessing all the ways in which humanity is continuously impacting our environment.

ANALYTICAL METHODOLOGIES TO ASSESS PARTICLES IN COMPLEX MATRICES

Understanding the biogeochemistry of anthropogenic particles [including nanoparticles (NPs) and their aggregates] requires advanced analytical methods. Nanometrology tools have continued to improve in the last several years developing increasingly performant and standardized materials and methods. Consequently, researchers can now track particles at very low particle concentrations and tackle research projects to understand the behavior of particles in a more environmentally relevant context. Nevertheless, implementing these methods in increasingly complex real-world scenarios remains analytically challenging, and the frontier of environmental nanometrology continues to be pushed forward. This is addressed in this Research Topic through three fundamental questions:

- **How can researchers detect particles in very low concentrations in complex matrices?** One strategy is preconcentration of particles. This approach was investigated for suspensions of nanoplastics by Hildebrandt et al.. Very sensitive and sufficiently selective detectors can also be used, namely inductively coupled plasma-atomic spectrometry (ICP-MS). In single particle (sp) mode, ICP-MS offers particle size distributions. Triple quad MS vs. simple quad enables size-based detection limits and selectivity to be improved, as illustrated by Wojcieszek et al. with the fate of TiO_2 NPs investigated in a model plant.
- **How can we identify the origins of nanoparticles?** For the analysis of inorganic particles, ICP-MS-based approaches remain powerful. In particular when considering particle composition and speciation, using multiple analytical techniques can be advantageous. This was approached in different ways in three studies in this Research Topic: (i) sp-ICP-MS (quadrupole)/imaging/X-ray spectroscopy; (ii) sp-ICP-MS (magnetic sector)/sp-ICP-MS(time-of-flight) to identify and determine the origins and behavior of CeO_2 NPs and TiO_2 NPs in natural waters in technical environments (Phalyvong et al.; Azimzada et al.); (iii) sample pre-fractionation/sp-ICP-MS(time-of-flight) to determine the speciation of Zn in colloidal phases of urban waters (Bevers et al.).
- **How can we validate analytical methods?** This question remains a challenge due to the lack of certified reference materials or standard suspensions for many nanomaterials and aggregates, especially in the case of plastics. In this context, labeled nanoplastics (e.g., with an incorporated metal-dopant) can be a solution, as they can be more easily traced. Their value is illustrated by the validation of the method of preconcentration of nanoplastics using metal-doped polymeric NPs (Hildebrandt et al.).

CONNECTING RESEARCH ACROSS PARTICLE CHEMISTRIES AND SOURCES

Research on the occurrence of particles and colloids in the natural environment has been conducted for many decades and is a principal component in the field of geochemistry. Some of these traditional principles and concepts may also be useful in the context of understanding the behavior of anthropogenic particles, but differences in particle material properties and chemistry changes how and what should be assessed. In this Research Topic, both engineered and incidental particles were investigated.

Improving industrial ecology is one decisive way in which the production of man-made materials can have fewer impacts at the start of a product life cycle. Slomberg et al. investigated the release of TiO_2 NPs from a production site, measuring industrial and urban wastewater treatment plant effluents and assessing how released particles distributed into receiving waters. The majority of the particles analyzed were confirmed to be anthropogenic, but they settled rapidly near the emission source and accumulated in the sediment. Environmental safety of engineered nanomaterials is a critical component of a "safer-by-design" approach, since we have the opportunity to control the material design and use of these materials, thereby selecting chemical properties and use scenarios which would have fewer negative environmental consequences. For the case of sunscreens, Labille et al. assessed a variety of UV-filters to review how material choice could minimize the environmental risk when particles are released into the environment during normal product use. Collectively, this information may provide industry and regulators with additional guidance on which materials should be used or avoided. Using advanced analytical tools to assess outdoor stains and paints, Azimzada et al. quantified and characterized TiO_2 particles which are released during weathering processes. Here the authors describe how incorporation of TiO_2 NPs in different products can result in different release profiles (amounts, aggregation states) and how seasonal differences in weathering changes particle release.

In some cases, the point sources of engineered NPs are not always clear, but the particles are nevertheless detected in the environment. Phalyvong et al. correlated potential engineered NP sources with their presence in the environment, where CeO_2 and TiO_2 NPs were measured up and downstream of wastewater treatment plants and near a freshwater recreation center. While particles surrounding the wastewater treatment plant may have included a mixture of natural and engineered NPs, those measured near the activity center were more clearly attributed to anthropogenic sources, such as runoff from a car parking lot. While studying particle behavior directly in the environment has its advantages, the impacts of geochemistry of surface waters on particle behavior can be more systematically studied in bench-top experiments. Supiandi et al. conducted a laboratory study to assess the geochemical factors which impact the behavior CdSe/ZnS quantum dots in surface waters.

Although some nano- and microplastics (small solid polymer particles <5 mm in size) are manufactured and used directly in products and applications, the vast majority of these particles in the environment originate from the abrasion of products during their lifecycle or breakdown of macroplastic litter. Halsband et al. assessed the chemical leaching profile of car tire crumb rubber to understand the potential impacts on coastal marine systems. While the leachate differed depending on tire composition and exposure scenario, organic components leached in the timespan of days while metals could still be released from the material over the 30-day test period.

Research on metals cycling processes in natural waters and their catchments has often focused on analyzing the "dissolved" fraction, which operationally is defined as the aqueous phase that passes through a $<0.45\,\mu$m filter. Biogeochemical cycling of elements can occur in a dissolved state, but many elements may also be bound to/be incorporated in natural nanoparticles (1–100 nm) and fine colloids (100–450 nm). Thanh-Nho et al. characterized the dynamics of trace metals in a tidal creek to assess their cycling in mangroves where complex biogeochemical processes of dissolution of metal bearing mineral phases resulted in high trace metal concentrations in pore waters. Under certain conditions, elements were exported to the estuary in particulate forms even though initially the elements (Fe, Mn, Co, and Ni) were put into the system in dissolved forms. This gives further evidence that identifying metal state and complexation is necessary to better understand the cycling and transport of elements in catchments and to determine their fate, transport, and biological availability.

CONNECTING FATE AND TRANSPORT MECHANISMS ACROSS ENVIRONMENTAL COMPARTMENTS

The transport of particles in environmental systems is driven by a combination of their intrinsic physico-chemical properties and their extrinsic properties which result from the interplay of particles and the conditions of the surrounding medium [e.g., in terms of pH, concentrations of various ions, presence and types of natural organic matter (NOM) or larger natural colloids]. The importance of studying particle fate as a function of a given environmental system to assess exposure and potential risks has been highlighted in several contributions to this Research Topic. Different freshwater systems have been investigated in field studies for the presence and transport of Ce-, Ti-, and Zn-containing NPs (Phalyvong et al.; Slomberg et al.; Phalyvong et al.), typically with several sampling points along a given river or watershed, sometimes covering different seasons and including the sediment compartment (Slomberg et al.). The effects of varying water chemistry on NP stability and the possible formation of heteroaggregates with larger natural mineral phases are discussed by Phalyvong et al.. Slomberg et al. found that most anthropogenic Ti-bearing particles occurred as aggregates in the water column, which explains the rapid sedimentation of a large fraction of the NPs close to the suspected emission sources. Additionally, they observed differences in aquatic concentrations in contrasting seasons, which may be attributed to differences in water chemistry.

Laboratory-based studies make it possible to more systematically discern effects of water chemistry on particle properties and behavior. Supiandi et al. used synthetic river water mimicking a natural river to study the effects of specific water constituents (i.e., fulvic acid and goethite) on the speciation of CdSe/ZnS Quantum Dots (QDs). They found that the presence of fulvic acid and goethite suppressed dissolution of Cd and Zn from the QDs, making them less bioavailable to sensitive organisms. Bour et al. used artificial seawater (salinity 30‰) and artificial freshwater (salinity 0‰) for studying interactions of plastic microbeads and microplastic fibers with fish, amongst other aquatic organisms, but found no significant difference in exposure for the fish in the different water types.

While freshwater systems are often considered one of the first entry points for anthropogenic particles into the water cycle, the importance of better understanding the behavior and impacts of anthropogenic particles in marine environments has been highlighted multiple times in this Research Topic (Halsband et al.; Corsi et al.; Gondikas et al.). A review on the behavior and fate of representative engineered metal oxide NPs (here TiO_2 NPs) and nanoplastics (here nano polystyrene) in artificial and real seawater is presented by Corsi et al. In particular, they highlight the importance of the possible formation of biomolecular coronas on the particles' surface and resulting changes in the physico-chemical properties of the NPs, as well as on their uptake by and interaction with organisms. In fact, Gondikas et al. demonstrate in their study that the presence of extracellular polymeric substances (EPS) resulting from seasonal biological activities such as algal bloom can lead to the intermittent stabilization of NPs in the marine water column. As a result, marine waters should not only be seen as a rapid sink for particles (due to the high salinity promoting aggregation and settling), but extended exposure times and further transport of NPs in the water column are possible in seasons of high biological activity. This, together with many other contributions to this Research Topic, highlights the importance of accounting for the complexity of possible processes affecting fate and sinks of anthropogenic particles in natural environments and to perform spatially and seasonally explicit fate (and risk) assessments.

CONNECTING RESEARCH ACROSS ECOLOGICAL IMPACTS

This Research Topic provides innovative insights and illustrates the large array of ongoing research on the biological assessment of the environmental impact of nano- and micro-sized anthropogenic particles that spans from aquatic (Halsband et al.; Bour et al.; Corsi et al.) to terrestrial environments (Wojcieszek et al.; Schöpfer et al.; Fringer et al.), from single-celled organisms (Fringer et al.) to biofilm communities (Desmau et al.), from plants (Wojcieszek et al.), to invertebrates and vertebrates (Bour et al.; Schöpfer et al.), from discrete nanoparticles (Wojcieszek et al.; Bour et al.; Corsi et al.; Schöpfer et al.; Fringer et al.; Desmau et al.) to more complex nanomaterials such as sunscreens (Labille et al.) or car tire crumb rubber leached chemical cocktails (Halsband et al.).

Interaction of NPs with biofilm microbial communities and consequences for NPs fate and impacts in the environment, as well as the need for further investigations were thoroughly discussed by Desmau et al.. The importance of the biofilm driven transformations such as dissolution, through ligand- or redox-mediated pathways, passivation or stabilization processes, and corona formation by EPS has the potential to strongly modify NP speciation and effects. Furthermore, biofilm-mediated NP synthesis in man-impacted systems were shown for the specific case of ZnS NPs. Using a gram-negative bacterium living in both anaerobic and aerobic environments, Fringer et al. showed that nano-polystyrene (nano-PS) were trapped by the EPS, associated to bacterial membranes and induced a specific and significant decrease in the secretion of riboflavin when exposed to nanoplastics without affecting cell viability, although the dosages used here are higher than expected for environmental concentrations nano-PS.

Wojcieszek et al. explored the uptake, translocation, and potential transformations of TiO_2 NPs with different sizes in hydroponically cultivated rooted radish. Small size NPs were measured in both leaves and roots, proving the plant's ability to translocate TiO_2 NPs. However, the root to shoot NP uptake ratio was low. Since NPs remained predominantly in the root, which is the edible portion of this plant, dietary exposure remains a possibility.

From a broader perspective, Corsi et al. provided an overview of the literature concerning the interaction of anthropogenic NPs with a range of marine microorganisms (from planktonic species to invertebrates and fish) and discussed the existing gaps toward a more realistic risk assessment of NPs in marine environment. TiO_2, and polystyrene (nano-PS), were used as case studies to illustrate the basic concept underlying the adsorption and absorption of NPs. Modifying factors enabling a better assessment of particle uptake and related cellular pathways leading to toxic effects were considered. Interactions of the anthropogenic NPs with various naturally occurring compounds was also highlighted by Lespes et al., as well as the need of a broader and integrated approach toward fate and impact of nano-sized particles in the environment.

Finally, a comprehensive review on the exposure and hazard of nanoparticulate UV-filters (TiO_2 or ZnO) of sunscreen products through the product lifecycle (manufacturing, usage, and disposal) in different compartments encountered was presented by Labille et al.. The importance of the development of realistic scenarios of environmental release and fate, as well as considering sunscreen filters and formulations which are used commercially was highlighted together with knowledge gaps. Collectively, this provides a scientific base for ecological risk assessment and toward safer by design products and sustainable nanotechnology.

Exposure to and ingestion of nano- and microplastics can impact the health, function and viability of organisms, both large and small, in a diversity of ecosystems. Halsband et al. presents the impacts of nanoplastic on a model bacterium and showed that while overall viability did not decrease, there were significant changes to cellular function, as evidenced by reduced riboflavin secretion. This impact was nanoplastic specific, since a similar finding was not observed when the bacteria were

exposed to colloidal TiO_2 or microplastic. Schöpfer et al. demonstrated that conventional and biodegradable microplastic particles were ingested by nematode, a key member of the soil food web, and induced sub-lethal effects. The alteration of the reproduction was confirmed even though other vitality metrics, such as body length, were not impacted (Thanh-Nho et al.). The observations were attributed to the physical and indirect nutritional effects rather than to chemical effects. Using a combination of microplastic morphologies (particles, fibers), feeding strategies (microplastic in presence and absence of food) and exposure conditions (fresh and salt waters), Phalyvong et al. assessed particle ingestion by fish. They found that gills were especially susceptible to microplastic exposure, and that ingestion and retention in the gut differed between particle morphologies. In many cases, the reason why microplastics are hazardous is not the polymer itself, but rather the leaching of plasticizers, additives and other compounds from the plastic over time. In addition, these same authors found that the ingestion and retention of polyethylene microbeads and doped dyed polyester microfibers differed in brine shrimp and fish (Bour et al.). Shrimps ingested large quantities of microbeads but very few microfibers, while fish ingested more microfibers than microbeads. These results suggested that particle selection can be based on size and shape, which has important implications for trophic transfer to predators.

Not only the particulate materials itself, but also different additives that can be leached from it can have significant effects on environmental biota as demonstrated by Halsband et al.. They provided a study assessing the impact of chemical additive leachates from crumb rubber granulate (CRG) produced from end of life tires exposing marine copepods. A dose-response relationship was found with smaller lipid-poor Acartia, which showed higher morality to leachates, opposed to the larger lipid-rich Calanus, indicating species-specific differences. Benzothiazole and Zn were two prevailing components in the leachates. Comparing relative impacts of organisms to particles can help to elucidate if effects are observed as a specific reaction to one material (i.e., microplastic) or if organisms are simply responding to the presence of particulate matter in their environment. Consequently, adverse effects may be observed when test organisms are subjected to turbid environments regardless of the source of the particulate matter; be it from a natural or anthropogenic source. Gorokhova et al. addressed this issue by exposing the unicellular alga *Raphidocelis subcapitata* to both natural particles (kaolin, cellulose) and microplastics, including in combination, to assess particle property specific effects. At lower doses (10–100 mg/L), no adverse effects were observed and in fact growth stimulation was seen for natural particles compared to the control, though at very high concentrations (1,000 mg/L), organisms suffered growth inhibition from all materials. Therefore, there was less dependence on the material of the particles the organisms were exposed to, but rather the total concentration.

OUTLOOK

The contributions to the Research Topic Biogeochemistry of Anthropogenic Particles in Frontiers in Environmental Science demonstrate the broad range of sources, particle types, environments, and species, which can play a role when assessing the fate and possible impacts of man-made particles to the natural environment. While ultimately particle chemistry will play an important role in biogeochemical of particle fluxes in the environment, researchers who study particle behavior of one class of materials can significantly advance their own studies by understanding the analytical toolboxes and concepts used by researchers who study different material types. Many parallels can be drawn between engineered, incidental and natural particles, as well as between different material types, such as metal/metal oxide NPs or nano- and microplastics. Fate, transport and (adverse) effects are impacted by particles size and shape, as well as by the interactions at the interface between particle surface and environment. These interactions are influenced by particle chemistry and by the conditions of the surrounding environment. Understanding and predicting these complex interactions will be instrumental in assessing potential risks posed by anthropogenic particles in the environment and help us design effective mitigation measures as well as more benign alternatives.

AUTHOR CONTRIBUTIONS

All authors collectively wrote and edited this editorial.

Conflict of Interest: The authors declare that the research was conducted in the absence of any commercial or financial relationships that could be construed as a potential conflict of interest.

frontiers in Environmental Science

BRIEF RESEARCH REPORT
published: 09 April 2020
doi: 10.3389/fenvs.2020.00041

Microplastics Effects on Reproduction and Body Length of the Soil-Dwelling Nematode *Caenorhabditis elegans*

Lion Schöpfer[1], Ralph Menzel[2], Uwe Schnepf[3], Liliane Ruess[2], Sven Marhan[1], Franz Brümmer[3], Holger Pagel[4] and Ellen Kandeler[1]*

[1] Soil Biology Department, Institute of Soil Science and Land Evaluation, Faculty of Agricultural Sciences, University of Hohenheim, Stuttgart, Germany, [2] Ecology Group, Institute of Biology, Humboldt-Universität zu Berlin, Berlin, Germany, [3] Research Unit Biodiversity and Scientific Diving, Institute of Biomaterials and Biomolecular Systems, Faculty of Energy, Process and Biotechnology, University of Stuttgart, Stuttgart, Germany, [4] Biogeophysics Department, Institute of Soil Science and Land Evaluation, Faculty of Agricultural Sciences, University of Hohenheim, Stuttgart, Germany

Microplastics (MP) are pervasive in the environment. There is ample evidence of negative MP effects on biota in aquatic ecosystems, though little is known about MP effects in terrestrial ecosystems. Given numerous entry routes of MP into soils, soil organisms are likely to be exposed to MP. We compared potential toxicological effects of MP from (i) low-density polyethylene (LDPE) (mean diameter ± standard deviation: 57 ± 40 μm) and (ii) a blend of biodegradable polymers polylactide (PLA) and poly(butylene adipate-co-terephthalate) (PBAT) (40 ± 31 μm) on the reproduction and body length of the soil-dwelling bacterivorous nematode *Caenorhabditis elegans*. Feed suspensions without (control) or with MP (treatments) at concentrations of 1, 10, and 100 mg MP L^{-1} were prepared and nematodes were exposed to those suspensions on agar plates until completion of their reproductive phase (~6 days). Using Nile red-stained PLA/PBAT MP particles and fluorescence microscopy, we demonstrated the ingestion of MP by *C. elegans* into pharynges and intestines. Under MP exposure, nematodes had fewer offspring (up to 22.9%) compared to nematodes in the control group. This decline was independent on the plastic type. We detected a tendency toward greater decreases in offspring at higher concentrations. Despite hints of negative effects on nematode body length under MP exposure, we could not derive a consistent pattern. We conclude that in MP-contaminated soils, the reproduction of nematodes, central actors in the soil food web, can be affected, with potentially negative implications for key soil functions, e.g., the regulation of soil biogeochemical cycles.

Keywords: plastic residues, Nematoda, ingestion, low-density polyethylene, polylactide, poly(butylene adipate-co-terephthalate)

OPEN ACCESS

Edited by:
Vera I. Slaveykova, Université de Genève, Switzerland

Reviewed by:
Moritz Bigalke, University of Bern, Switzerland
Defu He, East China Normal University, China

****Correspondence:***
Lion Schöpfer
l.schoepfer@uni-hohenheim.de

Specialty section:
This article was submitted to Biogeochemical Dynamics, a section of the journal Frontiers in Environmental Science

Received: *16 January 2020*
Accepted: *20 March 2020*
Published: *09 April 2020*

Citation:
Schöpfer L, Menzel R, Schnepf U, Ruess L, Marhan S, Brümmer F, Pagel H and Kandeler E (2020) Microplastics Effects on Reproduction and Body Length of the Soil-Dwelling Nematode Caenorhabditis elegans. Front. Environ. Sci. 8:41. doi: 10.3389/fenvs.2020.00041

INTRODUCTION

Microplastics (MP) have only recently been recognized as an environmental threat to terrestrial ecosystems. MP are plastic particles smaller than 5 mm, and with different shapes such as spheres, fibers, and fragments (de Souza Machado et al., 2018; Rillig et al., 2019). Although reliable data on the prevalence of MP in soils is scarce (Watteau et al., 2018), soils are presumably large sinks for MP and MP may harm soil organisms (Bläsing and Amelung, 2018; Hurley and Nizzetto, 2018).

It has been shown for aquatic organisms such as mussels, langoustines, copepods, short crabs, and lugworms that the ingestion of MP can lead to negative effects on growth, reproduction and survival (Galloway et al., 2017; Foley et al., 2018; Franzellitti et al., 2019). These detrimental effects can be nutritional, a result of lower food intake resulting in energy deficiencies (Franzellitti et al., 2019), but also physical, due to lacerations and inflammations (Horton et al., 2017). In contrast, little is known about MP effects on soil fauna (Chae and An, 2018). Early studies on earthworms under MP exposure indicated that some biological functions could be inhibited (Huerta Lwanga et al., 2016; Cao et al., 2017). One study documented histopathological damage, including congestion fibrosis and inflammatory infiltrates in earthworms in response to MP exposure, although no biological functions were affected (Rodriguez-Seijo et al., 2017). Wang et al. (2019) found oxidative stress in earthworms in response to artificially high MP exposure only. Translocation of MP by earthworms (Huerta Lwanga et al., 2017a; Rillig et al., 2017b) and collembola (Maaß et al., 2017) could increase the exposure of other soil-dwelling species to MP. In addition, evidence on the accumulation of MP from soil to earthworms to chicken feces (Huerta Lwanga et al., 2017b) indicates that MP may enter terrestrial food webs through trophic transfers.

Nematodes (roundworms) live in any terrestrial habitat, exhibit high diversity across soils (Yeates and Bongers, 1999), and have a wide range of diets (Yeates et al., 1993; Orgiazzi et al., 2016). By regulating biogeochemical cycles and ecosystem processes, including mineralization and decomposition of organic matter (Griffiths et al., 1998; Bardgett et al., 1999; Ferris, 2010), they are key organisms in the soil food web. The soil-dwelling bacterivorous nematode *Caenorhabditis elegans*, distributed world-wide, is a well-established model organism for ecotoxicological tests of different kinds of pollutants such as mycotoxins, persistent organic pollutants and endocrine-disrupting compounds (Leung et al., 2008; Keller et al., 2018; Chen et al., 2019) and has been used for biosafety assessments of nanoparticles (Wu et al., 2019). Fang-Yen et al. (2009) observed that *C. elegans* can ingest polystyrene beads that can further be transported into the intestine, a possible entry route of MP into the soil food web (Rillig et al., 2017a). An early study on exposure of *C. elegans* to MP reported that MP could lead to inhibition of survival rates, body length, and reproduction, as well as intestinal damage and oxidative stress. While MP effects were independent on plastic type, MP effects were dependent on particle size (Lei et al., 2018b): MP particles of one μm led to the strongest effects when three different sizes (0.1, 1, and 5 μm) were compared.

Biodegradable plastics are considered an environmentally friendly alternative to conventional plastics, as they theoretically can be completely metabolized by microorganisms without leaving plastic residues in the environment (Bandopadhyay et al., 2018; Sander, 2019). For instance, polylactide (PLA) and poly(butylene adipate-co-terephthalate) (PBAT) are common components of biodegradable plastic films which can be substituted for low-density polyethylene (LDPE) films (Künkel et al., 2016). However, there is some evidence that even nominally biodegradable plastics tend to disintegrate instead of being mineralized (de Souza Machado et al., 2018). A recent study demonstrated that even after 3 years, large quantities of commercially available, biodegradable plastic carrier bags were still present in soils and other environmental compartments (Napper and Thompson, 2019).

Our study aimed to compare possible effects of irregularly shaped MP particles of the conventional plastic type LDPE and a biodegradable blend of PLA/PBAT on nematodes. We evaluated the biological endpoints of reproduction and body length in the model organism *C. elegans* in response to MP exposure at different concentrations. We hypothesized that (i) *C. elegans* can ingest MP and (ii) MP adversely affect reproduction and body length of *C. elegans*, with stronger negative impacts at higher MP concentrations. Furthermore, we expected to observe comparable effects of both conventional and biodegradable MP.

MATERIALS AND METHODS

Microplastic Preparation and Characteristics

Two types of plastics were used in the experiment: (1) low-density polyethylene (LDPE) in the form of granules (Lupolen 2420 H, LyondellBasell Industries N.V., Rotterdam, Netherlands) and (2) a blend consisting of the polymers polylactide (PLA, Ingeo^{TM} Biopolymer 7001D, NatureWorks LLC, Minnetonka, MN, United States) and poly(butylene adipate-co-terephthalate) (PBAT, Ecoflex F Blend C1200, BASF SE, Ludwigshafen, Germany) with a mixing ratio of 80/20% w/w compounded at the "Institut für Kunststofftechnik" (University of Stuttgart, Stuttgart, Germany).

We used irregularly shaped MP particles because a non-spherical shape can be expected due to input of fragmented MP from mulch film and plastic bag residues in compost into soils. The particle size ingestible by *C. elegans* is smaller than 3 μm (Fang-Yen et al., 2009). However, it is very challenging, to produce irregularly shaped MP particles with defined size distribution <50 μm. For our experiments, plastic granules were first ground to MP particles <5 mm with a speed rotor mill (Pulverisette, Fritsch GmbH, Idar-Oberstein, Germany) and later milled to smaller fragments using a cryomill with liquid nitrogen (Cryomill, Retsch, Haan, Germany) at the Fraunhofer Institute for Chemical Technology (Pfinztal, Germany). This procedure yielded particle sizes of 57 ± 40 μm (LDPE) and 40 ± 31 μm (PLA/PBAT) (**Figure 1**). Due to light microscopy detection limits at ≤3 μm (see **Supplementary Material 1**), we could not differentiate particles ≤3 μm. The proportions of particles ≤3 μm (ingestible for *C. elegans*) were 8.0% (LDPE) and 7.4% (PLA/PBAT). Particles of both plastic types were similarly shaped, as shown by their form factors (**Supplementary Figure 1**). A detailed description of particle characteristics is given in **Supplementary Material 1**.

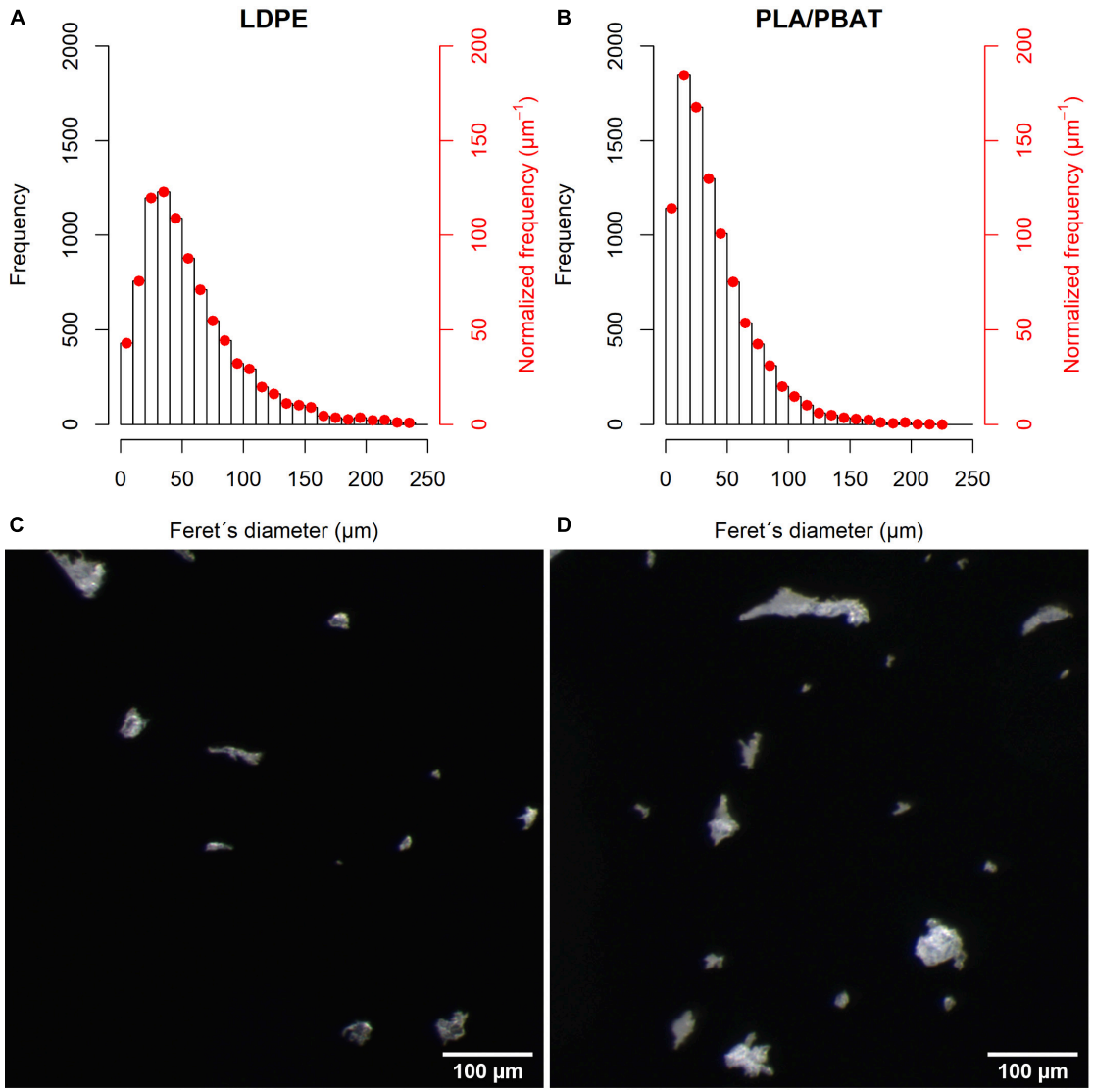

FIGURE 1 | The particle size distribution of **(A)** LDPE and **(B)** PLA/PBAT. The second ordinate shows the normalized frequency according to Filella (2015). Micrograph of **(C)** LDPE and **(D)** PLA/PBAT.

Cultivation of *C. elegans* and Preparation of MP Feed Suspensions

We used the *C. elegans* wild-type strain N2 in our assays, which was obtained from the Caenorhabditis Genetics Center (University of Minnesota). *C. elegans* was fed with *Escherichia coli* OP50 and cultivated on Nematode Growth Medium agar plates. For both assays, L1 nematodes were used. L1 refers to nematodes from the first of four larval stages in the life cycle of *C. elegans* before they become fertile adults (Gonzalez-Moragas et al., 2015).

For the treatments, MP feed suspensions were prepared at concentrations of 1, 10, and 100 mg MP L^{-1}. The MP feed suspensions consisted of M9 buffer, a common worm buffer for handling *C. elegans* (He, 2011), freshly harvested *E. coli* OP50 from overnight cultures and MP. For the control group, feed suspensions of M9 buffer and freshly harvested *E. coli* OP50 without MP were prepared. All feed suspensions (with and without MP) were then shaken for 30 min and placed in an ultrasonic bath for 15 min to prevent agglomeration of the particles in the treatments. Before an aliquot of 100 µl of the feed suspensions were added to the agar plates, the suspensions were vortexed for 10 s. Following the addition of the feed suspensions to the agar plates, they were dried under the laboratory hood and incubated at 19.5°C for 12 h. The entire procedure was performed under sterile conditions.

Ingestion Assay

Nematodes were exposed to Nile red (NR) stained PLA/PBAT particles at a concentration of 100 mg L^{-1}. For this purpose, PLA/PBAT particles were colored with the fluorescent dye NR

(72485, Sigma-Aldrich, St. Louis, MO, United States) that was recently used for the detection of MP in environmental samples (e.g., Shim et al., 2016; Maes et al., 2017). For staining of the MP particles, a NR stock solution of 1 mg L^{-1} methanol was first prepared. MP particles were stained with a NR working solution of 10 μg ml^{-1} by shaking the suspensions at 35 rpm for 1 h on a laboratory shaker (Roto-Shake Genie, Scientific Industries, Inc., New York, NY, United States). After incubation, the suspensions were transferred to glass Petri dishes where the solvents evaporated under the laboratory hood. The stained MP particles were used for the preparation of MP feed suspensions. Five nematodes were taken from a pre-culture and added to Nematode Growth Medium agar plates prepared with MP feed suspensions. The adult nematodes were transferred to new plates after 3 and 6 days, respectively. After 9 days of incubation, images were taken with a fluorescence microscope using an excitation wavelength of 510–560 nm and emission wavelength >590 nm (Axiophot with filter set 487914/analogous to current filter set 14, Carl Zeiss Microscopy GmbH, Jena, Germany). The Feret's diameter of MP particles incorporated by *C. elegans* was determined using Fiji 1.52p (Schindelin et al., 2012; Schneider et al., 2012). For better visualization, the particles were pseudo-colored on the images.

Reproduction and Body Length Assay

To exclude potential side effects of NR, here we only used non-stained MP particles. The experimental design consisted of two plastic types (LDPE or PLA/PBAT) at three different concentrations (1, 10, and 100 mg L^{-1}) and a control without MP addition (each $n = 8$).

L1 nematodes were individually picked from a pre-culture with a smoothed platinum picker and placed on the agar plates (one nematode per plate) prepared with feed suspensions with MP (treatments) or without (control). Subsequently, the nematodes were exposed to these feed suspensions on the agar plates at 19.5°C until oviposition (∼3 days). At intervals of 24 h the nematodes were transferred to new agar plates prepared with the nutrient suspensions with MP (treatments) or without (control) until the end of the reproduction phase (∼3 days). In total, nematodes of the treatment groups were exposed to MP for 6 days.

Nematode offspring per 24 h were counted optically with a stereomicroscope (Nikon SMZ1000, Nikon, Tokyo, Japan). The body length of the adult nematodes that survived the reproduction phase was determined using a stereomicroscope with camera (Zeiss Axio Scope.A1 & AxioCam ICc 5, Carl Zeiss Microscopy GmbH, Jena, Germany) and Fiji 1.52p. Before taking images, the nematodes were anesthetized with 20 mM tetramisole hydrochloride (L9756, Sigma-Aldrich, St. Louis, MO, United States).

Statistics

For data analysis, we used the statistical software R (R Core Team, 2018). To examine our hypotheses, we fitted a one-way analysis of variance model to our data and specified linear contrasts of interest as proposed by Mangiafico (2015) using the "glht" command from the R package "multcomp" (Hothorn et al., 2008). To test for an effect of MP on reproduction and body length, we compared each treatment to the control group. To clarify differences between the plastic types, we compared LDPE and PLA/PBAT per concentration level. To test the assumption that higher concentrations would lead to stronger effects, we compared the higher to the lower concentrations for each plastic type. We adjusted the *p*-values according to Benjamini and Hochberg (1995), to correct for several comparisons. Following the recommendation of Wasserstein et al. (2019), we did not define a significance level and deliberately omitted the term "statistically significant." The results of the statistical tests are given in **Supplementary Table 2**. We confirmed the model assumptions of the ANOVA visually by residual diagnostics plots (Kozak and Piepho, 2018).

We only considered nematodes that remained alive until the completion of the reproductive phase. Underdeveloped worms and worms that died before completing the reproductive phase from unexplained causes of death (e.g., mechanical damage) were excluded from the analysis. This resulted in an unbalanced design with at least $n = 5$ (**Supplementary Table 1**).

RESULTS

Ingestion Assay

We confirmed the uptake of NR stained PLA/PBAT MP particles in the pharynx and posterior intestinal lumen of *C. elegans* by fluorescence microscopy (**Figures 2A,B**). The particles ingested by *C. elegans* displayed in **Figure 2**, in the pharynx and intestine had a Feret's diameter of 2.3–5.1 μm and 1.3–2.5 μm, respectively.

Surprisingly, internal hatching of larvae was observed in a nematode with particles in the pharynx (**Figure 2C**). This phenomenon could also be observed in four nematodes from the reproduction assay exposed to 10 ($n = 1$) and 100 mg L^{-1} LDPE ($n = 2$) and 100 mg L^{-1} PLA/PBAT ($n = 1$). These individuals were not considered in the statistical analysis because they died before the completion of the reproductive phase. In the control group without MP, internal hatching did not occur.

Reproduction and Body Length Assay

Number of nematode offspring in the control group was 267 ± 6 (mean ± SE) (**Figure 3A**). Under MP exposure, nematodes produced 4.6–22.9% fewer offspring than nematodes in the control group. The strongest reduction in comparison to the control group was found at 10 mg L^{-1} LDPE ($p = 0.03$). For both plastic types, we observed a tendency toward stronger declines at higher concentrations. Under exposure to 10 and 100 mg L^{-1} compared to 1 mg L^{-1} LDPE, offspring declined by 18.4% ($p = 0.08$) and 9.9% ($p = 0.37$) stronger relative to the control. Exposure to 10 and 100 mg L^{-1} compared to 1 mg L^{-1} PLA/PBAT, resulted in declines relative to the control which were by 4.7% ($p = 0.63$) and 6.5% ($p = 0.49$) stronger. We found only marginal differences in offspring between LDPE and PLA/PBAT at all concentration levels (**Supplementary Table 2**). The coefficient of variation (CV) of the treatment groups (9.2–17.5%) was higher than the CV of the control group (5.5%).

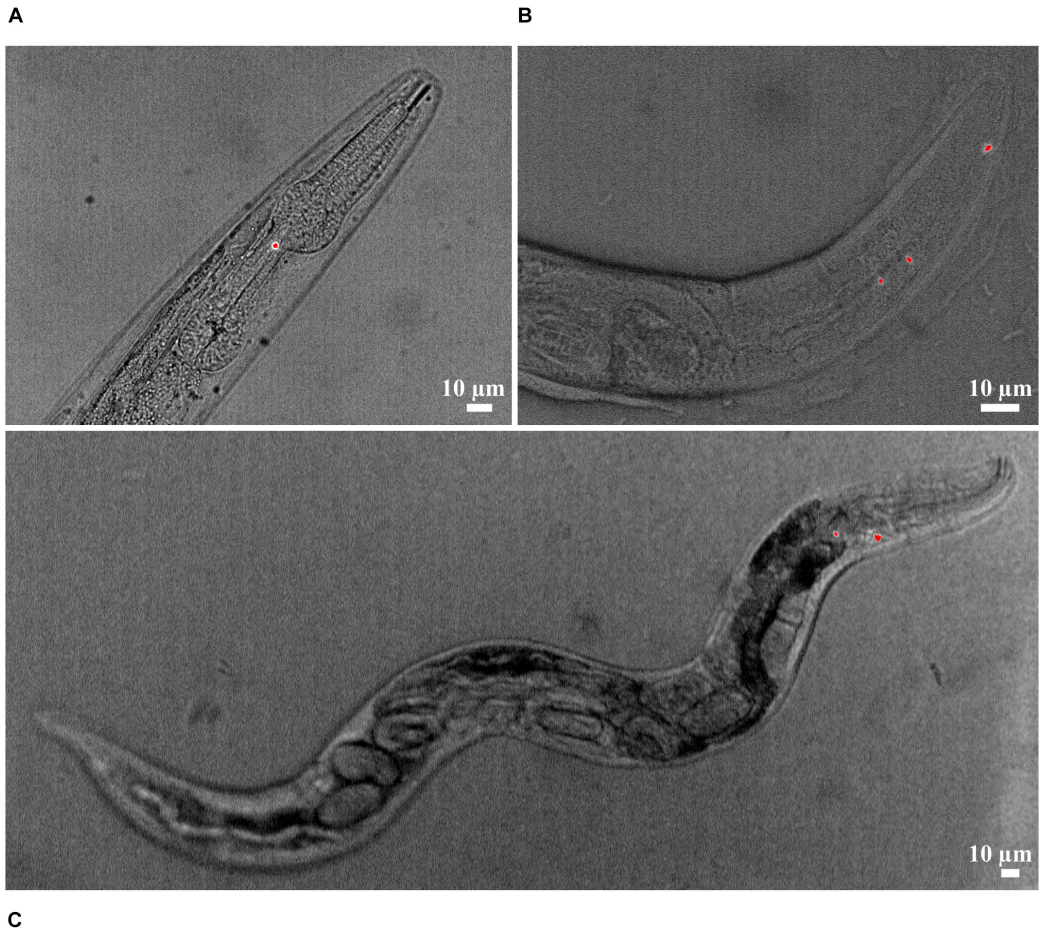

FIGURE 2 | Ingestion of NR-stained PLA/PBAT particles (red) in the **(A)** pharynx and **(B)** intestine lumen of *C. elegans*. **(C)** Nematode with NR-stained PLA/PBAT particles in the pharynx and internal hatching.

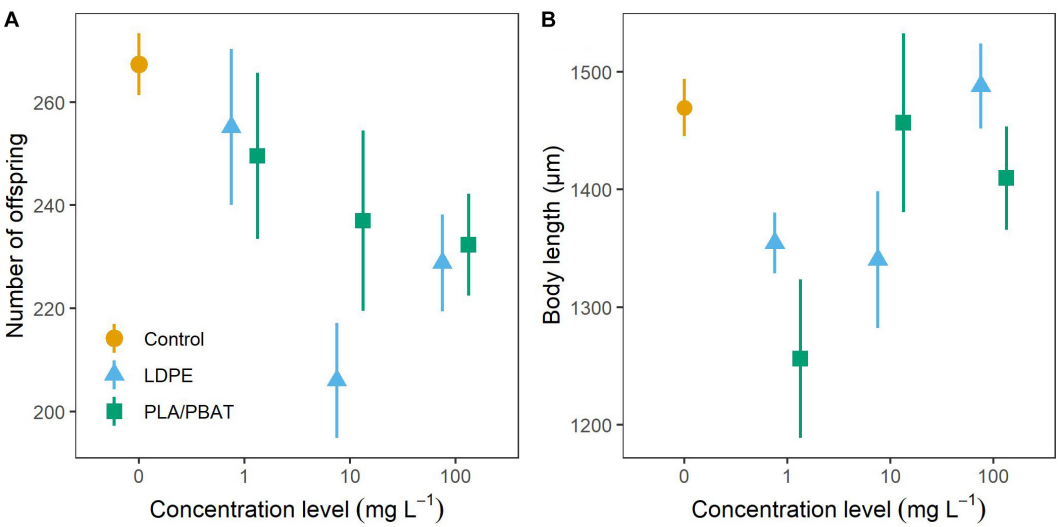

FIGURE 3 | (A) Number of offspring and **(B)** body length of *C. elegans* as a function of concentration and plastic type compared to the control group. Data are presented as means ± SE.

In the control group, body length of the nematodes was 1,470 ± 24 μm (**Figure 3B**). We could not observe a clear pattern for the body length of nematodes exposed to MP. Body length decreased most strongly relative to the control at exposure level of 1 mg L^{-1} PLA/PBAT (14.5%, $p = 0.06$) and at both 1 mg L^{-1} (7.8%, $p = 0.25$), and 10 mg L^{-1} (8.8%, $p = 0.21$) LDPE. Observed body lengths in all other treatments were close to the body length of the control group. Body length was not influenced by plastic type. With a CV of 4.1%, the control group exhibited lesser variance than the treatment groups, the CVs of which ranged from 4.7 to 14.2%.

DISCUSSION

By demonstrating that *C. elegans* can and does ingest MP particles, we established one prerequisite for the potential development of toxic effects (Horton et al., 2017; Kim and An, 2019) in *C. elegans*. Particle ingestion is generally controlled by a species-specific particle-to-mouth size ratio that defines the size of the particles which are ingestible by a particular species (Horton et al., 2017). Recently, Mueller et al. (2020) provided evidence for earlier findings from Fang-Yen et al. (2009) that the ingestible particle size of *C. elegans* is limited by the size of the buccal cavity, which in their study developed to 4.4 ± 0.5 μm. While polystyrene (PS) beads <3 μm entered the entire intestinal system of *C. elegans*, particles >6 μm did not enter the body of the nematodes at all (Mueller et al., 2020). In agreement with these findings, we detected in our study MP particles with sizes of 2.3–5.1 μm and 1.3–2.5 μm in the pharynges and intestines of *C. elegans*, respectively.

We found that MP reduced offspring of *C. elegans* by 4.5–22.9%, with a tendency toward greater declines in offspring at higher MP concentrations. The strong decline in offspring at 10 mg L^{-1} compared to the control might indicate the existence of a critical effect concentration of MP. Contra-intuitively, the decrease was more pronounced at 10 mg L^{-1} LDPE than at 100 mg L^{-1} LDPE which we attribute to the statistical uncertainties of the comparison between these treatments ($p = 0.44$, see **Supplementary Table 2**). The existence of a critical effect concentration is supported by observations in Lei et al. (2018a), who found clear lethal effects of PS beads in *C. elegans* at concentrations higher than 5 mg L^{-1}. Mueller et al. (2020) established clear dose-response curves for the reproduction of nematodes exposed to PS beads from 0.1 to 10 μm, with smaller particles exerting a stronger toxicity. Only 0.1 μm-sized particles caused effects on nematode reproduction with an EC_{50} at 77 mg L^{-1} (all units converted) below the highest concentration level of 100 mg L^{-1} used in our study, while larger particles caused inhibitions in reproduction at considerably higher concentrations (Mueller et al., 2020). Lei et al. (2018b) compared the toxic effects of five different MP types of irregular shape (mean diameter: ∼70 μm) on body length, embryo number, brood size, calcium levels in the intestine, and the expression of stress-indicating enzyme activity of *C. elegans*. Additionally, they compared the ingestion and toxic effects of PS beads of different sizes (0.1, 1, and 5 μm). Lei et al. (2018b) found offspring reductions of 2.4–28.0%, which were similar to the offspring reductions observed in our study. They found that body length was reduced by 4.9–11.4% when nematodes were exposed to MP, while we could not observe a clear MP effect pattern, as some MP treatments showed reductions compared to the control, while others did not.

Given the estimated fraction of MP particles <3 μm used in our experiments of 8.0 (LDPE) and 7.4% (PLA/PBAT), the concentration levels of 1, 10, and 100 mg L^{-1} in our study translate into 0.08, 0.8, 8.0 mg L^{-1} and 0.074, 0.74, to 7.4 mg L^{-1} in the ingestible range for *C. elegans*. Thus, in Mueller et al. (2020) the likelihood of an ingestion of MP by *C. elegans* was much higher than in our study, since they used spherical particles in the size range of 0.1–3 μm at concentrations of 40–12,500 mg L^{-1}. The authors found effects on reproduction at considerably higher concentrations than >100 mg L^{-1} (exception: 0.1 μm –sized particles with an EC_{50} of 77 mg L^{-1}), which indicates that the observed toxicity of MP in our study at much lower concentrations of ingestible particles was not solely attributed to the ingestion of particles. While direct toxicity of ingested MP particles was shown for 1 μm particles that were preferably ingested and accumulated in the intestines of *C. elegans* (Lei et al., 2018b), there is some experimental evidence that negative effects on reproduction of *C. elegans* are regulated by the ratio of the total surface area of MP particles to the volume of the medium, where the MP is contained (Mueller et al., 2020). Yet, the underlying mechanism of such a surface-related toxicity still needs to be clarified. Mueller et al. (2020) proposed as possible mechanisms of the surface-related toxicity the binding of food bacteria to MP and a dilution of food bacteria by MP, which could result in a limitation of food availability for the nematodes. In our study, surface-related toxicity could explain, why the MP particles reduced offspring although most of the particles were not directly ingestible by nematodes. Due to their higher specific surface area, irregularly shaped particles (used in our study) presumably lead to higher surface-related toxicity at lower concentrations compared to spherical MP particles (used in Mueller et al., 2020). Hence, toxic effects of MP are also likely to be controlled by particle shape.

In line with Lei et al. (2018b), negative effects on the reproduction of *C. elegans* under MP exposure occurred irrespective of the plastic type. Since LDPE and PLA/PBAT particles in our study had a similar shape and size, the observed reductions in offspring were probably attributable to physical effects, such as intestinal damage (Lei et al., 2018b) or indirect nutritional effects due to interaction of particles with the food bacteria (Mueller et al., 2020). Natural particles such as mesoporous SiO_2 particles, which can be found in soils, can also be ingested by *C. elegans* (Acosta et al., 2018). However, only exposure to nano-sized particles led to reductions in lifespan, mobility, and reproduction, while micro-sized particles showed no effect (Acosta et al., 2018). Mueller et al. (2020) compared the effects of SiO_2 particles to PS beads of equal size and showed that SiO_2 particles exhibited a clearly lower toxicity, which was indicated by toxic

effects at significantly higher particle to bacteria ratio. The authors claimed that the specific density of a material played an important role for the toxicity, because particles with specific density in the range of the bacteria like plastics would be taken up more readily.

We found a greater variance within our MP treatments than in the control treatment for both offspring and body length. One possible explanation is that not all nematodes exposed to MP had ingested them, such that only worms that ingested MP were affected. This was not possible to check, however, as we used non-stained MP in the reproduction and body length assay, and this was not detectable under the microscope inside the nematode bodies. Furthermore, it is possible that the total surface of the particles in the MP feed suspensions differed between the replications within and among the groups due to discrepancies in particle compositions present in the respective suspensions.

Studies of MP effects on other soil-dwelling animals have also reported negative effects of MP on some biological functions, with other functions unaffected. For instance, under high MP exposure, mortality level of the earthworm *Lumbricus terrestris* increased, growth inhibited, and biomass reduced, whereas even at higher concentrations no effect on reproduction was found (Huerta Lwanga et al., 2016). In comparison, Rodriguez-Seijo et al. (2017) observed no adverse effects on survival, reproduction, or body weight of the earthworm *Eisenia andrei*, but did find gut damage and histological alterations including congestion and fibrosis. Under MP exposure, the earthworm *Eisenia fetida* showed only marginal effects, with the anti-oxidase system negatively affected only at artificially high concentrations (Wang et al., 2019), while the isopod *Porcellio scaber* was not affected by MP at all (Jemec Kokalj et al., 2018). In view of our results and those from these studies, it appears that not all species or their biological endpoints are sensitive to MP, as our findings indicate that body length is a non-sensitive metric for MP toxicity in *C. elegans*. The fact that some biological endpoints were affected by MP and others were not may be explained by the disposable soma theory (Kirkwood, 1977). According to this theory, an organism can try to compensate for stress, in our case induced by MP. This stress and its compensation may lead to an imbalance of biological functions, as one function decreases at the expense of maintenance of another.

Remarkably, in the ingestion assay, we observed that several nematodes that ingested MP (not quantified, however) exhibited internal hatching (**Figure 2C**). In the reproduction assay, four nematodes which had been exposed to MP and died during the exposure also showed internal hatching. Generally, the phenomenon of internal hatching, also referred to as matricide, can occur under conditions of stress, e.g., starvation, exposure to toxins, or presence of bacteria (Mosser et al., 2011; Pestov et al., 2011). Nematodes, supposedly in response to stress, lay their eggs internally to ensure survival of their offspring, as the offspring receive sufficient nutrients in the body of the adult nematode. However, in our study, it was not clear whether internal hatching was induced directly by MP. Kiyama et al. (2012) observed that in the presence of food, uptake of MP was strongly reduced. Conversely, under the condition of food deficiency, more particles were taken up. A possible scenario in our study could have been that a combined effect of MP particle consumption and starvation would have led to internal hatching. The potential link of MP uptake and internal hatching should be investigated quantitatively in future studies.

We are aware that in our approach exposure of *C. elegans* to MP was rather artificial (MP feed suspensions on agar plates). We chose this exposure, though, because we aimed at understanding the general potential of MP to develop a toxicity in *C. elegans*. In soils, it would not have been possible to achieve a general process understanding. The design of more realistic experimental setups with soils is challenging because currently there are only few data on MP contamination in soils and it is not clear whether the MP concentrations found to date in urban (0.3–67.5 g kg^{-1}), riparian (0–0.055 g kg^{-1}), and agricultural soils (0–42,960 particles kg^{-1}) (Helmberger et al., 2019) lead to negative effects on soil biota. Due to detection limits, even less data is available in environmental samples for MP particles <10 μm (Haegerbaeumer et al., 2019) and thus for the ingestible size range of *C. elegans*. Given the aliquot of 100 μl that we gave to each nematode in our experiments, one nematode was effectively exposed to 0.1, 1, and 10 μg of MP. Based on a global median abundance of 12,030 individuals per 1 kg dry soil (van den Hoogen et al., 2019) and the mass-based MP concentrations reported in soil (see above), this translates into an exposure to 0–4.6 μg per nematode for riparian and 25–5,600 μg per nematode for soils in industrial areas. Thus, the applied MP amounts in our study are in a range typically found in natural soils.

CONCLUSION

We found that nematodes can ingest MP particles which might negatively affect their reproduction. Toxic effects of MP on nematode reproduction in soils cannot be ruled out. The toxicity risk for conventional and biodegradable MP particles is likely to be the same, as MP toxicity is rather attributable to physical and indirect nutritional effects rather than to chemical effects. Although we have hints of negative effects of MP on the body length of nematodes, our results are not conclusive. Since nematodes, as key members of the soil food web, may be at risk under MP exposure, our results suggest potentially negative implications for important soil functions, e.g., the regulation of biogeochemical cycles. Further studies are needed to estimate critical effect concentrations and to elucidate the influence of particle shape for nematodes under realistic exposure scenarios in soils.

DATA AVAILABILITY STATEMENT

The datasets generated for this study are available on request to the corresponding author.

AUTHOR CONTRIBUTIONS

LS, SM, EK, RM, HP, and LR contributed conception and design of the study. LS performed the ingestion assay as well as the

reproduction and body length assay supervised by RM and LR. LS conducted the data evaluation and statistics supported by HP. US determined the size distribution and characteristics of the microplastic particles supervised by FB. LS wrote the first draft of the manuscript. All authors contributed to manuscript revision, read and approved the submitted version.

FUNDING

The research is part of the project MiKoBo (Mikrokunststoffe in Komposten und Gärprodukten aus Bioabfallverwertungsanlagen und deren Eintrag in Böden – Erfassen, Bewerten, Vermeiden) which is funded by the Ministry of Environment, Climate and Energy Baden-Württemberg in the framework of BWPLUS – Baden-Württemberg Programm Lebensgrundlage Umwelt und ihre Sicherung (reference number: BWMK18003). HP was financially supported by the Ellrichshausen Foundation.

ACKNOWLEDGMENTS

We thank Julia Resch ("Institut für Kunststofftechnik," Stuttgart, Germany) and Ansilla Bayha (Fraunhofer Institute for Chemical Technology, Pfinztal, Germany) for the grinding and provision of the microplastic particles.

SUPPLEMENTARY MATERIAL

The Supplementary Material for this article can be found online at: https://www.frontiersin.org/articles/10.3389/fenvs.2020.00041/full#supplementary-material

REFERENCES

Acosta, C., Barat, J. M., Martínez-Máñez, R., Sancenón, F., Llopis, S., González, N., et al. (2018). Toxicological assessment of mesoporous silica particles in the nematode *Caenorhabditis elegans*. *Environ. Res.* 166, 61–70. doi: 10.1016/j.envres.2018.05.018

Bandopadhyay, S., Martin-Closas, L., Pelacho, A. M., and DeBruyn, J. M. (2018). Biodegradable plastic mulch films: impacts on soil microbial communities and ecosystem functions. *Front. Microbiol.* 9:819. doi: 10.3389/fmicb.2018.00819

Bardgett, R. D., Cook, R., Yeates, G. W., and Denton, C. S. (1999). The influence of nematodes on below-ground processes in grassland ecosystems. *Plant Soil* 212, 23–33. doi: 10.1023/A:1004642218792

Benjamini, Y., and Hochberg, Y. (1995). Controlling the false discovery rate: a practical and powerful approach to multiple testing. *J. R. Stat. Soc. Ser. B* 57, 289–300. doi: 10.1111/j.2517-6161.1995.tb02031.x

Bläsing, M., and Amelung, W. (2018). Plastics in soil: analytical methods and possible sources. *Sci. Total Environ.* 612, 422–435. doi: 10.1016/j.scitotenv.2017.08.086

Cao, D., Wang, X., Luo, X., Liu, G., and Zheng, H. (2017). Effects of polystyrene microplastics on the fitness of earthworms in an agricultural soil. *IOP Conf. Ser. Earth Environ. Sci.* 61, 012148. doi: 10.1088/1755-1315/61/1/012148

Chae, Y., and An, Y.-J. (2018). Current research trends on plastic pollution and ecological impacts on the soil ecosystem: a review. *Environ. Pollut.* 240, 387–395. doi: 10.1016/j.envpol.2018.05.008

Chen, H., Chen, W., Hui, L., Ruixue, M., Ziling, Y., Liangzhong, L., et al. (2019). A review of toxicity induced by persistent organic pollutants (POPs) and endocrine-disrupting chemicals (EDCs) in the nematode *Caenorhabditis elegans*). *J. Environ. Manag.* 237, 519–525. doi: 10.1016/j.jenvman.2019.02.102

de Souza Machado, A. A., Kloas, W., Zarfl, C., Hempel, S., and Rillig, M. C. (2018). Microplastics as an emerging threat to terrestrial ecosystems. *Global Change Biol.* 24, 1405–1416. doi: 10.1111/gcb.14020

Fang-Yen, C., Avery, L., and Samuel, A. D. T. (2009). Two size-selective mechanisms specifically trap bacteria-sized food particles in *Caenorhabditis elegans*. *Proc. Natl. Acad. Sci. U.S.A.* 106, 20093–20096. doi: 10.1073/pnas.0904036106

Ferris, H. (2010). Contribution of nematodes to the structure and function of the soil food web. *J. Nematol.* 42, 63–67.

Filella, M. (2015). Questions of size and numbers in environmental research on microplastics: methodological and conceptual aspects. *Environ. Chem.* 12:527. doi: 10.1071/EN15012

Foley, C. J., Feiner, Z. S., Malinich, T. D., and Höök, T. O. (2018). A meta-analysis of the effects of exposure to microplastics on fish and aquatic invertebrates. *Sci. Total Environ.* 63, 550–559. doi: 10.1016/j.scitotenv.2018.03.046

Franzellitti, S., Canesi, L., Auguste, M., Wathsala, R. H. G. R., and Fabbri, E. (2019). Microplastic exposure and effects in aquatic organisms: a physiological perspective. *Environ. Toxicol. Pharmacol.* 68, 37–51. doi: 10.1016/j.etap.2019.03.009

Galloway, T. S., Cole, M., and Lewis, C. (2017). Interactions of microplastic debris throughout the marine ecosystem. *Nat. Ecol. Evol.* 1:116. doi: 10.1038/s41559-017-0116

Gonzalez-Moragas, L., Roig, A., and Laromaine, A. (2015). C. elegans as a tool for in vivo nanoparticle assessment. *Adv. Colloid Interface Sci.* 219, 10–26. doi: 10.1016/j.cis.2015.02.001

Griffiths, B., Ritz, K., Ebblewhite, N., and Dobson, G. (1998). Soil microbial community structure: effects of substrate loading rates. *Soil Biol. Biochem.* 31, 145–153. doi: 10.1016/S0038-0717(98)00117-5

Haegerbaeumer, A., Mueller, M.-T., Fueser, H., and Traunspurger, W. (2019). Impacts of micro- and nano-sized plastic particles on benthic invertebrates: a literature review and gap analysis. *Front. Environ. Sci.* 7:1596.

He, F. (2011). Common worm media and buffers. *Bio Protoc.* 1:e55. doi: 10.21769/BioProtoc.55

Helmberger, M. S., Tiemann, L. K., and Grieshop, M. J. (2019). Towards an ecology of soil microplastics. *Funct. Ecol.* 7, 550–560.

Horton, A. A., Svendsen, C., Williams, R. J., Spurgeon, D. J., and Lahive, E. (2017). Large microplastic particles in sediments of tributaries of the river thames, uk - abundance, sources and methods for effective quantification. *Mar. Pollut. Bull.* 114, 218–226. doi: 10.1016/j.marpolbul.2016.09.004

Hothorn, T., Bretz, F., and Westfall, P. (2008). Simultaneous inference in general parametric models. *Biometr. J.. Biometr. Z.* 50, 346–363. doi: 10.1002/bimj.200810425

Huerta Lwanga, E., Gertsen, H., Gooren, H., Peters, P., Salánki, T., van der Ploeg, M., et al. (2016). Microplastics in the terrestrial ecosystem: implications for *Lumbricus terrestris* (oligochaeta, lumbricidae). *Environ. Sci. Technol.* 50, 2685–2691. doi: 10.1021/acs.est.5b05478

Huerta Lwanga, E., Gertsen, H., Gooren, H., Peters, P., Salánki, T., van der Ploeg, M., et al. (2017a). Incorporation of microplastics from litter into burrows of *Lumbricus terrestris*. *Environ. Pollut.* 220, 523–531. doi: 10.1016/j.envpol.2016.09.096

Huerta Lwanga, E., Mendoza Vega, J., Ku Quej, , V., Chi, J., de, L. A., Sanchez Del Cid, L., et al. (2017b).). Field evidence for transfer of plastic debris along a terrestrial food chain. *Sci. Rep.* 7, 14071. doi: 10.1038/s41598-017-14588-2

Hurley, R. R., and Nizzetto, L. (2018). Fate and occurrence of micro(nano)plastics in soils: knowledge gaps and possible risks. *Curr. Opin. Environ. Sci. Health* 1, 6–11. doi: 10.1016/j.coesh.2017.10.006

Jemec Kokalj, A., Horvat, P., Skalar, T., and Kržan, A. (2018). Plastic bag and facial cleanser derived microplastic do not affect feeding behaviour and energy reserves of terrestrial isopods. *Sci. Total Environ.* 615, 761–766. doi: 10.1016/j.scitotenv.2017.10.020

Keller, J., Antje, B., Hajo, H., Ralph, M., Liliane, R., and Matthias, K. (2018). Toxicity Assay for Citrinin, Zearalenone and Zearalenone-14-Sulfate using the

nematode *Caenorhabditis elegans* as model organism. *Toxins* 10:284. doi: 10.3390/toxins10070284

Kim, S. W., and An, Y.-J. (2019). Soil microplastics inhibit the movement of springtail species. *Environ. Int.* 126, 699–706. doi: 10.1016/j.envint.2019.02.067

Kirkwood, T. B. (1977). Evolution of ageing. *Nature* 270, 301–304. doi: 10.1038/270301a0

Kiyama, Y., Miyahara, K., and Ohshima, Y. (2012). Active uptake of artificial particles in the nematode *Caenorhabditis elegans*. *J, Exp. Biol.* 215, 1178–1183. doi: 10.1242/jeb.067199

Kozak, M., and Piepho, H.-P. (2018). What's normal anyway? Residual plots are more telling than significance tests when checking anova assumptions. *J. Agron. Crop Sci.* 204, 86–98. doi: 10.1111/jac.12220

Künkel, A., Becker, J., Börger, L., Hamprecht, J., Koltzenburg, S., Loos, R., et al. (2016). "Polymers, Biodegradable," in *Ullmann's Encyclopedia of Industrial Chemistry (American Cancer Society)* (Wiley-VCH Verlag GmbH & Co. KGaA: Weinheim), 1–29.

Lei, L., Liu, M., Song, Y., Lu, S., Hu, J., Cao, C., et al. (2018a). Polystyrene (nano)microplastics cause size-dependent neurotoxicity, oxidative damage and other adverse effects in *Caenorhabditis elegans*. *Environ. Sci. Nano* 5, 2009–2020. doi: 10.1039/C8EN00412A

Lei, L., Wu, S., Lu, S., Liu, M., Song, Y., Fu, Z., et al. (2018b). Microplastic particles cause intestinal damage and other adverse effects in zebrafish *Danio rerio* and nematode *Caenorhabditis elegans*. *Sci. Total Environ.* 61, 1–8. doi: 10.1016/j.scitotenv.2017.11.103

Leung, M. C. K., Williams, P. L., Benedetto, A., Au, C., Helmcke, K. J., Aschner, M., et al. (2008). *Caenorhabditis elegans*: an emerging model in biomedical and environmental toxicology. *Toxicol. Sci.*106, 5–28. doi: 10.1093/toxsci/kfn121

Maaß, S., Daphi, D., Lehmann, A., and Rillig, M. C. (2017). Transport of microplastics by two collembolan species. *Environ. Pollut.* 225, 456–459. doi: 10.1016/j.envpol.2017.03.009

Maes, T., Jessop, R., Wellner, N., Haupt, K., and Mayes, A. G. (2017). A rapid-screening approach to detect and quantify microplastics based on fluorescent tagging with nile red. *Sci. Rep.* 7, 44501. doi: 10.1038/srep44501

Mangiafico, S. S. (2015). *An r Companion for the Handbook of Biological Statistics, Version 1.3.2*. Available online at: rcompanion.org/documents/RCompanionBioStatistics.pdf (accessed August 06, 2019).

Mosser, T., Matic, I., and Leroy, M. (2011). Bacterium-induced internal egg hatching frequency is predictive of life span in *Caenorhabditis elegans* populations. *Appl. Environ. Microbiol.* 77, 8189–8192. doi: 10.1128/AEM.06357-11

Mueller, M.-T., Fueser, H., Trac, L. N., Mayer, P., Traunspurger, W., and Höss, S. (2020). Surface-related toxicity of polystyrene beads to nematodes and the role of food availability. *Environ. Sci. Technol.* 54, 1790–1798. doi: 10.1021/acs.est.9b06583

Napper, I. E., and Thompson, R. C. (2019). Environmental deterioration of biodegradable, oxo-biodegradable, compostable, and conventional plastic carrier bags in the sea, soil, and open-air over a 3-year period. *Environ. Sci. Technol.* 53, 4775–4783. doi: 10.1021/acs.est.8b06984

Orgiazzi, A., Bardgett, R. D., and Barrios, E. (2016). *Global Soil Biodiversity Atlas: Supporting the eu Biodiversity Strategy and the Global soil Biodiversity Initiative: Preserving Soil Organism Through Sustainable Land Management Practices and Environmental Policies for the Protection and Enhancement of Ecosystem Services. Global Soil Biodiversity Initiative*. Luxembourg: Publications Office of the European Union.

Pestov, N. B., Shakhparonov, M. I., and Korneenko, T. V. (2011). Matricide in *Caenorhabditis elegans* as an example of programmed death of an animal organism: the role of mitochondrial oxidative stress. *Russian J. Bioorganic Chem.* 37, 634–639. doi: 10.1134/S106816201105013X

R Core Team (2018). *R: A Language and Environment for Statistical Computing*. Vienna: R Core Team.

Rillig, M. C., Ingraffia, R., and de Souza Machado, A. A. (2017a). Microplastic incorporation into soil in agroecosystems. *Front. Plant Sci.* 8:1805. doi: 10.3389/fpls.2017.01805

Rillig, M. C., Ziersch, L., and Hempel, S. (2017b). Microplastic transport in soil by earthworms. *Sci. Rep.* 7:1362. doi: 10.1038/s41598-017-01594-7

Rillig, M. C., Lehmann, A., Ryo, M., and Bergmann, J. (2019). Shaping up: toward considering the shape and form of pollutants. *Environ. Sci. Technol.* 53, 7925–7926. doi: 10.1021/acs.est.9b03520

Rodriguez-Seijo, A., Lourenço, J., Rocha-Santos, T. A. P., da Costa, J., Duarte, A. C., Vala, H., et al. (2017). Histopathological and molecular effects of microplastics in Eisenia andrei bouché. *Environ. Pollut.* 220, 495–503. doi: 10.1016/j.envpol.2016.09.092

Sander, M. (2019). Biodegradation of polymeric mulch films in agricultural soils: concepts, knowledge gaps, and future research directions. *Environ. Sci. Technol.* 53, 2304–2315. doi: 10.1021/acs.est.8b05208

Schindelin, J., Arganda-Carreras, I., Frise, E., Kaynig, V., Longair, M., Pietzsch, T., et al. (2012). Fiji: an open-source platform for biological-image analysis. *Nat. Methods* 9, 676–682. doi: 10.1038/nmeth.2019

Schneider, C. A., Rasband, W. S., and Eliceiri, K. W. (2012). NIH image to ImageJ: 25 years of image analysis. *Nat. Methods* 9, 671–675. doi: 10.1038/nmeth.2089

Shim, W. J., Song, Y. K., Hong, S. H., and Jang, M. (2016). Identification and quantification of microplastics using Nile Red staining. *Mar. Pollut. Bull.* 113, 469–476. doi: 10.1016/j.marpolbul.2016.10.049

van den Hoogen, J., Geisen, S., Routh, D., Ferris, H., Traunspurger, W., Wardle, D. A., et al. (2019). Soil nematode abundance and functional group composition at a global scale. *Nature* 572, 194–198.

Wang, J., Coffin, S., Sun, C., Schlenk, D., and Gan, J. (2019). Negligible effects of microplastics on animal fitness and hoc bioaccumulation in earthworm *Eisenia fetida* in soil. *Environ. Pollut.* 249, 776–784. doi: 10.1016/j.envpol.2019.03.102

Wasserstein, R. L., Schirm, A. L., and Lazar, N. A. (2019). Moving to a world beyond " $p < 0.05$". *Am. Stat.* 73, 1–19.

Watteau, F., Dignac, M.-F., Bouchard, A., Revallier, A., and Houot, S. (2018). Microplastic detection in soil amended with municipal solid waste composts as revealed by transmission electronic microscopy and pyrolysis/gc/ms. *Front. Sustain. Food Syst.* 2:253. doi: 10.3389/fsufs.2018.00081

Wu, T., Xu, H., Liang, X., and Tang, M. (2019). *Caenorhabditis elegans* as a complete model organism for biosafety assessments of nanoparticles. *Chemosphere* 221, 708–726. doi: 10.1016/j.chemosphere.2019.01.021

Yeates, G. W., and Bongers, T. (1999). Nematode diversity in agroecosystems. *Agricu. Ecosyst. Environ.* 74, 113–135. doi: 10.1016/S0167-8809(99)00033-X

Yeates, G. W., Bongers, T., de Goede, R. G. M., Freckman, D. W., and Georgieva, S. S. (1993). Feeding habits in soil nematode families and genera—An outline for soil ecologists. *J. Nematol.* 25, 315–331.

Conflict of Interest: The authors declare that the research was conducted in the absence of any commercial or financial relationships that could be construed as a potential conflict of interest.

frontiers in Environmental Science

PERSPECTIVE
published: 29 May 2020
doi: 10.3389/fenvs.2020.00071

Natural Nanoparticles, Anthropogenic Nanoparticles, Where Is the Frontier?

Gaëtane Lespes[1]†, Stéphane Faucher[1]† and Vera I. Slaveykova[2]*†*

[1] University of Pau and Pays de l'Adour (E2S/UPPA), Institut des Sciences Analytiques et de Physico-Chimie pour l'Environnement et les Matériaux, UMR UPPA/CNRS, Pau, France, [2] Environmental Biogeochemistry and Ecotoxicology, Department F.-A. Forel for Environmental and Aquatic Sciences, School of Earth and Environmental Sciences, Faculty of Science, University of Geneva, Geneva, Switzerland

Nano-sized particles are important components of the Earth biogeochemical system. However, in the Anthropocene, the human activities disturbed their natural cycle and increased their abundance by (i) affecting their emissions and releases; (ii) altering the environmental processes involving nanoparticles; and (iii) introducing anthropogenic nanoparticles (ANPs). Intentionally or unintentionally released, the occurrence of the anthropogenic particles in the environment is continuously rising. Both natural and anthropogenic nanoparticles are recognized as important carriers for trace elements and organic micropollutants and key modifiers of their transport, speciation, bioavailability, and effects in the environment. Nevertheless, currently they are considered separately, despite the necessity of more integrated, broader, and non-sectorial perspective taking together particles of different origins and various processes likely to generate and involve them. The present paper provides a perspective on the environmental processes involving anthropogenic and natural nanoparticles (NNPs) and discusses the role of human activities in nanoparticle cycling, as well as the necessity to bridge the divide between the NNPs and ANPs. The discussion will be supported by the examples of our own research to ask, if there is still a frontier between NNPs and ANPs?

Keywords: nanoparticle biogeochemical cycle, pollution, nanoparticle sources, fate, toxicity, Anthropocene

OPEN ACCESS

Edited by:
Moritz Bigalke,
University of Bern, Switzerland

Reviewed by:
Arturo A. Keller,
University of California, Santa Barbara, United States
Michael Hochella,
Virginia Tech, United States

***Correspondence:**
Gaëtane Lespes
gaetane.lespes@univ-pau.fr
Vera I. Slaveykova
vera.slaveykova@unige.ch

†***ORCID**:*
Gaëtane Lespes
orcid.org/0000-0002-1752-8923
Stéphane Faucher
orcid.org/0000-0001-8887-6055
Vera I. Slaveykova
orcid.org/0000-0002-8361-2509

Specialty section:
This article was submitted to Biogeochemical Dynamics, a section of the journal Frontiers in Environmental Science

Received: *26 March 2020*
Accepted: *12 May 2020*
Published: *29 May 2020*

Citation:
Lespes G, Faucher S and Slaveykova VI (2020) Natural Nanoparticles, Anthropogenic Nanoparticles, Where Is the Frontier? Front. Environ. Sci. 8:71. doi: 10.3389/fenvs.2020.00071

INTRODUCTION

Nano-sized particles,[1] naturally present in the Earth, move through different compartments (biosphere, lithosphere, atmosphere, and hydrosphere) within global biogeochemical cycle. They play an important, but not fully understood, role in the dynamics of the overall Earth system. However, human activities disturbed the cycle of natural nanoparticles (NNPs) by (i) affecting their emissions and releases; (ii) altering the environmental processes involving nanoparticles; and (iii) introducing anthropogenic nanoparticles (ANPs). Both incidentally released nanoparticles (INPs)[2]

[1] Although still a question of debate, nano-sized particles definition used in the present paper involve any object (organic, inorganic, or organometallic) of nanometric size (or sub-micrometric size), which can be in dispersed form in a fluid (Faucher et al., 2019; IUPAC, 2019) and the small dimensions confer them peculiar physical and chemical properties that differ from larger objects made of the same material(s) (Maurice and Hochella, 2008). Natural nanoparticle describes a sub-set of the colloidal phase.

[2] Incidental nanoparticles are produced as a result of any form of direct or indirect anthropogenic activity or process.

and engineered nanoparticles (ENPs)[3] form the pool of the ANPs. It is estimated that 1000s of Tg of NNPs, 1–10 Tg of INPs and less than 1 Tg of ENPs from different natural and anthropogenic sources co-exist and move annually between the Earth compartments (Hochella et al., 2019). Despite their small proportion of the total nano-sized particle mass, the amount of ENPs in the environmental compartments continues to increase with ever growing use of nano-enabled materials (Keller and Lazareva, 2014). ENPs were recently considered within the frame of global anthropogenic cycling of elements, concluding that for elements such Ag, Al, Ce, Co, Cu, Fe, Ni, and Zn, ENPs had a minor impact on their cycling, whereas SiO_2 ENPs represented 3–25% of mined Si (Janković and Plata, 2019). However, such integrated Earth system approach has emerged only recently; NNPs and ANPs are thus in most cases considered separately. Only few examples can be found in the literature providing a comprehensive comparison of the behavior of NNPs and ENPs (Baalousha et al., 2011; Wagner et al., 2014; Sigmund et al., 2018). Therefore, broader and integrated approach toward fate and impact of nano-sized particles in the environment would be useful for better understanding Earth systems biogeochemical dynamics. This requires considering nano-sized particles of different origins together with the various processes likely to generate and involve them.

NANOPARTICLE CYCLING IN THE ENVIRONMENT

Natural nanoparticles are generated in different environmental compartments by various physical, chemical, and biological processes (**Figure 1**), such as (bio)chemical weathering of minerals, photo-oxidation, redox and precipitation reactions, (bio)mineralization, physical fragmentation, gas-solid nucleation in the atmosphere, etc. (Sharma et al., 2015). ANPs generation is a result of human-related activity or processes (e.g., combustion), due to the life cycle of products containing nanoparticles or accidental releases. Examples of such sources inherent for human activities include: (i) dust generation by various activities; typically mining, tillage, and demolition/construction. Atmospheric transport then constitutes a vector of long-distance transport (Jun et al., 2016); (ii) atmospheric release and nucleation (Lee et al., 2019); (iii) release of treated and untreated waste water (Brar et al., 2010); and (iv) storage in an insufficiently confined area or spreading of sludge from sewage treatment plants (Meier et al., 2016). Natural processes could also be responsible for the generation of the ANPs from different materials. For example, weathering of plastics could result in a formation of micro- and nano-plastics in waters and marine organisms (Ganesh Kumar et al., 2020; Kögel et al., 2020).

Independently on their origin, the nano-sized particles interact with different abiotic and biotic components, via various interconnected processes leading to their transformation in the environmental compartments. Processes such as aggregation, sedimentation, biological accumulation, biomagnification, dissolution, chemical and physical alterations, etc., are common for both NNPs and ANPs (Baalousha et al., 2011; Wagner et al., 2014; Sigmund et al., 2018). The nano-sized particles, regardless of their origin, participate in the same bio-physicochemical processes (**Figure 1**), which ultimate will determine their fate and impacts (Garner et al., 2017, 2018). The fate and behavior of bare ENPs was similar to their natural counterparts with the same composition (Garner and Keller, 2014; Wagner et al., 2014; Sigmund et al., 2018). Human activities also affect these processes by changing the surrounding physical and/or chemical conditions that govern them.

These processes depend on the multiple factors that can be grouped in three main categories intrinsic to: (i) nano-sized particles, including particle physicochemical speciation, size, shape, surface functionalization, etc.; (ii) environmental variables, including pH, water hardness, and alkalinity, presence and concentrations of different ligands from natural and anthropogenic origins, which may influence chemical and physicochemical speciation; and (iii) biological systems, including habitat, feeding pattern, etc. Abundant information on the environmental implications of ENPs can be found in recent review papers (Lead et al., 2018; Joonas et al., 2019; Mortimer and Holden, 2019; Kögel et al., 2020; Slaveykova et al., 2020).

It is out of the scope to provide a detailed overview on the fate and impact of the nano-sized materials in the environment. Hence, we make a parallel in some key properties and processes to consider toward bridging the gap between NNPs and ANPs.

TOWARD BRIDGING THE GAP BETWEEN NNPS AND ANPS

Whatever their origin, nano-sized particles are characterized by a greater fraction of atoms at the surface, which determine their enhanced surface energy and reactivity (Hochella et al., 2019). Purposely-made ENPs have controlled chemical composition, size, and properties. They therefore have less polydisperse character and some properties are enhanced as compared with NNPs. For example, due to their controlled surface structure and smaller sizes TiO_2 ENPs have catalytic and redox properties that natural ones do not present (Chin et al., 2011). In addition, the presence of persistent engineered coatings on the ENPs gives them properties which differ from the core material in terms of dissolution, stability and effects. Similarly to NNPs, the surface of ANPs is modified in the environmental and living systems, through the adsorption and desorption of organic and inorganic compounds of natural or anthropogenic origin. Such alterations can affect surface properties of nano-sized particles, hence their interactions with trace elements, organic micropollutants, colloids, surfaces, and biota (Wagner et al., 2014; Wang et al., 2015). Therefore, the pure synthetic identity of ENPs could also be questioned given their interactions with different naturally occurring compounds. The existence of "purely natural" NNPs is a source of interrogation insofar as the whole of the biosphere concerned by the processes of genesis and by materials/compounds qualified as natural are

[3]Engineered nanoparticles are purposely designed and produced by humans. Usually defined as particles with a size between 1 and 100 nm (IUPAC, 2019).

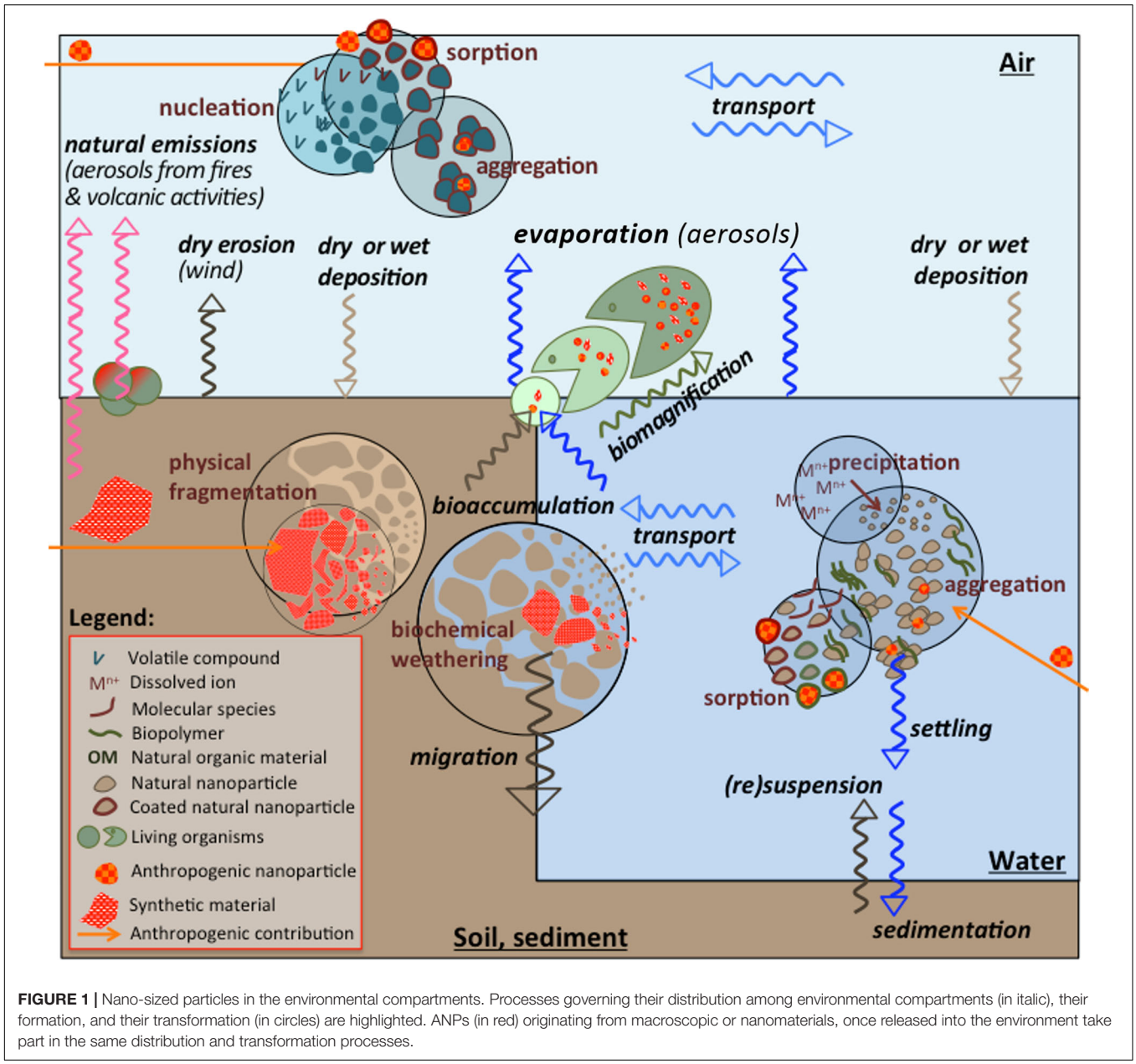

FIGURE 1 | Nano-sized particles in the environmental compartments. Processes governing their distribution among environmental compartments (in italic), their formation, and their transformation (in circles) are highlighted. ANPs (in red) originating from macroscopic or nanomaterials, once released into the environment take part in the same distribution and transformation processes.

possibly affected by human activities. It would therefore be useful to consider that "altered" nano-sized particles involve both anthropogenic and natural components and thus would have more complex environmental fate and impact. Hereafter, we provide shortly two examples considering the interactions of the ANPs with naturally occurred compounds and of the NNPs with inorganic and organic pollutants.

Interaction of ANPs With Naturally Occurring Compounds

Interaction of ANPs with various naturally occurring compounds (e.g., humic acid, extracellular polymeric substances, peptides) results in a formation of eco-corona and gives them new surface properties (Louie et al., 2016; Pulido-Reyes et al., 2017). This new "*environmental identity*" has a great influence on their fate by affecting their dissolution, aggregation/agglomeration, stability in the water column (Gigault et al., 2012; Wang et al., 2015; Louie et al., 2016), deposition to mineral surfaces (Louie et al., 2016), attachment to biological surfaces and bioavailability (von Moos et al., 2014; Louie et al., 2016), and toxicity (Ivask et al., 2014; von Moos and Slaveykova, 2014). For example, natural organic matter was shown to reduce the toxicity of metallic nanoparticles to many organisms (Wang et al., 2016).

Similarly, in biological environment, ANPs interact with various biomolecules (e.g., proteins, peptides, DNA, RNA, lipids, etc.) and earn a new "*biological identity*" determining nanoparticle fate and effects within living organisms. For

example, the antioxidant enzyme catalase formed a corona around AgNPs, and the released Ag together with AgNPs inhibited its enzymatic activity. However, AgNP–superoxide dismutase complex formation only slightly affected the protein conformation and had no impact on the enzymatic activity or AgNP dissolution (Liu et al., 2020). It is currently accepted that the formed bio-corona represents "what the cell sees" (Walczyk et al., 2010). Hence, it plays a critical role in modulation of the biological reactivity and nano-sized particle induced responses in living organisms, which may be significantly distinct from the expected one exclusively driven by the primary ENPs synthetic identity.

Interaction of NNPs With Inorganic and Organic Pollutants

Due to their small size and large specific surface area, NNPs play a key role in the transport, speciation, and bioavailability, and thus the ultimate impact of trace elements (Slaveykova and Wilkinson, 2005; Wilkinson and Lead, 2007; El Hadri et al., 2016), and organic micropollutants (Sigmund et al., 2018). NNPs possess a near infinite array of possible compositions and sizes and include principally oxides and oxyhydroxides of iron, manganese, and aluminum and aluminosilicates; humic-like substances, various biopolymers synthesized and released by living organisms involving various proteins, nucleic acids, and polysaccharides (Wilkinson and Lead, 2007; Hartland et al., 2011). Clear size dependence in a preferential binding of trace metals on NNPs was observed (Worms et al., 2010a,b). Following the adsorption of different inorganic and organic contaminants, the NNPs will acquire a new "*anthropogenic identity*," which will have an important consequence for the pollutant availability and biological outcomes. For example, in the aquatic environment, NNPs reduce the bioavailability of the trace metals to various organisms, including bacteria, fungus, phytoplankton, daphnia, and fish, in direct proportion to the free metal ion concentrations (Slaveykova and Wilkinson, 2005). NNPs could therefore play the role of Trojan horses for their associated pollutants and increase the trace metals bioavailability to filter feeders (e.g., clams, mussels, and oysters) (Luoma and Rainbow, 2005). Similarly, the adsorption of metallic pollutants on ENPs could result in their surface modification, which could change their properties and the way they interact with biota (Naasz et al., 2018; Li et al., 2020).

Overall, despite the existing differences between NNPs and ANPs, similar properties and processes control their fate and effects in the environment. Therefore, process-oriented knowledge has a potential to lead to sound progress in the understanding the nano-sized particles dynamics in the multifaceted Earth (sub-) systems, and feedbacks with human activity.

DATA AVAILABILITY STATEMENT

Publicly available datasets were analyzed in this study. Requests to access the data can be directed to gaetane.lespes@univ-pau.fr.

AUTHOR CONTRIBUTIONS

GL and VS took part in conceptualization, manuscript writing, and editing. SF drew the figure and took part in the manuscript writing. All authors read and agreed to the published version of the manuscript.

REFERENCES

Baalousha, M., Lead, J., Ju-Nam, Y., and Wilderer, P. (2011). Natural colloids and manufactured nanoparticles in aquatic and terrestrial systems. *Treat. Water Sci.* 3, 89–129. doi: 10.1016/b978-0-444-53199-5.00053-1

Brar, S. K., Verma, M., Tyagi, R. D., and Surampalli, R. Y. (2010). Engineered nanoparticles in wastewater and wastewater sludge – Evidence and impacts. *Waste Manag.* 30, 504–520. doi: 10.1016/j.wasman.2009.10.012

Chin, S., Park, E., Kim, M., Bae, G.-N., and Jurng, J. (2011). Synthesis and photocatalytic activity of TiO2 nanoparticles prepared by chemical vapor condensation method with different precursor concentration and residence time. *J. Coll. Interf. Sci.* 362, 470–476. doi: 10.1016/j.jcis.2011.06.034

El Hadri, H., Lespes, G., Chery, P., and Potin-Gautier, M. (2016). Asymmetric flow-field flow fractionation-multidetection coupling for assessing colloidal copper in drain waters from a bordeaux wine-growing area. *Anal. Bioanal. Chem.* 406, 1111–1119. doi: 10.1007/s00216-013-7104-x

Faucher, S., Le Coustumer, P., and Lespes, G. (2019). Nanoanalytics: history, concepts, and specificities. *Environ. Sci. Pollut. Res.* 26, 5267–5281. doi: 10.1007/s11356-018-1646-6

Ganesh Kumar, A., Anjana, K., Hinduja, M., Sujitha, K., and Dharani, G. (2020). Review on plastic wastes in marine environment – Biodegradation and biotechnological solutions. *Mar. Pollut. Bull.* 150:110733. doi: 10.1016/j.marpolbul.2019.110733

Garner, K. L., and Keller, A. A. (2014). Emerging patterns for engineered nanomaterials in the environment: a review of fate and toxicity studies. *J. Nanopart. Res.* 16:2503. doi: 10.1007/s11051-014-2503-2

Garner, K. L., Qin, Y., Cucurachi, S., Suh, S., and Keller, A. A. (2018). Linking exposure and kinetic bioaccumulation models for metallic engineered nanomaterials in freshwater ecosystems. *ACS Sustain. Chem. Eng.* 6, 12684–12694. doi: 10.1021/acssuschemeng.8b01691

Garner, K. L., Suh, S., and Keller, A. A. (2017). Assessing the risk of engineered nanomaterials in the environment: development and application of the nanofate model. *Environ. Sci. Technol.* 51, 5541–5551. doi: 10.1021/acs.est.6b05279

Gigault, J., Grassl, B., and Lespes, G. (2012). Size characterization of the associations between carbon nanotubes and humic acids in aqueous media by asymmetrical flow field-flow fractionation combined with multi-angle light scattering. *Chemosphere* 86, 177–182. doi: 10.1016/j.chemosphere.2011.10.009

Hartland, A., Fairchild, I. J., Lead, J. R., Zhang, H., and Baalousha, M. (2011). Size, speciation and lability of NOM-metal complexes in hyperalkaline cave dripwater. *Geochim. Cosmochim. Acta* 75, 7533–7551. doi: 10.1016/j.gca.2011.09.030

Hochella, M. F., Mogk, D. W., Ranville, J., Allen, I. C., Luther, G. W., Marr, L. C., et al. (2019). Natural, incidental, and engineered nanomaterials and their impacts on the Earth system. *Science* 363:eaau8299. doi: 10.1126/science.aau8299

IUPAC, (2019). *International Union of Pure and Applied Chemistry - Compendium of Chemical Terminology, Gold Book*. Research Triangle Park, CA: IUPAC.

Ivask, A., Juganson, K., Bondarenko, O., Mortimer, M., Aruoja, V., Kasemets, K., et al. (2014). Mechanisms of toxic action of Ag, ZnO and CuO nanoparticles to selected ecotoxicological test organisms and mammalian cells in vitro: a comparative review. *Nanotoxicology* 8, 57–71. doi: 10.3109/17435390.2013.855831

Janković, N. Z., and Plata, D. L. (2019). Engineered nanomaterials in the context of global element cycles. *Environ. Sci. Nano* 6, 2697–2711. doi: 10.1039/C9EN00322C

Joonas, E., Aruoja, V., Olli, K., and Kahru, A. (2019). Environmental safety data on CuO and TiO2 nanoparticles for multiple algal species in natural water: filling the data gaps for risk assessment. *Sci. Total Environ.* 647, 973–980. doi: 10.1016/j.scitotenv.2018.07.446

Jun, Y.-S., Kim, D., and Neil, C. W. (2016). Heterogeneous nucleation and growth of nanoparticles at environmental interfaces. *Acc. Chem. Res.* 49, 1681–1690. doi: 10.1021/acs.accounts.6b00208

Keller, A. A., and Lazareva, A. (2014). Predicted releases of engineered nanomaterials: from global to regional to local. *Environ. Sci. Technol. Lett.* 1, 65–70. doi: 10.1021/ez400106t

Kögel, T., Bjorøy, Ø, Toto, B., Bienfait, A. M., and Sanden, M. (2020). Micro- and nanoplastic toxicity on aquatic life: determining factors. *Sci. Total Environ.* 709:136050. doi: 10.1016/j.scitotenv.2019.136050

Lead, J. R., Batley, G. E., Alvarez, P. J. J., Croteau, M. N., Handy, R. D., McLaughlin, M. J., et al. (2018). Nanomaterials in the environment: behavior, fate, bioavailability, and effectsAn updated review. *Environ. Toxicol. Chem.* 37, 2029–2063. doi: 10.1002/etc.4147

Lee, S.-H., Gordon, H., Yu, H., Lehtipalo, K., Haley, R., Li, Y., et al. (2019). New particle formation in the atmosphere: from molecular clusters to global climate. *J. Geophys. Res. Atmos.* 124, 7098–7146. doi: 10.1029/2018jd029356

Li, M., Liu, W., and Slaveykova, V. I. (2020). Effects of mixtures of engineered nanoparticles and metallic pollutants on aquatic organisms. *Environments* 7:27. doi: 10.3390/environments7040027

Liu, W., Worms, I., and Slaveykova, V. I. (2020). Interaction of silver nanoparticles with antioxidant enzymes. *Environ. Sci. Nano* doi: 10.1039/C9EN01284B

Louie, S. M., Tilton, R. D., and Lowry, G. V. (2016). Critical review: impacts of macromolecular coatings on critical physicochemical processes controlling environmental fate of nanomaterials. *Environ. Sci. Nano* 3, 283–310. doi: 10.1039/C5EN00104H

Luoma, S. N., and Rainbow, P. S. (2005). Why is metal bioaccumulation so variable? Biodynamics as a unifying concept. *Environ. Sci. Technol.* 39, 1921–1931. doi: 10.1021/es048947e

Maurice, P. A., and Hochella, M. F. (2008). Chapter 5 nanoscale particles and processes: a new dimension in soil science. *Adv. Agron.* 100, 123–153. doi: 10.1016/s0065-2113(08)00605-6

Meier, C., Voegelin, A., Pradas del Real, A., Sarret, G., Mueller, C. R., and Kaegi, R. (2016). Transformation of silver nanoparticles in sewage sludge during incineration. *Environ. Sci. Technol.* 50, 3503–3510. doi: 10.1021/acs.est.5b04804

Mortimer, M., and Holden, P. A. (2019). "Chapter 3 - fate of engineered nanomaterials in natural environments and impacts on ecosystems," in *Exposure to Engineered Nanomaterials in the Environment*, eds N. Marmiroli, J. C. White, and J. Song (Amsterdam: Elsevier), 61–103. doi: 10.1016/b978-0-12-814835-8.00003-0

Naasz, S., Altenburger, R., and Kühnel, D. (2018). Environmental mixtures of nanomaterials and chemicals: The Trojan-horse phenomenon and its relevance for ecotoxicity. *Sci. Tot. Environ.* 635, 1170–1181. doi: 10.1016/j.scitotenv.2018.04.180

Pulido-Reyes, G., Leganes, F., Fernández-Piñas, F., and Rosal, R. (2017). Bio-nano interface and environment: a critical review. *Environ. Toxicol. Chem.* 36, 3181–3193. doi: 10.1002/etc.3924

Sharma, V. K., Filip, J., Zboril, R., and Varma, R. S. (2015). Natural inorganic nanoparticles – formation, fate, and toxicity in the environment. *Chem. Soc. Rev.* 44, 8410–8423. doi: 10.1039/C5CS00236B

Sigmund, G., Jiang, C., Hofmann, T., and Chen, W. (2018). Environmental transformation of natural and engineered carbon nanoparticles and implications for the fate of organic contaminants. *Environ. Sci. Nano* 5, 2500–2518. doi: 10.1039/C8EN00676H

Slaveykova, V. I., Li, M., Worms, I. A., and Liu, W. (2020). When environmental chemistry meets ecotoxicology: bioavailability of inorganic nanoparticles to phytoplankton. *CHIMIA* 74, 115–121. doi: 10.2533/chimia.2020.115

Slaveykova, V. I., and Wilkinson, K. J. (2005). Predicting the bioavailability of metals and metal complexes: critical review of the biotic ligand model. *Environ. Chem.* 2, 9–24. doi: 10.1071/en04076

von Moos, N., Bowen, P., and Slaveykova, V. I. (2014). Bioavailability of inorganic nanoparticles to planktonic bacteria and aquatic microalgae in freshwater. *Environ. Sci. Nano* 1, 214–232. doi: 10.1039/c3en00054k

von Moos, N., and Slaveykova, V. I. (2014). Oxidative stress induced by inorganic nanoparticles in bacteria and aquatic microalgae – state of the art and knowledge gaps. *Nanotoxicology* 8, 605–630. doi: 10.3109/17435390.2013.809810

Wagner, S., Gondikas, A., Neubauer, E., Hofmann, T., and von der Kammer, F. (2014). Spot the difference: engineered and natural nanoparticles in the environment—release, behavior, and fate. *Angewa. Chem. Intern. Edn.* 53, 12398–12419. doi: 10.1002/anie.201405050

Walczyk, D., Bombelli, F. B., Monopoli, M. P., Lynch, I., and Dawson, K. A. (2010). What the cell "sees" in bionanoscience. *J. Am. Chem. Soc.* 132, 5761–5768. doi: 10.1021/ja910675v

Wang, H., Adeleye, A. S., Huang, Y., Li, F., and Keller, A. A. (2015). Heteroaggregation of nanoparticles with biocolloids and geocolloids. *Adv. Coll. Interf. Sci.* 226, 24–36. doi: 10.1016/j.cis.2015.07.002

Wang, Z., Zhang, L., Zhao, J., and Xing, B. (2016). Environmental processes and toxicity of metallic nanoparticles in aquatic systems as affected by natural organic matter. *Environ. Sci. Nano* 3, 240–255. doi: 10.1039/C5EN00230C

Wilkinson, K. J., and Lead, J. R. (2007). *Environmental Colloids and Particles. Behaviour, Separation and Characterisation*. Chichester: John Wiley Sons, Ltd.

Worms, I. A. M., Szigeti, Z. A. G., Dubascoux, S., Lespes, G., Traber, J., Sigg, L., et al. (2010a). Colloidal organic matter from wastewater treatment plant effluents: characterization and role in metal distribution. *Water Res.* 44, 340–350. doi: 10.1016/j.watres.2009.09.037

Worms, I. A. M., Traber, J., Kistler, D., Sigg, L., and Slaveykova, V. I. (2010b). Uptake of Cd(II) and Pb(II) by microalgae in presence of colloidal organic matter from wastewater treatment plant effluents. *Environ. Pollut.* 158, 369–374. doi: 10.1016/j.envpol.2009.09.007

Conflict of Interest: The authors declare that the research was conducted in the absence of any commercial or financial relationships that could be construed as a potential conflict of interest.

frontiers in Environmental Science

REVIEW
published: 11 June 2020
doi: 10.3389/fenvs.2020.00060

Behavior and Bio-Interactions of Anthropogenic Particles in Marine Environment for a More Realistic Ecological Risk Assessment

Ilaria Corsi, Elisa Bergami and Giacomo Grassi*

Department of Physical, Earth and Environmental Sciences, University of Siena, Siena, Italy

Owing to production, usage, and disposal of nano-enabled products as well as fragmentation of bulk materials, anthropogenic nanoscale particles (NPs) can enter the natural environment and through different compartments (air, soil, and water) end up into the sea. With the continuous increase in production and associated emissions and discharges, they can reach concentrations able to exceed toxicity thresholds for living species inhabiting marine coastal areas. Behavior and fate of NPs in marine waters are driven by transformation processes occurring as a function of NP intrinsic and extrinsic properties in the receiving seawaters. All those aspects have been overlooked in ecological risk assessment. This review critically reports ecotoxicity studies in which size distribution, surface charges and bio–nano interactions have been considered for a more realistic risk assessment of NPs in marine environment. Two emerging and relevant NPs, the metal-based titanium dioxide (TiO_2), and polystyrene (PS), a proxy for nanoplastics, are reviewed, and their impact on marine biota (from planktonic species to invertebrates and fish) is discussed as a function of particle size and surface charges (negative vs. positive), which affect their behavior and interaction with the biological material. Uptake of NPs is related to their nanoscale size; however, *in vivo* studies clearly demonstrated that transformation (agglomerates/aggregates) occurring in both artificial and natural seawater drive to different exposure routes and biological responses at cellular and organism level. Adsorption of single particles or agglomerates onto the body surface or their internalization in feces can impair motility and affect sinking or floating behavior with consequences on populations and ecological function. Particle complex dynamics in natural seawater is almost unknown, although it determines the effective exposure scenarios. Based on the latest predicted environmental concentrations for TiO_2 and PS NPs in the marine environment, current knowledge gaps and future research challenges encompass the comprehensive study of bio–nano interactions. As such, the analysis of NP biomolecular coronas can enable a better assessment of particle uptake and related cellular pathways leading to toxic effects. Moreover, the formation of an environmentally derived corona (i.e., eco-corona) in seawater accounts for NP physical–chemical alterations, rebounding on interaction with living organisms and toxicity.

Keywords: anthropogenic particles, marine environment, ecological risk assessment, polystyrene, titanium dioxide, behavior, eco-corona, biomolecular corona

OPEN ACCESS

Edited by:
Antonia Praetorius,
University of Amsterdam, Netherlands

Reviewed by:
Julian Gallego Urrea,
University of Gothenburg, Sweden
Huacheng Xu,
Nanjing Institute of Geography and Limnology (CAS), China

****Correspondence:***
Ilaria Corsi
ilaria.corsi@unisi.it

Specialty section:
This article was submitted to Biogeochemical Dynamics, a section of the journal Frontiers in Environmental Science

Received: *07 January 2020*
Accepted: *28 April 2020*
Published: *11 June 2020*

Citation:
Corsi I, Bergami E and Grassi G (2020) Behavior and Bio-Interactions of Anthropogenic Particles in Marine Environment for a More Realistic Ecological Risk Assessment. Front. Environ. Sci. 8:60. doi: 10.3389/fenvs.2020.00060

INTRODUCTION

Engineered nanoscale materials (NMs) and particles (NPs) are used extensively in a wide range of emerging technologies and commercial applications including biomedicine, pharmaceuticals and personal care products, renewable energy, and electronic devices (Nel et al., 2006). According to EU recommendations, a nanomaterial is defined as "a material with one or more dimensions in the size range 1–100 nm" (European Commission [EU], 2011). Another commonly agreed definition is "any organic, inorganic, or organometallic materials presenting specific chemical, physical, and/or electrical properties that vary as a function of the size and shape of the material" (Hochella et al., 2019).

Owing to production, usage, and disposal of nano-enabled products as well as fragmentation of bulk materials, anthropogenic NPs can enter the natural environment, and through different compartments (air, soil, and water), end up into the sea (Corsi et al., 2014). With the continuous increase in production and associated emissions and discharges as well as due to weathering processes occurring during various stages of the product life cycle, they can reach concentrations able to exceed toxicity thresholds for living species inhabiting marine coastal areas (Garner et al., 2017; Lebreton and Andrady, 2019). Modeled predicted environmental concentrations (PECs) of the most common inorganic and organic engineered NMs in surface waters, based on production, usage, disposal, and fragmentation, have been estimated in the range of $<15\ \mu g\ L^{-1}$ for nanoplastics, around $\mu g\ L^{-1}$ for titanium dioxide (TiO_2) and zinc oxide (ZnO) NPs, and $ng\ L^{-1}$ for silver (Ag) NPs, fullerenes, carbon nanotubes (CNTs), and cerium oxide (CeO_2) (Gottschalk et al., 2013; Sun et al., 2014; Lenz et al., 2016; Renner et al., 2018). PECs are likely to increase in the near future due to the growing production and commercial applications of nano-enabled products and fragmentation of larger particles already present in the environment as for instance for nanoplastics (Andrady, 2017).

Particles reaching the sea may substantially differ in size as well as in physical chemical properties from primary particles incorporated in commercial products (Lowry et al., 2012; Mitrano et al., 2015; Nowack and Mitrano, 2018). During synthesis, attributes as chemical composition, size, geometry, crystallinity, porosity, roughness, hydrophobicity/hydrophilicity and surface coating are tightly controlled, resulting in small particles having unique chemical and physical properties. They reach the sea following the same routes of legacy and emerging chemical pollutants through domestic and industrial discharges and mismanaged waste disposal from which they ultimately are transported to wastewater treatment plants (WWTPs) and released in sewage effluents (Baalousha et al., 2016; Garner et al., 2017; Choi et al., 2018). Once reaching sea water, being rarely homogeneous, they interact with high amounts of ionic species (released by mineral salts) and inorganic and organic colloidal particles [i.e., iron oxides and natural organic matter (NOM)], which affect their fate and behavior (Keller et al., 2010; Petosa et al., 2010; von der Kammer et al., 2012; Praetorius et al., 2014).

Both heteroaggregation (i.e., the aggregation between non-homologous particles) and homoaggregation (i.e., aggregation of NPs among themselves) represent important processes (Praetorius et al., 2020) that will occur in the presence of relatively high pH (8) and ionic strength such as in sea water [mainly due to chloride (Cl^-), sodium (Na^+), sulfate (SO^{2-}), magnesium (Mg^{2+}), calcium (Ca^{2+}), and potassium (K^+)] (Therezien et al., 2014).

Biopolymers produced by marine phytoplankton, known as exopolymeric substances (EPS), can influence aggregation and transformation of NPs in aqueous media. Indeed, they can be present as dissolved organic matter (DOM) or as colloidal particles [particulate organic matter (POM)], namely, transparent exopolymer substances (TEP) (Long and Azam, 1996; Passow, 2002; Mari et al., 2017). Furthermore, NPs can promote the transition of such DOM molecules into suspended particles, thereby altering the DOM–POM balance of organic matter in seawater (Chen et al., 2011; Shiu et al., 2019). EPS can change their assembly kinetics in the presence of NPs, following both hydrophobic and electrostatic interactions, ultimately functioning as nucleation sites for phytoplanktonic exudates (Chen et al., 2011; Adeleye and Keller, 2014; Adeleye et al., 2014; Kadar et al., 2014). Given the abundance of natural colloids in coastal and oceanic waters, it is expected that heteroaggregation outclasses the contribution of homoaggregation in determining NP aquatic behavior and environmental fate. NP interplay with ubiquitous organic and inorganic colloids takes shape in highly complex heteroaggregation processes, whose outcomes were exhaustively delineated by Praetorius et al. (2020). In particular, the behavior of natural colloids will be more relevant in determining the expected environmental fate of NP in heteroaggregates than previsions based solely on homoaggregation processes. In this regard, different heteroaggregation pathways can be envisaged, starting with NP-colloid dimer formation and evolving toward more complex arrangements. Ultimately, however, natural colloid-attached NPs will generally follow the transport dictated by the larger suspended particulate matter, postulating consequences for interactions with living entities and ecotoxicity.

Differently, interaction of NPs with dissolved biomolecules can, in certain conditions, lead natural organic matter (NOM) into the formation of a nanoscale coating analogous to protein *corona* in mammalian systems, potentially affecting aggregation/deposition and transport of the NPs in fluids, but more importantly uptake and toxicity to marine species (Lundqvist et al., 2008; Monopoli et al., 2011). Such new extrinsic properties related to the formation of a *protein corona* may affect consistently the biological activity of NPs in terms of biodistribution, cellular uptake (biokinetics), and ultimate toxicity (Marques-Santos et al., 2018; Grassi et al., 2019).

Overall, a deeper understanding of NP eco-interactions is crucial for predicting their fate and ecotoxicity. Owing to the complexity in predicting and modeling NP properties and interactions in natural seawater (NSW), ecotoxicity could be a valuable tool for both screening and categorizing NPs for risk assessment purposes. On the other hand, more realistic

exposure studies and the formulation of *ad hoc* guidance protocols are required for a proper ecological risk assessment of nanoscale particles (Corsi et al., 2014, 2018; Petersen et al., 2015; Holden et al., 2016).

The lack of suitable analytical methods for a fast and cost-efficient detection of anthropogenic particles in aquatic matrices is one of the major constraints for the comprehensive understanding of the biogeochemistry of anthropogenic NPs, such as TiO_2 and PS NPs (da Silva et al., 2011; Huvet et al., 2016; Schwaferts et al., 2019).

In order to understand the potential effects and toxicity mechanisms of these anthropogenic NPs to the marine biota and provide methodologies for environmental risk assessment purposes, several ecotoxicity studies have focused on acute exposures of marine model organisms at the base of the food webs, ranging from phytoplankton and zooplankton to benthic filter feeders. Most of the studies reported are representative of worst-case scenarios in coastal areas, where these anthropogenic NPs have been predicted to reach high concentrations (Tovar-Sánchez et al., 2013; Labille et al., 2020).

This review critically reports ecotoxicity studies in which size distribution, surface charges, and bio–nano interactions have been considered for a more realistic risk assessment of anthropogenic NPs in marine environment. Two emerging and relevant NPs, the metal-based TiO_2 and polystyrene (PS) as a proxy for nanoplastics, are reviewed, and their impact on marine biota (from planktonic species to invertebrates and fish) is discussed as a function of particle size and surface charges (negative vs. positive), which affect their behavior and interaction with the biological material.

TiO_2 AND PS NANOPARTICLE PROPERTIES

Titanium dioxide NPs have been largely included in several commercial products (industrial, pharmaceutical, and food) due to their brightness, high refractive index, and UV resistance (Vance et al., 2015). Their photoelectronical properties allow solar energy conversion and photocatalytic chemical degradation piloting specific nanotechnological application as for instance in solar cells and in water and wastewater treatment including disinfection due to the generation of reactive species upon UV irradiation (390 nm) (Carp et al., 2004; Chong et al., 2010). Upon photoexcitation, nanoscale TiO_2 produces an electron-hole pair that may migrate to the particle surface where it is involved in surface oxidation reactions or remove an electron from hydroxide, producing the hydroxyl radical. Such photochemical properties rebound on their safety once reaching the natural environment both from direct application (e.g., water purification) or indirectly once released from commercial products (e.g., sunscreen, paints, and textiles) (Robichaud et al., 2009; Botta et al., 2011; Windler et al., 2012). Anionic species, mainly carbonate and chloride, naturally occurring in seawater media, have been shown to significantly reduce TiO_2 NP photoreactivity and increase aggregation, thus, having a strongest role in suppressing hydroxyl radical generation by substituting hydroxyl ions. Haynes et al. (2017) recently reviewed photocatalytic effects of TiO_2 NPs on aquatic species underlining how important it is to define environmental relevant factors in water media able to affect NP physico-chemical properties and, therefore, behavior and effects.

Polymeric-based NPs, such as PS NPs, may enter the environment both from primary sources, when present as newly synthesized nano-polymers, which are not retained by WWTPs (Blair et al., 2017), and secondary sources, as nanoscale polymers derived from the degradation of mismanaged products (Lambert et al., 2013; Andrady, 2017). Polymeric NPs have been used in several nanotechnology applications, ranging from biosensors and photonics (Velev and Kaler, 1999) to cosmetics (Guterres et al., 2007; Leslie, 2014; Hernandez et al., 2017), food nanocomposites (Silvestre et al., 2011; Hernandez et al., 2019), and drug nanocarriers (Jiménez-Fernández et al., 2014). In nanomedicine, many *in vitro* studies in human cell lines have been carried out using functionalized PS NPs to provide insights into the specific mechanisms of cell recognition, signaling cascade, and pathways of toxicity (e.g., Johnston et al., 2010; Bexiga et al., 2011; Liu et al., 2011; Salvati et al., 2011; Fröhlich et al., 2012; Wang et al., 2013; Loos et al., 2014). The most common PS NPs are carboxylate (PS-COOH) and amino-modified (PS-NH_2), corresponding to a negative and positive surface, charge respectively, usually associated to peculiar cellular pathways (Bexiga et al., 2011, 2014; Salvati et al., 2011; Wang et al., 2013).

From a wider environmental perspective, potential emissions of PS NPs are also associated with the slow and inevitable breakdown of large PS-based products once released in the marine environment, due to mechanical processes (Zhang et al., 2012; Kuo et al., 2014), weathering agents (e.g., UV radiation and high temperature) (Lambert and Wagner, 2016), and biota (Davidson, 2012).

An overwhelming part of the scientific research has been dedicated to the study of the occurrence, distribution, transformation, and impacts of marine litter. The continuous degradation of plastic debris in the water column, down to the nano-fraction, has been at first hypothesized (Cózar et al., 2014) and then confirmed by laboratory (Zhang et al., 2012; Gigault et al., 2016; Lambert and Wagner, 2016; Hernandez et al., 2019; Zhu et al., 2020) and *in situ* studies (Ter Halle et al., 2017; Schirinzi et al., 2019), raising concerns due to the potential harm to the marine biota associated to the lower plastic size (as reviewed by Chae and An, 2017). In this context, the term nanoplastics usually refers to polymers with various colors and shapes (e.g., fiber, film, spherule, and fragment), and sizes below 1 μm, thus, comprehensive of the sub-micron and nanometric fraction (Hartmann et al., 2019).

NP FATE AND BEHAVIOR IN SEA WATER

Owing to their growing production and continuous inflow into the environment (Gottschalk and Nowack, 2011; Garner et al., 2017), anthropogenic NPs such as TiO_2 and PS NPs are likely to be incorporated in natural biogeochemical cycles, though

it is difficult to determine their exact contribution alongside naturally occurring NPs. Once in the marine environment, anthropogenic NPs should not be conceived as single entities, but as a dynamic system of particles interacting with the surrounding ionic species and other colloids. To address these features, several heteroaggregation studies have investigated the individual role of monovalent (NaCl) and divalent salts ($MgCl_2$, $CaCl_2$) and their valences on NP behavior and stability as well as NOM model compounds such as fulvic acid (FA), tannic acid (TA), and humic acid (HA) in simplified systems (Romanello and Fidalgo de Cortalezzi, 2013; Cai et al., 2018; Danielsson et al., 2018; Singh et al., 2019).

In order to describe these complex interactions, the Derjaguin–Landau–Verwey–Overbeek (DLVO) theory is commonly applied (Romanello and Fidalgo de Cortalezzi, 2013; Cai et al., 2018), although it is restrictive to the balance between electrostatic and van der Waals forces. Several extensions of the DLVO theory have also been proposed to model inter-NP interactions in suspensions, for example, considering surface roughness, hydration forces, and steric effects (Wu et al., 1999; Walsh et al., 2012; Cardellini et al., 2019; Praetorius et al., 2020).

As a result of the NP intrinsic (e.g., size, shape, roughness, and crystallinity) and extrinsic (e.g., temperature, ionic strength and composition, NOM) properties (Petosa et al., 2010; Baalousha, 2017), NPs may undergo rapid transformations in NSW, which drive NP fate and determine the presence (or absence) of effects on the marine biota (Matranga and Corsi, 2012; Corsi et al., 2014; Blasco et al., 2015).

In order to ascertain NP features in natural exposure media, light scattering [i.e., dynamic light scattering (DLS)] and electrophoretic mobility (EM) analyses are among the most common techniques employed, providing information about NP hydrodynamic size, agglomeration kinetics, and surface charge (da Silva et al., 2011; Ribeiro et al., 2017; Cai et al., 2018; Mourdikoudis et al., 2018). The measurement of ζ-potential (mV) by EM can be used as an indicator of the NP surface charge and, thus, colloidal stability in the medium, with low absolute values usually associated with the screening of NP surface charge (Mourdikoudis et al., 2018). DLS and EM techniques are usually coupled with scanning or transmission electron microscopy (SEM/TEM), which allow to display the agglomeration state of colloidal suspensions and also the specific interactions occurring at the biological surfaces, such as bacteria (Gupta et al., 2016; Fu et al., 2018), microalgae (e.g., Chen et al., 2011; Wang et al., 2016; Bergami et al., 2017; González-Fernández et al., 2019; Seoane et al., 2019), and invertebrate cells (e.g., Canesi et al., 2016a,b; Ciacci et al., 2019). The limit of these techniques is the high concentration of the sample required (usually in the range of $\mu g\ ml^{-1}$) (Ribeiro et al., 2017), which often do not reflect PECs for the anthropogenic NPs, in the range of $\mu g\ L^{-1}$ for TiO_2NPs and $ng\ L^{-1}$ for PS NPs (da Silva et al., 2011; Gottschalk et al., 2013).

TiO_2NP Behavior in Seawater Media

One of the most common TiO_2 NPs tested in ecotoxicity studies is the P25 powder, characterized by a spheroid irregular structure, mostly containing anatase and with a primary size of 24 ± 7 nm (Brunelli et al., 2013; Della Torre et al., 2015b). Under controlled laboratory conditions, TiO_2 stock suspensions are extensively sonicated prior to use to ensure a good dispersion in the exposure media, as described by Brunelli et al. (2013). Once in NSW, TiO_2 NPs have been shown to quickly agglomerate, reaching micrometric sizes and wide size distribution within the first minutes after the preparation of the colloidal suspensions (Della Torre et al., 2015b; Hu et al., 2018; Ciacci et al., 2019). The same behavior has been observed in standard marine algal culture (F/2) medium, characterized by high salt content (Morelli et al., 2018). In solutions with high ionic strength, divalent cations (Ca^{2+} and Mg^{2+}) have a major role in TiO_2 aggregation, since they can adsorb onto NP surfaces, neutralizing the negative charge at pH values greater than the point of zero charge (French et al., 2009; Romanello and Fidalgo de Cortalezzi, 2013). On the contrary, TiO_2 nanoscale aggregates have been found soon after dispersion in media characterized by lower ionic strength, such as freshwater (Sillanpää et al., 2011), and absence of NOM, such as phosphate-buffered saline (PBS) (Grimaldi et al., 2013) and artificial sea water (ASW) (Brunelli et al., 2013). Both the agglomerate size and rate in NSW have been found to increase with TiO_2 NP concentration, due to the enhanced collision among NPs (Hu et al., 2018). The surface of TiO_2 NPs is dominated by three groups (i.e., $TiO^{-4/3}$, ${TiO_2}^{-2/3}$, and TiO_3) (Bourikas et al., 2001), displaying a point of zero charge at pH 6–8, depending on the electrolytes present in solution (Romanello and Fidalgo de Cortalezzi, 2013). In natural marine waters, TiO_2 NPs usually display a negative surface charge, which is strongly reduced (in absolute values) in NSW, due to the ionic strength-induced compression of NP electrical double layer (Brunelli et al., 2013; Romanello and Fidalgo de Cortalezzi, 2013; Morelli et al., 2018). Owing to their strong agglomeration behavior, TiO_2 NPs have been shown to settle in NSW in a concentration-dependent manner, with the removal of 50% up to 80% of the suspended NPs over 6 h observed at 10 and 50 $\mu g\ ml^{-1}$, respectively (Della Torre et al., 2015b). Doyle et al. (2015) observed that up to $97 \pm 5.1\%$ of TiO_2 NPs were present as heteroaggregates in NSW incorporated in the marine snow, with enhancing settling rates over 72 h. Similarly, Morelli et al. (2018) reported an initial constant sedimentation rate of TiO_2 NPs in the F/2 medium, with 58% of TiO_2 settling at 6 h after dispersion, followed by a 92% removal reached at 24 h. Although some nanoscale TiO_2 aggregates (200 nm) may still remain in suspension, as shown by DLS analysis of TiO_2 NPs at 1 $\mu g\ ml^{-1}$ after 24 h in NSW from the Adriatic Sea (Ciacci et al., 2019), the complete sedimentation of TiO_2 NPs can be reached after 50 h, regardless of the presence of NOM (Brunelli et al., 2013) or trace metals such as cadmium at 100 $\mu g\ L^{-1}$ (Della Torre et al., 2015b), indicating that high ionic strength (i.e., salinity from 35‰ to 41‰) mainly determines the behavior of TiO_2 NPs in the marine environment. On the opposite, TiO_2 suspensions in ultrapure water appear to be stable over time (6 h) (Della Torre et al., 2015b).

Several studies have explored the effect of NOM on TiO_2 stability and behavior in aquatic environments to correlate NOM–NP interactions to the toxicity observed in aquatic species (reviewed in Grillo et al., 2015). However, quantitative predictions are difficult due to the heterogeneity and variability of colloidal interactions, which are usually assessed in

simple systems with single ionic species and/or NOM analogs (Praetorius et al., 2020). NOM model compounds, such as FA, TA, and HA, generally exert a stabilizing effect of TiO_2 suspensions via adsorption or hydrophobic interactions, with an increase in NP ζ-potential toward more negative values (Romanello and Fidalgo de Cortalezzi, 2013; Mwaanga et al., 2014; Danielsson et al., 2018). For example, in the case of Suwannee River FA, functional carboxylic and phenolic groups may interact with TiO_2 (anatase) active surface sites upon adsorption, with consequent electrostatic repulsion and steric hindrance (Danielsson et al., 2018). Such NOM sorption is inversely pH dependent, with increasing electrostatic repulsion at pH > 8, since NOM molecules become highly ionized and thus negatively charged, similar to TiO_2 NPs (Mwaanga et al., 2014). Bioavailability (and toxicity) of TiO_2 NPs may also depend on the specific fraction of NOM, which preferentially sorb onto TiO_2 NPs. Mwaanga et al. (2014) reported a higher sorption of NOM compounds characterized by high molecular weight to TiO_2 NPs, regardless of NOM concentration. This is in agreement with studies on other engineered NPs, showing that NP stability increases in the presence of NOM with high molecular weight (Louie et al., 2015). However, the stabilizing effect of NOM can be masked in high ionic strength media, in which TiO_2 aggregation is favored by the interaction with divalent cations, which can lead to specific ion–NOM bridges (Romanello and Fidalgo de Cortalezzi, 2013; Luo et al., 2018).

The effect of ocean acidification on TiO_2 agglomeration dynamics in the marine environment has been evaluated by Shi et al. (2019). With respect to nanoscale agglomerates (average of 334.8 nm) formed in NSW at an ambient pH of 8.1, the authors observed an increase in TiO_2 NP size at lower pH, reaching an average of 439.8 and 537.1 nm at pH of 7.8 and 7.4, respectively. These results suggest that, under future ocean acidification scenarios, these anthropogenic NPs as large agglomerates could further change their behavior and are bioavailable to different species.

PS NP Behavior in Seawater Media

Several ecotoxicity studies reported the characterization of PS NP behavior in filtered NSW in simplified enclosed systems under controlled laboratory conditions, but with the attempt to mimic natural environmental conditions. These studies indicate that nanoplastic behavior and fate in temperate coastal regions mainly depend on their size and surface functionalization, with major differences observed between plain PS and PS-COOH vs. PS-NH_2 NPs, as reported below.

Negatively charged PS NPs, such as PS-COOH NPs, are usually prone to agglomerate in the range of 0.9–1.8 μm soon after dispersion in aqueous media characterized by high ionic strength (>38‰), basic pH, and NOM. Such agglomeration phenomena are largely supported by the DLVO theory and related extensions (Cai et al., 2018; Singh et al., 2019; Wu et al., 2019). Examples are represented by microalgae culture medium (Bergami et al., 2017) and NSW (Della Torre et al., 2014; Bergami et al., 2016; Manfra et al., 2017; Tallec et al., 2018; Grassi et al., 2019), where slight differences in NP agglomerates and size distribution are potentially related to the spatial and temporal variability in seawater chemical composition (i.e., organic matter and ions). In the studies mentioned above, large agglomerates of PS-COOH NPs were related to a wide size distribution and a reduced negative surface charge, as suggested by low ζ-potential values, corresponding to about −10 mV, compared to their values in ultrapure water, up to −66 mV (Bergami et al., 2017). Contrary to these previous works, González-Fernández et al. (2019) observed that PS-COOH NPs in seawater kept a small hydrodynamic size, which was stable for 5 h. The authors hypothesized that the different behavior in NSW was related to complex NP–environmental interactions, although the variability in PS NP intrinsic properties, such as particle density (1.03 g/cm^3 vs. 1.05–1.06 g/cm^3 in previous studies) or experimental conditions (constant rotation vs. static test in previous studies), might have dictated such different agglomeration.

Plain PS NPs with no functionalization typically exhibited a negative surface charge and a behavior in NSW similar to PS-COOH NPs, with a slight (Brandts et al., 2018) or pronounced (Tallec et al., 2018; Ciacci et al., 2019) increase in the average hydrodynamic size with respect to their optimal dispersion in ultrapure water, as well as a decrease in absolute ζ-potential. Stability of plain PS NPs in NSW has been reported in the first hours after the preparation of the suspensions (Mishra et al., 2019), though time-dependent agglomeration that occurred later at 24 and 48 h (Brandts et al., 2018; Tallec et al., 2018; Mishra et al., 2019). From DLS data, Brandts et al. (2018) also suggested the sorption capacity of carbamazepine, one of the most common pharmaceuticals found in the environment, onto PS NPs, while NP interaction with heavy metals mostly depends on their speciation in the aquatic environments (Singh et al., 2019). Differently from plain and PS-COOH NPs, once suspended in NSW, positively charged PS NPs usually display a hydrodynamic size close to their nominal diameter (Wu et al., 2019). For example, different batches of PS-NH_2 NPs (50 nm) from the Bangs Laboratories Inc., kept an average hydrodynamic size ranging from 58 to 196 nm in different NSW media from the Mediterranean region (Della Torre et al., 2014; Bergami et al., 2016, 2017; Manfra et al., 2017; Pinsino et al., 2017; Marques-Santos et al., 2018; Grassi et al., 2019), thus showing no or slight agglomeration soon after dispersion. However, time-resolved DLS measurements revealed a strong agglomeration behavior of PS-NH_2 in NSW after 48 and 72 h, with large aggregates up to 5 μm, which were more prone to sedimentation (Varó et al., 2019).

In terms of interaction with NOM, HA was found to stabilize negatively charged PS-based nanoplastics (100 nm), such as plain PS and PS-COOH NPs, due to electrostatic repulsion between negative charges and steric effect (Wu et al., 2019). On the contrary, once adsorbed onto positively charged PS-NH_2 NPs, HA was able to reverse the surface charge at HA concentrations above 5 mg L^{-1}, inducing PS-NH_2 to agglomerate at 10 mg L^{-1} HA (Wu et al., 2019). Divalent cations (e.g., Ca^{2+} and Mg^{2+}) present in seawater can induce higher agglomeration of PS NPs, compared to monovalent ones (Na^{+}) (Cai et al., 2018; Singh et al., 2019). In a $CaCl_2$ solution containing HA, high ionic valence was found to facilitate bridging effect between nanoplastics and HA, enhancing complexation (Singh et al., 2019). PS NPs (25 nm)

with different surface functionalization have also been shown to easily assemble with DOM in NSW due to hydrophobic interactions, with potential repercussions on carbon dynamics in marine environments even at low NP concentrations (10 $\mu g\ L^{-1}$) (Chen et al., 2018).

In nano-ecotoxicity studies, the analysis of NP aggregation kinetics and stability in aqueous suspensions over time is crucial to correctly interpret the biological effects observed, toward a more reliable environmental risk assessment. It is important to underline that the considerations from the studies reported are referred to temperate coastal regions and may be extended to tropical regions, although more case studies focusing on NP characterization under different environmental conditions are needed.

In polar marine environments, additional factors, such as the low sea surface temperature (below 0°C) and the interaction with sea ice may play an important role in determining the behavior and fate of anthropogenic NPs, although they have been poorly studied. Bergami et al. (2019) measured the size parameters of functionalized PS NPs in NSW collected from a coastal region in the maritime Antarctic. Secondary characterization in Antarctic NSW (salinity 34‰ and pH 8.0) revealed the initial formation of PS nano-scale agglomerates in NSW at 0°C, increasing over time until an average of 835 and 452 nm, for PS-COOH and PS-NH_2 NPs respectively. Additionally, when PS NP suspensions were incubated at −20°C for 12 h, broad size distributions were found, with a higher effect observed for positively charged PS-NH_2 (Bergami et al., 2019). On the contrary, the same batch of PS-COOH quickly reached micrometer agglomerates in filtered NSW from the Tyrrhenian Sea (Mediterranean region, salinity 38‰ and pH 8.3) at temperatures ranging from 18°C (Della Torre et al., 2014) to 25°C (Bergami et al., 2016). An explanation for this difference may be related to the increase in kinetic energy at higher temperatures, resulting in higher collision frequency and instability of the nanoplastics (Singh et al., 2019), which are more prone to agglomerate. The first data under Antarctic-like conditions suggest that low temperatures and salinity may significantly affect nanoplastic behavior, calling for further investigation.

INTERACTION WITH LIVING SYSTEMS: THE CORONA CONCEPT

Recent experimental evidence points out that many variables concur to determine the outcome of bio−nano interactions in seawater, both with a physical–chemical and biological relevance, and therefore delineating the ecotoxicity of NPs in such complex water matrices (**Figure 1**). With decreasing dimension, the surface area-to-volume ratio exponentially increases, leading to the presence of a higher number of atoms at the surface compared to the core of the NP. Interfacial properties are key determinants of NP reactivity, given the high portion of material exposed to the exterior and, hence, able to engage in chemical and physical reactions with other nanoscale objects or molecules. With such maximized exposure to the external environment, the particle interface is where all the processes defining the NP interaction with surrounding (biological) entities take place. The high surface free energy that characterizes NPs drives their interactions in order to lower such energy levels. Consequently, NPs are naturally prone to interact with biological and abiotic entities, which they encounter in the surrounding medium, as a means to achieve a more energetically favorable configuration (Petosa et al., 2010). The dynamics of protein adsorption onto surfaces has first been described by the Vroman effect (Vroman, 1962), which can be used to explain the interfacial interactions occurring when NPs are in biological milieus. On such basis, the interactions of NPs with biological molecules took shape in the biomolecule "corona" (also termed bio-corona) paradigm, as initially described by the coating of NPs by a layer of adsorbed proteins, derived from a biological environment (Cedervall et al., 2007b). Although foundational corona studies tackled the protein fraction, biomolecular coronas were shown to contain lipids (Lara et al., 2017) and saccharides (Wan et al., 2015). Moreover, as biomolecule adsorption onto NPs is a dynamic process, protein corona is regarded as a continuously evolving entity. Different protein species display distinct binding affinities for one specific NP surface, and an evolution of corona composition over time is usually observed. Generally, the most abundant proteins in the incubation media rapidly bind on the NP surface, often being displaced by species characterized by higher affinities (Cedervall et al., 2007a), until a "mature" protein corona composition is achieved (Casals et al., 2010; Monopoli et al., 2013). Commonly, the biomolecular corona is viewed as a slowly exchanging and tightly bound layer of biomolecules adsorbed on the NP surface, also termed the "hard" corona, whose composition is in equilibrium with the surrounding environment and sufficiently long lived to provide the NP with a molecular fingerprint, namely, the biological identity of NPs. Additionally, an outermost cloud of loosely bound molecules with lower binding affinities, called the "soft corona," is in rapid exchange with the environment (Milani et al., 2012; Winzen et al., 2015). Quantitative analysis reveals that only few protein species usually prevails in the overall corona composition (Kokkinopoulou et al., 2017). On top of peculiar molecule characteristics (e.g., isoelectric point, molecular weight, tertiary structure, charge distribution), NP physical–chemical features are key determinants of the biomolecular corona composition. The NP surface charge has been proven to exert a strong influence on the composition of biomolecular coronas due to electrostatic effects (Lundqvist et al., 2008; Walkey et al., 2012; Tenzer et al., 2013; Ritz et al., 2015). Moreover, NP surface charge interacts with the peculiar local charge distribution of proteins, determining their binding affinities and orientation when adsorbed on the NP surface (Shang and Nienhaus, 2017). NP size, determining the specific surface curvature, influences the amount and type of proteins forming the biomolecular corona, by spatial constraints and crowding effects (Dobrovolskaia et al., 2009; Tenzer et al., 2011; Goy-López et al., 2012; Piella et al., 2017). Accordingly, the peculiar NP shape and topology greatly influence the biomolecular corona qualitatively and quantitatively (Albanese et al., 2012; García-Álvarez et al., 2018). Along with intrinsic and extrinsic NP characteristics, factors defining the boundary conditions to NP–biomolecule interactions are important in determining their

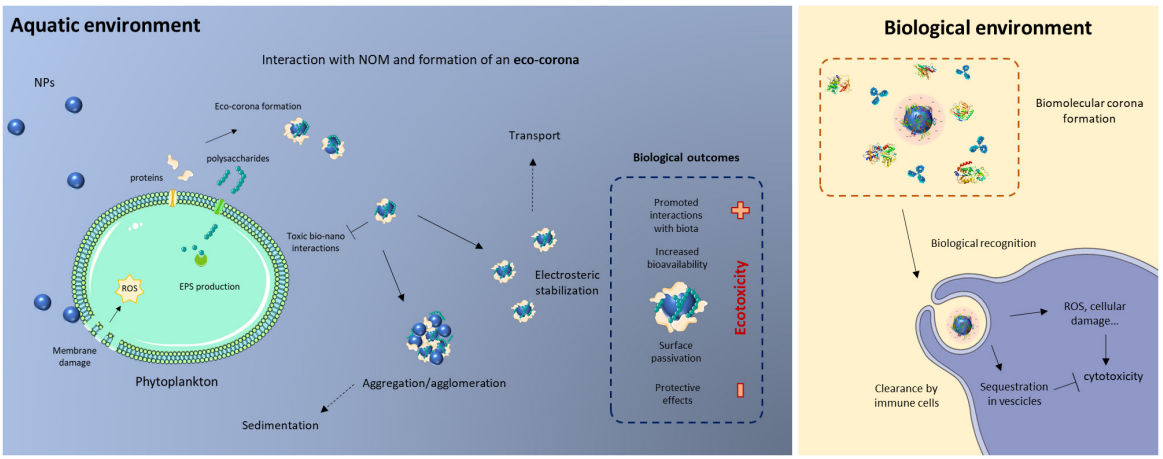

FIGURE 1 | Schematic illustration of the bio–nano interactions taking place in the marine environment. Left: possible interactions between nanoscale particles (NPs) dispersed in seawater and biomolecules making up the marine natural organic matter (NOM) pool, such as microalgal/cyanobacterial extracellular polymeric substances (EPS). Right: the cellular processes following biomolecular corona formation in biological fluids of marine invertebrate organisms.

outcomes. For instance, protein abundance and the relative ratio of NP surface area to the biological fluid volume can dictate the quantity and quality of adsorbed proteins (Caracciolo et al., 2011; Monopoli et al., 2011). Furthermore, exposure time (Casals et al., 2010), temperature (Mahmoudi et al., 2013), and chemical composition (Eigenheer et al., 2014) of the incubation medium play an important role in the corona formation. Moreover, such elements can determine the NP suspension stability and induce aggregation of NPs in the biological milieu, in turn influencing protein adsorption and organization within the aggregates, and finally the biodistribution of NP–protein complexes (Mohr et al., 2014; Kokkinopoulou et al., 2017; Lundqvist et al., 2017).

The Role of the Biomolecular Corona in Nanoecotoxicology

The introduction of the biomolecular corona concept, upon which has nowadays been reached a wide consensus among the scientific community, has led to a change in paradigm regarding how NPs are viewed in relation to biological systems. The rapid adsorption of proteins and other biomolecules can confer to NPs a new biological identity dictated by biomolecular species at the NP surface, remarkably different from the intrinsic, well-defined chemical one. By providing a first point of contact with cells, the biomolecular corona functions as a bridge in bio−nano interface. The fate of NPs in biological systems, be they cells, organs, or whole organism, is mediated by the adsorbed proteins species, which direct the NP toward specific pathways, deeply affecting subsequent events at the molecular level (Verma and Stellacci, 2010). Although the primary importance of biomolecular coronas has long been acknowledged in the biotechnological and biomedical fields, its potential in understanding nano-(eco)toxicology has only been recently recognized. Indeed, "traditional" ecotoxicity assessment, when applied to NPs, often fails to provide a comprehensive representation of toxicity, as objects at the nanoscale are intrinsically different entities compared to classical toxicants. In this regard, the protein corona paradigm can be incorporated into the field of ecotoxicology (Lynch et al., 2014). As reported in recent works, this concept has been fruitfully applied in the ecotoxicological studies concerning different NP types. For instance, the effect of protein adsorption on Ag NPs was found to be an important molecular determinant of toxicity toward fish gill cell lines in their physiological environment (Yue et al., 2015, 2016a). Moreover, the analysis of the protein corona formed in the intracellular environment of rainbow trout (*Oncorhynchus mykiss*) gill cells showed a fingerprint of the interactions of Ag NPs with different subcellular compartments and provided useful insight on mechanism of toxicity (Yue et al., 2016b). The incubation of PVP-coated Ag NPs in the blood plasma of male and female smallmouth bass *Micropterus dolomieu* resulted in the formation of a gender-specific corona and allowed for postulation of hypothetical distribution within different body compartments (Gao et al., 2017). Also, invertebrate species have been considered in ecotoxicity studies, encompassing the formation and characterization of biomolecular coronas. Hayashi and coworkers exposed SiO_2 and Ag NPs to the native protein repertoire of the earthworm *Eisenia fetida* demonstrating that the resulting protein corona assists cellular interactions (Hayashi et al., 2013). More recently, the importance of the study of biomolecular coronas in the biological fluids of invertebrate species as a means of understanding their environmental impact was stressed (Canesi et al., 2017).

Marine invertebrates are primary targets of NPs entering seawater coastal ecosystems and can provide insights in the mode of action of NP toxicity. Therefore, marine invertebrate species have been recommended and successfully employed in ecotoxicity studies with different NP types (Matranga and Corsi, 2012; Canesi and Corsi, 2016; Canesi et al., 2016a). As such, they provide an interesting platform to translate the study of biomolecular coronas into a concrete understanding of NP impact on the marine environment, advancing an ecological

risk assessment. For instance, marine mussels have been largely exploited in marine nano-ecotoxicology, and more recently, their biological fluids have been used for biomolecular corona studies (Canesi et al., 2015, 2017; Auguste et al., 2019). In the marine mussel *Mytilus galloprovincialis*, it was demonstrated that the presence of a biomolecular corona acquired in the organism hemolymph, composed by the Cu, Zn-SOD protein, clearly augmented toxicological responses in immune cells, compared to the corona-free counterparts (Sendra et al., 2018). In another study, cytotoxic effects toward *M. galloprovincialis* hemocytes, triggered by the exposure to aminated PS NPs (PS-NH_2), were ascribed to the extrapallial protein (EP) precursor (MgC1q6) that dominated the protein corona, which has known opsonization functions and is envisaged to facilitate NP–cell interactions (Canesi et al., 2016b). Marine mussels produce mucus as first line of defense from environmental stressors, with the ability to trap and sort exogenous particulate materials, as a means to prevent possible noxious interactions (Beninger and St-Jean, 1997; Espinosa et al., 2010). Therefore, mucus represents an important defense mechanism against NPs in seawater. It was demonstrated that a panel of TiO_2 NPs with different shapes, sizes, ζ potentials, and crystal structures (anatase vs. rutile), exposed to the same mucus protein repertoire of *Mytilus edulis*, formed biomolecular coronas with different protein patterns, depending on such characteristics (Bourgeault et al., 2017). In particular, adsorption of proteins was quantitatively different among TiO_2 NP types, and the protein signatures revealed the absence in the corona of the principal mucus component (the EP protein), unable to adsorb due to stiffness of its structure stemming from the high content of aromatic residues. On the contrary, the presence of some stress-related protein species, whose affinity for different TiO_2 NPs appeared to be crystal structure and shape dependent, suggested the acquisition of a new biological identity. Moreover, larger particles readily adsorbed higher protein amount per surface unit, suggesting that quantitative aspects of the protein corona should be accounted for in ecotoxicity studies.

Sea urchins have been largely employed in marine ecotoxicological studies. In this regard, the sea urchin immune system has been exploited in assessing the effect of various toxicants in marine ecosystems, being regarded as an exploratory tool for identifying the mechanism of immune response to environmental stresses (Matranga et al., 2005; Pinsino and Matranga, 2015). As to nano-ecotoxicology, sea urchin immune cells were used for probing the toxicity of different NP types (Falugi et al., 2012; Pinsino et al., 2015). The immunobiology of sea urchin has been defined as among the most complex within marine invertebrate species, qualifying the sea urchin as proxies for the study of NP-triggered immune reactions preluding to ecotoxic effects (Alijagic and Pinsino, 2017). NP–biomolecule complexes in environmentally relevant model species can be exploited to achieve a clearer image of NP ecotoxicology and advance our understanding of their environmental impact, and the use of sea urchins entails the potential to translate such findings to more complex organisms. In this light, Alijagic et al. (2020) depicted a comprehensive picture of the Mediterranean Sea urchin *Paracentrotus lividus* immune system adaptation to TiO_2 NP exposure by downregulating genes involved in the inflammatory immune response and increasing immune cell antioxidant capacity (Alijagic et al., 2020). Focusing on bio−nano interactions, Marques-Santos et al. (2018) described the effect of a calcium-binding, transferrin-like protein, adsorbed onto PS-NH_2 NPs incubated in coelomic fluid, on its immune system. Specifically, the toposome, with known cell adhesion functions, seemed to facilitate cell interactions and PS-NH_2 NP clearance from the coelomic fluid by phagocytic coelomocytes, which, in turn, sustained related cytotoxic effects. The biomolecular corona of positively and negatively charged PS NPs (PS-NH_2, 50 nm and PS-COOH, 62 nm) in *P. lividus* coelomic fluid was thoroughly assessed by a classical proteomic approach revealing a strikingly similar corona composition between the two particles. The abundance of cytoskeletal proteins and species involved in cell adhesion processes strengthened the hypothesis of an active role of the protein corona in the association with sea urchin immune cells and phagosome formation, as evidenced by the Kyoto Encyclopedia of Genes and Genomes (KEGG) pathway analysis, suggesting a similar internalization pathway of NP with different surface charges (Grassi et al., 2019). In a following similar study, the same protein species were recovered from the surface of P25 TiO_2 NPs incubated in *P. lividus* coelomic fluid (Alijagic et al., 2019). In particular, toposome, nectin and different actin isoforms were common constituents of both PS NPs, as previously identified, and TiO_2 NPs corona, suggesting a non-discriminative adsorption of *P. lividus* extracellular proteins on inherently different NPs, and postulating the same cell adhesion and internalization mechanisms toward by immune cells.

NP Bio-Interactions in Marine Waters: Introduction to the Eco-Corona Concept

Nanoscale particles entering aquatic ecosystems will likely be received by different environmental compartments prior to contacting biota. For instance, NPs entering natural water compartments will undergo substantial modifications as dictated by the characteristics of the receiving media. Along with the well-documented effects on colloidal stability with different outcomes on behavior and fate, increased emphasis has recently been placed on the processes occurring at the interface between NPs and the environment. Biomolecule-rich abiotic environmental compartments, such as marine water bodies, represent dynamic environments where NPs interact with biological entities. The organic component of natural waters is composed of a highly heterogeneous group of biomolecules which can be categorized as allochthonous and autochthonous compounds (Docter et al., 2015). The degradation byproducts of organic material of plant origin, mainly composed of high molecular weight HA and FA, belong to the former category. In contrast, autochthonous NOM is the ensemble of biomolecules produced *in situ* by living organisms, such as bacterial and microalgal communities, which are huge contributors to the organic macromolecule pool of natural waters (Gutierrez et al., 2018). Their exudates, collectively termed EPS (extracellular polymeric substances), mainly consist of a variety of high molecular weight polysaccharides, and

to a lesser extent of glycoproteins, lipids, and nucleic acids. The composition of the organic fractions encountered in seawater spans across a wide spectrum of molecular weights, taking shape in a continuum of sizes from amino acids to peptides and polysaccharides, encompassing truly dissolved and colloidal/macromolecular species (Verdugo et al., 2004; Wilkinson and Lead, 2007).

Additionally, due to the different contributions to the NOM pool, the chemical makeup of organic biomolecules is exceptionally heterogeneous, with tens of thousands of unique chemical species, contributing to the overall complexity of the marine water matrix (Mopper et al., 2007; Ortega-Morales et al., 2007). The interactions of NPs in natural waters with the totality of NOM can lead to the formation of diverse biomolecular coatings, collectively termed the "eco-corona," analogous to the bio-corona previously described in purely biological fluids (Lynch et al., 2014). For instance, the interaction of organic molecules with NPs dispersed in seawater can result in their inclusion into biomolecular matrices, occurring either as composite organic networks embedding single particles or aggregates into microgel-like structures (**Figures 2b,e**) or as tightly adsorbed layers at the surface (**Figures 2c,f**), as shown for TiO_2 and PS-COOH NPs.

Dispersion in natural waters usually confers some degree of polydispersity, complicating the interaction with natural biomolecules. Aggregation phenomena often occur, and NP aggregates/agglomerates will be present, together with monomers, giving rise to multifaceted interactions with the NOM matrix. In general, NOM molecules can either promote the aggregation of stable NP suspensions in natural waters or limiting the aggregation phenomena by providing steric stabilization (Nason et al., 2012; Surette and Nason, 2016, 2019; Danielsson et al., 2018). Therefore, aggregation and biomolecule adsorption can represent competing phenomena in seawater, where high salinity can induce aggregation, while eco-corona formation may disrupt such phenomena. Under such conditions, the result of NOM–NP interaction cannot be viewed simply as the formation of a uniform molecular layer at the particle surface, but rather a more complex organization of NPs in the NOM matrix can be expected.

The importance of an acquired eco-corona in shaping the nanotoxicity of different NP types has recently been acknowledged (He et al., 2018, 2015). In fact, the acquisition of an eco-corona from the surrounding environment is expected to modify key NP parameters, possibly rebounding on nanotoxicity (Ren et al., 2016), and the inclusion of such variables in the

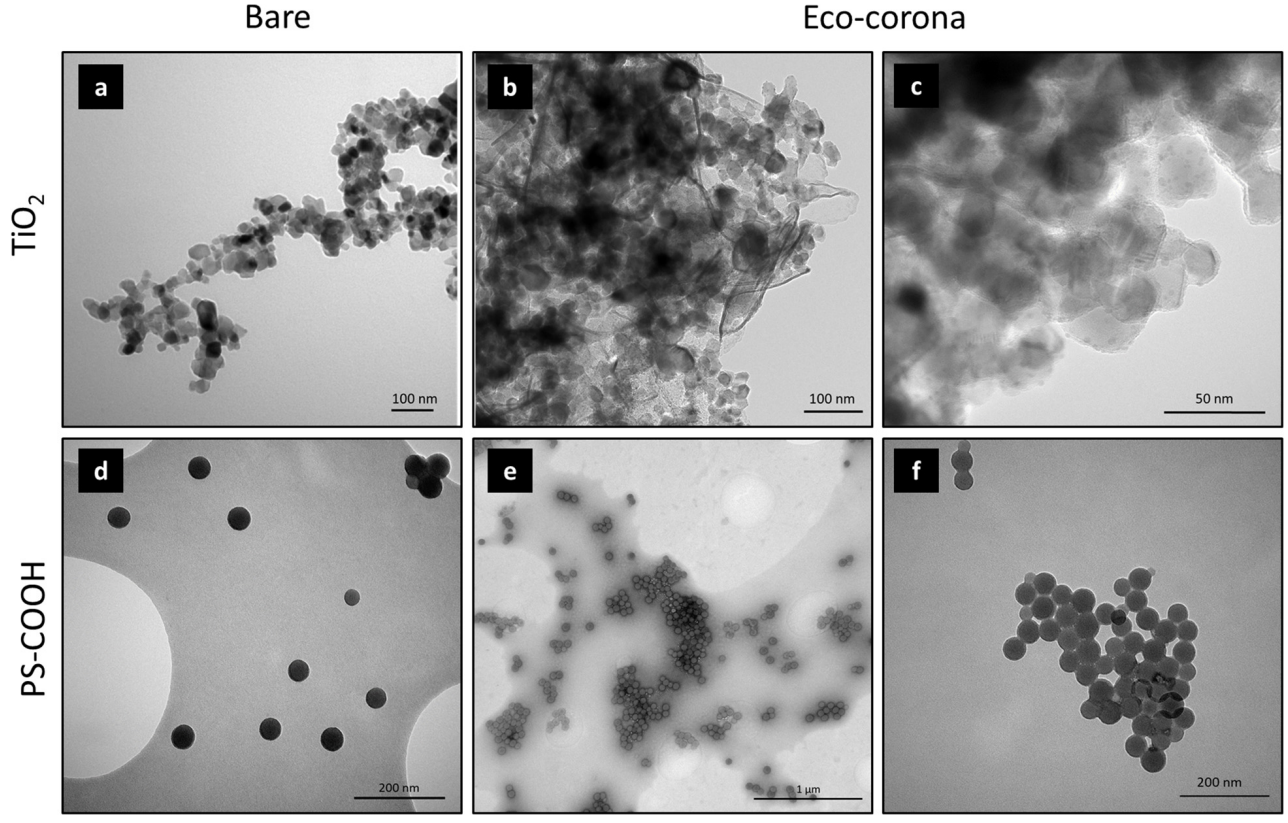

FIGURE 2 | Transmission electron microscopy (TEM) showing interactions of 25-nm titanium dioxide (TiO_2) P25 **(a,b,c)** and 60-nm carboxylate (PS-COOH) **(d,e,f)** NPs with marine NOM leading to eco-corona formation. Bare particles in deionized water are reported in panels **(a,d)**. **(b,c)** TiO_2 NP interactions with biomolecules form natural seawater. **(e,f)** PS-COOH NP interaction with EPS from the marine diatom *Phaeodactylum tricornutum*. Details of sample preparation are reported in the **Supplementary Material** section.

ecotoxicity testing of NP is strongly encouraged to gather ecologically meaningful results (Holden et al., 2016). Recently, proofs of concept were provided by supplementing ecotoxicity test media with exogenous NOM surrogates (e.g., commercially available humic/fulvic fractions and proteins), thus provoking eco-corona formation. In particular, NOM and BSA mitigated the toxicity induced by ZnO and MnO_2 NPs toward oyster (*Crassostrea gigas*) embryos by interfering with dissolution and bandgap mechanisms (Noventa et al., 2018). Morelli et al. (2018) isolated the EPS produced by the marine microalgae *Dunaliella tertiolecta*, probing the selective adsorption of proteins on the surface of P25 TiO_2 NPs, shaping an eco-corona (2018). The EPS from the marine bacterium *Pseudomonas aeruginosa* was able to clearly mitigate the toxic effect of the same NP type mainly by delaying the oxidative damage caused by reactive oxygen species (ROS) produced in seawater (Hessler et al., 2012).

EFFECTS ON MARINE ORGANISMS

According to the vast number of ecotoxicity studies on TiO_2 NP, oxidative stress is largely recognized as the main mechanism of toxicity in marine species, although other biological effects have been recorded (**Figure 3A**; Minetto et al., 2014, 2016; Xia et al., 2015). Based on most recent studies in which TiO_2NP characterization have been included in order to address exposure scenario in the observed toxicity, the largest efforts concentrated on both marine plankton (42.1%) and benthos (44.7%) and only a minority on marine fish (13.2%) (**Figure 3A**; see **Supplementary Material** section for literature cited).

The first record on TiO_2 ecotoxicity has been provided on marine phytoplanktonic species as cyanobacteria and green algae in which the role of light and consequently photoactivation has been linked to membrane damage, oxidative stress, genotoxicity, and inhibition of growth. According to Miller et al. (2010), no effect is observed in marine diatoms in the range between 10–1,000 $\mu g\ L^{-1}$ unless UV is inducting TiO_2 NP photoactivation (Miller et al., 2012). UV-A light is able to energize TiO_2 NP and to photoinduce the generation of reactive oxygen radicals in exposed cells (Uchino et al., 2002; Sayes et al., 2006). UV-A exposure (6 h per day), rather than visible light, is reported to strongly affect sensitivity of the marine algae *Phaeodactylum tricornutum* to TiO_2 NP compared to bulk form due to increased production of reactive oxygen species (ROS) (Sendra et al., 2017a). Chloroplasts of the algae *Karenia brevis* have been identified as the site of ROS induced by TiO_2 exposure with consequent increase in lipid peroxidation and cell damage leading to inhibition of algal growth (Li et al., 2015). On the other hand, according to Bhuvaneshwari et al. (2017), the formation in seawater of large TiO_2 agglomerates significantly reduced the TiO_2 phototoxicity under UV-A irradiation in brine shrimp *Artemia salina.* An increase in ROS generation and antioxidant enzymes is supposed to drive TiO_2 phototoxicity in green algae *Dunaliella salina* and brine shrimp larvae *A. salina* upon waterborne exposure (Bhuvaneshwari et al., 2018). Minetto et al. (2017) further support the role of light, which significantly affect TiO_2 toxicity on marine algae. According to Pellegrino et al. (2017), TiO_2 aggregation and agglomeration significantly reduce light adsorption by causing diffusion of the incoming radiation. Sun et al. (2014) previously demonstrated that UV irradiation of P25 TiO_2 water suspensions enhances particle aggregation by increasing surface concentration of hydroxyl groups, which lower the isolectric point and reduce positive charges of TiO_2. More recently, Budarz et al. (2017) showed that the photoreactivity and aggregation of TiO_2 NPs are strongly influenced by anionic species present in the water media with carbonate and chloride having a strongest role in suppressing hydroxyl radical generation by substituting hydroxyl ions. The fast agglomeration/aggregation of TiO_2 NPs in high ionic media such as sea water is also having a significant role in TiO_2 properties and therefore toxicity for marine species (Brunelli et al., 2013). A physical interaction of TiO_2 agglomerates by entrapping green algae *P. tricornutum* is considered the main driver of toxicity according to Deng et al. (2017); Wang et al. (2017). An increase in oxidative stress and the inhibition of the effective quantum yields are foreseen as a defense mechanism used by algae toward physical damage caused by TiO_2 agglomerates (Hu et al., 2018). Surface adhesion of TiO_2 agglomerates to the microalgae *Nitzschia closterium* is thought to be responsible for TiO_2 trophic transfer to the scallop *Chlamys farreri* (Wang et al., 2017). Fast sinking of TiO_2 agglomerates can explain the absence of toxicity to the larvae of rotifer *Brachionus plicatilis* and of the brine shrimp *A. salina* according to Nogueira et al. (2015). Moreover, no effect on embryo development was observed at concentrations above 1 $mg\ L^{-1}$ in marine bivalve *M. galloprovincialis* (Libralato et al., 2013; Balbi et al., 2014). A time-dependent process of TiO_2 agglomeration is reported by Morelli et al. (2018) as well as the mitigation role played by algal EPS in the fast TiO_2 NP agglomeration. Other sources of NOM, such as for instance the mucus secreted by bivalve's gills, can affect the formation of TiO_2 agglomerates, which are then translocated to the digestive gland by hemolymph and then excreted with pseudofeces (Wang et al., 2014; Canesi and Corsi, 2016). In this regard, evidence of TiO_2 NP localization in the cytoplasm and vacuoles of bivalve's immune cells raises further concern due to their widely reported TiO_2 NP immunomodulatory effects both *in vitro* and *in vivo* (i.e., endo-lysosomal system and phagocytic activity) (reviewed in Marisa et al., 2015; Canesi and Corsi, 2016; Shi et al., 2017; Guan et al., 2018; Canesi et al., 2019).

High and fast body clearance (<90% within 12 h) of two TiO_2 NP formulations (Titan and P25) is reported in blue mussel (*M. edulis*) and oyster (*Crassostrea virginica*) regardless of the form of delivery (marine snow vs. suspensions) upon waterborne exposure (6 h) (Doyle et al., 2015). In addition, less than 10% of the nominal concentration of TiO_2 is supposed to be available to marine species due to particle sedimentation and agglomeration/adsorption processes occurring in the presence of organic matter produced by marine organisms (EPS, mucus, pseudofeces).

Despite a certain number of studies that recognized TiO_2 ecotoxicity for marine species, a few of them investigated those TiO_2 formulations, which are released from commercial products, which also undergo such transformations (i.e., weathering and aging) able to affect their behavior and

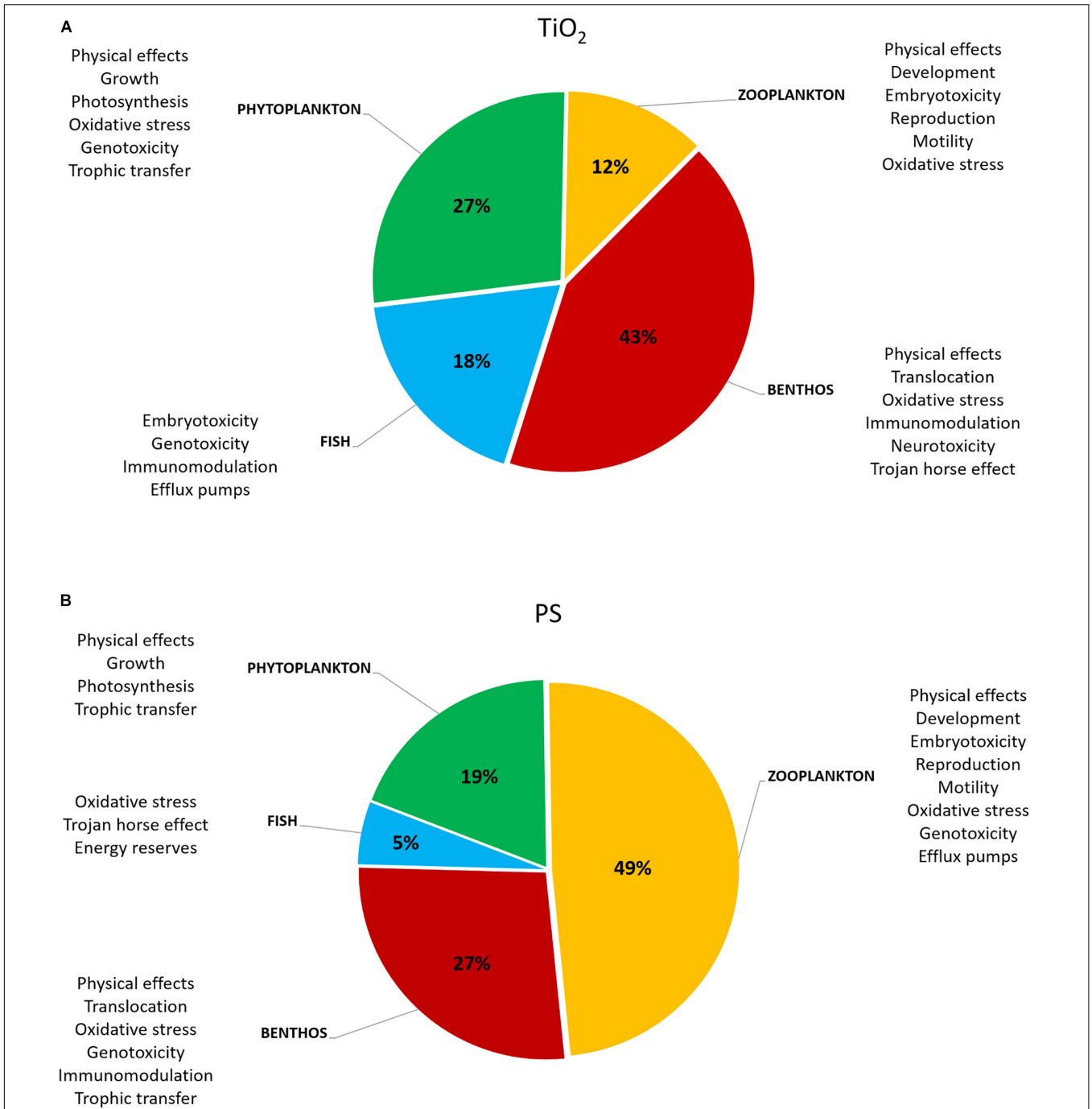

FIGURE 3 | Schematic representation of the distribution of taxa investigated in ecotoxicity studies [**(A)** TiO_2 and **(B)** polystyrene (PS) NPs] and related documented effects. Please refer to **Supplementary Material** section for details on literature used. Total number of studies was 37 for PS and 38 for TiO_2.

interaction with marine biota (Labille et al., 2010; Nowack and Mitrano, 2018). Gondikas et al. (2014) first showed the release of TiO_2 from sunscreen formulations in lake surface waters raising concern regarding effects on aquatic species. TiO_2-based sunscreen products have been shown to be more toxic to marine planktonic diatoms under direct sunlight exposure compared to classical formulation (Sendra et al., 2017b). Oxidative damage and hydrogen peroxide production have been recorded in marine diatoms upon TiO_2 exposure in association with organic compounds present in sunscreen formulation (Tovar-Sánchez et al., 2013). No effects of two TiO_2-based sunscreen formulations (Eusolex® T2000 and Optisol™) have been reported on tropical stony Acropora coral and symbionthic algae (i.e., *Symbiodinium* sp.) by Corinaldesi et al. (2018), while TiO_2

exposure was considered responsible for zooxanthellae expulsion in the Caribbean coral *Montastraea faveolata* (Jovanović and Guzmán, 2014). Therefore, more studies are urgently needed to disentangle the role of single nanoscale particle from the entire commercial formulation by addressing first the behavior of the particle, itself, in the natural media for defining real exposure scenarios. With this aim, several studies have been conducted for instance by evaluating the possible interactive effects of TiO_2 NPs with other existing marine pollutants. Antagonistic and interactive effects have been reported both *in vitro* and *in vivo* in marine bivalve *M. galloprovincialis* (immune system, digestive gland and gills) exposed to TiO_2 (Degussa P25) with cadmium and 2,3,7,8-tetrachlorodibenzo-*p*-dioxin (TCDD), respectively (Canesi et al., 2014; Della Torre et al., 2015b; Rocco et al., 2015; Banni et al., 2016). Co-exposure seemed to mitigate, rather than exacerbate, the adverse effect of single exposure with predominant antagonistic effects depending on experimental condition, cell/tissue, or type of measured response. Transcriptomic analysis in co-exposure conditions revealed transcriptional changes common to individual treatments (TiO_2 and TCDD) and identified newly generated processes and response to chemical stimulus without increasing overall stressful conditions (Banni et al., 2016). The negligible adsorption of Cd^{2+} to TiO_2 agglomerates reported upon incubation in artificial seawater probably explain the observed preferential accumulation of Cd^{2+} in the bivalve digestive gland and gills in the presence of n-TiO_2 (Della Torre et al., 2015b). In contrast, higher TCDD accumulation was observed in whole mussel tissues in the presence of n-TiO_2 but not in the digestive gland. A lower benzo(a)pyrene accumulation upon co-exposure to TiO_2 is reported by Farkas et al. (2015) in blue mussel *M. edulis*. Probably, B(a)P was less bioavailable to mussels due to adsorption to TiO_2 agglomerates. The presence of TiO_2 significantly increased the embryotoxicity of tributyltin (TBT) to the abalone (*Haliotis diversicolor*) (Zhu et al., 2011), and in the ark shell *Scapharca subcrenata*, enhanced uptake of phenanthrene is observed in the presence of TiO_2 (Tian et al., 2014). On the contrary, TiO_2 did not alter the bioaccumulation of several PBDE congeners in the same species (Tian et al., 2015). The few studies performed on marine fish species, underline that more studies should focus on this trophic level in order to better formulate risk assessment on marine biota. Sub-lethal adverse effects on the early life stages of the brackish *Oryzias latipes* as premature hatching, pericardial edema, and abnormal development have been reported (Paterson et al., 2011). Moreover, genotoxic and potentially cytotoxic effects were reported in *Trachinotus carolinus* exposed to 1.5–3 g of TiO_2 NP for 24, 48, and 72 h (Vignardi et al., 2015). In European sea bass *Dicentrarchus labrax*, higher levels of total Ti were found in liver upon waterborne co-exposure with TCDD (46 pg L^{-1}) and TiO_2 (1 mg L^{-1}) for 7 days (Della Torre et al., 2015b). At gene level, any influence of TiO_2 NP on TCDD ability to induce cyp1a and related EROD activity was found, which was further confirmed by similar levels of TCDD detected in the liver of fish upon single and co-exposure (Della Torre et al., 2015b; Vannuccini et al., 2015). On the opposite, exposure to the mixture caused a further significant downregulation of ATP-binding cassette transporter genes *abcb1* and *abcc2* compared to single exposure (n-TiO_2 and TCDD alone) suggesting an interactive effect on ABC, which could be a potential target of TiO_2 NP in liver of fish. Upon co-exposure with $CdCl_2$ in the same experimental conditions (0.1 mg L^{-1} and TiO_2 1 mg L^{-1} respectively), TiO_2-induced chromosomal damage and genome template instability in sea bass erythrocytes seemed reduced by the presence of Cd, thus, supporting the hypothesis of an interactive role in co-exposure scenarios (Nigro et al., 2015).

Several laboratory studies have shown that nanoplastics (below 1 μm following the classification from Hartmann et al., 2019) may cause both chemical and physical impacts to marine wildlife. In the last decade (2009–2019), PS NPs have been adopted in 85% of the ecotoxicity studies (n = 41, listed in **Supplementary Material**), alongside with other polymers, mainly polymethyl methacrylate (PMMA) NPs (Bhargava et al., 2018; Brandts et al., 2018) and polyethylene (PE) nano-sized fragments (Baudrimont et al., 2019). Functionalized PS NPs, such as PS-COOH and/or PS-NH_2, have been used in 44% of them to correlate the biological effects observed in the functionalization. The most common nanoplastics in the marine environment are expected to be negatively charged due to surface oxidation and acquisition of functionalities, such us the carbonyl groups, during the weathering (Fotopoulou and Karapanagioti, 2012; Gigault et al., 2016; Andrady, 2017). However, it is important to consider also positively charged nanoplastics as a counterpart since the functionalization and surface charge derived from plastic degradation products are yet to be fully determined. For example, amino modification may result from the hydrolyzation of polyamides (Merdas et al., 2003), although they are not expected to be found in high quantities in seas and oceans (Lehner et al., 2019).

The analysis of the species sensitivity to polymeric NPs, reported by Venâncio et al. (2019), showed that nanoplastics with a nominal size below 50 nm mainly affect marine model organisms depending on surface charge (positive vs. negative) and polymeric composition (PS vs. PMMA), suggesting that PS NPs may be more harmful than other polymers for the marine biota.

The main biological effects reported for marine model organisms exposed to PS NP suspensions are summarized in **Figure 3B**. Overall, a large effort has been made to study the effects on marine plankton (67.5%), while 27% of the studies has been carried out on benthic organisms and only 5.4% on marine fish, different from microplastic studies in which these two latter categories are far more represented (Chae and An, 2017).

Studies on PS NPs and phytoplankton have usually been performed following available standardized toxicity test protocols to determine the growth inhibition at 72 or 96 h of an algal culture in an exponential phase exposed to a contaminant (e.g., ISO, 2006; OECD 201, 2011). Interestingly, most of the studies reported no or limited effect on microalgal growth after exposure to increasing concentrations of plain PS and PS-COOH NPs (Bergami et al., 2017; Yi et al., 2019) up to 250 μg ml^{-1} (Sjollema et al., 2016), while many sub-lethal physiological alterations have been observed, such as a strong adsorption of nanoplastic agglomerates on microalgal surface

(Bergami et al., 2017; Sendra et al., 2019b; Yi et al., 2019), a decrease in photosynthesis efficiency and lipid content, as well as the production of reactive oxygen species (ROS) (González-Fernández et al., 2019; Sendra et al., 2019b; Seoane et al., 2019). Moreover, a significant increase in the DNA damage as well as depolarization of mitochondrial and cell membrane were found in the benthic diatom *Phaeodactylum tricornutum* exposed to increasing concentrations (in the range 0.1–50 $\mu g\ ml^{-1}$) of plain PS NPs, although toxicity was not affected by their nominal sizes of 50 and 100 nm (Sendra et al., 2019b). Recent findings also underline how PS-COOH (50 nm) adhesion onto a diatom's surface causes a reduction in their chain length with potential ecological implications as, for instance, changes in diatom's chain buoyancy as well as the formation and sinking of aggregates (Bellingeri et al., 2020).

Concerning PS-NH_2 NPs, Bergami et al. (2017) reported a significant growth inhibition in the unicellular green microalga *D. tertiolecta* [$EC_{50\ (72\ h)}$ of 12.97 $\mu g\ ml^{-1}$], while Seoane et al. (2019) found no effect on growth of the marine diatom *Chaetoceros neogracile*. This discrepancy can be explained by the different sizes of PS-NH_2 NPs (50 vs. 500 nm) used in the two studies and their behavior in the algal media, whereas 50 nm of PS-NH_2 NPs showed low aggregation and a positive surface charge (Bergami et al., 2017), 500 nm of PS-NH_2 NPs agglomerated (>3 μm) and resulted as negatively charged (Seoane et al., 2019). Different results in standard algal growth inhibition tests can also be related to the species sensitivity of phytoplankton toward nanoplastics. While marine diatoms are characterized by a silicified wall, green microalgae like *D. tertiolecta* present a thin cellular membrane (Oren, 2005), which may facilitate interactions with anthropogenic NPs with respect to other species.

Ecotoxicity studies on zooplankton mainly investigated the potential accumulation of PS NPs in the digestive tract of model organisms, by the detection of fluorescently labeled NPs under optical fluorescent or confocal microscopy through the thin transparent body of copepods (Lee et al., 2013; Jeong et al., 2017), anostracans (Bergami et al., 2016), rotifers (Snell and Hicks, 2009; Jeong et al., 2016, 2018; Manfra et al., 2017), and other planktonic larvae (Cole and Galloway, 2015; Della Torre et al., 2015b; Gambardella et al., 2017, 2018). Although egestion of large PS agglomerates, incorporated in fecal pellet structure, has been observed in several planktonic species (Lee et al., 2013; Bergami et al., 2016, 2017), some studies showed that PS NPs were still retained in the digestive tract of the exposed organisms after a 24-h recovery period (Bergami et al., 2016; Jeong et al., 2017; Manfra et al., 2017) and were removed less efficiently compared to micro-sized particles (Jeong et al., 2016). Plain PS and negatively charged PS-COOH NPs normally did not provoke mortality after acute (Della Torre et al., 2014; Cole and Galloway, 2015; Bergami et al., 2016; Gambardella et al., 2017; Manfra et al., 2017) or long-term (Bergami et al., 2017) exposures, although several sub-lethal effects have been reported, from the alteration in the swimming activity (Gambardella et al., 2017) to the decrease in fecundity, reproduction efficiency, and offspring fitness (Lee et al., 2013; Jeong et al., 2016, 2017). A concentration-dependent toxicity on growth and reproduction has been reported in the rotifer *Brachionus* spp., with a negative correlation between toxicity and NP size (Snell and Hicks, 2009; Jeong et al., 2016). In both studies, 50-nm PS NPs caused the most deleterious effects compared to larger NPs (100–500 nm) and microplastics (6 μm).

Some studies also reported the induction of oxidative stress (Jeong et al., 2016; González-Fernández et al., 2018) as well as mantle and shell malformations in the oyster *C. gigas* D-larvae following exposure to plain PS and PS-COOH NPs (Tallec et al., 2018).

In general, a higher toxicity in the marine zooplankton was associated to positively charged PS-NH_2 NPs, with average EC_{50} values ranging from 0.14 $\mu g\ ml^{-1}$ in the mussel *M. galloprovincialis* (Balbi et al., 2017) and 0.15 $\mu g\ ml^{-1}$ in the oyster *C. gigas* D-larva (Tallec et al., 2018), to 2.61 $\mu g\ ml^{-1}$ in the sea urchin *P. lividus* pluteus (Della Torre et al., 2014) and 6.62 $\mu g\ ml^{-1}$ in the rotifer *B. plicatilis* larva (Manfra et al., 2017). In *Artemia* spp. PS-NH_2 NPs provoked significant physiological alterations in the exposed larvae, including multiple molting (Bergami et al., 2016, 2017) as well as oxidative stress and neurotoxicity over short- and long-term exposure, as indicated by the significant decrease in the cholinesterase activity (Varó et al., 2019), leading to mortality after 14 days (Bergami et al., 2017; Varó et al., 2019). Long-term endpoints appeared thus more suitable to assess the toxicity of PS NPs to marine zooplankton (Lee et al., 2013; Bergami et al., 2017; Varó et al., 2019).

Marine mussels belonging to the *Mytilus* genus have been largely adopted as model organisms to investigate the biological effects of PS NPs through laboratory studies. Following short-term *in vivo* experiments (up to 72 h), ingestion and egestion of PS NP agglomerates have been confirmed in suspension-feeding bivalves (Ward and Kach, 2009), with the organisms starting to internalize NPs already in the first hour of exposure (Farrell and Nelson, 2013). In the mussel *M. edulis*, this has been associated with the production of pseudofeces (Wegner et al., 2012; Farrell and Nelson, 2013) and a reduced filtering activity, following exposure to high concentrations (up to 300 $\mu g\ ml^{-1}$) of sulfate-functionalized PS NPs (Wegner et al., 2012). Furthermore, trophic transfer of plain PS NPs of different sizes (30, 100, and 500 nm) from mussels to the crab *Carcinus maenas* has been demonstrated under laboratory conditions (Farrell and Nelson, 2013). Some studies reported the ability of PS NPs to translocate from the hemolymph to target tissues in benthic invertebrates (Farrell and Nelson, 2013) in a size-dependent manner, with 50 nm of PS NPs more internalized by hemocytes than larger particles (Sendra et al., 2019a), taken up in immune cells, and cause oxidative stress, immunotoxicity, and genotoxicity (Canesi et al., 2015; Brandts et al., 2018; Bergami et al., 2019; Ciacci et al., 2019; Sendra et al., 2019a). In a recent study on the benthic foraminifer *Ammonia parkinsoniana*, plain PS NPs tested at a concentration of 1 $\mu g\ ml^{-1}$ were internalized in the single-cell marine eukaryotes within 24 h, enhancing free-radical production and accumulation of intracellular neutral lipids (Ciacci et al., 2019). Furthermore, one study available on the Antarctic sea urchin *Sterechinus neumayeri* (Bergami et al., 2019) reported the sensitivity of this polar benthic

species to anthropogenic NPs, by investigating the effects of two functionalized PS NPs (at 1 and 5 $\mu g\ ml^{-1}$) on sea urchin coelomocytes following *in vitro* short-term exposure. PS-COOH NPs were able to induce an inflammatory response, with the modulation of genes having a role against oxidative stress and apoptosis, while a toxicity threshold was likely reached for PS-NH_2 NPs under the same experimental conditions.

For marine vertebrates, several studies have been conducted on freshwater species, in particular, on the zebrafish *Danio rerio* (as reviewed in Chae and An, 2017), while little information is available on marine model organisms. Yin et al. (2019) evaluated the alteration in behavior and metabolism of a marine demersal fish (*Sebastes schlegelii*) exposed to 190 $\mu g\ L^{-1}$ of PS NPs (nominal size of 500 nm) for 14 days. A significant decrease in protein and lipid content was observed, potentially associated with reduced fish energy reserve and altered feeding behavior. However, the negative impact appeared limited compared to the effects of larger micro-sized PS (15 μm). Almeida et al. (2019) reported that 100 nm of PS NPs was not cytotoxic to cell lines of two marine fish (*Sparus aurata* and *D. labrax*) after *in vitro* exposure (24 h), though they altered the lethality of human pharmaceuticals.

CURRENT GAPS AND FUTURE RECOMMENDATION

A comprehensive review of the major findings regarding the behavior, interactions with biological surfaces, and effects of TiO_2 and PS NPs in the marine environment is reported. Although several behavior patterns have been defined as well as major impacts and toxicity mechanisms determined on key marine species, some knowledge gaps remain and shape the future studies on this growing research field. The detection of anthropogenic NPs at trace levels in natural systems, such as seawater and sediments, remains the greatest challenge to monitor them in the marine environment and hone the probabilistic NP flow modeling (Sun et al., 2016). Analytical methods, such as stable isotope tracer and liquid chromatography coupled to high-resolution mass spectrometry, should be adapted and further implemented for anthropogenic NPs.

Future laboratory experiments should be carried out at environmentally realistic concentrations (i.e., $<\mu g\ L^{-1}$), for example using metal-doped nanoplastics (Koelmans, 2019; Mitrano et al., 2019) or radio-labeled NPs (Bourgeault et al., 2015; Al-Sid-Cheikh et al., 2018) that can be traced both in complex matrices and the biota, allowing for a more reliable environmental risk assessment. In an ecological perspective, long-term and chronic endpoints should be preferred over acute standard ecotoxicity tests, and multi-species studies are encouraged to understand the impacts of anthropogenic NPs over key ecological processes, such as algal bloom formation and particulate organic carbon flux. "Omics" approaches are promising tools to determine signaling cascade and toxicity mechanisms triggered by anthropogenic NPs in biological systems. Finally, gaining knowledge on the bio- and eco-corona(s) formation will be crucial to unveil the complex nano-bio interactions occurring in natural systems. Their study and consideration in the framework of ecotoxicity studies is of paramount importance to obtain meaningful outcomes and to extend to them real environmental scenarios.

AUTHOR CONTRIBUTIONS

IC conceived the outline of the review, and drafted the manuscript for the introduction and TiO_2 ecotoxicity state of the art. EB drafted the manuscript for the introduction, the behavior paragraph, and PS ecotoxicity state of the art. GG drafted the manuscript for the corona concept paragraph. All authors contributed to improving the manuscript and approved the submission.

FUNDING

This work was partly supported by the following funded projects: *Plastics in Antarctic Environment* (PLANET) and *Polymeric nanoparticles in the marine environment and in Antarctic organisms* (NANOPANTA), both funded by the Italian National Antarctic Program (PNRA: 14_00090; 16_00075).

SUPPLEMENTARY MATERIAL

The Supplementary Material for this article can be found online at: https://www.frontiersin.org/articles/10.3389/fenvs.2020.00060/full#supplementary-material

REFERENCES

Adeleye, A. S., Conway, J. R., Perez, T., Rutten, P., and Keller, A. A. (2014). Influence of extracellular polymeric substances on the long-term fate, dissolution, and speciation of copper-based nanoparticles. *Environ. Sci. Technol.* 48, 12561–12568. doi: 10.1021/es5033426

Adeleye, A. S., and Keller, A. A. (2014). Long-term colloidal stability and metal leaching of single wall carbon nanotubes: effect of temperature and extracellular polymeric substances. *Wat. Res.* 49, 236–250. doi: 10.1016/j.watres.2013.11.032

Albanese, A., Tang, P. S., and Chan, W. C. W. (2012). The effect of nanoparticle size, shape, and surface chemistry on biological systems. *Annu. Rev. Biomed. Eng.* 14, 1–16. doi: 10.1146/annurev-bioeng-071811-150124

Alijagic, A., Benada, O., Kofroňová, O., Cigna, D., and Pinsino, A. (2019). Sea urchin extracellular proteins design a complex protein corona on titanium dioxide nanoparticle surface influencing immune cell behavior. *Front. Immunol.* 10:2261. doi: 10.3389/fimmu.2019.02261

Alijagic, A., Gaglio, D., Napodano, E., Russo, R., Costa, C., Benada, O., et al. (2020). Titanium dioxide nanoparticles temporarily influence the sea urchin immunological state suppressing inflammatory-relate gene transcription and boosting antioxidant metabolic activity. *J. Hazard. Mater.* 384:389. doi: 10.1016/j.jhazmat.2019.121389

Alijagic, A., and Pinsino, A. (2017). Probing safety of nanoparticles by outlining sea urchin sensing and signaling cascades. *Ecotoxicol. Environ. Saf.* 144, 416–421. doi: 10.1016/j.ecoenv.2017.06.060

Almeida, M., Martins, M. A., Soares, A. M. V., Cuesta, A., and Oliveira, M. (2019). Polystyrene nanoplastics alter the cytotoxicity of human pharmaceuticals on marine fish cell lines. *Environ. Toxicol. Pharmacol.* 69, 57–65. doi: 10.1016/j.etap.2019.03.019

Al-Sid-Cheikh, M., Rowland, S. J., Stevenson, K., Rouleau, C., Henry, T. B., and Thompson, R. C. (2018). Uptake, whole-body distribution, and depuration of nanoplastics by the scallop pecten maximus at environmentally realistic concentrations. *Environ. Sci. Technol.* 52, 14480–14486. doi: 10.1021/acs.est.8b05266

Andrady, A. L. (2017). The plastic in microplastics: a review. *Mar. Pollut. Bull.* 119, 12–22. doi: 10.1016/j.marpolbul.2017.01.082

Auguste, M., Balbi, T., Montagna, M., Fabbri, R., Sendra, M., Blasco, J., et al. (2019). In vivo immunomodulatory and antioxidant properties of nanoceria (nCeO 2) in the marine mussel *Mytilus galloprovincialis*. *Comp. Biochem. Physiol. Part C Toxicol. Pharmacol.* 219, 95–102. doi: 10.1016/j.cbpc.2019.02.006

Baalousha, M. (2017). Effect of nanomaterial and media physicochemical properties on nanomaterial aggregation kinetics. *Nanoimpact* 6, 55–68. doi: 10.1016/j.impact.2016.10.005

Baalousha, M., Cornelis, G., Kuhlbusch, T. A. J., Lynch, I., Nickel, C., Peijnenburg, W., et al. (2016). Modeling nanomaterial fate and uptake in the environment: current knowledge and future trends. *Environ. Sci. Nano* 3, 323–345. doi: 10.1039/c5en00207a

Balbi, T., Camisassi, G., Montagna, M., Fabbri, R., Franzellitti, S., Carbone, C., et al. (2017). Impact of cationic polystyrene nanoparticles (PS-NH2) on early embryo development of Mytilus galloprovincialis: effects on shell formation. *Chemosphere* 186, 1–9. doi: 10.1016/j.chemosphere.2017.07.120

Balbi, T., Smerilli, A., Fabbri, R., Ciacci, C., Montagna, M., Grasselli, E., et al. (2014). Co-exposure to n-TiO2and Cd2+results in interactive effects on biomarker responses but not in increased toxicity in the marine bivalve *M. galloprovincialis*. *Sci. Tot. Environ.* 493, 355–364. doi: 10.1016/j.scitotenv.2014.05.146

Banni, M., Sforzini, S., Balbi, T., Corsi, I., Viarengo, A., and Canesi, L. (2016). Combined effectsof n-TiO2 and 2,3,7,8-TCDD in *Mytilus galloprovincialis* digestive gland: a transcriptomic and immunohistochemical study. *Environ. Res.* 145, 135–144. doi: 10.1016/j.envres.2015.12.003

Baudrimont, M., Arini, A., Guégan, C., Venel, Z., Gigault, J., Pedrono, B., et al. (2019). Ecotoxicity of polyethylene nanoplastics from the North Atlantic oceanic gyre on freshwater and marine organisms (microalgae and filter-feeding bivalves). *Environ. Sci. Pollut. Res.* 27, 3746–3755. doi: 10.1007/s11356-019-04668-3

Bellingeri, A., Casabianca, S., Cappellacci, S., Faleri, C., Paccagnigi, E., Lupetti, P., et al. (2020). Impact of polystyrene nanoparticles on marine diatom *Skeletonema marinoi* chain assemblages and consequences on their ecological role in marine ecosystems. *Environ. Pollut.* 262:114268. doi: 10.1016/j.envpol.2020.114268

Beninger, P. G., and St-Jean, S. D. (1997). The role of mucus in particle processing by suspension-feeding marine bivalves: unifying principles. *Mar. Biol.* 129, 389–397. doi: 10.1007/s002270050179

Bergami, E., Bocci, E., Vannuccini, M. L., Monopoli, M., Salvati, A., Dawson, K. A., et al. (2016). Nano-sized polystyrene affects feeding, behavior and physiology of brine shrimp *Artemia franciscana* larvae. *Ecotoxicol. Environ. Saf.* 123, 18–25. doi: 10.1016/j.ecoenv.2015.09.021

Bergami, E., Krupinski Emerenciano, A., González-Aravena, M., Cárdenas, C. A., Hernández, P., Silva, J. R. M. C., et al. (2019). Polystyrene nanoparticles affect the innate immune system of the Antarctic sea urchin *Sterechinus neumayeri*. *Polar Biol.* 42, 743–757. doi: 10.1007/s00300-019-02468-6

Bergami, E., Pugnalini, S., Vannuccini, M. L., Manfra, L., Faleri, C., Savorelli, F., et al. (2017). Long-term toxicity of surface-charged polystyrene nanoplastics to marine planktonic species *Dunaliella tertiolecta* and *Artemia franciscana*. *Aquat. Toxicol.* 189, 159–169. doi: 10.1016/j.aquatox.2017.06.008

Bexiga, M. G., Kelly, C., Dawson, K. A., and Simpson, J. C. (2014). RNAi-mediated inhibition of apoptosis fails to prevent cationic nanoparticle-induced cell death in cultured cells. *Nanomedicine* 9, 1651–1664. doi: 10.2217/nnm.13.151

Bexiga, M. G., Varela, J. A., Wang, F., Fenaroli, F., Salvati, A., Lynch, I., et al. (2011). Cationic nanoparticles induce caspase 3-, 7-and 9-mediated cytotoxicity in a human astrocytoma cell line. *Nanotoxicology* 5, 557–567. doi: 10.3109/17435390.2010.539713

Bhargava, S., Chen Lee, S. S., Min Ying, L. S., Neo, M. L., Lay-Ming Teo, S., and Valiyaveettil, S. (2018). Fate of nanoplastics in marine larvae: a case study using barnacles, *Amphibalanus amphitrite*. *ACS Sustain. Chem. Eng.* 6, 6932–6940. doi: 10.1021/acssuschemeng.8b00766

Bhuvaneshwari, M., Sagar, B., Doshi, S., Chandrasekaran, N., and Mukherjee, A. (2017). Comparative study on toxicity of ZnO and TiO2 nanoparticles on *Artemia salina*: effect of pre-UV-A and visible light irradiation. *Environ. Sci. Pollut. Res.* 24, 5633–5646. doi: 10.1007/s11356-016-8328-z

Bhuvaneshwari, M., Thiagarajan, V., Nemade, P., Chandrasekaran, N., and Mukherjee, A. (2018). Toxicity and trophic transfer of P25 TiO2 NPs from *Dunaliella salina* to *Artemia salina*: effect of dietary and waterborne exposure. *Environ. Res.* 160, 39–46. doi: 10.1016/j.envres.2017.09.022

Blair, R. M., Waldron, S., Phoenix, V., and Gauchotte-Lindsay, C. (2017). Micro- and nanoplastic pollution of freshwater and wastewater treatment systems. *Springer Sci. Rev.* 5, 19–30. doi: 10.1007/s40362-017-0044-7

Blasco, J., Corsi, I., and Matranga, V. (2015). Particles in the ocean, implications for a safe marine environment. *Mar. Environ. Res.* 111, 1–4. doi: 10.1016/j.marenvres.2015.10.001

Botta, C., Labille, J., Auffan, M., Bornscheck, D., Miche, H., Cabié, M., et al. (2011). TiO2-based nanoparticles released in water from commercialized sunscreeens in a life-cycle perspective: structures and quantities. *Environ. Poll.* 159, 1543–1550. doi: 10.1016/j.envpol.2011.03.003

Bourgeault, A., Cousin, C., Geertsen, V., Cassier-Chauvat, C., Chauvat, F., Durupthy, O., et al. (2015). The challenge of studying TiO2 nanoparticle bioaccumulation at environmental concentrations: crucial use of a stable isotope tracer. *Environ. Sci. Technol.* 49, 2451–2459. doi: 10.1021/es504638f

Bourgeault, A., Legros, V., Gonnet, F., Daniel, R., Paquirissamy, A., Bénatar, C., et al. (2017). Interaction of TiO2 nanoparticles with proteins from aquatic organisms: the case of gill mucus from blue mussel. *Environ. Sci. Pollut. Res.* 24, 13474–13483. doi: 10.1007/s11356-017-8801-3

Bourikas, K., Hiemstra, T., and Van Riemsdijk, W. H. (2001). Ion pair formation and primary charging behavior of titanium oxide (anatase and rutile). *Langmuir* 17, 749–756. doi: 10.1021/la000806c

Brandts, I., Teles, M., Gonçalves, A. P., Barreto, A., Franco-Martinez, L., Tvarijonaviciute, A., et al. (2018). Effects of nanoplastics on Mytilus galloprovincialis after individual and combined exposure with carbamazepine. *Sci. Total Environ.* 643, 775–784. doi: 10.1016/j.scitotenv.2018.06.257

Brunelli, A., Poiana, G., Callegaro, S., and Marcomini, A. (2013). Agglomeration and sedimentation of titanium dioxide nanoparticles (n-TiO2) in synthetic and realwaters. *J. Nanopart. Res.* 15, 1–10. doi: 10.1007/s11051-013-1684-4

Budarz, J. F., Turolla, A., Piasecki, A. F., Bottero, J., Antonelli, M., and Wiesner, M. R. (2017). Influence of aqueous inorganic anions on the reactivity of nanoparticles in TiO2 photocatalysis. *Langmuir* 33, 2770–2779. doi: 10.1021/acs.langmuir.6b04116

Cai, L., Hu, L., Shi, H., Ye, J., Zhang, Y., and Kim, H. (2018). Effects of inorganic ions and natural organic matter on the aggregation of nanoplastics. *Chemosphere* 197, 142–151. doi: 10.1016/j.chemosphere.2018.01.052

Canesi, L., Auguste, M., and Bebianno, M. J. (2019). "Sublethal effects of nanoparticles in aquatic invertebrates, from molecular to organism level," in *Ecotoxicology of Nanoparticles in Aquatic Systems*, eds J. Blasco and I. Corsi (Milton Park: CRC Taylor & Francis Group), 38–61. doi: 10.1201/9781315158761-2

Canesi, L., Balbi, T., Fabbri, R., Salis, A., Damonte, G., Volland, M., et al. (2017). Biomolecular coronas in invertebrate species: implications in the environmental impact of nanoparticles. *NanoImpact* 8, 89–98. doi: 10.1016/j.impact.2017.08.001

Canesi, L., Ciacci, C., and Balbi, T. (2016a). Invertebrate models for investigating the impact of nanomaterials on innate immunity: the example of the marine mussel *Mytilus* spp. *Curr. Bionanotechnol.* 2, 77–83. doi: 10.2174/2213529402666160601102529

Canesi, L., Ciacci, C., Fabbri, R., Balbi, T., Salis, A., Damonte, G., et al. (2016b). Interactions of cationic polystyrene nanoparticles with marine bivalve hemocytes in a physiological environment: role of soluble hemolymph proteins. *Environ. Res.* 150, 73–81. doi: 10.1016/j.envres.2016.05.045

Canesi, L., Ciacci, C., Bergami, E., Monopoli, M. P., Dawson, K. A., Papa, S., et al. (2015). Evidence for immunomodulation and apoptotic processes induced by cationic polystyrene nanoparticles in the hemocytes of the marine bivalve *Mytilus*. *Mar. Environ. Res.* 111, 34–40. doi: 10.1016/j.marenvres.2015.06.008

Canesi, L., and Corsi, I. (2016). Effects of nanomaterials on marine invertebrates. *Sci. Total Environ.* 565, 933–940. doi: 10.1016/j.scitotenv.2016.01.085

Canesi, L., Frenzilli, G., Balbi, T., Bernardeschi, M., Ciacci, C., Corsolini, S., et al. (2014). Interactive effects on n-TiO2 and 2,3,7,8-TCDD on the marine bivalve *Mytilus galloprovincialis*. *Aquat. Toxicol.* 153, 53–65. doi: 10.1016/j.aquatox.2013.11.002

Caracciolo, G., Pozzi, D., Capriotti, A. L., Cavaliere, C., Foglia, P., Amenitsch, H., et al. (2011). Evolution of the protein corona of lipid gene vectors as a function of plasma concentration. *Langmuir* 27, 15048–15053. doi: 10.1021/la202912f

Cardellini, A., Alberghini, M., Govind Rajan, A., Misra, R. P., Blankschtein, D., and Asinari, P. (2019). Multi-scale approach for modeling stability, aggregation, and network formation of nanoparticles suspended in aqueous solutions. *Nanoscale* 11, 3925–3932. doi: 10.1039/c8nr08782b

Carp, O., Huisman, C. L., and Reller, A. (2004). Photoinduced reactivity of titanium dioxide. *Prog. Solid State Chem.* 32, 33–77.

Casals, E., Pfaller, T., Duschl, A., Oostingh, G. J., and Puntes, V. (2010). Time evolution of the nanoparticle protein corona. *ACS Nano* 4, 3623–3632. doi: 10.1021/nn901372t

Cedervall, T., Lynch, I., Foy, M., Berggård, T., Donnelly, S. C., Cagney, G., et al. (2007a). Detailed identification of plasma proteins adsorbed on copolymer nanoparticles. *Angew. Chemie Int. Ed.* 46, 5754–5756. doi: 10.1002/anie.200700465

Cedervall, T., Lynch, I., Lindman, S., Berggard, T., Thulin, E., Nilsson, H., et al. (2007b). Understanding the nanoparticle-protein corona using methods to quantify exchange rates and affinities of proteins for nanoparticles. *Proc. Natl. Acad. Sci. U.S.A.* 104, 2050–2055. doi: 10.1073/pnas.0608582104

Chae, Y., and An, Y. J. (2017). Effects of micro- and nanoplastics on aquatic ecosystems: current research trends and perspectives. *Mar. Pollut. Bull.* 124, 624–632. doi: 10.1016/j.marpolbul.2017.01.070

Chen, C. S., Anaya, J. M., Zhang, S., Spurgin, J., Chuang, C. Y., Xu, C., et al. (2011). Effects of engineered nanoparticles on the assembly of exopolymeric substances from phytoplankton. *PLoS One* 6:e21865. doi: 10.1371/journal.pone.0021865

Chen, C. S., Le, C., Chiu, M. H., and Chin, W. C. (2018). The impact of nanoplastics on marine dissolved organic matter assembly. *Sci. Total Environ.* 634, 316–320. doi: 10.1016/j.scitotenv.2018.03.269

Choi, S., Johnston, M., Wang, G.-S., and Huang, C. P. (2018). A seasonal observation on the distribution of engineered nanoparticles in municipal wastewater treatment systems exemplified by TiO2 and ZnO. *Sci. Tot. Environ.* 625, 1321–1329. doi: 10.1016/j.scitotenv.2017.12.326

Chong, M. N., Jin, B., Chow, C. W. K., and Saint, C. (2010). Recent developments in photocatalytic water treatment technology: a review. *Water Res.* 44, 2997–3027. doi: 10.1016/j.watres.2010.02.039

Ciacci, C., Grimmelpont, M. V., Corsi, I., Bergami, E., Curzi, D., Burini, D., et al. (2019). Nanoparticle-biological interactions in a marine benthic foraminifer. *Sci. Rep.* 9:19441. doi: 10.1038/s41598-019-56037-2

Cole, M., and Galloway, T. S. (2015). Ingestion of nanoplastics and microplastics by pacific oyster larvae. *Environ. Sci. Technol.* 49, 14625–14632. doi: 10.1021/acs.est.5b04099

Corinaldesi, C., Marcellini, F., Nepote, E., Damiani, E., and Danovaro, R. (2018). Impact of inorganic UV filters contained in sunscreen products on tropical stony corals (*Acropora spp.*). *Sci. Tot. Environ.* 637–638, 1279–1285. doi: 10.1016/j.scitotenv.2018.05.108

Corsi, I., Cherr, G. N., Lenihan, H. S., Labille, J., Hassellov, M., Canesi, L., et al. (2014). Common strategies and technologies for the ecosafety assessment and design of nanomaterials entering the marine environment. *ACS Nano* 8, 9694–9709. doi: 10.1021/nn504684k

Corsi, I., Winther-Nielsen, M., Sethi, R., Punta, C., Della Torre, C., Libralato, G., et al. (2018). *Ecofriendly* nanotechnologies and nanomaterials for environmental applications: key issue and consensus recommendations for sustainable and ecosafe nanoremediation. *Ecotox. Environ. Saf.* 154, 237–244. doi: 10.1016/j.ecoenv.2018.02.037

Cózar, A., Echevarría, F., González-Gordillo, J. I., Irigoien, X., Úbeda, B., Hernández-León, S., et al. (2014). Plastic debris in the open ocean. *Proc. Natl. Acad. Sci. U.S.A.* 111, 10239–10244. doi: 10.1073/pnas.1314705111

da Silva, B. F., Pérez, S., Gardinalli, P., Singhal, R. K., Mozeto, A. A., and Barceló, D. (2011). Analytical chemistry of metallic nanoparticles in natural environments. *TrAC Trends Anal. Chem.* 30, 528–540. doi: 10.1016/j.trac.2011.01.008

Danielsson, K., Persson, P., Gallego-Urrea, J. A., Abbas, Z., Rosenqvist, J., and Jonsson, C. M. (2018). Effects of the adsorption of NOM model molecules on the aggregation of TiO2 nanoparticles in aqueous suspensions. *Nanoimpact* 10, 177–187. doi: 10.1016/j.impact.2018.05.002

Davidson, T. M. (2012). Boring crustaceans damage polystyrene floats under docks polluting marine waters with microplastic. *Mar. Pollut. Bull.* 64, 1821–1828. doi: 10.1016/j.marpolbul.2012.06.005

Della Torre, C., Balbi, T., Grassi, G., Frenzilli, G., Bernardeschi, M., Smerilli, A., et al. (2015a). Titanium dioxide nanoparticles modulate the toxicological response to cadmium in the gills of *Mytilus galloprovincialis*. *J. Haz. Mat.* 297, 92–100. doi: 10.1016/j.jhazmat.2015.04.072

Della Torre, C., Bergami, E., Salvati, A., Faleri, C., Cirino, P., Dawson, K. A., et al. (2014). Accumulation and embryotoxicity of polystyrene nanoparticles at early stage of development of sea urchin embryos *Paracentrotus lividus*. *Environ. Sci. Technol.* 48, 12302–12311. doi: 10.1021/es502569w

Della Torre, C., Buonocore, F., Frenzilli, G., Corsolini, S., Brunelli, A., Guidi, P., et al. (2015b). Influence of titanium dioxide nanoparticles on 2,3,7,8-tetrachlorodibenzo-*p*-dioxin bioconcentration and toxicity in the marine fish european sea bass (*Dicentrachus labrax*). *Environ. Pollut.* 196, 185–193. doi: 10.1016/j.envpol.2014.09.020

Deng, X. Y., Cheng, J., Hu, X. L., Wang, L., Li, D., and Gao, K. (2017). Biological effects of TiO2 and CeO2 nanoparticles on the growth, photosynthetic activity, and cellular components of a marine diatom *Phaeodactylum tricornutum*. *Sci. Total Environ.* 575, 87–96. doi: 10.1016/j.scitotenv.2016.10.003

Dobrovolskaia, M. A., Patri, A. K., Zheng, J., Clogston, J. D., Ayub, N., Aggarwal, P., et al. (2009). Interaction of colloidal gold nanoparticles with human blood: effects on particle size and analysis of plasma protein binding profiles. *Nanomed. Nanotechnol. Biol. Med.* 5, 106–117. doi: 10.1016/j.nano.2008.08.001

Docter, D., Westmeier, D., Markiewicz, M., Stolte, S., Knauer, S. K., and Stauber, R. H. (2015). The nanoparticle biomolecule corona: lessons learned – challenge accepted? *Chem. Soc. Rev.* 44, 6094–6121. doi: 10.1039/C5CS00217F

Doyle, J. J., Ward, E. J., and Mason, R. (2015). An examination of the ingestion, bioaccumulation, and depuration of titanium dioxide nanoparticles by the blue mussel (*Mytilus edulis*) and the eastern oyster (*Crassostrea virginica*). *Mar. Environ. Res.* 110, 45–52. doi: 10.1016/j.marenvres.2015.07.020

Eigenheer, R., Castellanos, E. R., Nakamoto, M. Y., Gerner, K. T., Lampe, A. M., and Wheeler, K. E. (2014). Silver nanoparticle protein corona composition compared across engineered particle properties and environmentally relevant reaction conditions. *Environ. Sci. Nano* 1:238. doi: 10.1039/c4en00002a

Espinosa, E. P., Hassan, D., Ward, J. E., Shumway, S. E., and Allam, B. (2010). Role of epicellular molecules in the selection of particles by the blue mussel, *Mytilus edulis*. *Biol. Bull.* 219, 50–60. doi: 10.1086/bblv219n1p50

European Commission [EU] (2011). European commission. 2011/696/EU commission recommendation of 18 October 2011 on the definition of nanomaterial. *Off. J. Eur. Union* 54:38.

Falugi, C., Aluigi, M. G., Chiantore, M. C., Privitera, D., Ramoino, P., Gatti, M. A., et al. (2012). Toxicity of metal oxide nanoparticles in immune cells of the sea urchin. *Mar. Environ. Res.* 76, 114–121. doi: 10.1016/j.marenvres.2011.10.003

Farkas, J., Bergum, S., Nilsen, E. W., Olsen, A. J., Salaberria, I., Ciesielski, T. M., et al. (2015). The impact of TiO2 nanoparticles on uptake and toxicity of benzo(a)pyrene in the blue mussel (*Mytilus edulis*). *Sci. Total Environ.* 511, 469–476. doi: 10.1016/j.scitotenv.2014.12.084

Farrell, P., and Nelson, K. (2013). Trophic level transfer of microplastic: *Mytilus edulis* (L.) to *Carcinus maenas* (L.). *Environ. Pollut.* 177, 1–3. doi: 10.1016/j.envpol.2013.01.046

Fotopoulou, K. N., and Karapanagioti, H. K. (2012). Surface properties of beached plastic pellets. *Mar. Environ. Res.* 81, 70–77. doi: 10.1016/j.marenvres.2012.08.010

French, R. A., Jacobson, A. R., Kim, B., Isley, S. L., Penn, L., and Baveye, P. C. (2009). Influence of ionic strength, pH, and cation valence on aggregation kinetics of titanium dioxide nanoparticles. *Environ. Sci. Technol.* 43, 1354–1359. doi: 10.1021/es802628n doi: 10.1021/es802628n

Fröhlich, E., Meindl, C., Roblegg, E., Ebner, B., Absenger, M., and Pieber, T. R. (2012). Action of polystyrene nanoparticles of different sizes on lysosomal function and integrity. *Part. Fibre Toxicol.* 9:1. doi: 10.1186/1743-8977-9-26

Fu, S. F., Ding, J. N., Zhang, Y., Li, Y. F., Zhu, R., Yuan, X. Z., et al. (2018). Exposure to polystyrene nanoplastic leads to inhibition of anaerobic digestion system. *Sci. Total Environ.* 625, 64–70. doi: 10.1016/j.scitotenv.2017.12.158

Gambardella, C., Morgana, S., Bramini, M., Rotini, A., Manfra, L., Migliore, L., et al. (2018). Ecotoxicological effects of polystyrene microbeads in a battery of marine organisms belonging to different trophic levels. *Mar. Environ. Res.* 141, 313–321. doi: 10.1016/j.marenvres.2018.09.023

Gambardella, C., Morgana, S., Ferrando, S., Bramini, M., Piazza, V., Costa, E., et al. (2017). Effects of polystyrene microbeads in marine planktonic crustaceans. *Ecotoxicol. Environ. Saf.* 145, 250–257. doi: 10.1016/j.ecoenv.2017.07.036

Gao, J., Lin, L., Wei, A., and Sepúlveda, M. S. (2017). Protein corona analysis of silver nanoparticles exposed to fish plasma. *Environ. Sci. Technol. Lett.* 4, 174–179. doi: 10.1021/acs.estlett.7b00074

García-Álvarez, R., Hadjidemetriou, M., Sánchez-Iglesias, A., Liz-Marzán, L. M., and Kostarelos, K. (2018). *In vivo* formation of protein corona on gold nanoparticles. the effect of their size and shape. *Nanoscale* 10, 1256–1264. doi: 10.1039/c7nr08322j

Garner, K. L., Suh, S., and Keller, A. A. (2017). Assessing the risk of engineered nanomaterials in the environment: development and application of the nanofate model. *Environ. Sci. Technol.* 51, 5541–5551. doi: 10.1021/acs.est.6b05279

Gigault, J., Pedrono, B., Maxit, B., and Ter Halle, A. (2016). Marine plastic litter: the unanalyzed nano-fraction. *Environ. Sci. Nano* 3, 346–350. doi: 10.1039/c6en00008h

Gondikas, A. P., von der Kammer, F., Reed, R. B., Wagner, S., Ranville, J. F., et al. (2014). Release of TiO2 nanoparticles from sunscreens into surface waters: a one-year survey at the old Danube recreational Lake. *Environ. Sci. Technol.* 48, 5415–5422. doi: 10.1021/es405596y

González-Fernández, C., Tallec, K., Le Goïc, N., Lambert, C., Soudant, P., Huvet, A., et al. (2018). Cellular responses of Pacific oyster (*Crassostrea gigas*) gametes exposed *in vitro* to polystyrene nanoparticles. *Chemosphere* 208, 764–772. doi: 10.1016/j.chemosphere.2018.06.039

González-Fernández, C., Toullec, J., Lambert, C., Le Goïc, N., Seoane, M., Moriceau, B., et al. (2019). Do transparent exopolymeric particles (TEP)affect the toxicity of nanoplastics on *Chaetoceros neogracile*? *Environ. Pollut.* 250, 873–882. doi: 10.1016/j.envpol.2019.04.093

Gottschalk, F., and Nowack, B. (2011). The release of engineered nanomaterials to the environment. *J. Environ. Monitor.* 13:1145. doi: 10.1039/c0em00547a

Gottschalk, F., Sun, T. Y., and Nowack, B. (2013). Environmental concentrations of engineered nanomaterials: review of modeling and analytical studies. *Environ. Pollut.* 181, 287–300. doi: 10.1016/j.envpol.2013.06.003

Goy-López, S., Juárez, J., Alatorre-Meda, M., Casals, E., Puntes, V. F., Taboada, P., et al. (2012). Physicochemical characteristics of protein-NP bioconjugates: the role of particle curvature and solution conditions on human serum albumin conformation and fibrillogenesis inhibition. *Langmuir* 28, 9113–9126. doi: 10.1021/la300402w

Grassi, G., Landi, C., Della Torre, C., Bergami, E., Bini, L., and Corsi, I. (2019). Proteomic profile of the hard corona of charged polystyrene nanoparticles exposed to sea urchin *Paracentrotus lividus* coelomic fluid highlights potential drivers of toxicity. *Environ. Sci. Nano.* 6, 2937–2947. doi: 10.1039/C9EN00824A

Grillo, R., Rosa, A. H., and Fraceto, L. F. (2015). Engineered nanoparticles and organic matter: a review of the state-of-the-art. *Chemosphere* 119, 608–619. doi: 10.1016/j.chemosphere.2014.07.049

Grimaldi, A. M., Belcari, P., Pagano, E., Cacialli, F., and Locatello, L. (2013). Immune responses of *Octopus vulgaris* (Mollusca: Cephalopoda) exposed to titanium dioxide nanoparticles. *J. Exp. Mar. Bio. Ecol.* 447, 123–127. doi: 10.1016/j.jembe.2013.02.018

Guan, X., Shi, W., Zha, S., Rong, J., Su, W., and Liu, G. (2018). Neurotoxic impact of acute TiO2 nanoparticle exposure on a benthic marine bivalve mollusk, *Tegillarca granosa*. *Aquat. Toxicol.* 200, 241–246. doi: 10.1016/j.aquatox.2018.05.011

Gupta, G. S., Kumar, A., Shanker, R., and Dhawan, A. (2016). Assessment of agglomeration, co-sedimentation and trophic transfer of titanium dioxide nanoparticles in a laboratory-scale predator-prey model system. *Sci. Rep.* 6, 1–13. doi: 10.1038/srep31422

Guterres, S. S., Alves, M. P., and Pohlmann, A. R. (2007). Polymeric nanoparticles, nanospheres and nanocapsules, for cutaneous applications. *Drug Target Insights* 2, 147–157. doi: 10.1177/117739280700200002

Gutierrez, T., Teske, A., Ziervogel, K., Passow, U., and Quigg, A. (2018). Editorial: microbial exopolymers: sources, chemico-physiological properties, and ecosystem effects in the marine environment. *Front. Microbiol.* 9:1822. doi: 10.3389/fmicb.2018.01822

Hartmann, N. B., Hüffer, T., Thompson, R. C., Hassellöv, M., Verschoor, A., Daugaard, A. E., et al. (2019). Are we speaking the same language? recommendations for a definition and categorization framework for plastic debris. *Environ. Sci. Technol.* 53, 1039–1047. doi: 10.1021/acs.est.8b05297

Hayashi, Y., Miclaus, T., Scavenius, C., Kwiatkowska, K., Sobota, A., Engelmann, P., et al. (2013). Species differences take shape at nanoparticles: protein corona made of the native repertoire assists cellular interaction. *Environ. Sci. Technol.* 47, 14367–14375. doi: 10.1021/es404132w

Haynes, V. N., Ward, J. E., Russell, B. J., and Agrios, A. G. (2017). Photocatalytic effects of titanium dioxide nanoparticles on aquatic organisms—current knowledge and suggestions for future research. *Aquat. Toxicol.* 185, 138–148. doi: 10.1016/j.aquatox.2017.02.012

He, X., Aker, W. G., Fu, P. P., and Hwang, H. (2015). Toxicity of engineered metal oxide nanomaterials mediated by nano–bio–eco–interactions: a review and perspective. *Environ. Sci. Nano* 2, 564–582. doi: 10.1039/C5EN00094G

He, X., Fu, P., Aker, W. G., and Hwang, H. M. (2018). Toxicity of engineered nanomaterials mediated by nano–bio–eco interactions. *J. Environ. Sci. Heal. Part C Environ. Carcinog. Ecotoxicol. Rev.* 36, 21–42. doi: 10.1080/10590501.2017.1418793

Hernandez, L. M., Xu, E. G., Larsson, H. C. E., Tahara, R., Maisuria, V. B., and Tufenkji, N. (2019). Plastic teabags release billions of microparticles and nanoparticles into tea. *Environ. Sci. Technol.* 53, 12300–12310. doi: 10.1021/acs.est.9b02540

Hernandez, L. M., Youse, N., and Tufenkji, N. (2017). Are there nanoplastics in your personal care products? *Cell* 7, 280–285. doi: 10.1021/acs.estlett.7b00187

Hessler, C. M., Wu, M. Y., Xue, Z., Choi, H., and Seo, Y. (2012). The influence of capsular extracellular polymeric substances on the interaction between TiO2 nanoparticles and planktonic bacteria. *Water Res.* 46, 4687–4696. doi: 10.1016/j.watres.2012.06.009

Hochella, M. F. Jr., Mogk, D. W., Ranville, J., Allen, I. C., Luther, G. W., Marr, L. C., et al. (2019). Natural, incidental, and engineered nanomaterials and their impacts on the Earth system. *Science* 363, 6434–8299. doi: 10.1126/science.aau8299

Holden, P. A., Gardea-Torresdey, J. L., Klaessig, F., Turco, R. F., Mortimer, M., Hund-Rinke, K., et al. (2016). Considerations of environmentally relevant test conditions for improved evaluation of ecological hazards of engineered nanomaterials. *Environ. Sci. Technol.* 50, 6124–6145. doi: 10.1021/acs.est.6b00608

Hu, J., Wang, J., Liu, S., Zhang, Z., Zhang, H., Cai, X., et al. (2018). Effect of TiO2 nanoparticle aggregation on marine microalgae *Isochrysis galbana*. *J. Environ. Sci.* 66:208. doi: 10.1016/j.jes.2017.05.026

Huvet, A., Paul-Pont, I., Fabioux, C., Lambert, C., Suquet, M., Thomas, Y., et al. (2016). Quantifying the smallest microplastics is the challenge for a comprehensive view of their environmental impacts. *Proc. Natl. Acad. Sci. U.S.A.* 113, E4123–E4124. doi: 10.1073/pnas.1607221113

ISO (2006). *Water Quality - Marine Algal Growth Inhibition Test With Skeletonema Costatum* and *Phaeodactylum tricornutum, ISO/TC 147/SC 5 10253*. London: ISO.

Jeong, C., Kang, H., Lee, Y. H., Kim, M., Lee, J., Seo, J. S., et al. (2018). Nanoplastic ingestion enhances toxicity of persistent organic pollutants (POPs) in the monogonont rotifer *Brachionus koreanus* via multixenobiotic resistance (MXR) disruption. *Environ. Sci. Technol.* 52, 11411–11418. doi: 10.1021/acs.est.8b03211

Jeong, C. B., Kang, H. M., Lee, M. C., Kim, D. H., Han, J., Hwang, D. S., et al. (2017). Adverse effects of microplastics and oxidative stress-induced MAPK/Nrf2 pathway-mediated defense mechanisms in the marine copepod *Paracyclopina nana*. *Sci. Rep.* 7, 1–11. doi: 10.1038/srep41323

Jeong, C. B., Won, E. J., Kang, H. M., Lee, M. C., Hwang, D. S., Hwang, U. K., et al. (2016). Microplastic size-dependent toxicity, oxidative stress induction, and p-JNK and p-p38 activation in the monogonont rotifer (*Brachionus koreanus*). *Environ. Sci. Technol.* 50, 8849–8857. doi: 10.1021/acs.est.6b01441

Jiménez-Fernández, E., Ruyra, A., Roher, N., Zuasti, E., Infante, C., and Fernández-Díaz, C. (2014). Nanoparticles as a novel delivery system for vitamin C administration in aquaculture. *Aquaculture* 432, 426–433. doi: 10.1016/j.aquaculture.2014.03.006

Johnston, H. J., Semmler-Behnke, M., Brown, D. M., Kreyling, W., Tran, L., and Stone, V. (2010). Evaluating the uptake and intracellular fate of polystyrene nanoparticles by primary and hepatocyte cell lines in vitro. *Toxicol. Appl. Pharmacol.* 242, 66–78. doi: 10.1016/j.taap.2009.09.015

Jovanović, B., and Guzmán, H. M. (2014). Effects of titanium dioxide (TiO2) nanoparticles on caribbean reef-building coral (*Montastraea faveolata*). *Environ. Toxicol. Chem.* 33, 1346–1353. doi: 10.1002/etc.2560

Kadar, E., Cunliffe, M., Fisher, A., Stolpe, B., Lead, J., and Shi, Z. (2014). Chemical interaction of atmospheric mineral dust-derived nanoparticles with natural seawater–EPS and sunlight-mediated changes. *Sci. Tot. Environ.* 468-469, 265–271. doi: 10.1016/j.scitotenv.2013.08.059

Keller, A. A., Wang, H., Zhou, D., Lenihan, H. S., Cherr, G., Cardinale, B. J., et al. (2010). Stability and aggregation of metal oxide nanoparticles in natural aqueous matrices. *Environ. Sci. Technol.* 44, 1962–1967. doi: 10.1021/es902987d doi: 10.1021/es902987d

Koelmans, A. A. (2019). Proxies for nanoplastic. *Nat. Nanotechnol.* 14, 307–308. doi: 10.1038/s41565-019-0416-z

Kokkinopoulou, M., Simon, J., Landfester, K., Mailänder, V., and Lieberwirth, I. (2017). Visualization of the protein corona: towards a biomolecular understanding of nanoparticle-cell-interactions. *Nanoscale* 9, 8858–8870. doi: 10.1039/c7nr02977b

Kuo, Y. Y., Zhang, H., Gerecke, A. C., and Wang, J. (2014). Chemical composition of nanoparticles released from thermal cutting of polystyrene foams and the associated isomerization of hexabromocyclododecane (HBCD) diastereomers. *Aerosol. Air Qual. Res.* 14, 1114–1120. doi: 10.4209/aaqr.2013.02.0059

Labille, J., Feng, J., Botta, C., Bornschneck, D., Sammut, M., Cabie, M., et al. (2010). Aging of TiO2 nanocomposites used in sunscreen. Dispersion and fate of the degradation products in aqueous environment. *Environ. Poll.* 158, 3482–3489. doi: 10.1016/j.envpol.2010.02.012

Labille, J., Slomberg, D., Catalano, R., Robert, S., Apers-Tremelo, M., Boudenne, J., et al. (2020). Assessing UV filter inputs into beach waters during recreational activity: A field study of three French Mediterranean beaches from consumer survey to water analysis. *Sci Tot. Environ.* 76:136010. doi: 10.1016/j.scitotenv.2019.136010

Lambert, S., Sinclair, C. J., Bradley, E. L., and Boxall, B. A. (2013). Effects of environmental conditions on latex degradation in aquatic systems. *Sci Tot. Environ*. 447, 225–234. doi: 10.1016/j.scitotenv.2012.12.067

Lambert, S., and Wagner, M. (2016). Formation of microscopic particles during the degradation of different polymers. *Chemosphere* 161, 510–517. doi: 10.1016/j.chemosphere.2016.07.042

Lara, S., Alnasser, F., Polo, E., Garry, D., Cristina, M., Giudice, L., et al. (2017). Identification of receptor binding to the biomolecular corona of nanoparticles. *ACS Nano* 11, 1884–1893. doi: 10.1021/acsnano.6b07933

Lebreton, L., and Andrady, A. (2019). Future scenarios of global plastic waste generation and disposal. *Palgrave Commun.* 5:6. doi: 10.1057/s41599-018-0212-7

Lee, K. W., Shim, W. J., Kwon, O. Y., and Kang, J. H. (2013). Size-dependent effects of micro polystyrene particles in the marine copepod *Tigriopus japonicus*. *Environ. Sci. Technol.* 47, 11278–11283. doi: 10.1021/es401932b

Lehner, R., Weder, C., Petri-Fink, A., and Rothen-Rutishauser, B. (2019). Emergence of nanoplastic in the environment and possible impact on human health. *Environ. Sci. Technol.* 53, 1748–1765. doi: 10.1021/acs.est.8b05512

Lenz, R., Enders, K., and Nielsen, T. G. (2016). Microplastic exposure studies should be environmentally realistic. *Proc. Natl. Acad. Sci U.S.A.* 113, E4121–E4122. doi: 10.1073/pnas.1606615113

Leslie, H. A. (2014). IVM Institute for Environmental Studies Review of Microplastics in Cosmetics. Environmental Chemistry and Toxicology AIMMS, VU University Amsterdam, Amsterdam.

Li, F., Liang, Z., Zheng, X., Zhao, W., Wu, M., and Wang, Z. (2015). Toxicity of nano-TiO2 on algae and the site of reactive oxygen species production. *Aquat. Toxicol.* 158, 1–13. doi: 10.1016/j.aquatox.2014.10.014

Libralato, G., Minetto, D., Totaro, S., Mičetić, I., Pigozzo, A., Sabbioni, E., et al. (2013). Embryotoxicity of TiO2 nanoparticles to *Mytilus galloprovincialis* (Lmk). *Mar. Environ. Res.* 92, 71–78. doi: 10.1016/j.marenvres.2013.08.015

Liu, Y., Li, W., Lao, F., Liu, Y., Wang, L., Bai, R., et al. (2011). Intracellular dynamics of cationic and anionic polystyrene nanoparticles without direct interaction with mitotic spindle and chromosomes. *Biomaterials* 32, 8291–8303. doi: 10.1016/j.biomaterials.2011.07.037

Long, R. A., and Azam, F. (1996). Abundant protein-containing particles in the sea. *Science* 10, 213–221. doi: 10.3354/ame010213

Loos, C., Syrovets, T., Musyanovych, A., Mailänder, V., Landfester, K., Ulrich Nienhaus, G., et al. (2014). Functionalized polystyrene nanoparticles as a platform for studying bio-nano interactions. *Beilstein J. Nanotechnol.* 5, 2403–2412. doi: 10.3762/bjnano.5.250

Louie, S. M., Spielman-Sun, E. R., Small, M. J., Tilton, R. D., and Lowry, G. V. (2015). Correlation of the physicochemical properties of natural organic matter samples from different sources to their effects on gold nanoparticle aggregation in monovalent electrolyte. *Environ. Sci. Technol.* 49, 2188–2198. doi: 10.1021/es505003d

Lowry, G. V., Gregory, K. B., Apte, S. C., and Lead, J. R. (2012). Transformations of nanomaterials in the environment. *Environ. Sci. Technol.* 46, 6893–6899. doi: 10.1021/es300839e

Lundqvist, M., Augustsson, C., Lilja, M., Lundkvist, K., Dahlbäck, B., Linse, S., et al. (2017). The nanoparticle protein corona formed in human blood or human blood fractions. *PLoS One* 12:0175871. doi: 10.1371/journal.pone.0175871

Lundqvist, M., Stigler, J., Elia, G., Lynch, I., Cedervall, T., and Dawson, K. A. (2008). Nanoparticle size and surface properties determine the protein corona with possible implications for biological impacts. *Proc. Natl. Acad. Sci. U.S.A.* 105, 14265–14270. doi: 10.1073/pnas.0805135105

Luo, M., Huang, Y., Zhu, M., Tang, Y., Ren, T., Ren, J., et al. (2018). Properties of different natural organic matter influence the adsorption and aggregation behavior of TiO2 nanoparticles. *J. Saudi Chem. Soc.* 22, 146–154. doi: 10.1016/j.jscs.2016.01.007

Lynch, I., Dawson, K. A., Lead, J. R., and Valsami-Jones, E. (2014). *Macromolecular Coronas and Their Importance in Nanotoxicology and Nanoecotoxicology*, 1st Edn, Amsterdam: Elsevier Ltd.

Mahmoudi, M., Abdelmonem, A. M., Behzadi, S., Clement, J. H., Dutz, S., Ejtehadi, M. R., et al. (2013). Temperature: the "ignored" factor at the nanobio interface. *ACS Nano* 7, 6555–6562. doi: 10.1021/nn305337c

Manfra, L., Rotini, A., Bergami, E., Grassi, G., Faleri, C., and Corsi, I. (2017). Ecotoxicology and environmental safety comparative ecotoxicity of polystyrene nanoparticles in natural seawater and reconstituted seawater using the rotifer *Brachionus plicatilis*. *Ecotoxicol. Environ. Saf.* 145, 557–563. doi: 10.1016/j.ecoenv.2017.07.068

Mari, X., Passow, U., Migon, C., Burd, A. B., and Legendre, L. (2017). Transparent exopolymer particles: effects on carbon cycling in the ocean. *Prog. Oceanogr.* 151, 13–37. doi: 10.1016/j.pocean.2016.11.002

Marisa, I., Marin, M. G., Caicci, F., Franceschinis, E., Martucci, A., and Matozzo, V. (2015). *In vitro* exposure of haemocytes of the clam *Ruditapes philippinarum* to titanium dioxide (TiO2) nanoparticles: nanoparticle characterization, effects on phagocytic activity and internalization of nanoparticles into haemocytes. *Mar. Environ. Res.* 103, 11–17. doi: 10.1016/j.marenvres.2014.11.002

Marques-Santos, L. F., Grassi, G., Bergami, E., Faleri, C., Balbi, T., Salis, A., et al. (2018). Cationic polystyrene nanoparticle and the sea urchin immune system: biocorona formation, cell toxicity, and multixenobiotic resistance phenotype. *Nanotoxicology* 12, 847–867. doi: 10.1080/17435390.2018.1482378

Matranga, V., and Corsi, I. (2012). Toxic effects of engineered nanoparticles in the marine environment: model organisms and molecular approaches. *Mar. Environ. Res.* 76, 32–40. doi: 10.1016/j.marenvres.2012.01.006

Matranga, V., Pinsino, A., Celi, M., Natoli, A., Bonaventura, R., Schröder, H. C., et al. (2005). Monitoring chemical and physical stress using sea urchin immune cells. *Echinodermata* 39, 85–110. doi: 10.1007/3-540-27683-1_5

Merdas, I., Thominette, F., and Verdu, J. (2003). Hydrolytic ageing of polyamide 11-Effect of carbon dioxide on polyamide 11 hydrolysis. *Polym. Degrad. Stab.* 79, 419–425. doi: 10.1016/s0141-3910(02)00358-0

Milani, S., Baldelli Bombelli, F., Pitek, A. S., Dawson, K. A., and Rädler, J. (2012). Reversible versus irreversible binding of transferrin to polystyrene nanoparticles: soft and hard corona. *ACS Nano* 6, 2532–2541. doi: 10.1021/nn204951s

Miller, R. J., Bennett, S., Keller, A. A., Pease, S., and Lenihan, H. S. (2012). TiO2 nanoparticles are phototoxic to marine phytoplankton. *PLoS One* 7:30321. doi: 10.1371/journal.pone.0030321

Miller, R. J., Lenihan, H. S., Muller, E. B., Tseng, N., Hanna, S. K., and Keller, A. A. (2010). Impacts of metal oxide nanoparticles on marine phytoplankton. *Environ. Sci. Technol.* 44, 7329–7334. doi: 10.1021/es100247x

Minetto, D., Ghirardini, A. V., and Libralato, G. (2016). Saltwater ecotoxicology of Ag, Au, CuO, TiO2, ZnO and C60 engineered nanoparticles: an overview. *Environ. Int* 92-93, 189–201. doi: 10.1016/j.envint.2016.03.041

Minetto, D., Libralato, G., and Ghirardini, A. V. (2014). Ecotoxicity of engineered TiO2 nanoparticles to saltwater organisms: an overview. *Environ. Int.* 66, 18–27. doi: 10.1016/j.envint.2014.01.012

Minetto, D., Libralato, G., Marcomini, A., and Volpi Ghirardini, A. (2017). Potential effects of TiO2 nanoparticles and TiCl4 in saltwater to *Phaeodactylum tricornutum* and *Artemia franciscana*. *Sci. Total Environ.* 579, 1379–1386. doi: 10.1016/j.scitotenv.2016.11.135

Mishra, P., Vinayagam, S., Duraisamy, K., Patil, S. R., Godbole, J., Mohan, A., et al. (2019). Distinctive impact of polystyrene nano-spherules as an emergent pollutant toward the environment. *Environ. Sci. Pollut. Res.* 26, 1537–1547. doi: 10.1007/s11356-018-3698-z

Mitrano, D. M., Beltzung, A., Frehland, S., Schmiedgruber, M., Cingolani, A., and Schmidt, F. (2019). Synthesis of metal-doped nanoplastics and their utility to investigate fate and behaviour in complex environmental systems. *Nat. Nanotechnol.* 14, 362–368. doi: 10.1038/s41565-018-0360-3

Mitrano, D. M., Motellier, S., Clavaguera, S., and Nowack, B. (2015). Review of nanomaterial aging and transformations through the life cycle of nano-enhanced products. *Environ. Int.* 77, 132–147. doi: 10.1016/j.envint.2015.01.013

Mohr, K., Sommer, M., Baier, G., Schöttler, S., Okwieka, P., Tenzer, S., et al. (2014). Aggregation behavior of polystyrene-nanoparticles in human blood serum and its impact on the in vivo distribution in mice. *J. Nanomedicine Nanotechnol.* 5:193. doi: 10.4172/2157-7439.1000193

Monopoli, M. P., Pitek, A. S., Lynch, I., and Dawson, K. A. (2013). Formation and characterization of the nanoparticle-protein corona. *Methods Mol. Biol.* 1025, 137–155. doi: 10.1007/978-1-62703-462-3_11

Monopoli, M. P., Walczyk, D., Campbell, A., Elia, G., Lynch, I., Baldelli Bombelli, F., et al. (2011). Physical-chemical aspects of protein corona: relevance to in vitro and in vivo biological impacts of nanoparticles. *J. Am. Chem. Soc.* 133, 2525–2534. doi: 10.1021/ja107583h

Mopper, K., Stubbins, A., Ritchie, J. D., Bialk, H. M., and Hatcher, P. G. (2007). Advanced instrumental approaches for characterization of marine dissolved organic matter: extraction techniques, mass spectrometry, and nuclear magnetic resonance spectroscopy. *Chem. Rev.* 107, 419–442. doi: 10.1021/cr050359b

Morelli, E., Gabellieri, E., Bonomini, A., Tognotti, D., Grassi, G., and Corsi, I. (2018). TiO2 nanoparticles in seawater: aggregation and interactions with the green alga *Dunaliella tertiolecta*. *Ecotoxicol. Environ. Saf.* 148, 184–193. doi: 10.1016/j.ecoenv.2017.10.024

Mourdikoudis, S., Pallares, R. M., and Thanh, N. T. K. (2018). Characterization techniques for nanoparticles: comparison and complementarity upon studying nanoparticle properties. *Nanoscale* 10, 12871–12934. doi: 10.1039/c8nr02278j

Mwaanga, P., Carraway, E. R., and Schlautman, M. A. (2014). Preferential sorption of some natural organic matter fractions to titanium dioxide nanoparticles: influence of pH and ionic strength. *Environ. Monit. Assess.* 186, 8833–8844. doi: 10.1007/s10661-014-4047-4

Nason, J. A., McDowell, S. A., and Callahan, T. W. (2012). Effects of natural organic matter type and concentration on the aggregation of citrate-stabilized gold nanoparticles. *J. Environ. Monit.* 14, 1885–1892. doi: 10.1039/c2em00005a

Nel, A., Xia, T., Madler, L., and Li, N. (2006). Toxic potential of materials at the nanolevel. *Science* 311:622. doi: 10.1126/science.1114397

Nigro, M., Berbardeschi, M., Costagliola, D., Della Torre, C., Frenzilli, G., Guidi, P., et al. (2015). n-TiO_2 and $CdCl_2$ co-exposure to titanium dioxide nanoparticles and cadmium: genomic, DNA and chromosomal damage evaluation in the marine fish European sea bass *Dicentrarchus labrax*. *Aquat. Toxicol.* 168, 72–77. doi: 10.1016/j.aquatox.2015.09.013

Nogueira, V., Lopes, I., Rocha-Santos, T. A. P., Rasteiro, M. G., Abrantes, N., Gonçalves, F., et al. (2015). Assessing the ecotoxicity of metal nano-oxides with potential for wastewater treatment. *Environ. Sci. Pollut. Res* 22, 13212–13224. doi: 10.1007/s11356-015-4581-9

Noventa, S., Rowe, D., and Galloway, T. (2018). Mitigating effect of organic matter on the in vivo toxicity of metal oxide nanoparticles in the marine environment. *Environ. Sci. Nano.* 5, 1764–1777. doi: 10.1039/c8en00175h

Nowack, B., and Mitrano, D. M. (2018). Procedures for the production and use of synthetically aged and product released nanomaterials for further environmental and ecotoxicity testing. *Nanoimpact* 10, 70–80. doi: 10.1016/j.impact.2017.12.001

OECD 201 (2011). *Test No. 201: Freshwater Alga and Cyanobacteria, Growth Inhibition Test, OECD Guidelines for the Testing of Chemicals, Section 2*. Paris: OECD Publishing, doi: 10.1787/9789264069923-en

Oren, A. (2005). A hundred years of dunaliella research: 1905-2005. *Saline Syst.* 1:2. doi: 10.1186/1746-1448-1-2

Ortega-Morales, B. O., Santiago-García, J. L., Chan-Bacab, M. J., Moppert, X., Miranda-Tello, E., Fardeau, M. L., et al. (2007). Characterization of extracellular polymers synthesized by tropical intertidal biofilm bacteria. *J. Appl. Microbiol.* 102, 254–264. doi: 10.1111/j.1365-2672.2006.03085.x

Passow, U. (2002). Transparent exopolymer particles (TEP) in aquatic environments. *Prog. Oceanogr.* 55, 287–333. doi: 10.1016/S0079-6611(02)00138-6

Paterson, G., Ataria, J. M., Hoque, E., and Metcalfe, C. D. (2011). The toxicity of titanium dioxide nanopowder to early life stages of the Japanese medaka (*Oryzias latipes*). *Chemosphere* 82, 1002–1009. doi: 10.1016/j.chemosphere.2010.10.068

Pellegrino, F., Pellutiè, L., Sordello, F., Minero, C., Ortel, H., Hodoroaba, V., et al. (2017). Influence of agglomeration and aggregation on the photocatalytic activity of TiO2 nanoparticles. *Appl. Catal. B Environ.* 216, 80–87. doi: 10.1016/j.apcatb.2017.05.046

Petersen, E. J., Diamond, S. A., Kennedy, A. J., Goss, G. G., Lead, J., Hanna, S. K., et al. (2015). Adapting OECD aquatic toxicity tests for use with manufactured nanomaterials: key issues and consensus recommendations. *Environ. Sci. Technol.* 49, 9532–9547. doi: 10.1021/acs.est.5b00997

Petosa, A. R., Jaisi, D. P., Quevedo, I. R., Elimelech, M., and Tufenkji, N. (2010). Aggregation and deposition of engineered nanomaterials in aquatic environments: role of physicochemical interactions. *Environ. Sci. Technol.* 44, 6532–6549. doi: 10.1021/es100598h

Piella, J., Bastús, N. G., and Puntes, V. (2017). Size-dependent protein-nanoparticle interactions in citrate-stabilized gold nanoparticles: the emergence of the protein corona. *Bioconjug. Chem.* 28, 88–97. doi: 10.1021/acs.bioconjchem.6b00575

Pinsino, A., Bergami, E., Della Torre, C., Vannuccini, M. L., Addis, P., Secci, M., et al. (2017). Amino-modified polystyrene nanoparticles affect signalling pathways of the sea urchin (*Paracentrotus lividus*) embryos. *Nanotoxicology* 11:360. doi: 10.1080/17435390.2017.1279360

Pinsino, A., and Matranga, V. (2015). Sea urchin immune cells as sentinels of environmental stress. *Dev. Comp. Immunol.* 49, 198–205. doi: 10.1016/j.dci.2014.11.013

Pinsino, A., Russo, R., Bonaventura, R., Brunelli, A., Marcomini, A., and Matranga, V. (2015). Titanium dioxide nanoparticles stimulate sea urchin immune cell phagocytic activity involving signalling pathway. *Sci. Rep.* 5, 1–12. doi: 10.1038/srep14492

Praetorius, A., Badetti, E., Brunelli, A., Clavier, A., Gallego-Urrea, J. A., Gondikas, A., et al. (2020). Strategies for determining heteroaggregation attachment efficiencies of engineered nanoparticles in aquatic environments. *Environ. Sci. Nano.* 7, 351–367. doi: 10.1039/c9en01016e

Praetorius, A., Labille, J., Scheringer, M., Thill, A., Hungerbuhler, K., and Bottero, J. Y. (2014). Heteroaggregation of titanium dioxide nanoparticles with model natural colloids under environmentally relevant conditions. *Environ. Sci. Technol.* 48, 10690–10698. doi: 10.1021/es501655v

Ren, C., Hu, X., and Zhou, Q. (2016). Influence of environmental factors on nanotoxicity and knowledge gaps thereof. *Nanoimpact* 2, 82–92. doi: 10.1016/j.impact.2016.07.002

Renner, G., Schmidt, T. C., and Schram, J. (2018). Analytical methodologies for monitoring micro(nano)plastics: which are fit for purposes? *Curr. Opin. Environ. Sci. Health* 1, 55–61. doi: 10.1016/j.coesh.2017.11.001

Ribeiro, A. R., Leite, P. E., Falagan-Lotsch, P., Benetti, F., Micheletti, C., Budtz, H. C., et al. (2017). Challenges on the toxicological predictions of engineered nanoparticles. *Nanoimpact* 8, 59–72. doi: 10.1016/j.impact.2017.07.006

Ritz, S., Schöttler, S., Kotman, N., Baier, G., Musyanovych, A., Kuharev, J., et al. (2015). Protein corona of nanoparticles: distinct proteins regulate the cellular uptake. *Biomacromolecules* 16, 1311–1321. doi: 10.1021/acs.biomac.5b00108

Robichaud, C. O., Uyar, A. E., Darby, M. R., Zucker, L. G., and Wiesner, M. R. (2009). Estimates of upper bounds and trends in nano-TiO2 production as

a basis for exposure assessment. *Environ. Sci. Technol.* 43, 4227–4233. doi: 10.1021/es8032549

Rocco, L., Santonastasio, M., Nigro, M., Mottola, F., Costagliela, D., Bernardeschi, M., et al. (2015). Genomic and chromosomal damage in the marine mussel *Mytilus galloprovincialis*: effects of the combined exposure titanium dioxide nanoparticles and cadmium chloride. *Mar. Environ. Res.* 111, 144–148. doi: 10.1016/j.marenvres.2015.09.004

Romanello, M. B., and Fidalgo de Cortalezzi, M. M. (2013). An experimental study on the aggregation of TiO2 nanoparticles under environmentally relevant conditions. *Water Res.* 47, 3887–3898. doi: 10.1016/j.watres.2012.11.061

Salvati, A., Åberg, C., dos Santos, T., Varela, J., Pinto, P., Lynch, I., et al. (2011). Experimental and theoretical comparison of intracellular import of polymeric nanoparticles and small molecules: toward models of uptake kinetics. *Nanomed. Nanotechnol. Biol. Med.* 7, 818–826. doi: 10.1016/j.nano.2011.03.005

Sayes, C. M., Wahi, R., Kurian, P. A., Liu, Y., West, J. L., Ausman, K. D., et al. (2006). Correlating nanoscale titania structure with toxicity: a cytotoxicity and inflammatory response study with human dermal fibroblasts and human lung epithelial cells. *Toxicol. Sci.* 92, 174–185. doi: 10.1093/toxsci/kfj197

Schirinzi, G. F., Llorca, M., Seró, R., Moyano, E., Barceló, D., Abad, E., et al. (2019). Trace analysis of polystyrene microplastics in natural waters. *Chemosphere* 236:52. doi: 10.1016/j.chemosphere.2019.07.052

Schwaferts, C., Niessner, R., Elsner, M., and Ivleva, N. P. (2019). Methods for the analysis of submicrometer- and nanoplastic particles in the environment. *Trend Anal. Chem.* 112, 52–65. doi: 10.1016/j.trac.2018.12.014

Sendra, M., Moreno-Garrido, I., Yeste, M. P., Gatica, J. M., and Blasco, J. (2017a). Toxicity of TiO2, in nanoparticle or bulk form to freshwater and marine microalgae under visible light and UV-A radiation. *Environ. Pollut.* 227, 39–48. doi: 10.1016/j.envpol.2017.04.053

Sendra, M., Sánchez-Quiles, D., Blasco, J., Moreno-Garrido, I., Lubián, L. M., Pérez-García, S., et al. (2017b). Effects of TiO2 nanoparticles and sunscreens on coastal marine microalgae: ultraviolet radiation is key variable for toxicity assessment. *Environ. Int.* 98, 62–68. doi: 10.1016/j.envint.2016.09.024

Sendra, M., Saco, A., Yeste, M. P., Romero, A., Novoa, B., and Figueras, A. (2019a). Nanoplastics: from tissue accumulation to cell translocation into *Mytilus galloprovincialis* hemocytes. resilience of immune cells exposed to nanoplastics and nanoplastics plus *Vibrio splendidus* combination. *J. Hazard. Mater.* 388:121788. doi: 10.1016/j.jhazmat.2019.121788

Sendra, M., Staf, E., Pilar, M., and Moreno-garrido, I. (2019b). Are the primary characteristics of polystyrene nanoplastics responsible for toxicity and ad / absorption in the marine diatom *Phaeodactylum tricornutum? Trend Anal. Chem.* 249, 610–619. doi: 10.1016/j.envpol.2019.03.047

Sendra, M., Volland, M., Balbi, T., Fabbri, R., Yeste, M. P., Gatica, J. M., et al. (2018). Cytotoxicity of CeO2 nanoparticles using in vitro assay with *Mytilus galloprovincialis* hemocytes: relevance of zeta potential, shape and biocorona formation. *Aquat. Toxicol.* 200, 13–20. doi: 10.1016/j.aquatox.2018.04.011

Seoane, M., González-Fernández, C., Soudant, P., Huvet, A., Esperanza, M., Cid, A., et al. (2019). Polystyrene microbeads modulate the energy metabolism of the marine diatom *Chaetoceros neogracile*. *Environ. Pollut.* 251, 363–371. doi: 10.1016/j.envpol.2019.04.142

Shang, L., and Nienhaus, G. U. (2017). In situ characterization of protein adsorption onto nanoparticles by fluorescence correlation spectroscopy. *Acc. Chem. Res.* 50, 387–395. doi: 10.1021/acs.accounts.6b00579

Shi, W., Han, Y., Guo, C., Su, W., Zhao, X., Zha, S., et al. (2019). Ocean acidification increases the accumulation of titanium dioxide nanoparticles (nTiO 2) in edible bivalve mollusks and poses a potential threat to seafood safety. *Sci. Rep.* 9, 1–10. doi: 10.1038/s41598-019-40047-1

Shi, W., Han, Y., Guo, C., Zhao, X., Liu, S., Su, W., et al. (2017). Immunotoxicity of nanoparticle nTiO2 to a commercial marine bivalve species, *Tegillarca granosa*. *Fish. Shellf. Immun.* 66, 300–306. doi: 10.1016/j.fsi.2017.05.036

Shiu, R.-F., Vazquez, C. I., Tsai, Y.-Y., Torres, G. V., Chen, C.-S., Santschi, P. H., et al. (2019). Nano-plastics induce aquatic particulate organic matter (microgels) formation. *Sci. Total Environ.* 706:135681. doi: 10.1016/j.scitotenv.2019.135681

Sillanpää, M., Paunu, T.-M., and Sainio, P. (2011). Aggregation and deposition of engineered TiO2 nanoparticles in natural fresh and brackish waters. *J. Phys. Conf. Ser.* 304, 1–8. doi: 10.1088/1742-6596/304/1/012018

Silvestre, C., Duraccio, D., and Cimmino, S. (2011). Food packaging based on polymer nanomaterials. *Prog. Polym. Sci.* 36, 1766–1782. doi: 10.1016/j.progpolymsci.2011.02.003

Singh, N., Tiwari, E., Khandelwal, N., and Darbha, G. K. (2019). Understanding the stability of nanoplastics in aqueous environments: effect of ionic strength, temperature, dissolved organic matter, clay, and heavy metals. *Environ. Sci. Nano* 6, 2968–2976. doi: 10.1039/c9en00557a

Sjollema, S. B., Redondo-hasselerharm, P., Leslie, H. A., Kraak, M. H. S., and Vethaak, A. D. (2016). Do plastic particles affect microalgal photosynthesis and growth? *Aquat. Toxicol.* 170, 259–261. doi: 10.1016/j.aquatox.2015.12.002

Snell, T. W., and Hicks, D. G. (2009). Assessing toxicity of nanoparticles using *Brachionus manjavacas* (Rotifera). *Environ. Toxicol.* 26, 146–152. doi: 10.1002/tox

Sun, J., Guo, L., Zhang, H., and Zhao, L. (2014). UV irradiation induced transformation of TiO2 nanoparticles in water: aggregation and photoreactivity. *Environ. Sci. Technol.* 48, 11962–11968. doi: 10.1021/es502360c

Sun, T. Y., Bornhöft, N. A., Hungerbühler, K., and Nowack, B. (2016). Dynamic probabilistic modeling of environmental emissions of engineered nanomaterials. *Environ. Sci. Technol.* 50, 4701–4711. doi: 10.1021/acs.est.5b05828

Sun, T. Y., Gottschalk, F., Hungerbuhler, K., and Nowack, B. (2014). Comprehensive probabilistic modelling of environmental emissions of engineered nanomaterials. *Environ. Pollut.* 185, 69–76. doi: 10.1016/j.envpol.2013.10.004

Surette, M. C., and Nason, J. A. (2016). Effects of surface coating character and interactions with natural organic matter on the colloidal stability of gold nanoparticles. *Environ. Sci. Nano* 3, 1144–1152. doi: 10.1039/C6EN00180G

Surette, M. C., and Nason, J. A. (2019). Nanoparticle aggregation in a freshwater river: the role of engineered surface coatings. *Environ. Sci. Nano* 6, 540–553. doi: 10.1039/C8EN01021H

Tallec, K., Huvet, A., Di, C., Gonz, C., Lambert, C., Petton, B., et al. (2018). Nanoplastics impaired oyster free living stages, gametes and embryos. *Environ. Pollut.* 242, 1226–1235. doi: 10.1016/j.envpol.2018.08.020

Tenzer, S., Docter, D., Kuharev, J., Musyanovych, A., Fetz, V., Hecht, R., et al. (2013). Rapid formation of plasma protein corona critically affects nanoparticle pathophysiology. *Nat. Nanotechnol.* 8, 772–781. doi: 10.1038/nnano.2013.181

Tenzer, S., Docter, D., Rosfa, S., Wlodarski, A., Kuharev, J., Rekik, A., et al. (2011). Nanoparticle size is a critical physicochemical determinant of the human blood plasma corona: a comprehensive quantitative proteomic analysis. *ACS Nano* 5, 7155–7167. doi: 10.1021/nn201950e

Ter Halle, A., Jeanneau, L., Martignac, M., Jardé, E., Pedrono, B., Brach, L., et al. (2017). Nanoplastic in the North Atlantic subtropical gyre. *Environ. Sci. Technol.* 51, 13689–13697. doi: 10.1021/acs.est.7b03667

Therezien, M., Thill, A., and Wiesner, M. R. (2014). Importance of heterogeneous aggregation for NP fate in natural and engineered systems. *Sci. Total. Environ.* 48, 309–318. doi: 10.1016/j.scitotenv.2014.03.020

Tian, S., Zhang, Y., Song, C., Zhu, X., and Xing, B. (2014). Titanium dioxide nanoparticles as carrier facilitate bioaccumulation of phenanthrene in marine bivalve, ark shell (*Scapharca subcrenata*). *Environ. Pollut.* 192, 59–64. doi: 10.1016/j.envpol.2014.05.010

Tian, S., Zhang, Y., Song, C., Zhu, X., and Xing, B. (2015). Bioaccumulation and biotransformation of polybrominated diphenyl ethers in the marine bivalve (*Scapharca subcrenata*): influence of titanium dioxide nanoparticles. *Mar. Poll. Bull.* 90, 48–53. doi: 10.1016/j.marpolbul.2014.11.031

Tovar-Sánchez, A., Sánchez-Quiles, D., Basterretxea, G., Benedé, J. L., Chisvert, A., Salvador, A., et al. (2013). Sunscreen products as emerging pollutants to coastal waters. *PLoS One* 8:e65451. doi: 10.1371/journal.pone

Uchino, T., Tokunaga, H., Ando, M., and Utsumi, H. (2002). Quantitative determination of OH radical generation and its cytotoxicity induced by TiO2-UVA treatment. *Toxicol. In Vitro* 16, 629–635. doi: 10.1016/s0887-2333(02)00041-3

Vance, M. E., Kuiken, T., Vejerano, E. P., McGinnis, S. P., and Hochella, M. F. (2015). Nanotechnology in the real world: redeveloping the nanomaterial

consumer products inventory. *Beilstein J. Nanotechnol.* 6, 1769–1780. doi: 10.3762/bjnano.6.181

Vannuccini, M. L., Grassi, G., Leaver, M. J., and Corsi, I. (2015). Combination effects of nano-TiO2 and 2,3,7,8-tetrachlorodibenzo-*p*-dioxin (TCDD) on biotransformation gene expression in the liver of European sea bass *Dicentrarchus labrax*. *Comp. Biochem. Physiol. Part C* 17, 71–78. doi: 10.1016/j.cbpc.2015.07.009

Varó, I., Perini, A., Torreblanca, A., Garcia, Y., Bergami, E., Vannuccini, M. L., et al. (2019). Time-dependent effects of polystyrene nanoparticles in brine shrimp *Artemia franciscana* at physiological, biochemical and molecular levels. *Sci. Total Environ.* 675:157. doi: 10.1016/j.scitotenv.2019.04.157

Velev, O. D., and Kaler, E. W. (1999). In situ assembly of colloidal particles into miniaturized biosensors. *Langmuir* 15, 3693–3698. doi: 10.1021/la981729c

Venâncio, C., Ferreira, I., Martins, M. A., Soares, A. M. V. M., Lopes, I., and Oliveira, M. (2019). The effects of nanoplastics on marine plankton: a case study with polymethylmethacrylate. *Ecotoxicol. Environ. Saf.* 184:109632. doi: 10.1016/j.ecoenv.2019.109632

Verdugo, P., Alldredge, A. L., Azam, F., Kirchman, D. L., Passow, U., and Santschi, P. H. (2004). The oceanic gel phase: a bridge in the DOM-POM continuum. *Mar. Chem.* 92, 67–85. doi: 10.1016/j.marchem.2004.06.017

Verma, A., and Stellacci, F. (2010). Effect of surface properties on nanoparticle-cell interactions. *Small* 6, 12–21. doi: 10.1002/smll.200901158

Vignardi, C. P., Hasue, F. M., Sartório, P. V., Cardoso, C. M., and Machado, A. S. (2015). Genotoxicity, potential cytotoxicity and cell uptake of titanium dioxide nanoparticles in the marine fish *Trachinotus carolinus* (Linnaeus, 1766). *Aquat. Toxicol.* 158, 218–229. doi: 10.1016/j.aquatox.2014.11.008

von der Kammer, F., Ferguson, P. L., Holden, P. A., Masion, A., Rogers, K. R., Klaine, S. J., et al. (2012). Analysis of engineered nanomaterials in complex matrices (environment and biota): general considerations and conceptual case studies. *Environ. Toxicol. Chem.* 31, 32–49. doi: 10.1002/etc.723

Vroman, L. (1962). Effect of adsorbed proteins on the wettability of hydrophilic and hydrophobic solids. *Nature* 196, 476–477. doi: 10.1038/196476a0

Walkey, C. D., Olsen, J. B., Guo, H., Emili, A., and Chan, W. C. W. (2012). Nanoparticle size and surface chemistry determine serum protein adsorption and macrophage uptake. *J. Am. Chem. Soc.* 134, 2139–2147. doi: 10.1021/ja2084338

Walsh, R. B., Nelson, A., Skinner, W. M., Parsons, D., and Craig, V. S. J. (2012). Direct measurement of Van der Waals and diffuse double-layer forces between titanium dioxide surfaces produced by atomic layer deposition. *J. Phys. Chem. C* 116, 7838–7847. doi: 10.1021/jp300533m

Wan, S., Kelly, P. M., Mahon, E., Stöckmann, H., Rudd, P. M., Caruso, F., et al. (2015). The "sweet" Side of the protein corona: effects of glycosylation on nanoparticle-cell interactions. *ACS Nano* 9, 2157–2166. doi: 10.1021/nn506060q

Wang, F., Bexiga, M. G., Anguissola, S., Boya, P., Simpson, J. C., Salvati, A., et al. (2013). Time resolved study of cell death mechanisms induced by amine-modified polystyrene nanoparticles. *Nanoscale* 5, 10868–10876. doi: 10.1039/c3nr03249c

Wang, Y., Hu, M., Li, Q., Li, J., Lin, D., and Lu, W. (2014). Immune toxicity of TiO_2 under hypoxia in the green-lipped mussel *Perna viridis* based on flow cytometric analysis of hemocyte parameters. *Sci. Total Environ.* 47, 791–799. doi: 10.1016/j.scitotenv.2013.09.060

Wang, Y., Zhu, X., Lao, Y., Lv, X., Tao, Y., Huang, B., et al. (2016). TiO2 nanoparticles in the marine environment: physical effects responsible for the toxicity on algae *Phaeodactylum tricornutum*. *Sci. Total Environ.* 565, 818–826. doi: 10.1016/j.scitotenv.2016.03.164

Wang, Z., Xia, B., Chen, B., Sun, X., Zhu, L., Zhao, J., et al. (2017). Trophic transfer of TiO2 nanoparticles from marine microalga (*Nitzschia closterium*) to scallop (*Chlamys farreri*) and related toxicity. *Environ. Sci. Nano* 4, 415–424. doi: 10.1039/C6EN00365F

Ward, J. E., and Kach, D. J. (2009). Marine aggregates facilitate ingestion of nanoparticles by suspension feeding bivalves. *Mar. Environ. Res.* 68, 137–142. doi: 10.1016/j.marenvres.2009.05.002

Wegner, A., Besseling, E., Foekema, E. M., Kamermans, P., and Koelmans, A. A. (2012). Effects of nanopolystyrene on the feeding behavior of the blue mussel (*Mytilus edulis* L.). *Environ. Toxicol. Chem.* 31, 2490–2497. doi: 10.1002/etc.1984

Wilkinson, K. J., and Lead, J. R. (2007). *Environmental Colloids and Particles: Behaviour, Separation and Characterisation*. Hoboken, NJ: John Wiley & Sons.

Windler, L., Lorenz, C., von Goetz, N., Hungerbuhler, K., Amberg, M., Heuberger, M., et al. (2012). Release of titanium dioxide from textiles during washing. *Environ. Sci. Technol.* 46, 8181–8188. doi: 10.1021/es301633b

Winzen, S., Schoettler, S., Baier, G., Rosenauer, C., Mailaender, V., Landfester, K., et al. (2015). Complementary analysis of the hard and soft protein corona: sample preparation critically effects corona composition. *Nanoscale* 7, 2992–3001. doi: 10.1039/C4NR05982D

Wu, J., Jiang, R., Lin, W., and Ouyang, G. (2019). Effect of salinity and humic acid on the aggregation and toxicity of polystyrene nanoplastics with different functional groups and charges. *Environ. Pollut.* 245, 836–843. doi: 10.1016/j.envpol.2018.11.055

Wu, W., Giese, R. F., and Van Oss, C. J. (1999). Stability versus flocculation of particle suspensions in water-correlation with the extended DLVO approach for aqueous systems, compared with classical DLVO theory. *Coll. Surf. B* 14, 47–55. doi: 10.1016/S0927-7765(99)00023-5

Xia, B., Chen, B., Sun, X., Qu, K., Ma, F., and Du, M. (2015). Interaction of TiO2 nanoparticles with the marine microalga *Nitzschia closterium*: growth inhibition, oxidative stress and internalization. *Sci. Total Environ.* 508, 525–533. doi: 10.1016/j.scitotenv.2014.11.066

Yi, X., Wang, J., Li, Z., Zhang, Z., Chi, T., Guo, M., et al. (2019). The effect of polystyrene plastics on the toxicity of triphenyltin to the marine diatom *Skeletonema costatum* — influence of plastic particle size. *Environ. Sci. Pollut. Res. Int.* 26, 25445–25451. doi: 10.1007/s11356-019-05826-3

Yin, L., Liu, H., Cui, H., Chen, B., Li, L., and Wu, F. (2019). Impacts of polystyrene microplastics on the behavior and metabolism in a marine demersal teleost, black rockfish (*Sebastes schlegelii*). *J. Hazard. Mater.* 380:120861. doi: 10.1016/j.jhazmat.2019.120861

Yue, Y., Behra, R., Sigg, L., Fernández Freire, P., Pillai, S., and Schirmer, K. (2015). Toxicity of silver nanoparticles to a fish gill cell line: role of medium composition. *Nanotoxicology* 9, 54–63. doi: 10.3109/17435390.2014.889236

Yue, Y., Behra, R., Sigg, L., and Schirmer, K. (2016a). Silver nanoparticles inhibit fish gill cell proliferation in protein-free culture medium. *Nanotoxicology* 10, 1075–1083. doi: 10.3109/17435390.2016.1172677

Yue, Y., Behra, R., Sigg, L., Suter, M. J.-F., Pillai, S., and Schirmer, K. (2016b). Silver nanoparticle–protein interactions in intact rainbow trout gill cells. *Environ. Sci. Nano* 3, 1174–1185. doi: 10.1039/C6EN00119J

Zhang, H., Kuo, Y. Y., Gerecke, A. C., and Wang, J. (2012). Co-release of hexabromocyclododecane (HBCD) and nano- and microparticles from thermal cutting of polystyrene foams. *Environ. Sci. Technol.* 46, 10990–10996. doi: 10.1021/es302559v

Zhu, L., Zhao, S., Bittar, T. B., and Stubbins, A. (2020). Photochemical dissolution of buoyant microplastics to dissolved organic carbon: rates and microbial impacts. *J. Hazard. Mater.* 383:121065. doi: 10.1016/j.jhazmat.2019.121065

Zhu, X., Zhou, J., and Cai, Z. (2011). TiO2 nanoparticles in the marine environment: impact on the toxicity of tributyltin to abalone (*Haliotis diversicolor supertexta*) embryos. *Environ. Sci. Technol.* 45, 3753–3758. doi: 10.1021/es103779h

Conflict of Interest: The authors declare that the research was conducted in the absence of any commercial or financial relationships that could be construed as a potential conflict of interest.

frontiers in Environmental Science

ORIGINAL RESEARCH
published: 16 June 2020
doi: 10.3389/fenvs.2020.00076

Anthropogenic Release and Distribution of Titanium Dioxide Particles in a River Downstream of a Nanomaterial Manufacturer Industrial Site

*Danielle L. Slomberg[1], Mélanie Auffan[1,2], Nelly Guéniche[1], Bernard Angeletti[1], Andrea Campos[3], Daniel Borschneck[1], Olivier Aguerre-Chariol[4] and Jérôme Rose[1,2]**

[1] CNRS, Aix-Marseille Univ., IRD, INRAE, Coll France, CEREGE, Aix-en-Provence, France, [2] Civil and Environmental Engineering Department, Duke University, Durham, NC, United States, [3] Aix-Marseille Univ., CNRS, Centrale Marseille, FSCM (FR1739), Marseille, France, [4] INERIS, Verneuil-en-Halatte, France

OPEN ACCESS

Edited by:
Denise M. Mitrano,
Swiss Federal Institute of Aquatic Science and Technology, Switzerland

Reviewed by:
Kevin Wilkinson,
Université de Montréal, Canada
Mohammed Baalousha,
University of South Carolina, United States

***Correspondence:**
Jérôme Rose
rose@cerege.fr

Specialty section:
This article was submitted to Biogeochemical Dynamics, a section of the journal Frontiers in Environmental Science

Received: 31 March 2020
Accepted: 18 May 2020
Published: 16 June 2020

Citation:
Slomberg DL, Auffan M, Guéniche N, Angeletti B, Campos A, Borschneck D, Aguerre-Chariol O and Rose J (2020) Anthropogenic Release and Distribution of Titanium Dioxide Particles in a River Downstream of a Nanomaterial Manufacturer Industrial Site. Front. Environ. Sci. 8:76. doi: 10.3389/fenvs.2020.00076

Several industries manufacture and process large quantities of engineered nanomaterials, thus increasing the potential for their environmental release during waste management and disposal. Herein, we quantified the release and spatial distribution of titanium dioxide nanomaterials (TiO_2 NMs) emitted from an industrial waste stream that flows into a nearby river. Two sampling campaigns were carried out on the river in fall 2017 and spring 2018 at selected sites upstream and downstream of the Industrial Effluent and an urban wastewater treatment plant (WWTP). Significant Ti accumulation was detected in the sediments at the Industrial Effluent and WWTP sites for both fall and spring samples, with measured Ti concentrations of 75–193 mg Ti/kg reaching 21–55× that of the local background upstream. X-ray diffraction analysis confirmed the anatase and rutile mineralogy of the inputs. River surface waters were filtered on-site to distinguish between particulate (>0.20 μm), colloidal (0.02–0.20 μm), and dissolved and/or small nanoparticulate (NP) (<0.02 μm) TiO_2. Up to 133 and 260 μg Ti/L were measured in the unfiltered waters for the Industrial Effluent and WWTP fall samples, respectively, while the spring samples exhibited Ti concentrations similar to the background concentration. Combining chemical analysis and scanning electron microscopy revealed that some Ti particles recovered from the Industrial Effluent and WWTP were clusters of TiO_2 NMs (~50 nm). Furthermore, anthropogenic TiO_2 was distinguished apart from natural Ti-containing minerals by comparing the concentration ratios between Ti and other naturally occurring elements (e.g., V, Al, and Fe). This study confirmed the release of manufactured TiO_2 NMs from the Industrial Effluent and the WWTP into the river, finding that almost all of the TiO_2 NMs are released in the particulate fraction (>0.20 μm), and that the particles sediment rapidly near the emission source and accumulate in the sediment.

Keywords: manufactured TiO_2 nanomaterials, anthropogenic emission, river ecosystem, environmental exposure, aggregation, sediment accumulation

INTRODUCTION

As advances in nanotechnology research and development continue, engineered nanomaterials are being increasingly manufactured for incorporation into consumer products destined for cosmetic, textile, coating, and plastic applications (Piccinno et al., 2012; Vance et al., 2015). Several recent studies have considered the environmental impacts of nanomaterials released from these consumer products during their use phase and end-of-life (Botta et al., 2011; Nowack et al., 2012; Mitrano et al., 2015; Auffan et al., 2018; Scifo et al., 2018), but another important consideration is the possible release and local environmental accumulation near nanomaterial manufacturing sites, especially those close to aquatic ecosystems such as rivers and lakes. Upon incidental or direct release into these natural systems, nanomaterial fate, and transport are governed by the water chemistry, particle aggregation state, and any transformation processes (e.g., dissolution, photochemical alteration, oxidation and reduction) (Nowack et al., 2012).

In the case of titanium dioxide nanomaterials (TiO_2 NMs), the second most-produced nanomaterial worldwide (Sun et al., 2014), previous research has already focused on evaluating their fate and behavior in model river waters, with the aim of determining their potential risk. Indeed, the aggregation and sedimentation of two of the most common TiO_2 NM forms, anatase and rutile, have been shown to depend on particle morphology, the point of zero charge, and water conditions (Liu et al., 2011; Ilina et al., 2017). Besides the physico-chemical characteristics of the TiO_2 NMs themselves and the pH of the aqueous environment, the presence of dissolved ions, suspended particulate matter (SPM), and natural organic matter (NOM) can also significantly influence NM stability through processes such as aggregation and sedimentation or dispersion and transport (Loosli et al., 2013; Labille et al., 2015; Slomberg et al., 2019). For example, increased ionic strength and divalent cation concentrations have been shown to facilitate TiO_2 NM homo-aggregate formation (Loosli et al., 2013; Ilina et al., 2017). However, in natural aqueous environments where SPM and NOM concentrations (mg/L) are likely much higher than the predicted TiO_2 NM concentration (μg/L), hetero-aggregation is expected to be the more dominant interaction driving NM fate and behavior (Labille et al., 2015). As such, Adam et al. evaluated both TiO_2 NM homo-aggregation and hetero-aggregation interactions with illite clay and Suwannee River fulvic acid (SRFA) in filtered river water (pH 8) sampled nearby the TiO_2 NM manufacturing site (Adam et al., 2016). In lower salinity conditions (0.25 mM Ca^{2+}) the 5 nm TiO_2 particles (40 mg/L) formed homo-aggregates (∼ 550 nm). The addition of SRFA (5–10 mg/L) slightly enhanced TiO_2 NM dispersion and decreased the overall TiO_2 aggregate size, and in the presence of illite (25 mg/L) no secondary hetero-aggregation was observed. Yet, when the river water Ca^{2+} concentration was increased to 3 mM, the decrease in TiO_2 NM homo-aggregate size was no longer observed in the presence of SRFA and the addition of illite resulted in hetero-aggregation, thus favoring NM sedimentation.

Multimedia environmental fate models have also been developed to investigate NM fate and transport in rivers as a complement to experimental approaches. Any NM inputs into river surface waters should be detected almost instantaneously, although their lifetime in the water column may be transient due to aggregation processes and changes in hydrological conditions. For NMs that are not stable in the water column, the riverbed sediment can act as a sink where the NMs will deposit and potentially accumulate as long as the NM emission continues. For example, river box models incorporating fixed or varied water conditions in time and space have examined TiO_2 NM fate in surface waters and sediment for two large European rivers, the Rhine, and the Rhone (Praetorius et al., 2012; Sani-Kast et al., 2015). In both cases, for a constant, point source TiO_2 NM emission of 0.39–1.5 kg/day, predicted TiO_2 NM concentrations were in the ng/L range for the water compartment and mg/kg in the sediment. TiO_2 NM fate was dependent on the water conditions near the emission source, with significant aggregation, sedimentation, and accumulation in the sediment layer occurring within a few km of NM release. However, these models also predicted that a fraction of TiO_2 NMs can remain stable in the water column, being transported up to ∼100 km from the source depending on river conditions.

While laboratory studies with simulated aquatic systems and the development of environmental fate models have allowed researchers to gain insight into TiO_2 NM transport, behavior, and fate, field studies to determine NM release and accumulation in real aqueous environments are still lacking. This is in part due to the fact that detecting and quantifying low concentrations of anthropogenic TiO_2 NMs apart from the natural background is analytically challenging. Recent approaches include a combination of size fractionation (e.g., filtration, field-flow fractionation) followed by identification and quantification using elemental analysis (i.e., inductively coupled plasma–mass spectrometry, ICP-MS) and electron microscopy coupled with X-ray energy dispersive spectroscopy (EDS) detection (Von der Kammer et al., 2011, 2012; Westerhoff et al., 2011; Labille et al., 2019). For example, three different sampling campaigns that analyzed filtered waters (<0.45 μm) near a wastewater treatment plant (WWTP) confirmed TiO_2 NM presence with electron microscopy and reported Ti values between 0.7 and 3 μg/L (Johnson et al., 2011; de Klein et al., 2016; Markus et al., 2018). Single particle (SP)-ICP-MS was utilized to target and detect smaller TiO_2 particles down to 100 nm in river surface waters without the need for filtration (Peters et al., 2018), and Hadioui et al. (2019) have now detected TiO_2 particle sizes down to 19.2 nm with the technique. While progress has been made in detecting low concentrations of TiO_2 NMs (μg/L) in complex environmental matrices, these analyses alone cannot confirm that the particles are anthropogenic. As such, the determination of elemental ratios between Ti and other naturally occurring elements such as V, Al, and Fe, or rare earth elements (Ga, Y, Nb, Eu, Ho, Er, Tm, Yb, Ta) has been employed to distinguish natural Ti-containing particles from the anthropogenic load in aquatic systems as well as soils (Gondikas et al., 2017; Reed et al., 2017; Labille et al., 2019; Baalousha et al., 2020; Wang et al., 2020). Building upon this approach, multi-element (ME)-SP-ICP-MS has been used to perform multi-element analysis of individual TiO_2 particles in

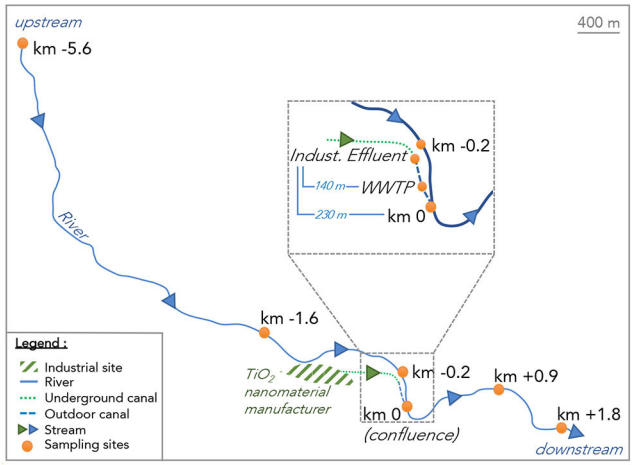

FIGURE 1 | Map of river sampling sites near TiO_2 nanomaterial manufacturing plant, with distances along the river given relative to the confluence of the industrial drainage canal and the river at km 0.

natural surface waters (Gondikas et al., 2018; Loosli et al., 2019). By identifying multi-element signatures of natural Ti-containing particles, anthropogenic TiO_2 NMs can be further distinguished apart from the natural background and quantified. Overall, these studies have demonstrated that TiO_2 NMs can be quantified in natural surface waters, while also providing insight as to their release from WWTPs or other anthropogenic sources. This knowledge is crucial for evaluating TiO_2 NM risk to aquatic ecosystems, yet a comprehensive assessment can only be obtained by also considering TiO_2 NM transport and accumulation in the sediment compartment in future field studies.

The present work reports the first quantification of TiO_2 NMs in a river next to a nanomaterial manufacturing plant, both upstream and downstream of the potential emission source (i.e., industrial drainage canal). Surface waters, sediments, and epilithic organisms were collected along the river and industrial drainage canal at two different time periods (October 2017 and March 2018) to assess any short-term, pulse occurrence vs. long-term accumulation in the different environmental compartments. In addition to TiO_2 quantification, anatase and rutile inputs into the river were distinguished from the local background using mineralogical analysis. Several elements (X = V, Al, and Fe) naturally co-occurring with Ti in suspended mineral particles were also quantified to determine Ti/X elemental ratios. Higher elemental ratios compared to the natural background were used as an indication of Ti of anthropogenic origin. By sampling the water and sediment compartments at multiple sites along the river, TiO_2 NM transport and fate were determined in a real release scenario.

MATERIALS AND METHODS

Sampling Campaigns

The samples were taken along a 7.4 km long transect in a watershed of about 160 km^2 at two different time periods, on October 18th, 2017 and March 22nd, 2018. For these dates, outflows of 0.98 ± 0.01 $m^3.s^{-1}$ and 4.89 ± 0.01 $m^3.s^{-1}$ were respectively measured in the river at a hydrology station located ∼7 km upstream from the confluence (http://hydro.eaufrance.fr/). The river is characterized by an average annual pH of 7.6–8.1, dissolved organic carbon (DOC) concentration of 1.8–2.3 mg/L, and total suspended sediment (TSS) concentration of ∼5 mg/L (Hissler and Probst, 2006; Adam et al., 2016). Eight sampling stations were selected: 6 along the river, upstream and downstream of the TiO_2 nanomaterial manufacturing site, and 2 along the drainage canal where treated industrial and urban effluents join the river (**Figure 1**). The confluence between the drainage canal and the river was referred to as km 0. The 6 sampling stations along the river were located at 5.6 km (km −5.6), 1.6 km (km −1.6), and 0.2 km (km −0.2) upstream of the confluence (km 0) as well as 0.9 km (km +0.9) and 1.8 km (km +1.8) downstream of the confluence. The effluents from the TiO_2 NM manufacturing site first flow through an underground canal (not accessible) for a distance of ∼1 km before the outdoor section of the drainage canal begins. The 2 sampling stations along this outdoor drainage canal were located at the beginning of the outdoor discharge of the manufacturing site's treated effluent (230 m upstream of the confluence, station called "Industrial Effluent") and at the outflow of the urban waste water treatment plant's (WWTP) treated effluent that also flows into the surface of the water column in the drainage canal (90 m upstream of the confluence, station called "WWTP"). No natural water sources are located along this drainage canal and it is surrounded by steep embankments. The distance between the drainage canal and the river at the Industrial Effluent sampling station is ∼35 m. The water depth was ∼20 cm in both the drainage canal and river in October 2017 and March 2018.

On-Site Water and Sediment Collection

Water samples were collected manually in the center of the riverbed. As soon as water samples are collected, the particle size distribution can change rapidly. It was therefore decided to filter on-site to avoid any modification of the size distribution. Water samples were filtered on-site using both 0.20 and 0.02 µm inorganic membrane syringe filters [Anodisc (Al_2O_3), Whatman, UK]. The raw, unfiltered waters and the 0.20 and 0.02 µm-filtered waters were then brought back to the laboratory and stored at 4°C for elemental analysis using inductively coupled plasma–mass spectrometry (ICP-MS). The membrane filters were dried 24 h at room temperature (protected from ambient dust particles) and stored at 4°C for scanning electron microscopy (SEM) observation. Water size fractionation was performed to quantify Ti in the particulate, colloidal, and dissolved fractions. The particulate and colloidal fractions were separated with 0.20 µm filters. Ideally, separation of the colloidal and dissolved fractions requires 1 or 3 K-Dalton membranes. The 0.02 µm inorganic membranes selected for the current work were therefore unable to isolate the "true" dissolved fraction, and instead resulted in a fraction composed of dissolved plus small nanoparticulate (NP) species. This choice was made due to the operational conditions needed for a fast separation on-site.

Surface sediment samples (down to ∼2 cm depth) were brought up from the center of the canal/river using a 50 mL syringe. These sediments were sieved at 1 mm and then 250 μm to remove larger grains and the fraction <250 μm was freeze-dried and homogenized for X-ray diffraction (XRD) and ICP-MS analysis. Natural epilithic organisms were also collected to evaluate TiO_2 accumulation. Briefly, a few grams of epilithic organisms were scraped from sedimentary river rocks at 3 sites along the river (km −5.6, 0, +1.8) (**Figure S1**). To remove any loosely adhered, small particles, the epilithic organisms were first gently rinsed with ultrapure water on a 20 μm sieve, then freeze-dried and homogenized before analysis with ICP-MS.

Mineralogical Analysis

X-ray diffraction (XRD) was performed on sediment fractions (<250, 1–250, and <1 μm) from 4 sites (km −5.6, Industrial Effluent, WWTP, km +1.8) for samples from October 18, 2017 to evaluate the river's background mineralogy of Ti-based phases and any anthropogenic TiO_2 contributions. The sediment samples from March 2018 were not included in the XRD analysis since they exhibited a similar distribution of Ti concentrations compared to those from October 2017. Based on previous analysis on the river sediment, we hypothesized that the <250 μm sediment fraction may contain background minerals exhibiting strong signals (e.g., quartz and feldspars) that could make it difficult to distinguish potentially less intense signals of anatase or rutile TiO_2 (Hissler and Probst, 2006). Thus, an additional size separation was performed to remove the larger background minerals and obtain a finer sediment fraction of <1 μm.

Briefly, the <1 μm fraction was recovered according to Stokes law by re-suspending the <250 μm sediment in ultrapure water (5.56 g/L), sonicating 30 min to break up aggregates, allowing the sample to settle for 186 min, and then collecting the top 4 cm (quartz density = 2.65 g/cm^3) (Rubey, 1933). The recovered <1 μm sediment, along with the remaining 1–250 μm fraction were freeze-dried and homogenized before XRD analysis.

The three sediment fractions (<250, 1–250, and <1 μm) were ground with a mortar and pestle before depositing them on XRD low-background silicon plates. The samples were then analyzed with a PANalytical X-Pert PRO (Limeil-Brevannes, France) diffractometer equipped with Co Kα radiation (1.79 Å) at 40 kV and 40 mA. Each fraction was spun at 15 rpm and scanned with a 2θ range of 4–75°, step size of 0.033° and time per step of 4.7 s. Quartz was used as an internal standard to correct displacement of peak positions.

Elemental Analysis

The fractioned sediment (<250 μm), surface waters, and epilithic organisms were subjected to total decomposition using microwave-assisted acid digestion before elemental analysis with ICP-MS. Fifty milligrams of the solid samples (i.e., sediments or epilithic organisms) were digested in an UltraWAVE microwave system (Milestone Inc.) with 1.5 mL HCl, 1 mL HNO_3, and 1 mL HF at 180°C. The raw and filtered surface water samples (2 mL) were digested in the same system with 1 mL HNO_3 and 0.5 mL HF. The digested residues were then diluted to 10 mL with ultrapure water before analysis for Ti, V, Al, and Fe concentrations using a PerkinElmer NexION 300X quadrupole ICP-MS (measured isotopes = ^{47}Ti, ^{51}V, ^{27}Al, and ^{56}Fe). A 94–96% Ti recovery was measured for the above protocol using TiO_2 NP standards prepared in ultrapure water (0, 10, 50, 100, 500, and 1,000 μg/L). The concentrations of Na^+, K^+, Mg^{2+}, and Ca^{2+} cations were determined by ICP-MS analysis (measured isotopes = ^{23}Na, ^{39}K, ^{24}Mg, and ^{43}Ca) of the 0.20 μm-filtered waters. The raw and filtered (0.20 and 0.02 μm) surface waters collected were analyzed for Ti concentration to provide insight into the real-time total, particulate (>0.20 μm), colloidal (0.02–0.20 μm), and dissolved and/or small nanoparticulate (<0.02 μm) Ti occurrence in the water column. The Ti concentrations in the particulate (>0.20 μm) fraction were calculated by subtracting the measured Ti in the 0.20 μm-filtered waters from the total Ti concentration in the raw surface waters. Likewise, the Ti concentration in the colloidal fraction (0.02–0.20 μm) was calculated by subtracting the Ti measured in the 0.02 μm-filtered waters from the Ti concentration measured in the 0.20 μm-filtered waters.

To distinguish natural and anthropogenic TiO_2 particles, we compared the elemental distributions of the collected natural samples (e.g., sediments and water) to two types of anthropogenic TiO_2 nanomaterials (NM1 and NM2) as well as 3 natural minerals (i.e., feldspar, clay, and quartz). NM1 and NM2 were provided as powders by the manufacturing plant located next to the sampled river. The anatase nanomaterials were well-crystallized and spherical, with a size of approximately 6.5 ± 2.0 nm (NM1) and 38.8 ± 2.0 nm (NM2) from transmission and scanning electron microscopy (**Figure S2**). It is also worth noting that the manufacturer not only produces nanomaterials, but also larger, submicron-sized pigments. The minerals analyzed were feldspar (albite and microcline of natural origin), clay (kaolinite), and quartz (<20 μm). The TiO_2 nanomaterials (i.e., NM1 and NM2) and minerals (50 mg) were digested using the same microwave-assisted procedure as that selected for the sediments and the resulting residues were diluted and analyzed with inductively coupled plasma–atomic emission spectroscopy (ICP-AES, Perkin Elmer 4300 DV) and ICP-MS for Ti, V, Al, and Fe concentrations.

Imagery and Elemental Detection

A Zeiss Gemini 500 scanning electron microscope (SEM) equipped with an EDAX Silicon Drift Detector was used to image and determine the elemental composition of surface water particles that had been collected on 0.20 μm inorganic membrane filters (Al_2O_3) on-site at the Industrial Effluent and WWTP discharge sites on October 18, 2017. One membrane filter from each site was attached directly to an aluminum pin stub with double-sided carbon tape and then analyzed without further preparation (e.g., sputter coating). In-lens secondary electron detection was employed for imaging and the microscope was operated at 1 kV with a working distance of 0.5 mm. Elemental analysis using Energy Dispersive Spectroscopy (EDS) was performed at 15 kV with a working distance of 12.3 mm to evaluate the presence of Ti, O, Al, Fe, and C.

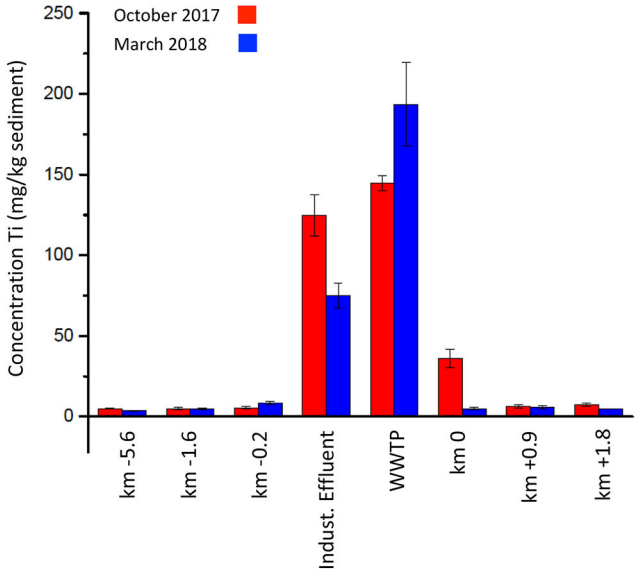

FIGURE 2 | Sediment (<250 μm) Ti concentrations (mg Ti/kg sediment) at each sampling site for October 2017 and March 2018. Error bars represent replicate sample digestions of the same sample ($n = 3$).

RESULTS AND DISCUSSION

Ti Accumulation in Sediment Downstream of the Manufacturing Plant

The Ti concentrations in the river sediment were determined first to assess potential TiO_2 nanomaterial accumulation over time. As shown in **Figure 2**, similar trends in sediment Ti concentration were observed for the samples collected in October 2017 and March 2018 despite the seasonal differences of the two sampling campaigns. Upstream of the confluence, at km −5.6, −1.6, and −0.2, the background Ti concentration in the river sediment was stable at ∼5.4 ± 1.5 mg/kg. However, along the industrial drainage canal, the Ti concentrations in the sediment were ∼21–25× and ∼29–55× higher than the background for the Industrial Effluent and WWTP sites, respectively. Specifically, concentrations of 124.6 ± 12.6 and 75.1 ± 7.9 mg Ti/kg sediment were measured at the Industrial Effluent site, while 144.5 ± 4.6 and 193.6 ± 25.8 mg Ti/kg sediment were detected at the WWTP site for October 2017 and March 2018, respectively. While the measured Ti concentrations in the canal sediments were higher at the WWTP site compared to the Industrial Effluent discharge site, there is no indication that this increase is related to more Ti-containing particles being discharged from the WWTP effluent. Ti-containing particles discharged from the Industrial Effluent site may be transported ∼90 m downstream before sedimenting at the WWTP site. Furthermore, although there appear to be significant differences in Ti sediment concentrations at the same site between October 2017 and March 2018, the presumed seasonal variations could also be due to difficulties in sampling the exact same sediment during both sampling campaigns. The two canal sites exhibited significant Ti accumulation, yet downstream of the confluence (km 0), the sediment Ti concentrations returned to levels similar to those observed upstream. For example, in October 2017, some Ti accumulation (36.1 ± 5.7 mg/kg) was still observed at km 0, but the sediment Ti concentration at km +0.9 was 6.4 ± 1.0 mg/kg, which was similar to the upstream background of 4.9 ± 0.3 mg/kg at km −5.6. The sediments collected in March 2018 also exhibited little evidence of Ti accumulation downstream of the confluence and in fact, the Ti sediment concentration measured at km 0 was comparable to that at km −5.6 (4.9 ± 0.8 vs. 3.5 ± 0.4 mg Ti/kg sediment). However, elemental analysis alone cannot be used to verify that this increased Ti concentration in the sediment resulted from the presence of TiO_2 and not another Ti-containing mineral. Furthermore, complementary analyses are required to confirm that the detected Ti results from anthropogenic TiO_2.

Anthropogenic vs. Natural Origin of TiO_2 in Sediment

Anatase and rutile were not detected apart from the sediment background upstream at km −5.6 in the <1 and 1–250 μm sample fractions from October 2017 (**Figure 3A**). The presence of TiO_2 in the canal sediments at the Industrial Effluent and WWTP discharge sites was confirmed, with clear signals observed from both the anatase and rutile main peaks at 29.443 and 31.982 $2\Theta[^\circ]$, respectively (**Figure 3A**) (Swanson et al., 1969). Of note, the main quartz peak at 31.035 $2\Theta[^\circ]$ is also shown for reference. While anatase TiO_2 was detected in both the <1 and 1–250 μm sediment fractions at the Industrial Effluent site, this form was only detected in the <1 μm sediment fraction at the WWTP site. Similarly, rutile TiO_2 was detected in both sediment fractions at the Industrial Effluent site. No significant rutile presence was observed in the <1 μm sediment fraction at the WWTP site, however a strong signal was present in the 1–250 μm fraction. Downstream at km +1.8, the presence of anatase was observed in the <1 and 1–250 μm fractions, but rutile was not detectable (**Figure S3**). Although anatase and rutile TiO_2 both accumulated in the canal sediments at the Industrial Effluent and WWTP discharge sites, the two forms were concentrated differently within the two sediment size fractions, implying that the anatase and rutile TiO_2 detected at the two sites may not have the same primary particle size or be distributed within the sediment in the same way (e.g., aggregate formation). The two TiO_2 forms may also exhibit different stability and transport in the river water, as suggested by the fact that only the anatase form was detected downstream at km +1.8 (Fazio et al., 2008; Liu et al., 2011; Iswarya et al., 2015).

To go further in determining the origin of the anatase and rutile phases identified with XRD, Ti/X molar ratios (with X = V, Al, and Fe) of manufactured NMs (NM1 and NM2) and natural minerals (feldspar, clay, and quartz) were compared to the ratios found in the collected river sediments, as shown in **Figure 3B** (Gondikas et al., 2017, 2018; Reed et al., 2017). The total element concentrations used to calculate these ratios can be found in **Table S2**. Such analysis of other naturally occurring elements in the sediment was essential for determining whether

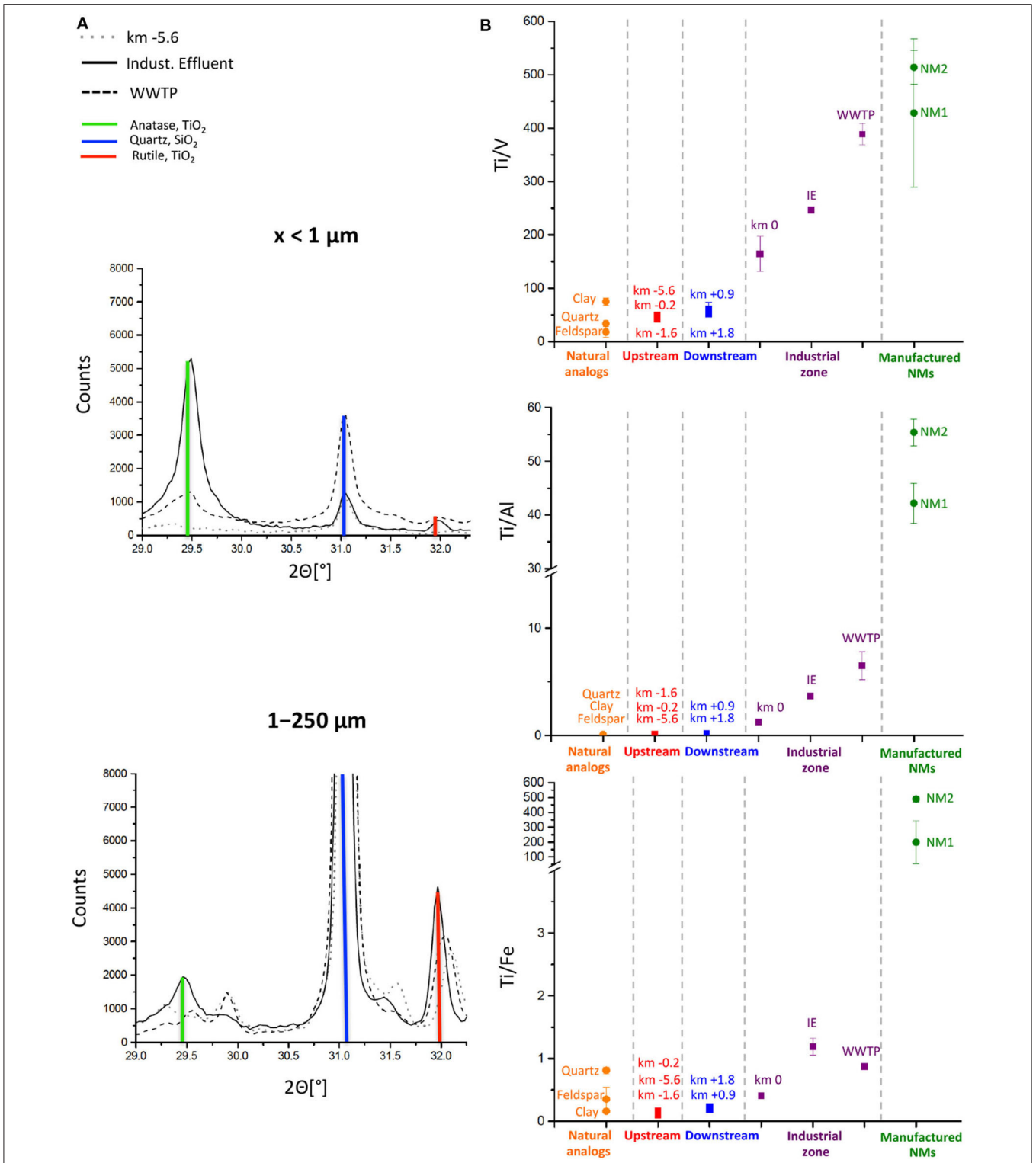

FIGURE 3 | Mineralogical and elemental analysis of sediments from October 2017: **(A)** XRD of fine fraction (x < 1 µm) and 1–250 µm fraction validating presence of anatase and rutile TiO_2 in Industrial Effluent and WWTP (Full XRD spectra in Supporting Information **Figure S3**). **(B)** Ratios of Ti/X (X = V, Al, and Fe) concentrations of analogs (e.g., NM1, NM2, clay) and river sediment to differentiate between anthropogenic inputs and natural TiO_2. IE, Industrial Effluent. Error bars represent replicate sample digestions of the same sample ($n = 3$).

these TiO_2 particles were anthropogenic or of natural origin. However, it must be considered that the comparison of Ti/X ratios using bulk elemental analysis measurements is based on the assumption that the natural background is best represented by individual, multi-element Ti-containing particles and not just the presence of numerous different particle compositions (e.g., $Fe_xAl_yTi_zO_a$ vs. Fe_xO_y, TiO_2, and Al_xO_y). NM1 and NM2 exhibited Ti/V, Ti/Al, and Ti/Fe ratios of 428–513, 42–55, and 199–490, respectively, in marked contrast to the ratios of 18–75, 0.01–0.1, and 0.16–0.81 measured in natural feldspar, clay, and quartz analogs. The manufactured NMs contain minimal amounts of V, Al, and Fe compared to Ti, which significantly increases the Ti/X ratio. In contrast, the feldspar, clay, and quartz contain naturally present V, Al, and Fe, resulting in a lower Ti/X ratio. Considering the natural river samples, the canal sediments at the Industrial Effluent and WWTP discharge sites exhibited much higher Ti/X ratios compared to the other sites. Specifically, Ti/V, Ti/Al, and Ti/Fe ratios of 246–389, 3.7–6.5, and 0.87–1.19 were determined for the Industrial Effluent and WWTP sites whereas at km −5.6 these same ratios were 49, 0.12, and 0.15. The sediment at km 0 (confluence of the industrial drainage canal and the river) was also characterized by elevated Ti/X ratios compared to the other sites. Of the element ratios tested here, Ti/V was the strongest indicator of anthropogenic Ti origin, due to a lower and less variable natural background of V compared to Al and Fe, as well as the possibility of Al and Fe contamination from the industrial canal sites. In fact, the manufacturing plant uses ilmenite ($FeTiO_3$) for TiO_2 NM production and WWTPs are known to use Al- and Fe-based salts in their treatment processes (Liu et al., 2013). The elemental analysis results shown here are for the sediments collected in October 2017, but the same trends were revealed for the sediments collected in March 2018 (**Figure S4**).

While the Ti/X ratios for the sediments at the Industrial Effluent and WWTP discharge sites, and at km 0 were not as high as those of the pure TiO_2 NMs, their significantly elevated values combined with the mineralogy determined by XRD support the anthropogenic and non-natural origin of the TiO_2 in the surface sediment. In order to elucidate the potential sources (e.g., industrial drainage canal or river) of this long-term anthropogenic TiO_2 sediment accumulation, the Ti concentrations in the surface waters were measured for each site.

Real-Time TiO_2 Occurrence in the Surface Waters

The total Ti concentrations measured in the raw surface waters collected in October 2017 exhibited a similar trend to that observed in the sediments, with low Ti background levels (3.4–7.0 μg/L) at km −5.6, −1.6, and −0.2, and significant increases in Ti at both the Industrial Effluent and WWTP sites, up to 133 and 260 μg Ti/L, respectively (**Figure 4**). Again, due to particle transport, TiO_2 particles originating from the Industrial Effluent likely contributed to increased Ti concentrations at the WWTP site (Praetorius et al., 2012; Sani-Kast et al., 2015). Downstream of the drainage canal, Ti concentrations in the water column did not return to upstream background levels, even at km +1.8 after the confluence, where the Ti concentration remained elevated (56.6 ± 8.6 μg /L). This finding is in support of river fate model predictions that have indicated that TiO_2 NMs can be transported several kilometers before settling into the sediment.

In March 2018, the Ti concentrations in the surface waters did not show any evolution along the industrial drainage canal or the river. At every sampling site, the Ti concentrations were comparable to that measured upstream at km −5.6 (4.9 ± 1.4 μg /L), even at the Industrial Effluent and WWTP discharge sites, where the measured concentrations were 3.4 ± 2.8 and 1.8 ± 0.5 μg /L, respectively. The disparate differences in total Ti detected in the surface waters between the two sampling dates could be the result of changes in waste management by the nanomaterial manufacturer (e.g., discharge), variations in canal flow, or due to seasonal dilution effects (e.g., rain or snowmelt) (Thompson, 1982; Carling et al., 2015). Indeed, changes in cation concentrations (**Table S1**) and the river outflow at km −5.6 between October 2017 and March 2018 suggest some dilution effects in the river. In October 2017 at km −5.6, the river outflow was 0.98 ± 0.01 $m^3.s^{-1}$ and Na^+ and Ca^{2+} concentrations were 0.497 and 0.207 mM, respectively, whereas in March 2018, the river outflow was ∼ 5× higher at 4.89 ± 0.01 $m^3.s^{-1}$ and the cation concentrations were lower (0.294 mM Na^+ and 0.157 mM Ca^{2+}). However, the low Ti concentrations detected in the surface waters at the Industrial Effluent and WWTP sites in March 2018 were more likely related to industrial waste management and differences in discharge since Na^+ (0.308–6.26 mM) and Ca^{2+} (0.204–0.219 mM) concentrations in March 2018 were either similar or higher than in October 2017 (0.5–2.07 mM Na^+ and 0.226–0.284 mM Ca^{2+}) and water depth was comparable between the two seasons.

Similar to the analysis conducted for the sediments, Ti/X ratios (X = V, Al, Fe) were also calculated for the surface waters collected in October 2017 to discriminate between an anthropogenic vs. natural origin of the detected Ti (**Figure 5**). The Ti/X ratios were not calculated for the surface waters from March 2018 since no significant Ti was detected. The total element concentrations in the surface waters can be found in **Table S3**. At the Industrial Effluent, the determined Ti/V, Ti/Al, and Ti/Fe ratios were ∼14× higher (ratios of 149, 1.13, and 1.27, respectively) than the ratios measured for the upstream sites (5–10, 0.05–0.08, and 0.08–0.09, respectively). Moving along the industrial drainage canal, Ti/X ratios in the WWTP surface water also remained elevated (4.5–15×) compared to those upstream. In contrast to the sediments where Ti/X ratios downstream of km 0 were similar to those upstream as a result of minimal anthropogenic Ti accumulation, in the surface waters Ti/V, Ti/Al, and Ti/Fe ratios remained elevated at km 0, +0.9, and +1.8 (31–51, 0.14–0.32, and 0.19–0.33). These complementary analyses of the surface water Ti/X ratios confirm the anthropogenic Ti emission from the Industrial Effluent and WWTP sites in October 2017. This demonstrates that the Ti measured in the surface waters downstream of the confluence resulted from the transport of anthropogenic material, not just the re-suspension of natural Ti in the sediment.

Using this data, the contribution of anthropogenic TiO_2 to the total Ti in the surface waters collected in October 2017 was

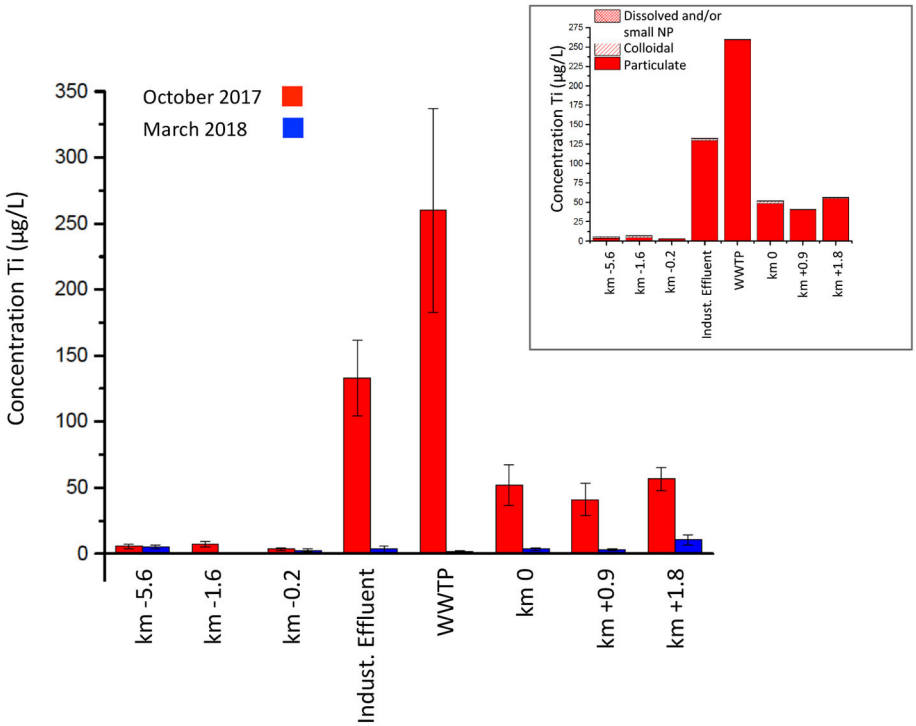

FIGURE 4 | Total Ti concentrations (µg/L) in raw surface waters. Inset: Ti concentrations (µg/L) measured in dissolved and/or nanoparticulate (NP) (<0.02 µm) fraction and Ti concentrations (µg/L) calculated for colloidal (0.02–0.20 µm) and particulate (>0.20 µm) fractions for October 2017 samples. Error bars represent replicate sample digestions of the same sample ($n = 3$).

estimated using Equation (1), as previously detailed in Loosli et al. (2019) These estimations are based on the assumption that all Ti measured above the background was in the form of pure TiO_2.

$$[TiO_2]_{anthropogenic} = \frac{TiO_{2MM}}{Ti_{MM}} \left[Ti_{sample} - V_{sample} \left(\frac{Ti}{V} \right)_{background} \right] \quad (1)$$

where $[TiO_2]_{anthropogenic}$ is the estimated concentration of anthropogenic TiO_2, Ti_{MM} and TiO_{2MM} are the molar masses (MM) of Ti and TiO_2, Ti_{sample} and V_{sample} are the total mass concentrations, and Ti/V is the molar mass ratio of Ti to V. The background Ti/V ratio was calculated using the average Ti/V ratios measured at the three upstream sampling locations (i.e., km −5.6, −1.6, −0.2). For the Industrial Effluent and WWTP sites along the drainage canal, estimated $TiO_{2anthropogenic}$ concentrations were 209 and 411 µg/L, representing 94 and 95% of the measured total Ti in the surface water, respectively. As expected, the estimated $TiO_{2anthropogenic}$ concentrations downstream at the km 0 and km +1.8 sites were lower at 73 and 71 µg/L, representing 85 and 76% of the measured total Ti in the surface water, respectively.

Beyond validating the origin of the TiO_2 release, evaluating the size of the emitted particles is crucial for predicting their transport, fate, and potential toxicity. The October 2017 surface waters were filtered to look for the presence of TiO_2 in the particulate (>0.20 µm), colloidal (0.02–0.20 µm), and dissolved and/or small nanoparticulate (<0.02 µm) fractions. Filtration and elemental analysis were also performed for the March 2018 samples, but due to low Ti concentrations in the raw surface waters, Ti in the filtrates was below 2 nM and not quantifiable (results not shown). As shown in the **Figure 4** inset, for the TiO_2 emitted from the Industrial Effluent and WWTP and then transported to the confluence at km 0, the majority of Ti was in the particulate form (98.6, 99.8, and 94% for the three sites, respectively), with a small contribution from the colloidal and dissolved and/or nanoparticulate fractions (0.2–6%). Specifically, Ti concentrations in the colloidal fraction were calculated to be 1.8, 0.4, and 3.1 µg/L for the Industrial Effluent, WWTP, and km 0 sites, whereas Ti concentrations measured in the dissolved/nanoparticulate fraction were 1.5, 0.3, and 0.4 ug/L for the respective sites. However, caution must be taken in interpreting these results, as previous work has shown that TiO_2 NMs can homo- and hetero- aggregate under river water conditions to form µm-sized aggregates (Loosli et al., 2013; Labille et al., 2015; Adam et al., 2016). Thus, the elemental analysis of the filtrates performed here cannot be used to distinguish between the presence of primary TiO_2 particles >0.20 µm and aggregates containing primary TiO_2 particles <0.20 µm.

Scanning electron microscopy (SEM) was used to visualize potential anthropogenic TiO_2 particles collected on 0.20 µm filter membranes from the Industrial Effluent and WWTP surface

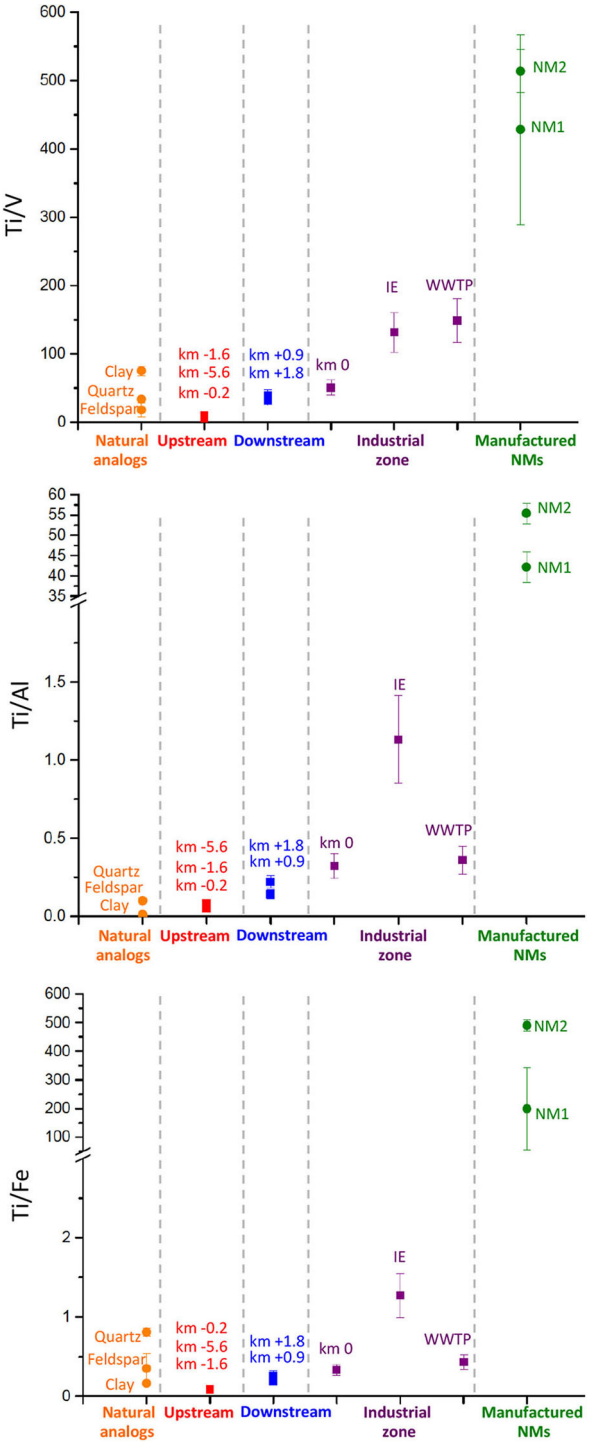

FIGURE 5 | Elemental analysis of surface waters from October 2017: Ratios of Ti/X (X = V, Al, and Fe) showing anthropogenic inputs. IE, Industrial Effluent. Error bars represent replicate sample digestions of the same sample ($n = 3$).

waters in October 2017. Although such an analysis remains challenging due to the low amount of Ti and considerable difficulty in providing statistically relevant data, it provided information on the primary particle size and morphology. The resulting SEM images revealed the presence of clusters of spherical nanomaterials in the waters collected from the Industrial Effluent and WWTP, with a shape and size consistent of TiO_2 synthesized for industrial and commercial applications (**Figure 6**) (Westerhoff et al., 2011). For the Industrial Effluent (**Figure 6A**), the nanomaterials in the imaged cluster had a primary particle size of 50 ± 13 nm (1 image, $n = 11$ particles), whereas for the WWTP (**Figure 6B**), the primary particle size was larger at 174 ± 43 nm (1 image, $n = 8$ particles). Furthermore, both EDS spectra exhibited Ti K and O K peaks, confirming that the particles were TiO_2. Of note, the presence of some P and Fe can be attributed to the surrounding environment, while the large Al signal resulted from the aluminum oxide membrane filter and the SEM pin stub. Additional SEM images and EDS spectra of other regions on the same 0.20 μm filter membranes also showed clusters of spherical TiO_2 nanomaterials, with primary particle sizes of ∼50–150 nm (**Figures S5–S7**).

While Ti elemental analysis of the surface water fractions suggested that >94% of the emitted TiO_2 particles were >0.20 μm, primary TiO_2 particles observed with SEM were <0.20 μm, and should have passed through the 0.20 μm membrane pores during filtration. These results indicate that the anthropogenic TiO_2 in the canal waters likely exists as aggregates of nanomaterials, at least in the Industrial Effluent. However, without further investigation it is not possible to discriminate between aggregates of fused TiO_2 nanomaterials formed during manufacturing from individual TiO_2 nanomaterials incorporated in homo- or hetero-aggregates formed in the canal waters under favorable ionic strength conditions (Loosli et al., 2013; Adam et al., 2016; Ilina et al., 2017; Slomberg et al., 2019). The formation of TiO_2 NM homo-aggregates over hetero-aggregates in the canal waters would only be probable if the NMs were present at a far greater concentration compared to that of natural colloids (**Figure S8**).

The significant differences in size of the TiO_2 particles collected at the Industrial Effluent and WWTP in October 2017 may result from temporal variations in particle manufacturing (production of nanomaterial and pigment), waste treatment, and effluent emissions. Furthermore, the disparity between the particles collected at the Industrial Effluent and the WWTP is coherent with the fact that the effluents from the NM manufacturing plant and the urban WWTP are unlikely to have the same composition. Any NMs present in the industrial effluent would be presumably composed of a mixture of unaged anatase and rutile TiO_2 based on plant production schedules, while those released in WWTP effluents most likely have a different origin and come from aged by-products of paints and personal care products (e.g., toothpaste, cosmetics) (Westerhoff et al., 2011).

Environmental Exposure Implications: TiO_2 Nanomaterial Release and Transport

The aggregation state of engineered nanomaterials in aqueous environments is a crucial parameter for predicting their residence time in the water column, their potential accumulation in the

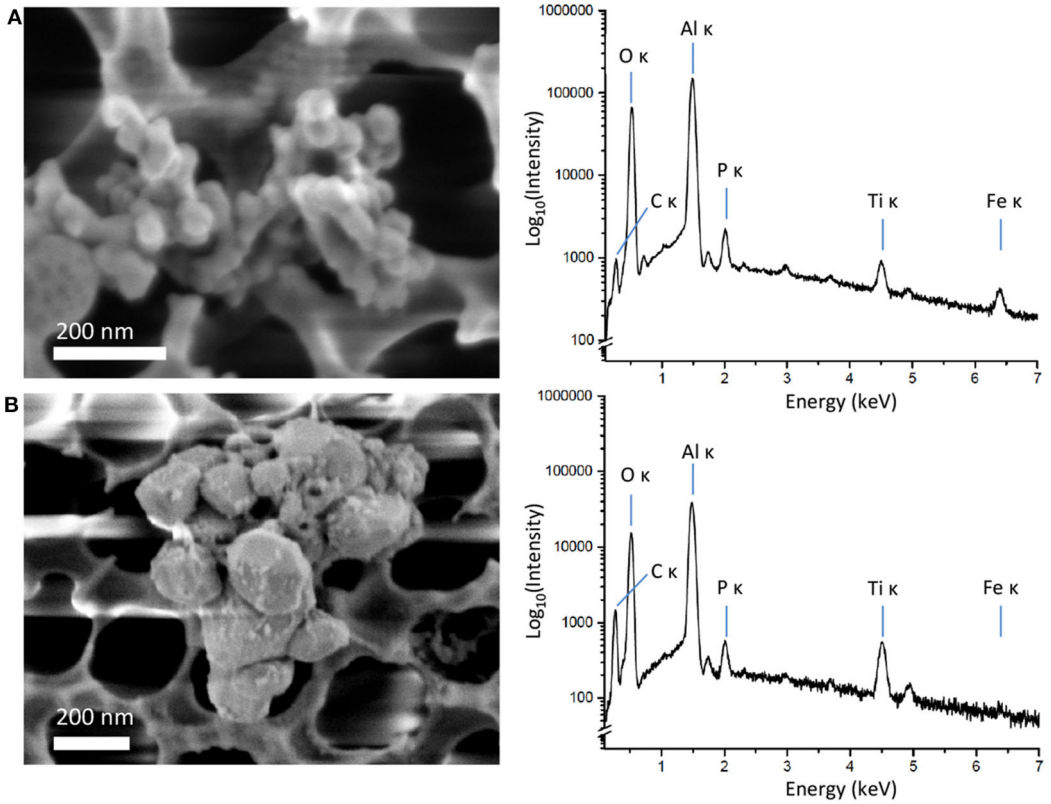

FIGURE 6 | SEM images (left) and corresponding EDS spectra (right) of particles recovered on 0.20 μm filters from **(A)** Industrial Effluent and **(B)** WWTP in October 2017. Some charging features present in SEM images as a result of no coating being applied to samples.

sediment layer, and determining which organisms are at risk of exposure. In addition to the TiO_2 NM clusters observed with SEM (**Figure 6**), the distributions of the measured Ti concentrations in the sediments and surface water fractions along the industrial drainage canal and river are also in support of the presence of TiO_2 NM aggregates that sediment close to the emission source. As evidenced in **Figure 2**, the TiO_2 NMs accumulate in the canal sediment close to the sources of the Industrial Effluent and WWTP discharge. Downstream of the confluence, the measured NM accumulation was not significant, with the TiO_2 detected at km +1.8 representing only ∼2% of that detected in the canal sediments near the two sources. However, due to the non-negligible TiO_2 background in the sediments (∼5 mg/kg), minor changes in accumulation can be difficult to verify with elemental analysis. The presence and accumulation of anatase TiO_2 in sediments at km +1.8 were thus confirmed by complementary XRD analysis (**Figure S3**), further supporting that there is some TiO_2 NM transport downstream even though the majority of TiO_2 sedimentation occurs near the emission source. We also evaluated the potential of epilithic organisms to accumulate Ti by scraping them from sedimentary river rocks and analyzing them for Ti concentration. These epilithic organisms (and possible associated sediment remaining after rinsing) from both October 2017 and March 2018 showed signs of significant Ti accumulation near the source, with concentrations of 3.3–5.8, 15.4–53.6, and 9.8–11.8 mg Ti/kg (dry weight) at km −5.6, 0, and +1.8. The Ti/V molar ratios of 53–68, 144–224, and 38–61 in the epilithic organisms at km −5.6, 0, and +1.8 also support an accumulation of anthropogenic Ti at km 0. As primary producers, these epilithic organisms represent the bottom of the trophic chain in the river ecosystem. Their TiO_2 accumulation thus provides a potential exposure pathway for primary consumers that feed on the sediments and subsequent entry into the food web.

Here, the canal and river sediments were a strong indicator of long-term NM accumulation, with similar TiO_2 concentrations observed for October 2017 and March 2018 along the various sites, including the Industrial Effluent, WWTP, and km 0. Yet, the sediment TiO_2 concentrations were not sensitive enough to provide information on real-time occurrence due to the difficulty in distinguishing small changes from a high background. The surface waters, having a low Ti background (3.4–7.0 μg Ti/L), offered a better indication of NM pulse release and transport mechanisms. As previously detailed, Ti concentrations in surface waters in October 2017 and March 2018 varied significantly (**Figure 4**), suggesting that NM emission in the canal was not constant and that environmental conditions (e.g., canal and river flow, seasonal dilution) may also play a role in NM detection. In October 2017, more significant transport was observed in the

surface water compared to what was revealed by the sediments. Downstream of the confluence at km +1.8, 20–40% of the TiO_2 detected at the emission sources remained in suspension. Thus, the processes of NM aggregation, sedimentation, and transport would likely continue further downstream of km +1.8. Indeed, TiO_2 NM fate model predictions have found that significant downstream transport is possible (Praetorius et al., 2012; Sani-Kast et al., 2015).

CONCLUSIONS

The thorough characterization of the surface water and sediment in a river next to a TiO_2 NM manufacturing plant highlighted both the presence and transport of anthropogenic TiO_2 NMs in the river ecosystem. Overall, the anthropogenic NMs exhibited rapid sedimentation near the TiO_2 emission source, but transport was still detected ∼2 km downstream. It was also evidenced that the anthropogenic Ti transport occurred mainly via the particulate fraction (>0.20 μm) as aggregates in the water column. Emissions into the surface waters were likely transient due to industrial/WWTP management, but differences in measured Ti concentrations could also result from contrasting seasonal conditions in October 2017 and March 2018. Despite differences in real-time surface water concentrations, long-term anthropogenic TiO_2 accumulation was observed in the sediments near the source of the treated industrial effluents, but further work is needed to confirm the presence and distribution of TiO_2 NMs in these sediments. Future studies should also include additional sampling sites near the emission sources and downstream to provide a more detailed and spatially resolved understanding of the TiO_2 NM transport and sedimentation. Sampling over several time periods will also be crucial for evaluating the transient nature of the TiO_2 NMs detected in the surface waters. The influence of these NMs on river organisms should also be further evaluated, investigating the effects of the TiO_2 NMs on several organisms in the trophic chain (primary producers and consumers) using relevant concentrations and considering pulse vs. chronic exposures.

DATA AVAILABILITY STATEMENT

The raw data supporting the conclusions of this article will be made available by the authors, without undue reservation.

AUTHOR CONTRIBUTIONS

MA and JR collected samples along the river and industrial drainage canal. DS prepared and conducted elemental analysis of the water, sediment, and epilithic organism samples with the help of NG and BA. DS and DB prepared and analyzed sediment samples with XRD. DS, MA, AC, and JR prepared and analyzed filter membranes with SEM. DS, MA, AC, DB, OA-C, and JR contributed to the interpretation of data. DS, MA, AC, OA-C, and JR contributed to the writing of the manuscript. All authors contributed to the article and approved the submitted version.

ACKNOWLEDGMENTS

This work was financed in part by the French Agency for the Environmental and Energetic Management (ADEME) under the contract number 1581C0027 called NANO-IDENT, funded by the 2015 CORTEA call. This work is a contribution to the OSU-Institut Pythéas, and to the Labex Serenade program (no. ANR-11-LABX-0064) funded by the Investissements d'Avenir program of the French National Research Agency (ANR) through the A*MIDEX project (no. ANR-11-IDEX-0001-02). The authors acknowledge the CNRS for the funding of the IRP iNOVE.

SUPPLEMENTARY MATERIAL

The Supplementary Material for this article can be found online at: https://www.frontiersin.org/articles/10.3389/fenvs.2020.00076/full#supplementary-material

REFERENCES

Adam, V., Loyaux-Lawniczak, S., Labille, J., Galindo, C., del Nero, M., Gangloff, S., et al. (2016). Aggregation behaviour of TiO_2 nanoparticles in natural river water. *J. Nanopart. Res.* 18:13. doi: 10.1007/s11051-015-3319-4

Auffan, M., Liu, W., Brousset, L., Scifo, L., Pariat, A., Sanles, M., et al. (2018). Environmental exposure of a simulated pond ecosystem to a CuO nanoparticle-based wood stain throughout its life cycle. *Environ. Sci. Nano* 5, 2579–2589. doi: 10.1039/C8EN00712H

Baalousha, M., Wang, J., Nabi, M. M., Loosli, F., Valenca, R., Mohanty, S. K., et al. (2020). Stormwater green infrastructures retain high concentrations of TiO2 engineered (nano)-particles. *J. Hazard Mater.* 392:122335. doi: 10.1016/j.jhazmat.2020.122335

Botta, C., Labille, J., Auffan, M., Borschneck, D., Miche, H., Cabié, M., et al. (2011). TiO_2-based nanoparticles released in water from commercialized sunscreens in a life-cycle perspective: structures and quantities. *Environ. Pollut.* 159, 1543–1550. doi: 10.1016/j.envpol.2011.03.003

Carling, G. T., Tingey, D. G., Fernandez, D. P., Nelson, S. T., Aanderud, Z. T., Goodsell, T. H., et al. (2015). Evaluating natural and anthropogenic trace element inputs along an alpine to urban gradient in the Provo River, Utah, USA. *Appl. Geochem.* 63, 398–412. doi: 10.1016/j.apgeochem.2015.10.005

de Klein, J. J., Quik, J. T., Bäuerlein, P. S., and Koelmans, A. A. (2016). Towards validation of the NanoDUFLOW nanoparticle fate model for the river Dommel, The Netherlands. *Environ. Sci. Nano* 3, 434–441. doi: 10.1039/C5EN00270B

Fazio, S., Guzman, J., Colomer, M., Salomoni, A., and Moreno, R. (2008). Colloidal stability of nanosized titania aqueous suspensions. *J. Eur. Ceram. Soc.* 28, 2171–2176. doi: 10.1016/j.jeurceramsoc.2008.02.017

Gondikas, A., von der Kammer, F., Kaegi, R., Borovinskaya, O., Neubauer, E., Navratilova, J., et al. (2018). Where is the nano? Analytical approaches for the detection and quantification of TiO_2 engineered nanoparticles in surface waters. *Environ. Sci. Nano* 5, 313–326. doi: 10.1039/C7EN00952F

Gondikas, A. P., Kammer, F., Reed, R. B., Wagner, S., Ranville, J. F., and Hofmann, T. (2017). Release of TiO2 nanoparticles from sunscreens into surface waters: a one-year survey at the old Danube recreational Lake. *Environ. Sci. Technol.* 48, 5415–5422. doi: 10.1021/es405596y

Hadioui, M., Knapp, G., Azimzada, A., Jreije, I., Frechette-Viens, L., and Wilkinson, K. J. (2019). Lowering the size detection limits of Ag and TiO_2

nanoparticles by single particle ICP-MS. *Anal. Chem.* 91, 13275–13284. doi: 10.1021/acs.analchem.9b04007

Hissler, C., and Probst, J.-L. (2006). Chlor-alkali industrial contamination and riverine transport of mercury: distribution and partitioning of mercury between water, suspended matter, and bottom sediment of the Thur River, France. *Appl. Geochem*. 21, 1837–1854. doi: 10.1016/j.apgeochem.2006.08.002

Ilina, S. M., Ollivier, P., Slomberg, D., Baran, N., Pariat, A., Devau, N., et al. (2017). Investigations into titanium dioxide nanoparticle and pesticide interactions in aqueous environments. *Environ. Sci. Nano* 4, 2055–2065. doi: 10.1039/C7EN00445A

Iswarya, V., Bhuvaneshwari, M., Alex, S. A., Iyer, S., Chaudhuri, G., Chandrasekaran, P. T., et al. (2015). Combined toxicity of two crystalline phases (anatase and rutile) of Titania nanoparticles towards freshwater microalgae: Chlorella sp. *Aquat. Toxicol.* 161, 154–169. doi: 10.1016/j.aquatox.2015.02.006

Johnson, A. C., Bowes, M. J., Crossley, A., Jarvie, H. P., Jurkschat, K., Jürgens, M. D., et al. (2011). An assessment of the fate, behaviour and environmental risk associated with sunscreen TiO_2 nanoparticles in UK field scenarios. *Sci. Tot. Environ.* 409, 2503–2510. doi: 10.1016/j.scitotenv.2011.03.040

Labille, J., Harns, C., Bottero, J.-Y., and Brant, J. (2015). Heteroaggregation of titanium dioxide nanoparticles with natural clay colloids under environmentally relevant conditions. *Environ. Sci. Technol.* 48, 10690–10698. doi: 10.1021/es501655v

Labille, J., Slomberg, D., Catalano, R., Robert, S., Apers-Tremelo, M.-L., Boudenne, J.-L., et al. (2019). Assessing UV filter inputs into beach waters during recreational activity: a field study of three French Mediterranean beaches from consumer survey to water analysis. *Sci. Tot. Environ.* 2019:136010. doi: 10.1016/j.scitotenv.2019.136010

Liu, X., Chen, G., and Su, C. (2011). Effects of material properties on sedimentation and aggregation of titanium dioxide nanoparticles of anatase and rutile in the aqueous phase. *J. Coll. Int. Sci*. 363, 84–91. doi: 10.1016/j.jcis.2011.06.085

Liu, Y., Zhang, W., Yang, X., Xiao, P., Wang, D., and Song, Y. (2013). Advanced treatment of effluent from municipal WWTP with different metal salt coagulants: contaminants treatability and floc properties. *Sep. Purif. Technol.* 120, 123–128. doi: 10.1016/j.seppur.2013.09.046

Loosli, F., Le Coustumer, P., and Stoll, S. (2013). TiO_2 nanoparticles aggregation and disaggregation in presence of alginate and Suwannee River humic acids: pH and concentration effects on nanoparticle stability. *Water Res*. 47, 6052–6063. doi: 10.1016/j.watres.2013.07.021

Loosli, F., Wang, J., Rothenberg, S., Bizimis, M., Winkler, C., Borovinskaya, O., et al. (2019). Sewage spills are a major source of titanium dioxide engineered (nano)-particle release into the environment. *Environ. Sci. Nano* 6, 763–777. doi: 10.1039/C8EN01376D

Markus, A., Krystek, P., Tromp, P., Parsons, J., Roex, E., de Voogt, P., et al. (2018). Determination of metal-based nanoparticles in the river Dommel in the Netherlands via ultrafiltration, HR-ICP-MS and SEM. *Sci. Tot. Environ.* 631, 485–495. doi: 10.1016/j.scitotenv.2018.03.007

Mitrano, D. M., Motellier, S., Clavaguera, S., and Nowack, B. (2015). Review of nanomaterial aging and transformations through the life cycle of nano-enhanced products. *Environ. Int.* 77, 132–147. doi: 10.1016/j.envint.2015.01.013

Nowack, B., Ranville, J. F., Diamond, S., Gallego-Urrea, J. A., Metcalfe, C., Rose, J., et al. (2012). Potential scenarios for nanomaterial release and subsequent alteration in the environment. *Environ. Toxicol. Chem.* 31, 50–59. doi: 10.1002/etc.726

Peters, R. J., van Bemmel, G., Milani, N. B., den Hertog, G. C., Undas, A. K., van der Lee, M., et al. (2018). Detection of nanoparticles in Dutch surface waters. *Sci. Tot. Environ.* 621, 210–218. doi: 10.1016/j.scitotenv.2017.11.238

Piccinno, F., Gottschalk, F., Seeger, S., and Nowack, B. (2012). Industrial production quantities and uses of ten engineered nanomaterials in Europe and the world. *J. Nanopart. Res.* 14:1109. doi: 10.1007/s11051-012-1109-9

Praetorius, A., Scheringer, M., and Hungerbühler, K. (2012). Development of environmental fate models for engineered nanoparticles—A case study of TiO_2 nanoparticles in the Rhine River. *Environ. Sci. Technol.* 46, 6705–6713. doi: 10.1021/es204530n

Reed, R., Martin, D., Bednar, A., Montaño, M., Westerhoff, P., and Ranville, J. (2017). Multi-day diurnal measurements of Ti-containing nanoparticle and organic sunscreen chemical release during recreational use of a natural surface water. *Environ. Sci. Nano* 4, 69–77. doi: 10.1039/C6EN00283H

Rubey, W. W. (1933). Settling velocity of gravel, sand, and silt particles. *Am. J. Sci.*25, 325–338. doi: 10.2475/ajs.s5-25.148.325

Sani-Kast, N., Scheringer, M., Slomberg, D., Labille, J., Praetorius, A., Ollivier, P., et al. (2015). Addressing the complexity of water chemistry in environmental fate modeling for engineered nanoparticles. *Sci. Tot. Environ.* 535, 150–159. doi: 10.1016/j.scitotenv.2014.12.025

Scifo, L., Chaurand, P., Bossa, N., Avellan, A., Auffan, M., Masion, A., et al. (2018). Non-linear release dynamics for a CeO_2 nanomaterial embedded in a protective wood stain, due to matrix photo-degradation. *Environ. Pollut*. 241, 182–193. doi: 10.1016/j.envpol.2018.05.045

Slomberg, D. L., Ollivier, P., Miche, H., Angeletti, B., Bruchet, A., Philibert, M., et al. (2019). Nanoparticle stability in lake water shaped by natural organic matter properties and presence of particulate matter. *Sci. Tot. Environ.* 656, 338–346. doi: 10.1016/j.scitotenv.2018.11.279

Sun, T. Y., Gottschalk, F., Hungerbühler, K., and Nowack, B. (2014). Comprehensive probabilistic modelling of environmental emissions of engineered nanomaterials. *Environ. Pollut*. 185, 69–76. doi: 10.1016/j.envpol.2013.10.004

Swanson, H. E., McMurdie, H. F., Morris, M. C., and Evans, E. H. (1969). *Standard X-Ray Diffraction Powder Patterns: Data for 81 Substances*. Washington, DC: National Bureau of Standards. doi: 10.6028/NBS.MONO.25-7

Thompson, M. E. (1982). "The cation denudation rate as a quantitative index of sensitivity of eastern Canadian rivers to acidic atmospheric precipitation," in *Long-Range Transport of Airborne Pollutants,* ed H. C. Martin (Dordrecht: Springer), 215–226. doi: 10.1007/978-94-009-7966-6_16

Vance, M. E., Kuiken, T., Vejerano, E. P., McGinnis, S. P., Hochella, M. F. Jr., Rejeski, D., et al. (2015). Nanotechnology in the real world: Redeveloping the nanomaterial consumer products inventory. *Beilstein J. Nanotechnol.* 6, 1769–1780. doi: 10.3762/bjnano.6.181

Von der Kammer, F., Ferguson, P. L., Holden, P. A., Masion, A., Rogers, K. R., Klaine, S. J.;, et al. (2012). Analysis of engineered nanomaterials in complex matrices (environment and biota): general considerations and conceptual case studies. *Environ. Toxicol. Chem*. 31, 32–49. doi: 10.1002/etc.723

Von der Kammer, F., Legros, S., Hofmann, T., Larsen, E. H., and Loeschner, K. (2011).Separation and characterization of nanoparticles in complex food and environmental samples by field-flow fractionation. *Trends Anal. Chem*. 30, 425–436. doi: 10.1016/j.trac.2010.11.012

Wang, J., Nabi, M. M., Mohanty, S. K., Nabiul Afrooz, A. R. M., Cantando, E., Aich, N., et al. (2020). Detection and quantification of engineered particles in urban runoff. *Chemosphere* 248, 126070. doi: 10.1016/j.chemosphere.2020.126070

Westerhoff, P., Song, G., Hristovski, K., and Kiser, M. A. (2011). Occurrence and removal of titanium at full scale wastewater treatment plants: implications for TiO_2 nanomaterials. *J. Environ. Monit.* 13, 1195–1203. doi: 10.1039/c1em10017c

Conflict of Interest: The authors declare that the research was conducted in the absence of any commercial or financial relationships that could be construed as a potential conflict of interest.

frontiers in Environmental Science

ORIGINAL RESEARCH
published: 18 June 2020
doi: 10.3389/fenvs.2020.00084

Quantification and Characterization of Nanoparticulate Zinc in an Urban Watershed

Shaun Bevers[1], Manuel David Montaño[2], Laya Rybicki[1], Thilo Hofmann[3], Frank von der Kammer[3] and James F. Ranville[1]*

[1] Department of Chemistry, Colorado School of Mines, Golden, CO, United States, [2] Department of Environmental Sciences, Western Washington University, Bellingham, WA, United States, [3] Centre for Microbiology and Environmental Systems, Department of Environmental Sciences, University of Vienna, Vienna, Austria

The recent expansion in the use of nanomaterials in consumer and industrial applications has led to a growing concern over their behavior, fate, and impacts in environmental systems. However, engineered nanoparticles comprise only a small fraction of the total nanoparticle mass in aquatic systems. Human activities, particularly in urban watersheds, are increasing the population of incidental nanoparticles and are likely altering the cycling of more abundant natural nanoparticles. Accurate detection, quantification, characterization, and tracking of these different populations is important for assessing both the ecological risks of anthropogenic particles, and their impact on environmental health. The urban portion of the South Platte watershed in Denver, Colorado (United States) was sampled for zinc to identify and quantify different nanomaterial sources. Single particle ICP-QMS was employed, to provide single elemental (Zn) signals arising from particle detection events. Coupling spICP-QMS to sample pre-fractionation (sedimentation, filtration) provided some insights into Zn association with nanoparticulate, colloidal, and suspended sediment phases. Single particle ICP-TOFMS (spICP-TOFMS) provided quantification across a large atomic mass range, yielding an even more detailed characterization (elemental ratios) on a particle-by-particle basis, providing some delineation of multiple sources of particles. Across the watershed, on average, 21% of zinc mass was present as zinc-only particles with a rather uniform mean size of 40.2 nm. Zinc that was detected with one or more other elements, primarily Al, Fe, and Si, is likely to be present as heteroagglomerates or within mineral colloids. Although spICP-TOFMS provides a substantial amount of information, it is still in its early stages as an analytical technique and currently lacks the requisite sensitivity to study the smallest of nanoparticles. As this technique continues to develop, it is anticipated that this methodology can be broadly applied to study sources, behavior and effects of a disparate variety of nanoparticles from both geogenic and anthropogenic origins.

Keywords: nanoparticles, single particle ICP-MS, ICP-TOFMS, urban runoff, suspended sediments

OPEN ACCESS

Edited by:
Denise M. Mitrano, Swiss Federal Institute of Aquatic Science and Technology, Switzerland

Reviewed by:
Anthony Bednar, United States Army Crops of Engineers, United States
Jeffrey M. Farner, University of Alberta, Canada

****Correspondence:***
Manuel David Montaño
montanm2@wwu.edu;
manuel.montano@wwu.edu

Specialty section:
This article was submitted to Biogeochemical Dynamics, a section of the journal Frontiers in Environmental Science

Received: *31 March 2020*
Accepted: *26 May 2020*
Published: *18 June 2020*

Citation:
Bevers S, Montaño MD, Rybicki L, Hofmann T, von der Kammer F and Ranville JF (2020) Quantification and Characterization of Nanoparticulate Zinc in an Urban Watershed. Front. Environ. Sci. 8:84. doi: 10.3389/fenvs.2020.00084

INTRODUCTION

The combination of increasing global human populations, combined with rising urbanization have placed stress on urban watersheds through the direct influx of anthropogenic contaminants and other man-made influences (Baalousha et al., 2016; Zheng et al., 2019). The concurrent rise of impermeable surfaces in an urban environment results in greater stormwater run-off into these water bodies, (Shuster et al., 2005) carrying a variety of contaminants ranging from automotive fluids and resuspended particulate emissions, (Lamprea et al., 2018) dissolved metals, (Zuo et al., 2012) and suspended solids (Toor et al., 2017), all of which having possible deleterious effects on human and ecological health (Young et al., 2018).

The increasing development of nano-enabled consumer and industrial products has resulted in a number of potential release pathways for engineered nanoparticles (ENPs) during use and disposal (Hendren et al., 2011; Sun et al., 2017; Giese et al., 2018). In addition to intentionally ENPs, urban centers serve as a source of incidental nanoparticles (INPs) that are unintentionally produced from human-driven processes such as vehicle emissions, (Gonet and Maher, 2019) tire wear, (Sommer et al., 2018) and road dust (Yang et al., 2016). These man-made particles infiltrate urban streams via storm water, adding to the naturally occurring nanoparticulates (NNP) load present from bio- and geogenic sources (Hochella et al., 2008, Hochella et al., 2019).

One nanomaterial of particular interest is zinc oxide (ZnO). As an ENP, it is used in large quantities (10,000 tons annually circa 2012; Piccinno et al., 2012) in tire manufacture, (Milani et al., 2004) sunscreens (Herzog et al., 2002; Osmond and McCall, 2010), and paints (Kaiser et al., 2013) with the potential to leach into the environment after use. There are several sources of Zn INPs as well, primarily generated from tire wear (Councell et al., 2004), and the resuspension of road dust (Ermolin et al., 2017). While not highly toxic, zinc's effect on aquatic species has led to EPA establishing hardness-dependent water quality criteria in the few tens to hundreds μg/L range (DeForest and Van Genderen, 2012). In order to protect our urban watersheds, it is necessary to develop risk managements strategies that can effectively mitigate the influx of these potential contaminants. However, the complexity of nano-scale zinc in the environment requires the development of new sophisticated means of detection, quantification, and differentiation of the different sources of particulate zinc.

Several techniques are available to examine the elemental composition of nanoparticles in the environment. Field flow fractionation coupled to ICP-MS (FFF-ICP-MS) is one such technique that can provide elemental composition on a hydrodynamic diameter basis (Stolpe et al., 2005; Plathe et al., 2010). However, in the analysis of multi-element particles, the co-elution of particle populations makes it difficult to discern between particles containing many elements, and distinct populations of similar sizes eluting simultaneously. In order to quantify particle composition on an individual particle basis, single particle ICP-MS (spICP-MS) has a widely demonstrated utility in the analysis of natural waters for ENPs (Furtado et al., 2014; Gondikas et al., 2014) and NNPs (Praetorius et al., 2017; Gondikas et al., 2018). In a study examining TiO_2 ENP release from sunscreens, spICP-MS was utilized to demonstrate an increase in particulate Ti from anthropogenic activity (Reed et al., 2017). Hadioui et al. (2015) used ICP-quadrupole-MS (ICP-QMS) coupled with ion exchange chromatography to measure ZnO nanoparticles in the presence of high dissolved Zn backgrounds. Expanding upon this work, Fréchette-Viens et al. (2019) employed a high-resolution, ICP-sector-field-MS instrument to push the size detection limits of ZnO nanoparticles in surface waters while noting the presence of larger heteroaggregate particles containing small amount of Zn. Nevertheless, these studies also highlight a fundamental weakness of quadrupole mass analyzers in their inability to monitor multiple ions simultaneously. Though some studies have shown the potential to monitor two or more elements in a given particle event, (Montaño et al., 2014; Heringer and Ranville, 2018) to accurately characterize the source of nanoparticulate Zn requires a means of analyzing multiple elements simultaneously. In recent years, commercially available ICP-time-of-flight-mass spectrometry (ICP-TOFMS) has shown the potential to significantly augment the utility of single particle analysis. The intrinsic nature of time-of-flight mass analysis permits the quasi-simultaneous detection of a wide mass range on microsecond time scales, the duration being bound to the extraction frequency. Typical acquisition times (33-46 μs; Gschwind et al., 2011; Borovinskaya et al., 2013; Hendriks et al., 2017) are on the same order as the nanoparticle detection events (500 μs) (Olesik and Gray, 2012). Recent studies have demonstrated its utility in characterizing a variety of nanomaterials ranging from simple core-shell ENPs (Naasz et al., 2018) and multi-element steel NPs (Hegetschweiler et al., 2018) to more complex atmospheric nanoparticulates (Erhardt et al., 2019). Given this capability, ascertaining the sources of NPs may be possible by monitoring the respective elemental or isotopic ratios on a particle-by-particle basis (Praetorius et al., 2017; Montaño et al., 2019).

In this study we demonstrate a multi-method approach for detecting and quantifying Zn NPs in the portion of the South Platte Watershed that encompasses Denver, CO (United States). Water samples were taken from multiple tributaries and the main stem of the South Platte River in mid-July 2018 within 2 days of a large storm event that significantly increased stream flow. Settling and filtration were used to separate different size fractions of particulate zinc, which were then quantified by spICP-QMS. Analysis by spICP-TOFMS provided particle-by-particle elemental associations of zinc to investigate the sources of Zn NPs across the watershed.

MATERIALS AND METHODS

Study Location

The urban reaches of the South Platte River, the primary water source for Denver (CO, United States), as well as several of

FIGURE 1 | Map of the urban South Platte watershed and sampling locations for July 16th and 17th, 2018.

its tributaries were examined (**Figure 1**). The South Platte River enters the metro area from the southwest corner and exits north of the city. Major tributaries that feed the South Platte River within the Denver metro area include Clear Creek (ClC), Cherry Creek (CC), and Sand Creek (SC). Chatfield Reservoir is the only significant impoundment on the South Platte River itself and it intercepts flow emanating from the mountains upstream of the study site. Cherry Creek Reservoir is the other significant impoundment in the watershed, existing on the Cherry Creek tributary also upstream of the sampling site. Streamflow throughout the basin is low during fall and winter months. Flow increases beginning in April and peaks in the months of June and July as a result of mountain snow melt. Water impoundment and release from the aforementioned reservoirs can have significant effects on streamflow along with agricultural diversion through numerous ditches during the growing season. Annual precipitation in the metro area ranges between 180–380 mm per year, which mostly falls during April to September. Notably, much of the summer precipitation occurs as brief-duration thunderstorms, resulting in short-term elevated stream flow. Sampling was timed to capture urban runoff following one such event in 2018.

Field Sampling

Sampling was performed on July 16th and 17th, 2018 following a rainfall event on July 14th–15th. Rainfall was not uniform across the basin and resulted in streamflow increases that varied among the sampling locations (hydrographs provided in ESI **Figure 1**). On July 16th five sites were sampled (**Figure 1**); three sites examined the confluence between the South Platte River downstream Denver (flow to the north), Clear Creek (flow from the west), and Sand Creek (flow from the east). Two samples were also taken from the South Platte River at points approximately 500 m upstream and downstream of the Robert W. Hite wastewater treatment plant, the largest such facility in Denver. Locations are labeled as: WSC (West Sand Creek), EClC (East Clear Creek), NSP (North South Platte), AWTTP (South Platte above the wastewater treatment plant), and BWTTP (South Platte below the wastewater treatment plant). To examine tributary inputs from outside the central urban area, sampling on

July 17th occurred at locations labeled ESC (East Sand Creek), WClC (West Clear Creek), SSP (South South Platte), and CC (Cherry Creek). Both EClC and NSP were also resampled on this date (**Figure 1**).

Grab samples were collected by submerging polyethylene bottles (1 L) approximately 10 cm or more below the surface, at a point at least 0.5 meter from the streambank. Bottles were filled and emptied three times to rinse the virgin bottles prior to collecting the sample. Subsamples were taken for chemical analysis in the laboratory at Colorado School of Mines. The remaining sample was stored at 4°C until further processing and single particle ICP-MS analysis.

Laboratory Analysis/Preparation

Subsamples (10 ml) were subjected to a modification of the EPA Total Recoverable (TR) Method, EPA 200.2 (United States Environmental Protection Agency [EPA], 1994). To accommodate our small-footprint digestion equipment, the method was modified by reducing the sample and acid volumes by a factor of 10. All other aspects of EPA 200.2 remained unchanged. All samples were shaken prior to subsampling. Cation concentrations were determined by ICP-OES (PerkinElmer Optima 7300 DV), the operational details and QA procedures being provided in ESI. Major anions (Cl and SO_4) were measured by ion chromatography (Dionex: ThermoFisher, ICS-900, Waltham, MA, United States). Turbidity measurements were made using a Hach DR 890 meter (HACH Method 8237), and results reported in formazin absorbance units (FAU). Results for metals, anions and turbidity are reported in **Table 1**.

Single Element, Single Particle ICP-QMS Analysis

Single particle ICP-QMS analysis was performed using an ICP-quadrupole mass spectrometer (NexION 300 D, Perkin Elmer, Waltham, MA, United States). For single particle analysis, the transport efficiency (TE) was determined using the mass-based method as described by Pace et al. (2011) and reported in **Supplementary Table S1**. A 60 nm Au nanoparticle (NIST SRM 8013, citrate-stabilized, mean size of 56.0 ± 0.5 nm by TEM) was used as a known mass standard. Dissolved standards of 0 to 100 μg/L Au [SPEX CertiPrep in 2% (v/v) hydrochloric acid] and Zn [SPEX CertiPrep in 2% (v/v) nitric acid] were prepared using nitric acid (Fisher Scientific, Optima grade, 32-35%) and were diluted in Milli-Q water (18.2 MΩ-cm, Barnstead International) on the day of each analysis. All unfiltered samples and Au NP standards were sonicated in a sonic bath for 5 min prior to analysis. ^{197}Au or ^{64}Zn were analyzed using a dwell time of 100 μs, no settling time, sample flow rate = 0.3 ml/min, a total data collection time of 60 s, and a very short detector dead time (35 ns) between readings. Data acquisition and data processing were performed using the Syngistix^{TM} Nano Application Module (PerkinElmer). TE determination is built into the software and is calculated in order to determine NP mass (from which size is computed) and the number concentration. Particle events were identified as ICP-MS responses that were deemed to above the threshold intensity, which was determined in real-time using the average background plus 3σ (Pace et al., 2011). The particle number concentration is computed from the number of NP events detected after adjustment for the sample flow rate and TE. In addition to particle analysis, data collected by spICP-QMS was integrated over the entire 60 s analysis and, through use of the calibration curves, the mass concentration of Zn (μg/L) was determined.

Additional Sampling Processing for spICP-QMS

Samples were also filtered through a 0.02 μm filter (Whatman Anotop) prior to spICP-QMS analysis to obtain an estimate of the dissolved elemental concentration (μg/L). Filtered samples also provided a means of evaluating the spICP-QMS baseline obtained for non-filtered samples. This is often assumed to represent the dissolved element mass concentration (μg/L). A crucial parameter in sizing nanomaterials by spICP-MS is the selection of particle composition (i.e., element mass fraction and density), and geometry. As a quadrupole mass analyzer is only capable of

TABLE 1 | Bulk water chemistry data for sample sites used in this study.

Sampling date	Turbidity (FAU)	Total recoverable metals (mg/L)					Anions (mg/L)		spICP-MS (μg/L)	
		Al	Si	Fe	Mn	Zn	Cl	SO_4	Zn	% recovery
16-Jul										
NSP	50	1.39	7.01	1.57	0.20	0.043	60	77	11.5	27
WSC	170	7.57	20.64	6.86	0.38	0.068	65	171	13.9	20
EClC	31	1.03	5.72	1.33	0.19	0.049	49	61	13.3	27
BWWTP	27	1.20	6.54	1.25	0.15	0.032	69	81	9.2	29
AWWTP	32	1.27	6.54	1.31	0.16	0.026	61	69	6.3	24
17-Jul										
NSP	29	1.00	6.87	0.99	0.20	0.050	93	151	13.7	27
ESC	258	10.67	27.88	9.03	0.35	0.072	42	196	19.9	28
EClC	13	0.16	4.10	0.31	0.19	0.022	75	86	8.4	38
WClC	7	0.17	3.20	0.34	0.05	0.061	14	35	23.2	38
SSP	19	0.61	3.79	0.62	0.40	0.009	67	73	1.8	20
CC	7	0.46	9.29	0.41	0.27	0.004	189	177	1.2	29

selecting for one mass-to-charge ratio at a time, it is necessary to utilize other means to approximate the values needed for particle sizing. To provide this additional information on the Zn-containing particles, each non-filtered sample was gently agitated and then subjected to settling in a 15 ml centrifuge tube (VWR, Falcon brand). Sampling from the upper 2 cm after 70 min provided a size separation at approximately 4.5 μm, assuming a spherical particle with a density of 2.65 g/cm^3, typical of sediment minerals. Using ZnO density 5.61 g/cm^3 gives an approximate size cutoff of 2.5 μm. Comparison of the observed changes in NP mass (size) and integrated concentration (number/ml and μg/L), to that predicted assuming the Zn was present as either ZnO or associated with sediment particles, provides insight into Zn form/mineralogy.

Multi Element, Single Particle ICP-TOFMS Analysis

Unfiltered samples were examined by multi-element analysis using single particle ICP- time-of-flight mass spectrometry (spICP-TOFMS) at the University of Vienna. Data were collected using an icpTOF 2R (TOFWERK AG, Thun, Switzerland). The ICP-TOF has a mass-resolving power of 6000 FWHM and a TOF extraction frequency of 46 kHz, measuring a majority of the atomic mass range (7–250 m/z$^+$). The operation of the ICP-TOF utilizes a notch filter, which allows for the attenuation of up to four chosen masses, typically chosen for their abundance, which can lead to signal suppression of ions of interest. In this case, $^{40}Ar^+$, $^{16}O_2^+$, $^{35}Cl^+$, and $^1H^+$ were chosen. To improve the signal-to-noise of $^{56}Fe^+$ and $^{28}Si^+$, both of which have isobaric interferences in $^{40}Ar^{16}O^+$ and $^{14}N_2^+$, respectively, a 7% H_2/He mixture was used for a collision gas. The flow parameters of this gas were optimized before analysis for maximum sensitivity. Dissolved calibration solutions were prepared from ESI stock solution of dissolved metals (Al, Si, Fe, Cu, Ti, Zn, Pb, Cd, Cu, Nd, Ni, and Au), analyzed prior to each sample run, with a continuing check verification standard (CCV) every 10 samples to account for any drift in instrument sensitivity. Additional and typical operating parameters are listed in supporting information (**Supplementary Table S1**). A 100 nm gold nanoparticle (BBI solution) was used as a known mass standard for obtaining TE. Due to limitations on data transfer from the data acquisition system to the laboratory computer, a 3 ms dwell time was used, despite the much shorter mass sweep time. To avoid particle coincidence for this long dwell time, a 1000× dilution of the samples was required. This was not required for the spICP-QMS analysis.

The raw mass spectrum data were initially processed using TofWare (TOFWERK AG, Thun, Switzerland) which allowed for peak integration after initial subtraction of the spectral baseline. The resulting data was then processed via a custom Python script which performed calibration and spectral correction of the data. The script also then processed the single particle data according to the previously established methodology (Pace et al., 2011; Laborda et al., 2014; Montano et al., 2016), which was similar to that used for spICP-QMS analysis. The subsequent data output resulted in a compiled list of particle events with time and their associated masses, which can then be converted into mass and size according to single particle theory.

RESULTS

Bulk Water Chemistry

Total recoverable mass concentrations (μg/L) for those elements that were also examined by spICP-MS are given in **Table 1**, with major cation concentrations provided in ESI. Although TR aggressively digests suspended sediments, in most cases particulate matter remained after the digestion and was removed by filtration (0.45 μm, nylon, GEI). Samples from Sand Creek contained considerably more suspended sediment than those from other sites. Chloride and sulfate were the major anions measured (**Table 1**). Alkalinity, representing another possible major anion, was not measured. Turbidity (**Table 1**) was used as a surrogate for suspended sediment concentration.

Single Element, spICP-QMS Results

Data collected for the unfiltered sample using spICP-QMS was integrated over the entire 60 s analysis to determine the mass concentration of Zn (**Table 1**). The number of particles measured in the raw samples (60 s analysis time) were, with one exception, always greater than 1000, and in most cases greater than 2000 (**Figure 2A**). Accounting for flow rate and transport efficiency resulted in calculated particle number concentrations for most samples of between 7500 and 170,000 particles/mL (**Table 2**). Integration of the particle-generated ^{64}Zn pulses yields a range of 0.5 to 9 femtograms for the number-weighted, geometric mean of the Zn mass contained in each particle (**Figure 2B**).

Analysis of unfiltered samples by spICP-QMS resulted in a series of pulses (representing NPs) over an elevated background (**Figure 3A**). We have applied a methodology that defines the Zn distribution as being composed of resolved, unresolved, and dissolved fractions. Resolved nanoparticulate Zn (RP) represents particles that have sufficient Zn content to be discriminated from the baseline signal when using the Syngistix software. In spICP-MS analysis, the baseline elemental signal is often considered to approximate the dissolved metal concentration (Montaño et al., 2014). Analysis of the 0.02 μm membrane-filtered sample gives a more direct approximation of dissolved Zn (**Figure 3B**) by removing a majority of particulate Zn, although smaller NPs could be present in this fraction. This pore size is well below the size detection limit of the spICP-QMS (approximately 50 nm as ZnO; Lee et al., 2014) and thus would not contain observable individual NPs. In this study, we also define an unresolved nanoparticle fraction (URNP) as the difference between the Zn baseline concentration in the raw sample [$(Zn)_{Raw,Diss.Baseline}$] minus the 0.02 μm filtered sample [$(Zn)_{0.02\ \mu m,Diss.Baseline}$].

$$[Zn]_{URNP}\left(\mu g/L\right) = [Zn]_{Raw,Diss.Baseline} - [Zn]_{0.02\ \mu m,Diss.Baseline} \quad (1)$$

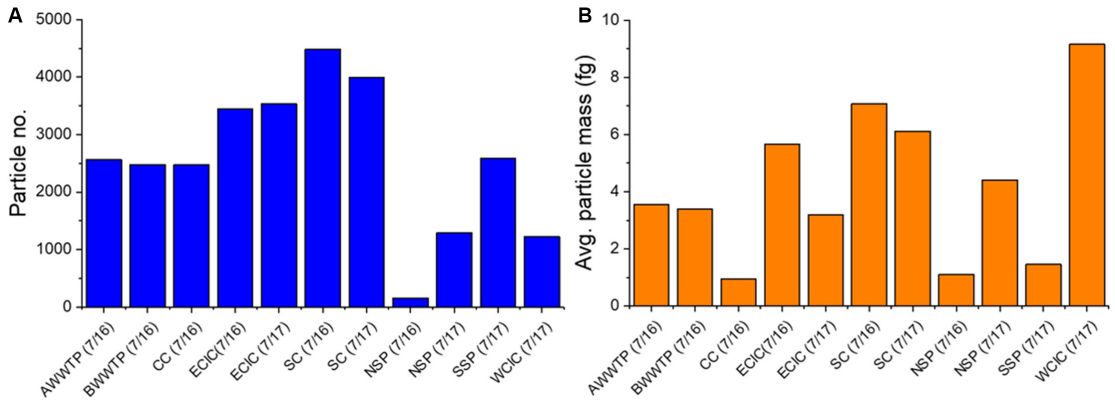

FIGURE 2 | (A) Number of Zn particles detected in a 60 s total acquisition time at each site, **(B)** Average Zn mass per particle.

TABLE 2 | spICP-MS quantification of Zn particle and dissolved fractions at the various sample sites used in this study.

Sampling date	Particle conc. (#/L)		Average diameter (ZnO eq.)		Background dissolved Zn (ppb)		
	Raw	Settled	Raw	Settled	Raw	Settled	0.02 filtered
16-Jul							
NSP	7.6E+03	1.4E+05	67	96	11.2	8.4	3.9
WSC	2.2E+03	2.4E+05	124	95	13.9	7.2	0.9
ECIC	1.7E+05	1.2E+05	115	102	13.3	10.1	4.0
BWWTP	1.2E+05	4.5E+04	97	91	9.2	7.9	5.2
AWWTP	1.3E+05	8.6E+04	98	86	6.3	4.6	1.7
17-Jul							
NSP	6.4E+04	1.4E+05	106	96	13.7	8.2	1.6
ESC	2.0E+05	1.9E+05	118	107	19.9	13.5	0.3
ECIC	1.7E+05	1.5E+05	95	90	8.4	6.6	5.2
WCIC	6.0E+05	3.8E+04	135	132	23.2	18.6	1.9
SSP	1.3E+05	1.1E+05	73	66	1.8	0.3	0.2
CC	1.2E+05	1.0E+05	63	62	1.2	0.8	0.4

Values reported for both raw and settled samples.

For the example shown (**Figure 3**), the peaks before filtration (**Figure 3A**) represent the RP fraction. The baseline in the raw and the 0.02 μm filtered samples (**Figure 3B**) give "dissolved" Zn concentrations of 6.1 μg/L and of 0.8 μg/L, respectively. Subsequently the difference of these two values give the URNP Zn concentration of 5.3 μg/L. The distribution in the Zn mass concentration of these three fractions across the watershed is shown in **Figure 4** (**Supplementary Table S3**).

Settling experiments were an attempt to examine Zn that might be present as ZnO (density = 5.61 g/cm^3) and as zinc-associated with mineral matter (density = 2.65 g/cm^3). Integration of Zn counts obtained by spICP-QMS for the settling experiments provided the mass concentrations of Zn (μg/L) in each of three fractions that were defined as particulate (i.e., subject to settling), colloidal (i.e., non-settleable), and dissolved (0.02 μm filtrate). Subtraction of the integrated Zn counts measured after settling from that of the raw sample was used to compute the particulate fraction. Likewise, subtraction of the integrated Zn counts for the 0.02 μm filtered sample from the counts for the sample after settling yields a colloidal fraction.

Figure 5A provides an example of this categorization for the mass concentration (μg/L) as well as the effect on the mean particle size determination, details provided in subsequent discussion of particle characterization. The distribution of these fractions across the watershed is shown in **Figure 6** (**Supplementary Table S4**).

Multiple Element, spICP-TOFMS Results

Results of the spICP-TOFMS analysis of samples collected from across the basin are presented as pie charts (**Figure 7**) with orange to represent particles that contained no detectable element other than Zn and blue as particles containing elements in addition to Zn, with Fe, Mn, Al, and Si being the other detected elements. The numerical values of detected events of ^{64}Zn in these two classes are also displayed in **Figure 7**.

Zn nanoparticles detected across all sites are represented in **Figure 8A** by the percent mass of Zn of which they are composed. Particles were detected primarily in two categories: those composed of high (>95%) and very low (<5%) proportions of Zn mass. With ICP-TOFMS we can use the observed elemental

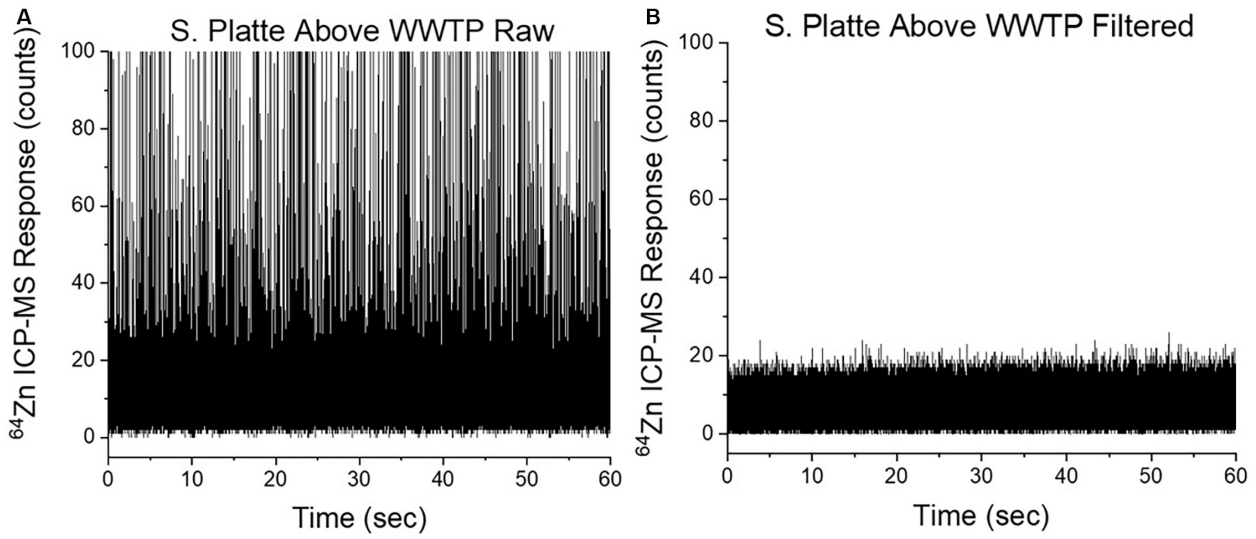

FIGURE 3 | (A) Raw spICP-MS spectrum of unfiltered Zn particles for sampling site above the wastewater treatment plant, **(B)** Raw spICP-MS spectrum of 0.02 μm filtered sample collected from the South Platte River above the wastewater treatment plant.

associations to make better estimates of overall particle size. Although the mineralogy is not known, it is a reasonable assumption that the Zn-only particles (>95%) present in fully oxygenated surface waters are ZnO. To approximate the size of the particles containing multiple elements (<5% and 5–95%) we converted the elements to their oxides (i.e., Al_2O_3, SiO_2, MnO_2, Fe_2O_3, and ZnO), calculated a volume for each oxide from the mass and density, summed the volumes of all oxides present in the particle and computed an average spherical size (**Figure 8B**). To examine spatial differences, the average and variation (box and whiskers plots) of particle diameters from each sample location were computed (**Figure 9**). Diameters were calculated assuming all Zn is present as ZnO (**Figure 9A**), as would be done for single element spICP-MS, and using the sum of the metal oxide mass, obtained by spICP-TOFMS (**Figure 9B**).

DISCUSSION

General Water Chemistry

Total Recoverable Metals and Turbidity Across Watershed

The TR metals concentrations (**Table 1**) varied little across the watershed, but for two notable exceptions. Elevated levels of Si, Al and Fe (2–5×) were found in samples from both Sand Creek sites as compared to all other sampling sites. This observation correlated with a higher turbidity measured at these two sites (East, 258 FAU; West, and 170 FAU), suggesting that these elements are present largely as part of the total suspended sediments. TR concentrations of each metal show strong correlations ($0.94 < R^2$) with turbidity (ESI **Figure 2**), consistent with their abundance in earth materials and their low solubility in neutral waters. TR Zn shows a weaker relationship to turbidity, but there are several observations that bear further examination. The West Clear Creek site has a high TR Zn concentration (0.068 mg/L) but a low turbidity (7 FAU), which could be attributed to dissolved Zn from mining inputs upstream of the watershed. Most of the urban waters have a moderate correlation (R^2 = 0.66) between these two parameters, if both sand creek sites are also excluded. These two sites show a combination of high TR Zn and turbidity, but the ratio of these two parameters is lower than for the other urban sites. This observation suggests that the high total suspended solids in Sand creek contains some amount of Zn, but not at the level seen in the other urban waters. The severe rainfall event on July 15th, 2018 (ESI **Figure 1**), which was more evident on the east side of the urban area, most likely mobilized sediment leading to the high measured turbidity. Although not investigated, we note that the central urban sites appear to have the higher levels of both sulfate and chloride, likely indicating generally poorer water quality than WClC, a less urbanized upstream site.

Settling Results for Mass Concentrations (Particulate, Colloidal, Dissolved)

A comparison of background dissolved Zn concentrations measured by spICP-MS is presented for the raw, settled, and 0.02 μm filtered samples (**Table 2**). The 0.02 μm sample approximates the truly dissolved fraction of Zn, as filtration removes all but the smallest of particulates. Differences in the Zn baseline between the raw and settled samples suggest that particles with low Zn mass (**Figure 2B**) are being removed by settling (**Table 2**). The total amount of Zn present in the settleable particulate fraction (**Figure 6** and **Supplementary Table S4**) varied anywhere from 15–83% of the total Zn across the watershed. The highest absolute particulate mass concentrations were found in Sand Creek (ESC, 6.4 μg/L; WSC, 6.7 μg/L, **Supplementary Table S3**). Sand creek also had the highest turbidity values and high TR Zn, suggesting that Zn

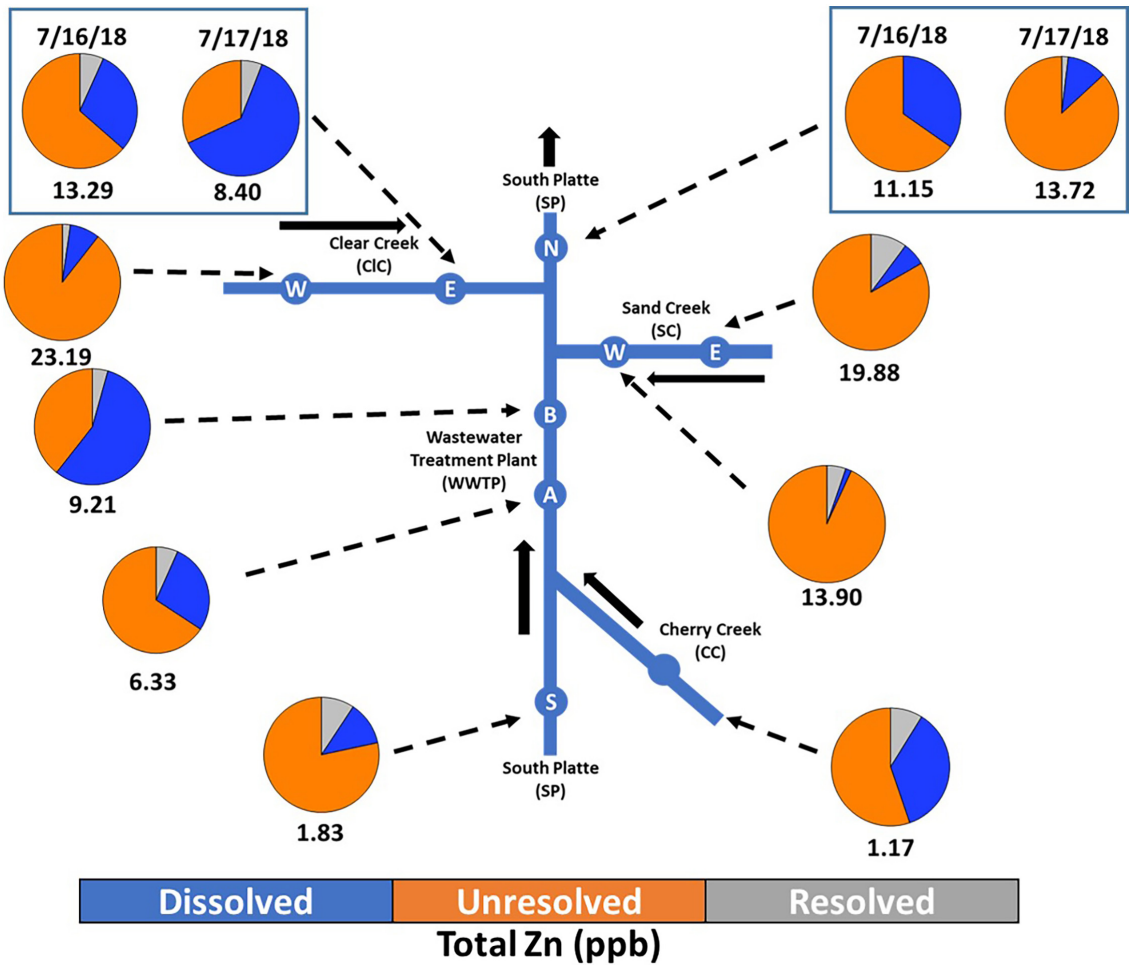

FIGURE 4 | Distribution of resolved, dissolved, and non-resolved zinc species at the various sampling locations. Bolded numbers represent total zinc concentrations in μg/L. N, S, E, and W represent the cardinal directions where "A" and "B" represent above and below the Wastewater Treatment plant, respectively.

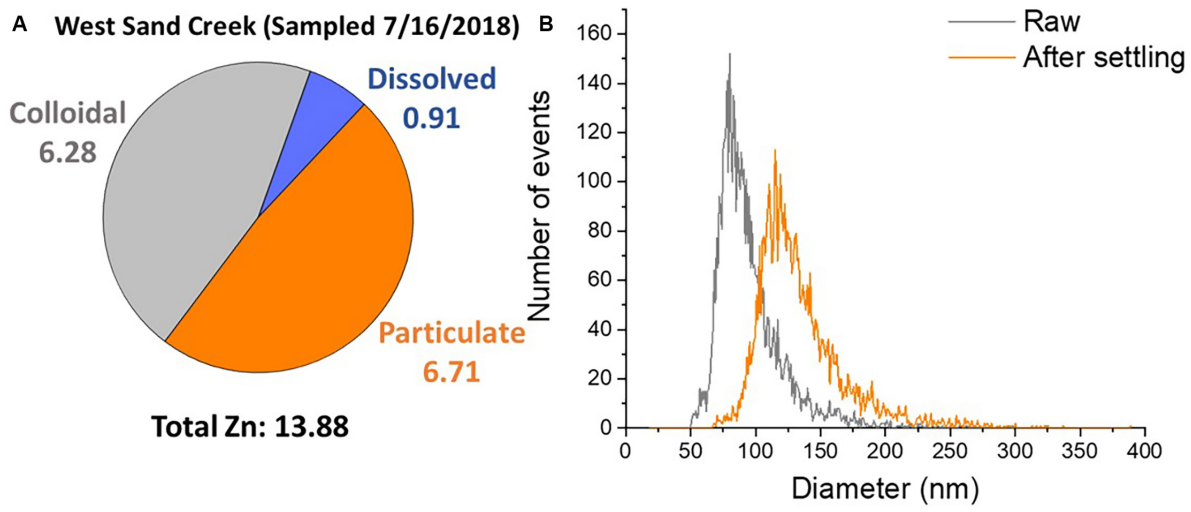

FIGURE 5 | (A) Distribution of zinc species in West sand creek (7/16/2018), concentrations in ppb, **(B)** Size distribution of raw vs. settled detected zinc events computed using ZnO density = 5.61 and a spherical geometry.

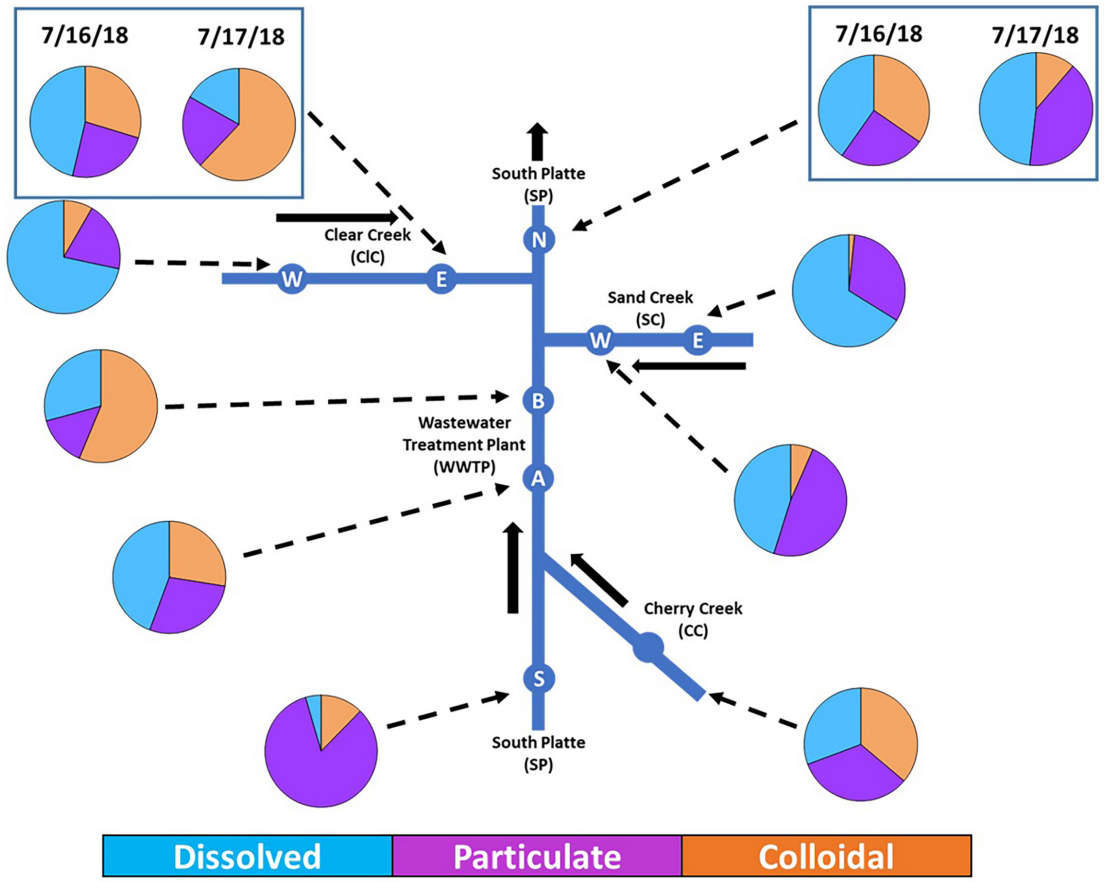

FIGURE 6 | Distribution of zinc speciation obtained by settling and 0.02 μm filtration across the watershed. N, S, E, and W represent the cardinal directions where "A" and "B" represent above and below the Wastewater Treatment plant, respectively.

may be present adsorbed to larger sediment particles. This is corroborated by the high concentrations of settleable Zn. As noted previously the ratio of Zn to turbidity is lowest for Sand Creek, perhaps reflecting the transport of sediment from the less-urbanized eastern side of the watershed.

The colloidal portion of the total Zn (**Figure 6**) varied greatly across the watershed from 5–72% with the highest concentrations in West Clear Creek and East Sand Creek (WClC, 16.62 μg/L; ESC 13.15 μg/L). Although the particulate and colloidal fractions form a higher proportion of the total Zn contributed by southern tributaries (SSP, CC), the higher absolute values of total Zn from the western and eastern inputs (WClC, WSC/ESC) makes these the significant sources of particulate Zn.

Particle Analysis (spICP-QMS)

Integrated Zn Mass Concentration Across Watershed (Recovery Compared to TR)

The percent recovery of Zn, defined as the total concentration measured by spICP-MS divided by the TR concentration measured by ICP-OES, varied from 20–38% with a mean of 28% across the watershed (**Table 1**). The low percent recovery measured for the spICP-MS could be attributed to Zn contained in particles larger than what can be measured by the ICP-MS. The maximum size limit for the sp-ICP-MS is based on both the need to avoid clogging of the nebulizer and the maximum-sized particle that can be completely transported through the spray chamber and ablated by the plasma. A study of silica nanoparticles in spICP-MS suggests that the maximum ablation size is upwards of 1200 nm (Olesik and Gray, 2012; Montano et al., 2016). Analysis of TR metal requires sample acidification, which liberates an indeterminate amount of the Zn contained in these larger particles, resulting in the higher TR Zn concentrations. As was previously noted, settled sediments were observed after acid digestion in some cases, especially the Sand Creek samples. Since the focus of this study is the nanoparticulate fraction, the low recovery is not of great concern but highlights that larger sediments need consideration if particulate-associated metal transport is of concern.

Resolved vs Unresolved Mass Concentration

Additional fractionation was performed to gain more insights into the speciation of colloidal/NP Zn. One such analysis was to measure the dissolved Zn concentration in 0.02 μm filtered samples. It was hypothesized that the Zn baseline "dissolved"

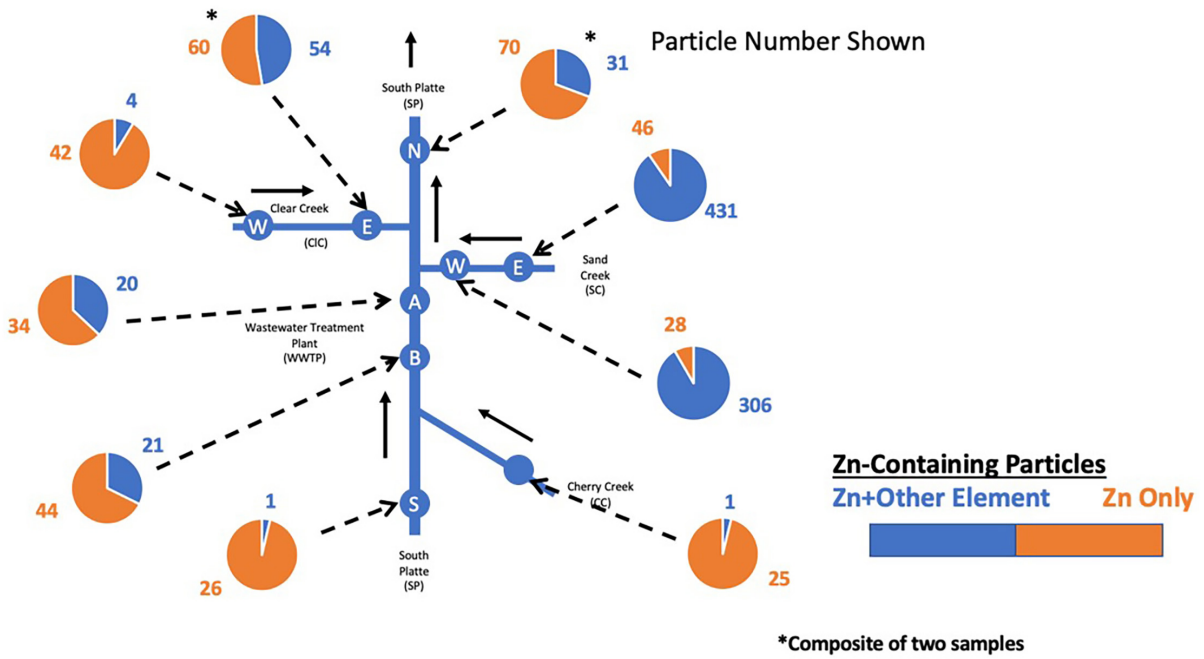

FIGURE 7 | Distribution of zinc species at different sampling sites as determined by spICP-TOFMS. Numbers represent the number of particles detected in 180 s of data collection.

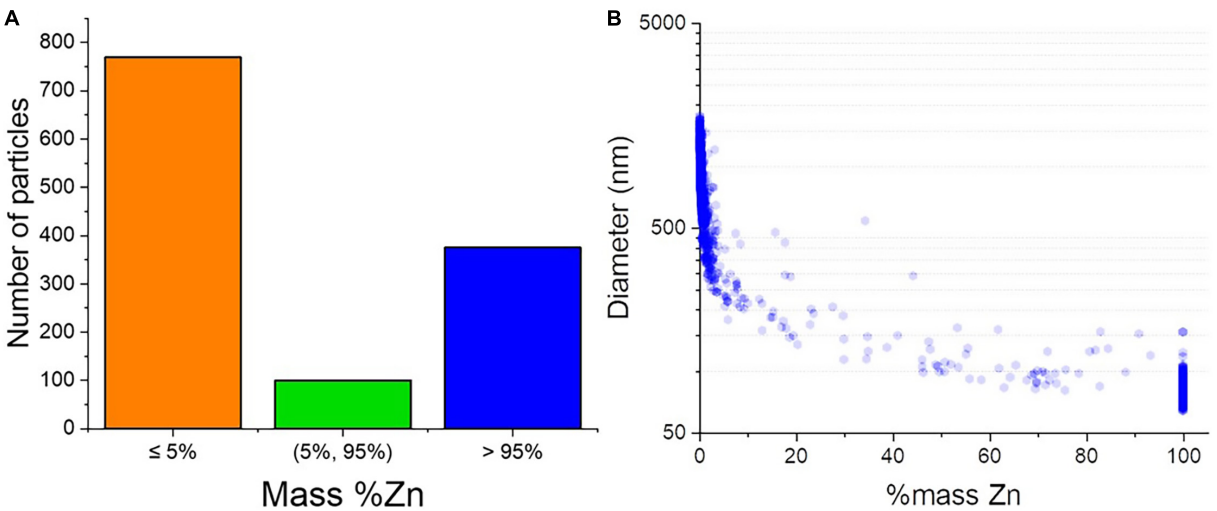

FIGURE 8 | (A) Number of particles detected defined by mass percent zinc, **(B)** Spherical diameters as related to the mass percent of zinc, and computed by summing of all elements converted to oxides.

signal, obtained for raw samples, contained a large fraction of colloidal Zn that was not massive enough to exceed the size detection limit required to be registered as a particle. Filtration was chosen over dilution for examining this size fraction, as dilution may cause dissolution and/or disaggregation of particles, resulting in artificial changes to the mass distributions (Baalousha, 2009). Although the amount of "dissolved" Zn (i.e., baseline concentration of raw samples) was greatly reduced through filtration, the 0.02 μm filtered samples still had particles roughly 50–60 nm in mean diameter suggesting that some particles can still pass. This may also be a consequence of non-spherical shapes passing through the filter. Moreover, these particle detections may also be false positives due to their proximity to the size detection limit (45 nm) (Lee et al., 2014). Though particle information (i.e., size and number) cannot be obtained for the URNP fraction in this approach, it does provide insight into the mass concentration. Characterization of this URNP fraction of Zn is important as these small particles

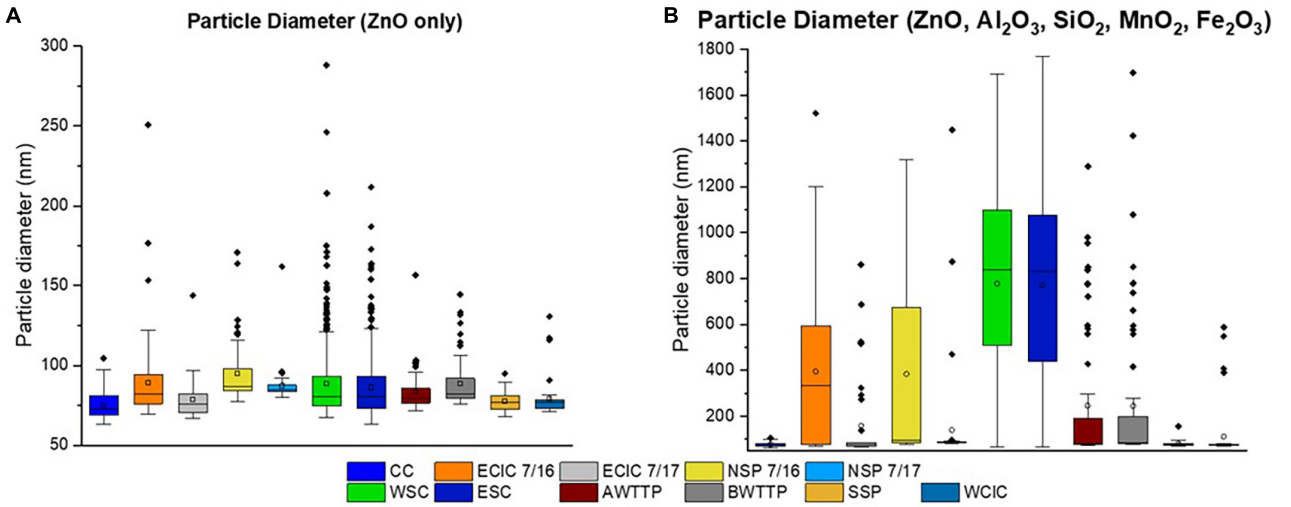

FIGURE 9 | (A) Particle diameters of zinc-containing particles at different sites if only ZnO is considered, **(B)** Particle diameters at different sites if all elements measured by spICP-TOFMS are considered and converted to oxides.

may possess nano-characteristics (high specific surface area, bioavailability) different than their ionic and suspended sediment counterparts (Nel et al., 2006, 2009). Across the watershed these unresolved fractions represent greater than 50% of the Zn mass concentration (**Figure 4**), highlighting the importance of the smaller size fraction of NPs. Based on these results, more studies comparing filtration and dilution as fractionation techniques to better resolve the smallest NPs might provide a deeper understanding of nanomaterial transport and potential ecotoxicological risk.

Particle Number, Particle Mass Concentration, and Particle Mass (Size) Distributions

Across the South Platte Watershed, the number concentrations of Zn-containing particles measured by spICP-QMS were all within an order of magnitude (~60,000–220,000 particles/mL) with no higher particle numbers measured in the South Platte as compared to its tributaries (**Figure 2A**). Included in the data is a number concentration recorded for the NSP sample collected on 7/16/18 that is not in agreement with the sample collected on 7/18/18 or consistent with the value for the total Zn in the 7/16/18 sample. This result is considered an error particle counting but does not affect the integrated mass concentrations (i.e., Zn counts). The highest number concentration was observed in the Sand Creek samples, consistent with the high turbidity measured for these samples. Mean particle Zn mass (**Figure 2B**) across all sites was within an order of magnitude (1–10 fg Zn/particle). Overall, the lack of increase in the NP number concentration or variation in NP Zn mass as the South Platte flows through the urban corridor suggests either no substantial anthropogenic contribution of resolvable Zn NPs or that these measures are insensitive to urban impacts.

One notable trend is that the total Zn mass concentrations (**Figure 4**) were lower in the southern inputs to the South Platte (CC and SSP) compared to the urban sites downstream (AWWTP, BWTTP, and NSP). The higher Zn mass concentrations in all three fractions (dissolved, unresolved, and resolved particles) in the downstream sites suggest that the urban environment is contributing Zn to the watershed. Both SSP and CC have a significant water impoundment upstream of them, Chatfield and Cherry Creek Reservoirs, respectively. These reservoirs likely act as a settling basin for particulate and sediment, reducing the background of NNP and increasing the magnitude of the urban effect. Chatfield Reservoir sits on the southwestern edge of the urbanized Denver metro area and thus could be expected to act as a settling basin for NNP but have little effect on anthropogenic or natural particles added to the watershed by the city itself. Among potential INPs, tire wear particles (Dahl et al., 2006; Klöckner et al., 2019) and brake dust (Adachi and Tainosho, 2004) are two likely sources of Zn particles in an urban watershed; as their presence in areas adjacent to roadways has been well-documented in soil, air and stormwater (Baalousha et al., 2016). The Sand Creek site produced two samples with high Zn mass concentrations, which were principally contained in the resolved and unresolved particle fractions. Examination of the hydrographs around the watershed (**Supplementary Figure S1**) shows that the rain event on July 15th. 2018 had considerable impact on Sand Creek. Flow increased by seven-fold from the event and this was the largest increase in flow of any South Platte tributary proportional to base flow. The increase in Zn particles, both resolved and non-resolved (**Figure 4**), could possibly thus be attributed to the rainfall pattern and the high volume of rainwater washing particles into Sand Creek and resuspending bed sediment. West Clear Creek is another tributary where high amounts of resolved and non-resolved Zn particles were observed (**Figure 4**) and these particles may be the result of widespread abandoned metal sulfide mines in the upper Clear Creek watershed (Butler, 2009).

Although the study focuses on the variation in concentration (mass and number) and chemical characteristics of Zn-containing particles within the urban watershed, it is useful to examine other information obtained by spICP-QMS, namely the particle mass (i.e., size) distributions (SI **Figure 3**). The lack of particles detected at small sizes (**Figure 5B**, computed for this example using a density of ZnO, 5.61 g/cm^3), despite the limit of detection being an ample distance below the mean measured size, resulted in size distributions that appear approximately gaussian. With high dissolved Zn backgrounds, smaller particles that register close to the average background can be obscured. However, in these data sets the dissolved background does not fully account for the absence of smaller NPs. For example, based on the instrumental noise and the dissolved background, for East Sand Creek, the limit of detection is estimated to be 55 nm, well below the leading edge of the particle distribution at roughly 77 nm (**Figure 5B**). Whether the measured particle size distributions are abnormal for this type of analysis is an open question. Pareto's law suggests that particle distributions in the environment should follow a power law relationship between size and number, namely as particles get smaller, their number should exponentially increase (Walther et al., 2006). Numerous studies have found that observed particle distributions can follow this law, (Baur et al., 2020) display a Poisson distribution (Dahl et al., 2006; Hadioui et al., 2015), or even be bimodal (Lin et al., 2005). These studies highlight many possible causes to explain distributions not following Pareto's law include influence of the type of sample (sediment vs. aqueous) or particle source (road wear vs. atmospheric). Thus, the lack of an observed monotonically decreasing number-based size distribution may arise from real effects or from analytical artifacts. ENP may not behave according to Pareto's law in that they are manufactured and perhaps introduced into the environment with a more defined size distribution. Natural processes such as weathering, that produce NP, could adhere to the law more closely as nanoparticles are not the starting material but a product of a bulk transformation. Another analytical explanation for the observed particle size distributions is that although NPs may be present in the "gap" between the DL and the maximum of the distribution, random variation in NP-generated signal results in their partial undercounting when close to the background noise level (i.e., some particle generate counts below the 3σ size DL). Regardless of cause, for very polydisperse natural samples, the counting statistics obtained in this study may not be sufficient to draw a conclusion regarding the distribution shape. Previous studies (Laborda et al., 2013) have suggested that 10^5 particles counted are necessary for a firm conclusion about particle size and have found a 3–10% variation in measured sizes. These are valid concerns that must be addressed in future field-based studies of NP size distributions.

Settling Particle Results (Number, Size, Background/Dissolved)

In addition to filtration, settling experiments were a means of discerning more about the speciation of Zn particles present in the resolved (RP) and unresolved URNP fractions. **Figure 5A** compares the distribution of particle masses for the settled and raw samples of West Sand Creek (7/16/18). Both raw and settled samples had approximately the same number of particles (Raw, 4482 particles; Settled, 4820 particles) but their mean diameter was different (Raw, 134 nm; Settled, 103 nm). In the time-frame used, the 100–200 nm particle distribution (**Figure 5B**) should not have been affected if particles were zinc metal or ZnO. Background Zn concentrations for the raw and settled samples were 13.90 and 7.19 ppb, respectively, with a dissolved Zn concentration for the site (0.02 μm filtered sample) was 0.91 ppb. It is apparent from the decrease in mean particle diameter and background Zn concentration in the settled sample, that settling removed Zn from solution even though the resolved Zn particles in the raw sample had a size distribution well below the calculated settleable size. A likely explanation is that part of the Zn measured in the raw sample is associated (either adsorbed or as a minor component) of larger minerals and hetero-aggregates. These larger particles containing low amounts of Zn could avoid detection as a resolvable Zn particle by the spICP-QMS. Thus, their absence from solution would be noted by a decrease in the background Zn concentration. This approach allows one to use spICP-QMS to gather more indirect evidence on the nature of metal-containing NPs but also leads direct to the obvious need for multi-element NP analysis.

Particle Analysis (spICP-TOFMS)

Given the varying morphologies and speciation of Zn, spICP-TOFMS was employed to quantify multiple elements within each particle (**Figure 7**). One inherent advantage of the ICP-TOFMS is the ability to distinguish between particles composed only of Zn (as the cation) and those that contain additional elements (excluding O, S, and other non-ionizable elements). This distinction is important in attempting to separate particles of anthropogenic origin from those of natural origin. Anthropogenic particles (i.e., tire wear, ENPs) are more likely to contain Zn as the only or primary metallic element. NNP with adsorbed Zn would contain other elements at amounts above that of Zn. Similarly, mineral NPs containing Zn within their lattice and hetero-aggregates of Zn-NPs and NNPs would also have some proportion of Zn but are likely to be principally composed of other elements.

It is important to note that fewer particles were counted by spICP-TOFMS, amounting to 10–20% that of the quadrupole instrument (**Figure 7**). Due to the difference in dwell times between the quadrupole and TOF instruments, 0.1 and 3 ms, respectively, considerable dilution for the TOF experiments was necessary to avoid coincidence of particles within one dwell time. The 1:1000 dilution used in these experiments for the TOF measurements is the most likely cause of the low particle numbers detected by the TOF, however, instrument sensitivity differences are also a possible cause. Data acquisition over a longer time period could be used to offset dilution differences and thus generate a comparable number of particles for both techniques.

Across all sites, similar average masses of Zn per particle were found in the Zn-only particles. Converting these masses to diameters, and assuming all the Zn is present as spherical ZnO NPs (**Figure 9A**), these particles were roughly 80 nm

in diameter, most values falling within 20 nm of this average value. We obtained a similar result for all Zn-containing NP when using an ICP-QMS, which provides only a single element analysis, concluding that the measured Zn NPs are relatively similar in size and composition across the South Platte watershed. However, with a TOF detector we can consider the other elements present in each particle, in this case Fe, Mn, Al, and Si, which imply a more complex mineralogy for the Zn-containing particles. Mineral particles can promote adsorption, particularly the common metal oxides (Fe, Mn; Trivedi and Axe, 2000), and aluminosilicate clays (Al, Si) (Sheikhhosseini et al., 2013). Converting the mass of each element to an oxide (Fe_2O_3, MnO_2, SiO_2, and Al_2O_3), assuming a density and spherical geometry, and combining them with mass of ZnO from the previous figure, we can approximate a more likely size of the particles (**Figure 9B**). It should be noted that some of these sizes are approaching the theoretical upper limit for spICP-MS, and thus might be underrepresenting the largest of the particle sizes. Plotting all particles by total oxide equivalent spherical size vs %m Zn (**Figure 8B**), we find a clear relationship with low % zinc being uniformly large (200–1000 nm) and high % zinc being uniformly small (60–100 nm).

The disconnect between the ZnO-only particle size and the particle size where all five elements are considered allows us to tease out differences in Zn particle speciation. Zn-containing particles where the Zn is adsorbed or hetero-agglomerated should show a large deviation between the particle radii calculated when considering ZnO only vs all five elements. It is expected that the Zn-adsorbed/aggregated particles would primarily be composed of other elements besides Zn and thus have only a small proportion of the total mass as Zn. This bears out for the size distributions of sampling sites such as Sand Creek, East Clear Creek and North South Platte (7/16/18), where the ZnO-only radius is much smaller than the radius of particles where all elements were considered (**Figures 9A,B**). For Sand Creek, the higher proportion of Zn possibly contained as an adsorbate also supports the settling experiments utilizing the ICP-QMS. A high proportion of the Zn particles present in the Sand Creek samples could thus be classified as sediment particles with adsorbed Zn. Conversely, the small difference between Zn-only and multi-element particle size (**Figures 9A,B**) suggest that NPs primarily composed of Zn dominated other locations along the South Platte such as the wastewater treatment plant sites (AWTTP, BWTTP). This may be some indication of a greater anthropogenic contribution.

Separating particles based on the percentage of their % Zn mass also allowed for better speciation of the particle-associated Zn in a sample. The different chemical properties of nanoparticulate Zn as compared to dissolved metal ions or adsorbed Zn is well known. ZnO and other metal oxide nanoparticles are potent reactive oxygen species generators and have ecotoxicity characteristics distinct from the dissolved forms of the metals (Xia et al., 2008). Adsorption of heavy metals to nanoparticles is an important component of many biogeochemical cycles and identifying the prevalence of adsorbed metal can be a boon to modeling and environmental remediation (Hochella et al., 2005).

Dissolution studies have shown ZnO can be soluble (7–16 mg/mL; Franklin et al., 2007; Reed et al., 2012a; Domingos et al., 2013; Ma et al., 2013) at the pH values expected for these surface waters (pH 7-8). However, ZnO dissolution can be affected by inorganic factors including water hardness (Reed et al., 2012b), and pH (Miao et al., 2010; Domingos et al., 2013) or organic species such as fulvic acids, NOM (Domingos et al., 2013) or protein (Moreau et al., 2007). Also, ZnO may compose up to 1% by weight of the total tire mass (Milani et al., 2004) and ZnO particles from tire wear may be embedded in rubber, protecting them from solubilization. ZnO may also be protected from dissolution by being coated by a less soluble Zn mineral such as $ZnCO_3$ (Reed et al., 2012b). Based on the host of factors that can affect ZnO particle dissolution, it seems highly possible that ZnO NP could be present in natural waters.

Future studies might be improved by including transmission electron microscopy (TEM) or scanning electron microscopy (SEM) to identify the chemical speciation of Zn particles be they ZnO, ZnS, $ZnCO_3$, or a more exotic metal compound. However, the ppb levels, which results in low particle numbers, make observing these particles by EM very difficult. Other particle characterization techniques, such as FFF, might also provide valuable information by providing an additional means by which to verify the size of the particles whilst characterizing their elemental composition. Employing fraction collection of the FFF eluent would also permit additional characterization by spICP-MS (Kly et al., 2020). The identification of the exact Zn particle mineralogy could also aid in determination of their origin and determining a truer particle size. Similarly, Fe, Mn, Al, and Si were assumed to be oxides for the purposes of calculating a particle size. This assumption was made for simplicity sake but does not reflect the probability that these elements are most likely present as a variety of aluminosilicate minerals. More detailed analysis of the mineralogy present in these samples would allow for more accurate representations of particle size where these elements are considered, although determining the association of Zn with the observed minerals is problematic at the low (<5%) Zn contents observed in these waters.

CONCLUSION

By utilizing sp-ICP-MS, using both a quadrupole and a time-of-flight detector, the NP populations present in an urban watershed could be more fully characterized. The unique use of settling and filtration experiments combined with an ICP-QMS provided further speciation of metal-containing particles using single element data. ICP-TOFMS analysis provided invaluable insights into the elemental abundances (i.e., mineralogy) present on a particle-by-particle basis. The totality of these analyses allows for the further speciation of metal-containing particles into particles composed completely of a given metal, and those with the metal adsorbed to, or incorporated within, colloidal mineral matter. This survey of the South Platte watershed found that Zn-only particles were more abundant in the central, more urbanized parts of the watershed, suggesting, but not confirming, anthropogenic origin. ZnO nanoparticles from tire wear particles

were hypothesized, but not investigated, as the most likely source. If regulation is in the future for nanomaterial emissions, the ability to distinguish between particle types will be invaluable. Most significantly, the study demonstrates that multi-elemental information, provided by an ICP-TOFMS, may form the future basis for developing the field of particle-by-particle geology, utilizing each particles elemental composition. Furthermore, a variety of different information about metal speciation can be derived from the application of settling and filtration as fractionation tools prior to ICP-QMS analysis.

DATA AVAILABILITY STATEMENT

The raw data supporting the conclusions of this article will be made available upon request by the authors, without undue reservation, to any qualified researcher.

AUTHOR CONTRIBUTIONS

SB, MM, and JR equally contributed to the writing of this manuscript. SB and LR performed sampling, filtration and settling experiments, and ICP-QMS measurements under the direction of JR. MM performed the spICP-TOFMS experiments and measurements under the guidance of TH and FK. All authors contributed to the article and approved the submitted version.

FUNDING

The authors would like to acknowledge funding from the National Science Foundation (NSF-CBET 1512695) and from the European Union Horizon 2020 project ACEnano (Grant Agreement No. 720952).

ACKNOWLEDGMENTS

The authors would like to acknowledge the contributions of Sara El-Youbi (University of Vienna) and Katie Challis (Colorado School of Mines) for their assistance in the sample preparation for ICP-MS measurements and Star Summer (Western Washington University) for assistance in data processing. The authors would also like to thank Drs. Olga Borovinskaya and Martin Tanner (tofWERK) for their assistance regarding any software and maintenance issues relating to the icpTOF 2R. Watershed graphics provided by Karoline Lambert (University of Colorado).

SUPPLEMENTARY MATERIAL

The Supplementary Material for this article can be found online at: https://www.frontiersin.org/articles/10.3389/fenvs.2020.00084/full#supplementary-material

REFERENCES

Adachi, K., and Tainosho, Y. (2004). Characterization of heavy metal particles embedded in tire dust. *Environ. Int.* 30, 1009–1017. doi: 10.1016/j.envint.2004.04.004

Baalousha, M. (2009). Aggregation and disaggregation of iron oxide nanoparticles: influence of particle concentration, pH and natural organic matter. *Sci. Total Environ.* 407, 2093–2101. doi: 10.1016/j.scitotenv.2008.11.022

Baalousha, M., Yang, Y., Vance, M. E., Colman, B. P., McNeal, S., Xu, J., et al. (2016). Outdoor urban nanomaterials: the emergence of a new, integrated, and critical field of study. *Sci. Total Environ.* 557, 740–753. doi: 10.1016/j.scitotenv.2016.03.132

Baur, S., Reemtsma, T., Stärk, H.-J., and Wagner, S. (2020). Surfactant assisted extraction of incidental nanoparticles from road runoff sediment and their characterization by single particle-ICP-MS. *Chemosphere* 246, 125765. doi: 10.1016/j.chemosphere.2019.125765

Borovinskaya, O., Hattendorf, B., Tanner, M., Gschwind, S., and Gunther, D. (2013). A prototype of a new inductively coupled plasma time-of-flight mass spectrometer providing temporally resolved, multi-element detection of short signals generated by single particles and droplets. *J. Anal. Atomic Spectrom.* 28, 226–233. doi: 10.1039/c2ja30227f

Butler, B. A. (2009). Effect of pH, ionic strength, dissolved organic carbon, time, and particle size on metals release from mine drainage impacted streambed sediments. *Water Res.* 43, 1392–1402. doi: 10.1016/j.watres.2008.12.009

Councell, T. B., Duckenfield, K. U., Landa, E. R., and Callender, E. (2004). Tire-wear particles as a source of zinc to the environment. *Environ. Sci. Technol.* 38, 4206–4214. doi: 10.1021/es034631f

Dahl, A., Gharibi, A., Swietlicki, E., Gudmundsson, A., Bohgard, M., Ljungman, A., et al. (2006). Traffic-generated emissions of ultrafine particles from pavement–tire interface. *Atmosp. Environ.* 40, 1314–1323. doi: 10.1016/j.atmosenv.2005.10.029

DeForest, D. K., and Van Genderen, E. J. (2012). Application of US EPA guidelines in a bioavailability-based assessment of ambient water quality criteria for zinc in freshwater. *Environ. Toxicol. Chem.* 31, 1264–1272. doi: 10.1002/etc.1810

Domingos, R. F., Rafiei, Z., Monteiro, C. E., Khan, M. A., and Wilkinson, K. J. (2013). Agglomeration and dissolution of zinc oxide nanoparticles: role of pH, ionic strength and fulvic acid. *Environ. Chem.* 10, 306–312.

Erhardt, T., Jensen, C. M., Borovinskaya, O., and Fischer, H. (2019). Single particle characterization and total elemental concentration measurements in polar ice using continuous flow analysis-inductively coupled plasma time-of-flight mass spectrometry. *Environ. Sci. Technol.* 53, 13275–13283. doi: 10.1021/acs.est.9b03886

Ermolin, M., Fedotov, P., Ivaneev, A., Karandashev, V., Fedyunina, N., and Eskina, V. (2017). Isolation and quantitative analysis of road dust nanoparticles. *J. Anal. Chem.* 72, 520–532. doi: 10.1134/s1061934817050057

Franklin, N. M., Rogers, N. J., Apte, S. C., Batley, G. E., Gadd, G. E., and Casey, P. S. (2007). Comparative toxicity of nanoparticulate ZnO, bulk ZnO, and ZnCl2 to a freshwater microalga (Pseudokirchneriella subcapitata): the importance of particle solubility. *Environ. Sci. Technol.* 41, 8484–8490. doi: 10.1021/es071445r

Fréchette-Viens, L., Hadioui, M., and Wilkinson, K. J. (2019). Quantification of ZnO nanoparticles and other Zn containing colloids in natural waters using a high sensitivity single particle ICP-MS. *Talanta* 200, 156–162. doi: 10.1016/j.talanta.2019.03.041

Furtado, L. M., Hoque, M. E., Mitrano, D. F., Ranville, J. F., Cheever, B., Frost, P. C., et al. (2014). The persistence and transformation of silver nanoparticles in littoral lake mesocosms monitored using various analytical techniques. *Environ. Chem.* 11, 419–430. doi: 10.1071/En14064

Giese, B., Klaessig, F., Park, B., Kaegi, R., Steinfeldt, M., Wigger, H., et al. (2018). Risks, release and concentrations of engineered nanomaterial in the environment. *Sci. Rep.* 8, 1–18.

Gondikas, A., von der Kammer, F., Kaegi, R., Borovinskaya, O., Neubauer, E., Navratilova, J., et al. (2018). Where is the nano? Analytical approaches for the detection and quantification of TiO 2 engineered nanoparticles in surface waters. *Environ. Sci. Nano* 5, 313–326. doi: 10.1039/c7en00952f

Gondikas, A. P., von der Kammer, F., Reed, R. B., Wagner, S., Ranville, J. F., and Hofmann, T. (2014). Release of TiO2 nanoparticles from sunscreens into surface waters: a one-year survey at the old danube Recreational Lake. *Environ. Sci. Technol.* 48, 5415–5422. doi: 10.1021/es405596y

Gonet, T., and Maher, B. A. (2019). Airborne, vehicle-derived fe-bearing nanoparticles in the urban environment: a review. *Environ. Sci. Technol.* 53, 9970–9991. doi: 10.1021/acs.est.9b01505

Gschwind, S., Flamigni, L., Koch, J., Borovinskaya, O., Groh, S., Niemax, K., et al. (2011). Capabilities of inductively coupled plasma mass spectrometry for the detection of nanoparticles carried by monodisperse microdroplets. *J. Anal. Atomic Spectrom.* 26, 1166–1174. doi: 10.1039/c0ja00249f

Hadioui, M., Merdzan, V., and Wilkinson, K. J. (2015). Detection and characterization of ZnO nanoparticles in surface and waste waters using single particle ICPMS. *Environ. Sci. Technol.* 49, 6141–6148. doi: 10.1021/acs.est.5b00681

Hegetschweiler, A., Borovinskaya, O., Staudt, T., and Kraus, T. (2018). Single-particle mass spectrometry of titanium and niobium carbonitride precipitates in steels. *Anal. Chem.* 91, 943–950. doi: 10.1021/acs.analchem.8b04012

Hendren, C. O., Mesnard, X., Droge, J., and Wiesner, M. R. (2011). Estimating production data for five engineered nanomaterials as a basis for exposure assessment. *Environ. Sci. Technol.* 45, 2562–2569. doi: 10.1021/es103300g

Hendriks, L., Gundlach-Graham, A., Hattendorf, B., and Guther, D. (2017). Characterization of a new ICP-TOFMS instrument with continuous and discrete introduction of solutions. *J. Anal. Atom. Spectrom.* 32, 548–561. doi: 10.1039/c6ja00400h

Heringer, R. D., and Ranville, J. F. (2018). Gunshot residue (GSR) analysis by single particle inductively coupled plasma mass spectrometry (spICP-MS). *For. Sci. Int.* 288, e20–e25. doi: 10.1016/j.forsciint.2018.05.010

Herzog, B., Mongiat, S., Deshayes, C., Neuhaus, M., Sommer, K., and Mantler, A. (2002). In vivo and in vitro assessment of UVA protection by sunscreen formulations containing either butyl methoxy dibenzoyl methane, methylene bis-benzotriazolyl tetramethylbutylphenol, or microfine ZnO. *Int. J. Cosmetic Sci.* 24, 170–185. doi: 10.1046/j.1467-2494.2002.00137.x

Hochella, M. F. Jr., Lower, S. K., Maurice, P. A., Penn, R. L., Sahai, N., Sparks, D. L., et al. (2008). Nanominerals, mineral nanoparticles, and Earth systems. *Science* 319, 1631–1635. doi: 10.1126/science.1141134

Hochella, M. F. Jr., Moore, J. N., Putnis, C. V., Putnis, A., Kasama, T., and Eberl, D. D. (2005). Direct observation of heavy metal-mineral association from the clark fork river superfund complex: implications for metal transport and bioavailability. *Geochim. Cosmochim. Acta* 69, 1651–1663. doi: 10.1016/j.gca.2004.07.038

Hochella, M. F., Mogk, D. W., Ranville, J., Allen, I. C., Luther, G. W., Marr, L. C., et al. (2019). Natural, incidental, and engineered nanomaterials and their impacts on the Earth system. *Science* 363:eaau8299. doi: 10.1126/science.aau8299

Kaiser, J.-P., Zuin, S., and Wick, P. (2013). Is nanotechnology revolutionizing the paint and lacquer industry? A critical opinion. *Sci. Total Environ.* 442, 282–289. doi: 10.1016/j.scitotenv.2012.10.009

Klöckner, P., Reemtsma, T., Eisentraut, P., Braun, U., Ruhl, A. S., and Wagner, S. (2019). Tire and road wear particles in road environment–Quantification and assessment of particle dynamics by Zn determination after density separation. *Chemosphere* 222, 714–721. doi: 10.1016/j.chemosphere.2019.01.176

Kly, S., Moffitt, M., Rand, L., and Ranville, J. F. (2020). Coupling single particle ICP-MS with field-flow fractionation for characterizing metal nanoparticles contained in nanoplastic colloids. *Environ. Sci.* 43, 7277–7284.

Laborda, F., Bolea, E., and Jimenez-Lamana, J. (2014). Single particle inductively coupled plasma mass spectrometry: a powerful tool for nanoanalysis. *Anal. Chem.* 86, 2270–2278. doi: 10.1021/ac402980q

Laborda, F., Jimenez-Lamana, J., Bolea, E., and Castillo, J. R. (2013). Critical considerations for the determination of nanoparticle number concentrations, size and number size distributions by single particle ICP-MS. *J. Anal. Atomic Spectrom.* 28, 1220–1232. doi: 10.1039/c3ja50100k

Lamprea, K., Bressy, A., Mirande-Bret, C., Caupos, E., and Gromaire, M.-C. (2018). Alkylphenol and bisphenol A contamination of urban runoff: an evaluation of the emission potentials of various construction materials and automotive supplies. *Environ. Sci. Pollut. Res.* 25, 21887–21900. doi: 10.1007/s11356-018-2272-z

Lee, S., Bi, X., Reed, R. B., Ranville, J. F., Herckes, P., and Westerhoff, P. (2014). Nanoparticle size detection limits by single particle ICP-MS for 40 elements. *Environ. Sci. Technol.* 48, 10291–10300. doi: 10.1021/es502422v

Lin, C.-C., Chen, S.-J., Huang, K.-L., Hwang, W.-I., Chang-Chien, G.-P., and Lin, W.-Y. (2005). Characteristics of metals in nano/ultrafine/fine/coarse particles collected beside a heavily trafficked road. *Environ. Sci. Technol.* 39, 8113–8122. doi: 10.1021/es048182a

Ma, R., Levard, C., Michel, F. M., Brown, G. E. Jr., and Lowry, G. V. (2013). Sulfidation mechanism for zinc oxide nanoparticles and the effect of sulfidation on their solubility. *Environ. Sci. Technol.* 47, 2527–2534. doi: 10.1021/es3035347

Miao, A. J., Zhang, X. Y., Luo, Z., Chen, C. S., Chin, W. C., Santschi, P. H., et al. (2010). Zinc oxide–engineered nanoparticles: dissolution and toxicity to marine phytoplankton. *Environ. Toxicol. Chem.* 29, 2814–2822. doi: 10.1002/etc.340

Milani, M., Pucillo, F., Ballerini, M., Camatini, M., Gualtieri, M., and Martino, S. (2004). First evidence of tyre debris characterization at the nanoscale by focused ion beam. *Mater. Characteriz.* 52, 283–288.

Montaño, M. D., Badiei, H. R., Bazargan, S., and Ranville, J. (2014). Improvements in the detection and characterization of engineered nanoparticles using spICP-MS with microsecond dwell times. *Environ. Sci.* 1, 338–346. doi: 10.1039/c4en00058g

Montano, M. D., Olesik, J. W., Barber, A. G., Challis, K., and Ranville, J. F. (2016). Single Particle ICP-MS: advances toward routine analysis of nanomaterials. *Anal. Bioanal. Chem.* 408, 5053–5074. doi: 10.1007/s00216-016-9676-8

Montaño, M. D., von der Kammer, F., Cuss, C. W., and Ranville, J. F. (2019). Opportunities for examining the natural nanogeochemical environment using recent advances in nanoparticle analysis. *J. Anal. Atom. Spectrom.* 34, 1768–177. doi: 10.1039/c9ja00168a

Moreau, J. W., Weber, P. K., Martin, M. C., Gilbert, B., Hutcheon, I. D., and Banfield, J. F. (2007). Extracellular proteins limit the dispersal of biogenic nanoparticles. *Science* 316, 1600–1603. doi: 10.1126/science.1141064

Naasz, S., Weigel, S., Borovinskaya, O., Serva, A., Cascio, C., Undas, A. K., et al. (2018). Multi-element analysis of single nanoparticles by ICP-MS using quadrupole and time-of-flight technologies. *J. Anal. Atom. Spectrom.* 33, 835–845. doi: 10.1039/c7ja00399d

Nel, A., Xia, T., Madler, L., and Li, N. (2006). Toxic potential of materials at the nanolevel. *Science* 311, 622–627. doi: 10.1126/science.1114397

Nel, A. E., Madler, L., Velegol, D., Xia, T., Hoek, E. M., Somasundaran, P., et al. (2009). Understanding biophysicochemical interactions at the nano-bio interface. *Nat. Mater.* 8, 543–557. doi: 10.1038/nmat2442

Olesik, J. W., and Gray, P. J. (2012). Considerations for measurement of individual nanoparticles or microparticles by ICP-MS: determination of the number of particles and the analyte mass in each particle. *J. Anal. Atom. Spectrom.* 27, 1143–1155. doi: 10.1039/c2ja30073g

Osmond, M. J., and McCall, M. J. (2010). Zinc oxide nanoparticles in modern sunscreens: an analysis of potential exposure and hazard. *Nanotoxicology* 4, 15–41. doi: 10.3109/17435390903502028

Pace, H. E., Rogers, N. J., Jarolimek, C., Coleman, V. A., Higgins, C. P., and Ranville, J. F. (2011). Determining transport efficiency for the purpose of counting and sizing nanoparticles via single particle inductively coupled plasma mass spectrometry. *Anal. Chem.* 83, 9361–9369. doi: 10.1021/ac201952t

Piccinno, F., Gottschalk, F., Seeger, S., and Nowack, B. (2012). Industrial production quantities and uses of ten engineered nanomaterials in Europe and the world. *J.Nanopart. Res.* 14, 1–11. doi: 10.1007/s11051-012-1109-9

Plathe, K. L., von der Kammer, F., Hassellov, M., Moore, J., Murayama, M., Hofmann, T., et al. (2010). Using FlFFF and aTEM to determine trace metal-nanoparticle associations in riverbed sediment. *Environ. Chem.* 7, 82–93. doi: 10.1071/En09111

Praetorius, A., Gundlach-Graham, A., Goldberg, E., Fabienke, W., Navratilova, J., Gondikas, A., et al. (2017). Single-particle multi-element fingerprinting (spMEF) using inductively-coupled plasma time-of-flight mass spectrometry (ICP-TOFMS) to identify engineered nanoparticles against the elevated natural background in soils. *Environ. Sci. Nano* 4, 307–314. doi: 10.1039/c6en00455e

Reed, R. B., Higgins, C. P., Westerhoff, P., Tadjiki, S., and Ranville, J. F. (2012a). Overcoming challenges in analysis of polydisperse metal-containing nanoparticles by single particle inductively coupled plasma mass spectrometry. *J. Anal. Atom. Spectrom.* 27, 1093–1100. doi: 10.1039/c2ja30061c

Reed, R. B., Ladner, D. A., Higgins, C. P., Westerhoff, P., and Ranville, J. F. (2012b). Solubility of nano-zinc oxide in environmentally and biologically important matrices. *Environ. Toxicol. Chem.* 31, 93–99. doi: 10.1002/etc.708

Reed, R. B., Martin, D. P., Bednar, A. J., Montano, M. D., Westerhoff, P., and Ranville, J. F. (2017). Multi-day diurnal measurements of Ti-containing nanoparticle and organic sunscreen chemical release during recreational use of a natural surface water. *Environ. Sci. Nano* 4, 69–77. doi: 10.1039/c6en00283h

Sheikhhosseini, A., Shirvani, M., and Shariatmadari, H. (2013). Competitive sorption of nickel, cadmium, zinc and copper on palygorskite and sepiolite silicate clay minerals. *Geoderma* 192, 249–253. doi: 10.1016/j.geoderma.2012.07.013

Shuster, W. D., Bonta, J., Thurston, H., Warnemuende, E., and Smith, D. (2005). Impacts of impervious surface on watershed hydrology: a review. *Urban Water J.* 2, 263–275. doi: 10.1080/15730620500386529

Sommer, F., Dietze, V., Baum, A., Sauer, J., Gilge, S., Maschowski, C., et al. (2018). Tire abrasion as a major source of microplastics in the environment. *Aerosol Air Qual. Res.* 18, 2014–2028. doi: 10.4209/aaqr.2018.03.0099

Stolpe, B., Hassellov, M., Andersson, K., and Turner, D. R. (2005). High resolution ICPMS as an on-line detector for flow field-flow fractionation; multi-element determination of colloidal size distributions in a natural water sample. *Anal. Chim. Acta* 535, 109–121. doi: 10.1016/j.aca.2004.11.067

Sun, T. Y., Mitrano, D. M., Bornhöft, N. A., Scheringer, M., Hungerbühler, K., and Nowack, B. (2017). Envisioning nano release dynamics in a changing world: using dynamic probabilistic modeling to assess future environmental emissions of engineered nanomaterials. *Environ. Sci. Technol.* 51, 2854–2863. doi: 10.1021/acs.est.6b05702

Toor, G. S., Occhipinti, M. L., Yang, Y.-Y., Majcherek, T., Haver, D., and Oki, L. (2017). Managing urban runoff in residential neighborhoods: nitrogen and phosphorus in lawn irrigation driven runoff. *PLoS One* 12:e0179151. doi: 10.1371/journal.pone.0179151

Trivedi, P., and Axe, L. (2000). Modeling Cd and Zn sorption to hydrous metal oxides. *Environ. Sci. Technol.* 34, 2215–2223. doi: 10.1021/es991110c

United States Environmental Protection Agency [EPA] (1994). *Method 200.2: Sample Preparation Procedure for Spectrochemical Determination of Total Recoverable Elements*. Washington, DC: US Environmental Protection Agency.

Walther, C., Büchner, S., Filella, M., and Chanudet, V. (2006). Probing particle size distributions in natural surface waters from 15 nm to 2 μm by a combination of LIBD and single-particle counting. *J. Coll. Interface Sci.* 301, 532–537. doi: 10.1016/j.jcis.2006.05.039

Xia, T., Kovochich, M., Liong, M., Madler, L., Gilbert, B., Shi, H., et al. (2008). Comparison of the mechanism of toxicity of zinc oxide and cerium oxide nanoparticles based on dissolution and oxidative stress properties. *ACS Nano* 2, 2121–2134. doi: 10.1021/nn800511k

Yang, Y., Vance, M., Tou, F., Tiwari, A., Liu, M., and Hochella, M. F. (2016). Nanoparticles in road dust from impervious urban surfaces: distribution, identification, and environmental implications. *Environ. Sci. Nano* 3, 534–544. doi: 10.1039/c6en00056h

Young, A., Kochenkov, V., McIntyre, J. K., Stark, J. D., and Coffin, A. B. (2018). Urban stormwater runoff negatively impacts lateral line development in larval zebrafish and salmon embryos. *Sci. Rep.* 8, 1–14.

Zheng, Y., Mutzner, L., Ort, C., Kaegi, R., and Gottschalk, F. (2019). Modelling engineered nanomaterials in wet-weather discharges. *NanoImpact* 16:100188. doi: 10.1016/j.impact.2019.100188

Zuo, X., Fu, D., and Li, H. (2012). Speciation distribution and mass balance of copper and zinc in urban rain, sediments, and road runoff. *Environ. Sci. Pollut. Res.* 19, 4042–4048. doi: 10.1007/s11356-012-0907-z

Conflict of Interest: The authors declare that the research was conducted in the absence of any commercial or financial relationships that could be construed as a potential conflict of interest.

frontiers in Environmental Science

ORIGINAL RESEARCH
published: 26 June 2020
doi: 10.3389/fenvs.2020.00083

Synthetic Microfiber and Microbead Exposure and Retention Time in Model Aquatic Species Under Different Exposure Scenarios

Agathe Bour[1], Shahadat Hossain[1], Mark Taylor[2], Mark Sumner[2] and Bethanie Carney Almroth[1]*

[1] Department of Biological and Environmental Sciences, University of Gothenburg, Gothenburg, Sweden, [2] School of Design, University of Leeds, Leeds, United Kingdom

OPEN ACCESS

Edited by:
Denise M. Mitrano, Swiss Federal Institute of Aquatic Science and Technology, Switzerland

Reviewed by:
Alice Horton, University of Southampton, United Kingdom
Sinja Rist, Technical University of Denmark, Denmark
Gerardo Pulido-Reyes, Swiss Federal Institute of Aquatic Science and Technology, Switzerland

***Correspondence:**
Agathe Bour
agathe.bour@bioenv.gu.se

Specialty section:
This article was submitted to Biogeochemical Dynamics, a section of the journal Frontiers in Environmental Science

Received: *23 January 2020*
Accepted: *26 May 2020*
Published: *26 June 2020*

Citation:
Bour A, Hossain S, Taylor M, Sumner M and Carney Almroth B (2020) Synthetic Microfiber and Microbead Exposure and Retention Time in Model Aquatic Species Under Different Exposure Scenarios. Front. Environ. Sci. 8:83. doi: 10.3389/fenvs.2020.00083

Synthetic microfibers have been reported in most aquatic environments and represent a large proportion of environmental microplastics. However, they remain largely under-represented in microplastic ecotoxicity studies. The present study aims to investigate particle interaction with, and retention time in, aquatic organisms comparing microfibers, and microbeads. We used brine shrimp (*Artemia sp.*) and fish (*Gasterosteus aculeatus*) as invertebrate and vertebrate models, respectively. Organisms were exposed to a mixture of microbeads (polyethylene, 27–32 μm) and microfibers (dope dyed polyester; 500 μm-long) for 2 h, at high concentrations (100,000 part./L) in order to maximize organism-particles interaction. *Artemia* were exposed in the presence or absence of food. Fish were exposed either via the trophic route or directly via water, and water exposures were performed either in freshwater or seawater. In the absence of food, *Artemia* ingested high numbers of microbeads, retained in their digestive tract for up to 96 h. Microfiber ingestion was very limited, and its egestion was fast. In the presence of food, no microfiber was ingested, microbead ingestion was limited, and egestion was fast (48 h). Limited particle ingestion was observed in fish exposed via water, and particle retention time in gut did not exceed 48 h, both for direct and trophic exposure. However, water exposures resulted in a higher number of particles present in gills, and average retention time was higher in gills, compared to gut. This suggests that gills are organs susceptible to microplastic exposure and should be taken into account in fish exposure and effect studies. Our results show that particle ingestion and retention by organisms differ between microbeads and microfibers, suggesting particle selection based on size, shape, and/or color and species-specific selective feeding. We also showed that the presence of food results in limited particle ingestion and retention in *Artemia* and that microbeads are more likely to be transferred to organisms from upper trophic levels than microfibers. Finally, fish exposure to particles was not significantly different between freshwater and seawater conditions.

Keywords: microplastic, fish, invertebrates, ingestion, depuration, trophic transfer, ecotoxicity

INTRODUCTION

The presence of synthetic microfibers has been reported in most aquatic environments—from deep sea to intertidal sediments (Mathalon and Hill, 2014; Woodall et al., 2014; Sanchez-Vidal et al., 2018), and in every ocean (Desforges et al., 2014; Lusher et al., 2015). In marine environments, synthetic fibers mostly originate from the degradation of discarded maritime equipment (e.g., nets and ropes), and release during textile production and use (Carney Almroth et al., 2018; Henry et al., 2019; Cai et al., 2020). The highest fiber concentrations have been observed close to urban areas, with up to 200–800 fibers/kg of sediment and up to 4100 fibers/m^3 in rivers (Mathalon and Hill, 2014; Zhao et al., 2015). Overall, synthetic fibers represent a significant proportion of microplastics in aquatic environments. Based on a literature review, Burns and Boxall (2018) found that 52% of microplastics are fibers [marine water and fresh water (FW) combined]. Other studies found that 75% (Desforges et al., 2014) and more than 95% (Lusher et al., 2014, 2015) of microplastics found in oceanic waters are fibers. Synthetic microfibers have also been shown to be ingested by organisms. Field studies report their presence in zooplankton, polychaetes, bivalves, crustaceans (Phuong et al., 2016; Bour et al., 2018; Avio et al., 2020), deep-sea organisms (Taylor et al., 2016), fish (Halstead et al., 2018; Avio et al., 2020) and FW fish species (Sanchez et al., 2014; Pazos et al., 2017; Silva-Cavalcanti et al., 2017; Horton et al., 2018). Moreover, many authors do not include fibers in their analyses since they could result from air-borne contamination. Therefore, the presence of fibers in field organisms could currently be underestimated.

Effects studies showed that exposure to microfibers can impact growth, reproduction and survival of FW water fleas, and amphipods (Au et al., 2015; Jemec et al., 2016; Ziajahromi et al., 2017). Decreased food consumption, energy and body condition were observed in shore crabs and langoustine (Watts et al., 2015; Welden and Cowie, 2016). Damaged gill epithelium was also observed in Japanese medaka following long-term exposure to microfibers (Hu et al., 2020). The effects of fiber exposure to soil invertebrates was also investigated, with lower cast production observed for exposed earthworms (Prendergast-Miller et al., 2019), while limited effects were observed on enchytraeids, springtails, isopods and oribatid mites (Selonen et al., 2020). Studies focusing on fiber retention and gut residence time showed that retention time for synthetic microfiber varies from a few hours to a couple of days for small invertebrates, like daphnids, gammarids, sea anemones, and shrimps (Blarer and Burkhardt-Holm, 2016; Jemec et al., 2016; Gray and Weinstein, 2017; Romanó de Orte et al., 2019), and from a few hours to up to 3 weeks for crabs and fish species (Watts et al., 2015; Grigorakis et al., 2017; Ory et al., 2018).

Retention time is an important parameter that directly influences microplastic accumulation in organisms. High retention time and accumulation can lead to increased effects over time, increased chemical transfer from particles to organisms (Koelmans, 2015; Rochman, 2015), and increased potential for trophic transfer. Although the number of studies providing data on microplastic ingestion and retention is continuously growing, most studies use microbeads as model particle. However, there is currently no evidence that organisms present similar ingestion patterns and retention times for microbeads and microfibers. Trophic transfer is also an important parameter to consider, since it can result in increased fiber accumulation in species of higher trophic levels, and can also lead to adverse effects occurring at the food web scale. Despite the relevance of this parameter, the number of studies investigating the trophic transfer of microplastics, all shapes considered, is still limited (Farrell and Nelson, 2013; Setälä et al., 2014; Batel et al., 2016; Au et al., 2017; Rochman et al., 2017; Tosetto et al., 2017).

The present study aims to compare exposure to and retention time of plastic microfibers and microbeads in fish and invertebrate species under different exposure scenarios. Specifically, we tested the following hypotheses: (i) exposure and retention by organisms are different between microbeads and microfibers; (ii) the presence of food influences particle ingestion and retention by invertebrates; (iii) particle ingestion and filtration through the gills are different between FW and seawater (SW) fish; and (iv) microbeads and microfibers can be transferred through the trophic chain. Previous studies suggest that the presence of food can influence microplastic ingestion and retention by invertebrates (Wang et al., 2019; Chae and An, 2020). FW and SW fish present different physiologies, especially concerning the functions, and organizations of gill epithelia and the volumes of water swallowed (Eckert et al., 1988). Marine fish ingest larger volumes of water, potentially resulting in higher particle ingestion (Rochman, 2018). It can therefore be expected that fish gills and digestive tracts present different exposure patterns to contaminants, depending on the environment. For this study, we selected the three-spined stickleback *Gasterosteus aculeatus* as a model species for its ability to adapt its physiology to different salinity conditions (Bell and Foster, 1994). This species is also broadly used in ecotoxicology and naturally occupies a wide range of aquatic habitats (Jutfelt et al., 2013; Marchand et al., 2017). To test our hypotheses, we exposed brine shrimps (*Artemia sp.*) to identical concentrations of microbeads and microfibers in the presence or absence of food and quantified particle ingestion and depuration time. We also exposed sticklebacks in FW or SW to the same particle concentrations, and quantified the presence of particles in gills and gut following exposure and over depuration time. In a second step, we combined *Artemia* and stickleback in the same experiment to study particle trophic transfer. Since microfiber ingestion by *Artemia* was not concluding, trophic transfer was assessed with microbeads only.

MATERIALS AND METHODS

Organisms

Three-spined sticklebacks (*Gasterosteus aculeatus*) were collected in a reference site (Skaftö, Sweden; water salinity: 16–18‰) with a hand-operated net and immediately brought to the laboratory in aerated, thermally isolated boxes containing water from the sampling site. They were then randomly divided in two groups, acclimatized to and kept in either artificial SW (13°C ± 1°C,

30‰) or FW (13°C ± 1°C, 0‰) for a month prior to the start of the experiment. Fish were fed daily with red mosquito larvae. Continuous water flow and aeration ensured good water quality, and environmental enrichment was provided.

Brine shrimps (*Artemia sp.*) were obtained from commercially available dry cysts (HOBBY Aquaristik, Germany). Cysts were placed in artificial SW (35‰) for 48 h and supplied with strong aeration. After hatching, nauplii were transferred in 30‰ artificial SW and fed everyday with dried phytoplankton powder (HOBBY Aquaristik, Germany). *Artemia* reached their adult size after 3 weeks.

Microparticles and Suspension Preparation

Microbeads (opaque blue polyethylene microspheres) were purchased from Cospheric (Santa Barbara, United States; lot #120328-2–1). According to the manufacturer, they are spherical (>90%), with a 27–32 μm diameter (>90% of particles in size range), and a density of 1.00 *g*/cc. The polyester microfibers were extracted from a commercially manufactured yarn. This yarn is a solution dyed black, textured, filament yarn, which is very similar to yarns used in a wide range of clothing products. The yarn has a linear density of 75 denier, with 72 filaments in its cross section. The individual filaments within the cross section are approximately 12 μm in diameter. Black microfibers were used to improve identification and tracking during experimentation. The yarn was further manually cut into 500 μm-long fibers. Microscopic measurement of microfibers (n = 100) indicates median length of 483 ± 13 μm. Particle suspensions were prepared in artificial SW (salinity 30‰) or in FW (salinity 0‰), and specific concentrations were obtained either by weighing microbeads and diluting suspension or by counting microfibers while cutting. Gentle sonication ensured suspensions homogeneity.

Organismal Exposure and Retention Time Determination

Brine Shrimps (*Artemia*)

Before exposure, *Artemia* were starved for 24 h. Adult *Artemia* were exposed in artificial SW to a combination of microbeads and microfibers (50,000 part./L each, 100,000 part./L in total) for 2 h, in the presence or absence of food. These concentrations are not environmentally relevant and were selected to maximize interaction between organisms and particles. Exposures were carried out in triplicate, each replicate comprising 10 individuals, in 100 ml glass flasks.

For the exposure in the absence of food, an initial suspension was prepared (300 ml total volume, comprising 15,000 microfibers and 15,000 microbeads), homogenized by gentle sonication, and distributed between replicates. *Artemia* were then added to the flasks. After 2 h of exposure, individuals were gently picked, rinsed in clean medium and placed on a petri dish for microscopic observation (Leica EZ4HD stereomicroscope). The number of ingested particles was manually counted, and individuals were placed in clean SW for depuration (grouped by replicate). The number of particles present in *Artemia* digestive tract was determined at 2, 6, 24, 48, 72, and 96 h of depuration. Individual microbeads and microfibers could easily be detected through the *Artemia*'s transparent cuticle (**Figure 1**).

For the exposure in the presence of food, a similar initial suspension was prepared and supplemented with 100 mg of *Artemia* food (phytoplankton powder, final concentration 333.3 mg/L) before homogenization and distribution between replicates. After 2 h of exposure, the presence of food in *Artemia*'s digestive tract prevented assessing the presence of microparticles. Therefore, individuals were gently picked, rinsed and individually placed in petri dishes containing clean SW supplemented with food (333.3 mg/L). Microparticles were then

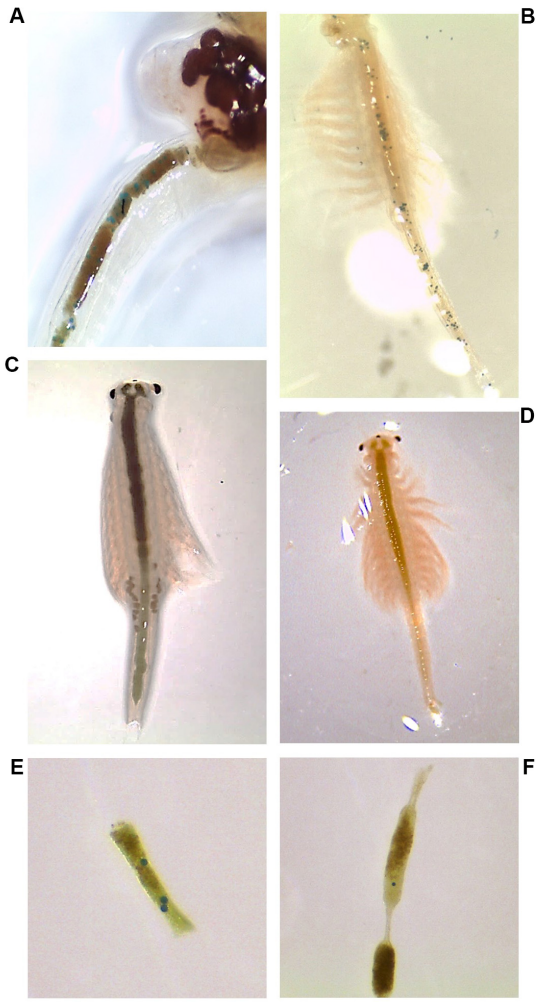

FIGURE 1 | Particle ingestion and egestion by *Artemia*. **(A)** Particles present in the *Artemia* digestive tract after 2 h of exposure. One black microfiber can be seen close to blue microbeads. **(B)** Trophic chain experiment: *Artemia* after exposure to microbeads and before being fed to fish. **(C)** *Artemia* exposed to particles in the presence of food: the upper digestive tract is filled with food, preventing the observation of microbeads, and microfibers potentially ingested. **(D)** *Artemia* after 96 h of depuration. **(E,F)** Microbeads observed in *Artemia* feces.

quantified in depuration SW and fecal pellets by microscopic observation at 2, 6, 24, and 48 h. Depuration medium was changed after every observation. Individual particles could easily be detected in SW and fecal pellets (**Figure 1**). Fecal pellets that were too dense to be fully transparent were mechanically torn to ensure the absence of particle. For each individual, the number of ingested microbeads was expressed as the sum of microbeads egested, counted at each observation time.

For both experiments, after 2 h of exposure the water column was sampled from each replicate in order to quantify microparticles in suspension. In the case of the absence of food, visual observation indicated that no particle was present at the bottom of the flasks; therefore the whole volume was sampled. In the case of the presence of food, sedimented microfibers and food were observed at the bottom of the flasks; therefore, only the water column was sampled, excluding the solid deposit. Water samples were filtered on gridded cellulose nitrate filters (12 μm pore size). Particles were counted in five representative cells, and the total number of particles was estimated based on average numbers per cell.

Fish Exposed *via* Water

Sticklebacks were exposed to a combination of beads and fibers (50,000 part./L each, 100,000 part./L in total) either in SW or FW (20 cm × 12 cm × 13 cm tanks; 4 L). Fish from the same exposure condition (SW: $n = 27$; FW: $n = 26$) were grouped in a single replicate. Control conditions (clean SW and FW) were also included (SW: $n = 4$; FW: $n = 8$). After 2 h of exposure, fish were transferred to clean water (SW or FW, respectively) for 3 min to allow removal of particles potentially present on their body. Fish from control (SW: $n = 1$; FW: $n = 2$) and exposed (SW: $n = 6$; FW: $n = 7$) groups were immediately euthanized, and the digestive tracts and gills were sampled. The remaining fish were transferred in new clean water for depuration. Fish from exposed groups were euthanized, and organs were sampled after 2, 24, or 48 h depuration ($n = 7$ per condition and sampling time). Fish from control groups were euthanized, and organs were sampled after 2 h of depuration. Samples were stored at 4°C before further analysis (see section *Fish Samples Processing and Analysis*). Water samples (two replicates per condition; 15 ml per sample) were taken from exposure waters immediately after fish exposure, filtered on gridded cellulose nitrate filters (12 μm pore size), and particles were counted.

Fish Exposed *via* Trophic Chain

Due to the very limited ingestion of microfibers by *Artemia*, trophic exposure was carried out with microbeads only. As a first step, *Artemia* were placed for 5 min in 15 ml flasks (six *Artemia*/flask) containing either microbeads suspension (500,000 particle/L in SW) or SW only (control group). Individuals were then gently rinsed in SW and photographed under microscopic condition for further microbead quantification: pictures were analyzed with ImageJ® software to count the number of ingested microbeads, easily detected through the organisms' cuticles. Each *Artemia* was attributed a number, corresponding to the fish it would be fed. In a second step, fish were individualized to ensure equal prey ingestion between individuals. Every fish was fed three *Artemia*, either pre-exposed to microbead suspension ($n = 18$ fish) or to SW only ($n = 12$ fish). All the *Artemia* were eaten within 5 min, so microbead egestion by *Artemia* is considered negligible. Three fish from control and exposed groups were immediately euthanized and their digestive tract was sampled. The remaining fish were allowed to depurate in clean SW. Fish from the microbead group were taken at 2, 8, 12, 24, and 48 h of depuration. Fish from the control group were taken at 2, 24, and 48 h of depuration. At each sampling time, three fish per condition were taken and their gills and gut were sampled and stored at 4°C before further analysis (see section *Fish Samples Processing and Analysis*).

Fish Samples Processing and Analysis

Samples were digested overnight in 10% KOH at 50°C then filtered on 10 μm nylon mesh. This digestion method has been validated for different plastic polymers (Dehaut et al., 2016), and a pilot study was conducted in our laboratory to ensure that it would not alter the microbeads or microfibers' physical properties (**Supplementary Figure 1**). Filters were observed under a stereomicroscope, and particles were counted. The polyester fibers studied here have a specific shape, color, and size and were easily distinguished from potential air-borne fibers.

Statistics

All statistical analyses were performed using GraphPad Prism 8 software. For *Artemia* exposure, ANOVAs were performed to compare the number of ingested microbeads between replicates at each observation time. When the required assumptions were not satisfied, ANOVAs on ranks (Kruskal–Wallis test) were performed instead. For fish water exposure, four factors were considered to compare the number of particles found in samples: depuration time, particle shape (i.e. fiber or bead), organ (i.e. gills or gut) and water salinity (i.e. FW or SW). Since data did not satisfy the assumptions required to perform multi-factor analyses, each factor was analyzed separately in all possible combinations of other factors. ANOVA on ranks (Kruskal–Wallis test) was performed to compare the number of particles found in samples based on depuration time. Particle shape, organ and water salinity were analyzed with *t*-test or the corresponding non-parametric test (Mann-Whitney) when the required assumptions were not met. Levels of significance were set at $p < 0.05$.

RESULTS

Artemia

Exposure in the Absence of Food

Ingestion of microfibers was very limited, with only four individuals presenting one fiber each in their gut. Egestion of microfiber was fast, occurring between 2 h and 72 h of depuration. Microbead ingestion rate was much higher, with 100% of individuals having microbeads in their gut (30 ± 3 microbeads/individual on average) after 2 h of exposure. The number of microbeads ingested per individual did not significantly differ between replicates. Complete microbead

egestion occurred within 96 h for most individuals, and was almost complete for others: only one or two beads were still present in gut for seven individuals at 96 h of depuration. On average, more than 50% of the ingested microbeads were excreted in less than 24 h (**Figure 2A**). Detailed particle counts are presented in **Supplementary Table 1**.

Following filtration of exposure water, 5,220 ± 765 (average ± SE) microbeads and 5,069 ± 64 (average ± SE) microfibers were recovered, indicating concentrations of approximately 52,200 beads/L and 50,690 fibers/L.

Exposure in the Presence of Food

No fiber ingestion was observed when particles were presented in the presence of food. Microbead ingestion was low, with 4 ± 1 part./individual (average ± SE), and 10% of individuals not having ingested any particle. The number of microbeads ingested per individual did not significantly differ between replicates. Microbead egestion was complete in 48 h for all the individuals, and more than 50% of the ingested microbeads were excreted in less than 2 h on average (see **Figure 2B** and **Supplementary Table 1**). Following filtration of exposure water (water column), 4,439 ± 178 (average ± SE) microbeads and 339 ± 53 (average ± SE) microfibers were recovered.

Fish Exposed via Water

In gills, microfibers were more abundant than microbeads: an average of 31 and 18 microfibers/individuals were observed for SW and FW fish, respectively, while only 18 and 0.2 microbeads/individuals were observed for SW and FW fish, respectively. Contrary to gills, very few particles were observed in the gut: samples containing fibers had a maximum of two fibers (1 and 0.6 fibers/individual on average for SW and FW fish, respectively), and only one sample contained microbeads (two beads present in one SW fish). In both FW and SW conditions, most particles were depurated in 2 h, and complete depuration was achieved in 48 h (**Figure 3** and **Supplementary Table 2**). Group comparison based on particle shape indicates that in FW, a significantly higher number of fibers was found in both gills and gut immediately after exposure, compared to microbeads ($p = 0.02$, both in gills and gut). More specifically, microbeads were totally absent from gut samples and nearly totally absent from gills samples (only two FW fish were positive for the presence of beads in the gills). From 2 h of depuration, no significant difference between shapes was observed (**Figures 3C,D**). In SW, beads were nearly totally absent from gut samples (only one SW fish was positive for beads) but were found in gills samples (**Figures 3A,B**). However, the difference between shapes was not statistically significant in SW fish ($p = 0.37$ and 0.25 at T0 in gills and gut, respectively, and $p = 0.06$ in both gills and gut, at 2 h).

Group comparison based on fish organs (i.e., gills and gut) indicated significantly higher numbers of particles found in gills, compared to gut, both in FW and SW conditions and until 2 h of depuration (SW: $p < 0.03$ and $p < 0.02$ at 0 and 2 h of depuration, respectively; FW: $p < 0.02$ and $p < 0.05$ at 0 and 2 h of depuration, respectively).

No difference in the number of particle was observed when groups were compared based on water salinity (i.e. SW and FW).

Following filtration of exposure waters, 646 ± 43 (average ± SE) microbeads and 646 ± 23 (average ± SE) microfibers were recovered in SW conditions, and 373 ± 26 (average ± SE) microbeads and 486 ± 43 (average ± SE) microfibers in FW conditions. This indicates approximate concentrations of 43,033 part./L for both microbeads and microfibers in SW and 24,867 microbeads/L, and 32,367 microfibers/L in FW. Although these concentrations are below the theoretical concentration of 50,000 part./L, they confirm fish exposure to both microbeads and microfibers, in SW and FW.

Following processing and filtration of samples from the control groups, eight microfibers were observed in the case of one gut sample from an SW fish. No microbead or microfiber was observed in any other sample from control groups neither in SW nor in FW, gut or gills, and at any sampling time.

Fish Exposed via Trophic Chain

The method used to perform trophic exposures allowed us to quantify the number of ingested microbeads for each fish. Detailed numbers are presented in **Supplementary Table 3**. The presence of microbeads in fish gut is therefore expressed as the percentage of ingested particle. Similarly to water exposure, fast depuration was observed: more than 50% depuration was achieved within 2 h and complete depuration was observed in 48 h (**Figure 4**). Detailed numbers of microbeads recovered over time are presented in **Supplementary Table 3**. No microbead was observed in fish from the control group.

DISCUSSION

Particle Ingestion and Retention Time in *Artemia*

Artemia are filter-feeders that can feed on a wide range of particle sizes (Bergami et al., 2016): they continuously ingest particles present in the surrounding water. The very high particle concentration used for this study is not representative of environmental concentrations but was chosen to maximize interactions between particles and organisms. The microbead ingestion (30 particle/individual on average) observed in the absence of a food source is therefore not surprising and has previously been observed (Batel et al., 2016; Peixoto et al., 2019). The observed microbead retention time was also longer than normal retention time for *Artemia* (48 h, determined with food). Despite the high particle concentration, fiber ingestion was very low. Although microfiber diameter (12.5 μm) is much smaller than that in *Artemia* (∼1 cm), the fibers can be long enough to limit their ingestion. Other studies observed higher ingestion rates for microbeads than for fibers, by gammarids (Blarer and Burkhardt-Holm, 2016), shrimps (Gray and Weinstein, 2017), and daphnids (Ziajahromi et al., 2017). One study found higher ingestion rates for fibers, in *Hyalella azteca* (Au et al., 2015).

In the presence of food, no microfiber ingestion was observed and microbead ingestion was very limited (approximately

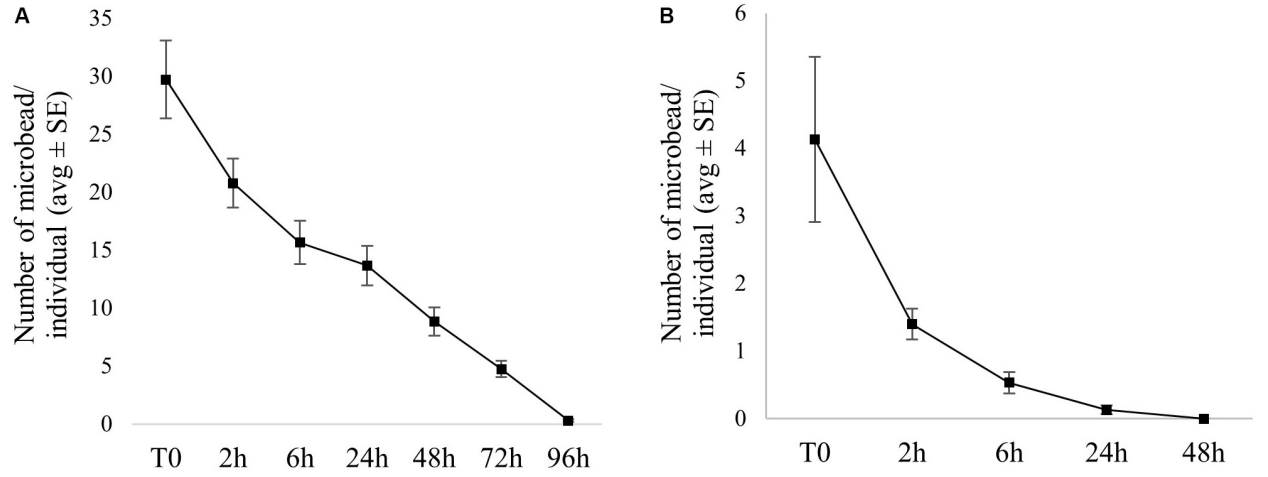

FIGURE 2 | Microbead uptake (T0) and depuration over time in *Artemia* exposed **(A)** without food and **(B)** in the presence of food (average number/individual ± SE).

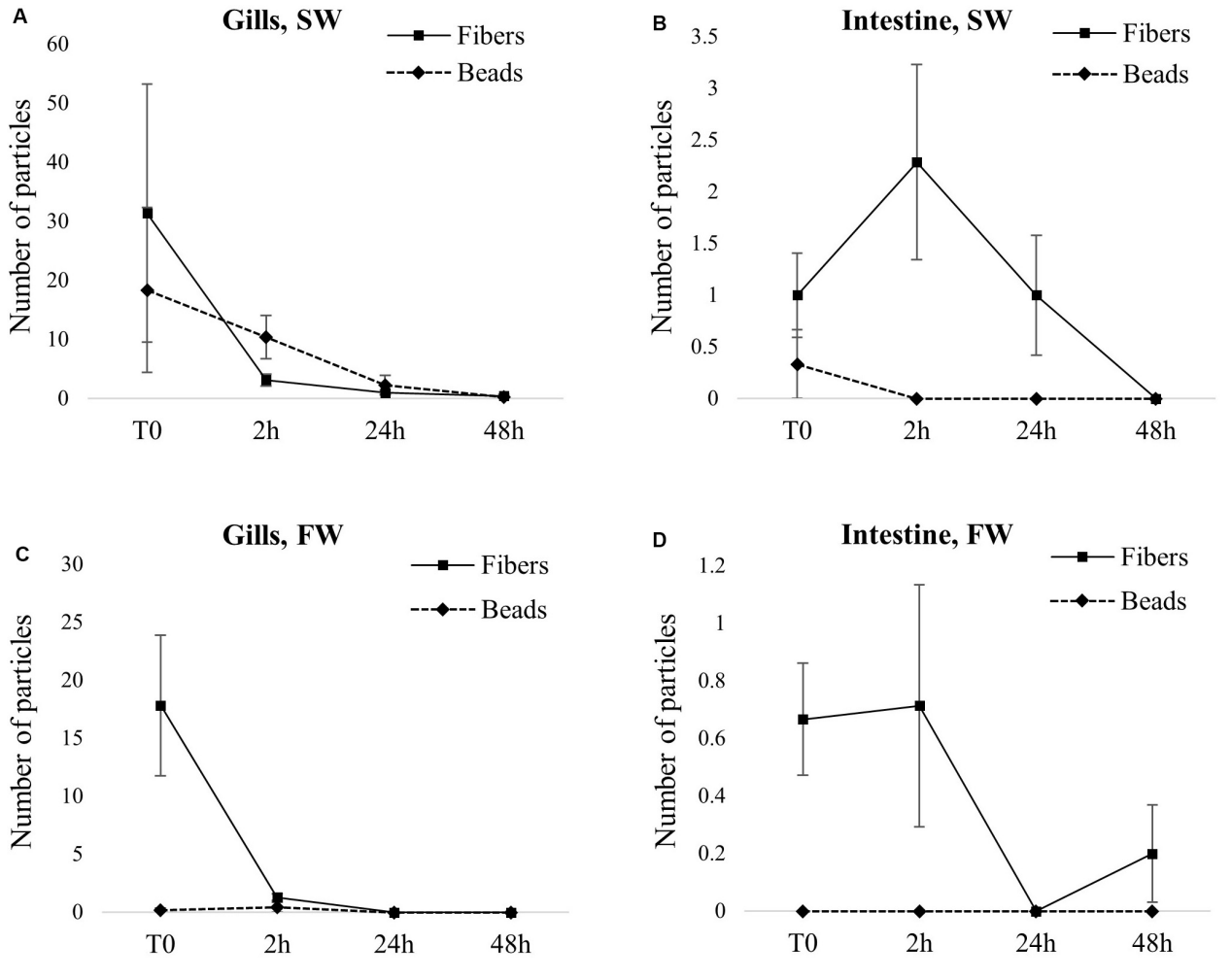

FIGURE 3 | Particle uptake (T0) and depuration over time in fish exposed *via* water [seawater (SW) or freshwater (FW)]. Results are expressed as the average number of particles found in tissue ± SE. **(A)** gills from SW fish. **(B)** Intestine from SW fish. **(C)** Gills from FW fish. **(D)** Intestine from FW fish.

four microbeads/individual), while food ingestion was fast. In the exposure water, visual observation indicated microfiber flocculation with food and sedimentation, which was further confirmed by particle quantification: a low proportion of fibers was left in the water column (<7%). However, the number of microfibers in suspension was still high enough to allow interaction with *Artemia*. The number of microbeads in the suspension was high (89% of nominal concentration) and similar to concentrations measured in the absence of food. Therefore, the limited particle ingestion by *Artemia* in the presence of food is not likely to be due to limited numbers of particles, and suggests instead selective feeding and avoidance of plastic microparticles. Complete microbead egestion was faster in the presence of food, corresponding to the normal food retention time (48 h). Similarly to our result, limited ingestion of plastic microparticles in presence of food has been observed in *Artemia parthenogenetica* (Wang et al., 2019). On the contrary, a similar study conducted with blue mussel showed that plastic microbead retention time increased in the presence of food (Chae and An, 2020), suggesting species-specific ingestion, and egestion patterns.

These results also highlight the importance of the experimental design when assessing microplastic ingestion and retention time. The total absence of food in natural environments seems unlikely, and very high microplastic concentrations are not expected, except in specific hotspots (Van Cauwenberghe et al., 2013). Our results show that microbeads can be ingested by *Artemia* and retained for a couple of days and are therefore likely to be transferred to organisms from upper trophic levels.

Microbead Trophic Transfer to Fish

Microbead egestion by fish exposed via trophic chain was fast, with more than 50% depuration achieved within 2 h and complete depuration was achieved in 48 h. This corresponds to stickleback's normal gut retention time (estimated at 48 h) and suggests that plastic microbeads do not accumulate when transferred from contaminated preys. Similarly to our results, a short retention time of microplastic was previously observed in goldfish exposed via food (33 h), with no significant differences between microplastic and natural food (Grigorakis et al., 2017). The short microplastic retention time in fish, seen in light of field studies' results, highlights an important feature of environmental exposure. Currently, most field studies report high proportions of fish positive for the presence of microplastics. Short microplastic retention time implies that the probability of fish ingesting microplastic shortly before sampling is high, suggesting that fish are continuously, or at least very frequently, exposed to microplastics in the environment.

Particle Interaction With Fish Exposed via Water

Particle quantification in exposure waters showed concentrations lower than nominal concentrations, especially in FW. This could be due to initial suspension preparation. However, the concentrations measured in *Artemia* exposure waters were very close to nominal concentrations, suggesting that our methods enable accurate preparation of both microbead and microfiber suspensions. Moreover, we performed pilot studies to ensure that particle suspension in water, ingestion by organism and processing with 10% KOH (cf. section *Fish Samples Processing and Analysis*) would not alter particles' physical properties (e.g., color loss) and result in lowered recovery rates (see **Supplementary Figure 1**). It is therefore more likely that after 2 h of exposure, particles are not homogeneously distributed in the water column. Since the water samples were taken at mid-depth of the water column, it can be hypothesized that plastic microparticles tend to float (case of SW) or sink, potentially flocculating with fish feces (case of FW). The quantities of particles recovered from water samples indicate that fish were still exposed to high particle concentrations and that concentrations were similar for microbeads and microfibers.

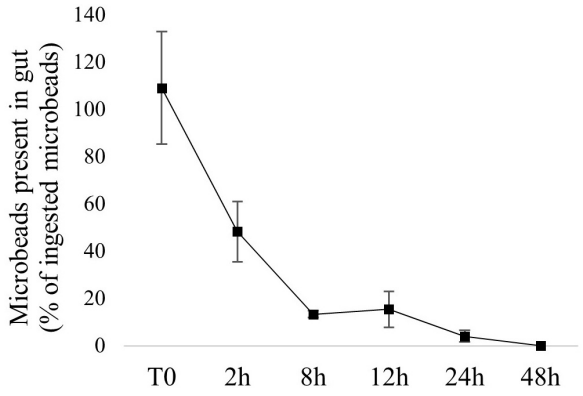

FIGURE 4 | Microbead depuration over time in fish exposed *via* trophic chain. Values are numbers of microbeads recovered in fish gut, expressed as a percentage of ingested microbeads (average ± SE; $n = 3$).

However, significant differences between microbeads and microfibers recovered from fish samples were observed in FW. This difference was not significant in SW, but the important individual variations at T0 and the low p-values (0.06) at 2 h of depuration suggest that the non-significance could be due to a low statistical power. Eight microfibers were found in a gut sample from one control SW fish. This is by far the highest number of microfibers observed in all gut samples and suggests a contamination of the filter during sample processing rather than contamination of fish during exposure. Since this is the only case of control contamination, it was decided to not include it in the calculations, by removing it as background contamination for instance. The almost complete absence of microbeads in the gut in both SW and FW conditions suggests that fish could selectively avoid microbeads. Stickleback are capable of actively selecting their prey based on shape and prefer straight prey over globular ones (Ibrahim and Huntingford, 2010), which supports the hypothesis of fibers selection over beads in our experiment. However, prey selection is also based on other factors, such as size, color, and movement, and color has been shown to be the predominant one, followed by movement, shape, and size (Ibrahim and Huntingford, 2010). Especially, stickleback can perceive blue colors (Rick and Bakker, 2008) and could have therefore distinguished the microbeads and actively avoided

them. In another study where fish were exposed to microplastics of different colors, authors observed that fish avoided colored particles, whereas they ingested black particles that looked more similar to their food (Ory et al., 2018). Although the blue color of microbeads may have resulted in their selective avoidance by fish, it is important to note that in environmental conditions, rapid biofouling of microplastics (Harrison et al., 2014) can alter their physical appearance, including color. Color-based selection of microparticles may therefore not be as relevant in environmental conditions.

The significantly higher numbers of particles found in gills, compared to gut, show that gills are the most exposed organ when fish are directly exposed via water. Therefore, gills should be considered a highly relevant organ when investigating microplastic exposure and effects in fish. Currently, the vast majority of field studies conducted on fish focus solely on gut. Based on our results, we recommend that future field studies include gills when assessing the presence of microplastics in fish. Similarly, when considering effect studies at the organ level following water exposure, data on gills are under-represented, compared to those of gut (Karami et al., 2016, 2017; Choi et al., 2018; Jin et al., 2018; Lei et al., 2018). More effect studies on gills are therefore necessary to fill this gap.

Finally, our results indicate that in our specific exposure conditions, water salinity (i.e. SW or FW) do not influence exposure to and retention time of particles, therefore invalidating our initial hypothesis. Although the present results are unambiguous and represent valuable data on the comparison of FW and SW systems, they should not be extrapolated to the whole FW and SW ecosystems, and complementary studies comprising different species would be needed.

CONCLUSION

Our results confirmed that ingestion and retention by organisms are different between microbeads and microfibers, suggesting particle selection based on size, shape, and/or color. Invertebrates and fish exhibited different patterns—*Artemia* ingesting large quantities of microbeads but very few microfibers, while stickleback ingested more microfibers than microbeads. For *Artemia*, selective feeding was also confirmed with decreased particle ingestion when exposed in the presence of food. Our results also show that microfiber trophic transfer from *Artemia* to predator species is not likely, contrarily to microbeads. In fish, particle ingestion directly via water is limited, and ingested particles, either directly from water or from contaminated prey, have a short gut retention time. On the contrary, gills are more susceptible to microparticle exposure, with higher numbers of particles- and longer retention times. This highlights the importance of gills in fish exposure and effect studies. We therefore recommend that both field and laboratory studies include gills in their experimental design. Finally, we initially hypothesized that fish exposure to particle would differ between FW and SW conditions, but our results invalidated this hypothesis.

DATA AVAILABILITY STATEMENT

All datasets generated for this study are included in the article/**Supplementary Material**.

ETHICS STATEMENT

The animal study was reviewed and approved by Swedish Board of Agriculture (Jordbruks Verket). Animal husbandry and experiments were conducted in compliance with ethical practices from the Swedish Board of Agriculture (Ethical permit number #15986-2018).

AUTHOR CONTRIBUTIONS

AB and BC conceived the study. AB and SH conducted the experiments. MT and MS provided the yarn samples and textile expertise. AB wrote the manuscript, which all authors approved before submission.

FUNDING

This research was supported by the Swedish Research Council FORMAS (2016-00895).

ACKNOWLEDGMENTS

The authors are grateful to the reviewers for their thorough review of this work and their constructive comments which helped improve and clarify this manuscript.

SUPPLEMENTARY MATERIAL

The Supplementary Material for this article can be found online at: https://www.frontiersin.org/articles/10.3389/fenvs.2020.00083/full#supplementary-material

REFERENCES

Au, S. Y., Bruce, T. F., Bridges, W. C., and Klaine, S. J. (2015). Responses of Hyalella azteca to acute and chronic microplastic exposures. *Environ. Toxicol. Chem.* 34, 2564–2572. doi: 10.1002/etc.3093

Au, S. Y., Lee, C. M., Weinstein, J. E., van den Hurk, P., and Klaine, S. J. (2017). Trophic transfer of microplastics in aquatic ecosystems: identifying critical research needs. *Integr. Environ. Assess. Manag.* 13, 505–509. doi: 10.1002/ieam.1907

Avio, C. G., Pittura, L., d'Errico, G., Abel, S., Amorello, S., Marino, G., et al. (2020). Distribution and characterization of microplastic particles and textile microfibers in Adriatic food webs: general insights for biomonitoring strategies. *Environ. Pollut.* 258:113766. doi: 10.1016/j.envpol.2019.113766

Batel, A., Linti, F., Scherer, M., Erdinger, L., and Braunbeck, T. (2016). Transfer of benzo[a]pyrene from microplastics to *Artemia nauplii* and further to zebrafish

via a trophic food web experiment: CYP1A induction and visual tracking of persistent organic pollutants: trophic transfer of microplastics and associated POPs. *Environ. Toxicol. Chem.* 35, 1656–1666. doi: 10.1002/etc.3361

Bell, M. A., and Foster, S. A. (1994). *The Evolutionary Biology of the Threespine Stickleback*. New York, NY: Oxford University Press.

Bergami, E., Bocci, E., Vannuccini, M. L., Monopoli, M., Salvati, A., Dawson, K. A., et al. (2016). Nano-sized polystyrene affects feeding, behavior and physiology of brine shrimp *Artemia franciscana* larvae. *Ecotoxicol. Environ. Saf.* 123, 18–25. doi: 10.1016/j.ecoenv.2015.09.021

Blarer, P., and Burkhardt-Holm, P. (2016). Microplastics affect assimilation efficiency in the freshwater amphipod *Gammarus fossarum*. *Environ. Sci. Pollut. Res.* 23, 23522–23532. doi: 10.1007/s11356-016-7584-2

Bour, A., Avio, C. G., Gorbi, S., Regoli, F., and Hylland, K. (2018). Presence of microplastics in benthic and epibenthic organisms: influence of habitat, feeding mode and trophic level. *Environ. Pollut.* 243, 1217–1225. doi: 10.1016/j.envpol.2018.09.115

Burns, E. E., and Boxall, A. B. A. (2018). Microplastics in the aquatic environment: evidence for or against adverse impacts and major knowledge gaps: microplastics in the environment. *Environ. Toxicol. Chem.* 37, 2776–2796. doi: 10.1002/etc.4268

Cai, Y., Yang, T., Mitrano, D. M., Heuberger, M., Hufenus, R., and Nowack, B. (2020). Systematic study of microplastic fiber release from 12 different polyester textiles during washing. *Environ. Sci. Technol.* 54, 4847–4855. doi: 10.1021/acs.est.9b07395

Carney Almroth, B. M., Åström, L., Roslund, S., Petersson, H., Johansson, M., and Persson, N.-K. (2018). Quantifying shedding of synthetic fibers from textiles; a source of microplastics released into the environment. *Environ. Sci. Pollut. Res.* 25, 1191–1199. doi: 10.1007/s11356-017-0528-7

Chae, Y., and An, Y.-J. (2020). Effects of food presence on microplastic ingestion and egestion in Mytilus galloprovincialis. *Chemosphere* 240:124855. doi: 10.1016/j.chemosphere.2019.124855

Choi, J. S., Jung, Y.-J., Hong, N.-H., Hong, S. H., and Park, J.-W. (2018). Toxicological effects of irregularly shaped and spherical microplastics in a marine teleost, the sheepshead minnow (*Cyprinodon variegatus*). *Mar. Pollut. Bull.* 129, 231–240. doi: 10.1016/j.marpolbul.2018.02.039

Dehaut, A., Cassone, A.-L., Frère, L., Hermabessiere, L., Himber, C., Rinnert, E., et al. (2016). Microplastics in seafood: benchmark protocol for their extraction and characterization. *Environ. Pollut.* 215, 223–233. doi: 10.1016/j.envpol.2016.05.018

Desforges, J.-P. W., Galbraith, M., Dangerfield, N., and Ross, P. S. (2014). Widespread distribution of microplastics in subsurface seawater in the NE Pacific Ocean. *Mar. Pollut. Bull.* 79, 94–99. doi: 10.1016/j.marpolbul.2013.12.035

Eckert, R., Randall, R., and Augustine, G. (1988). *Animal Physiology: Mechanisms and Adaptations*. New York, NY: W. H. Freeman and Co.

Farrell, P., and Nelson, K. (2013). Trophic level transfer of microplastic: *Mytilus edulis* (L.) to *Carcinus maenas* (L.). *Environ. Pollut.* 177, 1–3. doi: 10.1016/j.envpol.2013.01.046

Gray, A. D., and Weinstein, J. E. (2017). Size- and shape-dependent effects of microplastic particles on adult daggerblade grass shrimp (*Palaemonetes pugio*): uptake and retention of microplastics in grass shrimp. *Environ. Toxicol. Chem.* 36, 3074–3080. doi: 10.1002/etc.3881

Grigorakis, S., Mason, S. A., and Drouillard, K. G. (2017). Determination of the gut retention of plastic microbeads and microfibers in goldfish (*Carassius auratus*). *Chemosphere* 169, 233–238. doi: 10.1016/j.chemosphere.2016.11.055

Halstead, J. E., Smith, J. A., Carter, E. A., Lay, P. A., and Johnston, E. L. (2018). Assessment tools for microplastics and natural fibres ingested by fish in an urbanised estuary. *Environ. Pollut.* 234, 552–561. doi: 10.1016/j.envpol.2017.11.085

Harrison, J. P., Schratzberger, M., Sapp, M., and Osborn, A. M. (2014). Rapid bacterial colonization of low-density polyethylene microplastics in coastal sediment microcosms. *BMC Microbiol.* 14:232. doi: 10.1186/s12866-014-0232-4

Henry, B., Laitala, K., and Klepp, I. G. (2019). Microfibres from apparel and home textiles: prospects for including microplastics in environmental sustainability assessment. *Sci. Total Environ.* 652, 483–494. doi: 10.1016/j.scitotenv.2018.10.166

Horton, A. A., Jürgens, M. D., Lahive, E., van Bodegom, P. M., and Vijver, M. G. (2018). The influence of exposure and physiology on microplastic ingestion by the freshwater fish Rutilus rutilus (roach) in the River Thames, UK. *Environ. Pollut.* 236, 188–194. doi: 10.1016/j.envpol.2018.01.044

Hu, L., Chernick, M., Lewis, A. M., Ferguson, P. L., and Hinton, D. E. (2020). Chronic microfiber exposure in adult Japanese medaka (*Oryzias latipes*). *PLoS One* 15:e0229962. doi: 10.1371/journal.pone.0229962

Ibrahim, A. A., and Huntingford, F. A. (2010). The Role of Visual Cues in Prey Selection in Three-spined Sticklebacks (*Gasterosteus aculeatus*). *Ethology* 81, 265–272. doi: 10.1111/j.1439-0310.1989.tb00772.x

Jemec, A., Horvat, P., Kunej, U., Bele, M., and Kržan, A. (2016). Uptake and effects of microplastic textile fibers on freshwater crustacean *Daphnia magna*. *Environ. Pollut.* 219, 201–209. doi: 10.1016/j.envpol.2016.10.037

Jin, Y., Xia, J., Pan, Z., Yang, J., Wang, W., and Fu, Z. (2018). Polystyrene microplastics induce microbiota dysbiosis and inflammation in the gut of adult zebrafish. *Environ. Pollut.* 235, 322–329. doi: 10.1016/j.envpol.2017.12.088

Jutfelt, F., Bresolin de Souza, K., Vuylsteke, A., and Sturve, J. (2013). Behavioural Disturbances in a Temperate Fish Exposed to Sustained High-CO2 Levels. *PLoS One* 8:e0065825. doi: 10.1371/journal.pone.0065825

Karami, A., Groman, D. B., Wilson, S. P., Ismail, P., and Neela, V. K. (2017). Biomarker responses in zebrafish (*Danio rerio*) larvae exposed to pristine low-density polyethylene fragments. *Environ. Pollut.* 223, 466–475. doi: 10.1016/j.envpol.2017.01.047

Karami, A., Romano, N., Galloway, T., and Hamzah, H. (2016). Virgin microplastics cause toxicity and modulate the impacts of phenanthrene on biomarker responses in African catfish (*Clarias gariepinus*). *Environ. Res.* 151, 58–70. doi: 10.1016/j.envres.2016.07.024

Koelmans, A. A. (2015). "Modeling the role of microplastics in bioaccumulation of organic chemicals to marine aquatic organisms. a critical review," in *Marine Anthropogenic Litter*, eds M. Bergmann, L. Gutow, and M. Klages (Cham: Springer International Publishing), 309–324. doi: 10.1007/978-3-319-16510-3_11

Lei, L., Wu, S., Lu, S., Liu, M., Song, Y., Fu, Z., et al. (2018). Microplastic particles cause intestinal damage and other adverse effects in zebrafish *Danio rerio* and nematode *Caenorhabditis elegans*. *Sci. Total Environ.* 619–620, 1–8. doi: 10.1016/j.scitotenv.2017.11.103

Lusher, A. L., Burke, A., O'Connor, I., and Officer, R. (2014). Microplastic pollution in the Northeast Atlantic Ocean: validated and opportunistic sampling. *Mar. Pollut. Bull.* 88, 325–333. doi: 10.1016/j.marpolbul.2014.08.023

Lusher, A. L., Tirelli, V., O'Connor, I., and Officer, R. (2015). Microplastics in Arctic polar waters: the first reported values of particles in surface and sub-surface samples. *Sci. Rep.* 5:14947. doi: 10.1038/srep14947

Marchand, A., Porcher, J.-M., Turies, C., Chadili, E., Palluel, O., Baudoin, P., et al. (2017). Evaluation of chlorpyrifos effects, alone and combined with lipopolysaccharide stress, on DNA integrity and immune responses of the three-spined stickleback, *Gasterosteus aculeatus*. *Ecotoxicol. Environ. Saf.* 145, 333–339. doi: 10.1016/j.ecoenv.2017.07.025

Mathalon, A., and Hill, P. (2014). Microplastic fibers in the intertidal ecosystem surrounding Halifax Harbor, Nova Scotia. *Mar. Pollut. Bull.* 81, 69–79. doi: 10.1016/j.marpolbul.2014.02.018

Ory, N. C., Gallardo, C., Lenz, M., and Thiel, M. (2018). Capture, swallowing, and egestion of microplastics by a planktivorous juvenile fish. *Environ. Pollut.* 240, 566–573. doi: 10.1016/j.envpol.2018.04.093

Pazos, R. S., Maiztegui, T., Colautti, D. C., Paracampo, A. H., and Gómez, N. (2017). Microplastics in gut contents of coastal freshwater fish from Río de la Plata estuary. *Mar. Pollut. Bull.* 122, 85–90. doi: 10.1016/j.marpolbul.2017.06.007

Peixoto, D., Amorim, J., Pinheiro, C., Oliva-Teles, L., Varó, I., de Medeiros Rocha, R., et al. (2019). Uptake and effects of different concentrations of spherical polymer microparticles on *Artemia franciscana*. *Ecotoxicol. Environ. Saf.* 176, 211–218. doi: 10.1016/j.ecoenv.2019.03.100

Phuong, N. N., Zalouk-Vergnoux, A., Poirier, L., Kamari, A., Châtel, A., Mouneyrac, C., et al. (2016). Is there any consistency between the microplastics found in the field and those used in laboratory experiments? *Environ. Pollut.* 211, 111–123. doi: 10.1016/j.envpol.2015.12.035

Prendergast-Miller, M. T., Katsiamides, A., Abbass, M., Sturzenbaum, S. R., Thorpe, K. L., and Hodson, M. E. (2019). Polyester-derived microfibre impacts on the soil-dwelling earthworm *Lumbricus terrestris*. *Environ. Pollut.* 251, 453–459. doi: 10.1016/j.envpol.2019.05.037

Rick, I. P., and Bakker, T. C. (2008). Color signaling in conspicuous red sticklebacks: do ultraviolet signals surpass others? *BMC Evol. Biol.* 8:189. doi: 10.1186/1471-2148-8-189

Rochman, C. M. (2015). "The complex mixture, fate and toxicity of chemicals associated with plastic debris in the marine environment," in *Marine Anthropogenic Litter*, eds M. Bergmann, L. Gutow, and M. Klages (Cham: Springer International Publishing), 117–140. doi: 10.1007/978-3-319-16510-3_5

Rochman, C. M. (2018). Microplastics research—from sink to source. *Science* 360, 28–29. doi: 10.1126/science.aar7734

Rochman, C. M., Parnis, J. M., Browne, M. A., Serrato, S., Reiner, E. J., Robson, M., et al. (2017). Direct and indirect effects of different types of microplastics on freshwater prey (*Corbicula fluminea*) and their predator (*Acipenser transmontanus*). *PLoS One* 12:e0187664. doi: 10.1371/journal.pone.0187664

Romanó de Orte, M., Clowez, S., and Caldeira, K. (2019). Response of bleached and symbiotic sea anemones to plastic microfiber exposure. *Environ. Pollut.* 249, 512–517. doi: 10.1016/j.envpol.2019.02.100

Sanchez, W., Bender, C., and Porcher, J.-M. (2014). Wild gudgeons (*Gobio gobio*) from French rivers are contaminated by microplastics: preliminary study and first evidence. *Environ. Res.* 128, 98–100. doi: 10.1016/j.envres.2013.11.004

Sanchez-Vidal, A., Thompson, R. C., Canals, M., and de Haan, W. P. (2018). The imprint of microfibres in southern European deep seas. *PLoS One* 13:e0207033. doi: 10.1371/journal.pone.0207033

Selonen, S., Dolar, A., Jemec Kokalj, A., Skalar, T., Parramon Dolcet, L., Hurley, R., et al. (2020). Exploring the impacts of plastics in soil – The effects of polyester textile fibers on soil invertebrates. *Sci. Total Environ.* 700:134451. doi: 10.1016/j.scitotenv.2019.134451

Setälä, O., Fleming-Lehtinen, V., and Lehtiniemi, M. (2014). Ingestion and transfer of microplastics in the planktonic food web. *Environ. Pollut.* 185, 77–83. doi: 10.1016/j.envpol.2013.10.013

Silva-Cavalcanti, J. S., Silva, J. D. B., de França, E. J., de Araújo, M. C. B., and Gusmão, F. (2017). Microplastics ingestion by a common tropical freshwater fishing resource. *Environ. Pollut.* 221, 218–226. doi: 10.1016/j.envpol.2016.11.068

Taylor, M. L., Gwinnett, C., Robinson, L. F., and Woodall, L. C. (2016). Plastic microfibre ingestion by deep-sea organisms. *Sci. Rep.* 6:33997. doi: 10.1038/srep33997

Tosetto, L., Williamson, J. E., and Brown, C. (2017). Trophic transfer of microplastics does not affect fish personality. *Anim. Behav.* 123, 159–167. doi: 10.1016/j.anbehav.2016.10.035

Van Cauwenberghe, L., Vanreusel, A., Mees, J., and Janssen, C. R. (2013). Microplastic pollution in deep-sea sediments. *Environ. Pollut.* 182, 495–499. doi: 10.1016/j.envpol.2013.08.013

Wang, Y., Mao, Z., Zhang, M., Ding, G., Sun, J., Du, M., et al. (2019). The uptake and elimination of polystyrene microplastics by the brine shrimp, Artemia parthenogenetica, and its impact on its feeding behavior and intestinal histology. *Chemosphere* 234, 123–131. doi: 10.1016/j.chemosphere.2019.05.267

Watts, A. J. R., Urbina, M. A., Corr, S., Lewis, C., and Galloway, T. S. (2015). Ingestion of plastic microfibers by the crab carcinus maenas and its effect on food consumption and energy balance. *Environ. Sci. Technol.* 49, 14597–14604. doi: 10.1021/acs.est.5b04026

Welden, N. A. C., and Cowie, P. R. (2016). Long-term microplastic retention causes reduced body condition in the langoustine, *Nephrops norvegicus*. *Environ. Pollut.* 218, 895–900. doi: 10.1016/j.envpol.2016.08.020

Woodall, L. C., Sanchez-Vidal, A., Canals, M., Paterson, G. L. J., Coppock, R., Sleight, V., et al. (2014). The deep sea is a major sink for microplastic debris. *R. Soc. Open Sci.* 1, 140317–140317. doi: 10.1098/rsos.140317

Zhao, S., Zhu, L., and Li, D. (2015). Microplastic in three urban estuaries. *China Environ. Pollut.* 206, 597–604. doi: 10.1016/j.envpol.2015.08.027

Ziajahromi, S., Kumar, A., Neale, P. A., and Leusch, F. D. L. (2017). Impact of microplastic beads and fibers on waterflea (*Ceriodaphnia dubia*) survival, growth, and reproduction: implications of single and mixture exposures. *Environ. Sci. Technol.* 51, 13397–13406. doi: 10.1021/acs.est.7b03574

Conflict of Interest: The authors declare that the research was conducted in the absence of any commercial or financial relationships that could be construed as a potential conflict of interest.

The reviewer SR declared a past co-authorship with one of the authors BC to the handling Editor.

frontiers in Environmental Science

ORIGINAL RESEARCH
published: 30 June 2020
doi: 10.3389/fenvs.2020.00097

Impacts of Nanoplastics on the Viability and Riboflavin Secretion in the Model Bacteria *Shewanella oneidensis*

*Victoria S. Fringer[1], Liam P. Fawcett[1], Denise M. Mitrano[2] and Melissa A. Maurer-Jones[1]**

[1] Department of Chemistry and Biochemistry, University of Minnesota Duluth, Duluth, MN, United States, [2] Department of Process Engineering, Eawag, Swiss Federal Institute of Aquatic Science and Technology, Dübendorf, Switzerland

Characterizing the impact of nanoplastics to organism health is important to understand the consequences of the environmental plastic waste problem. This article examines the impact of nano-polystyrene (nano-PS; 159 ± 0.9 nm diameter) to ecologically relevant bacteria *Shewanella oneidensis*. Bacterial viability was evaluated using a growth-based assay. Riboflavin secretion is a critical cell function of *S. oneidensis*, serving as an electron mediator in anaerobic respiration and/or as a signaling molecule when the bacteria are under stress. Thus, changes in cellular function were monitored through riboflavin secretion in order to evaluate toxic responses that may not result in cell death. Under aerobic and anaerobic exposures (4, 8, or 12 h), the viability of the *S. oneidensis* was minimally changed as compared to the control, while the concentration of riboflavin secreted varied with exposure dose. In order to determine if this was a specific response to nanoplastic particles, opposed to a response to either particles or plastic more generally, we exposed the system to colloidal TiO_2 nanoparticles and polystyrene and polyethylene thin films. We confirmed that riboflavin secretion trends were specific to nano-PS and not to these other materials, which showed no significant changes. We investigated the association of the nano-PS with ICP-MS using Pd that was chemically incorporated into the model nanoplastics. While 59.2% of the nano-PS were found in the non-cellular culture media, 7.0 and 6.6% was found associated with the loosely and tightly bound extracellular polymeric substance, respectively. There was significantly more nano-PS (10.9%) strongly associated with the cells. Taken together, we found that nano-PS had minimal impacts to viability but caused a significant change in the function of *S. oneidensis* that can be related to the nano-PS attached or in proximity to the bacterium. These trends are consistent between aerobic and anaerobic cultures, signifying that the stress response of *S. oneidensis* can be generalized between different environmental compartments. This work highlights that the association of nanoplastic materials with microorganisms may modify the cellular function that could ultimately be an impact to ecosystem health.

Keywords: nanoplastic, viability, functional response, polystyrene, association

OPEN ACCESS

Edited by:
Alexandre J. Poulain, University of Ottawa, Canada

Reviewed by:
Ilaria Corsi, University of Siena, Italy
Andrew Mark Osborn, RMIT University, Australia

***Correspondence:**
Melissa A. Maurer-Jones
maujones@d.umn.edu

Specialty section:
This article was submitted to Biogeochemical Dynamics, a section of the journal Frontiers in Environmental Science

Received: *09 April 2020*
Accepted: *09 June 2020*
Published: *30 June 2020*

Citation:
Fringer VS, Fawcett LP, Mitrano DM and Maurer-Jones MA (2020) Impacts of Nanoplastics on the Viability and Riboflavin Secretion in the Model Bacteria Shewanella oneidensis. Front. Environ. Sci. 8:97. doi: 10.3389/fenvs.2020.00097

INTRODUCTION

Plastic-particle distributions in marine and freshwater systems are an active area of research, with most current work centered on the size distribution, polymer type, and number of particles above 1 micron (Wagner et al., 2014; Zbyszewski et al., 2014; Driedger et al., 2015; Hendrickson et al., 2018; Allen et al., 2019), and estimates suggest there could be up to 125 trillion microplastics in ocean water (Lindeque et al., 2020). Particulate plastics (nano- and microplastic particles, fragments and fibers) pose a concern for organisms in our environment because they can cause a myriad of health outcomes, such as impacting the gill cavity of crab *Carcinus maenas* causing altered O_2 consumption (Watts et al., 2016) or causing inflammation of the liver tissue of zebrafish (Lu et al., 2016). Exposure to microplastics is often through the ingestion pathway because the size range overlaps with that of phytoplankton in both fresh and salt waters, which has resulted in the ingestion of microplastic particles by invertebrates and fish (Imhof et al., 2016). Ingestion is thought to pose challenges to various organisms such as false satiation, leading to nutritional deficits, (Welden and Cowie, 2016; Yin et al., 2018) tissue inflammation (Lu et al., 2016) or toxicity of additives leaching from plastic into tissue (Rochman et al., 2012; Tanaka et al., 2015). While environmental microplastic hazards are concerning, there is growing worry for the impact of nanoplastics in the environment as laboratory studies have shown that they are likely prevalent within these natural systems (Koelmans et al., 2015; Gangadoo et al., 2020; Hebner and Maurer-Jones, 2020). Nanoplastics are particularly concerning with regard to ecosystem health because they have the potential to permeate cell membranes and disrupt cellular behavior (Rossi et al., 2014) while also having a larger surface area-to-volume ratio, increasing the additive leaching potential (Bouwmeester et al., 2015; Hermabessiere et al., 2017).

Nanoparticle toxicity, largely focused on engineered inorganic materials, has been widely studied with the growing demand of novel nanomaterials along with their incorporation into commercially available products. Efforts in this arena have established the framework for studying the interaction between nanoparticles and organisms at various trophic levels (Maurer-Jones et al., 2013b; Zhang et al., 2018) and there are substantial efforts to have the toxicity response to inorganic nanomaterials inform nanoparticle design (Buchman et al., 2019a). Yet, there is much less understood about the toxicity of nanoplastics. The most studied nanoplastic in terms of toxicity is nanoparticle polystyrene (nano-PS) because of its commercial availability with a variety of controlled size ranges and surface chemistries. Many nano-PS toxicity studies have focused on a range of ecologically relevant, multi-cellular model organisms (Besseling et al., 2014; Della Torre et al., 2014; Greven et al., 2016; Chen et al., 2017; Pitt et al., 2018) but there is a gap in knowledge in the toxicity of nano-PS to single-celled organisms.

Toxicity evaluation of single-celled microorganisms is critical because these organisms provide a bedrock of the ecosystems. To date, studies of nano-PS toxicity has primarily focused on algal species. For example, algae exposed to nano-PS have demonstrated a decrease in photosynthetic activity due to their adsorption onto the surface of the algae, and thus screening sunlight (Bhattacharya et al., 2010). Beyond the toxic implications for the algae itself, sorption to the surface can also be the first step within the food web for bioaccumulation of nanoplastic, moving from algae to water fleas to carp (Cedervall et al., 2012). These studies of photosynthetic activity changes and trophic transfer highlight the important role that microorganisms play within the context of nanoplastic hazards to larger organisms. It is expected, due to the close algal-bacterial relationship (Ramanan et al., 2016), that the influence of nano-PS to bacteria systems could be similar, including changes to the primary productivity from these organisms, the transfer of nano-PS to larger organisms through ingestion, or changes in health to other organisms that rely on the cellular function of the microorganisms (Azam and Malfatti, 2007). Yet, there is not a wide understanding of the impact of nano-PS to ecologically relevant bacteria. In bacteria models, Fu et al. (2018) showed nano-PS causes a decrease in growth and metabolism of *Acetobacteroides hydrogenigenes*, a species relevant to anaerobic digestion. Qu and coworkers studied the impact of micro- and nano-PS to marine bacteria *Halomonas alkaliphilia* and showed both sizes of particles inhibited growth at high concentrations but that nano-PS also negatively impacted the ammonia conversion efficiencies of the bacteria (Sun et al., 2018). There is still a lot to be understood about the impact of nano-PS to other ecologically relevant bacteria, including where the nanoplastics are in relationship to the bacteria (i.e., associated to or localized within the bacteria) and/or the response to nano-PS from a bacterial species in a range of growing conditions such as aerobic and anaerobic settings.

Shewanella oneidensis is an ideal model bacterium for nanoplastic studies because they are a facultative anaerobe (i.e., they can switch between anaerobic and aerobic respiration), are distributed worldwide and live in varied environmental conditions (e.g., variable salt concentrations and/or temperatures) (Hau and Gralnick, 2007). The fact that these bacteria live in such diverse conditions means it is likely that the organism will encounter nano-PS in a natural system. Additionally, their adaptability may aid in ecosystem modeling as their response may inform our understanding of the impact of nano-PS to similar organisms. In anaerobic conditions, *Shewanellae* have a unique ability to respire on compounds found in the environment, such as reducing iron to its bioavailable state [Fe(III) to Fe(II)] (Valls and De Lorenzo, 2002; Hau and Gralnick, 2007; Shi et al., 2007), which contribute to the process of metal cycling that other organisms within the environment rely on for their survival (Sheng and Fein, 2014; Wang et al., 2016). The metal reduction function is facilitated through the secretion of flavin mediators, including riboflavin and flavin mononucleotide. Riboflavin secretion is a critical cell function of *S. oneidensis*, serving as both an electron mediator in anaerobic respiration and as a signaling molecule when the bacteria are under stress in both aerobic and anaerobic environments (Brutinel et al., 2013; Oram and Jeuken, 2019). Finally, this model organism has been used in previous nanoparticle toxicity assessments and thus provides precedent benchmarks for toxicity responses that go beyond only live versus dead cell counts, with

evaluation of how substances induce changes of cellular function and gene expression (Maurer-Jones et al., 2013a,c; Zhi et al., 2019; Buchman et al., 2020; Clement et al., 2020). Taken together, these advantages provide an improved understanding as to what cellular processes are most impacted and how this will in turn influence the surrounding environment.

To address the gaps in knowledge of nanoplastic toxicity to single-celled organisms, we evaluated the impacts of nano-PS on the model bacteria *S. oneidensis* MR-1. The toxicity evaluation included assessments of the viability and riboflavin secretion and iron reduction upon exposure to varied concentrations of nano-PS under both aerobic and anaerobic culture conditions. These sublethal endpoints are critical to more completely evaluate the environmental risk of nanoplastics. While previous work discussed above had characterized inorganic nanoparticle toxicity in aerobic conditions, this is the first study of toxicity to *S. oneidensis* under anaerobic conditions. We hypothesized that the markers of respiration (i.e., riboflavin secretion) would be varied between the two culture conditions, thus suggesting that nano-PS interrupts the signaling and iron reduction capabilities. To better understand the changes observed in cellular function, we evaluated the association of the nano-PS with the cells using ICP-MS, taking advantage of a Pd-label incorporated into the particle. While increasing understanding of nano-PS impacts to bacteria, this work provides an example of toxicity evaluation that considers diverse culture conditions (aerobic and anaerobic) that could enable generalization of the nano-PS toxicity response.

MATERIALS AND METHODS

A suite of analyses was used to assess the impact of nano-PS to *S. oneidensis*. The approach of our analyses is shown in **Figure 1**.

Exposure Materials

Nano-PS was synthesized and characterized as previously described in Mitrano et al. (2019). Briefly, a polyacrylonitrile material containing a chemically entrapped Pd-tracer was capped with crosslinked polystyrene shell, ultimately resulting in a core/shell nanoplastic, which was approximately 160 nm in diameter. On average, the nano-PS contained 0.49% Pd, which equated to 5.1×10^{-9} ng Pd per nano-PS particle. The nanoplastic particle demonstrated a high stability, with no leaching of the Pd tracer in complex matrices. Therefore, we are confident the interaction of the bacteria is with the polystyrene shell material and all impacts to bacterial cell viability and function is due to the plastic, and not the metal tracer. *S. oneidensis* were exposed to other materials including TiO_2 nanoparticles (25 nm, anatase; Aldrich, Burlington, MA, United States) and polystyrene (30 μm thick) and polyethylene (25 μm thick) thin films (Goodfellow, Huntington England). Thin films were pre-processed by soaking in n-hexane, methanol, and water, each for 24 h prior to bacteria experiments to remove potential contaminants from the commercially acquired films that could cause bacterial toxicity. A single 1 × 1 cm piece (∼3 mg) of pre-soaked and dried film was placed directly into the bacterial culture.

Bacterial Cell Culture

S. oneidensis MR-1(ATCC BAA-1096, Manassas VA, United States) was inoculated in Luria-Burtani (LB, Fisher Scientific) growth media overnight at 30°C with shaking at 200 rpm under aerobic conditions. After inoculation, cells were washed in triplicate with M4 growth media via centrifugation at 1500 rpm for 15 min followed by resuspension in fresh media. After washing, cells were diluted with M4 to a specific optical density by monitoring the absorbance at 600 nm (OD_{600}). M4 broth is a media with little bioavailable carbon and is optimized to sustain bacteria, though does not encourage growth (detailed preparation of M4 in **Supplementary Information**). M4 was chosen to prevent artificially nutrient rich conditions of the LB and also encourage an interaction of *S. oneidensis* with the nano-PS because there it has minimal bioavailable carbon.

Growth Based Viability Assay

Using an adapted growth-based viability assay developed by Qiu et al. (2017) the viability of *S. oneidensis* was quantified after exposure to nano-PS. Briefly, the assay relates the onset of exponential growth of *S. oneidensis* to calibrate viability, using a mathematical model to fit the exponential growth phase. Bacteria exposure was performed under aerobic and anaerobic environments with nano-PS suspended in MQ water at concentrations ranging from 18.75 to 300 mg/L for periods of 4, 8, or 12 h. These dosages were chosen as they cover the exposure ranges previously studied in other nanoplastic toxicity evaluations (Sun et al., 2018; Shen et al., 2019). The exposure times were chosen because the bacteria were able to be sustained for this period of time in the M4 broth without displaying stress caused from lack of bioavailable carbon. For aerobic growth studies, cells were diluted to an OD_{600} of 0.5 in M4 broth, which corresponds to approximately 5×10^8 cells/mL. For anaerobic growth, where the doubling rate of *S. oneidensis* is significantly slowed, the M4 media was supplemented with 15 mM lactate to allow for cell survival during the prolonged experiments, while the LB was supplemented with 20 mM lactate and 20 mM fumarate to allow for anaerobic growth. Anaerobic conditions were achieved by purging samples with an $N_2/CO_2/H_2$ [85:10:5] gas mixture in an anaerobic chamber (Coy Lab Products, Grass Lake MI, United States) and cells were equilibrated for 4 h prior to exposure. Growth was monitored by optical density readings at 600 nm. A Biotek Synergy two (Winooski, VT, United States) plate reader was used to take optical density measurements every 20 min for 13 h under aerobic environments. Alternatively, anaerobic growth measurements were observed approximately every 3 h for 48 h with a SpectraMax Plus 384 Microplate Reader (Molecular Devices, San Jose CA, United States). Anaerobic measurements required the transfer of plates from the anaerobic chamber to aerobic conditions and a subsequent transfer back to the anaerobic chamber. Anaerobic conditions in the 96-well plates were maintained by sealing the plates with an adhesive film cover.

Growth curves were modeled using R coding (RStudio, Boston, MA, United States). Under aerobic conditions the exponential growth phase of bacterial growth was modeled to

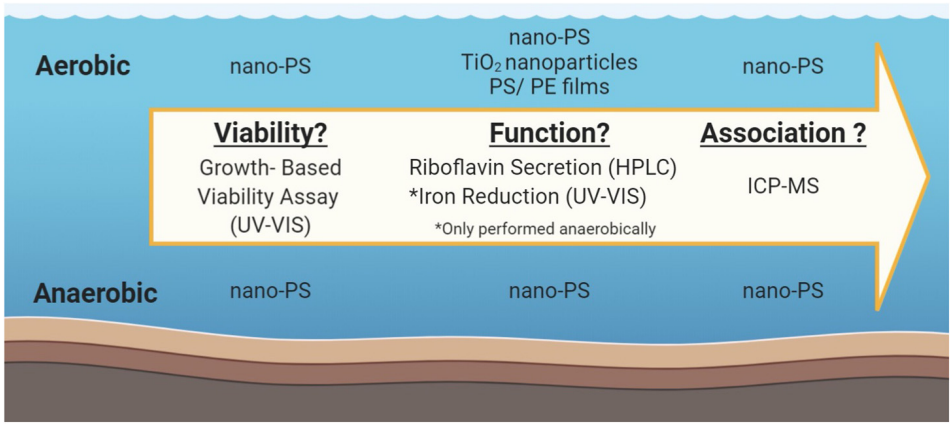

FIGURE 1 | Schematic of experimental workflow, including the exposure materials studied in the various assays.

evaluate viability through the onset of exponential growth (Qiu et al., 2017). Anaerobic growth lacked a noticeable lag phase, requiring an alternative model. A Gompertz model was chosen and viability was evaluated using the end of exponential growth (Zwietering et al., 1990). A detailed data analysis code is provided in the **Supplementary Information** along with example growth curves for 12 h exposure conditions (**Supplementary Figure S1**). Results of nano-PS exposure were compared to a negative control where the nano-PS exposure volume was replaced by an equivalent volume of MQ water without nano-PS, as the nano-PS stock was suspended in MQ water. A serial dilution of the negative control was performed after the exposure period for the construction of a calibration curve.

Cellular Function

The impact of nano-PS to bacterial cell function was evaluated by secretion of the external electron mediator, riboflavin. Suspended cells were diluted to an OD_{600} of 0.1 in media containing 1 mM iron hydroxide to a final volume of 3.2 mL. Aerobic studies were performed with LB broth, while anaerobic studies were performed with M4 broth supplement 9 mM lactate. After a 5-day exposure to nano-PS with concentrations ranging from 18.75 to 300 mg/L, riboflavin concentration in the supernatant was determined by isolating the non-cellular media by centrifugation for 5 min at 13000 rpm (Eppendorf Minispin Microcentrifuge Z606235) and quantifying using a Dionex UltiMate 3000 Series UHPLC (LPG-3400SD) with a 50 × 4.6 mm ID, Phenomenex Gemini C18 (3 μm particles) column. The mobile phase consisted of 85% Milli-Q water/15% acetonitrile v/v (Millipore Sigma; Sigma-Aldrich, Darmstadt Germany) with a flow rate of 0.5 mL/min. Riboflavin eluted after approximately 10 min and detected using fluorescence with excitation and emission wavelengths of 450 and 525 nm, respectively. A comparative analysis of riboflavin secretion after exposure to the same mass-based concentrations (18.75–300 mg/L) of TiO_2 nanoparticles was performed under aerobic conditions. The cell density of the bacteria after exposure was measured through changes in the OD_{600} in comparison to the control after exposure and used as an estimation of viability.

Beyond quantification of the riboflavin, the anaerobic cultures described above were also used to evaluate the reduction of iron. That is, while 1 mL sample of each exposure was taken for riboflavin and optical density analysis, the remainder of the culture was used to evaluate the reduction of iron. Iron reduction was halted before analysis by the addition of 0.56 mL of 12 M HCl. Reduced iron concentrations in the supernatants of lysed cells were quantified by the ferrozine (Sigma-Aldrich, Darmstadt Germany) assay, which used UV–Visible spectroscopy to selectively monitor the formation of a Fe(II)-ferrozine complex at 562 nm (Lies et al., 2005).

Sample Preparation and Digestion for ICP-MS Analysis

Various components of the cellular culture were evaluated for the presence of nano-PS. Specifically, nano-PS was quantified in the non-cellular portions of the growth media, lightly bound extracellular polymeric substance (LB-EPS), tightly bound extracellular polymeric substance (TB-EPS), and in the cell biomass, using the Pd-label as means for detection of the nano-PS with ICP-MS analysis. Collection of the ICP-MS samples relied on the physical extraction of the TB-EPS maintained intact cells, as opposed to chemical extractions that increase the risk of lysing the cells. Initially, the non-cellular growth broth solution was collected via centrifugation at 5000 × *g* for 10 min. The cell-containing pellet was then washed twice with 0.9% NaCl at 5000 × *g* for 10 min each, with the supernatant of each NaCl wash being collected and analyzed as the LB-EPS. The cell-containing pellet was resuspended in 0.9% NaCl and incubated at 30°C for 30 min to dislodge the TB-EPS from the cells. Samples were centrifuged at 5000 × *g* for 10 min and the supernatant containing the TB-EPS was collected while the pellet was resuspended in M4 growth media and collected as the cell biomass.

Upon collection of the culture components, the samples were digested to dissolve and homogenize the bacteria and nano-PS.

Specifically, an acid digestion was performed where 8 mL of each component of the cellular culture were mixed with 4.8 mL of a 1:10:1 (H_2O_2 (30%, Fisher): HNO_3(69.2% Fischer): H_2SO_4(95%, Arcos) acid mixture. Samples were added to a glass digestion tube (N9308049, Perkin Elmer) with H_2O_2 and allowed to stand for 30 min to initiate the digestion of the organic matter. HNO_3 was then added, followed by a 30-min standing period to allow for gas formation to slow. Finally, H_2SO_4 was added followed by a final 30-min standing period. H_2SO_4 was added slowly as it reacts with H_2O_2 to produce perania acid, which causes off-gassing and bubbling. The samples were then covered with aluminum foil and placed into the autoclave with the chamber temperature set at 270°C and a pressure of approximately 15 psi for 135 min. During the heating phase, the temperature fluctuated around 250°C. Two heating phases, which were deemed necessary upon visual inspection of the samples for particle presence, were performed on each sample.

A Shimadzu ICP-MS-2030 was used to detect the Pd label of the nano-PS. Pd standards (Inorganic Ventrures, Christiansburg VA, United States) were prepared at a range of 0.5–50 ppb from a 1000 ppb stock to a final volume of 10 mL. Culture components were quantified as a percent recovery of Pd by normalizing results to nano-PS control samples analyzed with ICP-MS that were of the same nano-PS concentration as the exposure. For some samples, a conversion factor of 5.1×10^{-9} ng Pd/nano-PS particle was used to quantify the number of nano-PS particles within each sample.

Statistical Analysis

Numerical representations of the data are presented as mean ± standard error. Single factor ANOVA analyses (alpha = 0.95) were used to determine the overall statistical significance of the varied concentrations for the different exposure conditions. ANOVA analyses that were statistically different (i.e., $p < 0.05$) were subsequently evaluated with Tukey posthoc to determine the pairwise p-values between the different exposure levels.

RESULTS AND DISCUSSION

Viability of *S. oneidensis*

The impact to *S. oneidensis* viability was evaluated with a growth-based viability assay (Qiu et al., 2017). The viability of the suspended bacteria was determined by calibrating to a point on the bacterial growth curve, either at the onset or at the end of exponential phase for aerobic and anaerobic growth, respectively. The viability of *S. oneidensis* exposed to increasing doses of nano-PS for varying exposure times showed minimal changes compared to the control (**Figure 2**), where values were normalized to the calibration samples for the 100% viability. In aerobic conditions (**Figure 2A**), there are slight, but significant ($p < 0.05$), decreases in viability between control viability (dashed line) and the viability of *S. oneidensis* aerobically exposed to 75, 150, and 300 mg/L nano-PS for 8 h. However, this decrease in viability was not observed with the other aerobic exposure times, so it was concluded the impact of nano-PS on aerobically grown *S. oneidensis* is small. For anaerobic conditions, there were no significant changes to the cell viability as compared to the control (**Figure 2B**). There is larger error associated with the viabilities determined under anaerobic conditions that could be the result of small, but variable amounts of O_2 entering the sealed samples over the course of the experiment. Considering both aerobic and anaerobic cultures, nano-PS caused minimal changes to cell survival under either growth environment. Previously, bacterial viability has shown a significant negative correlation with the presence of nano-PS. Both marine bacterium *Halomonas alkaliphila*, after 2 h of exposure (Sun et al., 2018), and fermentation bacterium *Acetobacteroides hydrogenigenes*, after over 3 days of exposure (Fu et al., 2018), experienced significant decreases in growth or viability upon exposure to 55 nm nano-PS. Our findings are not consistent with these observations as there is not a significant decrease in the viability observed consistently for the all exposure conditions. Due to the lack of single-species literature studies, we cannot conclude if our results vary from literature because of experimental parameters such as nanoparticle size, exposure length, or species differences.

Riboflavin Secretion

While the viability of *S. oneidensis* was minimally affected by the presence of nano-PS in our exposure conditions, we sought to also evaluate changes in cellular function. The exuded riboflavin concentration upon exposure to various concentrations of nano-PS in aerobic and anaerobic growth conditions is shown in **Figure 3A**. Aerobic exposure conditions (diagonal lines) showed significant increases in riboflavin secretion of cells with doses up to and including 150 mg/L nano-PS, but there was a significant ($p < 0.05$) decrease at the highest (300 mg/L) exposure concentration as compared to the control. It should be noted that 300 mg/L would be an unexpectedly high dose in ecologically relevant conditions. This increase in riboflavin secretion with a decrease at 300 mg/L nano-PS exposure was also observed in anaerobic conditions (solid gray bars), although the effect size was much smaller overall when compared to aerobic conditions. It is interesting to note that while the absolute value of riboflavin per cell was different, secretion trends were similar for aerobic and anaerobic conditions. *S. oneidensis* exudes riboflavin and other flavin mediators for a number of bacterial functions (Marsili et al., 2008; Mcanulty and Wood, 2014; Kim et al., 2016). Primarily, these flavin mediators act as part of the anaerobic respiratory pathway resulting in the reduction of a variety of metals. However, upon quantifying the bacterially reduced iron in anaerobic conditions, we observed no significant change in iron reduction in the presence of the nano-PS (**Figure 3B**). This signifies that there is not a correlation between riboflavin secretion and iron reduction after exposure to nano-PS. Therefore, we conclude that riboflavin is being secreted by *S. oneidensis* for a purpose beyond acting as an electron mediator itself. There is evidence that *S. oneidensis* also uses riboflavin as a signaling molecule, where riboflavin activates the cells for a number of different cellular behaviors, including repulsion of foreign bodies (Moriyama et al., 2008; Brutinel et al., 2013) or chemotaxis of other *S. oneidensis* bacteria (Li et al., 2012; Kim et al., 2016; Oram and Jeuken, 2019). To elucidate the purpose of

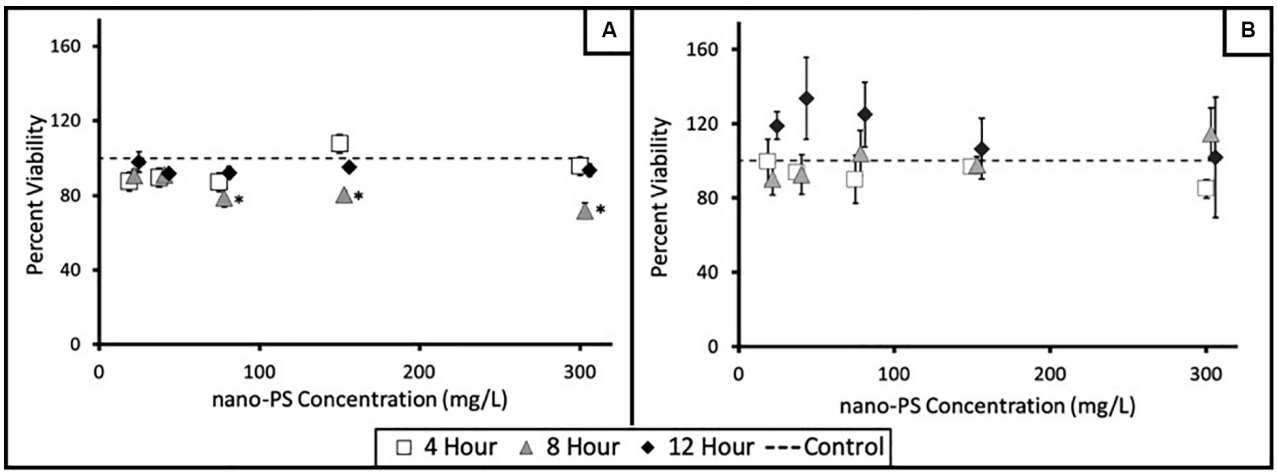

FIGURE 2 | Viability of *S. oneidensis* exposed to nano-PS as measured with a growth-based viability assay. Cells were exposed to varied concentrations of nano-PS (18.75–300 mg mg/L) for varying exposure lengths (4, 8, 12 h) in **(A)** aerobic and **(B)** anaerobic conditions. Markers at each of the nano-PS exposure concentrations are slightly staggered to highlight the viabilities for exposure length. The dashed line represents the control wells, which were normalized to the 100% viable calibration wells (*$p < 0.05$). Biological triplicates were performed for each exposure condition, where one assay was considered a single biological replicate containing four exposure wells for each nano-PS exposure concentration. Error bars represent the SEM of biological triplicates.

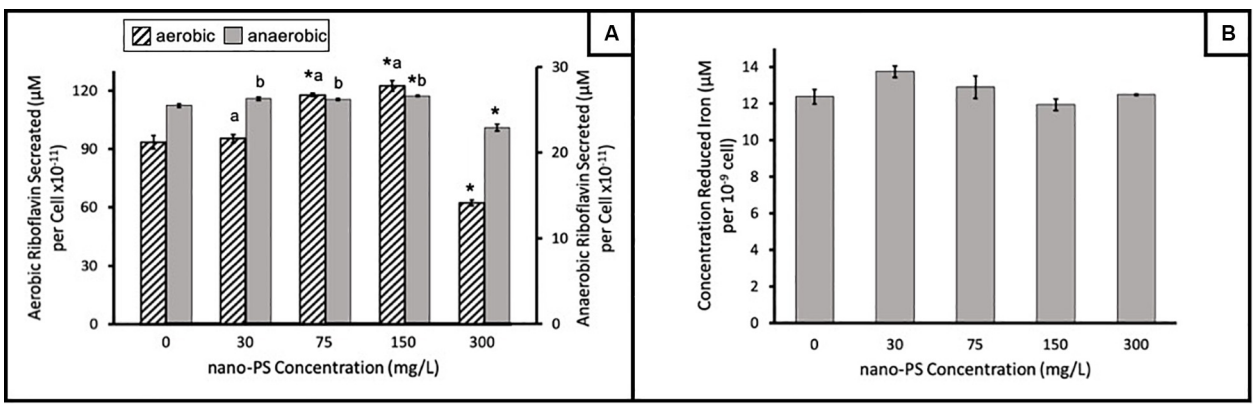

FIGURE 3 | (A) Riboflavin secreted per cell from *S. oneidensis* as a function of exposure concentration of nano-PS in aerobic (diagonal lines) and anaerobic (solid gray) conditions. A significant increase (*$p < 0.05$) was observed as compared to the control (0 mg/L nano-PS) for aerobic 75, and 150 mg/L nano-PS and anaerobic 150 mg/mL. However, 300 mg/mL was significantly decreased riboflavin secreted per cell as compared to the control. The highest exposure concentration, 300 mg/L nano-PS, was significantly different ($^{a \text{ or } b}p < 0.05$) in secreted riboflavin compared to the other exposure concentration. The SEM among triplicate trials is represented by the error bars. **(B)** Iron reduced by *S. oneidensis* under anaerobic conditions exposed to varying concentrations of nano-PS does not show significant differences from the control (i.e., non-exposed) cells (single-factor ANOVA, $p = 0.26$). Error bars present the SEM of triplicate trials.

the flavin response, future transcriptomics work is being pursued. In comparing aerobic and anaerobic exposures, we have shown that the observed stress response to nano-PS is consistent, no matter the culture conditions. Consequently, we hypothesize that the interactions (e.g., association) of the nano-PS with *S. oneidensis* would be similar between culture conditions.

To confirm that these cellular responses were the result of the particulate polymer, and not simply a response to particulate matter in solution more generally, aerobic riboflavin production was quantified in the presence of TiO_2 nanoparticles (**Figure 4A**). The optical density of the bacteria was measured to roughly estimate changes in viability at the end of exposure for all exposure doses. Like the nano-PS, TiO_2 did not induce a change in optical density as compared to the control (see **Supplementary Figure S5**), which is interpreted as minimal changes in viability, but unlike nano-PS, there was no significant difference in the secretion of riboflavin. The difference in chemical makeup and size could potentially contribute to the observed response, but previous work with nickel manganese cobalt oxide(NMC) nanosheets (Mitchell et al., 2019) and iron oxide nanoparticles (Buchman et al., 2019b) were similar, where exposure did not result in a significant changes in the amount of riboflavin secretion from *S. oneidensis*. Considering these inorganic nanomaterials, with varied sizes and shapes, cause a similar secretion behavior from *S. oneidensis,* our results of nano-PS significantly changing the riboflavin secretion is unique. This

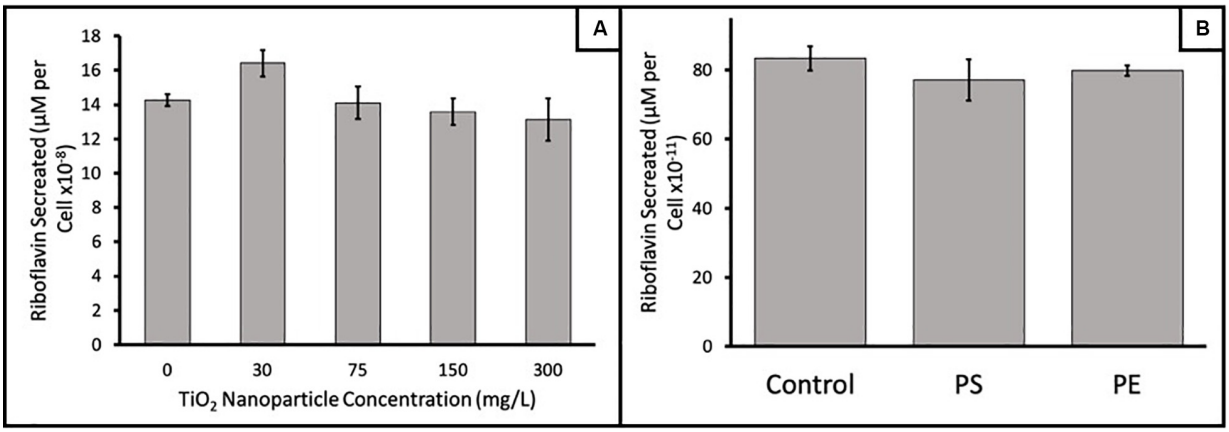

FIGURE 4 | (A) Riboflavin secreted from *S. oneidensis* upon aerobic exposure to varying concentrations of 25 nm TiO_2 nanoparticles were not statistically different than control cultures (single-factor ANOVA, $p = 0.69$). **(B)** Riboflavin secreted by *S. oneidensis* after aerobic exposure to sheets of polystyrene (PS) and polyethylene (PE) thin films. No statistical difference was observed (single-factor ANOVA, $p = 0.58$). Trials were performed in triplicate; error bars represent the SEM in triplicate values. Note the different order of magnitudes on the riboflavin secretion for panels **(A,B)**.

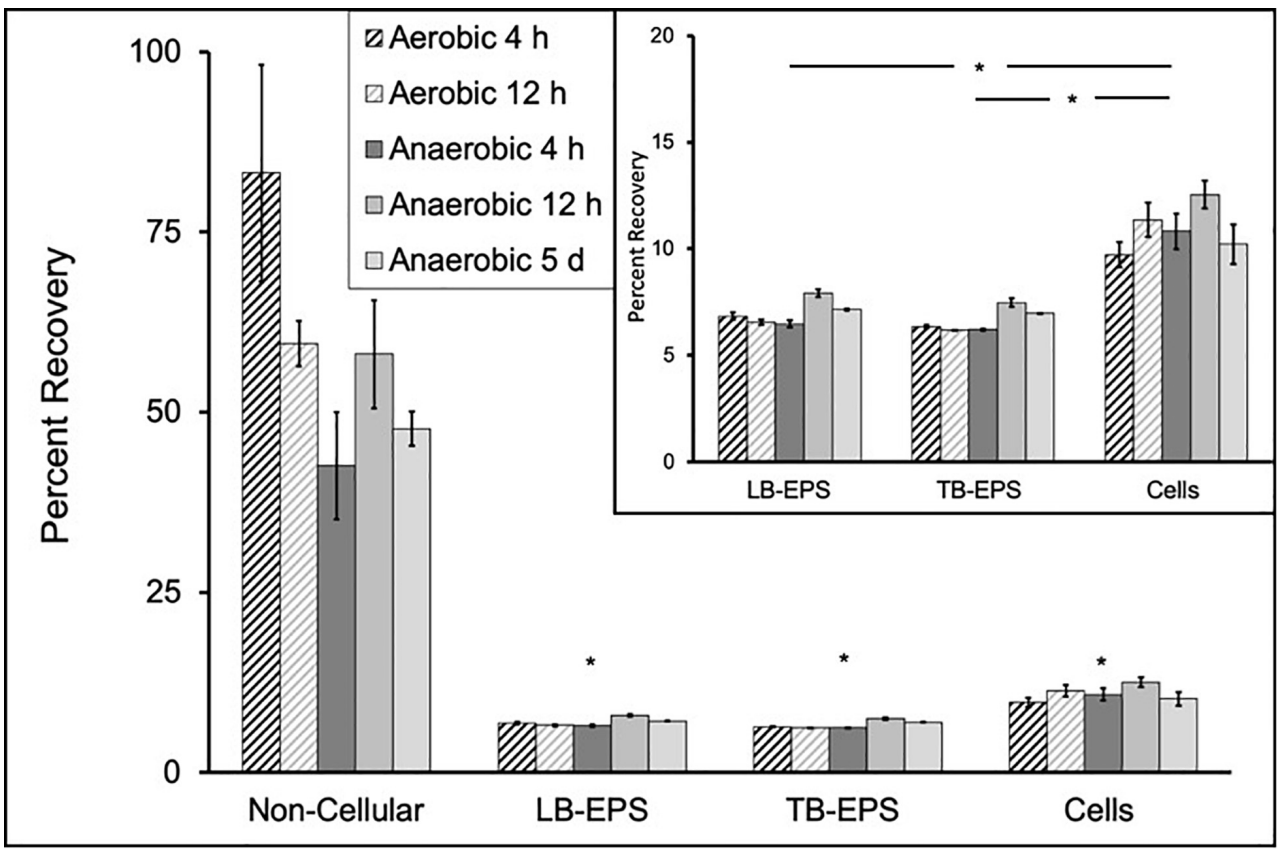

FIGURE 5 | The distribution of nano-PS in the four components of the exposed bacterial culture after exposure to 150 mg/L nano-PS, including the non-cellular growth broth, which is significantly greater ($p < 0.05$) than lightly bound (LB)-EPS, tightly bound (TB)-EPS and association with cells. Inset shows statistical comparison of the nano-PS in LB-EPS and TB-EPS to the cells (*$p < 0.05$). Error bars represent the SEM of triplicate biological replicates.

suggests that the nano-PS material itself, and not simply bacterial interactions with particles, is important in inducing changes in cellular behavior for S. *oneidensis*.

Beyond particulate matter, no significant differences in the secretion of riboflavin was measured when bacteria were exposed to polystyrene or polyethylene thin films, indicating that the

material and/or size in which the bacteria are exposed to the material impacts its response (**Figure 4B**). For context of the size comparison, the surface area of the thin films is 2.0×10^{14} nm^2 is very similar to the nano-PS exposure concentration of 75 mg/L that has a surface area of 2.2×10^{14} nm^2. This highlights the significance of the elevated riboflavin secretion in the presence of nano-PS. While the thin film polystyrene and polyethylene induced a similar result, it remains unclear if nano-polyethylene would elicit the same size-dependent response that was observed with nano-PS. Polystyrene and polyethylene are both considered to have fairly recalcitrant backbones and would be harder for microorganisms to degrade compared to polymers such as polylactic acid (Amaral-Zettler et al., 2020). Based on this similarity, we would predict that nano-polyethylene may similarly increase riboflavin secretion, although studies of natural microbial communities show that microbes respond differently to these polymers (Zettler et al., 2013; Debroas et al., 2017).

Characterizing Association of Nano-PS With *S. oneidensis*

To understand the association of nano-PS with respect to the bacteria in an effort to interpret the observed changes in functionality, we analyzed various components of the bacterial culture and organisms by ICP-MS. After exposure, the majority of the nano-PS remained in the non-cellular culture media under all experimental conditions (averaging 59.2 ± 15.7% of the recovered nano-PS), which was significantly greater ($p < 0.05$) than all the other culture components (**Figure 5**). The remaining fractions of nano-PS were found in the LB-EPS (7.0 ± 0.6%), TB-EPS (6.6 ± 0.6%), and directly associated with the cellular biomass (10.9 ± 1.1%) (**Figure 5**, inset). The mass balance for nano-PS was ranged between 66 and 106% of the total nano-PS in the exposure, which was the result of efforts to separate the aggregated nano-PS from the pelleted bacteria cell (see **Supplementary Figure S6**). Collectively, our results suggest that nano-PS interact both indirectly with the bacteria through entrapment in the EPS and directly with the bacterial membranes. Particles which were associated with the membrane were presumed to be strongly bound because the associated nano-PS remained attached after a series of cell washing steps. Bacteria exude EPS as a mechanism for improved chemical reactions, nutrient capture, and protection (Costa et al., 2018). This work supports previous nanoparticle toxicity studies, where nanoparticles are shown associated with the EPS, likely a protective response by the bacteria (Kang et al., 2014; Nomura et al., 2016). Interestingly, though, there is a significant increase ($p < 0.05$) of nano-PS associated with the bacterial biomass as was as compared to the LB-EPS or TB-EPS samples. While it would be unusual for a particle with a diameter of 160 nm to cross the bacterial membranes (Neal, 2008; Ivask et al., 2014), an association with the membrane is supported by previous work with a variety of materials and bacterial organisms (Ivask et al., 2012, 2014; Zhao et al., 2013). Specifically, for *S. oneidensis*, Jacobson et al. (2015) has shown that Au nanoparticles (12.8 nm) associate with the bacteria as a function of the lipopolysaccharide (LPS) within the outer cell membrane, we would hypothesize *S. oneidensis* would have a similar mechanism for our nano-PS results. The exposure times did not influence the percent of associated nano-PS, suggesting that the interaction with the EPS and membranes occurs within the first 4 h of exposure. Other nanoparticle association studies have suggested that this association could be even faster, within the first 60 min of exposure (Butler et al., 2014; Moore et al., 2017).

The presence of nano-PS associated to the cell biomass indicates that a direct interaction occurs between the nano-PS and the bacteria. To determine if there is a correlation between the amount of nano-PS particles associated with the cell and the changes in riboflavin secretion, we quantified the amount of nano-PS in the cell biomass upon increased exposure doses (**Figure 6**). An increase in the number of nano-PS associated with the cell was observed with increased exposure concentrations. There was a significant increase in the nanoparticles per cell at 300 mg/L in comparison to the 75 and 150 mg/L exposure results, although we did not observe a doubling in membrane nano-PS concentration with a doubled exposure concentration. The 300 mg/L exposure concentration correlates with the nano-PS exposure concentration in which the riboflavin secretion had significant decreases in comparison to the control. Based on the determined low number of nano-PS/cell (12–15 nano-PS particles/cell), we do not anticipate nano-PS aggregates on the cell surface but that the particles would be individually bound onto the cell membrane. This association behavior has been observed by Jahnke et al. (2016) in which *S. oneidensis* was exposed to 50 and 100 nm gold nanoparticle at similar nanoparticles/cell dosages. The corresponding surface area coverage between the cells exposed to 150 mg/L and 300 mg/L nano-PS was 13.4 and

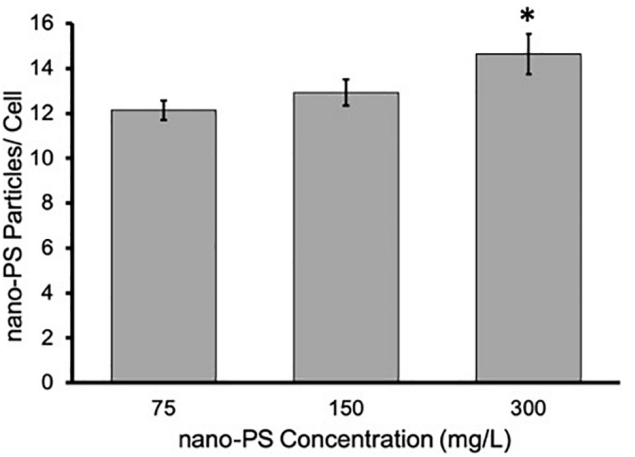

FIGURE 6 | Comparison of the number of nano-PS normalized to the number of cells for samples exposed to 75, 150, and 300 mg/L nano-PS in anaerobic conditions for 12 h. A significant increase (*$p < 0.05$) in the number of nano-PS particles/cell for samples exposed to 300 mg/L nano-PS was observed in comparison to bacteria exposed to 75 and 150 mg/L nano-PS. Error bars represent SEM of biological triplicates.

15.2%, respectively. The significant increase in the nano-PS coverage of membrane surface area paired with the observed significant decrease of riboflavin secretion, suggests that there is a concentration at which the association of nano-PS with the bacterial membrane results in alterations of the bacteria's riboflavin secretion ability. Nanoparticles have been shown to perturb the structural integrity of the cell membranes, resulting in changes within the local lipid environment (Rossi et al., 2014; Contini et al., 2018). Membrane proteins are often sensitive to protein-lipid interactions that may be altered by changes in the morphology of the membrane caused by nanoparticle presence (Lee, 2004; Dowhan and Bogdanov, 2011; Battle et al., 2015; Muller et al., 2019). While the experimental dosages are higher than what would be expected in natural systems, the increase in the number of nano-PS particles associated with cells at higher concentrations may result in the disruption of the membrane shape impacting protein function responsible for riboflavin secretion.

CONCLUSION

Overall, exposing *S. oneidensis* to nano-PS causes a stress response that is not related to viability. Specifically, riboflavin secretion, a critical cell function, is altered in the presence of nano-PS. This work highlights the importance of this riboflavin stress response because it is observed in both anaerobic and aerobic conditions, indicating that the secretion behavior is not a result of its metal reducing function. The observed similar aerobic and anaerobic response is interesting as it indicates that the interaction with nano-PS will be consistent in many different environmental compartments. Furthermore, we reveal that nano-PS associates indirectly with the EPS and directly with the bacteria membranes. This is the first study to characterize *S. oneidensis* nanoplastic or nanoparticle response in both aerobic and anaerobic cultures. By understanding the response of this adaptable single-celled organism under varied conditions, this work has contributed to a better understanding of the impact of plastic waste to the bedrock of our ecosystems.

DATA AVAILABILITY STATEMENT

The datasets presented in this study can be found in online repositories. The names of the repository/repositories and accession number(s) can be found below: https://conservancy.umn.edu/handle/11299/166578.

AUTHOR CONTRIBUTIONS

VF contributed the data collection and analysis of growth-based viability assays and ICP-MS. LF contributed the data collection and analysis of the riboflavin secretion and iron reduction assays. DM synthesized and characterized nano-PS particles. MM-J and DM contributed the conception of the work. All authors contributed to data interpretation and writing and editing of the manuscript.

FUNDING

Financial support of this work was provided to MM-J by the University of Minnesota and the Swiss National Science Foundation, Ambizione Grant number PZP002_168105 to DM.

ACKNOWLEDGMENTS

We gratefully acknowledge Jessica Sieber for use of her lab space and discussion of results, Zhihua Xu for providing the TiO_2 nanoparticles, Amanda Klein for use of her lab space, and the Shama Mirza research group for performing ICP-MS measurements.

SUPPLEMENTARY MATERIAL

The Supplementary Material for this article can be found online at: https://www.frontiersin.org/articles/10.3389/fenvs.2020.00097/full#supplementary-material

REFERENCES

Allen, S., Allen, D., Phoenix, V. R., Le Roux, G., Durántez Jiménez, P., Simonneau, A., et al. (2019). Atmospheric transport and deposition of microplastics in a remote mountain catchment. *Nat. Geosci.* 12, 339–344. doi: 10.1038/s41561-019-0335-5

Amaral-Zettler, L. A., Zettler, E. R., and Mincer, T. J. (2020). Ecology of the plastisphere. *Nat. Rev. Microbiol.* 18, 139–151. doi: 10.1038/s41579-019-0308-0

Azam, F., and Malfatti, F. (2007). Microbial structuring of marine ecosystems. *Nat. Rev. Microbiol.* 5, 782–791. doi: 10.1038/nrmicro1747

Battle, A. R., Ridone, P., Bavi, N., Nakayama, Y., Nikolaev, Y. A., and Martinac, B. (2015). Lipid-protein interactions: lessons learned from stress. *Biochim. Biophys. Acta Biomemb.* 18, 1744–1756. doi: 10.1016/j.bbamem.2015.04.012

Besseling, E., Wang, B., Lürling, M., and Koelmans, A. A. (2014). Nanoplastic affects growth of *S. obliquus* and reproduction of *D. magna*. *Environ. Sci. Technol.* 48, 12336–12343. doi: 10.1021/es503001d

Bhattacharya, P., Lin, S., Turner, J. P., and Ke, P. C. (2010). Physical adsorption of charged plastic nanoparticles affects algal photosynthesis. *J. Phys. Chem. C* 114, 16556–16561. doi: 10.1021/jp1054759

Bouwmeester, H., Hollman, P. C. H., and Peters, R. J. B. (2015). Potential health impact of environmentally released micro- and nanoplastics in the human food production chain: experiences from nanotoxicology. *Environ. Sci. Technol.* 49, 8932–8947. doi: 10.1021/acs.est.5b01090

Brutinel, E. D., Dean, A. M., and Gralnick, J. A. (2013). Description of a riboflavin biosynthetic gene variant prevalent in the phylum *Proteobacteria*. *J. Bacteriol.* 195:5479. doi: 10.1128/jb.00651-13

Buchman, J. T., Bennett, E. A., Wang, C., Abbaspour Tamijani, A., and Bennett, J. W. (2020). Nickel enrichment of next-generation NMC nanomaterials alters material stability, causing unexpected dissolution behavior and observed toxicity to *S. oneidensis MR*-1 and *D. magna*. *Environ. Sci. Nano* 7, 571–587. doi: 10.1039/c9en01074b

Buchman, J. T., Hudson-Smith, N. V., Landy, K. M., and Haynes, C. L. (2019a). Understanding nanoparticle toxicity mechanisms to inform redesign strategies

to reduce environmental impact. *Acc. Chem. Res.* 52, 1632–1642. doi: 10.1021/acs.accounts.9b00053

Buchman, J. T., Pho, T., Rodriguez, R. S., Feng, Z. V., and Haynes, C. L. (2019b). Coating iron oxide nanoparticles with mesoporous silica reduces their interaction and impact on *S. oneidensis* MR-1. *Chemosphere* 237:124511. doi: 10.1016/j.chemosphere.2019.124511

Butler, K. S., Casey, B. J., Garborcauskas, G. V. M., Dair, B. J., and Elespuru, R. K. (2014). Assessment of titanium dioxide nanoparticle effects in bacteria: association, uptake, mutagenicity, co-mutagenicity and DNA repair inhibition. *Mutat. Researchagen.* 768, 14–22. doi: 10.1016/j.mrgentox.2014.04.008

Cedervall, T., Hansson, L. A., Lard, M., Frohm, B., and Linse, S. (2012). Food chain transport of nanoparticles affects behaviour and fat metabolism in fish. *PLoS One* 7:e32254. doi: 10.1371/journal.pone.0032254

Chen, Q., Yin, D., Jia, Y., Schiwy, S., Legradi, J., Yang, S., et al. (2017). Enhanced uptake of BPA in the presence of nanoplastics can lead to neurotoxic effects in adult zebrafish. *Sci. Total Environ.* 609, 1312–1321. doi: 10.1016/j.scitotenv.2017.07.144

Clement, P. L., Kuether, J. E., Borgatta, J. R., Buchman, J. T., Cahill, M. S., Qiu, T. A., et al. (2020). Cobalt release from a nanoscale multiphase lithiated cobalt phosphate dominates interaction with *Shewanella oneidensis* MR-1 and *Bacillus subtilis* SB491. *Chem. Res. Toxicol.* 33, 806–816. doi: 10.1021/acs.chemrestox.9b00465

Contini, C., Schneemilch, M., Gaisford, S., and Quirke, N. (2018). Nanoparticle-membrane interactions. *J. Exp. Nanosci.* 13, 62–81.

Costa, O. Y. A., Raaijmakers, J. M., and Kuramae, E. E. (2018). Microbial extracellular polymeric substances: ecological function and impact on soil aggregation. *Front. Microbiol.* 9:1636. doi: 10.3389/fmicb.2018.01636

Debroas, D., Mone, A., and Ter Halle, A. (2017). Plastics in the North Atlantic garbage patch: a boat-microbe for hitchhikers and plastic degraders. *Sci. Total Environ.* 59, 1222–1232. doi: 10.1016/j.scitotenv.2017.05.059

Della Torre, C., Bergami, E., Salvati, A., Faleri, C., Cirino, P., Dawson, K. A., et al. (2014). Accumulation and embryotoxicity of polystyrene nanoparticles at early stage of development of sea urchin embryos *Paracentrotus lividus*. *Environ. Sci. Technol.* 48, 12302–12311. doi: 10.1021/es502569w

Dowhan, W., and Bogdanov, M. (2011). Lipid-protein interactions as determinants of membrane protein structure and function. *Biochem. Soc. Trans.* 39, 767–774. doi: 10.1042/bst0390767

Driedger, A. G. J., Dürr, H. H., Mitchell, K., and Van Cappellen, P. (2015). Plastic debris in the laurentian great lakes: a review. *J. Great Lakes Res.* 41, 9–19. doi: 10.1016/j.jglr.2014.12.020

Fu, S.-F., Ding, J.-N., Zhang, Y., Li, Y.-F., Zhu, R., Yuan, X.-Z., et al. (2018). Exposure to polystyrene nanoplastic leads to inhibition of anaerobic digestion system. *Sci. Total Environ.* 625, 64–70. doi: 10.1016/j.scitotenv.2017.12.158

Gangadoo, S., Owen, S., Rajapaksha, P., Plaisted, K., Cheeseman, S., Haddara, H., et al. (2020). Nano-plastics and their analytical characterisation and fate in the marine environment: from source to sea. *Sci. Total Environ.* 732:138792. doi: 10.1016/j.scitotenv.2020.138792

Greven, A.-C., Merk, T., Karagöz, F., Mohr, K., Klapper, M., Jovanoviæ, B., et al. (2016). Polycarbonate and polystyrene nanoplastic particles act as stressors to the innate immune system of fathead minnow (*Pimephales promelas*). *Environ. Toxicol. Chem.* 35, 3093–3100. doi: 10.1002/etc.3501

Hau, H. H., and Gralnick, J. A. (2007). Ecology and biotechnology of the genus *Shewanella*. *Annu. Rev. Microbiol.* 61, 237–258.

Hebner, T. S., and Maurer-Jones, M. A. (2020). Characterizing microplastic size and morphology of photodegraded polymers placed in simulated moving water conditions. *Environ. Sci. Process. Impacts* 22, 398–407. doi: 10.1039/c9em00475k

Hendrickson, E., Minor, E. C., and Schreiner, K. (2018). Microplastic abundance and composition in western lake superior as determined via microscopy, Pyr-GC/MS, and FTIR. *Environ. Sci. Technol.* 52, 1787–1796. doi: 10.1021/acs.est.7b05829

Hermabessiere, L., Dehaut, A., Paul-Pont, I., Lacroix, C., Jezequel, R., Soudant, P., et al. (2017). Occurrence and effects of plastic additives on marine environments and organisms: a review. *Chemosphere* 182, 781–793. doi: 10.1016/j.chemosphere.2017.05.096

Imhof, H. K., Laforsch, C., Wiesheu, A. C., Schmid, J., Anger, P. M., Niessner, R., et al. (2016). Pigments and plastic in limnetic ecosystems: a qualitative and quantitative study on microparticles of different size classes. *Water Res.* 98, 64–74. doi: 10.1016/j.watres.2016.03.015

Ivask, A., Kurvet, I., Kasemets, K., Blinova, I., Aruoja, V., Suppi, S., et al. (2014). Size-dependent toxicity of silver nanoparticles to bacteria, yeast, algae, crustaceans and mammalian cells in vitro. *PLoS One* 9:e102108. doi: 10.1371/journal.pone.00102108

Ivask, A., Suarez, E., Patel, T., Boren, D., Ji, Z., and Holden, P. (2012). Genome-wide bacterial toxicity screening uncovers the mechanisms of toxicity of a cationic polystyrene nanomaterial. *Environ. Sci. Technol.* 46, 2398–2405. doi: 10.1021/es203087m

Jacobson, K. H., Gunsolus, I. L., Kuech, T. R., Troiano, J. M., Melby, E. S., and Lohse, S. E. (2015). Lipopolysaccharide density and structure govern the extent and distance of nanoparticle interaction with actual and model bacterial outer membranes. *Environ. Sci. Technol.* 49, 10642–10650. doi: 10.1021/acs.est.5b01841

Jahnke, J. P., Cornejo, J. A., Sumner, J. J., Schuler, A. J., Atanassov, P., and Ista, L. K. (2016). Conjugated gold nanoparticles as a tool for probing the bacterial cell envelope: the case of *Shewanella oneidensis* MR-1. *Biointerphases* 11:011003. doi: 10.1116/1.4939244

Kang, F., Alvarez, P. J., and Zhu, D. (2014). Microbial extracellular polymeric substances reduce Ag+ to silver nanoparticles and antagonize bactericidal activity. *Environ. Sci. Technol.* 48, 316–322. doi: 10.1021/es403796x

Kim, B. J., Chu, I., Jusuf, S., Kuo, T., Teravest, M. A., Angenent, L. T., et al. (2016). Oxygen tension and riboflavin gradients cooperatively regulate the migration of *Shewanella oneidensis* MR-1 revealed by a hydrogel-based microfluidic device. *Front. Microbiol.* 7:1438. doi: 10.3389/fmicb.2018.01438

Koelmans, A. A., Besseling, E., and Shim, W. J. (2015). "Nanoplastics in the aquatic environment. critical review," in *Marine Anthropogenic Litter*, eds M. Bergmann, L. Gutow, and M. Klages (Cham: Springer International Publishing), 325–340. doi: 10.1007/978-3-319-16510-3_12

Lee, A. G. (2004). How lipids affect the activities of integral membrane proteins. *Biochim. Biophys. Acta* 1666, 62–87. doi: 10.1016/j.bbamem.2004.05.012

Li, R., Tiedje, J. M., Chiu, C., and Worden, R. M. (2012). Soluble electron shuttles can mediate energy taxis toward insoluble electron acceptors. *Environ. Sci. Technol.* 46, 2813–2820. doi: 10.1021/es204302w

Lies, D. P., Hernandez, M. E., Kappler, A., Mielke, R. E., Gralnick, J. A., and Newman, D. K. (2005). *Shewanella Oneidensis* MR-1 uses overlapping pathways for iron reduction at a distance and by direct contact under conditions relevant for biofilms. *Appl. Environ. Microbiol.* 71:4414. doi: 10.1128/aem.71.8.4414-4426.2005

Lindeque, P. K., Cole, M., Coppock, R. L., Lewis, C. N., Miller, R. Z., and Watts, A. J. R. (2020). Are we underestimating microplastic abundance in the marine environment? A comparison of microplastic capture with nets of different mesh-size. *Environ. Pollut.* 2020:114721. doi: 10.1016/j.envpol.2020.114721

Lu, Y., Zhang, Y., Deng, Y., Jiang, W., Zhao, Y., Geng, J., et al. (2016). Uptake and accumulation of polystyrene microplastics in zebrafish (*Danio rerio*) and toxic effects in liver. *Environ. Sci. Technol.* 50, 4054–4060. doi: 10.1021/acs.est.6b00183

Marsili, E., Baron, D. B., Shikhare, I. D., Coursolle, D., Gralnick, J. A., and Bond, D. R. (2008). Shewanella secretes flavins that mediate extracellular electron transfer. *Proc. Natl. Acad. Sci. U.S.A.* 105:3968. doi: 10.1073/pnas.0710525105

Maurer-Jones, M. A., Gunsolus, I. L., Meyer, B. M., Christenson, C. J., and Haynes, C. L. (2013a). Impact of TiO2 nanoparticles on growth, biofilm formation, and flavin secretion in *Shewanella oneidensis*. *Analyt. Chem.* 85, 5810–5818. doi: 10.1021/ac400486u

Maurer-Jones, M. A., Gunsolus, I. L., Murphy, C. J., and Haynes, C. L. (2013b). Toxicity of engineered nanoparticles in the environment. *Analyt. Chem.* 85, 3036–3049.

Maurer-Jones, M. A., Mousavi, M. P. S., Chen, L. D., Bühlmann, P., and Haynes, C. L. (2013c). Characterization of silver ion dissolution from silver nanoparticles using fluorous-phase ion-selective electrodes and assessment of resultant toxicity to *Shewanella oneidensis*. *Chem. Sci.* 4, 2564–2572.

Mcanulty, M. J., and Wood, T. K. (2014). YeeO from *Escherichia coli* exports flavins. *Bioengineered* 5, 386–392. doi: 10.4161/21655979.2014.969173

Mitchell, S. L., Hudson-Smith, N. V., Cahill, M. S., Reynolds, B. N., Frand, S. D., Green, C. M., et al. (2019). Chronic exposure to complex metal oxide nanoparticles elicits rapid resistance in *Shewanella oneidensis* MR-1. *Chem. Sci.* 10, 9768–9781. doi: 10.1039/c9sc01942a

Mitrano, D. M., Beltzung, A., Frehland, S., Schmiedgruber, M., Cingolani, A., and Schmidt, F. (2019). Synthesis of metal-doped nanoplastics and their utility to investigate fate and behaviour in complex environmental systems. *Nat. Nanotechnol.* 14, 362–368. doi: 10.1038/s41565-018-0360-3

Moore, J. D., Avellan, A., Noack, C. W., Guo, Y., Lowry, G. V., and Gregory, K. B. (2017). Time-dependent bacterial transcriptional response to CuO nanoparticles differs from that of Cu2+ and provides insights into CuO nanoparticle toxicity mechanisms. *Environ. Sci. Nano* 4, 2321–2335. doi: 10.1039/c7en00600d

Moriyama, Y., Hiasa, M., Matsumoto, T., and Omote, H. (2008). Multidrug and toxic compound extrusion (MATE)-type proteins as anchor transporters for the excretion of metabolic waste products and xenobiotics. *Xenobiotica* 38, 1107–1118. doi: 10.1080/00498250701883753

Muller, M. P., Jiang, T., Sun, C., Lihan, M., Pant, S., Mahinthichaichan, P., et al. (2019). Characterization of lipid-protein interactions and lipid-mediated modulation of membrane protein function through molecular simulation. *Chem. Rev.* 119, 6086–6161. doi: 10.1021/acs.chemrev.8b00608

Neal, A. L. (2008). What can be inferred from bacterium-nanoparticle interactions about the potential consequences of environmental exposure to nanoparticles? *Ecotoxicology* 17:362. doi: 10.1007/s10646-008-0217-x

Nomura, T., Fujisawa, E., Itoh, S., and Konishi, Y. (2016). Comparison of the cytotoxic effect of polystyrene latex nanoparticles on planktonic cells and bacterial biofilms. *J. Nanopart. Res.* 18:157.

Oram, J., and Jeuken, L. J. C. (2019). Tactic response of *Shewanella oneidensis* MR-1 toward insoluble electron acceptors. *mBio* 10:e002490-18.

Pitt, J. A., Kozal, J. S., Jayasundara, N., Massarsky, A., Trevisan, R., and Geitner, N. (2018). Uptake, tissue distribution, and toxicity of polystyrene nanoparticles in developing zebrafish (*Danio rerio*). *Aquat. Toxicol.* 194, 185–194. doi: 10.1016/j.aquatox.2017.11.017

Qiu, T. A., Nguyen, T. H. T., Hudson-Smith, N. V., Clement, P. L., Forester, D. C., Frew, H., et al. (2017). Growth-based bacterial viability assay for interference-free and high-throughput toxicity screening of nanomaterials. *Analyt. Chem.* 89, 2057–2064. doi: 10.1021/acs.analchem.6b04652

Ramanan, R., Kim, B. H., Cho, D. H., Oh, H. M., and Kim, H. S. (2016). Algae-bacteria interactions: Evolution, ecology and emerging applications. *Biotechnol. Adv.* 34, 14–29. doi: 10.1016/j.biotechadv.2015.12.003

Rochman, C. M., Hoh, E., Hentschel, B. T., and Kaye, S. (2012). Long-term field measurement of sorption of organic contaminants to five types of plastic pellets: implications for plastic marine debris. *Environ. Sci. Technol.* 47, 1646–1654.

Rossi, G., Barnoud, J., and Monticelli, L. (2014). Polystyrene nanoparticles perturb lipid membranes. *J. Phys. Chem. Lett.* 5, 241–246. doi: 10.1021/jz402234c

Shen, M., Zhang, Y., Zhu, Y., Song, B., Zeng, G., Hu, D., et al. (2019). Recent advances in toxicological research of nanoplastics in the environment: a review. *Environ. Pollut.* 252, 511–521. doi: 10.1016/j.envpol.2019.05.102

Sheng, L., and Fein, J. B. (2014). Uranium reduction by *Shewanella oneidensis* MR-1 as a function of nahco3 concentration: surface complexation control of reduction kinetics. *Environ. Sci. Technol.* 48, 3768–3775. doi: 10.1021/es5003692

Shi, L., Squier, T. C., Zachara, J. M., and Fredrickson, J. K. (2007). Respiration of metal (hydr)oxides by *Shewanella* and *Geobacter*: a key role for multihaem c-type cytochromes. *Mol. Microbiol.* 65, 12–20. doi: 10.1111/j.1365-2958.2007.05783.x

Sun, X., Chen, B., Li, Q., Liu, N., Xia, B., Zhu, L., et al. (2018). Toxicities of polystyrene nano- and microplastics toward marine bacterium *Halomonas alkaliphila*. *Sci. Total Environ.* 642, 1378–1385. doi: 10.1016/j.scitotenv.2018.06.141

Tanaka, K., Takada, H., Yamashita, R., Mizukawa, K., Fukuwaka, M.-A., and Watanuki, Y. (2015). Facilitated leaching of additive-derived PBDEs from plastic by seabirds' stomach oil and accumulation in tissues. *Environ. Sci. Technol.* 49, 11799–11807. doi: 10.1021/acs.est.5b01376

Valls, M., and De Lorenzo, V. (2002). Exploiting the genetic and biochemical capacities of bacteria for the remediation of heavy metal pollution. *FEMS Microbiol. Rev.* 26, 327–338. doi: 10.1016/s0168-6445(02)00114-6

Wagner, M., Scherer, C., Alvarez-Muñoz, D., Brennholt, N., Bourrain, X., Buchinger, S., et al. (2014). Microplastics in freshwater ecosystems: what we know and what we need to know. *Environ. Sci. Eur.* 26:12.

Wang, J., Wu, M., Lu, G., and Si, Y. (2016). Biotransformation and biomethylation of arsenic by *Shewanella oneidensis* MR-1. *Chemosphere* 145, 329–335. doi: 10.1016/j.chemosphere.2015.11.107

Watts, A. J. R., Urbina, M. A., Goodhead, R., Moger, J., Lewis, C., and Galloway, T. S. (2016). Effect of microplastic on the gills of the shore crab *Carcinus maenas*. *Environ. Sci. Technol.* 50, 5364–5369. doi: 10.1021/acs.est.6b01187

Welden, N. A. C., and Cowie, P. R. (2016). Long-term microplastic retention causes reduced body condition in the langoustine, *Nephrops norvegicus*. *Environ. Pollut.* 218, 895–900. doi: 10.1016/j.envpol.2016.08.020

Yin, L., Chen, B., Xia, B., Shi, X., and Qu, K. (2018). Polystyrene microplastics alter the behavior, energy reserve and nutritional composition of marine jacopever (*Sebastes schlegelii*). *J. Hazard. Mater.* 360, 97–105. doi: 10.1016/j.jhazmat.2018.07.110

Zbyszewski, M., Corcoran, P. L., and Hockin, A. (2014). Comparison of the distribution and degradation of plastic debris along shorelines of the Great Lakes, North America. *J. Great Lakes Res.* 40, 288–299. doi: 10.1016/j.jglr.2014.02.012

Zettler, E. R., Mincer, T. J., and Amaral-Zettler, L. A. (2013). Life in the "Plastisphere": microbial communities on plastic marine debris. *Environ. Sci. Technol.* 47, 7137–7146. doi: 10.1021/es401288x

Zhang, W., Xiao, B., and Fang, T. (2018). Chemical transformation of silver nanoparticles in aquatic environments: mechanism, morphology and toxicity. *Chemosphere* 191, 324–334. doi: 10.1016/j.chemosphere.2017.10.016

Zhao, J., Wang, Z., Dai, Y., and Xing, B. (2013). Mitigation of CuO nanoparticle-induced bacterial membrane damage by dissolved organic matter. *Water Res.* 47, 4169–4178. doi: 10.1016/j.watres.2012.11.058

Zhi, B., Yang, Y., Hudson-Smith, N. V., Kortshagen, U. R., and Haynes, C. L. (2019). Bacterial toxicity of germanium nanocrystals induced by doping with boron and phosphorus. *ACS Appl. Nano Mater.* 2, 4744–4755. doi: 10.1021/acsanm.9b00525

Zwietering, M. H., Jongenburger, I., Rombouts, F. M., Van, T., and Riet, K. (1990). Modeling of the bacterial growth curve. *Appl. Environ. Microbiol.* 56:1875.

Conflict of Interest: The authors declare that the research was conducted in the absence of any commercial or financial relationships that could be construed as a potential conflict of interest.

frontiers in Environmental Science

ORIGINAL RESEARCH
published: 30 June 2020
doi: 10.3389/fenvs.2020.00091

Single- and Multi-Element Quantification and Characterization of TiO_2 Nanoparticles Released From Outdoor Stains and Paints

*Agil Azimzada[1,2], Jeffrey M. Farner[2], Ibrahim Jreije[1], Madjid Hadioui[1], Carolyn Liu-Kang[1], Nathalie Tufenkji[2], Phil Shaw[3] and Kevin J. Wilkinson[1]**

[1] Department of Chemistry, University of Montreal, Montreal, QC, Canada, [2] Department of Chemical Engineering, McGill University, Montreal, QC, Canada, [3] Nu Instruments Ltd, Wrexham, United Kingdom

With growing applications of TiO_2 nanoparticles (NPs) in outdoor surface coatings, notably in paints and stains, their release into the environment is inevitable. While NP release has potential ecotoxicological risk, reliable risk assessments are often complicated by the near absence of analytical data on release rates under natural weathering scenarios, and the lack of a chemical characterization of the NPs following their release. This work measured NPs released from painted and stained surfaces and characterized them by size and composition using magnetic sector single particle inductively coupled plasma mass spectrometry (SP-ICP-MS) and SP-ICP-time-of-flight-MS (SP-ICP-TOF-MS). Two *in situ* experimental plans were examined in which natural precipitation interacted with nano-enhanced surfaces to varying degrees during the fall and winter. Weathering data showed that longer contact times of the precipitation (snow and rain) resulted in greater NP release. Although the stained surfaces had far fewer NPs per unit area, they lost a much higher fraction of their NP load (max 6% leached, as opposed to $<10^{-4\%}$ in paints), over similar exposure times. NP release was particularly enhanced for conditions of frequent rainfall and spring snow melt (i.e., slushy snow). SP-ICP-TOF-MS measurements on the Ti NPs indicated that they were often associated with a secondary metal in both the liquid paint (Al was detected in ∼20% of the Ti NPs; Zr in about ∼1% of the NP) and the liquid stain (Fe was detected in ∼7%, Si in ∼8% and Al in ∼3% of the Ti NPs). In contrast, for the vast majority of Ti NPs being leached out of the painted/stained surfaces, only Ti was detected. Metal interactions in the paint were explained by binding of the TiO_2 within a complex paint matrix; while in the stain, TiO_2 NPs were hypothesized to be found in heteroagglomerates, potentially with aluminosilicates (Fe, Si, and Al). In rain and snow, Ti was the only element detected in about half of the Ti NPs; in the other half, Ti often co-occurred with Fe, Si and Al. The results indicate that single element, likely anthropogenic, Ti NPs are already prevalent in the natural precipitation and that NP release from surface coatings will further increase their presence in the environment.

Keywords: nanomaterial, release, paint, stain, titania, SP-ICP-TOF-MS, weathering, environment

OPEN ACCESS

Edited by:
Vera I. Slaveykova, Université de Genève, Switzerland

Reviewed by:
Francisco Laborda, University of Zaragoza, Spain
Mohammed Baalousha, University of South Carolina, United States

****Correspondence:***
Kevin J. Wilkinson
kj.wilkinson@umontreal.ca

Specialty section:
This article was submitted to Biogeochemical Dynamics, a section of the journal Frontiers in Environmental Science

Received: *30 March 2020*
Accepted: *03 June 2020*
Published: *30 June 2020*

Citation:
Azimzada A, Farner JM, Jreije I, Hadioui M, Liu-Kang C, Tufenkji N, Shaw P and Wilkinson KJ (2020) Single- and Multi-Element Quantification and Characterization of TiO_2 Nanoparticles Released From Outdoor Stains and Paints. Front. Environ. Sci. 8:91. doi: 10.3389/fenvs.2020.00091

INTRODUCTION

A rapid increase in the adoption of nanotechnologies across numerous industries has been a major driver in the production and use of engineered nanomaterials (ENMs) (Robichaud et al., 2009; Vance et al., 2015). Paints and stains represent two important applications of ENMs, for which TiO_2 nanoparticles (NPs) are extensively used for improved UV protection and self-cleaning properties (Hincapié et al., 2015; Hischier et al., 2015). The increasing development of nano-enabled coatings will invariably lead to increased environmental release of TiO_2 NPs, prompting questions about their fate and bioavailability (Auffan et al., 2009; Van Broekhuizen et al., 2011; Nowack et al., 2012; Sun et al., 2014; Hischier et al., 2015; Mitrano et al., 2015; Coll et al., 2016).

Although some environmental and health hazards have been associated with TiO_2 NPs (Zhu et al., 2011; Simonin et al., 2017; Farner et al., 2019; Liu et al., 2019), the extent of their release from different outdoor coatings has not been well investigated, especially under variable climatic conditions. The near absence of measured environmental concentrations of TiO_2 (or any other) NPs greatly complicates their risk assessment. Indeed, most laboratory and *in situ* studies on NP release from coatings have been limited to a qualitative or semi-quantitative demonstration of release (e.g., with microscopy) or quantitative measurements based on the total metal content (Kägi et al., 2008; Olabarrieta et al., 2012; Al-Kattan et al., 2013; Zuin et al., 2014; Hincapié et al., 2015; Hischier et al., 2015; Kaegi et al., 2017; Zhang et al., 2017; Clar et al., 2018, 2019) – rather than a specific determination of the NP forms. Using a sensitive, magnetic-sector ICP-MS, we were recently (Azimzada et al., 2020) able to quantify mass and number release rates of TiO_2 NPs from painted surfaces during natural weathering cycles. While that study provided valuable information on real-life NP release quantities and particle size distributions, the data was mainly relevant for surfaces that were likely to retain the incoming snow or rainwater. It showed that the wet surface interaction time (i.e., contact time between the precipitation and the surface) was a critical environmental variable affecting NP release. Nonetheless, the study did not look at other outdoor surfaces, notably façades, or other nano-enhanced surfaces, such as stains. Furthermore, a major difficulty was the ability to distinguish Ti-rich natural colloids from TiO_2 NPs (Wagner et al., 2014; del Real et al., 2018).

Both exposure conditions and the nature of the coating will influence NP leaching and their interactions with other chemical constituent(s). For example, paint-released NPs have been shown to be embedded in their original paint matrix (Kaegi et al., 2010; Al-Kattan et al., 2014), which may result in them acting as a vector for the release and transport of other potentially toxic chemicals. Furthermore, while metal-based, manufactured NPs are often assumed to be composed of single elements or metal oxides (Loosli et al., 2019), only limited datasets are available with respect to their actual chemical identities, including metallic impurities, surface coatings, etc. While quantitative measurements of NP exposure concentrations are necessary for risk determinations, characterization of the released NP and their associations with other elements is necessary in order to define chemical hazard.

ICP-MS based techniques are well-suited for NP quantification as they are extremely sensitive, high-throughput and analyte-specific techniques that can quantify metal-based NPs and determine their size distributions on a single particle basis (Montaño et al., 2016; Azimzada et al., 2017; Gondikas et al., 2018; Meermann and Nischwitz, 2018). By analyzing the transient ICP-MS signal, NPs are identified as high-intensity spikes against a continuous background signal that is attributed to dissolved metals and background interferences (Degueldre et al., 2006; Tharaud et al., 2017). While single-particle ICP-MS (SP-ICP-MS) provides targeted single-element analysis of the NPs, SP-ICP-time-of-flight-MS (SP-ICP-TOF-MS) is able to simultaneously identify and quantify a full spectrum of elements in single particles (Hendriks et al., 2017, 2018; Praetorius et al., 2017). Nonetheless, due to the nature of the technology and the multiplicity of analytes in a single particle, SP-ICP-TOF-MS generally has higher size detection limits than SP-ICP-MS (Meermann and Nischwitz, 2018; Mozhayeva and Engelhard, 2020). For example, for Ti-containing NPs in surface waters, minimum detectable sizes of $<$20 nm have been determined using a high-resolution SP-ICP-MS (Hadioui et al., 2019; Azimzada et al., 2020), whereas size detection limits are typically above 60 nm when using SP-ICP-TOF-MS (Gondikas et al., 2018; Mozhayeva and Engelhard, 2020).

Given the above knowledge gaps, this study was designed to analyze TiO_2 NP release from two nano-enhanced surfaces under different weathering scenarios. Technical challenges were addressed by using recent improvements (Hadioui et al., 2019) in sensitivity and data treatment for both SP-ICP-MS and SP-ICP-TOF-MS. The specific objectives were: (i) to quantify and characterize TiO_2 NP release from a paint and a stain under natural weathering scenarios, and (ii) to distinguish TiO_2 NPs from the high quantity of colloidal Ti particles found in natural precipitation.

MATERIALS AND METHODS

Weathering Panels

Untreated oak slats were cut to obtain panels that were 0.64 cm thick, 6.4 cm wide and 8.4 cm long. They were subsequently painted (Behr Premium Plus Ultra Exterior Satin Enamel Ultra-Pure White paint) or stained (SICO exterior semi-transparent wood stain) with products that were advertised for their Nanoguard Technology and/or nano-sized pigments. The paint was uniformly distributed by applying 15 mL per side of each panel using a film applicator (Bird Film Applicator, Inc., Washington, United States) (Azimzada et al., 2020) with removal of the excess paint. Due to its lower viscosity, 5 mL of stain was applied per side using a paintbrush. Panel surfaces were coated twice on each side and at least two days was allowed for drying between each coat. The final dry paint or stain loadings were similar among panels for each coating type: 400 $\pm$ 40 g-paint

m^{-2} (or 4.4 g-paint per panel) and 36 ± 3 g-stain m^{-2} (or 0.4 g-stain per panel).

Natural Weathering Setups

The outdoor weathering setup consisted of two experimental designs – namely, vertical and slanted designs – that simulated two environmentally relevant weathering scenarios. The vertical design was designed to be more representative of a scenario where a surface is weathered by stationary water or snow accumulation (e.g., puddle or snow on a deck), whereas the slanted design was designed to represent the weathering of outdoor façades where precipitation does not accumulate on the surface. In the ***vertical design***, painted/stained panels were vertically positioned in pre-weighed, wide-mouth polypropylene containers (500 mL, Fisher Scientific) (**Figure 1A**). Every 2,3 weeks, panels were removed from the containers, and then placed outside in a new (empty) container. In the ***slanted design***, two polypropylene containers were fixed on top of each other and separated by a polypropylene mesh (**Figure 1B**). The mesh supported the panel, which was fixed in a slanted position in the top section. Rain came into contact with the panel and then flowed into the bottom container (the leachate collector), whereas snow had a tendency to sometimes collect on the surface of the panel. For each timepoint, the bottom container was removed, capped and replaced by another pre-labeled, pre-weighed and pre-cleaned container.

Due to the ubiquitous presence of nano- and micron-sized particles in the precipitation (Hochella et al., 2019; Rahim et al., 2019; Azimzada et al., 2020), one critical challenge in the experiments was to quantitatively distinguish NPs that were leached out of painted surfaces from background NPs in the natural precipitation (Wagner et al., 2014). Control experiments were thus critical to accurately determining NP release, with sufficient replication at each timepoint (n = 4). The use of untreated wooden panels was ruled out based on the preliminary observations that they rapidly disintegrated when subjected to natural weathering. Thus, for both designs, controls consisted of empty containers that were placed alongside exposure samples in order to collect the incoming precipitation (Azimzada et al., 2020). Containers were randomly placed in plastic bins, which protected them from tipping over by minimizing the impact of side winds. Bins were then placed outdoors on a 7th floor roof (Pavillon Roger-Gaudry, University of Montreal, Montreal, Canada). Samples were left undisturbed, unless they were buried by snow, in which case, excess snow was carefully scraped off the top of the containers (Azimzada et al., 2020). Fall weathering experiments started at the beginning of October 2018 and lasted for 11 weeks, while winter weathering experiments extended from late January (2019) until early April for a duration of 12 weeks. All exposure and control samples included 4 replicates. For the last two timepoints of the fall weathering series, the slanted samples tipped over and thus, the results for those timepoints are not available.

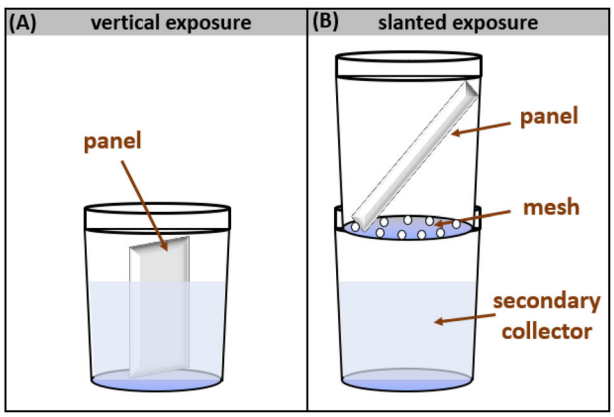

FIGURE 1 | Experimental setups for two weathering scenarios: **(A)** vertical exposure – consisting of a painted/stained panel vertically positioned in a polypropylene container, **(B)** slanted exposure – made up of two containers stacked on top of each other and separated by a polypropylene mesh, where the top container contains a painted/stained panel fixed in a slanted position. The vertical exposure is more representative of a surface in more sustained contact with precipitation whereas the slanted exposure is designed to be more representative of the weathering of an outdoor façade. Panels did not extend out of the containers, but rather they were custom cut to fit in the containers, while leaving an overhead space equivalent to 15% of the container height.

Indoor Weathering

To characterize surface-leached NPs using SP-ICP-TOF-MS, painted and stained (each with four replicates) panels were placed vertically into pre-weighed polypropylene containers, which were filled with 380 mL of Milli-Q water (i.e., panels fully immersed). Surfaces were then subjected to accelerated aging under freeze-thaw conditions, which involved successive cycles of 24 h freezing and 24 h thawing over 3 weeks (Azimzada et al., 2020). Following the freeze-thaw cycles, leachates were collected and prepared for SP-ICP-TOF-MS analysis.

Sample Preparation for SP-ICP-MS/SP-ICP-TOF-MS

At each timepoint, samples (exposure and controls) were brought inside the lab, left to melt and then gently mixed. The samples were then weighed and placed in a sonicator bath for 30 minutes (Branson Ultrasonic Cleaner, 5510R-DTH Model, 135 W, 42 kHZ ± 6%). Eight (8) to 10 mL of the samples were filtered (0.45 μm cut-off) through a 33 mm diameter PVDF (Polyvinylidene fluoride) syringe filter (Sigma-Aldrich) that had been pre-rinsed with 12 mL Milli-Q water and 6 mL of sample (Azimzada et al., 2020). The filtration step is designed to protect the nebulizers by avoiding build-up and blockage, while being large enough to minimize exclusion of the NPs. While pre-rinsing the filter with sample minimizes adsorptive losses, the 0.45 μm cutoff is nonetheless operationally defined- particle losses would lead to an underestimation of particle numbers.

SP-ICP-MS Analysis and Data Acquisition

SP-ICP-MS measurements were performed on a magnetic sector ICP-MS (AttoM ES, Nu Instruments, United Kingdom), at low

resolution (300), using single ion acquisition in fast-scan mode (Shaw and Donard, 2016). To further enhance the sensitivity, the ICP-MS used a desolvator (Aridus II, Teledyne Cetac Technologies), which utilized a PFA (perfluoroalkoxy) micro-flow nebulizer (self-aspiration rate of 200 μL min^{-1} at 1 L min^{-1} of Ar) (Fréchette-Viens et al., 2019; Hadioui et al., 2019). Optimized membrane sweep gas (argon) flow rates typically ranged between 3–7 L min^{-1}, while the nebulizer gas (argon) flow was between 0.7–1.0 L min^{-1}. In accordance with previously optimized strategies (Hadioui et al., 2019) to lower the size detection limits (SDL) 49Ti was chosen for analysis. With an acquisition time of 50 s per sample and an optimized dwell time of 50 μs (Hadioui et al., 2019), ca. 10 (Hischier et al., 2015) datapoints were obtained per replicate. Sensitivity calibrations for 49Ti were based on ionic standards (High Purity Standards) and transport efficiency (TE) measurements were performed using a suspension of ultra-uniform 30 nm Au NPs (NanoComposix, AUXU30-1M) that were previously validated using a second standard reference material (60 nm Au NPs, NIST8013) (Hadioui et al., 2019). Standards for TE measurements were prepared daily at 50 ng L^{-1}. TE values ranged between 13–15%, corresponding to an actual sample injection into the plasma of 0.45–0.55 μL s^{-1}. Filtered samples were diluted up to 10× to ensure that the incidences of concurrent peaks were minimized (less than 10,000 events or 1% of total datapoints), while ensuring a statistically significant number of NPs (>500 events). Matrix effects were not observed (Azimzada et al., 2020).

SP-ICP-TOF-MS Analysis and Data Acquisition

SP-ICP-TOF-MS measurements were performed on a time-of-flight ICP-MS (Nu Vitesse, Nu Instruments, United Kingdom), using a segmented reaction cell with ca. 4–6 cm^3 min^{-1} of He and ca. 4 cm^3 min^{-1} of H_2 gas introduced to eliminate argon and nitrogen-based interferences. This method improved the sensitivity of the technique by allowing the higher abundance isotopes of elements like Si, K, Ca, Cr, Fe, and Se to be monitored without interference. A near full range of time of flight mass spectra (23–238 amu) were acquired every 25.5 μs, and three acquisitions were combined before electronics noise was subtracted and isotope signals were integrated over their defined mass positions to produce individually stored measurements for Na to U, every 76 μs. Data were acquired for a total sampling time of about 30 s, for the most concentrated samples, to a maximum of 2 min for dilute samples. Mass spectra were acquired continuously, in an uninterrupted manner and without loss of data. Sensitivity was further improved by using an Aridus II desolvator as above, with similar parameters as the magnetic sector instrument. TE was determined using the particle size method (Pace et al., 2011) by measuring the instrument sensitivity (counts s^{-1} ng L^{-1}) for ionic gold standards and mass sensitivity (counts ng^{-1}) for a highly monodisperse Au NP standard (known size and density). This led to TE values ranging between 10–15%. An ultra-uniform NP standard of 30 nm (NanoComposix, AUXU30-1M) was used to calculate TE, while 60 nm Au NP (NanoComposix) and 40 nm Ag (NanoComposix) standards were used for validation of the TE values. A multi-element standard (SPEX CertiPrep) containing all metals was used for ionic sensitivity determinations.

SP-ICP-MS/SP-ICP-TOF-MS Data Processing

SP-ICP-MS data were analyzed using NuQuant software version 2.2 (Nu Instruments, United Kingdom), based on the methodology described in Hadioui et al. (2019) and Shaw and Donard (2016). In summary, the data analysis algorithm used data smoothing to reduce baseline fluctuations; created rolling search windows where it searched for NP peaks based on maximum intensities; and calculated local backgrounds for each peak based on data preceding the pre-inflection points. For each detected NP, the local background was subtracted from the integrated raw data, while the average of local peak backgrounds was used to calculate dissolved metal contents.

For SP-ICP-TOF-MS data, a modified version of NuQuant software (NuQuant Vitesse prototype, Nu Instruments, United Kingdom) was used, where the algorithm searched for a target isotope, here 48Ti, using similar smoothing and peak detection parameters as in the single-particle analysis. The start and end timestamps for each detected particle event were determined and used to identify counts for all isotopes. The full width half maximum (FWHM) values, along with the standard deviation of the background (for each isotope) were used to estimate the noise threshold, above which particle events were reported. This threshold, typically consisting of 5–7 multiples of the standard deviation of the background, was applied to filter out background artifacts while optimizing the detection of real NP peaks. Elements of interest (especially those with low intensities) were visually checked to ensure that background artifacts were avoided (i.e., very slender or very wide peaks with low intensity).

NP masses (and sizes if density and shape can be assumed) were calculated using calibrated multi-element sensitivities and transport efficiency measurements obtained for the monodisperse Au NPs (Pace et al., 2011). Size calculations for TiO_2 were performed by assuming a spherical particle with a density of 4.23 g cm^{-3}, corresponding to rutile (Azimzada et al., 2020).

Ti Analysis by Quantitative ICP-MS

Given the very low Ti concentrations in the precipitation samples (i.e., ng L^{-1} levels) and dilutions required to reduce acid concentrations prior to ICP-MS analysis, the use of digestion protocols (Gondikas et al., 2014; Loosli et al., 2019) to obtain total Ti was unfortunately not viable here. Ti measurements were nonetheless performed on leachate samples, following filtration over a 0.45-μm PVDF filter and addition of 67–70% HNO_3 (ultratrace grade, BDH Aristar Ultra) in polypropylene tubes to obtain a final acid content of 20% v/v. Samples were left for 16 h at 85 °C in a DigiPREP digestion system (SCP Science) (Azimzada et al., 2020) and

then diluted 5–10× with Milli-Q water to obtain a final HNO_3 content of 2–4% v/v for the ICP-MS analysis. The measured Ti nominally included dissolved Ti as well as any of the sub-0.45-μm particles. Although the addition of concentrated HNO_3 is not sufficient for the complete digestion of the TiO_2 (De la Calle et al., 2016), measurements were performed to provide some additional validation of the single-particle techniques for which particle concentrations are determined from the number of transient peaks, using a non-acidified sample (i.e., greater potential for adsorptive losses). Digested Ti thus represents an operationally defined fraction (Azimzada et al., 2020) that may not capture all of the colloidal Ti in the sample.

RESULTS AND DISCUSSION

Technical Considerations in the SP-ICP-MS and SP-ICP-TOF-MS Measurements

Fewer than three spikes per min were generally observed for a Milli-Q water blank (Fréchette-Viens et al., 2019). By assuming

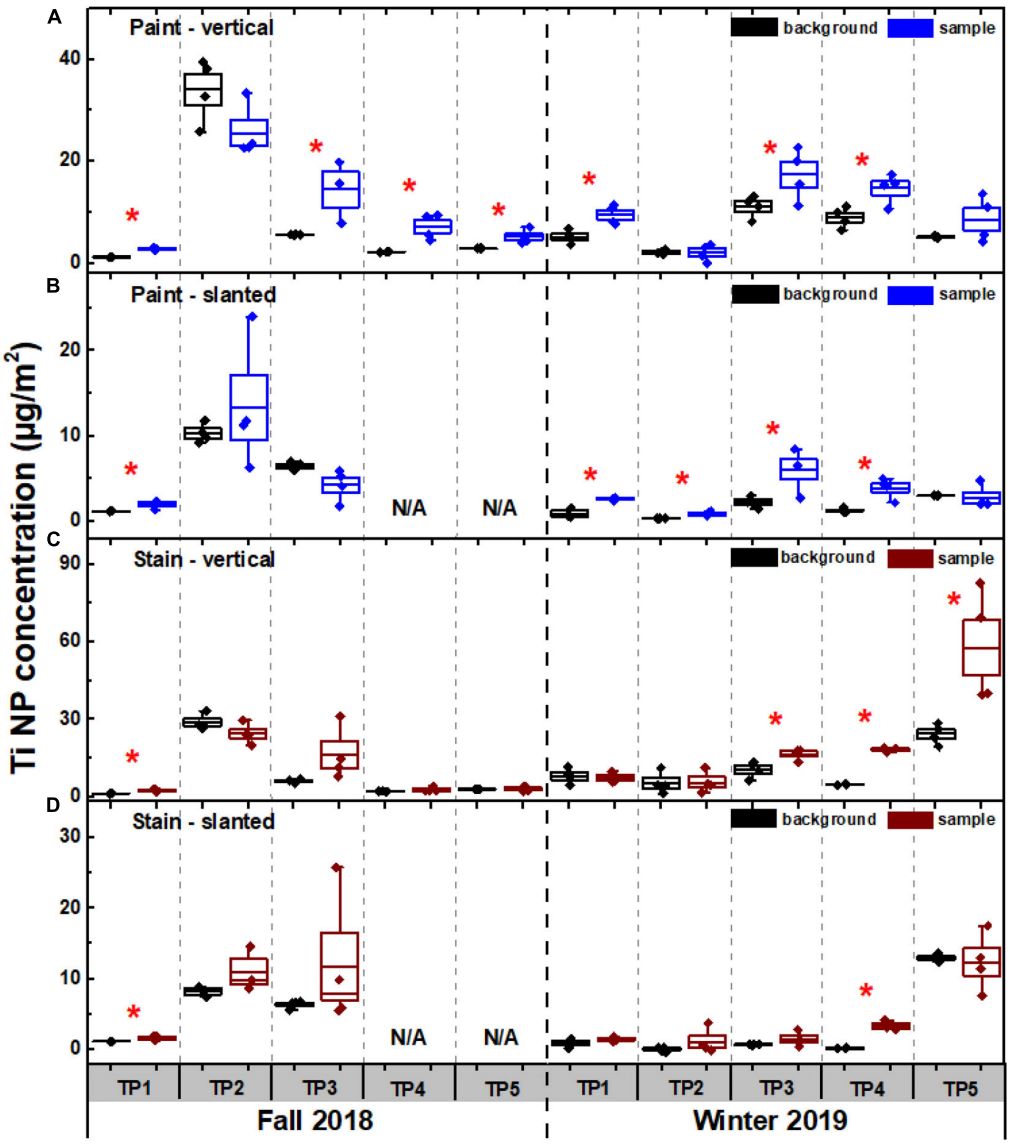

FIGURE 2 | Quantification of Ti containing NPs in the precipitation (i.e. background) and in the precipitation following its contact with **(A,B)** painted and **(C,D)** stained panels. Weathering experiments were conducted using two exposure designs (**Figure 1**), **(A,C)** vertical and **(B,D)** slanted, for painted and stained panels. A red star indicates a significant difference ($N = 4$, student t-test, $p < 0.05$) between the NP content in the background and the NP content in the sample. NP concentrations were normalized by the surface area of the painted/stained panels subjected to weathering. Containers were renewed at each timepoint (TP). Measurements were performed using a magnetic sector ICP-MS in single particle mode. Measured NP content includes particles between the instrumental size detection limit of ∼15 nm and the filtration cut-off (0.45 μm). N/A denotes two samples that were lost.

that the detection of 10 NPs during a 50 s acquisition would be required in order to have sufficient confidence that particles were being detected (Laborda et al., 2019), one can estimate a detection threshold of ca. 360 NP mL^{-1} with a minimum detectable (TiO_2 equivalent) particle size of ∼15 nm (**Supplementary Figure S1A**). The size detection limit compare favorably with those that have generally been determined by SP-ICP-MS [∼60 nm (Gondikas et al., 2014; Lee et al., 2014)]. The SP-TOF-ICP-MS had higher, matrix-sensitive size detection limits, ranging from 30 nm (in Milli-Q water) to 46 nm (in the rain) (i.e., assuming spherical TiO_2 particles, **Supplementary Figure S2**). In that case, minimum detectable particle numbers were kept <1000 mL^{-1} by increasing the acquisition time to 120 s. For both techniques, raw data corresponding to NPs that are close to instrumental size detection limits have been provided in **Supplementary Figures S1B**, **S2B,D,F** for the different matrices. In all cases, NP concentrations in the samples were consistently above 10,000 mL^{-1}, well above the detection limits. While these detection limits are among the lowest in the literature for TiO_2, it is important to note that "nanoparticle" number measurements presented below are necessarily for particles that are larger than the lower size detection limits (e.g., 15 nm by magnetic sector SP-ICP-MS; 34 nm by SP-TOF-ICP-MS) but smaller than the filtration cut-off (i.e., 0.45 μm).

Characterization of TiO_2 NPs in the Paint and Stain

Immediately prior to analysis by SP-ICP-MS, liquid acrylic paint was diluted $2 \times 10^7\times$ in Milli-Q water, while stain was diluted $2 \times 10^5\times$. TiO_2 NPs in the paint were fairly polydisperse with a particle size distribution extending from about 20 nm (just above the size detection limit) to beyond 200 nm (**Supplementary Figure S3A**), with a concentration of $(6.8 \pm 0.1) \times 10^{15}$ NPs kg-paint^{-1}. TiO_2 NPs in the stain were smaller with a majority (>95%) of the particles between 20 and 100 nm (**Supplementary Figure S3B**) and a

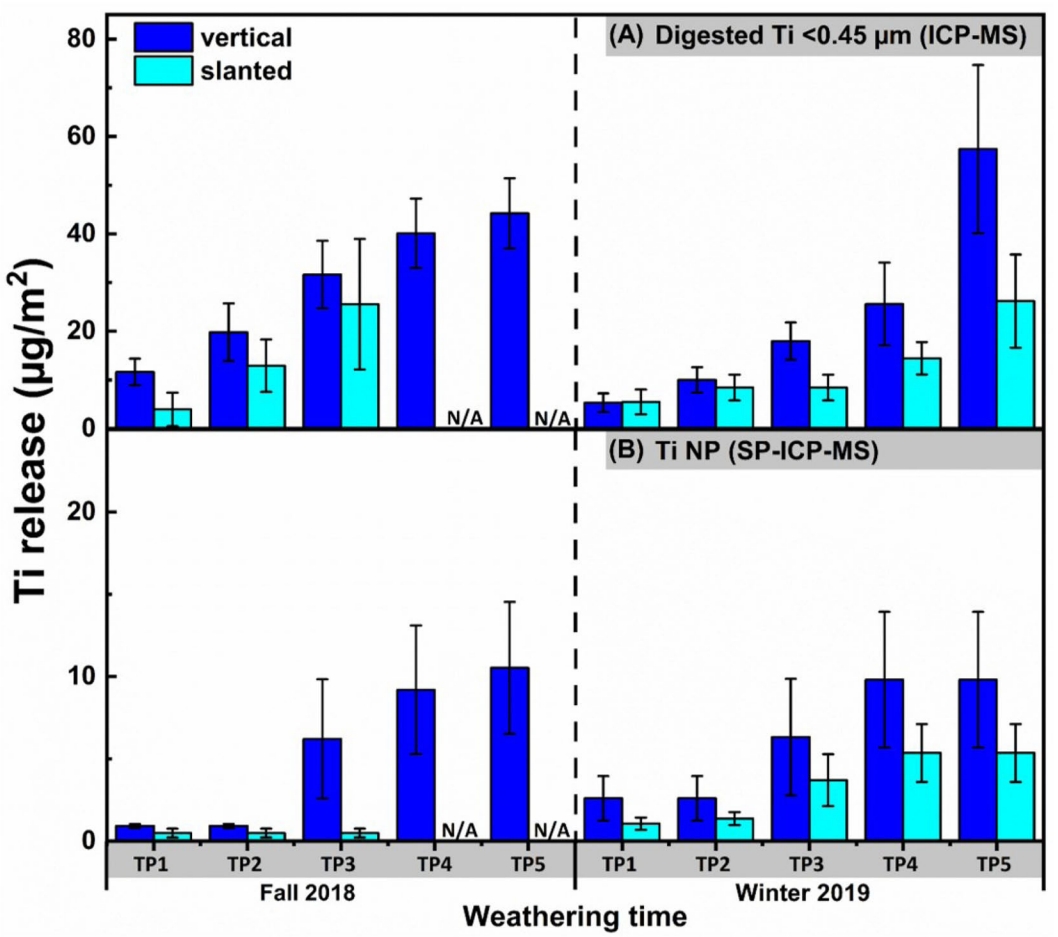

FIGURE 3 | Cumulative concentrations of sub-0.45-μm Ti determined by **(A)** ICP-MS on acidified samples and **(B)** SP-ICP-MS, obtained by integration of the NP peaks. Ti was measured following its release from the **painted** surfaces in vertical and slanted exposure modes (N = 4 for each condition). Release was normalized by the surface area of the painted panels that were subject to weathering and corrected for the pre-existing natural background in the precipitation. Measurements were performed using a magnetic sector ICP-MS. N/A denotes two samples that were lost.

concentration of $(2.9 \pm 0.4) \times 10^{13}$ NPs kg-stain^{-1}. Number-based average particle sizes corresponded to 131 ± 53 nm in the liquid paint and 42 ± 24 nm in the stain, where standard deviations reflected polydispersities, rather than errors determined on repeated measurements (typically ∼3 nm). Particle concentrations corresponded to about 5% w/w in the paint and 0.001% w/w NP in the stain.

Release of NPs From Painted and Stained Surfaces

In spite of precautions that included the use of four replicates for samples and controls; their randomization in the protective bins and the lowering of detection limits of the SP-ICP-MS technique; there were still cases where NPs in the leachates were quantitatively indistinguishable from those in the precipitation (t-test, $p > 0.05$). This result was more frequently observed for the slanted exposures (**Figure 2**) and was primarily due to relatively high background concentrations with respect to the low quantities of released NPs. In agreement with Azimzada et al. (2020), while no or low release appeared to occur during specific weathering conditions, such as a lack of precipitation (**Supplementary Figure S4**), background concentrations were also highly episodic. Given that the errors were cumulative, detection of NP release was only significant for cases where release was high, and background was low (**Figure 2**). This implies that the measured release quantities are minimum values only, since low release quantities can easily be masked by pre-existing high background concentrations of the Ti containing NPs.

In addition to characterizing the NPs by SP-ICP-MS, Ti in the 0.45-μm filtrate was measured using quantitative ICP-MS, following acidification and heating of the samples. The concentration of NPs determined by integration of the SP-ICP-MS peaks corresponded to about 10–30% of the values determined based on the digested filtrates of the paint and stain leachates. While the remaining fraction of Ti could be dissolved forms or Ti NPs below the instrumental detection limits, it is also important to acknowledge that a fraction of the missing mass balance could be attributed to sorptive losses in the sample introduction system (Azimzada et al., 2017; Fréchette-Viens et al., 2017; Hadioui et al., 2019) and losses due to incomplete ionization (Goodall et al., 1993; Meermann and Nischwitz, 2018; Hadioui et al., 2019) (recall that SP-ICP-MS is necessarily performed on non-acidified samples).

The size distributions of the NPs released from the painted (**Supplementary Figure S5B**) and stained (**Supplementary Figure S5C**) surfaces were similar to NPs found in the natural precipitation (**Supplementary Figure S5A**). For example, paint-released NPs were mostly <60 nm, with a size range from

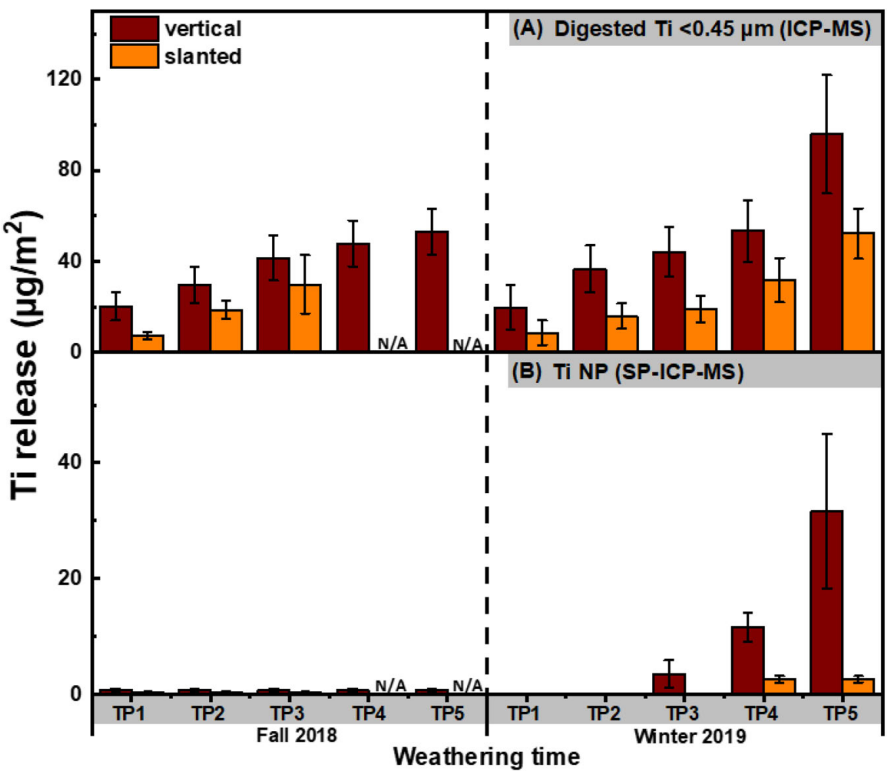

FIGURE 4 | Cumulative concentrations of sub-0.45-μm Ti determined by **(A)** ICP-MS on acidified samples and **(B)** SP-ICP-MS, obtained by integration of the NP peaks. Ti was measured following its release from the **stained** surfaces in vertical and slanted exposure modes (N = 4 for each condition). Release was normalized by the surface area of the painted panels that were subject to weathering and corrected for the pre-existing natural background in the precipitation. Measurements were performed using a magnetic sector ICP-MS. N/A denotes two samples that were lost.

15–120 nm in agreement with our previous results (Azimzada et al., 2020). Generally, they had smaller sizes than those originally found in the liquid paint (**Supplementary Figure S3A**), indicating that there was some agglomeration in the original paint mixture. In contrast, NPs released from the stained surfaces ranged from 15–100 nm with a size distribution (**Supplementary Figure S5C**) that was similar to the original particles in the stain (**Supplementary Figure S3B**).

Role of Exposure Mode (Vertical or Slanted), Season (Fall or Winter) and Coating Type (Paint or Stain)

Generally speaking, less TiO_2 NP release was observed for the slanted exposures where precipitation was not allowed to remain in contact with the panels (**Figures 3**, **4**). Furthermore, NP release from the vertical painted surfaces was still several times less than that observed in Azimzada et al. (2020) and others (Kägi et al., 2008; Olabarrieta et al., 2012; Zuin et al., 2014; Zhang et al., 2017), where much longer weathering times or accelerated weathering conditions were used in a similar experimental design. The results show that NPs are more likely to be leached from surfaces that have a prolonged exposure to precipitation.

While comparable NP release was observed for the painted surfaces that were weathered in fall or winter; for the stain, NP release was clearly greater in the winter (t-test, $p < 0.05$) (**Figures 3B**, **4B**). It is also notable that most NP release did not occur in the initial stages of the exposure (<3 μg-Ti m^{-2} over the first 4,5 weeks, corresponding to timepoints 1 and 2), but rather during the final 6,7 weeks (i.e., last three timepoints) of the weathering period. This observation could be attributed to two possible explanations: (i) an initial weathering period rendered

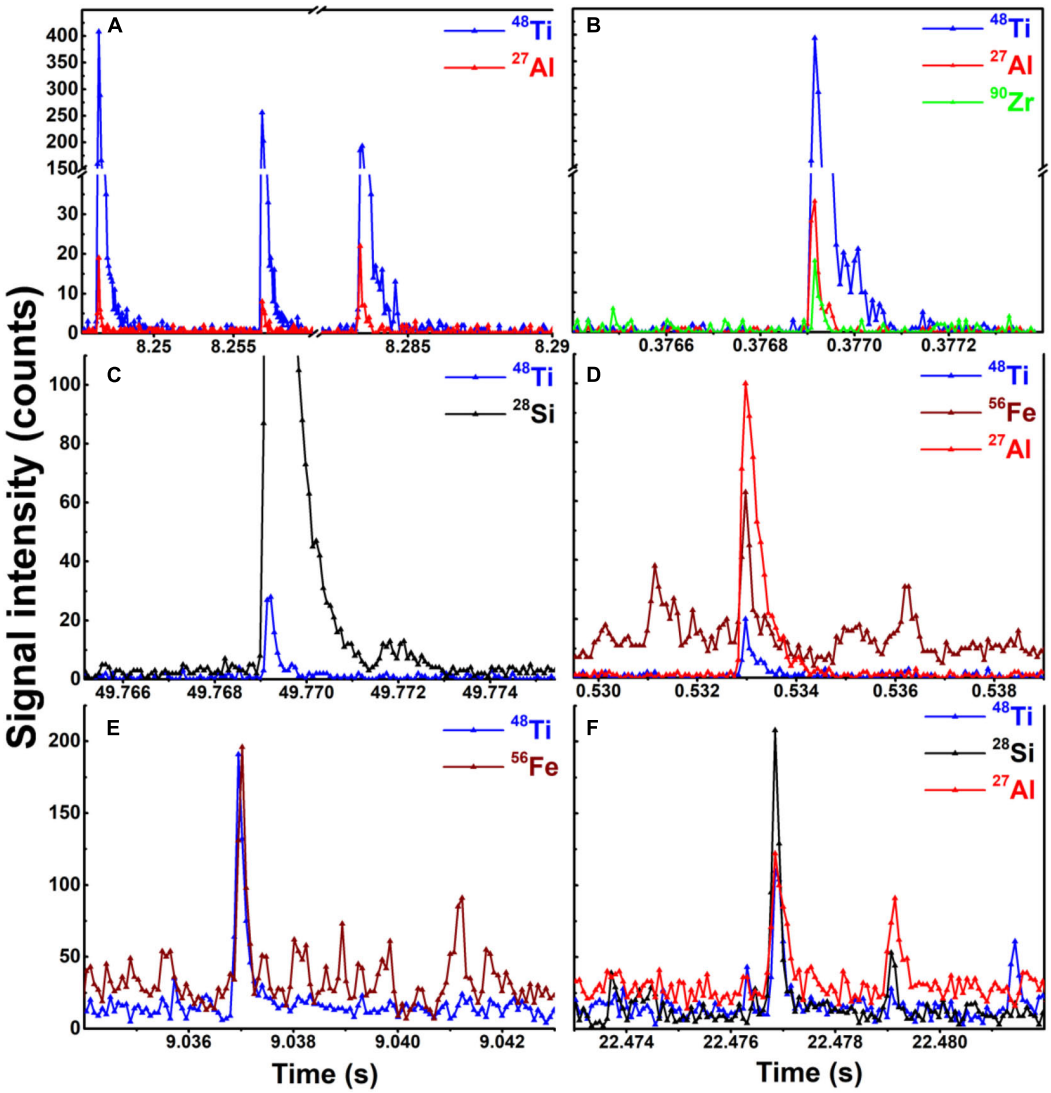

FIGURE 5 | Examples of SP-ICP-TOF-MS raw peak data corresponding to Ti-containing NPs detected in the different matrices. Association of Ti with **(A)** Al or with **(B)** Al and Zr in the liquid paint. Association of Ti with **(C)** Si or with **(D)** Fe and Al in the liquid stain. Association of Ti with **(E)** Fe and **(F)** Si and Al in Montreal rain.

the samples more vulnerable to NP release in the subsequent weeks, or (ii) the samples were exposed to conditions that were more conducive to NP release during the final weeks of the fall and winter exposure period (Azimzada et al., 2020). Indeed, weather data (**Supplementary Figure S4**) reveals that more numerous incidents of precipitation, slushy snow and freeze-thaw conditions (about 20 rainy/snowy days with temperatures fluctuating between +10°C and −10°C) were observed near the end of fall and winter seasons. Irrespective of the NP release trend, Ti NPs in the leachate consistently increased over time in both the fall and winter (**Figures 3A**, **4A**).

NP release from painted surfaces was fairly small, eventually surpassing 10 μg-Ti m^{-2} by the end of the 11-week fall weathering experiment and remaining slightly below 10 μg-Ti m^{-2} during the winter exposure (**Figure 3B**). Release from stained surfaces was very low (<1 μg-Ti m^{-2}) and neither increased throughout fall, nor during the first 4 weeks of the winter exposure (**Figure 4B**). During the spring snowmelt period, however, the quantities of NPs released from the stain greatly surpassed those released from paint, eventually exceeding 30 μg-Ti m^{-2}. While the absolute quantities (mass normalized by surface area) released from painted and stained surfaces were generally on the same order of magnitude, when given as a proportion of the total Ti NPs in the coatings, Ti release from the stained surfaces (max release about 6%) was several orders of magnitude greater than that released from painted surfaces (max release about 5×10^{-5}%). This result might be related to the size distribution in the original coating, as smaller particles are thought to be more easily released from the matrix due to weathering/crack formation, etc. (Bossa et al., 2017) which could also help explain the similarity of the release histograms observed in **Supplementary Figure S5**. Overall, it is clear that NP leaching is strongly influenced by the chemistry of the coating and that some nano-enhanced surfaces (e.g., stained surfaces) are much more vulnerable to NP release than others.

Distinguishing the Engineered NPs From Background NPs in the Precipitation Using SP-ICP-TOF-MS

SP-ICP-TOF-MS measurements on the NPs in the diluted paint and stain showed that in addition to Ti-containing NPs, several other particle types were observed including those containing Fe, Al, Zr, Ce, and Si. In both paints and stains, Ce (i.e., CeO_2) (Piccinno et al., 2012; Clar et al., 2018; Scifo et al., 2018) and Si (i.e., SiO_2) (Zhou et al., 2002; Mizutani et al., 2006; Al-Kattan et al., 2015) are known to impart thermal/mechanical resistance and weathering durability (e.g., against UV) to the coatings, while Al, Fe and Zr NPs could be purposefully added to improve coating properties (Piccinno et al., 2012) or could simply be present as impurities from the manufacturing process. Clear differences were observed when comparing the nature of the particles in the paint (**Supplementary Figure S6**) to those in the stain (**Supplementary Figure S7**). Peak co-incidences indicated that the Ti-containing NPs in the liquid paint (**Figures 5A,B**) were often associated with Al (<20% of TiO_2 NPs) and rarely with Zr (<1% of TiO_2 NPs) (**Figure 6A**). Nonetheless, over 70% of the particles had Ti/Al or Ti/Zr mass ratios above 10, when calculated on a particle by particle basis (**Figures 7A,B**). Three alternative explanations are proposed to explain these high ratios in the paint: (i) traces of Al or Zr, whether in dissolved or small NP forms, were bound to Ti-containing NPs or their agglomerates; (ii) these metals (or their oxides) were used as coatings on Ti-containing NPs (Loosli et al., 2019); or (iii) there were impurities in the Ti-containing NPs. In contrast to measurements on the liquid paint, no Al and almost no Zr were detected in the Ti-containing NPs in the paint leachate (**Figure 6B**), even though high amounts of dissolved Al were observed as compared to the controls (**Supplementary Figure S8**). The absence of Al in the Ti NPs found in the leachate suggests that during the weathering of the painted surface, TiO_2 NPs were separated from an Al-containing matrix (hypothesis i), resulting in increased dissolved Al concentrations. The low detection of Zr in the leachate could simply be explained by its low concentration (relative to instrument detection limits).

In the liquid stain, Ti-containing NPs were often associated with Fe (∼7%) and Si (∼8%) and less often with Al (∼3%, **Figures 5C,D**). This result is not direct evidence that Fe, Si, or

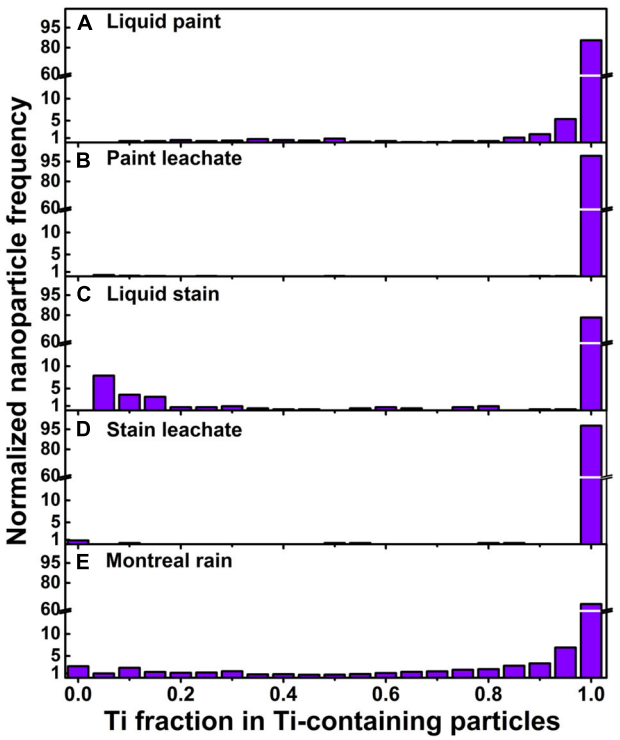

FIGURE 6 | Elemental fractions of Ti in Ti-containing NPs for **(A)** liquid paint (diluted in Milli-Q water), **(B)** paint leachate, **(C)** liquid stain (diluted in Milli-Q water), **(D)** stain leachate, and **(E)** Montreal rainwater. Measurements were performed using a SP-ICP-TOF-MS. Under the described conditions, a Ti fraction of 1 implies that the NP is primarily composed of Ti (or TiO_2, i.e., single metal), whereas fractions < 1 indicate the presence of additional metals within the NP or agglomerate. Paint and stain leachates were collected during accelerated weathering experiments of the coated panels in Milli-Q water.

Al co-occurred with the Ti of a given NP, since Ti-containing NPs could have simply been associated with particles such as aluminosilicates within heteroagglomerates. Indeed, given that the Ti fraction was often below 0.2 (**Figure 6C**), it is possible that small TiO_2 NPs (often <50 nm, **Supplementary Figure S3B**) were associated with larger Fe and Si based particles in the liquid stain (**Figures 7C,D**). This hypothesis of heteroagglomeration was reinforced by the relatively high particle numbers that were found for the Fe and Si NPs, i.e., 1 Ti NP was detected per 25 Fe NPs/10 Si NPs. Given that the vast majority of Ti NPs in the leachate (>95% of NPs) were not associated with any other metals (including Fe or Si) (**Figure 6D**), the results are another indication that the nature of the Ti NPs within the painted or stained surfaces is different from that found in the leachate, following the weathering process. The observation that Ti NPs in the leachate are primarily "pure" particles is important from the perspective of risk analysis.

SP-ICP-MS measurements showed a significant presence of Ti-containing NPs in the rain and snow, which are thought to result from both anthropogenic activities and natural processes (Hochella et al., 2019; Rahim et al., 2019). Generally, engineered NPs are assumed to contain a single element with trace impurities (if any) (Praetorius et al., 2017), whereas NPs of natural origin are believed to more often contain multiple elements. Using elemental purity as an indicator for the origin of the NPs, up to 50% of the Ti-containing NPs in Montreal rain/snowmelt could be classified as engineered NPs (with >99% purity), while the rest had multi-element identities (**Figure 6E**). In the multi-element particles, Ti typically co-occurred with Fe and less often with Al and Si (**Figures 5E,F**, **7E,F**), further supporting the hypothesis

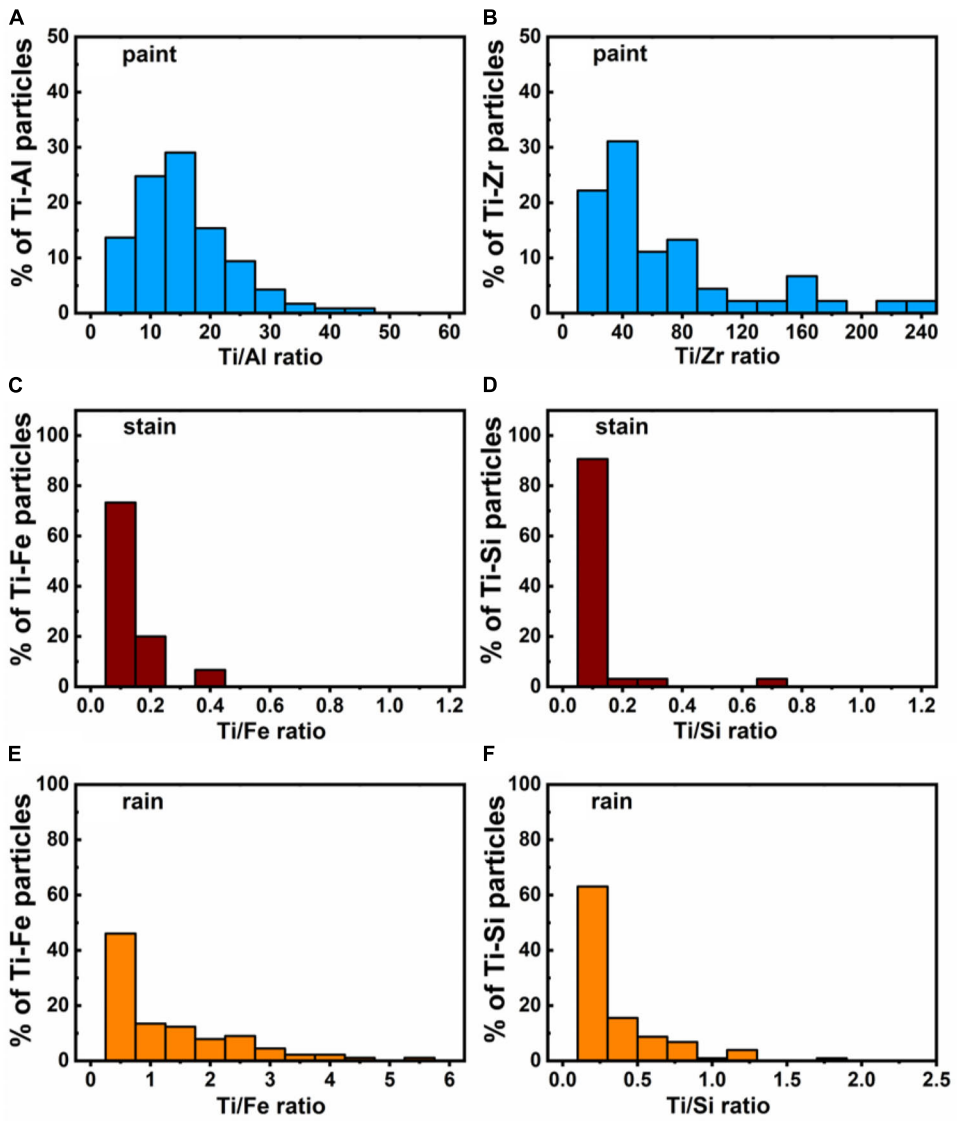

FIGURE 7 | Elemental mass ratios measured on individual particles for major associations of the Ti in **(A,B)** liquid paint, **(C,D)** liquid stain and **(E,F)** Montreal rain samples. Measurements were performed using a SP-ICP-TOF-MS.

that they were naturally occurring particulates (Hochella et al., 2008; Plathe et al., 2013). Nonetheless, the ratio of single element particles should be used carefully when distinguishing NP source since it will vary geographically and temporally, as a function of urban, industrial or natural setting of the location and/or episodic events. While multi-element Ti particles predominate in nature, it is possible for TiO_2 nanoparticles to occur naturally. The environmental release of anthropogenic TiO_2, including those from the paints and stains, will nevertheless increase the overall proportion of Ti in the Ti-containing particles (**Figure 6**), providing an indication of particle source.

Environmental Implications

TiO_2 NPs were leached out of both painted and stained surfaces under natural weathering conditions. For the products tested here, absolute release quantities were comparable (i.e., within one order of magnitude), although this was mainly because there were initially far more NPs in the paint and far greater release by the stain. NP release dynamics were largely driven by the nature of contact with the precipitation. For instance, for scenarios where the panels were in extended contact with sitting water or snow (e.g., on a deck), stronger NP release was observed as compared to the weathering of surfaces where precipitation was not allowed to accumulate (e.g., outdoor facades). While the weathering experiments were performed under realistic environmental scenarios, losses of the NP due to agglomeration (Azimzada et al., 2020; Farner et al., 2020) and a potential underestimation of the measured NP concentrations (Azimzada et al., 2017; Hadioui et al., 2019) implies that the actual release rates could be higher in environmental systems. On the other hand, the recovered (measured) NP concentrations are likely to represent the most mobile and bioavailable fraction that is likely to be of highest environmental relevance.

It is of note that the individual NP appeared to be associated with multiple elements in the pure stain and paint, whereas after weathering of the dried compounds from the surfaces, particles were more elementally pure, suggesting dissociation from a complex matrix. The results also indicated that the particles in the leachates were smaller than NPs detected in the rain, which often had multi-element identities, and thus, larger sizes than those estimated using analysis with a single isotope (i.e., SP-ICP-MS). This implies that, in addition to NPs, other compounds, including potentially toxic ones, are being released during the degradation of these nano-enhanced surfaces. Finally, while anthropogenic NPs already appear to have a significant presence in precipitation, NP release from consumer products, such as paints and stain, will only contribute further to their presence in the environment.

DATA AVAILABILITY STATEMENT

The raw data supporting the conclusions of this article will be made available by the authors, without undue reservation, to any qualified researcher.

AUTHOR CONTRIBUTIONS

KW, JF, NT, and AA conceived the study and designed the experimental plan. AA, JF, IJ, and CL-K prepared the weathering setups, collected the samples and prepared them for single particle and total metal analysis. AA and MH conducted SP-ICP-MS analysis. AA and PS conducted SP-ICP-TOF-MS analysis. AA, MH, and PS performed the SP-ICP(-TOF)-MS data treatment. AA organized all data and performed statistics. AA and KW wrote the manuscript, with complementary input from other authors. All authors contributed to the article and approved the submitted version.

FUNDING

This research was supported by the Natural Sciences and Engineering Research Council of Canada (NSERC), Environment and Climate Change Canada, a McGill Engineering Doctoral Award (MEDA), Pollution in Urban Environments (PURE CREATE) and an EcotoQ Excellence Scholarship.

ACKNOWLEDGMENTS

We thank Prof. Ghoshal (McGill University) for providing access to a film applicator.

SUPPLEMENTARY MATERIAL

The Supplementary Material for this article can be found online at: https://www.frontiersin.org/articles/10.3389/fenvs.2020.00091/full#supplementary-material

REFERENCES

Al-Kattan, A., Wichser, A., Vonbank, R., Brunner, S., Ulrich, A., Zuin, S., et al. (2013). Release of TiO2 from paints containing pigment-TiO2 or nano-TiO2 by weathering. *Environ. Sci. Process. Impacts* 15, 2186–2193.

Al-Kattan, A., Wichser, A., Vonbank, R., Brunner, S., Ulrich, A., Zuin, S., et al. (2015). Characterization of materials released into water from paint containing nano-SiO2. *Chemosphere* 119, 1314–1321. doi: 10.1016/j.chemosphere.2014.02.005

Al-Kattan, A., Wichser, A., Zuin, S., Arroyo, Y., Golanski, L., Ulrich, A., et al. (2014). Behavior of TiO2 released from nano-TiO2-containing paint and comparison to pristine nano-TiO2. *Environ. Sci. Technol.* 48, 6710–6718. doi: 10.1021/es5006219

Auffan, M., Rose, J., Wiesner, M. R., and Bottero, J.-Y. (2009). Chemical stability of metallic nanoparticles: a parameter controlling their potential cellular toxicity in vitro. *Environ. Pollut.* 157, 1127–1133. doi: 10.1016/j.envpol.2008.10.002

Azimzada, A., Farner, J. M., Hadioui, M., Liu-Kang, C., Jreije, I., Tufenkji, N., et al. (2020). Release of TiO2 nanoparticles from painted surfaces in cold climates: characterization using a high sensitivity single-particle ICP-MS. *Environ. Sci. Nano* 7, 139–148. doi: 10.1039/c9en00951e

Azimzada, A., Tufenkji, N., and Wilkinson, K. J. (2017). Transformations of silver nanoparticles in wastewater effluents: links to Ag bioavailability. *Environ. Sci. Nano* 4, 1339–1349. doi: 10.1039/c7en00093f

Bossa, N., Chaurand, P., Levard, C., Borschneck, D., Miche, H., Vicente, J., et al. (2017). Environmental exposure to TiO2 nanomaterials incorporated in building material. *Environ. Pollut.* 220, 1160–1170. doi: 10.1016/j.envpol.2016.11.019

Clar, J. G., Platten, W. E. III, Baumann, E., Remsen, A., Harmon, S. M., Rodgers, K., et al. (2019). Release and transformation of ZnO nanoparticles used in outdoor surface coatings for UV protection. *Sci. Total Environ.* 670, 78–86. doi: 10.1016/j.scitotenv.2019.03.189

Clar, J. G., Platten, W. E. III, Baumann, E. J. Jr., Remsen, A., Harmon, S. M., Bennett-Stamper, C. L., et al. (2018). Dermal transfer and environmental release of CeO2 nanoparticles used as UV inhibitors on outdoor surfaces: implications for human and environmental health. *Sci. Total Environ.* 613, 714–723. doi: 10.1016/j.scitotenv.2017.09.050

Coll, C., Notter, D., Gottschalk, F., Sun, T., Som, C., and Nowack, B. (2016). Probabilistic environmental risk assessment of five nanomaterials (nano-TiO2, nano-Ag, nano-ZnO, CNT, and fullerenes). *Nanotoxicology* 10, 436–444. doi: 10.3109/17435390.2015.1073812

De la Calle, I., Menta, M., and Seby, F. (2016). Current trends and challenges in sample preparation for metallic nanoparticles analysis in daily products and environmental samples: a review. *Spectrochim. Acta Part B At. Spectrosc.* 125, 66–96. doi: 10.1016/j.sab.2016.09.007

Degueldre, C., Favarger, P.-Y., and Wold, S. (2006). Gold colloid analysis by inductively coupled plasma-mass spectrometry in a single particle mode. *Anal. Chim. Acta* 555, 263–268. doi: 10.1016/j.aca.2005.09.021

del Real, A. E. P., Castillo-Michel, H., Kaegi, R., Larue, C., de Nolf, W., Reyes-Herrera, J., et al. (2018). Searching for relevant criteria to distinguish natural vs. anthropogenic TiO2 nanoparticles in soils. *Environ. Sci. Nano* 5, 2853–2863. doi: 10.1039/c8en00386f

Farner, J. M., Cheong, R. S., Mahé, E., Anand, H., and Tufenkji, N. (2019). Comparing TiO2 nanoparticle formulations: stability and photoreactivity are key factors in acute toxicity to *Daphnia magna*. *Environ. Sci. Nano* 6, 2532–2543. doi: 10.1039/c9en00666d

Farner, J. M., De Tommaso, J., Mantel, H., Cheong, R. S., and Tufenkji, N. (2020). Effect of freeze/thaw on aggregation and transport of nano-TiO2 in saturated porous media. *Environ. Sci. Nano* 7, 1781–1793.

Fréchette-Viens, L., Hadioui, M., and Wilkinson, K. J. (2017). Practical limitations of single particle ICP-MS in the determination of nanoparticle size distributions and dissolution: case of rare earth oxides. *Talanta* 163, 121–126. doi: 10.1016/j.talanta.2016.10.093

Fréchette-Viens, L., Hadioui, M., and Wilkinson, K. J. (2019). Quantification of ZnO nanoparticles and other Zn containing colloids in natural waters using a high sensitivity single particle ICP-MS. *Talanta* 200, 156–162. doi: 10.1016/j.talanta.2019.03.041

Gondikas, A., von der Kammer, F., Kaegi, R., Borovinskaya, O., Neubauer, E., Navratilova, J., et al. (2018). Where is the nano? Analytical approaches for the detection and quantification of TiO2 engineered nanoparticles in surface waters. *Environ. Sci. Nano* 5, 313–326. doi: 10.1039/c7en00952f

Gondikas, A. P., Kammer, F. V. D., Reed, R. B., Wagner, S., Ranville, J. F., and Hofmann, T. (2014). Release of TiO2 nanoparticles from sunscreens into surface waters: a one-year survey at the old Danube recreational Lake. *Environ. Sci. Technol.* 48, 5415–5422. doi: 10.1021/es405596y

Goodall, P., Foulkes, M. E., and Ebdon, L. (1993). Slurry nebulization inductively coupled plasma spectrometry-the fundamental parameters discussed. *Spectrochim. Acta Part B At. Spectrosc.* 48, 1563–1577. doi: 10.1016/0584-8547(93)80143-i

Hadioui, M., Knapp, G. V., Azimzada, A., Jreije, I., Frechette-Viens, L., and Wilkinson, K. J. (2019). Lowering the size detection limits of Ag and TiO2 nanoparticles by Single Particle ICP-MS. *Anal. Chem.* 91, 13275–13284. doi: 10.1021/acs.analchem.9b04007

Hendriks, L., Gundlach-Graham, A., and Günther, D. (2018). Analysis of inorganic nanoparticles by single-particle inductively coupled plasma time-of-flight mass spectrometry. *Chim. Int. J. Chem.* 72, 221–226. doi: 10.2533/chimia.2018.221

Hendriks, L., Gundlach-Graham, A., Hattendorf, B., and Günther, D. (2017). Characterization of a new ICP-TOFMS instrument with continuous and discrete introduction of solutions. *J. Anal. At. Spectrom.* 32, 548–561. doi: 10.1039/c6ja00400h

Hincapié, I., Caballero-Guzman, A., Hiltbrunner, D., and Nowack, B. (2015). Use of engineered nanomaterials in the construction industry with specific emphasis on paints and their flows in construction and demolition waste in Switzerland. *Waste Manag.* 43, 398–406. doi: 10.1016/j.wasman.2015.07.004

Hischier, R., Nowack, B., Gottschalk, F., Hincapie, I., Steinfeldt, M., and Som, C. (2015). Life cycle assessment of façade coating systems containing manufactured nanomaterials. *J. Nanopart. Res.* 17:68.

Hochella, M. F., Lower, S. K., Maurice, P. A., Penn, R. L., Sahai, N., Sparks, D. L., et al. (2008). Nanominerals, mineral nanoparticles, and earth systems. *Science* 319, 1631–1635. doi: 10.1126/science.1141134

Hochella, M. F., Mogk, D. W., Ranville, J., Allen, I. C., Luther, G. W., Marr, L. C., et al. (2019). Natural, incidental, and engineered nanomaterials and their impacts on the Earth system. *Science* 363:eaau8299. doi: 10.1126/science.aau8299

Kaegi, R., Englert, A., Gondikas, A., Sinnet, B., von der Kammer, F., and Burkhardt, M. (2017). Release of TiO2–(Nano) particles from construction and demolition landfills. *Nanoimpact* 8, 73–79. doi: 10.1016/j.impact.2017.07.004

Kaegi, R., Sinnet, B., Zuleeg, S., Hagendorfer, H., Mueller, E., Vonbank, R., et al. (2010). Release of silver nanoparticles from outdoor facades. *Environ. Pollut.* 158, 2900–2905. doi: 10.1016/j.envpol.2010.06.009

Kägi, R., Ulrich, A., Sinnet, B., Vonbank, R., Wichser, A., Zuleeg, S., et al. (2008). Synthetic TiO2 nanoparticle emission from exterior facades into the aquatic environment. *Environ. Pollut.* 156, 233–239. doi: 10.1016/j.envpol.2008.08.004

Laborda, F., Gimenez-Ingalaturre, A. C., Bolea, E., and Castillo, J. R. (2019). Single particle inductively coupled plasma mass spectrometry as screening tool for detection of particles. *Spectrochim. Acta Part B At. Spectrosc.* 159:105654.

Lee, S., Bi, X., Reed, R. B., Ranville, J. F., Herckes, P., and Westerhoff, P. (2014). Nanoparticle size detection limits by single particle ICP-MS for 40 elements. *Environ. Sci. Technol.* 48, 10291–10300. doi: 10.1021/es502422v

Liu, S., Zeng, P., Li, X., Thuyet, D. Q., and Fan, W. (2019). Effect of chronic toxicity of the crystalline forms of TiO2 nanoparticles on the physiological parameters of *Daphnia magna* with a focus on index correlation analysis. *Ecotoxicol. Environ. Saf.* 181, 292–300. doi: 10.1016/j.ecoenv.2019.06.014

Loosli, F., Wang, J., Rothenberg, S., Bizimis, M., Winkler, C., Borovinskaya, O., et al. (2019). Sewage spills are a major source of titanium dioxide engineered (nano)-particle release into the environment. *Environ. Sci. Nano* 6, 763–777. doi: 10.1039/c8en01376d

Meermann, B., and Nischwitz, V. (2018). ICP-MS for the analysis at the nanoscale–a tutorial review. *J. Anal. At. Spectrom.* 33, 1432–1468. doi: 10.1039/c8ja00037a

Mitrano, D. M., Motellier, S., Clavaguera, S., and Nowack, B. (2015). Review of nanomaterial aging and transformations through the life cycle of nano-enhanced products. *Environ. Int.* 77, 132–147. doi: 10.1016/j.envint.2015.01.013

Mizutani, T., Arai, K., Miyamoto, M., and Kimura, Y. (2006). Application of silica-containing nano-composite emulsion to wall paint: a new environmentally safe paint of high performance. *Prog. Organ. Coat.* 55, 276–283. doi: 10.1016/j.porgcoat.2005.12.001

Montaño, M. D., Olesik, J. W., Barber, A. G., Challis, K., and Ranville, J. F. (2016). Single particle ICP-MS: advances toward routine analysis of nanomaterials. *Anal. Bioanal. Chem.* 408, 5053–5074. doi: 10.1007/s00216-016-9676-8

Mozhayeva, D., and Engelhard, C. (2020). A critical review of single particle inductively coupled plasma mass spectrometry–A step towards an ideal method for nanomaterial characterization. *J. Anal. At. Spectrom.* doi: 10.1039/C9JA00206E

Nowack, B., Ranville, J. F., Diamond, S., Gallego-Urrea, J. A., Metcalfe, C., Rose, J., et al. (2012). Potential scenarios for nanomaterial release and subsequent alteration in the environment. *Environ. Toxicol. Chem.* 31, 50–59. doi: 10.1002/etc.726

Olabarrieta, J., Zorita, S., Peña, I., Rioja, N., Monzón, O., Benguria, P., et al. (2012). Aging of photocatalytic coatings under a water flow: long run performance and TiO2 nanoparticles release. *Appl. Catal. B Environ.* 123, 182–192. doi: 10.1016/j.apcatb.2012.04.027

Pace, H. E., Rogers, N. J., Jarolimek, C., Coleman, V. A., Higgins, C. P., and Ranville, J. F. (2011). Determining transport efficiency for the purpose of counting and sizing nanoparticles via single particle inductively coupled plasma mass spectrometry. *Anal. Chem.* 83, 9361–9369. doi: 10.1021/ac201952t

Piccinno, F., Gottschalk, F., Seeger, S., and Nowack, B. (2012). Industrial production quantities and uses of ten engineered nanomaterials in Europe and the world. *J. Nanopart. Res.* 14:1109.

Plathe, K. L., Von Der Kammer, F., Hassellöv, M., Moore, J. N., Murayama, M., Hofmann, T., et al. (2013). The role of nanominerals and mineral nanoparticles in the transport of toxic trace metals: field-flow fractionation and analytical TEM analyses after nanoparticle isolation and density separation. *Geochim. Cosmochim. Acta* 102, 213–225. doi: 10.1016/j.gca.2012.10.029

Praetorius, A., Gundlach-Graham, A., Goldberg, E., Fabienke, W., Navratilova, J., Gondikas, A., et al. (2017). Single-particle multi-element fingerprinting (spMEF) using inductively-coupled plasma time-of-flight mass spectrometry (ICP-TOFMS) to identify engineered nanoparticles against the elevated natural background in soils. *Environ. Sci. Nano* 4, 307–314. doi: 10.1039/c6en00455e

Rahim, M. F., Pal, D., and Ariya, P. A. (2019). Physicochemical studies of aerosols at Montreal Trudeau Airport: the importance of airborne nanoparticles containing metal contaminants. *Environ. Pollut.* 246, 734–744. doi: 10.1016/j.envpol.2018.12.050

Robichaud, C. O., Uyar, A. E., Darby, M. R., Zucker, L. G., and Wiesner, M. R. (2009). Estimates of upper bounds and trends in nano-TiO2 production as a basis for exposure assessment. *Environ. Sci. Technol.* 43, 4227–4233. doi: 10.1021/es8032549

Scifo, L., Chaurand, P., Bossa, N., Avellan, A., Auffan, M., Masion, A., et al. (2018). Non-linear release dynamics for a CeO2 nanomaterial embedded in a protective wood stain, due to matrix photo-degradation. *Environ. Pollut.* 241, 182–193. doi: 10.1016/j.envpol.2018.05.045

Shaw, P., and Donard, A. (2016). Nano-particle analysis using dwell times between 10 μs and 70 μs with an upper counting limit of greater than 3× 10 7 and a gold nanoparticle detection limit of less than 10 nm diameter. *J. Anal. At. Spectrom.* 31, 1234–1242. doi: 10.1039/c6ja00047a

Simonin, M., Martins, J. M., Le Roux, X., Uzu, G., Calas, A., and Richaume, A. (2017). Toxicity of TiO2 nanoparticles on soil nitrification at environmentally relevant concentrations: lack of classical dose–response relationships. *Nanotoxicology* 11, 247–255. doi: 10.1080/17435390.2017.1290845

Sun, T. Y., Gottschalk, F., Hungerbühler, K., and Nowack, B. (2014). Comprehensive probabilistic modelling of environmental emissions of engineered nanomaterials. *Environ. Pollut.* 185, 69–76. doi: 10.1016/j.envpol.2013.10.004

Tharaud, M., Gondikas, A. P., Benedetti, M. F., von der Kammer, F., Hofmann, T., and Cornelis, G. (2017). TiO2 nanomaterial detection in calcium rich matrices by spICPMS. A matter of resolution and treatment. *J. Anal. At. Spectrom.* 32, 1400–1411. doi: 10.1039/c7ja00060j

Van Broekhuizen, P., van Broekhuizen, F., Cornelissen, R., and Reijnders, L. (2011). Use of nanomaterials in the European construction industry and some occupational health aspects thereof. *J. Nanopart. Res.* 13, 447–462. doi: 10.1007/s11051-010-0195-9

Vance, M. E., Kuiken, T., Vejerano, E. P., McGinnis, S. P., Hochella, M. F. Jr., Rejeski, D., et al. (2015). Nanotechnology in the real world: redeveloping the nanomaterial consumer products inventory. *Beilstein J. Nanotechnol.* 6, 1769–1780. doi: 10.3762/bjnano.6.181

Wagner, S., Gondikas, A., Neubauer, E., Hofmann, T., and von der Kammer, F. (2014). Spot the difference: engineered and natural nanoparticles in the environment—release, behavior, and fate. *Angew. Chem. Int. Ed.* 53, 12398–12419.

Zhang, X., Wang, M., Guo, S., Zhang, Z., and Li, H. (2017). Effects of weathering and rainfall conditions on the release of SiO2, Ag, and TiO2 engineered nanoparticles from paints. *J. Nanopart. Res.* 19:338.

Zhou, S., Wu, L., Sun, J., and Shen, W. (2002). The change of the properties of acrylic-based polyurethane via addition of nano-silica. *Prog. Organ. Coat.* 45, 33–42. doi: 10.1016/s0300-9440(02)00085-1

Zhu, X., Zhou, J., and Cai, Z. (2011). TiO2 nanoparticles in the marine environment: impact on the toxicity of tributyltin to abalone (*Haliotis diversicolor supertexta*) embryos. *Environ. Sci. Technol.* 45, 3753–3758. doi: 10.1021/es103779h

Zuin, S., Gaiani, M., Ferrari, A., and Golanski, L. (2014). Leaching of nanoparticles from experimental water-borne paints under laboratory test conditions. *J. Nanopart. Res.* 16:2185.

Conflict of Interest: PS is an employee of Nu Instruments, United Kingdom.

The remaining authors declare that the research was conducted in the absence of any commercial or financial relationships that could be construed as a potential conflict of interest.

frontiers in Environmental Science

ORIGINAL RESEARCH
published: 30 June 2020
doi: 10.3389/fenvs.2020.00089

A Nanoplastic Sampling and Enrichment Approach by Continuous Flow Centrifugation

*Lars Hildebrandt[1,2], Denise M. Mitrano[3], Tristan Zimmermann[1] and Daniel Pröfrock[1]**

[1] Marine Bioanalytical Chemistry, Helmholtz-Zentrum Geesthacht, Centre for Materials and Coastal Research, Geesthacht, Germany, [2] Department of Chemistry, Inorganic and Applied Chemistry, Universität Hamburg, Hamburg, Germany, [3] Process Engineering, Eawag, Swiss Federal Institute of Aquatic Science and Technology, Dübendorf, Switzerland

Substantial efforts have been undertaken to isolate and characterize plastic contaminants in different sample matrices in the last years as the ubiquitous presence of particulate plastic in the environment has become evident. In comparison, plastic particles <1 µm (nanoplastic) in the environment remain mostly unexplored. Adequate techniques for the enrichment, as well as the detection of nanoplastic, are lacking but are urgently needed to assess the full scope of (potential) nanoplastic pollution. Use of Pd-doped nanoplastic particles constitutes a powerful tool to develop new analytical approaches, as they can be traced accurately and with ease in a variety of complex matrices by highly sensitive, time-efficient and robust ICP-MS(/MS) techniques. In this lab-scale study, for the first time, the capability of continuous flow centrifugation to retain nanoplastic particles (∼160 nm) from ultrapure water, as well as from filtered and unfiltered water from the German Elbe River was evaluated. Depending on the pump rate, the retention efficiency for the nanoplastic particles in ultrapure water ranged from 92% ± 8% (1 L h^{-1}) to 53% ± 5% (5 L h^{-1}) [u_C (n = 3)] and from 75% ± 5% to 65% ± 6% (u_C) (2.5 L h^{-1}) in river water. Recirculating the water through the system two and three times at the highest tested flow rate led to retention efficiencies >90%. In a proof-of-principle setup, it was demonstrated that operating two continuous flow centrifuges sequentially at different rotational speeds bears the potential to enable size- and density-selective sampling of the colloidal fraction. A significant fraction of the spiked nanoplastic particles [76% ± 5% (u_C)] could be separated from a model mixture of natural particles with a well-defined mean size of approximately 3 µm. While the certified reference plankton material used here was quantitatively retained in the first centrifuge rotor together with 23.0% ± 2.2% of the effective dose of the spiked nanoplastic, the remaining fraction of the nanoplastic could be recovered in the second rotor (53% ± 5%) and the effluent [24.4% ± 2.4% (u_C)]. Based on the good retention efficiencies and the demonstrated separation potential, continuous flow centrifugation has proven to be a very promising technique for nanoplastic sampling and enrichment from natural water samples.

Keywords: metal-doped nanoplastic, nanoplastic sampling, nanoplastic separation, nanoplastic enrichment, submicrometer plastic, plastic contaminants, particulate plastic

OPEN ACCESS

Edited by:
John Crusius, United States Geological Survey, United States

Reviewed by:
Jes Vollertsen, Aalborg University, Denmark
Ulrike Braun, Federal Institute for Materials Research and Testing (BAM), Germany

****Correspondence:***
Daniel Pröfrock
daniel.proefrock@hzg.de

Specialty section:
This article was submitted to Biogeochemical Dynamics, a section of the journal Frontiers in Environmental Science

Received: *28 February 2020*
Accepted: *02 June 2020*
Published: *30 June 2020*

Citation:
Hildebrandt L, Mitrano DM, Zimmermann T and Pröfrock D (2020) A Nanoplastic Sampling and Enrichment Approach by Continuous Flow Centrifugation. Front. Environ. Sci. 8:89. doi: 10.3389/fenvs.2020.00089

INTRODUCTION

Particulate plastic has gained high importance as an emerging environmental contaminant for researchers, authorities and society as a whole (Stöven et al., 2015; Gago et al., 2016; Rochman et al., 2016; Peng et al., 2017; Burns and Boxall, 2018; Science Advice for Policy by European Academies, 2019). Notwithstanding research on other engineered nanoparticles (e.g., inorganic nanoparticles) (Hüffer et al., 2017), evidence on nanoplastic particles [NPPs, defined as 1 nm to 1000 nm in size for this article (Gigault et al., 2018)] and even on particles smaller than 10 µm in natural systems is very scarce (Ter Halle et al., 2017; Meyns et al., 2019). NPPs are contained in many consumer products and can additionally be released as secondary NPPs from macro- and microplastic (MP, 1 µm – 5 mm) due to UV-induced and mechanical degradation processes (Lambert and Wagner, 2016; Lehner et al., 2019; Mitrano et al., 2019). Furthermore, NPPs are expected to exhibit different properties than particles >1 µm (Mattsson et al., 2015) as easier translocation and uptake into cells are also probable. Nanoplastic beads were shown to enhance toxicity of persistent organic pollutants toward Rotifers (Jeong et al., 2018), hinder algal photosynthesis (Bhattacharya et al., 2010) and exhibit different adverse effects on human lung epithelial cells (Xu et al., 2019).

Due to analytical challenges related with sampling and analysis, there is no definite proof of NPPs being present in the environment so far. Currently, there are also no validated standard operation procedures to analyze particulate plastic (Löder and Gerdts, 2015; Besley, 2017), despite some activities aiming at methodological standardization from institutions such as the International Organization for Standardization (ISO/TC 61/SC 14) and JPI Oceans. Furthermore, no certified reference materials exist which could enable a valid comparison of the performance of different sampling, sample processing and characterization approaches (Frias et al., 2019).

The quantification of NPPs is highly challenging. Well-established techniques for MP particle analysis, such as FTIR and Raman microspectroscopy, have size detection limits of approximately 10 µm and 1 µm, respectively (Käppler et al., 2016; Ivleva et al., 2017; Primpke et al., 2017). Method optimization can slightly decrease these limits (to a few micrometer for FTIR and several hundred nanometers for Raman microscopy), but analyzing submicron plastic particles still requires combination of FTIR spectroscopy with atomic force microscopy (AFM), or SEM-EDX in order to achieve the necessary lateral resolution and chemical information (Shim et al., 2017; Meyns et al., 2019). However, these kinds of analysis are very time-consuming and inefficient in terms of spatial coverage (Koelmans, 2019). Methods which determine mass concentrations of particulate plastic based on separation of characteristic combustion products by gas chromatography hyphenated to mass spectrometry require extensive sample purification and high preconcentration of colloidal plastic to meet the current quantification limits (Dümichen et al., 2017; Fischer and Scholz-Böttcher, 2017).

Some techniques which are technically capable of measuring particles in the nanometer range are inadequate for assessing NPP concentration or sizes in complex matrices. For example, Dynamic light scattering (DLS) and asymmetric flow field-flow fractionation (AF4) coupled with multi-angle light scattering (MALS) provide size-related information, but no information on the polymer type and potential aggregation. Quantitative plastic-specific isolation from the matrix and in addition *a priori* knowledge of the refractive index would be required (Correia and Loeschner, 2018; Ekvall et al., 2019).

Chemically labeled particles have previously been used to circumvent these analytical limitations to mechanistically understand NPP fate, transport and biological interactions (Cole et al., 2013; Lusher et al., 2017). Fluorescence-labeled particles, for instance, can easily be identified in tissues and complex structures using fluorescence microscopes. However, in biological exposure experiments, it was reported that these dyes can leach out and lead to fluorescence in examined organisms without particle uptake (Schür et al., 2019). A second problem related with fluorescence-labeled particles is photobleaching (Sullivan and Gugliada, 2018).

Using metal-doped particles is a promising new approach. Even with a trace metal content embedded in the polymer of <0.5% *w*/*w*, the sensitivity of ICP-MS enables particle detection at lower concentrations in a variety of complex matrices (Keller et al., 2019; Mitrano et al., 2019; Schmiedgruber et al., 2019) after total microwave-assisted acid digestion (MWAD) of the bulk sample. While only a model, metal-doped particles can also be a valuable tool when it comes to the investigation of potential techniques for environmental NPP extraction and enrichment.

Though a high percentage of NPPs occur as heteroaggregates in the environment with either natural organic or inorganic materials (Hüffer et al., 2017; Oriekhova and Stoll, 2018), sampling techniques for the colloidal fraction still need to be developed with NPPs in mind. Suitable sampling and concentration techniques are understudied but crucial aspects of the analytical method development workflow (Koelmans et al., 2015; Schwaferts et al., 2019; Zhou et al., 2019). Schwaferts et al. (2019) presume that the mass of NPPs in the aquatic environment is likely very low (Schwaferts et al., 2019). Thus, for NPP analysis considerable pre-concentration may be necessary in order to have enough material to analyze and characterize as well as to meet the *LOD*s/*LOQ*s of the currently used analytical techniques. Using conventional nanofiltration is technically not feasible due to the low volume flows (Hernandez et al., 2017; Mintenig et al., 2018) (i.e., small sample sizes are not likely to capture the NPPs). Even in the range of 10 µm – 20 µm, filtration is quite problematic when high contents of suspended particulate matter (SPM) are present and large volumes need to be processed to obtain representative samples (Enders et al., 2015; Lenz and Labrenz, 2018; Bannick et al., 2019).

Alternatives to filtration-based approaches are needed which enable nanometer-size-selective and time-efficient sampling. The application of continuous flow centrifugation (CFC) for efficient sampling of the fine particulate fraction (1 µm – 25 µm) in natural water at high flow rates of several hundred liters per hour has already been shown (Douglas et al., 1993; Ran et al., 2000; Conn et al., 2016). Recently, CFC proved to be a suitable technique to quantitatively enrich small MP (model MP ranged from 1 µm to 1 mm) of a variety of polymer types with densities ranging

from 0.94 g mL^{-1} to 1.63 g mL^{-1} (Hildebrandt et al., 2019). In a second step, it was applied to sample small MP particles from the German Elbe estuary. After the sampling, the content of the centrifuge had to be subjected to a purification protocol including oxidative-chemical treatment and density separation for matrix reduction prior to final spectroscopic analysis.

From a physical perspective, CFC is also capable of retaining particles in the submicron range when the flow rate is further reduced (see section "Data processing and calculations"). It poses a promising option whenever particles with a sedimentation coefficient >50 Svedberg must be separated from volumes >2 L (Dorin and Cummings, 2015). If the density of the particles, the viscosity and density of the medium and the geometry of the CFC rotor are known, the optimal flow rate for maximum particle removal can be estimated (see section "Data processing and calculations").

The good performance of CFC for MP sampling (Hildebrandt et al., 2019) and its wide application in the biomedical sector to pellet subcellular components (Goodenough, 1974; Kahane et al., 1976; Cacace et al., 1977; Turk et al., 1988) and viruses (Shibley et al., 1980; Wheeler et al., 1986; Anderson et al., 1991) were a motivation to test the enrichment of NPPs by CFC as well. In this study, Pd-doped NPPs were spiked into ultrapure water to assess the efficiency of CFC in retaining NPPs and evaluate the effect of different pump rates (1) and recirculation (2), into natural water to test NPP retention under realistic environmental conditions (3) and into a model matrix suspension with a high concentration of micrometer-sized SPM to evaluate the potential of a serial CFC approach for nanometer-size-selective sampling (separation) (4). Through this procedure, we could assess which conditions are most applicable to concentrate NPPs under laboratory conditions, and propose a workflow for enriching NPPs from environmental water samples.

MATERIALS AND METHODS

Nanoplastic Particles

Pd-doped nanoplastic particles were previously developed and characterized, as described by Mitrano et al. (2019), with additional characterization of the particles used in this study as detailed below. Briefly, the particles had a core/shell structure featuring a polyacrylonitrile core doped with Pd and a polystyrene shell. The hydrodynamic diameter of the particles was 175 nm ± 1.3 nm, with a low polydispersity (PDI: 0.02) as measured by dynamic light scattering. A slightly smaller diameter (approximately 160 nm) was measured by transmission electron microscopy. A 1:10 dilution of the original stock suspension was performed to a final volume of 50 mL, to which 2 drops of Triton X-100 (VWR Life Science, Darmstadt, Germany) were added to ensure particle stability through storage. This dilution served as a working stock suspension for all experiments. To confirm that the Pd was completely incorporated into the polymer matrix and there was not free Pd remaining from particle synthesis, 100 µL of the suspension was filled up to 10 mL with Milli-Q water (MQW) and centrifuged at 10000 rpm for 7 h (Centrifuge 5804 R, Eppendorf AG, Hamburg, Germany). Measurement of the supernatant showed that at maximum 0.767% ± 0.017% [1 *SD* (n = 3)] of the Pd was not associated with the particles. The solid content in the NPP suspension was determined gravimetrically after freeze-drying (Gamma 1–16 LSC plus Christ, Osterode, Germany). The stock suspension used for all spiking experiments contained 0.848% ± 0.021% (w/w) [1 *SD* (n = 3)] NPPs. The Pd content of the working stock suspension was 22.8 mg L^{-1} ± 1.3 mg L^{-1} [u_c (n = 12)]. Consequently, the Pd mass fraction of the NPPs was approximately 0.27% (w/w).

Reagents and Standards

Preparatory laboratory work was performed in a class 10,000 clean room inside a class 100 clean bench. Type I reagent-grade water (18.2 MΩ cm) was obtained from a Milli-Q Integral water purification system (Merck-Millipore, Darmstadt, Germany), equipped with a Q-Pod Element. Suprapur® nitric acid [65% (w/w), Merck-Millipore] and suprapur® hydrochloric acid [30% (w/w), Merck-Millipore] were further purified by double sub-boiling in PFA stills (Savillex, Eden Prairie, United States) operated under clean room conditions. Polyethylene and polypropylene flasks, tubes and pipette tips (VWR International, Radnor, United States), as well as perfluoroalkoxy (PFA) screw cap vials (Savillex, Eden Prairie, United States) were pre-cleaned in a two-stage washing procedure using nitric acid [10% (w/w) and 1% (w/w), respectively]. A single-element standard of Pd (C = 1 g L^{-1}) obtained from Agilent Technologies (Santa Clara, CA, United States) was used for external calibration.

River Water Sampling and Nanoplastic Spiking

Elbe river water was sampled from a dock in the Elbe river located in Geesthacht, Germany (53° 24.6′ N, 10° 25.6′ E, 12/17/2019) with a cleaned 25 L HDPE bottle (Kautex Textron, Bonn, Germany). As we aimed to specifically only quantify nanoplastics with the Pd-doping, any potential plastic contamination during the sampling procedure was inconsequential. An aliquot of the water was directly filled into 5 L glass bottles with PFA screw caps (Schott AG, Mainz, Germany). A second aliquot was filtered over bottle-top SCFA filters (0.2 µm; Nalgene, Rochester, NY, United States) directly into 5 L glass bottles. The SPM concentration was determined gravimetrically prior to (2.60 mg L^{-1} ± 0.23 mg L^{-1}) and after [6.5 mg L^{-1} ± 0.7 mg L^{-1} (1 *SD;* n = 3)] the incubation, by filtration of 1 L over glass fiber membrane filters (0.7 µm, Merck, Darmstadt, Germany). A Multi 3430© sensor system (WTW GmbH, Weilheim, Germany) was employed to determine physical water parameters, such as temperature, conductivity, oxygen content and pH (T = 4.3°C, EC = 1084 mS cm^{-1}, C_{O2} = 12.33 mg L^{-1}, pH = 8.165). 1 mL of the working stock Pd-doped NPP suspension was spiked into replicates of 5 L of the filtered and unfiltered river water and stirred for 31 days (magnetic stirrer at 500 rpm, T_{mean} = 20°C) prior to being pumped through the CFC system. The number of added NPPs was chosen based on achieving a sufficient mass of Pd for straightforward tracing in different scenarios.

Microwave-Assisted Acid Digestion of Nanoplastic and Suspended Particulate Matter

MWAD was utilized to determine the concentration of the certified elements in BCR-414 (As, Cd, Cr, Cu, Hg, Mn, Ni, Pb, Se, V, and Zn) and ERM®-EC680m (As, Cd, Cr, Hg, Pb, Sb, Sn, and Zn) (both Joint Research Centre (JRC), European Commission) and the Pd concentration for all fractions that could not be introduced directly into the ICP-MS/MS due to the presence of SPM in the micrometer size range. After freeze-drying (Gamma 1–16 LSC plus Christ), residues were digested with 4 mL HNO_3 and 1 mL HCl in pre-cleaned 35 mL Quartz vials (Discover-SP-D 35; CEM Corp., Kamp Lintfort, Germany) at 230°C (20 min ramp and 5 min hold time). After digestion, the clear solutions were transferred quantitatively to 50 mL pre-cleaned DigiTubes® (SCP Science) and diluted to 50 mL with MQW. The plastic certified reference material (CRM) ERM®-EC680m (JRC, Geel, Belgium) was utilized to validate the MWAD protocol in terms of complete dissolution of the polymeric matrix and quantitative elemental recoveries. BCR-414 was used to as a model for interfering matrix particles and traced by its Ni content using ICP-MS/MS (see section "Dependence of Retention Efficiency in MQW on Number of Cycles").

Metal Analysis in Nanoplastic and CRMs

Metal content determination of all samples was performed using an inductively coupled plasma tandem mass spectrometry (ICP-MS/MS) instrument (Agilent 8800, Agilent Technologies, Tokyo, Japan) coupled to an ESI SC-4 DX FAST autosampler (Elemental Scientific, Omaha, United States). The instrument was tuned in a daily routine using a tune solution containing Li, Co, Y, Ce and Tl. Quantification was conducted by an external calibration, covering a concentration range from 0.1 μg L^{-1} to 100 μg L^{-1} for all analytes. Solutions were prepared volumetrically on a daily basis from a combination of multi-element standards (Inorganic Ventures, Christiansburg, United States) made in-house. Wash blanks were measured after each sample triplicate to minimize carry over effects. ICP-MS/MS operating parameters, cell gas modes used and a list of measured isotopes and their detection modes for all analytes can be found in **Supplementary Tables S2, S3**. Selection of the optimal isotope and measurement mode for Pd quantification was based on analysis of all six stable isotopes in all gas modes (including mass-shift) in a multielement solution (C_{Pd} = 500 μg L^{-1}) containing 51 other metals (C = 25 – 250 μg L^{-1}) (**Supplementary Table S1**). Multi-elemental data were processed using Mass Hunter version 4.2 (Agilent Technologies) and a custom written Excel© spreadsheet.

Continuous Flow Centrifugation

Two continuous flow centrifuges (Contifuge Stratos, Thermo Scientific, Waltham, United States) in conjunction with two titanium rotors with a sedimentation capacity of 300 mL (Continuous Flow Rotor 3049, Thermo Scientific) were available for all experiments.

In the first three variants of the experiment (see section "Experimental Setups Using One Centrifuge"), the setup comprised only of one centrifuge, whereas for the fourth objective two centrifuges were sequentially connected. For all experiments, peristaltic pumps (Masterflex L/S, Cole-Parmer, Vernon Hills, United States) were applied to pump 5.22 L ± 0.22 L (1 *SD*, n = 18) of NPP-spiked ultrapure or natural water from a 5 L bottle through the rotating centrifuge rotor. The final spiked water contained 1 mL of working stock suspension. The temperature of the centrifuge was kept constant at 20°C. Before the sample was pumped through the rotor, it was filled with MQW at 4000 rpm and accelerated to the final rotational speed (17000 rpm). To avoid air bubbles entering the centrifuge, the experiments were stopped at a residual volume of 0.29 L ± 0.06 L (1 *SD*, n = 14) remaining in the glass sample bottle.

Experimental Setups Using One Centrifuge

The first experiments focusing on the retention of nanoplastic from MQW and river water in a linear setup as well as from MQW in a circular setup were based on usage of one centrifuge (**Figure 1**). A setup based on a single CFC system leads to enrichment of all retained particulate material ranging from the micrometer to the nanometer size in the system's rotor. Therefore, no separation of only NPPs is achieved with this configuration.

Linear setup: influence of the pump rate

The water was pumped from the suspension bottle by a peristaltic pump through the CFC rotor into an effluent beaker (**Figure 1A**). The peristaltic pump was placed between the suspension bottle and the centrifuge. After the procedure, the three fractions of the original spiked water were separated into "residual water in suspension bottle," "rotor content," and "effluent". Using this linear setup, the influence of the pump rate (1 L h^{-1}, 2.5 L h^{-1}, and 5 L h^{-1}) was investigated, as its importance for the degree of retention has previously been explored (Berman, 1966; Brown, 1989). These experiments were run with MQW which allowed direct introduction of the resulting fractions into the ICP-MS/MS, as there was no organic matter and it was tested that the plasma could fully decompose/atomize the NPPs without prior digestion. For all experimental runs, the rotational speed was set to the maximum of 17000 rpm (∼24200 g-forces). After centrifugation, ∼ 5 μL of the detergent Triton X-100 were added (for stabilization) to each of the fractions prior to ultrasonication for 15 min to avoid adhesion to the vessels. Replicates of 50 mL of the fractions suspension bottle (n = 3), rotor content (n = 6) and effluent (n = 6) were taken with a glass pipette and transferred to DigiTubes® (SCP Science, Quebec, Canada). Thorough shaking of the tubes prior to the measurement ensured homogeneous mixing.

Linear setup: recovery of nanoplastic from river water

The NPP-spiked filtered and unfiltered river water was pumped through the centrifuge at a rate of 2.5 L h^{-1} and a rotational speed of 17000 rpm. The same pumping procedure as used for the MQW samples was used. However, due to the presence of SPM in the fractions, the content of the suspension bottle and the rotor body were subjected to MWAD prior to ICP-MS/MS measurement to avoid blockages of the nebulizer and other unwanted matrix-based effects. Therefore, replicates (n_{bottle} = 3, n_{rotor} = 6) of 20 mL were transferred to pre-cleaned 35 mL Quartz vials (CEM Corp., Kamp Lintfort, Germany) and freeze-dried.

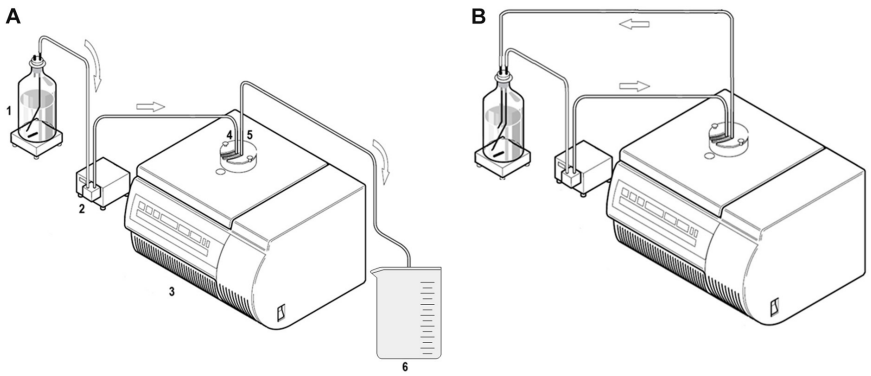

FIGURE 1 | Schematic drawing of the experimental setup for CFC. **(A)**: Linear setup (1: Suspension bottle containing the NPPs on a magnetic stirrer. 2: Peristaltic pump. 3: Flow Centrifuge. 4: Inflow. 5: Outflow. 6: Collected effluent fraction). **(B)** Circular setup (Heraeus Instruments GmbH, 1998, modified) © Thermo Scientific.

The effluent was sampled and analyzed without need for MWAD, as it was highly clarified through the centrifugation process.

Circular setup: influence of additional pumping cycles

The water was pumped from the suspension bottle by a peristaltic pump through the CFC rotor (17000 rpm) and then back into the suspension bottle (**Figure 1B**). In this instance, the impact of one and two additional pumping cycles (i.e., by recycling water 2-times and 3-times through the centrifuge) on the retention efficiency was evaluated at 5 L h^{-1}. The peristaltic pump was placed at the same position as in the linear approach.

For the circular approach, only samples from the rotor content and the suspension bottle were obtained and sampled analogously (n = 6). This experimental variant was also run with MQW enabling direct introduction of the resulting fractions into the ICP-MS/MS without MWAD.

Experimental Setup Using Two Centrifuges

The use of a sequence of two CFC systems is our concept for size- and density-selective nanoplastic sampling from water. The goal was to evaluate to what extent separation of nanoparticles from microparticles can be achieved by using a sequence of the two CFC systems operated at different rotational speeds.

Separation of Nanoplastic From Micrometer-Sized Suspended Particulate Matter

In the sequential CFC setup, the sample suspension was pumped from the bottle through the first CFC system and subsequently through a second CFC (**Figure 2**). The clarified liquid that passed both centrifuges was collected in the effluent beaker. Hereby, a peristatic pump with a dual-channel pump head, which was placed between the bottle and the first centrifuge as well as between both centrifuges, was utilized.

In order to mimic natural particles which may aggregate with nanoplastic in environmental samples, BCR-414 [Plankton (trace elements)] was added into the solution which passed through the sequential CFC system. BCR-414 is a powder [d_{mean} = 2.894 µm ± 0.003 µm (1 *SD*)] of milled organisms such as *cladocera* and Si-, Ca, CaP-rich, organic and clay particles with a C_{org}-content of 30% ± 5% [1 *SD* (n = 6)]. Certified mass fractions for the elements As, Cd, Cr, Hg, Mn, Ni, Pb, Se, V and Zn were provided by the supplier. 5 L MQW were spiked with 500 mg of the CRM. The suspension was stirred for 15 min before spiking 1 mL of NPP suspension and conducting sequential CFC at a pump rate of 2.5 L h^{-1} (**Figure 2**). The two centrifuges were operated at different rotational speeds (CFC 1 at 4000 rpm and CFC 2 at 17000 rpm). Subsamples of 20 mL (n = 6) of the fractions suspension bottle and rotor content 1 were transferred to 35 mL Quartz vials (CEM Corp.) and freeze-dried (for MWAD). Subsamples of 50 mL (n = 6) of the clarified fractions rotor content 2 and effluent were sampled and analyzed by ICP-MS/MS directly without MWAD.

Data Processing and Calculations

The calculation of retention efficiencies (RE) (Eq. 1) is based on the effective dose of particles (using the Pd mass fraction) that entered the centrifuge and that could be recovered in the rotor content and effluent. The recoveries in all fractions and cumulative recoveries can be found in **Supplementary Table S5**.

$$RE = \frac{m_{Pd}^{Rotor\ content}}{m_{Pd}^{Effluent} + m_{Pd}^{Rotor\ content}}$$

Equation 1: Formula for the calculation of the retention efficiency (RE) based on the effective NPP dose.

Eq. 2 was used to estimate the optimal flow rate for maximum particle retention. Knowledge and/or estimates of the rotor geometry, the medium's density and viscosity as well as of the NPPs' diameter and density were required for the calculations.

$$F = \pi \frac{\rho_p - \rho_m}{18\ \eta} D^2\ h\ \omega^2 \frac{r_{max}^2 - \left(\frac{r_t - r_b}{\ln\left(\frac{r_t}{r_b}\right)}\right)^2}{ln\left(\frac{r_{max}}{\left(\frac{r_t - r_b}{\ln\left(\frac{r_t}{r_b}\right)}\right)}\right)}$$

Equation 2: Formula for the calculation of the optimal flow rate F [$m^3\ s^{-1}$] for CFC with ρ_p: density of the particles [kg m^{-3}],

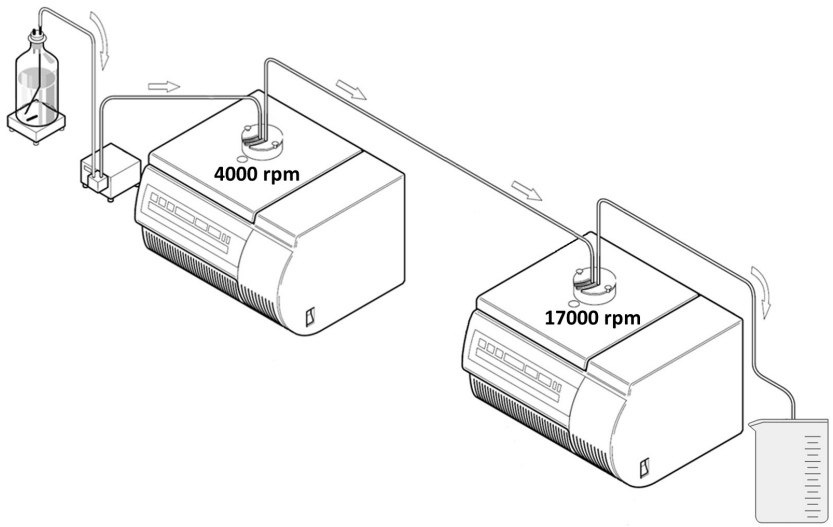

FIGURE 2 | Schematic drawing of the experimental setup for sequential CFC. In our experimental design, the first centrifuge was operated at 4000 rpm and the second one at 17000 rpm (modified, © Thermo Scientific).

ρ_m: density of the medium [kg m^{-3}], η: viscosity of the medium [kg m^{-1} s^{-1}], D: diameter of the particles [m], h: height of the rotor core [m], ω: angular velocity [s^{-1}], r_{max}: maximum radius of the core [m], r_t: radius at top of core [m], r_b: radius at bottom of core [m] (Svedberg and Pedersen, 1940; Berman, 1966; Dorin and Cummings, 2015).

Combined uncertainties (u_c) (calculated according to the "Guide to the expression of uncertainty in measurement" [GUM (JCGM 100:2008)] comprise instrument replicates (measurement precision), sample replicates (repeatability), experiment replicates using different centrifuge systems (reproducibility) (u_c: square root of sums of squared errors), and their propagation in the calculation of the retention efficiencies. If certified values in conjunction with expanded uncertainties are provided, these uncertainties are also considered (Ellison and Williams, 2012).

RESULTS AND DISCUSSION

Four CFC experiments were conducted which focused on the influence of the pump rate on the retention efficiency (1) under simplified conditions and (2) under realistic environmental conditions, (3) the influence of recirculation and (4) the potential of CFC to enable nanometer-size-selective sampling. Except for experiment 4, for which a sequence of two CFC systems was used, all experiments were based on application of one CFC system.

Stock Nanoplastic Analysis and Digestion Methods

The MWAD protocol proved suitable for complete polymer digestion. The obtained digests were completely clear and the recoveries for the certified metals (As, Cd, Cr, Hg, Pb, Sn, and Zn) ranged from 97.4% ± 1.5% to 103% ± 4% (**Supplementary Table S4**). Only Sb posed a slight outlier with a recovery of 115.9% ± 1.5% [1 *SD* (n = 3)].

Measuring ^{105}Pd in helium mode was determined to be optimal in terms of trueness and precision of Pd concentration. Recovery for the ICP-MS standard solution was 100.0% ± 1.2% [n = 4 (1 *SD*)]. The determined Pd concentration in the working stock NPP suspension (1:10 dilution of the suspension as synthesized) was 22.8 mg L^{-1} ± 1.3 mg L^{-1} [u_c (n = 12)]. Direct measurements of diluted NPP suspension based on instrument calibration using the Pd standard solution was possible.

The optimized protocol including surfactant and ultrasonication led to good agreement between the calibration and the corresponding dilution series of the NPP suspension (**Supplementary Figure S1**). Near perfect linearity in the working range was achieved, with $R^2 \geq 99.98\%$. The instrumental *LOD* was 0.0017 µg L^{-1} (3 × *SD* of the Blank) which equated to approximately 3.3 × 10^8 particles L^{-1}.

Dependence of Retentions Efficiency in MQW on Pump Rate

Except for the flow rate, all other relevant parameters influencing the retention behavior of particles during CFC depend on either the medium and particles of interest, the angular velocity or the geometry of the used CFC rotor. Thus, the flow rate is the decisive parameter to vary size- and density-selectivity of the applied setup (Eq. 2). The lower the flow is set, the more time the medium needs to pass the centrifugal field and the higher the achievable retention of small particles in the rotor is. Correct adjustment and optimization of the pump rate will ultimately lead to maximum particle removal.

The pump rate was assessed using the known geometry of the rotor, the angular velocity, the density and viscosity of the liquid, and estimating the density of the plastics (details in **Supplementary Material**). Using assumption of a NPP density

between 1.14 g mL^{-1} and 1.18 g mL^{-1} and a particle diameter of 160 nm led to ideal estimated pump rates between 2.6 L h^{-1} and 3.4 L h^{-1} (**Figure 3**).

In order to evaluate the fitness of the calculated flow rates according to Equation 2, three different pump rates were tested. The retention efficiency for the NPPs in MQW in the linear setup was 92% ± 8% for 1 L h^{-1}, 67% ± 6% for 2.5 L h^{-1} and 53% ± 5% for 5 L h^{-1} [u_c (n = 3)] (**Table 1**). The results show that, despite the calculations, a pump rate of 2.5 L h^{-1} was not sufficient for quantitative retention, whereas 1 L h^{-1} led to efficient NPP removal. Nevertheless, as the flow rate of the CFC systems used in these experiments can be adjusted between a few mL h^{-1} and 66 L h^{-1}, the calculations gave a good estimate which could be further refined experimentally. The gap between the estimations and the experimental findings refers either to a counterflow induced by diffusional drift, which is described by Brownian dynamics (which is applicable to particles <1 µm in diameter) (Meireles et al., 2010; Minoura et al., 2010; de la Torre et al., 2018), or slight deviations of particle density and/or size. The retention efficiency values describe the partitioning of the effective NPP dose between the rotor content and the effluent fraction. Thus, for a pump rate of 5 L h^{-1}, approximately half of the NPPs were retained in the rotor and half passed through. It is important not to confuse the retention efficiency with the overall recovery. For the linear setup, the spiked NPPs could be quantitatively recovered in the three fractions: (1) suspension bottle, (2) rotor content and (3) effluent {85% ± 5% – 98% ± 4% [u_c (n = 3)]; **Table 1**}. This is encouraging, since such high recoveries are not always achieved when working with (sub)micron particles (Imhof et al., 2012; Nguyen et al., 2019).

Dependence of Retention Efficiency in MQW on Number of Cycles

In the circular setup (**Figure 1B**), the retention efficiency rose to 91% ± 10% for two cycles and 95% ± 8% for three cycles [u_c (n = 2)] (**Table 1**). This is an >40% gain from the linear setup. On the other hand, the overall recoveries were significantly lower in this setup, 60% ± 5% and 68% ± 4% for two and three cycles, respectively. We hypothesize that in this configuration a considerable fraction of the NPPs adhered to the walls of the suspension bottle and/or the tubing, which was only evident when the NPPs spent extended times in the system. Nevertheless, by increasing the number of pumping cycles the retention efficiency of NPPs in the CFC system can be significantly enhanced.

Retentions Efficiency in Filtered and Unfiltered River Water

Heteroaggregation of NPPs with inorganic and organic natural matter was observed in various environmental circumstances (Koelmans et al., 2015; Gigault et al., 2018; Oriekhova and Stoll, 2018; Li et al., 2019). Therefore, the influence of suspending the NPPs in water from the German Elbe River (∼1 month

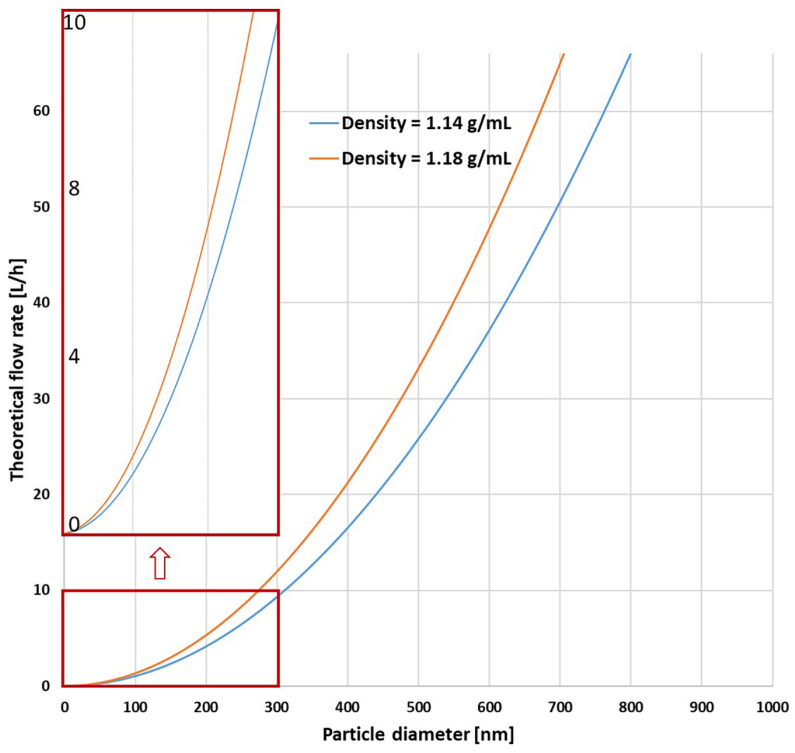

FIGURE 3 | Parabolic relationship (based on Eq. 2) between the flow rates required for quantitative retention and the particle diameter for operation of the CFC Rotor at 17000 rpm with water as medium (for the density range of polyacrylonitrile).

TABLE 1 | Retention efficiencies and recoveries for the Pd-doped NPPs in the different fractions in the different setup using one CFC system (17000 rpm).

Setup	Pump rate [L h^{-1}]	Medium ($V \sim 5$ L)	Retention Efficiency [%]	Total Recovery [%]
Linear (**Figure 1A**)	1	MQW	92 ± 8	85 ± 5
	2.5	MQW	67 ± 6	98 ± 4
	5	MQW	53 ± 5	90 ± 4
	2.5	filtered river water	65 ± 6	74 ± 3
	2.5	unfiltered river water	75 ± 5	77.8 ± 2.9
Circular (**Figure 1B**)	5	MQW (2 cycles)	91 ± 10	60 ± 5
	5	MQW (3 cycles)	95 ± 8	68 ± 4

Errors correspond to combined uncertainties (u_c with n = 2; 3).

incubation time) on the retention efficiency of the CFC system run at 2.5 L h^{-1} was investigated. Two reasons led to selecting this flow rate instead of 1 L h^{-1}, which had a higher retention in the linear system with one rotor:

1. It poses a tradeoff between the possibility to process larger volumes (necessary for sufficient preconcentration under environmental conditions) and a high retention.
2. It enabled identification of an increase in the retention efficiency due to the formation of larger particles by heteroaggregation (in contrast to a flow rate that already leads to quantitative retention in MQW).

An equal percentage of NPPs were retained for filtrated river water (65% ± 6%) and MQW at 2.5 L h^{-1} [67% ± 6% (n = 3)] in the linear setup. This indicates that no influence of the natural colloids (i.e., particles <0.2 μm) and humic substances led to formation of larger heteroaggregates. Moreover, the mean retention efficiency was higher for the unfiltered water (75% ± 5%) than for NPPs spiked into the filtered river water.

Longer incubation times and higher concentrations of SPM and dissolved organic substances, whose interactions with different nanoparticles have previously been shown (Grillo et al., 2015; Milne et al., 2017; Wu et al., 2019), could be an explanation for the increase in the retention efficiencies. Future experiments can give further insights into the aggregation kinetics of NPPs with SPM in real-world scenarios. In this way, CFC may be an additional way to assess NPP attachment to larger particles, as particles which are attached to SPM would be efficiently removed in the centrifuge and those which remain unattached would pass it to a higher extent.

Separation of Nanoplastic From Micrometer-Sized Suspended Particulate Matter

The dependence between the flow rates and retention efficiency was demonstrated for NPPs with the same density. However, in an environmental situation, density differences can be used for separation of particles of different materials and sizes. It was calculated, that at 4000 rpm, particles with a diameter of 3 μm and a density >1.01 g mL^{-1} can be quantitatively retained at flow rates of approximately 4 L h^{-1} (**Supplementary Figure S2**). Thus, we hypothesize that in a sequence of two CFC systems, plankton particles ($d \approx 3$ μm) should be retained in the first centrifuge at the operative pump rate of 2.5 L h^{-1}. Moreover, the calculations indicate quantitative retention of ∼ 200 nm particles with a density >1.1 g mL^{-1} at a flow rate of ∼ 3 L h^{-1} at 17000 rpm in centrifuge 2. Therefore, the separation of the NPPs from the natural particles appeared feasible.

Separation efficiency of the NPPs from natural particles in the micrometer-range was evaluated by using a sequence of two CFC systems with differential rotation speeds between rotors and a pump rate of 2.5 L h^{-1}. A plankton CRM (BCR-414), that is certified for a variety of metals, was used as a model for undesired interfering matrix constituents (high load of organic carbon and minerals). The micron-sized plankton particles were retained in the first rotor as it can be seen in **Figure 4** (left panel). Results of this experiment are shown in **Table 2**.

According to calculations, the entire free NPPs should have passed the first rotor, as very low flow rates of 0.15 L h^{-1} to 0.19 L h^{-1} are theoretically required for NPP retention at 4000 rpm (**Supplementary Figure S2**). However, only 77% ± 5% of the effective NPP dose passed rotor 1 (23.0% ± 2.2% retention efficiency). The NPPs retained in rotor 1 were likely bound to the SPM in the short amount of time between spiking and passing through the sequential CFF system. The entire contact time between SPM and NPPs was 120 min throughout the whole CFC procedure. 53% ± 5% of NPPs was retained in the second rotor.

In order to estimate the amount of plankton CRM retained by centrifugation, an element which was associated by the CRM was chosen to be measured as a proxy according to the following criteria: (1) no detectable background concentration in the Pd-doped NPPs, (2) negligible background value (contamination) stemming from the CFC setup and MWAD and (3) quantitative cumulative recovery. Based on these requirements, Ni was chosen to track the plankton CRM through the separation process. Accordingly, 89% ± 9% (n = 12) of BCR-414 were retained in rotor 1, whereas 3% ± 4% and 2% ± 4% (probably dissolved Ni) were recovered in rotor 2 and the effluent ($Recovery_{total}$ = 113% ± 12%). The ratio of the Ni mass fractions detected in Rotor 1 and Rotor 2 was >30.

Extended Utility of CFC for Field Sampling and Concentration of Nanoplastics in Environmental Media

The lab-scale study emphasizes the potential of a sequence of CFC systems for separation of the micron fraction from the colloidal fraction (**Figure 5**). The results show CFC's potential for the preconcentration of colloidal plastic particles, which is of high

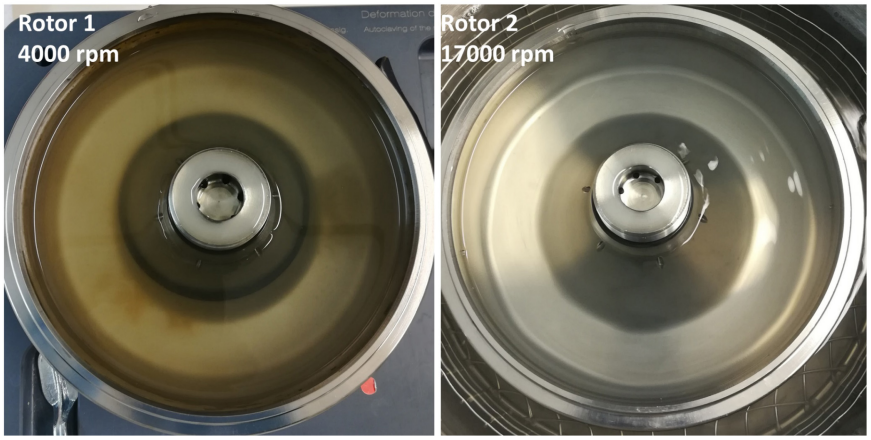

FIGURE 4 | Left: Rotor 1 (4000 rpm) containing most of the plankton particles. **Right:** Rotor 2 (17000 rpm) containing primarily NPPs.

TABLE 2 | Retention efficiencies and recoveries for the Pd-doped NPPs and the plankton CRM BCR-414 for a sequential setup of two centrifuges operated at 4000 rpm and 17000 rpm.

Analyte (tracer)	Retention Efficiency 1st rotor [%]	Retention Efficiency 2nd rotor [%]	Effluent [%]	Total Recovery [%]
NPPs (Pd)	23.0 ± 2.2	53 ± 5	24.4 ± 2.4	88.4 ± 2.9
BCR-414 (Ni)	89 ± 9	3 ± 4	2 ± 4	113 ± 12

Errors correspond to combined uncertainties (u_c).

importance for the future detection of NPPs in environmental aquatic systems. For mechanistic experiments, the Pd-labeled particles served as a valuable model to accurately show the high NPP retention rates under optimal conditions. However, in practice, polymer-specific techniques such as Py-GC-MS or TED-GC-MS (Dümichen et al., 2017; Fischer and Scholz-Böttcher, 2017) would be additionally needed to quantify the enriched colloidal plastic particle sample.

This study focused on the development of a feasible separation and preconcentration method for NPPs, further optimization of NPP quantification was beyond the scope of this study. Nevertheless, some additional sample preparation steps can be recommended. As the CFC enrichment technique would lead to pre-concentration of both NPPs and natural organic colloids contained in environmental waters, purification (i.e., organic matrix digestion) protocols will be required to better isolate NPPs from this heterogeneous mixture (Hurley et al., 2018). The experiments have shown a tendency that heteroaggregation can occur quickly. If only one rotor is used, natural micro- and nanoparticles, MP, free colloidal plastic particles and NPPs included in micron-sized heteroaggregates will be sampled as a mixture.

The sequential CFC setup opens up the possibility to fractionate different sizes of plastic particles and natural colloids. **Figure 5** visually expands on this concept. To sample particles in the desired size range from natural waters, the rotational speeds of both centrifuges have to be coordinated. For example, at a flow rate of 2.5 L h^{-1}, adjusting CFC 1 to 2000 rpm would quantitatively remove particles of ≥3 μm with a density >1.02 g mL^{-} and particles ≥1 μm with a density >1.24 g mL^{-1}. One striking advantage would be the additional removal of all particles ≥500 nm with a density ≥2 g mL^{-1} (online density separation), which includes all minerals but no polymers of interest (Schön, 2011). As SPM contains a high weight fraction of small sediment particles (Imhof et al., 2012; Vidmar et al., 2017), which cannot be removed by oxidative treatments, samples obtained by filtration approaches usually have to be subjected to density separation before their analysis.

Results indicate a linear CFC setup may be preferable over the circular CFC approach for environmental samples. The natural water can be pumped through the CFC directly on-site without any storage in a container where particle sedimentation and adhesion to walls may occur. A second important argument for omitting an intermediary container is minimizing contamination, which is a tremendous issue for research on particulate plastic (Löder and Gerdts, 2015; Wesch et al., 2017; Hermsen et al., 2018). Furthermore, using a rotor of titanium in conjunction with perfluorinated sealing and tubing keeps the potential contamination to a minimum.

The centrifuge can be run in the continuous operation mode for multiple days with ease. In contrast to filtration approaches, no permanent observation is necessary. Operation of the centrifuge for 5 days at a pump rate of 5 L h^{-1} would enable time-integrated sampling of 600 L of source water. Thus, the larger volumes which can be processed compared to ultracentrifugation (10 mL – 100 mL) and the avoidance of membrane blockages compared to ultrafiltration are the main advantages of CFC compared to other centrifugation techniques (De Bruijn et al., 2005; Schwaferts et al., 2019; Enfrin et al., 2020).

The application in the field has already been tested for MP sampling (Hildebrandt et al., 2019). Due to the system's weight (>100 kg), operation on a stationary basis is beneficial. In order to enrich NPPs from water, which presumably contains very low

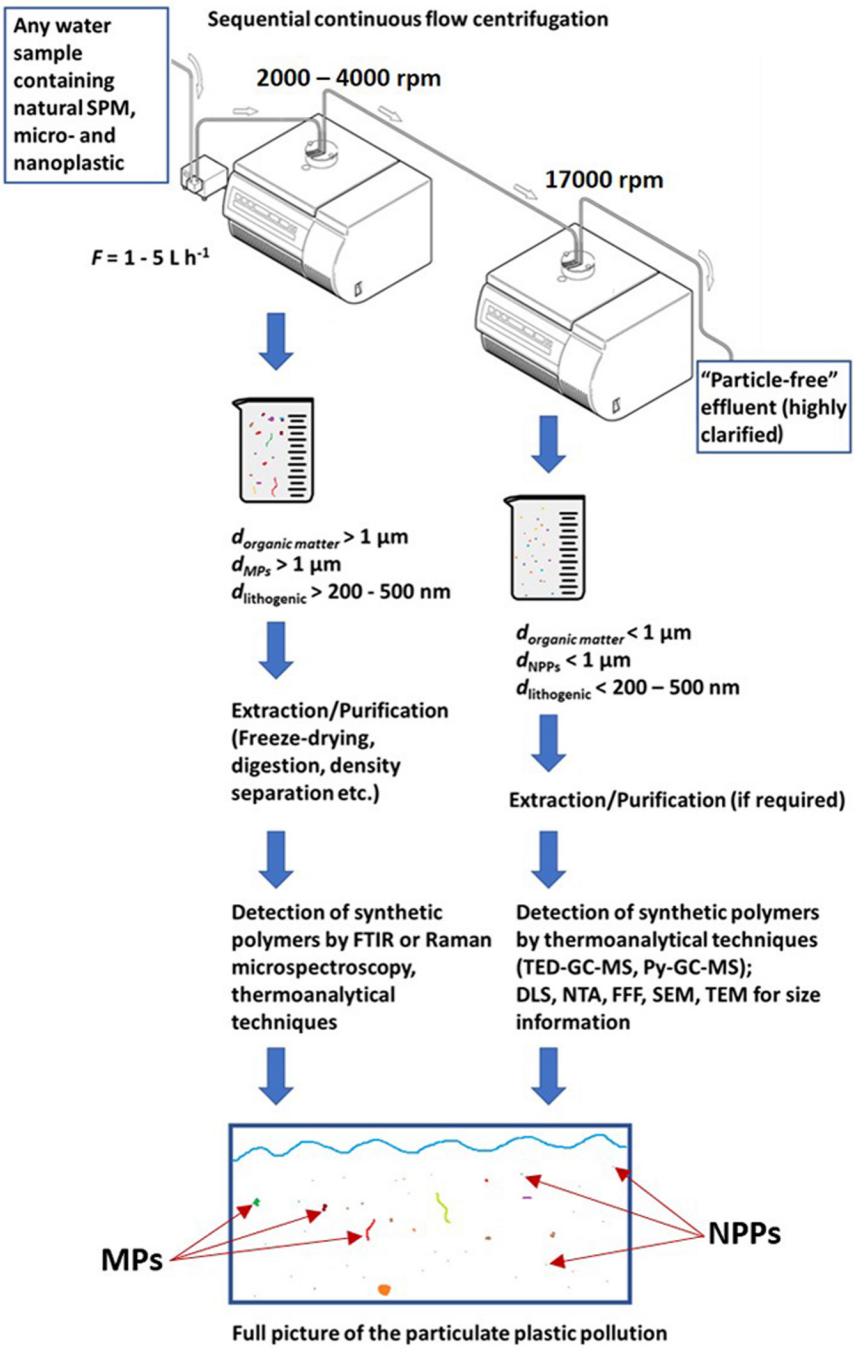

FIGURE 5 | Schematic explanation of the extended utility of the sequential CFC setup as a tool for size- and density selective MP and nanoplastic sampling (modified, © Thermo Scientific).

amounts of NPPs, it may be necessary to implement a high-performance CFC with ∼100,000 g (compared to ∼24,000 g) to enable higher sampling flow rates (e.g., CF-32-Ti, Beckman Coulter, Brea, United States).

As the proof-of-principle has been made, CFC can be tested in even more demanding scenarios. Though application to natural waters is still hypothetical due to challenges arising from other stages of the analytical workflow (e.g., chemical identification of the polymers), the authors would suggest the sequential use of two CFC systems. MP and micron-sized matrix particles would be retained in the first centrifuge, as well as mineral particles down to a few hundred nanometers. In the second rotor, colloidal particles with a density <2 g mL^{-1} could further be enriched. Waters which contain a high concentration of particulate matter, such as water from wastewater treatment plants or street run-off, should be subjected to CFC sampling first. Subsequently,

evaluation of the degree of preconcentration necessary to meet the *LOD* of e.g., TED-GC-MS, to which the freeze-dried sample could be subjected directly, has to be conducted. This requires further method development with respect to both nanoplastic-specific sample preparation and thermoanalytical detection.

CONCLUSION AND OUTLOOK

There is high public, political and scientific interest in environmental plastic pollution, but the smaller the polymer pieces are, the greater the analytical challenges become. This leaves severe data gaps in understanding the occurrence, concentration and identity of nanoplastics and finally their impact on the environment.

In exposure studies, the colloidal plastic fraction was shown to potentially be the most hazardous (Koelmans et al., 2015; Burns and Boxall, 2018). However, a meaningful ecological risk assessment also requires knowledge of relevant exposure levels. As of yet, crossflow ultrafiltration was considered the only technique suitable for nanometer-size-selective sampling of representative volumes. Our results prove that continuous flow centrifugation (CFC) is a valuable alternative for nanoplastic sampling and enrichment, as it does not use a polymer membrane, features a high retention of NPPs and can be used for time-integrated sampling of several hundred liters of source water (Hildebrandt et al., 2019). The proof-of-principle-experiments presented here, in conjunction with expanded theoretical calculations underpin the techniques' potential for size- and density-selective preconcentration of colloidal plastic particles. >90% retention of model NPPs ($d \approx 160$ nm) at a relatively low flow rate in MQW (1 L h^{-1}) and good retention efficiencies (>75%) in river water at higher flow rates (2.5 L h^{-1}) can be achieved. High-performance CFC systems (>100,000 g) (Dorin and Cummings, 2015) may enable higher water throughput with considerably greater flow rates. The scientific community already knows a lot about macro and microplastic pollution (Lorenz et al., 2019), but to successfully answer the question "Where is all the plastic?" (Thompson et al., 2004) it is crucial to also understand the distribution and fate of NPPs.

DATA AVAILABILITY STATEMENT

All datasets generated for this study are included in the article/**Supplementary Material**.

AUTHOR CONTRIBUTIONS

LH has conducted the major part or the experimental work and the data evaluation and the writing. DM has synthesized and provided the Pd-doped-nanoplastic as an analytical key element of the experiments and substantially contributed to the planning of the experimental setup and the experiments. TZ has substantially contributed to the planning of the experiments and with the instrumental analysis as well as data evaluation. DP has considerably contributed to the experimental design and conception of the manuscript. DM, TZ, and DP have also extensively helped with revising and proof-reading the manuscript. All authors contributed to the article and approved the submitted version.

FUNDING

DM was supported by the Swiss National Science Foundation, Ambizione Grant number PZP002_168105.

SUPPLEMENTARY MATERIAL

The Supplementary Material for this article can be found online at: https://www.frontiersin.org/articles/10.3389/fenvs.2020.00089/full#supplementary-material

REFERENCES

Anderson, K. P., Low, M.-A. L., Lie, Y. S., Keller, G.-A., and Dinowitz, M. (1991). Endogenous origin of defective retroviruslike particles from a recombinant Chinese hamster ovary cell line. *Virology* 181, 305–311. doi: 10.1016/0042-6822(91)90496-x

Bannick, C. G., Szewzyk, R., Ricking, M., Schniegler, S., Obermaier, N., Barthel, A. K., et al. (2019). Development and testing of a fractionated filtration for sampling of microplastics in water. *Water Res.* 149, 650–658. doi: 10.1016/j.watres.2018.10.045

Berman, A. S. (1966). *The Development of Zonal Centrifuges and Ancillary Systems for Tissue Fractionation and Analysis*. Washington, DC: U. S. Government Printing Office.

Besley, A. (2017). A standardized method for sampling and extraction methods for quantifying microplastics in beach sand. *Mar. Pollut. Bull.* 114, 77–83. doi: 10.1016/j.marpolbul.2016.08.055

Bhattacharya, P., Lin, S., Turner, J., and Ke, C. (2010). Physical adsorption of charged plastic nanoparticles affects algal photosynthesis. *J. Phys. Chem. C* 114, 16556–16561. doi: 10.1021/jp1054759

Brown, R. I. (1989). The physics of continuous flow centrifugal cell separation. *Artif. Organs* 13, 4–20. doi: 10.1111/j.1525-1594.1989.tb02827.x

Burns, E. E., and Boxall, A. B. A. (2018). Microplastics in the aquatic environment: evidence for or against adverse impacts and major knowledge gaps. *Environ. Toxicol. Chem.* 37, 2776–2796. doi: 10.1002/etc.4268

Cacace, M. G., Nucci, R., and Reckert, H. (1977). Large scale preparation of calf liver nuclei by continuous flow centrifugation. *Experientia* 33, 855–857. doi: 10.1007/bf01951241

Cole, M., Lindeque, P., Fileman, E., Halsband, C., Goodhead, R., Moger, J., et al. (2013). Microplastic ingestion by zooplankton. *Science* 47, 6646–6655. doi: 10.1021/es400663f

Conn, K. E., Dinicola, R. S., Black, R. W., Cox, S. E., Sheibley, R. W., Foreman, J. R., et al. (2016). "Continuous-flow centrifugation to collect suspended sediment for chemical analysis," in *Techniques and Methods,* Plus Appendixes, (Reston, VA: U.S. Geological Survey), 1–D6. doi: 10.3133/tm1D6

Correia, M., and Loeschner, K. (2018). Detection of nanoplastics in food by asymmetric flow field-flow fractionation coupled to multi-angle light scattering: possibilities, challenges and analytical limitations. *Analyt. Bioanalyt. Chem.* 410, 5603–5615. doi: 10.1007/s00216-018-0919-8

De Bruijn, J. P. F., Salazar, F. N., and Bórquez, R. (2005). Membrane blocking in ultrafiltration: a new approach to fouling. *Food Bioprod. Proc.* 83, 211–219. doi: 10.1205/fbp.04012

de la Torre, J. G., Cifre, J. G. H., and Peña, A. I. D. (2018). Prediction and analysis of analytical ultracentrifugation experiments for heterogeneous macromolecules and nanoparticles based on Brownian dynamics simulation. *Eur. Biophys. J.* 47, 845–854. doi: 10.1007/s00249-018-1322-2

Dorin, M., and Cummings, J. (2015). *Principles of Continuous Flow Centrifugation. Technical Application Note*. Indianapolis, IN: Beckman Coulter Lifer Sciences.

Douglas, G. B., Beckett, R., and Hart, B. T. (1993). Fractionation and concentration of suspended particulate matter in natural waters. *Hydrol. Process.* 7, 177–191. doi: 10.1002/hyp.3360070208

Dümichen, E., Eisentraut, P., Bannick, C. G., Barthel, A.-K., Senz, R., and Braun, U. (2017). Fast identification of microplastics in complex environmental samples by a thermal degradation method. *Chemosphere* 174, 572–584. doi: 10.1016/j.chemosphere.2017.02.010

Ekvall, M. T., Lundqvist, M., Kelpsiene, E., Šileikis, E., Gunnarsson, S. B., and Cedervall, T. (2019). Nanoplastics formed during the mechanical breakdown of daily-use polystyrene products. *Nanoscale Adv.* 1, 1055–1061. doi: 10.1039/c8na00210j

Ellison, S. L. R., and Williams, A. (2012). *Quantifying Uncertainty in Analytical Measurement*, 3rd Edn, Washington, DC: CITAC.

Enders, K., Lenz, R., Stedmon, C. A., and Nielsen, T. G. (2015). Abundance, size and polymer composition of marine microplastics $\geq$ 10μm in the Atlantic Ocean and their modelled vertical distribution. *Mar. Pollut. Bull.* 100, 70–81. doi: 10.1016/j.marpolbul.2015.09.027

Enfrin, M., Lee, J., Le-Clech, P., and Ludovic, D. (2020). Kinetic and mechanistic aspects of ultrafiltration membrane fouling by nano- and microplastics. *J. Memb. Sci.* 601:117890. doi: 10.1016/j.memsci.2020.117890

Fischer, M., and Scholz-Böttcher, B. M. (2017). Simultaneous trace identification and quantification of common types of microplastics in environmental samples by pyrolysis-gas chromatography–mass spectrometry. *Environ. Sci. Technol.* 51, 5052–5060. doi: 10.1021/acs.est.6b06362

Frias, J., Filgueiras, A., Gago, J., Pedrotti, M. L., Suaria, G., Tirelli, V., et al. (2019). Standardised protocol for monitoring microplastics in seawater. *Techincal Report*. doi: 10.13140/RG.2.2.14181.45282

Gago, J., Galgani, F., Maes, T., and Thompson, R. C. (2016). Microplastics in seawater: recommendations from the marine strategy framework directive implementation process. *Front. Mar. Sci.* 3:219. doi: 10.3389/fmars.2016.00219

Gigault, J., Ter Halle, A., Baudrimont, M., Pascal, P.-Y., Gauffre, F., Phi, L., et al. (2018). Current opinion: what is a nanoplastic?. *Environ. Pollut.* 235, 1030–1034. doi: 10.1016/j.envpol.2018.01.024

Goodenough, D. A. (1974). Bulk isolation of mouse hepatocyte gap junctions : characterization of the principal protein, connexin. *J. Cell Biol.* 61, 557–563. doi: 10.1083/jcb.61.2.557

Grillo, R., Rosa, A. H., and Fraceto, L. F. (2015). Engineered nanoparticles and organic matter: a review of the state-of-the-art. *Chemosphere* 119, 608–619. doi: 10.1016/j.chemosphere.2014.07.049

Heraeus Instruments GmbH (1998). *Continuous Flow Rotors 3049 (Titanium) and 3054 (Aluminium)*. Hanau: Heraeus.

Hermsen, E., Mintenig, S. M., Besseling, E., and Koelmans, A. A. (2018). Quality criteria for the analysis of microplastic in biota samples: a critical review. *Environ. Sci. Technol.* 52, 10230–10240. doi: 10.1021/acs.est.8b01611

Hernandez, L. M., Yousefi, N., and Tufenkji, N. (2017). Are there nanoplastics in your personal care products? *Environ. Sci. Technol. Lett.* 4, 280–285. doi: 10.1021/acs.estlett.7b00187

Hildebrandt, L., Voigt, N., Zimmermann, T., Reese, A., and Proefrock, D. (2019). Evaluation of continuous flow centrifugation as an alternative technique to sample microplastic from water bodies. *Mar. Environ. Res.* 151:104768. doi: 10.1016/j.marenvres.2019.104768

Hüffer, T., Praetorius, A., Wagner, S., Von Der, Kammer, F., and Hofmann, T. (2017). Microplastic exposure assessment in aquatic environments: learning from similarities and differences to engineered nanoparticles. *Environ. Sci. Technol.* 51, 2499–2507. doi: 10.1021/acs.est.6b04054

Hurley, R. R., Lusher, A. L., Olsen, M., and Nizzetto, L. (2018). Validation of a method for extracting microplastics from complex, organic-rich, environmental matrices. *Environ. Sci. Technol.* 52, 7409–7417. doi: 10.1021/acs.est.8b01517

Imhof, H. K., Schmid, J., Niessner, R., Ivleva, N. P., and Laforsch, C. (2012). A novel, highly efficient method for the separation and quantification of plastic particles in sediments of aquatic environments. *Limnol. Oceanogr. Methods* 10, 524–537. doi: 10.4319/lom.2012.10.524

Ivleva, N. P., Wiesheu, A. C., and Niessner, R. (2017). Microplastic in aquatic ecosystems. *Angew. Chem. Intern. Edn.* 56, 1720–1739. doi: 10.1002/anie.201606957

Jeong, C.-B., Kang, H.-M., Lee, Y. H., Kim, M.-S., Lee, J.-S., Seo, J. S., et al. (2018). Nanoplastic ingestion enhances toxicity of persistent organic pollutants (POPs) in the monogonont rotifer brachionus koreanus via multixenobiotic resistance (MXR) disruption. *Environ. Sci. Technol.* 52, 11411–11418. doi: 10.1021/acs.est.8b03211

Kahane, I., Furthmayr, H., and Marchesi, V. T. (1976). Isolation of membrane glycoproteins by affinity chromatography in the presence of detergents. *Biochim. Biophys. Acta Biomemb.* 426, 464–476. doi: 10.1016/0005-2736(76)90391-6

Käppler, A., Fischer, D., Oberbeckmann, S., Schernewski, G., Labrenz, M., Eichhorn, K.-J., et al. (2016). Analysis of environmental microplastics by vibrational microspectroscopy: FTIR, Raman or both? *Analyt. Bioanalyt. Chem.* 408, 8377–8391. doi: 10.1007/s00216-016-9956-3

Keller, A., Jimenez-Martinez, J., and Mitrano, D. (2019). Transport of nano- and microplastic through unsaturated porous media from sewage sludge application. *Environ. Sci. Technol.* 54, 911–920. doi: 10.1021/acs.est.9b06483

Koelmans, A. A. (2019). Proxies for nanoplastic. *Nat. Nanotechnol.* 14, 307–308. doi: 10.1038/s41565-019-0416-z

Koelmans, A. A., Besseling, E., and Shim, W. J. (2015). "Nanoplastics in the aquatic environment. critical review," in *Marine Anthropogenic Litter*, eds M. Bergmann, L. Gutow, and M. Klages (Cham: Springer International Publishing), 325–340. doi: 10.1007/978-3-319-16510-3_12

Lambert, S., and Wagner, M. (2016). Characterisation of nanoplastics during the degradation of polystyrene. *Chemosphere* 145, 265–268. doi: 10.1016/j.chemosphere.2015.11.078

Lehner, R., Weder, C., Petri-Fink, A., and Rothen-Rutishauser, B. (2019). Emergence of nanoplastic in the environment and possible impact on human health. *Environ. Sci. Technol.* 53, 1748–1765. doi: 10.1021/acs.est.8b05512

Lenz, R., and Labrenz, M. (2018). Small microplastic sampling in water: development of an encapsulated filtration device. *Water* 10:1055. doi: 10.3390/w10081055

Li, Y., Wang, X., Fu, W., Xia, X., Liu, C., Min, J., et al. (2019). Interactions between nano/micro plastics and suspended sediment in water: Implications on aggregation and settling. *Water Res.* 161, 486–495. doi: 10.1016/j.watres.2019.06.018

Löder, M. G. J., and Gerdts, G. (2015). "Methodology used for the detection and identification of microplastics—a critical appraisal," in *Marine Anthropogenic Litter*, eds M. Bergmann, L. Gutow, and M. Klages (Cham: Springer International Publishing), 201–227. doi: 10.1007/978-3-319-16510-3_8

Lorenz, C., Roscher, L., Meyer, M. S., Hildebrandt, L., Prume, J., Löder, M. G. J., et al. (2019). Spatial distribution of microplastics in sediments and surface waters of the southern North Sea. *Environ. Pollut.* 252, 1719–1729. doi: 10.1016/j.envpol.2019.06.093

Lusher, A. L., Welden, N. A., Sobral, P., and Cole, M. (2017). Sampling, isolating and identifying microplastics ingested by fish and invertebrates. *Analyt. Methods* 9, 1346–1360. doi: 10.1039/c6ay02415g

Mattsson, K., Hansson, L.-A., and Cedervall, T. (2015). Nano-plastics in the aquatic environment. *Environ. Sci.* 17, 1712–1721. doi: 10.1039/c5em00227c

Meireles, M., Bourgeois, F., Tourbin, M., Guiraud, P., and Frances, C. (2010). Review: Removal of oversize & recovery of particles from suspensions in the nano size range. [Research Report] CNRS. hal-01186033.

Meyns, M., Primpke, S., and Gerdts, G. (2019). Library based identification and characterisation of polymers with nano-FTIR and IR-sSNOM imaging. *arXiv* [Preprint], Available online at: https://ui.adsabs.harvard.edu/abs/2019arXiv190610243M (accessed June 01, 2019).

Milne, C. J., Lapworth, D. J., Gooddy, D. C., Elgy, C. N., and Valsami-Jones, É (2017). Role of humic acid in the stability of ag nanoparticles in suboxic conditions. *Environ. Sci. Technol.* 51, 6063–6070. doi: 10.1021/acs.est.6b06054

Minoura, I., Katayama, E., Sekimoto, K., and Muto, E. (2010). One-dimensional brownian motion of charged nanoparticles along microtubules: a model system

for weak binding interactions. *Biophys. J.* 98, 1589–1597. doi: 10.1016/j.bpj.2009.12.4323

Mintenig, S. M., Bäuerlein, P. S., Koelmans, A. A., Dekker, S. C., and Van Wezel, A. P. (2018). Closing the gap between small and smaller: towards a framework to analyse nano- and microplastics in aqueous environmental samples. *Environ. Sci. Nano* 5, 1640–1649. doi: 10.1039/c8en00186c

Mitrano, D. M., Beltzung, A., Frehland, S., Schmiedgruber, M., Cingolani, A., and Schmidt, F. (2019). Synthesis of metal-doped nanoplastics and their utility to investigate fate and behaviour in complex environmental systems. *Nat. Nanotechnol.* 14, 362–368. doi: 10.1038/s41565-018-0360-3

Nguyen, B., Claveau-Mallet, D., Hernandez, L. M., Xu, E. G., Farner, J. M., and Tufenkji, N. (2019). Separation and analysis of microplastics and nanoplastics in complex environmental samples. *Acc. Chem. Res.* 52, 858–866. doi: 10.1021/acs.accounts.8b00602

Oriekhova, O., and Stoll, S. (2018). Heteroaggregation of nanoplastic particles in presence of inorganic colloids and natural organic matter. *Environ. Sci. Nano* 5, 792–799. doi: 10.1039/c7en01119a

Peng, J., Wang, J., and Cai, L. (2017). Current understanding of microplastics in the environment: occurrence, fate, risks, and what we should do. *Integr. Environ. Assess. Manag.* 13, 476–482. doi: 10.1002/ieam.1912

Primpke, S., Lorenz, C., Rascher-Friesenhausen, R., and Gerdts, G. (2017). An automated approach for microplastics analysis using focal plane array (FPA) FTIR microscopy and image analysis. *Analyt. Methods* 9, 1499–1511. doi: 10.1039/c6ay02476a

Ran, Y., Fu, J. M., Sheng, G. Y., Beckett, R., and Hart, B. T. (2000). Fractionation and composition of colloidal and suspended particulate materials in rivers. *Chemosphere* 41, 33–43. doi: 10.1016/s0045-6535(99)00387-2

Rochman, C. M., Cook, A.-M., and Koelmans, A. A. (2016). Plastic debris and policy: using current scientific understanding to invoke positive change. *Environ. Toxicol. Chem.* 35, 1617–1626. doi: 10.1002/etc.3408

Schmiedgruber, M., Hufenus, R., and Mitrano, D. M. (2019). Mechanistic understanding of microplastic fiber fate and sampling strategies: synthesis and utility of metal doped polyester fibers. *Water Res.* 155, 423–430. doi: 10.1016/j.watres.2019.02.044

Schön, J. H. (2011). "Chapter 4 - density," in *Handbook of Petroleum Exploration and Production*, ed. J. H. Schön (Amsterdam: Elsevier), 97–105.

Schür, C., Rist, S., Baun, A., Mayer, P., Hartmann, N., and Wagner, M. (2019). When fluorescence is not a particle: the tissue translocation of microplastics in Daphnia magna seems an artIfact. *Environ. Toxicol. Chem.* 38, 1495–1503. doi: 10.1002/etc.4436

Schwaferts, C., Niessner, R., Elsner, M., and Ivleva, N. P. (2019). Methods for the analysis of submicrometer- and nanoplastic particles in the environment. *TrAC Trends Analyt. Chem.* 112, 52–65. doi: 10.1016/j.trac.2018.12.014

Science Advice for Policy by European Academies (2019). *A Scientific Perspective on Microplastics in Nature and Society*. Berlin: SAPEA. doi: 10.26356/microplastics

Shibley, G. P., Manousos, M., Munch, K., Zelljadt, I., Fisher, L., Mayyasi, S., et al. (1980). New method for large-scale growth; and concentration of the Epstein-Barr viruses. *Appl. Environ. Microbiol.* 40, 1044–1048.

Shim, W. J., Hong, S. H., and Eo, S. E. (2017). Identification methods in microplastic analysis: a review. *Analyt. Methods* 9, 1384–1391. doi: 10.1039/c6ay02558g

Stöven, K., Jacobs, F., and Schnug, E. (2015). Microplastic: a selfmade environmental problem in the plastic age. *J. Fur Kulturpflanzen* 67, 241–250. doi: 10.5073/JFK.2015.07.01

Sullivan, K. D., and Gugliada, V. (2018). Fluorescence photobleaching of microplastics: a cautionary tale. *Mar. Pollut. Bull.* 133, 622–625. doi: 10.1016/j.marpolbul.2018.06.019

Svedberg, T., and Pedersen, K. (1940). *The Ultracentrifuge*. Oxford: The Clarendon Press.

Ter Halle, A., Jeanneau, L., Martignac, M., Jardé, E., Pedrono, B., Brach, L., et al. (2017). Nanoplastic in the North Atlantic subtropical gyre. *Environ. Sci. Technol.* 51, 13689–13697. doi: 10.1021/acs.est.7b03667

Thompson, R. C., Olsen, Y., Mitchell, R. P., Davis, A., Rowland, S. J., John, A. W. G., et al. (2004). Lost at sea: where is all the plastic? *Science* 304, 838–838. doi: 10.1126/science.1094559

Turk, E., Teplow, D. B., Hood, L. E., and Prusiner, S. B. (1988). Purification and properties of the cellular and scrapie hamster prion proteins. *Eur. J. Biochem.* 176, 21–30. doi: 10.1111/j.1432-1033.1988.tb14246.x

Vidmar, J., Zuliani, T., Novak, P., Drinčić, A., Ščančar, J., and Milačič, R. (2017). Elements in water, suspended particulate matter and sediments of the Sava River. *J. Soils Sediments* 17, 1917–1927. doi: 10.1007/s11368-016-1512-4

Wesch, C., Elert, A., Wörner, M., Braun, U., Klein, R., and Paulus, M. (2017). Assuring quality in microplastic monitoring: about the value of clean-air devices as essentials for verified data. *Sci. Rep.* 7:5424. doi: 10.1038/s41598-017-05838-4

Wheeler, C. M., Robertson, B. H., Van Nest, G., Dina, D., Bradley, D. W., and Fields, H. A. (1986). Structure of the hepatitis a virion: peptide mapping of the capsid region. *J. Virol.* 58, 307–313. doi: 10.1128/jvi.58.2.307-313.1986

Wu, J., Jiang, R., Lin, W., and Ouyang, G. (2019). Effect of salinity and humic acid on the aggregation and toxicity of polystyrene nanoplastics with different functional groups and charges. *Environ. Pollut.* 245, 836–843. doi: 10.1016/j.envpol.2018.11.055

Xu, M., Halimu, G., Zhang, Q., Song, Y., and Fu, X. (2019). Internalization and toxicity: a preliminary study of effects of nanoplastic particles on human lung epithelial cell. *Sci. Total Environ.* 694:133794. doi: 10.1016/j.scitotenv.2019.133794

Zhou, X.-X., Hao, L.-T., Wang, H.-Y.-Z., Li, Y.-J., and Liu, J.-F. (2019). Cloud-point extraction combined with thermal degradation for nanoplastic analysis using pyrolysis gas chromatography–mass spectrometry. *Analyt. Chem.* 91, 1785–1790. doi: 10.1021/acs.analchem.8b04729

Conflict of Interest: The authors declare that the research was conducted in the absence of any commercial or financial relationships that could be construed as a potential conflict of interest.

frontiers in Environmental Science

REVIEW
published: 03 July 2020
doi: 10.3389/fenvs.2020.00082

How Microbial Biofilms Control the Environmental Fate of Engineered Nanoparticles?

*Morgane Desmau[1], Andrea Carboni[2], Maureen Le Bars[3], Emmanuel Doelsch[4,5], Marc F. Benedetti[6], Mélanie Auffan[2], Clément Levard[2] and Alexandre Gelabert[6]**

[1] Department of Civil and Environmental Engineering, Northwestern University, Evanston, IL, United States, [2] Aix Marseille Univ, Centre National de la Recherche Scientifique (CNRS), Institut de Recherche pour le Dŕveloppement (IRD), Institut National de Recherche pourl'agriculture, l'alimentation et l'environnement (INRAE), Coll France, Centre Européen de Recherche et d'Enseignement en Géosciences de l'Environnement (CEREGE), Aix-en-Provence, France, [3] Université de Pau et des Pays de l'Adour, E2S Université de Pau et des Pays de l'Adour (UPPA), Centre National de la Recherche Scientifique (CNRS), Institut des Sciences Analytiques et de Physico-Chimie pour l'Environnement et les Matériaux (IPREM), UMR 5254, Pau, France, [4] Centre de coopération International en Recherche Agronomique pourle Développement (CIRAD), Unité Propre de Recherche (UPR) Recyclage et Risque, Montpellier, France, [5] Recyclage et Risque, University of Montpellier, Centre de coopération International en Recherche Agronomique pour le Développement (CIRAD), Montpellier, France, [6] Université de Paris, Institut de Physique du Globe de Paris, UMR 7154, Centre National de la Recherche Scientifique (CNRS), Paris, France

Predicting the fate of engineered nanoparticles (ENPs) once they are released in the environment is essential to evaluate their impacts to ecosystems. Microbial biofilms, as highly reactive compartments in soils and sediments, have the potential to impose strong controls on ENPs life cycle in natural settings. However, information regarding impacts of biofilms toward ENPs environmental fate are not easily accessible, and such evidences are collected and discussed in this review, in order to identify common trends and to better constrain the role played by these microbial structures. Biofilms are reported to exhibit important ENPs accumulation capacities, and short to long-term ENPs immobilization can thus be expected. Mechanisms that govern such accumulation and ENPs migration within biofilms depend strongly on electrostatic and hydrophobic interactions, as well as biofilm structural properties, such as density and permeability. They are a combination of key parameters that include ENPs size and surface properties, mineral substrate reactivity, ability to develop organic corona around ENPs, or formation of aggregates within the biofilm thickness. In addition, these microbial structures exhibit highly reactive microenvironments, and are consequently able to impose major ENPs transformations such as dissolution, through ligand- or redox-mediated pathways, as well as passivation or stabilization processes. Interestingly, exposure to toxic ENPs can even trigger a response from micro-organisms biofilms which has the potential to strongly modify ENPs speciation. Promising approaches to investigate the role of microbial biofilms for ENPs cycling in realistic systems are introduced through the use of mesocosms, medium-size replicated ecosystems that allow to integrate the complexity of natural settings. Finally, biofilm-mediated nanoparticles synthesis in man-impacted systems is presented. This raises important questions regarding biofilms role as secondary sources of nanoparticles.

Keywords: biofilm, engineered nanoparticles, mesocosm, microenvironment, ZnS, passivation, dissolution

OPEN ACCESS

Edited by:
Denise M. Mitrano, Swiss Federal Institute of Aquatic Science and Technology, Switzerland

Reviewed by:
Ilaria Corsi, University of Siena, Italy
Elisa Bergami, University of Siena, Italy

****Correspondence:***
Alexandre Gelabert
gelabert@ipgp.fr

Specialty section:
This article was submitted to Biogeochemical Dynamics, a section of the journal Frontiers in Environmental Science

Received: *11 April 2020*
Accepted: *25 May 2020*
Published: *03 July 2020*

Citation:
Desmau M, Carboni A, Le Bars M, Doelsch E, Benedetti MF, Auffan M, Levard C and Gelabert A (2020) How Microbial Biofilms Control the Environmental Fate of Engineered Nanoparticles? Front. Environ. Sci. 8:82. doi: 10.3389/fenvs.2020.00082

INTRODUCTION

Since their generalized synthesis in the late 1980s, the use and production of engineered nanoparticles (ENPs) have grown steadily (Giese et al., 2018). This specific class of material, defined as particles with at least one dimension inferior to 100 nm, present an important variety of compositions (both organic and inorganic), shapes (spheres, rods, nanotubes), sizes, and functionalized capping agents at their surface (various types of polymers or inorganic coatings). Attached to their nanometric dimensions, the unique physico-chemical properties of ENPs have been widely exploited in numerous fields including electronics, optics, medicine, cosmetics, energy or informatics (Auffan et al., 2009; Piccinno et al., 2012). However, the increasing number of products incorporating ENPs over the past 20 years (Vance et al., 2015) combined to high production volumes of approximately 300,000 metric tons per year (Keller et al., 2013), have raised important concerns regarding the release of these highly reactive ENPs in the environment, and subsequently their potential impacts on ecosystems. Keller et al. (2013) estimated that 63–91% of all produced ENPs were entering landfills, soil, water, and air annually, either during their utilization or at the end of life of ENPs-containing products (Mueller and Nowack, 2008).

Although some studies have recently been able to directly measure the concentration of ENPs in rivers (Peters et al., 2018; Wang et al., 2020), there are still major technical limitations to quantify accurately ENPs presence in the environment. To circumvent these difficulties, material flow models have been developed in the last years (Mueller and Nowack, 2008; Gottschalk et al., 2009; Keller et al., 2013) in order to estimate the flows and sinks of different ENPs types in the environment. These approaches based on production volumes and, more recently, time-dependent ENPs release from nano-products provided estimations of ENPs release in natural systems (Sun et al., 2016; Wang and Nowack, 2018). Thanks to those models, landfills, soils and sediments have been identified as the main environmental compartments acting as sinks for ENPs (Sun et al., 2016; Wang and Nowack, 2018). However, these approaches are mostly designed to quantify fluxes entering environmental and technical compartments and do not provide any information regarding ENPs fate and impact once in the environment. The high degree of complexity inherent to soils and sediments significantly complexifies studies on ENPs transformations and transport in such environmental matrices (Levard et al., 2012; Montano et al., 2014; Layet et al., 2017; Xu, 2018). Rodrigues et al. (2016) listed the principal factors and processes that control the behavior of ENPs in those matrices, which are homoaggregation, heteroaggregation with organic matter (OM), pore straining, oxidation/dissolution reactions, complexation with OM, and interaction with the mineral surfaces. In particular, the latter is considered of first importance when considering metal(loid)s, OM, colloids and even ENPs cycling in the environment (Brown et al., 1999). Moreover, the development of a microorganisms-based coating at the mineral surfaces creates a highly reactive interface that strongly impacts the fate of toxic and essential elements in the environment (Brown, 2001; Templeton et al., 2001, 2003a). In all subsurface environments where they can develop, i.e., from soils to several kilometers depth below the surface, microorganisms tend to form biofilms, structures in which microorganisms are encased in highly hydrated 3D-matrix composed of exopolymeric substances (EPS) (Costerton et al., 1995; Ménez et al., 2012; Flemming and Wuertz, 2019). The transport limitations attached to these structures in addition with metabolic activity favor the creation of microenvironments within the biofilm thickness (Stewart, 2003), which, in association to the high density of functional groups, confers a very high and specific reactivity at the mineral/biofilm/solution interface.

While a large amount of studies exists on ENPs toxicity toward microorganisms and microbial biofilms (Fulaz et al., 2019b), research focusing on biofilms impacts on ENPs fate in the environment are scarce and systematic information is not easily accessible. Herein, we report the current knowledge relative to controls exerted by microbial biofilms on ENPs transformations in soils, sediments or sludge systems. A critical analysis of biofilm organization and reactivity is introduced, as well as a description of the physical interactions between microbial biofilms and ENPs. Mechanisms of ENPs dissolution, passivation, and stabilization when in contact with microbial biofilms, or their EPS matrix, are thoroughly discussed. Promising strategies based on the use of mesocosms to investigate biofilms impacts in realistic dynamic ecosystems are presented. Finally, the generation of ENPs by biofilms as a defense mechanism when associated with anthropogenic activities are also discussed.

MICROBIAL BIOFILMS IN NATURAL SYSTEMS

Occurrence, Structure, and Overall Reactivity

Bacteria and archaea constitute major phylogenetic groups with reported concentrations around 10^7–10^{12} cells/g of soils (Watt et al., 2006), and a total biomass estimated at 77 Gt C on Earth (Bar-On et al., 2018). They are ubiquitous in all environments, from subsurface aquatic systems to locations several kilometers deep in the lithosphere. In most cases, soil microorganisms are organized as communities called biofilms, where microbial cells are encased in a 3-dimensional organic matrix (Costerton et al., 1987; Flemming and Wuertz, 2019). However, despite their high occurrence in soils, biofilms are mostly concentrated in small scale microhabitats that encompass less than 1% of total soil volume (Young et al., 2008). There, biofilms are found as 2–10 μm thick structures, mainly located at the surfaces of soil pores (Young et al., 2008; Flemming and Wuertz, 2019). The resulting microbial hotspots and high cell densities (Kuzyakov and Blagodatskaya, 2015; Nunan, 2017) are correlated to specific reactive microenvironments (**Figure 1**), which are associated with either metabolic activities or to the specific organization of these structures (Kuzyakov and Blagodatskaya, 2015; Nunan, 2017).

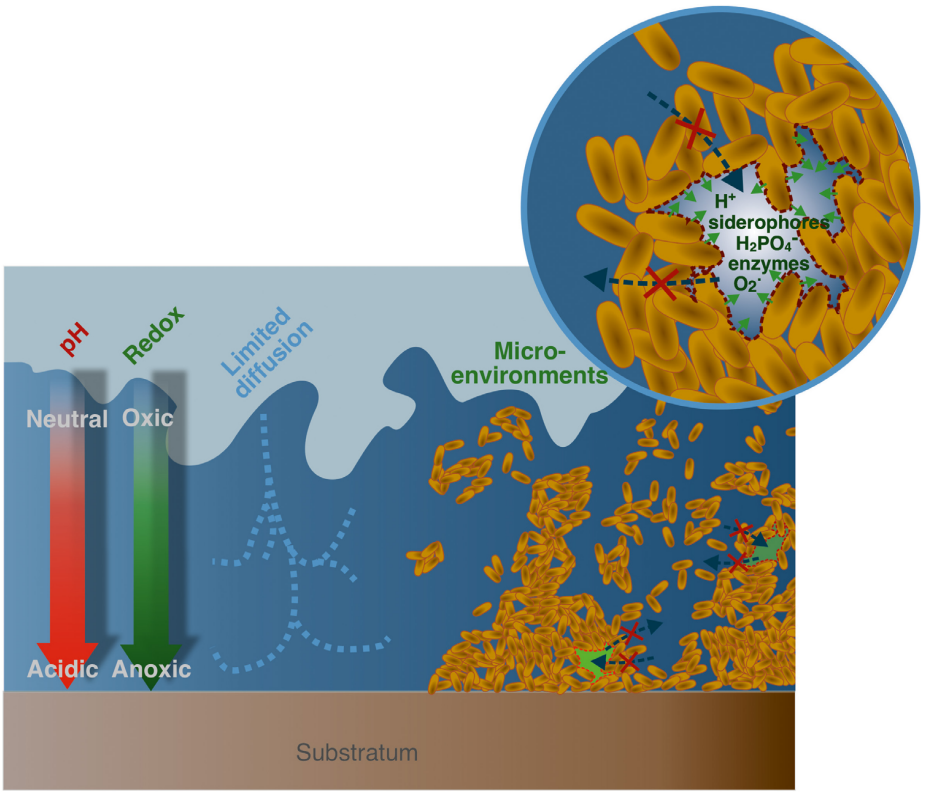

FIGURE 1 | Physico-chemical properties of microbial biofilms. From left to right, existence of gradients in pH and redox conditions with depth; diffusion limited transport of nutriments, molecules (such as siderophores, enzymes), and metabolites; existence of microenvironments within the biofilm thickness that exhibit specific physico-chemical conditions (for instance low pH, high siderophore, superoxide, enzymes, or phosphate concentrations) at the local scale.

Indeed, microbial cell walls and membranes are known to exhibit very elevated specific surface areas, as well as high reactive site densities (Fein et al., 1998; Borrok et al., 2005). For bacteria, the overall surface charge is usually reported to originate from the presence of carboxyl moieties (pK_a in the range 3–4.5) and phosphoryl groups (pK_a in the range 7–8), both functions that exhibit a negative charge when deprotonated, as well as positively charged amino groups at neutral pH (pK_a in the range 8–11). In addition, some recent studies highlighted a strong affinity of thiol groups toward soft metals (e.g., Hg, Cd), despite their lower density at the cell surfaces in comparison to other functional sites (Yu et al., 2014; Mishra et al., 2017). In general, the external surface charge of microbes exposed to the solution is dominated by negatively charged groups, with reported electrophoretic mobilities for bacteria suspensions generally negative at pH higher than 3 (Ha et al., 2010). Moreover, to create and maintain biofilms, microbial cells secrete an exopolymeric matrix (EPS), which in turns provides additional functional sites, mostly negatively charged (Tourney and Ngwenya, 2014), and confers specific density and permeability properties to the whole structure. Thus, biofilms and their EPS matrix as well as the substrate where they are attached to, can act as competing sorbents in all natural systems and are considered a major driver for various environmental processes such as metal(loid)s cycling (Ha et al., 2010; Wang et al., 2016a,b). As such, biofilms play a relevant role in metals and metalloids cycling, and are therefore of first importance from an environmental perspective.

Microenvironments Within Biofilm Thickness

Biofilms structure is intrinsically highly complex, and has been thoroughly investigated, especially in the context of biomedical applications (Costerton et al., 1999; Donlan, 2002). Their organization is highly variable, depending on the strain, growth condition, or even the substrate type on which these colonies develop (Sutherland, 2001). Microbial biofilm matrices are described as gel-like structures surrounding a high density of cells, where the diffusion of chemical elements is limited by the low porosity and permeability of the system (Warren and Haack, 2001). Consequently, because of their metabolic activities, microorganisms within these structures create and maintain micro-environments that are intrinsically different from the surrounding bulk solution (**Figure 1**). As a result, they impose concentration gradients for organic or inorganic compounds such as phosphate (Couasnon et al., 2019), enzymes or EPS (Flemming and Wingender, 2010), as well as physico-chemical gradients (pH, Eh, pO_2...) (Hunter and Beveridge, 2005; Hidalgo et al., 2009). For instance, *Pseudomonas fluorescens* WCS 365 biofilms were reported to exhibit low pH regions (down to

pH 5.1) in cells clusters located at the inner-core of microcolonies, which gradually evolved to neutral pH in vicinity of the bulk solution at the biofilm surface (Fulaz et al., 2019a). These pH variations within relatively short spatial scales could be explained by the fast production of metabolic residues combined with a limited solute transfer through the EPS matrix, resulting in a local accumulation of acidic by-products (Fulaz et al., 2019a). Multi-species biofilms, presenting an array of different metabolisms, could generate more acidic by-products under oxygen-limiting conditions compared to single-species biofilms, resulting in lower minimal pH values, reported between 4 and 5 for multi-species oral biofilms (Schlafer et al., 2018). In addition, extracellular medium within biofilms can be considered as an external digestive system, where extracellular enzymes are in close vicinity with cells, and can thus metabolize dissolved, colloidal and solid biopolymers (Flemming and Wingender, 2010). These physico-chemical modifications at the local scale in biofilms' micro-environments constitute a key parameter regarding their reactivity, and they are known to impact the metal(loid)s cycling in environmental systems. For instance, numerous evidences point out the major control microbial communities exert on mineral and rock weathering. As such, a 20-fold increase in dissolution rates is reported for soil bacteria (Kalinowski et al., 2000), and up to 2 orders of magnitude for groundwater bacteria (Barker and Banfield, 1998). Local acidification as well as siderophore, organic acids, and metabolites produced in vicinity of microorganisms are usually invoked to explain this increase in weathering rates when microbial communities are present (Dehner et al., 2010; Gadd, 2010).

However, local physico-chemical conditions and the nature of gradients imposed, as well as metal(loid)s dynamic in biofilms, remain poorly understood and certainly need further investigation. It can be expected that the improvement of existing techniques to accurately probe specific patterns in biofilm microenvironments, such as confocal laser scanning microscopy (CLSM), will allow a better characterization and more precise description of the mechanisms of metal(loid)s dynamic in biofilms. Understanding these processes is particularly relevant in the case of ENPs that are potentially very sensitive to physico-chemical gradients. For example, these microbial structures can drive ENPs dissolution under low pH or high complexing ligands concentrations (ligand-assisted dissolution) but can also stabilize ENPs surfaces. Conversely, biofilms are also able to impose local oversaturations relative to mineral phases (Finlay et al., 1999; Templeton et al., 2003b; Nancharaiah et al., 2010; Couasnon et al., 2019), that were kept undersaturated in the overlying bulk solution, resulting in the formation of incidental NPs. As a result, biofilms may constitute an important accumulator for ENPs or a source of incidental NPs that can strongly impact their fate through a number of bio-physico-chemical processes that will be discussed in this review.

Biofilms: Important Environmental Accumulators

As stated previously, biofilms have a 3-dimensional organization which is close to a gel-like structure, and exhibit high reactive site densities of cells and EPS. As a result, biofilms are frequently regarded as filters or even sinks for a variety of inorganic, organic and biological components (Ikuma et al., 2015). Actually, their sequestration capacity has been extensively studied for metal(loid)s by Templeton et al. (2003b) and Wang et al. (2016a; 2016b), that identified biofilms as accumulative compartments in the environment. Similarly, a large variety of ENPs are trapped in significant amounts by biofilms (Battin et al., 2009; Burns et al., 2013; Avellan et al., 2018). It was also observed in column transport experiments where retention of ENPs increases in presence of these microbial structures: latex NPs and CdSe/ZnS quantum dots (QDs) (Tripathi et al., 2012), zerovalent Fe-NPs (Lerner et al., 2012; Crampon et al., 2018), nano-ZnO (Jiang et al., 2013), biogenic nano-Se (Wang et al., 2019), nano-Ag (Xiao and Wiesner, 2013). This increased retention in column experiments is generally explained by changes in roughness, surface charge and hydrophobicity at the surface of aquifer grains (Donlan, 2002; Kurlanda-Witek et al., 2015) in addition to the intrinsic accumulation properties of these microbial structures.

In addition, a mesocosm-based study showed that microbial biofilms constituted the biggest NPs accumulation reservoir on a per mass basis for gold nanorods (Ferry et al., 2009). However, the reported degree of accumulation is variable, depending on the biofilm and ENPs types as well as parameters such as ENPs concentration, pH or presence of organic ligands. Nano-CeO_2 accumulation in *P. fluorescens* biofilms and *Mycobacterium smegmatis* biofilms were estimated at approximately 20 and 50% respectively, for initial concentration ranging between 5 and 30 $mg.L^{-1}$ (Jing et al., 2014). Multi-species biofilms seem to be more efficient nano-Ag accumulators compared to single-species biofilms, suggesting that higher structural heterogeneity and density in multi-species biofilm are important parameters for ENPs trapping (Walden and Zhang, 2018). *Shewanella oneidensis* MR1 biofilms exposed to 31.22 μg nano-Ag exhibit an accumulation extent of 1.7% at pH 7 (Desmau et al., 2018), while *Pseudomonas putida* exposed to 22.8 μg nano-Ag has an accumulation level of 0.4% at pH 7.5, and 5.3% at pH 6.0 (Fabrega et al., 2009). Interestingly, accumulation in *P. putida* biofilms becomes largely predominant when going to low ENPs concentrations, relevant to most expected concentrations in environmental systems (Gottschalk et al., 2009; Sun et al., 2016), reaching levels as high as 93% for an exposure to 20 $\mu g.L^{-1}$ (total 2.28 μg) nano-Ag (Fabrega et al., 2009).

Regarding ENPs accumulation kinetics, a pseudo-first order was used to model adsorption and desorption rate of nano-CeO_2 onto bacteria biofilms (Jing et al., 2014). Usually, interactions between ENPs and biofilms are reported as being fast, occurring in less than 30 min (Jing et al., 2014; Walden and Zhang, 2018). However, in some studies, the evolution at longer times varies among different experimental systems, either quickly reaching an apparent steady-state (Jing et al., 2014), or experiencing a continuous accumulation and ENPs migration at the mineral/biofilm/solution interface over 24 h (Desmau et al., 2018). A decrease in accumulation rate was also reported for nano-Fe_3O_4, with a maximum accumulation of 17% reached after 5 h of exposure, dropping to 0.5% after 24 h, potentially due to cells detachment (Herrling et al., 2016).

Nevertheless, accumulation trends over longer time periods, on the order of months, remain mostly unexplored despite their high environmental importance.

The significant accumulation of ENPs in biofilms raises the question of considering biofilms as a potential secondary source for ENPs in other environmental compartments (Walden and Zhang, 2018). In soils, if biofilms are temporarily exposed to high ENPs concentrations on short time periods, they are likely to accumulate these objects to a relatively high extent. Then, biofilms could gradually release ENPs, or ENPs products of degradation, in ENPs-free pore waters. This process, potentially important when considering ENPs spreading in the environment on the longer term, specifically regarding their mobility and their associated toxicity to ecosystems, has remained largely overlooked up to now.

ENPs RETENTION AND MIGRATION MECHANISMS WITHIN BIOFILMS

Retention properties imposed by biofilms are critical when evaluating the environmental fate of ENPs. As a result, several reviews specifically report the types of interactions existing between ENPs and these microbial structures (Ikuma et al., 2015; Joo and Aggarwal, 2018; Walden and Zhang, 2018). Ikuma et al. (2015) provide an extensive description of such interactions following a three-step process: (1) ENPs transport to the vicinity of the biofilm, (2) ENPs attachment to the biofilm surface, (3) migration within the biofilm thickness. For the authors, if ENPs transport to the biofilm and its initial attachment are relatively well-documented, they point out the lack of comprehensive understanding regarding the processes that govern ENPs migration within biofilms. However, this last factor is absolutely essential since it determines to a large extent the retention properties imposed by biofilms, and is thus partly responsible for ENPs behavior in natural systems. As a result, the identified key parameters that control the migration and retention of ENPs within biofilm structures are reported here (**Figure 2**).

Biofilm Structural Properties and Effect on Size-Dependent ENPs Transport

Porosity and permeability of biofilms constitute major parameters for ENPs migration since they govern any solute transport within the structure. As such, ENPs diffusion coefficients are calculated to be much smaller (up to 50 times) than the values in aqueous solutions for a variety of model NPs (Au-, Ti-, latex-, and silicone-based NPs) and biofilms (*P. fluorescens*, *Lactococcus lactis*, *Stenotrophonas maltophilia*) (Guiot et al., 2002; Golmohamadi et al., 2013). Porosity and permeability are linked to the type, composition, thickness, age and roughness of the biofilm (Joo and Aggarwal, 2018). In more details, the presence of water channels, submitted to advective transport and simple diffusion, as well as smaller pores and conduits (Costerton et al., 1995) constitute the template that could allow the migration of ENPs at the mineral/biofilm/solution interface. In that case, the overall

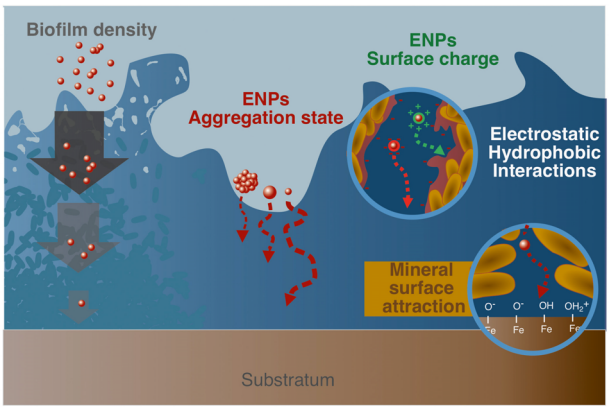

FIGURE 2 | Parameters controlling ENPs migration within biofilms. From left to right, biofilm density and permeability that can limit access to the deepest layers; aggregation state and size of ENPs; ENPs surface charge that controls associations with the biofilm matrix (EPS and cells) through electrostatic and hydrophobic interactions, with for instance positively charged ENPs that tend to interact strongly with the negatively charged biofilm matrix; complexation of ENPs with the mineral substrate surface that partly drives ENPs transport through the biofilm thickness.

density variations in the biofilm, channel sections, but also ENPs size constitute critical factors, associated to size exclusion and diffusion limited processes (Golmohamadi et al., 2013).

For instance, when using silica NPs sensors as stains to generate high-resolution maps of *Escherichia coli* biofilms, only the smallest 10 nm diameter particles allowed to access fine details in biofilm structure, while 70 and 30 nm only displayed a limited access to this 3-dimensional organization (Hidalgo et al., 2009). Also, relative self-diffusion coefficients of 2 and 10 nm nano-Ag was shown to decrease exponentially with the square of the radius of the ENPs (Peulen and Wilkinson, 2011). This size effect as a control of diffusion was critical for nano-Ag interacting with biofilm, when investigating their migration through a *S. oneidensis* MR1 biofilm (Desmau et al., 2018). Actually, it is recognized that ENPs penetration is more efficient in less dense biofilms, or biofilm parts, since they exhibit higher pore space more readily accessible (Peulen and Wilkinson, 2011; Joo and Aggarwal, 2018). Similarly, more mature biofilms, usually displaying elevated structural densities, are expected to lower ENPs penetration (Mitzel and Tufenkji, 2014). However, there are evidence that ENPs tend to accumulate preferentially in dense rather than loosely attached biofilms (Peulen and Wilkinson, 2011), with higher structural heterogeneity and density being critical parameters for ENPs accumulation (Walden and Zhang, 2018). This may be explained by the fact that denser biofilms exhibit a more developed extracellular matrix (EPS) that fills the spaces between cells, composed of polysaccharides, proteins and other molecules, either hydrophilic or hydrophobic. As a result, dense biofilms are likely to display higher reactive site densities, enabling more efficient interactions with ENPs through electrostatic or chemical bonding in addition to steric immobilization, leading to strong ENPs trapping. On the contrary, if ENPs transport is favored in

loose biofilms, a significant part of trapped ENPs is also submitted to advective transport out of the biofilm, thus disabling long term sequestration.

Electrostatic and Hydrophobic Interactions

Effect of Surface Properties of ENPs on ENPs-Biofilm Interactions

Interactions between ENPs and biofilms are usually described as governed by electrostatic and hydrophobic factors (Fulaz et al., 2019b). In this regard, a critical parameter to understand ENPs-biofilm interactions is surface properties of ENPs, such as hydrophobicity or type of coatings, and more specifically surface charge. The importance of the ENPs surface properties was demonstrated for different types of ENPs, (un)coated or with various capping agents. The uncoated ENPs showed a much higher retention compared to the coated ones (Li et al., 2013). The significantly higher attachment to *Pseudomonas aeruginosa* biofilms, for sulfate-functionalized model NPs compared to their carboxylated counterparts, illustrates how surface chemistry and NPs functionalization is an important parameter (Tripathi et al., 2012).

As noted earlier (cf. section "Occurrence, Structure, and Overall Reactivity"), microbial biofilms exhibit an overall negative charge (Ha et al., 2010; Tourney and Ngwenya, 2014). Based on electrostatic considerations, interactions with positively charged ENPs are thus expected to be favored, while ENPs of negative charge should only poorly interact with the biofilm. This general trend is globally observed in many ENPs-biofilms systems (Peulen and Wilkinson, 2011; Lerner et al., 2012; Ikuma et al., 2014, 2015; Dzumedzey et al., 2017; Crampon et al., 2018; Wang et al., 2019). Interestingly, electrostatic repulsion energy is also size dependent and is reported to be roughly proportional to the particle's surface area. For instance, 70 nm particles are submitted to approximately a 50-fold increase in repulsion compared to 10 nm particles (Hidalgo et al., 2009). Functionalized QDs (Cdse/ZnS) of cationic charge were shown to fully penetrate into *E. coli* biofilms, while neutral and anionic QDs did not efficiently accumulate in the structure (Li et al., 2015). Similarly, a low retention of negatively charged nano-Ag [polyvinylpyrrolidone (PVP) coating] onto *P. aeruginosa* PAO1 biofilms was explained as the result of repulsive electrostatic forces (Mitzel and Tufenkji, 2014). Noticeably, although electrostatic interactions constituted a critical parameter in numerous studies, they could reveal to be inadequate to describe ENPs-biofilm interactions in some systems (Peulen and Wilkinson, 2011; Golmohamadi et al., 2013). Indeed, this electrostatic attraction or repulsion rule is not always accurate, and negatively charged ENPs have been shown to interact with biofilms despite their general negative charge (Tong et al., 2010; Tripathi et al., 2012; Desmau et al., 2018). This could be related to local positive charges or domains, e.g., the presence of positive functional moieties such as amino groups (Ha et al., 2010), or due to other attraction forces (attraction from the mineral surface, chemical binding and stabilization, hydrophobicity, advective transport).

In addition, ENPs hydrophobicity constitutes also an important parameter for their sequestration and subsequent migration within the biofilm thickness (Habimana et al., 2011; Xiao and Wiesner, 2013; Mitzel et al., 2016). This property is likely to be related to the existence of hydrophobic domains in biofilms (Aldeek et al., 2011; Jian-Zhou et al., 2015; Flemming et al., 2016), such as protein-rich zones for some microbial consortia (Xiao and Wiesner, 2013). Also, an increase in ENPs coating hydrophobicity could favor retention (Lerner et al., 2012). Li et al. (2015). reported distinct localization for hydrophobic and hydrophilic QDs throughout *E. coli* biofilms, with hydrophobic particles being more homogeneously distributed than hydrophilic ones. This example illustrates that dynamics of ENPs partitioning within different domains of biofilms can be, at least partly, impacted by hydrophobic interactions.

Effect of Biofilm and Corona-Formation on ENPs Aggregation

Aggregation state, which is related to ENPs surface properties, is a critical factor affecting ENPs' reactivity, such as their penetration capacities in biofilms (Wirth et al., 2012). Indeed, nano-Ag were found to aggregate when exposed to *E. coli*, with an increase in average particle size by a factor of 40 in biofilms, and only by a factor of 15 for planktonic cells (Choi et al., 2010). Given the size of the aggregates, it is expected that aggregated ENPs will experience lower penetration and interaction with the biofilm (Peulen and Wilkinson, 2011). Within biofilm thickness, the presence of microenvironments is likely to modify the overall ENPs reactivity, and thus, their aggregation (**Figure 3**). For instance, nano-Ag suspensions are efficiently stabilized by EPS at low $Ca(NO_3)_2$ concentrations while at higher $Ca(NO_3)_2$ concentrations, the formation of EPS intermolecular bridging favors the connection of EPS-caped nano-Ag together (Fernando et al., 2020). The corona formation process, which consists in the association of organic (bio)molecules, natural OM or EPS to the ENPs surface (Navarro et al., 2009; Ikuma et al., 2015; Zhu et al., 2016; Ouyang et al., 2017), plays an important role in controlling ENPs aggregation by modifying the colloidal stability of the nanoparticles, and in turn their interactions properties with biofilms (Fabrega et al., 2009). This corona formation is likely to happen within the biofilm itself, given the existence of microenvironments along the biofilm thickness (cf. section "Occurrence, Structure, and Overall Reactivity"), that may locally expose ENPs to high concentrations of organic molecules (EPS, biopolymers, metabolic residues). The formation of an EPS coating layer surrounding the ENPs (Khan et al., 2011b), is reported to increase the ENPs hydrodynamic diameter (Kroll et al., 2014) but also to decrease the ENPs rate of aggregation (Khan et al., 2011a; Adeleye et al., 2014; Kroll et al., 2014; Miao et al., 2015; Wang and Nowack, 2018), In addition, the electrostatic repulsion between ENPs can be favored when the surface charge is becoming more negative in presence of EPS (Khan et al., 2011a; Wang and Nowack, 2018). Steric repulsions and hydrophobic interactions also need to be considered regarding the aggregation rate of ENPs in presence of EPS (Lin et al., 2016; Wei et al., 2019). One of the main consequences of the ENPs stabilization in presence of EPS

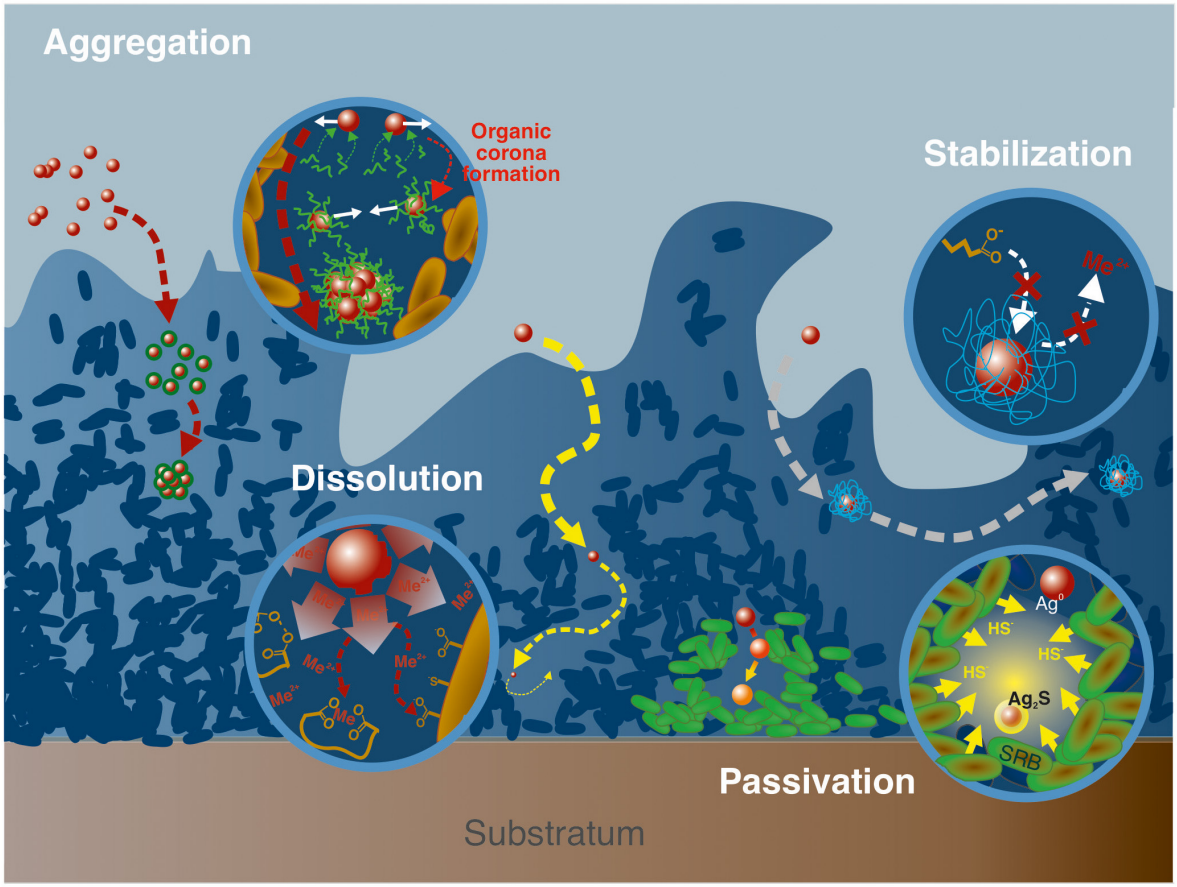

FIGURE 3 | Examples of processes associated to ENPs transformations and aggregation. From left to right, aggregation mediated by the formation, in the biofilm matrix, of an organic corona, that modifies ENPs surface properties and promotes interactions between ENPs; ligand-mediated dissolution involving the presence of highly complexing ligands (such as siderophores) that complex free metals in solution and thus promotes ENPs dissolution; passivation of silver NPs in vicinity of sulfato-reducing bacteria (SRB) that increase locally HS- concentrations, and favors sulfidation processes at the ENPs surface; ENPs stabilization through the formation of an organic corona that isolates ENPs from the surrounding solution thus limiting dissolution processes.

would be the favored transport of ENPs in aquatic environments (Wang and Nowack, 2018).

The presence of functional groups in EPS, their composition (protein, carboxylate, polysaccharide, and lipid contents) and concentration will also strongly condition the interactions with ENPs (Adeleye and Keller, 2016; Xu et al., 2016; Zhou et al., 2016; Morelli et al., 2018; Wang and Nowack, 2018; Fernando et al., 2020). As such, investigations were conducted on the stabilization potential of three EPS types, soluble, loosely bound, and tightly bound EPS, characterized by different protein to polysaccharide ratio (Fernando et al., 2020). All three EPS-types were found to prevent nano-Ag aggregation, but loosely bound EPS were the most efficient, due to its lower content in hydrophilic dissolved OM. In addition, EPS hydrophobic properties can be important when considering sorption at ENPs surfaces (Wei et al., 2019).

Noticeably, EPS composition is strongly determined by the type of microorganisms considered (Sutherland, 2001; Flemming and Wingender, 2010), and conditions in which they develop. As a result, dynamic changes in ENPs reactivity when interacting with biofilms can be expected for some specific conditions, but such mechanism remains today largely overlooked.

Mineral Substrate Reactivity

Mineral surfaces are known to exhibit strong complexing capacities toward metal(loid)s and organic matter in most ecosystems (Brown et al., 1999). In soils, they can serve as substrates on which biofilms develop, but doing so, they maintain their high complexing capacities despite the overlying microbial community, as reported for different mineral/biofilm/solution interfaces (Templeton et al., 2001, 2003a,b; Wang et al., 2016a,b). In these studies, focused on the partitioning of metal(loid)s at the mineral/biofilm/solution interface, mineral substrates constitute a strong complexing compartment able to drive the dynamics of free metal transport within the whole interface, biofilm included. Regarding ENPs, a study by Desmau et al. (2018) on *S. oneidensis* MR1 biofilms exposed to nano-Ag shows that the mineral surface remains highly reactive and tends to accumulate negatively charged ENPs (PVP coated nano-Ag). As a result, the ENPs dynamics of accumulation and further transport at

the mineral/biofilm/solution interface are strongly driven by the mineral surface. However, in most studies the reactivity of the mineral substrate was poorly or not considered and future research will need to elucidate its role.

ENPs CHEMICAL TRANSFORMATIONS IN BIOFILMS

As previously discussed (cf. section "ENPs Retention and Migration Mechanisms Within Biofilms"), ENPs fate in natural systems is strongly controlled by retention mechanisms imposed by microbial biofilms. To this perspective, another critical factor that needs to be considered is the transformation that ENPs can undergo when in contact with these biological structures (Holden et al., 2016). At a first approximation, ENPs potential for speciation changes could be considered similar to that of free metals that are subjected to strong chemical modifications in biofilms (Templeton et al., 2003a; Couasnon et al., 2019). It is thus likely that ENPs experience similar transformations, driven by the high reactivity of local microenvironments and the important functional sites density spread within the biofilm thickness.

Dissolution and stabilization by surface passivation are reported here as the main processes able to drastically modify ENPs speciation (**Figure 3**). In addition, response to toxic stress from cells caused by ENPs exposure is discussed since the related processes are potentially impacting their environmental life cycle.

Dissolution

Toxicity of various ENPs comes from their dissolution and the subsequent exposure of organisms to free metals. This toxic pathway is usually evoked for known soluble ENPs such as nano-Ag or nano-ZnO (Franklin et al., 2007; Xia et al., 2008; Auffan et al., 2009; Gelabert et al., 2015; Le Ouay and Stellacci, 2015). In that case, ENPs in close vicinity of bacteria cell walls become a continuous source of novel metal species through dissolution processes. This can result in high concentrations of toxic ions and cause toxicity to the bacteria (Slavin et al., 2017). The extent of dissolution and the associated kinetics generally depend on the size, shape, surface characteristics of the ENPs, as well as the solvent properties (pH, ionic strength, presence of ligands), and is well-documented even in complex matrices (Gelabert et al., 2014; Sivry et al., 2014). In natural systems, dissolution kinetics can be largely enhanced in contact with highly reactive environmental compartments, such as biofilms. Even NPs known as stable could be submitted to dissolution. As such, some studies report a significant ENPs dissolution when in contact with microbial biofilms (Wirth et al., 2012; Gil-Allué et al., 2015; Avellan et al., 2018; Wang and Nowack, 2018; Alizadeh et al., 2019; McGivney et al., 2019).

Even if the associated processes remain poorly documented, two main factors are likely to be responsible for ENPs dissolution in microbial biofilms: (i) the high density of reactive ligands in these bio-structures favoring ligand assisted dissolution, and (ii) the strong redox activities of microorganisms. These dissolution processes are certainly favored in biofilm microenvironments that exhibit specific physico-chemical properties at the local scale.

Ligand-Mediated Dissolution

In microbial biofilms, the high reactive site densities result from the association of numerous functional sites present on the cell walls of microorganisms (Ngwenya et al., 2003; Borrok et al., 2004a,b, 2005), and on the EPS matrix (Ha et al., 2010; Tourney and Ngwenya, 2014). Regarding microbial surfaces, the compilation of several studies on Gram-positive and Gram-negative bacteria in planktonic suspension reported functional sites densities in the range of $4.5 \pm 0.8.10^{-3}$ mol.g^{-1} (dry weight) (Yee and Fein, 2001). On the other hand, EPS reactivity is a function of the types of molecules included in their compositions, such as their polysaccharides/proteins ratio. Regarding ENPs forced dissolution, the high sites density in biofilms, cell walls and EPS included, tends to complex metal(loid)s to high extent (Tourney and Ngwenya, 2014; Wang et al., 2016a,b), resulting in a decrease in local concentrations of free metal(loid)s in solution within the biofilm matrix. In order to restore thermodynamics equilibria, ENPs will in turn dissolve and release free metal(loid)s (Bian et al., 2011; Wirth et al., 2012). If the density of complexing sites is in high excess, ENPs total dissolution could thus be expected. This process can be facilitated by formation of strong metal-organic complexes at the ENPs surface that weakens metal-oxygen bonds.

Focusing specifically on EPS reactivity in absence of biofilm, Adeleye et al. (2014) noted a more important dissolution of nano-CuO in presence of EPS after 90 days compared to EPS-free control. By extension, the EPS role is likely to be critical when investigating biofilm impact reactivity. As a result, EPS are considered by many authors a reasonably good analog to evaluate the biofilm impact onto ENPs fate (Tong et al., 2010; Jiang et al., 2013). However, it must be noted that since cells metabolic activity constitutes also an important part of the biofilms' reactivity, which in association with their specific 3-dimensional structure that creates microenvironments, is likely to strongly impact the ENPs fate in the environment.

The extracellular matrix is known to contain enzymes and other proteins secreted by living cells in the biofilm, leading to the notion of "external digestion system" that partly controls organic molecules and polymers degradation, as well as certain extracellular redox process (Flemming and Wingender, 2010, Flemming et al., 2016). As a result, degradation of organic polymers that coat (and protect in a certain way) functionalized ENPs may arise from exposure to such enzymes (Ikuma et al., 2015). Interestingly, the type of capping agents constitutes an important factor regarding dissolution rate (Mitrano et al., 2014). Siderophores, metal-complexing molecules of high affinity, are also produced by bacteria in biofilms (Visca et al., 2007; Saha et al., 2013). Siderophore production by bacteria, including the ligands catecholate, hydroxamate, and carboxylate, is extensively reviewed (Springer and Butler, 2016; Albelda-Berenguer et al., 2019), and present the central role of this class of molecules for metal scavenging. Other highly complexing ligands are also secreted by bacteria, such as cysteine-containing molecules and glutathione that exhibit thiol groups of high affinity toward soft metals (Brown et al., 2006; Mugerfeld et al., 2009). Oxalic acid (Palmieri et al., 2019) produced by *P. fluorescens* (Hamel et al., 1999) or *Burkholderia*

glumae (Nakata and He, 2010) were also reported. Presence of complexing ligands such as siderophores is frequently invoked when considering mineral dissolution mediated by bacteria, and can be extended to ENPs, with ligand-promoted dissolution kinetics being higher than proton-promoted dissolution above pH 4 (Kraemer, 2004; Reichard et al., 2007; Wang et al., 2015).

The biofilm structure is known to induce microenvironments formation (cf. section "Microenvironments Within Biofilm Thickness"), that are able to strongly impact local thermodynamics equilibria and favor both ligand-mediated and redox-mediated dissolution. Existence of gradients in pH or redox state are both reported, and take place at very short spatial scales within the biofilm structure (Yu and Bishop, 2001; Billings et al., 2015; Flemming et al., 2016; Kataky and Knowles, 2018). However, despite their importance, the nature and properties of such microenvironments are still poorly known regarding ligands or metal(loid)s concentrations, even if few studies suggest strong and dynamic changes in local physico-chemical conditions (Couasnon et al., 2019). Nonetheless, it can be anticipated that these "hot spots" of high reactivity exhibit low pHs, important redox changes, and locally concentrate to high extent siderophores and other complexing ligands as well as enzymes. Since metal-based ENPs dissolution is usually favored at low pH (Bian et al., 2011; Han et al., 2016) and in the presence of high affinity complexing molecules (cf. section "Ligand-Mediated Dissolution"), it is likely that microenvironments strongly impact ENPs dissolution.

Redox-Mediated Dissolution

As a second factor, many microorganisms are known to exhibit strong redox activities, thoroughly reported in numerous studies, as for *Acidothiobacillus ferrooxidans* which is able to oxidize sulfur species by direct contact or indirect mechanisms (Monachon et al., 2019). Generally, microorganisms in biofilms secrete a high variety of redox-active molecules associated to the EPS matrix (Tourney and Ngwenya, 2014), and some studies propose that some types of EPS could be electron shuttles in biofilms. Production of riboflavin or c-type cytochrome (Xiao et al., 2017; Kataky and Knowles, 2018), and cyanide residues (Avellan et al., 2018) have been reported. Also, the production of extracellular superoxide, a reactive oxygen species, has been reported for an important variety of microorganisms such as *Firmicutes*, *Actinobacteria*, *Bacteroidetes*, *Gammaproteobacteria*, and *Alphaproteobacteria* (Diaz et al., 2013). As a result, the collection of redox-active molecules in the extracellular matrix is also likely to play an important role for dissolution of redox-sensitive ENPs, such as nano-CeO_2, nano-Ag or nano-Au, in microbial biofilms.

For instance, Nano-Au are thought to remain inert in abiotic conditions. However, presence of soil bacterium *Chromobacterium violaceum*, that produces cyanide residues, is able to provoke oxidative dissolution of nano-Au (McGivney et al., 2019). Similarly, nano-Au was shown to dissolve in contact with freshwater macrophyte biofilm through oxidation processes involving cyanide release (Avellan et al., 2018). Nano-CeO_2 exposed to wastewater biofilm experience higher dissolution rates, following Ce(IV) reduction (Wang and Nowack, 2018), with associated mechanism involving either direct contact between the NPs and bacteria surface or liberation of electron shuttle molecules in the extracellular medium (Thill et al., 2006). It is also proposed that light-induced production of reactive oxygen species (ROS) at the EPS surface can also play a role for ENPs dissolution through oxidation of Ce(III) to Ce(IV) in solution, lowering the concentration of dissolved Ce(III) (Kroll et al., 2014).

ENPs Surface Passivation

Biofilms can favor ENPs dissolution as discussed above but can also induce surface passivation through either (i) chemical transformation of the surface to a more thermodynamically stable phase, or (ii) formation of a corona shell that will limit surface interactions with the surrounding environment.

Passivation of ENPs surface through phase transformation, lowering their reactivity and solubility, is observed when in contact with biofilm and microorganisms. For instance, in anaerobic conditions, typically at the bottom of biofilms, sulfate-reducing bacteria can reduce sulfate to bisulfide (HS^-) which is in turn able to promote nano-Ag sulfidation at the surface of the NPs (Levard et al., 2011, 2013). Such sulfidation is reported in water resource recovery facilities biofilms (Alizadeh et al., 2019), with the creation of such an Ag_2S passivation layer at the surface of nano-Ag that reduces the NP solubility, and consequently its toxicity (Levard et al., 2013).

Organic polymers originally present as coatings on ENPs can also be destabilized in the biofilm thickness by ligand exchange processes involving EPS molecules, with strong consequences on ENPs stability. Although the adsorption of EPS to the surface of ENPs can favor their dissolution or their aggregation, as presented previously, they may also promote their passivation. This depends on the type of EPS and complexing ligands considered, their charge and hydrophobic properties, as well as the mode of interaction with ENPs. Strong metal-organic complexes at the ENPs surface are expected to lower the strength of surrounding metal-oxygen bonds thus favoring dissolution, while weaker EPS interactions with ENPs can drastically modify ENPs surface properties, and potentially promote aggregation depending on local physico-chemical conditions (through intermolecular bridging for instance). Finally, ENPs enhanced passivation takes place when the organic corona formed by EPS either isolates ENPs from the surrounding solution, thus disabling their dissolution, or promotes repulsion among ENPs, lowering their aggregation.

Cellular Toxicity Response as a Strong Modifier of ENPs Speciation

ENPs toxicity to biofilm cells is clearly related to the penetration of these particles and the effectiveness of interaction with microbial cells. As a result, several studies linked ENPs toxicity to biofilm physico-chemical properties such as thickness or roughness (Thuptimdang et al., 2017). Actually, bacteria encased in biofilms structures are usually reported as more resistant to toxic substances than the corresponding planktonic analogs, and a significant amount of studies and reviews exist that discuss this

topic (Wirth et al., 2012; Flemming et al., 2016). However, what is more important regarding the ENPs environmental fate is the microbial cells response after exposure to NPs, since some of them are known toxic agents.

Multi-species communities exposed to ENPs may experience important changes in microbial consortium structure with significant evolutions in microbial diversity (Binh et al., 2014, 2016; Echavarri-Bravo et al., 2015; Jomini et al., 2015; Tang et al., 2017; Miao et al., 2018; Zhu et al., 2018a,b, 2019). These remodeling of microbial consortia can potentially modify the types of metabolisms expressed in these communities and impact the environmental ENPs fate. Noticeably, mechanisms of cell toxicity resistance to ENPs will differ from one microorganism to the other, as is the case of *E. coli* and *Pseudomonas aeruginosa* exposed to nano-Ag (Saleh et al., 2015), or even among two different strains of the same bacteria, such as *E. coli* MG1655 and W3110 exposed to ZnO-NPs (Gelabert et al., 2015). This suggests the existence of numerous metabolic pathways, potentially generating the extracellular release of a variety of substances.

Nevertheless, whereas NPs impact on biofilms viability and toxicity have been extensively studied, only a few articles focus on ENPs effects on microbial biofilms functioning. Exposure to photocatalytic ENPs (CdS, TiO_2, Fe_2O_3) result in different adaptations in peryphitic biofilms (Zhu et al., 2019). While no decrease in biomass, chlorophyll content and ATPase activity were detected, a significant increase in EPS production and secretion of superoxide dismutase have been observed. The microbial community is also evolving due to an increase in the proportion of phototrophic and high nutrient metabolic microorganisms. Such an evolution in microbial community composition was also shown for periphytic biofilms exposed to nano-TiO_2, with an increase in the abundance of denitrifying bacteria (Zhu et al., 2018a) and a significant production of EPS enriched in proteins. Exposure to nano-TiO_2 and nano-CeO_2 also lead to changes in bacteria consortium for surficial sediment microbial communities, with an observed inhibition of microbial-mediated oxygen consumption, and strong changes in local redox state (Miao et al., 2018). Nano-CdS have been shown to induce an increase in overall metabolic activity (ATPase activity), and to stimulate EPS production (Zhu et al., 2018b), while exposure to nano-CuO resulted in the production of polysaccharides-rich loosely bound-EPS (Hou et al., 2015).

Interestingly, the production or inhibition of key molecules that could modify ENPs speciation were also reported. *S. oneidensis* MR-1 biofilms exposed to nano-TiO_2 showed an increased production of riboflavin (Maurer-Jones et al., 2013). This molecule is related to metal reduction capacity in bacteria, accounting for approximately 75% of extracellular electron transfer to insoluble substrates by *S. oneidensis* (Kotloski and Gralnick, 2013). Similarly, a riboflavin production was reported for planktonic *S. oneidensis* exposed to lithium nickel manganese cobalt oxide nanosheets (Mitchell et al., 2019), whereas nano-Fe oxide did not induce any increase in riboflavin expression (Buchman et al., 2019). The production of pyoverdine, an important siderophore exhibiting a high affinity for Fe, was shown to be inhibited following exposure to nano-CuO on *Pseudomonas chlororaphis* 06 (Dimkpa et al., 2012), or to Te nanorods for *P. aeruginosa* (Mohanty et al., 2014, 2015). In bacterial communities, the activity of key extracellular enzymes such as alkaline phosphatase and ß-glucosidase was also restrained by the combined exposure to nano-TiO_2 and Cu (Fan et al., 2016) or polystyrene NPs (Awet et al., 2018). However, denitrification enzyme activity and respiration were shown to increase after addition of nano-TiO_2 (Ozaki et al., 2016). Importantly, a common metal-resistance mechanism by bacteria, such as *S. oneidensis,* to resist oxidative stress is the production of enzymes containing cysteine residues and glutathione (Brown et al., 2006; Mugerfeld et al., 2009), molecules that usually exhibit high affinities toward soft metals and could thus promote ligand-mediated dissolution for ENPs containing such metals.

Regarding specific impacts on EPS matrix, several studies report the extracellular production of molecules by microbes exposed to ENPs (Maurer-Jones et al., 2013; Zhu et al., 2018a,b, 2019). Particularly, the formation of more compacted biofilms and higher active site densities was observed, following a significant increase in EPS production after exposure to ENPs (Hou et al., 2015; Tang et al., 2017; Liu et al., 2018; Miao et al., 2018; Zhu et al., 2018a,b, 2019). Interestingly, this increased EPS production is thought to reduce cells damage (Hessler et al., 2012), particularly when most metal-bearing ENPs are known to produce ROS at their surface (Nel et al., 2006) which promotes oxidative stress at the cellular level. However, a denser and more functionalized EPS matrix provides more attachment sites to ENPs, thus drastically limiting their interactions with cell membranes and thus lowering exposure to ROS (Joshi et al., 2012; Zhou et al., 2016). Concurrently, even ROS generation at the ENPs surface is reported to be lowered in presence of an EPS coating, potentially due to a limited contact between NPs inorganic surface and solution (Hessler et al., 2012). However, if ENPs toxicity is too high, structural damages will occur and biofilms will, on the contrary, tend to get thinner and less dense.

All these studies show that ENPs can significantly impact microbial biofilms functioning by inducing changes in EPS composition and by promoting EPS production. Such changes can result in more packed biofilms and a significant increase in active site densities, simultaneously promoting ENPs trapping and an increased dissolution of metallic ENPs due to the presence of higher local concentrations of complexing ligands. Also, changes in the enzymes production as well as the synthesis of strong metal complexants such as cysteine residues, or molecules involved in metal reduction (e.g., flavins and riboflavins), can drastically govern changes in ENPs speciation through dissolution processes.

LONG-TERM FATE OF ENPs IN NATURAL ENVIRONMENT: THE MESOCOSM APPROACH

As stated previously, microbial biofilms control to high extents the environmental fate of ENPs. Most studies devoted to these questions of biofilm-ENPs interactions focus on model systems,

providing invaluable information regarding the associated processes at the biofilm scale. However, these approaches lack the complexity of natural settings as well as the intricate interplay between the different environmental compartments. As such, in complement to these small-scale studies, more integrative approaches are required that evaluate the biofilms impact in global environmental systems.

Understanding the long-term fate and biotransformation of ENPs in the environment is challenging due to the complexity of the bio-physical-chemical interactions within natural systems including aggregation and sorption of (in)organic substances, oxidation and reduction, as well as ecological factors such as interacting organisms [e.g., microorganisms, (in)vertebrates, plants, fungi], trophic levels present (e.g., primary producer, primary consumer, secondary consumer) and trophic and transgenerational transfer potentials (Auffan et al., 2009). Taking into account this complexity requires a diverse collection of expertise, including but not limited to physical chemistry, (micro)biology, and ecology. Particularly well-suited experimental units with which to engage such multidisciplinary teams are mesocosms, that consist in medium-size replicated ecosystems (Crossland and La Point, 1992; Shaw and Kennedy, 1996; Food and Agriculture Organization, 2009). Mesocosms experiments can be designed to mimic any ecological scenarios of exposure (Auffan et al., 2019) and in the scope of ENP studies, have been defined as indoor or outdoor experimental systems containing a portion of the natural environment which is (i) self–sustaining once set up and acclimatized without any additional input of nutrients or resources, and (ii) that allows monitoring of all (or the maximum of) input and output parameters to measure changes in the environment, and in the concentration and speciation of ENPs over time, space, and ecosystem compartments (**Figure 4**).

This set of information is used to discern the kinetics of (bio)transformation, (bio)distribution and impacts of the ENPs to better inform studies on their fate and modeling of their environmental risks. Biotransformation of the ENPs exerted by micro-organisms, as well as macro-organisms, is one of the main drivers of the ENPs fate and impacts on the long-term. For instance, sulfidation in the sediments is a major transformation pathway for ENPs such as Ag and Cu, that are enhanced by the activity of microbial consortia as the modulation of anoxic/anaerobic conditions in soils/sediments, or also the release of exudates and organic material during metabolism, respiration or death (e.g., Bone et al., 2012; Lowry et al., 2012). Such a release of exudates by microbial biofilms and macro-organisms is important in inducing dissolution, homo- and hetero-aggregation, and by modulating their toxic effects on the mid- to long-term, as presented previously in this review. Although the formation of bio-corona shortly after introduction in mesocosms governed the persistency of ENPs in the water column (Espinasse et al., 2018), this will depend on the size and surface properties of the pristine ENPs (Unrine et al., 2012; Geitner et al., 2018). For instance, PVP coated Ag ENPs were colloidally stabilized by plant-derived and biofilm-derived dissolved organic matter. On the contrary, gum Arabic-coated Ag ENPs were rapidly removed from the water column at the same conditions through deposition or dissolution of the particles and subsequent binding of ions to plant or biofilm on the sediment surfaces (Bone et al., 2012; Unrine et al., 2012).

Macrophytes, surficial sediments and associated microorganisms were often reported as two major sinks for ENPs. Regarding aquatic plants, studies reported extensive change in the speciation of ENMs following their adsorption or internationalization by aquatic plants. For instance, the majority of nano-Au introduced in freshwater mesocosms (outdoor, 300 L volume, 180 d exposure) were found associated to the biofilm growing on *Egeria densa*, where the totality of Au was complexed with cyanide (43 ± 8%), hydroxide (38 ± 4%) and thiol (19 ± 4%) ligands (Avellan et al., 2018). The driving biodissolution mechanism was the Au oxidation and subsequent complexation with cyanide [$Au(CN)_2^-$], produced as secondary metabolites by the microbiome in the periphyton associated with leaves. The displacement of CN ligands by S-R groups, led to the formation of soluble thiol-Au species such as [R-S-Au-CN]$^-$ or [R-S_2-Au]$^-$ complexes. These complexes were stable at the environmental physico-chemical conditions tested and likely represent major transformation pathways for other redox active ENPs. Stegemeier et al. (2017) also investigated the speciation of nano-Ag and -Cu in wetland mesocosms (outdoor, 400 L volume, 270 d exposure). Ag(0) ENPs added to the ecosystem were found in the plant tissues as Ag(0), Ag_2S, and Ag bound to thiol whereas major transformation products for Cu ENPs were identified in Cu–O–R and Cu–S–R. Such products differed from those measured in the surrounding sediments compartment and the authors suggested that plants natural defense, such as glutathione, may play an important role. Similarly, in freshwater pond mesocosms contaminated with Ce ENPs, metals speciation and redox reactions were associated with the benthic (micro)biota activity and were not measured in the surrounding natural matrices (Tella et al., 2014). A protein storage mechanism for Cu ENPs was also proposed to explain the transformation of $Cu(OH)_2$ nano-pesticide in Cu-S, and Cu-O/N-R products in plant tissues (Avellan et al., 2020). Changes in the redox state following interactions with the micro-organisms/macrophytes systems were also observed for CeO_2 ENPs, where up to 57% of the pristine Ce(IV) atoms were reduced to Ce(III). In this case, the degree of reduction was observed to increase at decreasing ENPs size, likely due to an intrinsic higher reactivity of the smaller ENPs and their greater association with reducing microbes (Geitner et al., 2018).

These studies, conducted in complex realistic systems, confirm the important impact exerted by microbial biofilms toward ENPs fate, and allow investigating their role among the different reactive environmental compartments. However, it must be noted that although mesocosms experiments were able to provide comprehensive data regarding mid-term/long-term ENPs (bio)transformation in realistic environmental conditions, these strategies were seldom applied in environmental fate studies, in comparison with standard methodologies (e.g., single-species ecotoxicity tests) (Bour et al., 2015). Nonetheless, similar

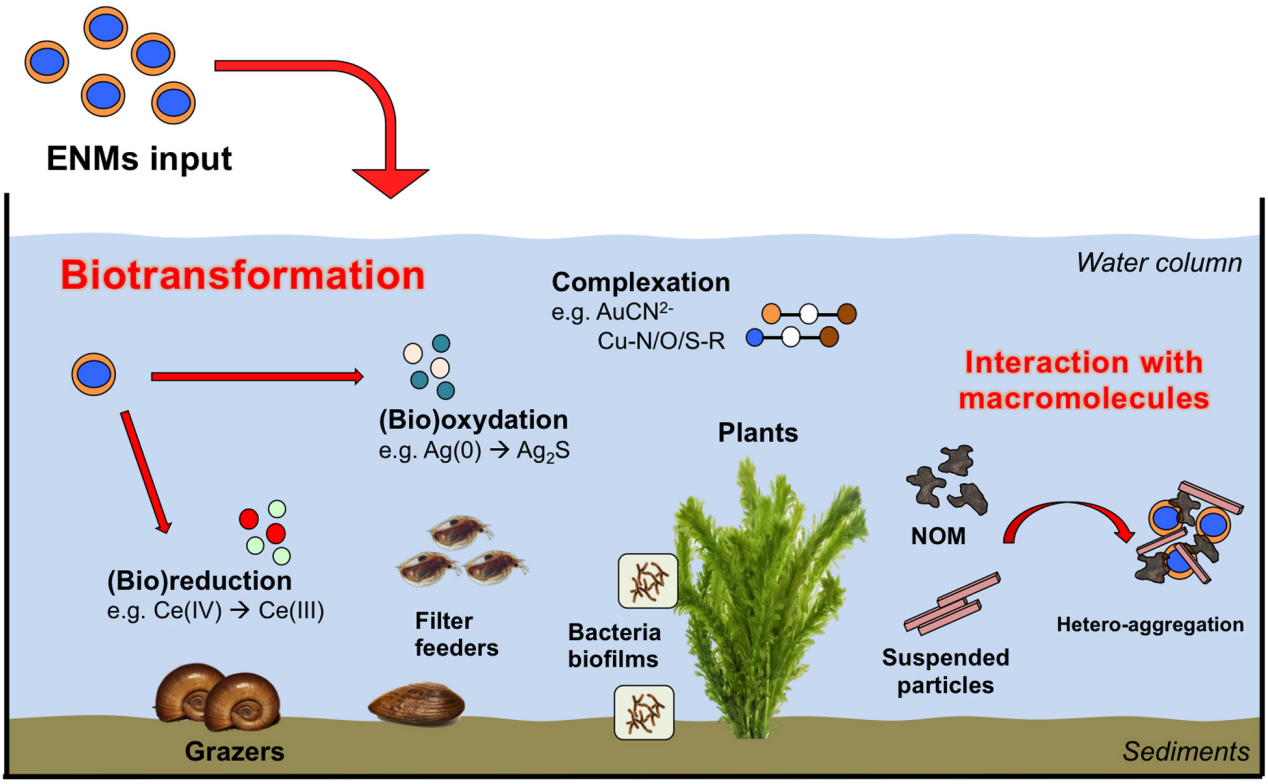

FIGURE 4 | Major ENPs (bio)transformation pathways observed in aquatic mesocosms studies.

approaches are needed in order to investigate ENPs fate and effects that could not be observed in less complex systems, with shorter exposure periods and at higher ENPs doses (Avellan et al., 2018). These advantages can help investigating ENPs ecological processes at a higher level of complexity, and with regard to microbiota and biofilms. They can also help defining the role played by these microbial communities for ENPs fate in complex ecosystem submitted to realistic environmental exposure conditions. Mesocosms also offer many strengths when evaluating ecological hazards and could be seen as alternative testing strategies (ATS) for complementing existing procedures in the environmental risk assessment of ENPs (Hjorth et al., 2017). By simultaneously creating representative conditions for environmental transformation and ecosystem exposure, mesocosm platforms facilitate the integration of reliable exposure and hazard data into an environmental risk assessment framework. As a next step, mesocosms could also be used to study ENPs release from nano–enabled products (e.g., cement, paint, stains, diesel additives) throughout their life cycle, especially during their uses and their end of life. This could contribute to the development of nano–enabled products, which are safer by design, as well as innovative applications. Future aging protocols used to estimate the impact of such nano–enabled products should eventually be based on realistic exposure scenarios taking into account illumination, rainfall, temperature variation, leaching in biotic conditions. Mesocosms are, and will remain extremely useful on our way to understand the behavior of nano–products over the long term in realistic environments.

BIO-MEDIATED FORMATION AND STOCK OF INCIDENTAL NPs IN THE ENVIRONMENT: THE CASE OF ZnS NPs

If biofilms are key environmental compartments affecting the fate of ENPs, they are also able to generate NPs from secondary precipitation of metal(oid)s within their thickness, thus favoring and enhancing metal(loid)s immobilization in environmental systems. For instance, bacteria can release inorganic phosphates (Jarosławiecka and Piotrowska-Seget, 2014) that can be extracellularly trapped into the biofilm structure, and induce metal-bearing phosphate precipitation such as pyromorphite [$Pb_5(PO_4)_3(OH,Cl)$] (Templeton et al., 2003b), HUO_2PO_4 (Finlay et al., 1999), or Cr(III)-phosphates (Nancharaiah et al., 2010). The dynamics of secondary minerals formation can also be strongly modified on short time scales, along with changes in micro-environments physico-chemical conditions. This has been reported for *S. oneidensis* MR1 biofilms simultaneously exposed to lead and molybdenum. In this case, although thermodynamics calculations predicted the formation of wulfenite ($PbMoO_4$) only, a fast precipitation of nanoscale pyromorphite crystals was observed in hot spots distributed within the biofilm thickness, while wulfenite

production was observed only after 7 days of exposure to lead (Couasnon et al., 2019). Another example concerns Sulfate-Reducing bacteria (SRB), mentioned before, that are known to play a major role in the precipitation of metal sulfide minerals through the reduction of sulfate to sulfide. Sulfides (mostly as HS- at neutral pH) readily precipitate with soft metals to form metal sulfides. Among the variety of bio-mediated NPs formed from anthropic metal(oid)s sources (also called incidental NPs), the case of ZnS NPs is a good example, relatively well-documented, and will be presented here as a case-study. As such, several examples are reported including ZnS NPs generated in abandoned mine sites, contaminated sediments and organic wastes.

Bio-Mediated Formation of ZnS-NPs in Contaminated Sites

Banfield's group has been a pioneer in the discovery of ZnS NPs formed by SRB in abandoned tunnels and drainage system of the Piquette Pb-Zn mine in southwest Wisconsin (Labrenz et al., 2000; Druschel et al., 2002; Labrenz and Banfield, 2004; Moreau et al., 2004). ZnS NPs biofilm concentration was found to be about 106 times that of associated groundwater (Labrenz et al., 2000). ZnS NPs of the order of 3–5 nm, mostly sphalerite, were observed within micron-sized spheroids. The authors proposed that the spheroids were induced by microbially derived extracellular proteins, which potentially plays an important role in limiting NP dispersion in natural environments (Moreau et al., 2007). These proteins can interact with ZnS during and after their formation. Indeed, thiol containing compounds play a key role to limit ZnS NPs aggregation and was hypothesized to be a key factor contributing to their persistence in the environment (Lau and Hsu-Kim, 2008).

In another context, the formation of ZnS NPs in a variety of organic waste (OW) has long been overlooked. The main reason lies in the fact that extreme precaution should be given for sampling and storage of samples before their analyses to avoid change in Zn speciation (Le Bars et al., 2018). OWs, used as a fertilizer for crops in many countries, is a major source of input of NPs in the environment. While several studies investigated ENPs accumulation and transformation in wastewater sludges, it has recently been shown that a considerable amount of ZnS NPs was non-intentionally produced in a variety of OWs. Among them, sewage sludge and livestock manures used as amendment have relatively high concentrations of Zn (40–4000 $mg.kg^{-1}$) (Alburquerque et al., 2012; Romeo et al., 2014; Zirkler et al., 2014; Alvarenga et al., 2015). Zn in OW is mostly anthropogenic. For example, high Zn concentrations in livestock manures are explained by important quantities of Zn added in animal feed compared to their ability to assimilate it (Legros et al., 2010). Nanosized ZnS is a major Zn species in raw liquid OWs and in anaerobically digested OWs (Le Bars et al., 2018). The reductive conditions combined with high sulfur content in these systems are a favorable environment for SRB (Santegoeds et al., 1999; Tang et al., 2004; Chen et al., 2008). Therefore, it is likely that these ZnS NPs are formed because of sulfide release by SRB. Crystallite size of ZnS formed in OW was estimated around 3 nm using X-ray Absorption Spectroscopy (Formentini et al., 2017; Le Bars et al., 2018). This is consistent with the identification of 2.5–7.5 nm ZnS in digested sewage sludge by Transmission Electron Microscopy (Kim et al., 2014). Interestingly, these particles transformed within months during composting (Donner et al., 2011; Lombi et al., 2012; Le Bars et al., 2018) or after land application (Formentini et al., 2017). These results suggest a high reactivity of bio-mediated ZnS NPs compared to micrometer ZnS analog which are stable over years in soils (Robson et al., 2014). The high reactivity of ZnS NPs formed in OW could be related to their small size. Indeed, Gilbert et al. (2004) highlighted contracted interatomic distances (1%) for ZnS NPs of this range of size (3.4 nm) compared to their bulk analog. Such structural disorder can increase NP surface reactivity (Yang et al., 2016) and enhance ZnS dissolution. A better understanding of potential impacts of ZnS NPs transformation on the ecosystem and in particular on cultivated lands is needed.

Structural Properties of Biogenic ZnS NPs

It seems that SRB-induced ZnS NPs are bigger than ZnS-NPs formed in abiotic systems at similar conditions (Peltier et al., 2011; da Costa et al., 2012; Xu et al., 2016; Eskelsen et al., 2018). It could be explained by the progressive production of sulfide by SRB leading to a lower saturation index, since a lower saturation index favors particle growth (Mersmann, 1999). In the same way, ligands either initially present in the culture media, or produced metabolites by bacteria, could bind to Zn, thus lowering the saturation index. However, factors controlling the size of biogenic ZnS NPs are not clear and would require further investigation.

Biogenic ZnS NPs tend to exhibit structural defects. Indeed, Xu et al. (2016) showed stacking faults and twins on the (111) face of biogenic ZnS NPs, the only polar face, i.e., prone to interact with polar molecules such as water, phospholipids head or amino acids. This suggests that surface interaction with surrounding compounds influences ZnS NPs structure. Eskelsen et al. (2018) also observed structural defaults (twins) on the (111) face of biogenic ZnS NPs, to a lower extent because of the unfavorable particles's orientation. The authors detected carbon traces in biogenic ZnS NPs aggregates and assumed a microbial metabolite interaction with ZnS NPs.

However, the effect of structural defects on their reactivity is unclear. For hematite NPs, Echigo et al. (2012) have shown that surface defects enhance their dissolution. Regarding ZnS NPs, Xu et al. (2016) highlighted by electronic microscopy that biogenic ZnS NPs dissolution starts where the structural defects are observed. Also, Eskelsen et al. (2018) have calculated a higher surface energy for biogenic ZnS NPs, compared with the abiotic ones, suggesting a higher reactivity. In contrast, smaller abiotic ZnS NPs have a higher available specific surface area for oxidative dissolution. Despite the gathered information regarding their properties, further investigations are needed to evaluate biotic influence on ZnS NPs reactivity, in order to predict their fate when released in the environment.

Biogenic ZnS NPs: An Underestimated Stock in the Environment That Needs Further Investigation

Although biofilms have been identified as a key compartment governing in part the environmental fate of ENPs, it also hosts favorable conditions for the formation of biogenic NPs in particular from anthropic metal(oid)s inputs. The latter is clearly overlooked despite concentrations that can reach the orders of magnitude of the expected ENPs environmental release. As an example, the concentrations of ZnS NPs observed in the studies described above are up to 4 orders of magnitudes higher than the predicted concentrations of ZnO ENPs in soils, sediments and biosolids (about 0.1, 0.1, and 10–100 $mg.kg^{-1}$, respectively) (Gottschalk et al., 2013). Indeed, although ZnO ENPs was shown to transform into ZnS NPs in wastewater treatment plants (Ma et al., 2013, 2014), a large variety of other Zn sources can potentially be transformed into ZnS NPs within biofilms. In this regard, better understanding of biomediated formation of NPs in biofilms needs further attention in particular when associated with anthropic activities that potentially affect biofilm and therefore NPs stabilities. It includes the use of OW as amendments or sediment dredging for example that in both cases involve strong physico-chemical changes (e.g., oxidation) that can potentially release significant amounts of free Zn with unknown effects for ecosystems. Thus, in addition to the control they exert on ENPs fate, biofilms can also become secondary sources of NPs release in the environment, showing the central role these microbial structures are likely to play in general NPs cycling. However, numerous questions remain opened that deserve further investigation in order to better constrain their environmental impact.

CONCLUDING REMARKS

This review highlights the central role played by biofilms regarding ENPs fate in the environment. In details, these microbial structures exert a control on ENPs cycling at multiple levels, by exhibiting relatively high retention capacities and by enforcing ENPs transformations. Accumulation and migration properties within biofilms are governed by a combination of key parameters, including biofilm density, ENPs size and surface properties, creation of electrostatic and hydrophobic interactions, mineral substrate reactivity, and formation of aggregates within the biofilm thickness. Interestingly, the effects of some of these key parameters remain poorly defined despite evidence of their strong impact on ENPs accumulation and transport within biofilms. This is for instance the case of mineral substrates, on which biofilms develop, that are likely to exhibit strong complexation capacity toward ENPs. In addition, given the relatively high accumulation capacities of biofilms, these microbial structures could be considered as secondary sources of ENPs and products of ENPs transformations, able to release them gradually in ENPs-free pore waters. This problematic remains an open question of important environmental significance that needs further investigations.

ENPs are also submitted to speciation changes in biofilms. They can experience dissolution, either mediated by strong complexing ligands produced by microorganisms (siderophores, cysteine-containing molecules) or redox conditions, as well as changes in local physico-chemical properties in microenvironments. Passivation mechanisms can also happen through the precipitation of an inert secondary mineral layer, as well as through ENPs stabilization following the interactions with organic ligands from the EPS matrix. Finally, exposure to toxic ENPs can trigger a response from micro-organisms in biofilms (for instance riboflavin production), which in turn has the potential to strongly impact the ENPs fate within these microbial structures.

Mesocosms-based approaches allow to consider biofilms activity in complex ecosystems, in some ways similar to the environment, and submitted to realistic exposure conditions. As such, these approaches are extremely valuable to better constrain the role of microbial biofilms for ENPs fate, and certainly need to be developed for future research devoted to that topic.

Finally, the case of nano-ZnS shows that biofilms can also synthesize NPs in man-impacted systems. This raises important questions regarding the impact of such processes on a global NPs cycling in natural systems. However, these questions have been largely overlooked and certainly require further investigation.

Some other important points deserve direct attention. First, the general lack of established standardized protocols strongly limits inter-comparison between studies whether at the small-scale or in larger systems. Then, even if considering single-species biofilm as a model system provides important advantages to investigate complex mechanisms of interaction between ENPs and biofilms, this approach presents also some limitations. Natural biofilms function as important microbial consortia that usually include a high variety of strains. To that perspective, efforts should be conducted to investigate more realistic multi-species biofilms. Also, metagenomic approaches could help understanding the dynamic role of the different microbial communities and metabolisms in biofilms, and the complex interplay among them, during their interactions with ENPs. Finally, a vast majority of the studies compiled in this review were focused on the interactions between ENPs and bacteria biofilms. Nevertheless, in the environment, fungi and archaea play also important roles, and more studies should investigate their ability to impact ENPs cycling.

AUTHOR CONTRIBUTIONS

MD, CL, and AG contributed to the conception of the study. MD and AG wrote the first draft of the manuscript. MA, AC, CL, and ML wrote sections of the manuscript. MB, AC, and ED revised it critically. All authors contributed to the article and approved the submitted version.

FUNDING

This work has received funding from Excellence Initiative of Aix – Marseille University – A*MIDEX, a French "Investissements d'Avenir" program, through its associated Labex SERENADE project, and from the MAMBA ANR project (ANR-18-CE01-0001-01). This work was also a contribution to the OSU-Institut Pytheìas. The authors thank the PIREN-Seine program for the funding.

ACKNOWLEDGMENTS

We acknowledge the CNRS for the funding of the IRP iNOVE.

REFERENCES

Adeleye, A. S., Conway, J. R., Perez, T., Rutten, P., and Keller, A. A. (2014). Influence of extracellular polymeric substances on the long-term fate, dissolution, and speciation of copper-based nanoparticles. *Environ. Sci. Technol.* 48, 12561–12568. doi: 10.1021/es5033426

Adeleye, A. S., and Keller, A. A. (2016). Interactions between algal extracellular polymeric substances and commercial TiO2 nanoparticles in aqueous media. *Environ. Sci. Technol.* 50, 12258–12265. doi: 10.1021/acs.est.6b03684

Albelda-Berenguer, M., Monachon, M., and Joseph, E. (2019). Siderophores: from natural roles to potential applications. *Adv. Appl. Microbiol.* 106, 193–225. doi: 10.1016/bs.aambs.2018.12.001

Alburquerque, J. A., de la Fuente, C., Ferrer-Costa, A., Carrasco, L., Cegarra, J., Abad, M., et al. (2012). Assessment of the fertiliser potential of digestates from farm and agroindustrial residues. *Biomass Bioenergy* 40, 181–189. doi: 10.1016/j.biombioe.2012.02.018

Aldeek, F., Mustin, C., Balan, L., Roques-Carmes, T., Fontaine-Aupart, M. P., and Schneider, R. (2011). Surface-engineered quantum dots for the labeling of hydrophobic microdomains in bacterial biofilms. *Biomaterials* 32, 5459–5470. doi: 10.1016/j.biomaterials.2011.04.019

Alizadeh, S., Ghoshal, S., and Comeau, Y. (2019). Fate and inhibitory effect of silver nanoparticles in high rate moving bed biofilm reactors. *Sci. Total Environ.* 647, 1199–1210. doi: 10.1016/j.scitotenv.2018.08.073

Alvarenga, P., Mourinha, C., Farto, M., Santos, T., Palma, P., Sengo, J., et al. (2015). Sewage sludge, compost and other representative organic wastes as agricultural soil amendments: benefits versus limiting factors. *Waste Manage.* 40, 44–52. doi: 10.1016/j.wasman.2015.01.027

Auffan, M., Masion, A., Mouneyrac, C., de Garidel-Thorona, C., Hendren, C. O., Thiery, A., et al. (2019). Contribution of mesocosm testing to a single-step and exposure-driven environmental risk assessment of engineered nanomaterials. *Nanoimpact* 13, 66–69. doi: 10.1016/j.impact.2018.12.005

Auffan, M., Rose, J., Bottero, J., Lowry, G. V., Jolivet, J., and Wiesner, M. R. (2009). Towards a definition of inorganic nanoparticles from an environmental, health and safety perspective. *Nat. Nanotechnol.* 4, 634–641. doi: 10.1038/NNANO.2009.242

Avellan, A., Simonin, M., Anderson, S. M., Geitner, N. K., Bossa, N., Spielman-Sun, E., et al. (2020). Differential reactivity of copper- and gold-based nanomaterials controls their seasonal biogeochemical cycling and fate in a freshwater wetland mesocosm. *Environ. Sci. Technol.* 54, 1533–1544. doi: 10.1021/acs.est.9b05097

Avellan, A., Simonin, M., McGivney, E., Bossa, N., Spielman-Sun, E., Rocca, J. D., et al. (2018). Gold nanoparticle biodissolution by a freshwater macrophyte and its associated microbiome. *Nat. Nanotechnol.* 13, 1072–1077. doi: 10.1038/s41565-018-0231-y

Awet, T. T., Kohl, Y., Meier, F., Straskraba, S., Grün, A. L., Ruf, T., et al. (2018). Effects of polystyrene nanoparticles on the microbiota and functional diversity of enzymes in soil. *Environ. Sci. Eur.* 30:11. doi: 10.1186/s12302-018-0140-6

Barker, W., and Banfield, J. F. (1998). Zones of chemical and physical interaction at interfaces between microbial communities and minerals. A model. *Geomicrobiol. J.* 15, 223–244. doi: 10.1080/014904598093078078

Bar-On, Y. M., Phillips, R., and Milo, R. (2018). The biomass distribution on Earth. *Proc. Natl. Acad. Sci. U.S.A.* 115, 6506–6511. doi: 10.1073/pnas.1711842115

Battin, T. J., Kammer, F. V. D., Weilhartner, A., Ottofuelling, S., and Hofmann, T. (2009). Nanostructured TiO2: transport behavior and effects on aquatic microbial communities under environmental conditions. *Environ. Sci. Technol.* 43, 8098–8104. doi: 10.1021/es9017046

Bian, S. W., Mudunkotuwa, I. A., Rupasinghe, T., and Grassian, V. H. (2011). Aggregation and dissolution of 4 nm ZnO nanoparticles in aqueous environments: influence of pH, Ionic Strength, Size, and Adsorption of Humic Acid. *Langmuir* 27, 6059–6068. doi: 10.1021/la200570n

Billings, N., Birjiniuk, A., Samad, T. S., Doyle, P. S., and Ribbeck, K. (2015). Material properties of biofilms - A review of methods for understanding permeability and mechanics. *Rep. Prog. Phys.* 78:036601. doi: 10.1088/0034-4885/78/3/036601

Binh, C. T. T., Adams, E., Vigen, E., Tong, T., Alsina, M. A., Gaillard, J.-F., et al. (2016). Chronic addition of a common engineered nanomaterial alters biomass, activity and composition of stream biofilm communities. *Environ. Sci. Nano* 3, 619–630. doi: 10.1039/c5en00274e

Binh, C. T. T., Tong, T., Gaillard, J.-F., Gray, K. A., and Kelly, J. J. (2014). Acute effects of TiO2 nanomaterials on the viability and taxonomic composition of aquatic bacterial communities assessed via high-throughput screening and next generation sequencing. *PLos One* 9:e106280. doi: 10.1371/journal.pone.0106280

Bone, A. J., Colman, B. P., Gondikas, A. P., Newton, K. M., Harrold, K. H., Cory, R. M., et al. (2012). Biotic and abiotic interactions in aquatic microcosms determine fate and toxicity of Ag nanoparticles: part 2-toxicity and Ag speciation. *Environ. Sci. Technol.* 46, 6925–6933. doi: 10.1021/es204683m

Borrok, D., Fein, J. B., and Kulpa, C. F. (2004a). Cd and proton adsorption onto bacterial consortia grown from industrial wastes and contaminated geologic settings. *Environ. Sci. Technol.* 38, 5656–5664. doi: 10.1021/es049679n

Borrok, D., Fein, J. B., and Kulpa, C. F. (2004b). Proton and Cd adsorption onto natural bacterial consortia: testing universal adsorption behavior. *Geochim. Cosmochim. Acta* 68, 3231–3238. doi: 10.1016/j.gca.2004.02.003

Borrok, D., Turner, B. F., and Fein, J. B. (2005). Universal surface complexation framework for modeling proton binding onto bacterial surfaces in geological settings. *Am. J. Sci.* 305, 826–853. doi: 10.2475/ajs.305.6-8.826

Bour, A., Mouchet, F., Silvestre, J., Gauthier, L., and Pinelli, E. (2015). Environmentally relevant approaches to assess nanoparticles ecotoxicity: a review. *J. Hazard. Mater.* 283, 764–777. doi: 10.1016/j.jhazmat.2014.10.021

Brown, G. E. (2001). How minerals react with water. *Science* 294, 67–69. doi: 10.1126/science.1063544

Brown, G. E., Henrich, V. E., Casey, W. H., Clark, D. L., Eggleston, C., Felmy, A., et al. (1999). Metal oxide surfaces and their interactions with aqueous solutions and microbial organisms. *Chem. Rev.* 99, 77–174. doi: 10.1021/cr980011z

Brown, S. D., Thompson, M. R., VerBerkmoes, N. C., Chourey, K., Shah, M., Zhou, J., et al. (2006). Molecular dynamics of the *Shewanella oneidensis* response to chromate stress. *Mol. Cell. Proteomics* 5, 1054–1071. doi: 10.1074/mcp.M500394-MCP200

Buchman, J. T., Pho, T., Rodriguez, R. S., Feng, Z. V., and Haynes, C. L. (2019). Coating iron oxide nanoparticles with mesoporous silica reduces their interaction and impact on *S. oneidensis MR*-1. *Chemosphere* 237:124511. doi: 10.1016/j.chemosphere.2019.124511

Burns, J. M., Pennington, P. L., Sisco, P. N., Frey, R., Kashiwada, S., Fulton, M. H., et al. (2013). Surface charge controls the fate of Au nanorods in saline estuaries. *Environ. Sci. Technol.* 47, 12844–12851. doi: 10.1021/es402880u

Chen, Y., Cheng, J. J., and Creamer, K. S. (2008). Inhibition of anaerobic digestion process: a review. *Bioresour. Technol.* 99, 4044–4064. doi: 10.1016/j.biortech.2007.01.057

Choi, O., Yu, C.-P., Fernandez, G. E., and Hu, Z. (2010). Interactions of nanosilver with *Escherichia coli* cells in planktonic and biofilm cultures. *Water Res.* 44, 6095–6103. doi: 10.1016/j.watres.2010.06.069

Costerton, J. W., Cheng, K. J., Geesey, G. G., Ladd, T. I., Nickel, J. C., Dasgupta, M., et al. (1987). Bacteria biofilms in nature and disease. *Annu. Rev. Microbiol.* 41, 435–464. doi: 10.1146/annurev.mi.41.100187.002251

Costerton, J. W., Lewandowski, Z., Caldwell, D. E., Korber, D. R., and Lappin-Scott, H. M. (1995). Microbial biofilms. *Annu. Rev. Microbiol.* 49, 711–745. doi: 10.1146/annurev.mi.49.100195.003431

Costerton, J. W., Stewart, P., and Greenberg, E. P. (1999). Bacterial biofilms: a common cause of persistent infections. *Science* 284, 1318–1322. doi: 10.1126/science.284.5418.1318

Couasnon, T., Gelabert, A., Menez, B., and Guyot, F. (2019). Experimental assessment of occurrences and stability of lead-bearing minerals in bacterial biofilms. *Chem. Geol.* 505, 23–35. doi: 10.1016/j.chemgeo.2018.11.023

Crampon, M., Hellal, J., Mouvet, C., Wille, G., Michel, C., Wiener, A., et al. (2018). Do natural biofilm impact nZVI mobility and interactions with porous media? A column study. *Sci. Total Environ.* 610, 709–719. doi: 10.1016/j.scitotenv.2017.08.106

Crossland, N. O., and La Point, T. W. (1992). The design of mesocosms experiments. *Environ. Toxicol. Chem.* 11, 1–4. doi: 10.1002/etc.5620110101

da Costa, J. P., Girao, A. V., Lourenco, J. P., Monteiro, O. C., Trindade, T., and Costa, M. C. (2012). Synthesis of nanocrystalline ZnS using biologically generated sulfide. *Hydrometallurgy* 117, 57–63. doi: 10.1016/j.hydromet.2012.02.005

Dehner, C. A., Awaya, J. D., Maurice, P. A., and DuBois, J. L. (2010). Roles of siderophores, oxalate, and ascorbate in mobilization of iron from hematite by the aerobic bacterium *Pseudomonas* mendocina. *Appl. Environ. Microbiol.* 76, 2041–2048. doi: 10.1128/AEM.02349-09

Desmau, M., Gélabert, A., Levard, C., Ona-Nguema, G., Vidal, V., Stubbs, J. E., et al. (2018). Dynamics of silver nanoparticles at the solution/biofilm/mineral interface. *Environ. Sci. Nano* 5, 2394–2405. doi: 10.1039/c8en00331a

Diaz, J. M., Hansel, C. M., Voelker, B. M., Mendes, C. M., Andeer, P. F., and Zhang, T. (2013). Widespread production of extracellular superoxide by Heterotrophic Bacteria. *Science* 340, 1223–1226. doi: 10.1126/science.123

Dimkpa, C. O., McLean, J. E., Britt, D. W., Johnson, W. P., Arey, B., Lea, S. A., et al. (2012). Nanospecific inhibition of pyoverdine siderophore production in *Pseudomonas chlororaphis* O6 by CuO nanoparticles. *Chem. Res. Toxicol.* 25, 1066–1074. doi: 10.1021/tx3000285

Donlan, R. M. (2002). Biofilms: microbial life on surfaces. *Emerg. Infect. Dis.* 8, 881–890. doi: 10.3201/eid0809.020063

Donner, E., Howard, D. L., Jonge, M. D. D., Paterson, D., Cheah, M. H., Naidu, R., et al. (2011). X-ray absorption and micro X-ray fluorescence spectroscopy investigation of copper and zinc speciation in biosolids. *Environ. Sci. Technol.* 45, 7249–7257. doi: 10.1021/es201710z

Druschel, G. K., Labrenz, M., Thomsen-Ebert, T., Fowle, D. A., and Banfield, J. F. (2002). Geochemical Modeling of ZnS in biofilms: an example of ore depositional processes. *Econ. Geol. Bull. Soc. Econ. Geol.* 97, 1319–1329. doi: 10.2113/gsecongeo.97.6.1319

Dzumedzey, Y., Labille, J., Cathala, B., Moreau, C., and Santaella, C. (2017). Polysaccharide coating on environmental collectors affects the affinity and deposition of nanoparticles. *Nanoimpact* 5, 83–91. doi: 10.1016/j.impact.2016.12.004

Echavarri-Bravo, V., Paterson, L., Aspray, T. J., Porter, J. S., Winson, M. K., Thornton, B., et al. (2015). Shifts in the metabolic function of a benthic estuarine microbial community following a single pulse exposure to silver nanoparticles. *Environ. Pollut.* 201, 91–99. doi: 10.1016/j.envpol.2015.02.033

Echigo, T., Aruguete, D. M., Murayama, M., and Hochella, M. F. Jr. (2012). Influence of size, morphology, surface structure, and aggregation state on reductive dissolution of hematite nanoparticles with ascorbic acid. *Geochim. Cosmochim. Acta* 90, 149–162. doi: 10.1016/j.gca.2012.05.008

Eskelsen, J. R., Xu, J., Chiu, M., Moon, J.-W., Wilkins, B., Graham, D. E., et al. (2018). Influence of structural defects on biomineralized ZnS nanoparticle dissolution: an in-situ electron microscopy study. *Environ. Sci. Technol.* 52, 1139–1149. doi: 10.1021/acs.est.7b04343

Espinasse, B. P., Geitner, N. K., Schierz, A., Therezien, M., Richardson, C. J., Lowry, G. V., et al. (2018). Comparative persistence of engineered nanoparticles in a complex aquatic ecosystem. *Environ. Sci. Technol.* 52, 4072–4078. doi: 10.1021/acs.est.7b06142

Fabrega, J., Renshaw, J. C., and Lead, J. R. (2009). Interactions of silver nanoparticles with *Pseudomonas putida* biofilms. *Environ. Sci. Technol.* 43, 9004–9009. doi: 10.1021/es901706j

Fan, W., Liu, T., Li, X., Peng, R., and Zhang, Y. (2016). Nano-TiO2 affects cu speciation, extracellular enzyme activity, and bacterial communities in sediments. *Environ. Pollut.* 218, 77–85. doi: 10.1016/j.envpol.2016.08.018

Fein, J. B., Daughney, C. J., Yee, N., and Davis, T. A. (1998). A chemical equilibrium model for metal adsorption onto bacterial surfaces. *Geochim. Cosmochim. Acta* 61, 3319–3328. doi: 10.1016/S0016-7037(97)00166-X

Fernando, I., Lu, D., and Zhou, Y. (2020). Interactive influence of extracellular polymeric substances (EPS) and electrolytes on the colloidal stability of silver nanoparticles. *Environ. Sci. Nano* 7, 186–197. doi: 10.1039/c9en00861f

Ferry, J. L., Craig, P., Hexel, C., Sisco, P., Frey, R., Pennington, P. L., et al. (2009). Transfer of gold nanoparticles from the water column to the estuarine food web. *Nat. Nanotechnol.* 4, 441–444. doi: 10.1038/NNANO.2009.157

Finlay, J. A., Allan, V. J. M., Conner, A., Callow, M. E., Basnakova, G., and Macaskie, L. E. (1999). Phosphate release and heavy metal accumulation by biofilm-immobilized and chemically-coupled cells of a *citrobacter* sp. pre-grown in continuous culture. *Biotechnol. Bioeng.* 63, 87–97. doi: 10.1002/(sici)1097-0290(19990405)63:1<87::aid-bit9>3.0.co;2-0

Flemming, H. C., and Wingender, J. (2010). The biofilm matrix. *Nat. Rev. Microbiol.* 8, 623–633. doi: 10.1038/nrmicro2415

Flemming, H.-C., Wingender, J., Szewzyk, U., Steinberg, P., Rice, S. A., and Kjelleberg, S. (2016). Biofilms: an emergent form of microbial life. *Nat. Rev. Microbiol.* 14, 563–575. doi: 10.1038/nrmicro.2016.94

Flemming, H. C., and Wuertz, S. (2019). Bacteria and archaea on Earth and their abundance in biofilms. *Nat. Rev. Microbiol.* 17, 247–260. doi: 10.1038/s41579-019-0158-9

Food and Agriculture Organization [FAO] (2009). *Biosafety of Genetically Modified Organisms: Basic Concepts, Methods and Issues*. Rome: FAO.

Formentini, T. A., Legros, S., Fernandes, C. V. S., Pinheiro, A., Le Bars, M., Levard, C., et al. (2017). Radical change of Zn speciation in pig slurry amended soil: Key role of nano-sized sulfide particles. *Environ. Pollut.* 222, 495–503. doi: 10.1016/j.envpol.2016.11.056

Franklin, N. M., Rogers, N. J., Apte, S. C., Batley, G. E., Gadd, G. E., and Casey, P. S. (2007). Comparative toxicity of nanoparticulate ZnO, bulk ZnO, and ZnCl2 to a freshwater microalga (*Pseudokirchneriella subcapitata*): the importance of particle solubility. *Environ. Sci. Technol.* 41, 8484–8490. doi: 10.1021/es071445r

Fulaz, S., Hiebner, D., Barros, C. H. N., Devlin, H., Vitale, S., et al. (2019a). Ratiometric imaging of the in situ pH distribution of biofilms by use of fluorescent mesoporous silica nanosensors. *ACS Appl. Mater. Interfaces* 11, 32679–32688. doi: 10.1021/acsami.9b09978

Fulaz, S., Vitale, S., Quinn, L., and Casey, E. (2019b). Nanoparticle–biofilm interactions: the role of the EPS matrix. *Trends Microbiol.* 27, 915–926. doi: 10.1016/j.tim.2019.07.004

Gadd, G. M. (2010). Metals, minerals and microbes: geomicrobiology and bioremediation. *Microbiology* 156, 609–643. doi: 10.1099/mic.0.037143-0

Geitner, N. K., Cooper, J. L., Avellan, A., Castellon, B. T., Perrotta, B. G., Bossa, N., et al. (2018). Size-based differential transport, uptake, and mass distribution of ceria (CeO2) nanoparticles in wetland mesocosms. *Environ. Sci. Technol.* 52, 9768–9776. doi: 10.1021/acs.est.8b02040

Gelabert, A., Sivry, Y., Ferrari, R., Akrout, A., Cordier, L., Nowak, S., et al. (2014). Uncoated and coated ZnO nanoparticles life cycle in synthetic seawater. *Environ. Toxicol. Chem.* 22, 341–349. doi: 10.1002/etc.2447

Gelabert, A., Sivry, Y., Gobbi, P., Mansour, N., Menguy, N., Brayner, R., et al. (2015). Testing nano effect onto model bacteria: impact of speciation and genotypes. *Nanotoxicology* 10, 216–25. doi: 10.3109/17435390.2015.1048323

Giese, B., Klaessig, F., Park, B., Kaegi, R., Steinfeldt, M., Wigger, H., et al. (2018). Risks, release and concentrations of engineered nanomaterial in the environment. *Sci. Rep.* 8:1565. doi: 10.1038/s41598-018-19275-4

Gil-Allué, C., Schirmer, K., Tlili, A., Gessner, M. O., and Behra, R. (2015). Silver nanoparticle effects on stream periphyton during short-term exposures. *Environ. Sci. Technol.* 49, 1165–1172. doi: 10.1021/es5050166

Gilbert, B., Huang, F., Zhang, H., Waychunas, G. A., and Banfield, J. F. (2004). Nanoparticles: strained and stiff. *Science* 305, 651–654. doi: 10.1126/science.1098454

Golmohamadi, M., Clark, R. J., Veinot, J. G. C., and Wilkinson, K. J. (2013). The role of charge on the diffusion of solutes and nanoparticles (silicon nanocrystals, nTiO2, nAu) in a biofilm. *Environ. Chem.* 10, 34–41. doi: 10.1071/EN12106

Gottschalk, F., Sonderer, T., Scholz, R. W., and Nowack, B. (2009). Modeled environmental concentrations of engineered nanomaterials (TiO2, ZnO, Ag, CNT, fullerenes) for Different Regions. *Environ. Sci. Technol.* 43, 9216–9222. doi: 10.1021/es9015553

Gottschalk, F., Sun, T., and Nowack, B. (2013). Environmental concentrations of engineered nanomaterials: review of modeling and analytical studies. *Environ. Pollut.* 181, 287–300. doi: 10.1016/j.envpol.2013.06.003

Guiot, E., Georges, P., Brun, A., Fontaine-Aupart, M. P., Bellon-Fontaine, M. N., and Briandet, R. (2002). Heterogeneity of diffusion inside microbial biofilms determined by fluorescence correlation spectroscopy under two-photon excitation. *Photochem. Photobiol.* 75, 570–578. doi: 10.1562/0031-8655(2002)0750570hodimb2.0.co2

Ha, J., Gelabert, A., Spormann, A., and Brown, G. E. Jr. (2010). Role of extracellular polymeric substances in metal ion complexation on *Shewanella oneidensis*: batch uptake, thermodynamic modeling, ATR-FTIR, and EXAFS study. *Geochim. Cosmochim. Acta* 74, 1–15. doi: 10.1016/j.gca.2009.06.031

Habimana, O., Steenkeste, K., Fontaine-Aupart, M. P., Bellon Fontaine, M. N., Kulakauskas, S., and Briandet, R. (2011). Diffusion of nanoparticles in biofilms is altered by bacterial cell wall hydrophobicity. *Appl. Environ. Microbiol.* 77, 367–368. doi: 10.1128/AEM.02163-10

Hamel, R., Levasseur, R., and Apana, V. D. (1999). Oxalic acid production and aluminum tolerance in *Pseudomonas fluorescens*. *J. Inorg. Biochem.* 76, 99–104. doi: 10.1016/S0162-0134(99)00120-8

Han, Y., Hwang, G., Kim, D., Bradford, S. A., Lee, B., Eom, I., et al. (2016). Transport, retention, and long-term release behavior of ZnO nanoparticle aggregates in saturated quartz sand: role of solution pH and biofilm coating. *Water Res.* 90, 247–257. doi: 10.1016/j.watres.2015.12.009

Herrling, M. P., Lackner, S., Tatti, O., Guthausen, G., Delay, M., Franzreb, M., et al. (2016). Short and long term biosorption of silica-coated iron oxide nanoparticles in heterotrophic biofilms. *Sci. Total. Environ.* 544, 722–729. doi: 10.1016/j.scitotenv.2015.11.174

Hessler, C. M., Wu, M. Y., Xue, Z., Choi, H., and Seo, Y. (2012). The influence of capsular extracellular polymeric substances on the interaction between TiO2 nanoparticles and planktonic bacteria. *Water Res.* 46, 4687–4696. doi: 10.1016/j.watres.2012.06.009

Hidalgo, G., Burns, A., Herz, E., Hay, A. G., Houston, P. L., Wiesner, U., et al. (2009). Functional tomographic fluorescence imaging of pH microenvironments in microbial biofilms by use of silica nanoparticle sensors. *Appl. Environ. Microbiol.* 75, 7426–7435. doi: 10.1128/AEM.01220-09

Hjorth, R., Holden, P. A., Hansen, S. F., Colman, B. P., Grieger, and Hendren, C. O. (2017). The role of alternative testing strategies in environmental risk assessment of engineered nanomaterials. *Environ. Sci. Nano* 4, 292–301. doi: 10.1039/c6en00443a

Holden, P. A., Gardea-Torresdey, J. L., Klaessig, F., Turco, R. F., Mortimer, M., Hund-Rinke, K., et al. (2016). Considerations of Environmentally Relevant Test Conditions for Improved Evaluation of Ecological Hazards of Engineered Nanomaterials. *Environ. Sci. Technol.* 50, 6124–6145. doi: 10.1021/acs.est.6b00608

Hou, J., Miao, L. Z., Wang, C., Wang, P. F., Ao, Y. H., and Lv, B. W. (2015). Effect of CuO nanoparticles on the production and composition of extracellular polymeric substances and physicochemical stability of activated sludge flocs. *Bioresour. Technol.* 176, 65–70. doi: 10.1016/j.biortech.2014.11.020

Hunter, R. C., and Beveridge, T. J. (2005). Application of a pH-sensitive fluoroprobe (C-SNARF-4) for pH microenvironment analysis in *Pseudomonas aeruginosa* biofilms. *Appl. Environ. Microbiol.* 71, 2501–2510. doi: 10.1128/AEM.71.5.2501-2510.2005

Ikuma, K., Decho, A. W., and Lau, B. L. T. (2015). When nanoparticles meet biofilms-interactions guiding the environmental fate and accumulation of nanoparticles. *Front. Microbiol.* 6:591. doi: 10.3389/fmicb.2015.00591

Ikuma, K., Madden, A. S., Decho, A. W., and Lau, B. L. T. (2014). Deposition of nanoparticles onto polysaccharide-coated surfaces: implications for nanoparticle–biofilm interactions. *Environ. Sci. Nano* 1, 117–122. doi: 10.1039/c3en00075c

Jarosławiecka, A., and Piotrowska-Seget, S. (2014). Lead resistance in micro-organisms. *Microbiology* 160, 12–25. doi: 10.1099/mic.0.070284-0

Jiang, X., Wang, X., Tong, M., and Kim, H. (2013). Initial transport and retention behaviors of ZnO nanoparticles in quartz sand porous media coated with *Escherichia coli* biofilm. *Environ. Pollut.* 174, 38–49. doi: 10.1016/j.envpol.2012.11.016

Jian-Zhou, H., Cheng-Cheng, L., Deng-Jun, W., and Zhou, D.-M. (2015). Biofilms and extracellular polymeric substances mediate the transport of graphene oxide nanoparticles in saturated porous media. *J. Hazard. Mater.* 300, 467–474. doi: 10.1016/j.jhazmat.2015.07.026

Jing, H., Mezgebe, B., Hassan, A. A., Sahle-Demessie, E., Sorial, G. A., and Bennett-Stamper, C. (2014). Experimental and modeling studies of sorption of ceria nanoparticle on microbial biofilms. *Bioresour. Technol.* 161, 109–117. doi: 10.1016/j.biortech.2014.03.015

Jomini, S., Clivot, H., Bauda, P., and Pagnout, C. (2015). Impact of manufactured TiO2 nanoparticles on planktonic and sessile bacterial communities. *Environ. Pollut.* 202, 196–204. doi: 10.1016/j.envpol.2015.03.022

Joo, S. H., and Aggarwal, S. (2018). Factors impacting the interactions of engineered nanoparticles with bacterial cells and biofilms: mechanistic insights and state of knowledge. *J. Environ. Manag.* 225, 62–74. doi: 10.1016/j.jenvman.2018.07.084

Joshi, N., Ngwenya, B. T., and French, C. E. (2012). Enhanced resistance to nanoparticle toxicity is conferred by overproduction of extracellular polymeric substances. *J. Hazard. Mater.* 241-242, 363–370. doi: 10.1016/j.jhazmat.2012.09.057

Kalinowski, B. E., Liermann, L. J., Givens, S., and Brantley, S. L. (2000). Rates of bacteria-promoted solubilization of Fe from minerals: a review of problems and approaches. *Chem. Geol.* 169, 357–370. doi: 10.1016/S0009-2541(00)00214-X

Kataky, R., and Knowles, E. (2018). Biofilm formation on abiotic surfaces and their redox activity. *Curr. Opin. Electrochem.* 12, 121–128. doi: 10.1016/j.coelec.2018.07.007

Keller, A. A., McFerran, S., Lazareva, A., and Suh, S. (2013). Global life cycle releases of engineered nanomaterials. *J. Nanopart. Res.* 15:1692. doi: 10.1007/s11051-013-1692-4

Khan, S. S., Mukherjee, A., and Chandrasekaran, N. (2011a). Impact of exopolysaccharides on the stability of silver nanoparticles in water. *Water Res.* 45, 5184–5190. doi: 10.1016/j.watres.2011.07.024

Khan, S. S., Srivatsan, P., Vaishnavi, N., Mukherjee, A., and Chandrasekaran, N. (2011b). Interaction of silver nanoparticles (SNPs) with bacterial extracellular proteins (ECPs) and its adsorption isotherms and kinetics. *J. Hazard Mater.* 192, 299–306. doi: 10.1016/j.colsurfa.2011.03.032

Kim, B., Levard, C., Murayama, M., Brown, G. E., and Hochella, M. F. (2014). Integrated approaches of X-ray absorption spectroscopic and electron microscopic techniques on zinc speciation and characterization in a final sewage sludge product. *J. Environ. Qual.* 43, 908–916. doi: 10.2134/jeq2013.10.0418

Kotloski, N. J., and Gralnick, J. A. (2013). Flavin electron shuttles dominate extracellular electron transfer by *Shewanella oneidensis*. *mBio* 4:e00553-12. doi: 10.1128/mBio.0055312

Kraemer, S. M. (2004). Iron oxide dissolution and solubility in the presence of siderophores. *Aquat. Sci.* 66, 3–18. doi: 10.1007/s00027-003-0690-5

Kroll, A., Behra, R., Kaegi, R., and Sigg, L. (2014). Extracellular polymeric substances (EPS) of freshwater biofilms stabilize and modify CeO2 and Ag nanoparticles. *PLoS One* 9:e110709. doi: 10.1371/journal.pone.0110709

Kurlanda-Witek, H., Ngwenya, B., and Butler, I. (2015). The influence of biofilms on the mobility of bare and capped zinc oxide nanoparticles in saturated sand and glass beads. *J. Cont. Hydrol.* 179, 160–170. doi: 10.1016/j.jconhyd.2015.06.009

Kuzyakov, Y., and Blagodatskaya, E. (2015). Microbial hotspots and hot moments in soil: concept & review. *Soil Biol. Biochem.* 83, 184–199. doi: 10.1016/j.soilbio.2015.01.025

Labrenz, M., and Banfield, J. F. (2004). Sulfate-reducing bacteria-dominated biofilms that precipitate ZnS in a subsurface circumneutral-pH mine drainage system. *Microb. Ecol.* 47, 205–217. doi: 10.1007/s00248-003-1025-8

Labrenz, M., Druschel, G. K., Thomsen-Ebert, T., Gilbert, B., Welch, S. A., Kemner, K. M., et al. (2000). Formation of Sphalerite (ZnS) deposits in natural biofilms of sulfate-reducing Bacteria. *Science* 290, 1744–1747. doi: 10.1126/science.290.5497.1744

Lau, B. L., and Hsu-Kim, H. (2008). Precipitation and growth of zinc sulfide nanoparticles in the presence of thiol-containing natural organic ligands. *Environ. Sci. Technol.* 42, 7236–7241. doi: 10.1021/es801360b

Layet, C., Auffan, M., Santaella, C., Chevassus-Rosset, C., Montes, M., Ortet, P., et al. (2017). Evidence that soil properties and organic coating drive the

phytoavailability of cerium oxide nanoparticles. *Environ. Sci. Technol.* 51, 9756–9764. doi: 10.1021/acs.est.7b02397

Le Bars, M., Legros, S., Levard, C., Chaurand, P., Tella, M., Rovezzi, M., et al. (2018). Drastic change in zinc speciation during anaerobic digestion and composting: instability of nanosized zinc sulfide. *Environ. Sci. Technol.* 52, 12987–12996. doi: 10.1021/acs.est.8b02697

Le Ouay, B., and Stellacci, F. (2015). Antibacterial activity of silver nanoparticles: a surface science insight. *Nano Today* 10, 339–354. doi: 10.1016/j.nantod.2015.04.002

Legros, S., Doelsch, E., Masion, A., Rose, J., Borshneck, D., Proux, O., et al. (2010). Combining size fractionation, scanning electron microscopy, and X-ray absorption spectroscopy to probe zinc speciation in pig slurry. *J. Environ. Qual.* 39, 531–540. doi: 10.2134/jeq2009.0096

Lerner, R. N., Lu, Q., Zeng, H., and Liu, Y. (2012). The effects of biofilm on the transport of stabilized zerovalent iron nanoparticles in saturated porous media. *Water Res.* 46, 975–985. doi: 10.1016/j.watres.2011.11.070

Levard, C., Hotze, E. M., Colman, B. P., Dale, A. L., Truong, L., Yang, X. Y., et al. (2013). Sulfidation of silver nanoparticles: natural antidote to their toxicity. *Environ. Sci. Technol.* 47, 13440–13448. doi: 10.1021/es403527n

Levard, C., Hotze, E. M., Lowry, G. V., and Brown, G. E. (2012). Environmental Transformations of Silver nanoparticles: impact on stability and toxicity. *Environ. Sci. Technol.* 46, 6900–6914. doi: 10.1021/es2037405

Levard, C., Reinsch, B. C., Michel, F. M., Oumahi, C., Lowry, G. V., and Brown, G. E. Jr. (2011). Sulfidation processes of PVP-coated silver nanoparticles in aqueous solution: impact on dissolution rate. *Environ. Sci. Technol.* 45, 5260–5266. doi: 10.1021/es2007758

Li, X., Yeh, Y. C., Giri, K., Mout, R., Landis, R. F., Prakash, Y. S., et al. (2015). Control of nanoparticle penetration into biofilms through surface design. *Chem. Commun.* 51, 282–285. doi: 10.1039/c4cc07737g

Li, Z., Aly Hassan, A., Sahle-Demessie, E., and Sorial, G. A. (2013). Transport of nanoparticles with dispersant through biofilm coated drinking water sand filters. *Water Res.* 47, 6457–6466. doi: 10.1016/J.WATRES.2013.08.026

Lin, D., Story, S. D., Walker, S. L., Huang, Q., and Cai, P. (2016). Influence of extracellular polymeric substances on the aggregation kinetics of TiO2 nanoparticles. *Water Res.* 104, 381–388. doi: 10.1016/j.watres.2016.08.044

Liu, S., Cao, S., Guo, J., Luo, L., Zhou, Y., Lin, C., et al. (2018). Graphene oxide–silver nanocomposites modulate biofilm formation and extracellular polymeric substance (EPS) production. *Nanoscale* 10, 19603–19611. doi: 10.1039/c8nr04064h

Lombi, E., Donner, E., Tavakkoli, E., Turney, T. W., Naidu, R., Miller, B. W., et al. (2012). Fate of zinc oxide nanoparticles during anaerobic digestion of wastewater and post-treatment processing of sewage sludge. *Environ. Sci. Technol.* 46, 9089–9096. doi: 10.1021/es301487s

Lowry, G. V., Espinasse, B. P., Badireddy, A. R., Richardson, C. J., Reinsch, B. C., Lee, D. B., et al. (2012). Long-term transformation and fate of manufactured Ag nanoparticles in a simulated large scale freshwater emergent wetland. *Environ. Sci. Technol.* 46, 7027–7036. doi: 10.1021/es204608d

Ma, R., Levard, C., Judy, J. D., Unrine, J. M., Durenkamp, M., Martin, B., et al. (2014). Fate of zinc oxide and silver nanoparticles in a pilot wastewater treatment plant and in processed biosolids. *Environ. Sci. Technol.* 48, 104–112. doi: 10.1021/es403646x

Ma, R., Levard, C., Michel, F. M., Brown, G. E. Jr., and Lowry, G. V. (2013). Sulfidation mechanism for zinc oxide nanoparticles and the effect of sulfidation on their solubility. *Environ. Sci. Technol.* 47, 2527–2534. doi: 10.1021/es3035347

Maurer-Jones, M. A., Gunsolus, I. L., Meyer, B. M., Christenson, C. J., and Haynes, C. L. (2013). Impact of TiO2 nanoparticles on growth, biofilm formation, and flavin secretion in *Shewanella oneidensis*. *Anal. Chem.* 85, 5810–5818. doi: 10.1021/ac400486u

McGivney, E., Gao, X., Liu, Y., Lowry, G. V., Casman, E. A., and Gregory, K. B. (2019). Biogenic cyanide production promotes dissolution of gold nanoparticles in soil. *Environ. Sci. Technol.* 53, 1287–1295. doi: 10.1021/acs.est.8b05884

Ménez, B., Pasini, V., and Brunelli, D. (2012). Life in the hydrated suboceanic mantle. *Nat. Geosci.* 5, 133–137. doi: 10.1038/NGEO1359

Mersmann, A. (1999). Crystallization and precipitation. *Chem. Eng. Process.* 38, 345–353. doi: 10.1016/S0255-2701(99)00025-2

Miao, L., Wang, C., Hou, J., Wang, P., Ao, Y., Li, Y., et al. (2015). Enhanced stability and dissolution of CuO nanoparticles by extracellular polymeric substances in aqueous environment. *J. Nanopart. Res.* 17:404. doi: 10.1007/s11051-015-3208-x

Miao, L., Wang, P., Wang, C., Hou, J., Yao, Y., Liu, J., et al. (2018). Effect of TiO2 and CeO2 nanoparticles on the metabolic activity of surficial sediment microbial communities based on oxygen microelectrodes and high-throughput sequencing. *Water Res.* 129, 287–296. doi: 10.1016/j.watres.2017.11.014

Mishra, B., Shoenfelt, E., Yu, Q., Yee, N., Fein, J. B., and Myneni, S. C. B. (2017). Stoichiometry of mercury-thiol complexes on bacterial cell envelopes. *Chem. Geol.* 464, 137–146. doi: 10.1016/j.chemgeo.2017.02.015

Mitchell, S. L., Hudson-Smith, N. V., Cahill, M. S., Reynolds, B. N., Frand, S. D., Green, C. M., et al. (2019). Chronic exposure to complex metal oxide nanoparticles elicits rapid resistance in *Shewanella oneidensis* MR-1. *Chem. Sci.* 10, 9768–9781. doi: 10.1039/c9sc01942a

Mitrano, D. M., Ranville, J., Bednar, A., Kazor, K., Hering, A. S., and Higgins, C. (2014). Tracking dissolution of silver nanoparticles at environmentally relevant concentrations in laboratory, natural and processed waters using single particle ICP-MS (spICP-MS). *Environ. Sci. Nano* 1, 248–259. doi: 10.1039/c3en00108c

Mitzel, M. R., Sand, S., Whalen, J. K., and Tufenkji, N. (2016). Hydrophobicity of biofilm coatings influences the transport dynamics of polystyrene nanoparticles in biofilm-coated sand. *Water Res.* 92, 113–120. doi: 10.1016/j.watres.2016.01.026

Mitzel, M. R., and Tufenkji, N. (2014). Transport of Industrial PVP-Stabilized Silver Nanoparticles in Saturated Quartz Sand Coated with *Pseudomonas aeruginosa* PAO1 Biofilm of Variable Age. *Environ. Sci. Technol.* 48, 2715–2723. doi: 10.1021/es404598v

Mohanty, A., Kathawala, M. H., Zhang, J., Chen, W. N., Loo, J. S. C., Kjelleberg, S., et al. (2014). Biogenic tellurium nanorods as a novel antivirulence agent inhibiting pyoverdine production in *Pseudomonas aeruginosa*. *Biotechnol. Bioeng.* 111, 858–865. doi: 10.1002/bit.25147

Mohanty, A., Liu, Y., Yang, L., and Cao, B. (2015). Extracellular biogenic nanomaterials inhibit pyoverdine production in *Pseudomonas aeruginosa*: a novel insight into impacts of metal(loid)s on environmental bacteria. *Appl. Microbiol. Biotechnol.* 99, 1957–1966. doi: 10.1007/s00253-014-6097-5

Monachon, M., Albelda-Berenguer, M., and Joseph, E. (2019). Biological oxidation of iron sulfides. *Adv. Appl. Microbiol.* 107, 1–27. doi: 10.1016/bs.aambs.2018.12.002

Montano, M. D., Lowry, G. V., von der Kammer, F., Blue, J., and Ranville, J. F. (2014). Current status and future direction for examining engineered nanoparticles in natural systems. *Environ. Chem.* 11, 351–366. doi: 10.1071/EN14037

Moreau, J. W., Webb, R. I., and Banfield, J. F. (2004). Ultrastructure, aggregation-state, and crystal growth of biogenic nanocrystalline sphalerite and wurtzite. *Am. Mineral.* 89, 950–960. doi: 10.2138/am-2004-0704

Moreau, J. W., Weber, P. K., Martin, M. C., Gilbert, B., Hutcheon, I. D., and Banfield, J. F. (2007). Extracellular proteins limit the dispersal of biogenic nanoparticles. *Science* 316, 1600–1603. doi: 10.1126/science.1141064

Morelli, E., Gabellieri, E., Bonomini, A., Tognotti, D., Grassi, G., and Corsi, I. (2018). TiO2 nanoparticles in seawater: aggregation and interactions with the green alga *Dunaliella tertiolecta*. *Ecotoxicol. Environ. Saf.* 148, 184–193. doi: 10.1016/j.ecoenv.2017.10.024

Mueller, N. C., and Nowack, B. (2008). Exposure modeling of engineered nanoparticles in the environment. *Environ. Sci. Technol.* 42, 4447–4453. doi: 10.1021/es7029637

Mugerfeld, I., Law, B. A., Wickham, G. S., and Thompson, D. K. (2009). A putative azoreductase gene is involved in the *Shewanella oneidensis* response to heavy metal stress. *Appl. Microbiol. Biotechnol.* 82, 1131–1141. doi: 10.1007/s00253-009-1911-1

Nakata, P. A., and He, C. (2010). Oxalic acid biosynthesis is encoded by an operon in *Burkholderia glumae*. *FEMS Microbiol. Lett.* 304, 177–182. doi: 10.1111/j.1574-6968.2010.01895.x

Nancharaiah, Y. V., Dodge, C., Venugopalan, V. P., Narasimhan, S. V., and Francis, A. J. (2010). Immobilization of Cr(VI) and its reduction to Cr(III) phosphate by granular biofilms comprising a mixture of microbes. *Appl. Environ. Microbiol.* 76, 2433–2438. doi: 10.1128/AEM.02792-09

Navarro, D. A. G., Watson, D. F., Aga, D. S., and Banerjee, S. (2009). Natural organic matter-mediated phase transfer of quantum dots in the aquatic environment. *Environ. Sci. Technol.* 43, 677–682. doi: 10.1021/es8017623

Nel, A., Xia, T., Mädler, L., and Li, N. (2006). Toxic potential of materials at the nanolevel. *Science* 311, 622–627. doi: 10.1126/science.1114397

Ngwenya, B. T., Sutherland, I. W., and Kennedy, L. (2003). Comparison of the acid–base behaviour and metal adsorption characteristics of a Gram-negative bacterium with other strains. *Appl. Geochem.* 18, 527–538. doi: 10.1016/S0883-2927(02)00118-X

Nunan, N. (2017). Game changer in soil science The microbial habitat in soil: scale, heterogeneity and functional consequences. *J. Plant Nutr. Soil Sci.* 180, 425–429. doi: 10.1002/jpln.201700184

Ouyang, K., Yu, X. Y., Zhu, Y., Gao, C., Huang, Q., and Cai, P. (2017). Effects of humic acid on the interactions between zinc oxide nanoparticles and bacterial biofilms. *Environ. Pollut.* 231(Pt 1), 1104–1111. doi: 10.1016/j.envpol.2017.07.003

Ozaki, A., Adams, E., Binh, C., Tong, T. Z., Gaillard, J. F., Gray, K. A., et al. (2016). One-time addition of nano-TiO2 triggers short-term responses in benthic bacterial communities in artificial streams. *Microb. Ecol.* 71, 266–275. doi: 10.1007/s00248-015-0646-z

Palmieri, F., Estoppey, A., House, G. L., Lohberger, A., Bindschedler, S., Chain, P. S. G., et al. (2019). Chapter Two - Oxalic acid, a molecule at the crossroads of bacterial-fungal interactions. *Adv. Appl. Microbiol.* 106, 49–77. doi: 10.1016/bs.aambs.2018.10.001

Peltier, E., Ilipilla, P., and Fowle, D. (2011). Structure and reactivity of zinc sulfide precipitates formed in the presence of sulfate-reducing bacteria. *Appl. Geochem.* 26, 1673–1680. doi: 10.1016/j.apgeochem.2011.04.024

Peters, R. J. B., van Bemmel, G., Milani, N. B. L., den Hertog, G. C. T., Undas, A. K., van der Lee, M., et al. (2018). Detection of nanoparticles in Dutch surface waters. *Sci. Total Environ.* 621, 210–218. doi: 10.1016/j.scitotenv.2017.11.238

Peulen, T. O., and Wilkinson, K. J. (2011). Diffusion of Nanoparticles in a Biofilm. *Environ. Sci. Technol.* 45, 3367–3373. doi: 10.1021/es103450g

Piccinno, F., Gottschalk, F., Seeger, S., and Nowack, B. (2012). Industrial production quantities and uses of ten engineered nanomaterials in Europe and the world. *J. Nanopart. Res.* 14:1109. doi: 10.1007/s11051-012-1109-9

Reichard, P., Kretzschmar, R., and Kraemer, S. (2007). Dissolution mechanisms of goethite in the presence of siderophores and organic acids. *Geochim. Cosmochim. Acta* 71, 5635–5650. doi: 10.1016/j.gca.2006.12.022

Robson, T. C., Braungardt, C. B., Rieuwerts, J., and Worsfold, P. (2014). Cadmium contamination of agricultural soils and crops resulting from sphalerite weathering. *Environ. Pollut.* 184, 283–289. doi: 10.1016/j.envpol.2013.09.001

Rodrigues, S. M., Trindade, T., Duarte, A. C., Pereira, E., Koopmans, G. F., and Römkens, P. F. A. M. (2016). A framework to measure the availability of engineered nanoparticles in soils: trends in soil tests and analytical tools. *Trends Anal. Chem.* 75, 129–140. doi: 10.1016/j.trac.2015.07.003

Romeo, A., Vacchina, V., Legros, S., and Doelsch, E. (2014). Zinc fate in animal husbandry systems. *Metallomics* 6, 1999–2009. doi: 10.1039/C4MT00062E

Saha, R., Saha, N., Donofrio, R. S., and Bestervelt, L. L. (2013). Microbial siderophores: a mini review. *J. Basic Microbiol.* 53, 303–317. doi: 10.1002/jobm.201100552

Saleh, N. B., Chambers, B., Aich, N., Plazas-Tuttle, J., Phung-Ngoc, H. N., and Kirisits, M. J. (2015). Mechanistic lessons learned from studies of planktonic bacteria with metallic nanomaterials: implications for interactions between nanomaterials and biofilm bacteria. *Front. Microbiol.* 6:677. doi: 10.3389/fmicb.2015.00677

Santegoeds, C. M., Damgaard, L. R., Hesselink, G., Zopfi, J., Lens, P., Muyzer, G., et al. (1999). Distribution of sulfate-reducing and methanogenic bacteria in anaerobic aggregates determined by microsensor and molecular analyses. *Appl. Environ. Microbiol.* 65, 4618–4629. doi: 10.1128/aem.65.10.4618-4629.1999

Schlafer, S., Baelum, V., and Dige, I. (2018). Improved pH-ratiometry for the three-dimensional mapping of pH T microenvironments in biofilms under flow conditions. *J. Microbiol. Methods* 152, 194–200. doi: 10.1016/j.mimet.2018.08.007

Shaw, J. L., and Kennedy, J. H. (1996). The use of aquatic field mesocosm studies in risk assessment. *Environ. Toxicol. Chem.* 15, 605–607. doi: 10.1002/etc.5620150501

Sivry, Y., Gelabert, A., Cordier, L., Ferrari, R., Lazar, H., Juillot, F., et al. (2014). Behavior and fate of industrial zinc oxide nanoparticles in a carbonate-rich river water. *Chemosphere* 95, 519–526. doi: 10.1016/j.chemosphere.2013.09.110

Slavin, Y. N., Asnis, J., Hafeli, U. O., and Bach, H. (2017). Metal nanoparticles: understanding the mechanisms behind antibacterial activity. *J. Nanobiotechnology* 15:65. doi: 10.1186/s12951-017-0308-z

Springer, S. D., and Butler, A. (2016). Microbial ligand coordination: consideration of biological significance. *Coord. Chem. Rev.* 306(Pt 2), 628–635. doi: 10.1016/j.ccr.2015.03.013

Stegemeier, J. P., Avellan, A., and Lowry, G. V. (2017). Effect of initial speciation of copper- and silver-based nanoparticles on their long-term fate and phytoavailability in freshwater wetland mesocosms. *Environ. Sci. Technol.* 51, 12114–12122. doi: 10.1021/acs.est.7b02972

Stewart, P. S. (2003). Diffusion in biofilms. *J. Bacteriol.* 185, 1485–1491. doi: 10.1128/JB.185.5.1485-1491.2003

Sun, T. Y., Bornhöft, N. A., Hungerbühler, K., and Nowack, B. (2016). Dynamic probabilistic modeling of environmental emissions of engineered nanomaterials. *Environ. Sci. Technol.* 50, 4701–4711. doi: 10.1021/acs.est.5b05828

Sutherland, I. W. (2001). The biofilm matrix – an immobilized but dynamic microbial environment. *Trends Microbiol.* 9, 222–227. doi: 10.1016/s0966-842x(01)02012-1

Tang, J., Zhu, N., Zhu, Y., Liu, J., Wu, C., Kerr, P., et al. (2017). Responses of periphyton to Fe2O3 nanoparticles: a physiological and ecological basis for defending nanotoxicity. *Environ. Sci. Technol.* 51, 10797–10805. doi: 10.1021/acs.est.7b02012

Tang, Y., Shigematsu, T., Morimura, S., and Kida, K. (2004). The effects of micro-aeration on the phylogenetic diversity of microorganisms in a thermophilic anaerobic municipal solid-waste digester. *Water Res.* 38, 2537–2550. doi: 10.1016/S0043-1354(04)00136-8

Tella, M., Auffan, M., Brousset, L., Issartel, J., Kieffer, I., Pailles, C., et al. (2014). Transfer, transformation, and impacts of ceria nanomaterials in aquatic mesocosms simulating a pond ecosystem. *Environ. Sci. Technol.* 48, 9004–9013. doi: 10.1021/es501641b

Templeton, A. S., Trainor, T. P., Spormann, A. M., and Brown, G. E. Jr. (2003a). Selenium speciation and partitioning within *Burkholderia cepacia* biofilms formed on α-Al2O3 surfaces. *Geochim. Cosmochim. Acta* 67, 3547–3557. doi: 10.1016/S0016-7037(03)00212-6

Templeton, A. S., Trainor, T. P., Spormann, A. M., Newville, M., Sutton, S. R., Dohnalkova, A., et al. (2003b). Sorption versus biomineralization of Pb(II) within *Burkholderia cepacia* biofilms. *Environ. Sci. Technol.* 37, 300–307. doi: 10.1021/es025972g

Templeton, A. S., Trainor, T. P., Traina, S. J., Spormann, A. M., and Brown, G. E. (2001). Pb(II) distributions at biofilm–metal oxide interfaces. *Proc. Natl. Acad. Sci. U.S.A.* 98, 11897–11902. doi: 10.1073/pnas.201150998

Thill, A., Zeyons, O., Spalla, O., Chauvat, F., Rose, J., Auffan, M., et al. (2006). Cytotoxicity of CeO2 nanoparticles for *Escherichia coli*: physico-chemical insight of the cytotoxicity mechanism. *Environ. Sci. Technol.* 40, 6151–6156. doi: 10.1021/es060999b

Thuptimdang, P., Limpiyakorn, T., and Khan, E. (2017). Dependence of toxicity of silver nanoparticles on *Pseudomonas* putida biofilm structure. *Chemosphere* 188, 199–207. doi: 10.1016/j.chemosphere.2017.08.147

Tong, M., Ding, J., Shen, Y., and Zhu, P. (2010). Influence of biofilm on the transport of fullerene (C60) nanoparticles in porous media. *Water Res.* 44, 1094–1103. doi: 10.1016/j.watres.2009.09.040

Tourney, J., and Ngwenya, B. T. (2014). The role of bacterial extracellular polymeric substances in geomicrobiology. *Chem. Geol.* 386, 115–132. doi: 10.1016/j.chemgeo.2014.08.011

Tripathi, S., Champagne, D., and Tufenkji, N. (2012). Transport behavior of selected nanoparticles with different surface coatings in granular porous media coated with *Pseudomonas aeruginosa* biofilm. *Environ. Sci. Technol.* 46, 6942–6949. doi: 10.1021/es202833k

Unrine, J. M., Colman, B. P., Bone, A. J., Gondikas, A. P., and Matson, C. W. (2012). Biotic and abiotic interactions in aquatic microcosms determine fate and toxicity of Ag nanoparticles, Part 1. Aggregation and Dissolution. *Environ. Sci. Technol.* 46, 6915–6924. doi: 10.1021/es204682q

Vance, M. E., Kuiken, T., Vejerano, E. P., McGinnis, S. P., Hochella, M. F. Jr., Rejeski, D., et al. (2015). Nanotechnology in the real world: redeveloping the nanomaterial consumer products inventory. *Beilstein J. Nanotechnol.* 6, 1769–1780. doi: 10.3762/bjnano.6.181

Visca, P., Imperi, F., and Lamont, I. L. (2007). Pyoverdine siderophores: from biogenesis to biosignificance. *Trends Microbiol.* 15, 22–30. doi: 10.1016/j.tim.2006.11.004

Walden, C., and Zhang, W. (2018). Bioaccumulation of silver nanoparticles in model wastewater biofilms. *Environ. Sci. Water Res. Technol.* 4, 1163–1171. doi: 10.1039/C8EW00102B

Wang, J.-L., Alasonati, E., Tharaud, M., Gelabert, A., Fisicaro, P., and Benedetti, M. F. (2020). Flow and fate of silver nanoparticles in small French catchments under different land-uses: the first one-year study. *Water Res.* 176, 115722. doi: 10.1016/j.watres.2020.115722

Wang, X., Liu, B., Pan, X., and Gadd, G. M. (2019). Transport and retention of biogenic selenium nanoparticles in biofilm-coated quartz sand porous media and consequence for elemental mercury immobilization. *Sci. Total Environ.* 692, 1116–1124. doi: 10.1016/j.scitotenv.2019.07.309

Wang, Y., Gélabert, A., Michel, F. M., Choi, Y., Gescher, J., Ona-Nguema, G., et al. (2016a). Effect of biofilm coatings at metal-oxide/water interfaces I: Pb(II) and Zn(II) partitioning and speciation at *Shewanella oneidensis*/metal-oxide/water interfaces. *Geochim. Cosmochim. Acta* 188, 368–392. doi: 10.1016/j.gca.2016.04.052

Wang, Y., Gélabert, A., Michel, F. M., Choi, Y., Peter, E., Spormann, A. M., et al. (2016b). Effect of biofilm coatings at metal-oxide/water interfaces II: competitive sorption between Pb(II) and Zn(II) at *Shewanella oneidensis*/metal-oxide/water interfaces. *Geochim. Cosmochim. Acta* 188, 396–406. doi: 10.1016/j.gca.2016.04.054

Wang, Y., and Nowack, B. (2018). Dynamic probabilistic material flow analysis of nano-SiO2, nano iron oxides, nano-CeO2, nano-Al2O3, and quantum dots in seven European regions. *Environ. Pollut.* 235, 589–601. doi: 10.1016/j.envpol.2018.01.004

Wang, Z., Schenkeveld, W. D., Kraemer, S. M., and Giammar, D. E. (2015). Synergistic effect of reductive and ligand-promoted dissolution of goethite. *Environ. Sci. Technol.* 49, 7236–7244. doi: 10.1021/acs.est.5b01191

Warren, L. A., and Haack, E. A. (2001). Biogeochemical controls on metal behaviour in freshwater environments. *Earth Sci. Rev.* 54, 261–320. doi: 10.1016/S0012-8252(01)00032-0

Watt, M., Hugenholtz, P., White, R., and Vinall, K. (2006). Numbers and locations of native bacteria on field-grown wheat roots quantified by fluorescence in situ hybridization (FISH). *Environ. Microbiol.* 8, 871–884. doi: 10.1111/j.1462-2920.2005.00973.x

Wei, L., Ding, J., Xue, M., Qin, K., Wang, S., Xin, M., et al. (2019). Adsorption mechanism of ZnO and CuO nanoparticles on two typical sludge EPS: effect of nanoparticle diameter and fractional EPS polarity on binding. *Chemosphere* 214, 210–219. doi: 10.1016/j.chemosphere.2018.09.093

Wirth, S. M., Lowry, G. V., and Tilton, R. D. (2012). Natural organic matter alters biofilm tolerance to silver nanoparticles and dissolved silver. *Environ. Sci. Technol.* 46, 12687–12696. doi: 10.1021/es301521p

Xia, T., Kovochich, M., Liong, M., Madler, L., Gilbert, B., Shi, H., et al. (2008). Comparison of the mechanism of toxicity of zinc oxide and cerium oxide nanoparticles based on dissolution and oxidative stress properties. *ACS Nano* 2, 2121–2134. doi: 10.1021/nn800511k

Xiao, Y., and Wiesner, M. R. (2013). Transport and retention of selected engineered nanoparticles by porous media in the presence of a biofilm. *Environ. Sci. Technol.* 47, 2246–2253. doi: 10.1021/es304501n

Xiao, Y., Zhang, E., Zhang, J., Dai, Y., Yang, Z., Christensen, H. E., et al. (2017). Extracellular polymeric substances are transient media for microbial extracellular electron transfer. *Sci. Adv.* 3:e1700623. doi: 10.1126/sciadv.1700623

Xu, F. (2018). Review of analytical studies on TiO2 nanoparticles and particle aggregation, coagulation, flocculation, sedimentation, stabilization. *Chemosphere* 212, 662–677. doi: 10.1016/j.chemosphere.2018.08.108

Xu, J., Murayama, M., Roco, C. M., Veeramani, H., Michel, F. M., Rimstidt, J. D., et al. (2016). Highly-defective nanocrystals of ZnS formed via dissimilatory bacterial sulfate reduction: a comparative study with their abiogenic analogues. *Geochim. Cosmochim. Acta* 180, 1–14. doi: 10.1016/j.gca.2016.02.007

Yang, S., Liu, F., Wu, C., and Yang, S. (2016). Tuning surface properties of low dimensional materials via strain engineering. *Small* 12, 4028–4047. doi: 10.1002/smll.201601203

Yee, N., and Fein, J. (2001). Cd adsorption onto bacterial surfaces: a universal adsorption edge? *Geochim. Cosmochim. Acta* 65, 2037–2042. doi: 10.1016/S0016-7037(01)00587-7

Young, I. M., Crawford, J. W., Nunan, N., Otten, W., and Spiers, A. (2008). Chapter 4 Microbial distribution in soils: physics and scaling. *Adv. Agron.* 100, 81–121. doi: 10.1016/S0065-2113(08)00604-4

Yu, Q., Szymanowski, J., Myneni, S. C. B., and Fein, J. B. (2014). Characterization of sulfhydryl sites within bacterial cell envelopes using selective site-blocking and potentiometric titrations. *Chem. Geol.* 373, 50–58. doi: 10.1016/j.chemgeo.2014.02.027

Yu, T., and Bishop, P. L. (2001). Stratification and oxidation–reduction potential change in an aerobic and sulfate-reducing biofilm studied using microelectrodes. *Water Environ. Res.* 73, 368–373. doi: 10.2175/106143001X139399

Zhou, K., Hu, Y., Zhang, L., Yang, K., and Lin, D. (2016). The role of exopolymeric substances in the bioaccumulation and toxicity of Ag nanoparticles to algae. *Sci. Rep.* 6:32998. doi: 10.1038/srep32998

Zhu, N., Tang, J., Tang, C., Duan, P., Yao, L., Wu, Y., et al. (2018a). Combined CdS nanoparticles-assisted photocatalysis and periphytic biological processes for nitrate removal. *Chem. Eng. J.* 353, 237–245. doi: 10.1016/j.cej.2018.07.121

Zhu, N., Wang, S., Tang, C., Duan, P., Yao, L., Tang, J., et al. (2019). Protection mechanisms of Periphytic biofilm to photocatalytic nanoparticle exposure. *Environ. Sci. Technol.* 53, 1585–1594. doi: 10.1021/acs.est.8b04923

Zhu, N., Wu, Y., Tang, J., Duan, P., Yao, L., Rene, E. R., et al. (2018b). A new concept of promoting nitrate reduction in surface waters: simultaneous supplement of denitrifiers, electron donor pool and electron mediators. *Environ. Sci. Technol.* 52, 8617–8626. doi: 10.1021/acs.est.8b01605

Zhu, T., Lawler, D. F., Chen, Y., and Lau, B. L. T. (2016). Effects of natural organic matter and sulfidation on the flocculation and filtration of silver nanoparticles. *Environ. Sci. Nano* 3, 1436–1446. doi: 10.1039/C6EN00266H

Zirkler, D., Peters, A., and Kaupenjohann, M. (2014). Elemental composition of biogas residues: variability and alteration during anaerobic digestion. *Biomass Bioenergy* 67, 89–98. doi: 10.1016/j.biombioe.2014.04.021

Conflict of Interest: The authors declare that the research was conducted in the absence of any commercial or financial relationships that could be construed as a potential conflict of interest.

frontiers in Environmental Science

REVIEW
published: 10 July 2020
doi: 10.3389/fenvs.2020.00101

Assessing Sunscreen Lifecycle to Minimize Environmental Risk Posed by Nanoparticulate UV-Filters – A Review for Safer-by-Design Products

Jérôme Labille[1], Riccardo Catalano[1], Danielle Slomberg[1], Sylvie Motellier[2], Annalisa Pinsino[3], Pierre Hennebert[4], Catherine Santaella[5] and Vincent Bartolomei[2]*

[1] CNRS, IRD, INRAe, Coll France, CEREGE, Aix Marseille University, Aix-en-Provence, France, [2] University Grenoble Alpes, Commissariat á l'Energie Atomique et aux Energies Alternatives, DRT/LITEN/DTNM/STDC/Laboratory of Measure, Safety, and Environment, Grenoble, France, [3] Istituto per la Ricerca e l'Innovazione Biomedica, Consiglio Nazionale delle Ricerche, Palermo, Italy, [4] National Institute for Industrial Environment Risk (INERIS), Aix-en-Provence, France, [5] Aix Marseille Univ, CEA, CNRS, BIAM, Laboratory of Microbial Ecology of the Rhizosphere, Saint-Paul-lès-Durance, France

OPEN ACCESS

Edited by:
Denise M. Mitrano, Swiss Federal Institute of Aquatic Science and Technology, Switzerland

Reviewed by:
Veronique Adam, Swiss Federal Laboratories for Materials Science and Technology, Switzerland
Yousuf Hussain Mohammed, The University of Queensland, Australia

***Correspondence:**
Jérôme Labille
labille@cerege.fr

Specialty section:
This article was submitted to Biogeochemical Dynamics, a section of the journal Frontiers in Environmental Science

Received: *30 March 2020*
Accepted: *10 June 2020*
Published: *10 July 2020*

Citation:
Labille J, Catalano R, Slomberg D, Motellier S, Pinsino A, Hennebert P, Santaella C and Bartolomei V (2020) Assessing Sunscreen Lifecycle to Minimize Environmental Risk Posed by Nanoparticulate UV-Filters – A Review for Safer-by-Design Products. Front. Environ. Sci. 8:101. doi: 10.3389/fenvs.2020.00101

Sunscreens are of emerging concern regarding environmental effect. After leaving the skin either through bathing or washing, the ingredients contained in the product formulation can be released into rivers, lakes, seashores, and/or sewage treatment plants. Nanomaterials used as UV-filters are of particular concern in this context as they may have a negative effect on these systems. To assess the risks posed, the exposure and hazard of nanoparticulate UV-filters must be considered through the entire lifecycle of the sunscreen product. This includes not only usage, but also manufacturing and disposal at the end of life of the product, as some nanomaterials may be released into the environment at each stage. This includes also developing relevant approaches that take into account realistic scenarios of environmental release and fate. Nanoparticulate UV-filters typically consist of a mineral nanoparticle core (TiO_2 or ZnO) coated with surface layers aimed at optimizing the dispersion in the formulation and at supressing any photo-sensibility. This coating plays a key role in the associated risk since it affects the nanoparticle surface properties, which control both fate and hazard. At present, knowledge gaps remain regarding the safety of nanomaterials used in sunscreen, as very few studies have focused on real sunscreen filters and formulations throughout their lifecycle so far. A literature review is proposed here from the design of nanoparticulate UV-filters and formulations, to the release, fate, and effect in the different compartments encountered along the product lifecycle. The resulting state of the art highlights knowledge gaps and will likely help regulators, manufacturers, and consumers choose appropriate guidance. By considering each development stage of the sunscreen, from the choice of the UV-filter(s) and its (their) integration into a cosmetic

formulation to the knowledge of the risk involved in this choice all along the product lifecycle, an eco-design approach can be achieved where release or toxicity are reduced. Sustainability can thus be accounted for, during the design process, by making the appropriate choices (in advance) that help minimize or prevent the environmental impact of the sunscreen.

Keywords: UV filter (sunscreen), nano risk, lifecycle, fate and transport model, safe by design, nanoparticle, environment pollution

INTRODUCTION

Our modern lifestyle implies frequent exposure to the sun's rays, during everyday and recreational activities. Sunscreen usage is often needed to protect our skin against the damaging effects of UV rays, that include accelerated aging and skin cancer. Sunscreen products are conceived by the cosmetic industry in a way that composition, labeling, and efficacy to block UV rays are in accordance with local regulations. Nowadays, in the context of global changes, the multiple impacts of anthropic activities on the environment are of rising concern, and the case of sunscreens has come into consideration. While their usage must remain a health priority, sunscreen composition can be formulated to minimize its effects on the environment, in relation with the ingredients they contain. Sunscreens typically consist of a complex oil-in-water (o/w) or water-in-oil (w/o) emulsion in which UV-filters, the major active ingredients, are incorporated at high concentration. The UV-filters can be organic or mineral in nature, and provide the desired solar protection factor (SPF) that is labeled on the product packaging (Steinberg, 2007). Some organic UV-filters found in many sunscreens have been blamed for having endocrine disrupting capacities inducing adverse effects on fecundity and reproduction (Schlumpf et al., 2004; Kunz and Fent, 2006; Calafat et al., 2008; Bluthgen et al., 2012), as well as causing adverse effects on marine systems (Calafat et al., 2008; Danovaro et al., 2008; Kunz and Fent, 2009; Sanchez-Quiles and Tovar-Sanchez, 2014; Downs et al., 2016; Sendra et al., 2017; Fel et al., 2019; Rodriguez-Romero et al., 2019; Tovar-Sanchez et al., 2019). While mineral UV-filters may offer an alternative to synthetic organic UV-filters, their toxicity, fate, and overall impact on the environment are still under consideration, and their resulting acceptance by the consumers is largely related to the potential risks of nanotechnology-based products. Bombarded with alarmist information about nanomaterials, consumers are now wary of spreading products containing these substances on their skin, as they question the benefit-risk ratio of the product. What about the toxicity that this implies for their health and for the environment?

Nanometric titanium dioxide (TiO_2) or zinc oxide (ZnO) UV-filters have many advantages in terms of sun protection and aesthetics and thus constitute a main active ingredient of sunscreens. However, after leaving the skin either through bathing or washing, such engineered nanomaterials (ENM) contained in the sunscreen can be released into rivers, lakes, seashores, and/or sewage treatment plants. In order to assess the related risks posed and the global environmental footprint of the product, their fate and effect in these different systems must be considered along with the product lifecycle.

Here we discuss how safe-by-design sunscreens can be developed by considering and minimizing the risk associated with ENMs at all stages of the cream lifecycle, from its manufacture to its end of life, through the consumer use and its effects on the exposed environment. In this review, the impact of sunscreen components on the consumer health via topical application and direct transcutaneous exposure is not considered, because this constitutes a priority point of consideration and evaluation for the respective country regulators and has thus been systematically studied (see e.g., Osmond and McCall, 2010; Schneider and Lim, 2019 and references therein). Here, we focus on the scientific questions regarding the environmental effects of sunscreen products, and particularly of nanoparticulate UV-filters. Key stages of the sunscreen lifecycle and the related scientific literature are developed in this review. This includes (i) the sunscreen design at both scales of UV-filter selection and formulation optimization; (ii) the aquatic environment directly exposed via bathing activity, or indirectly exposed via domestic wastewater pathways; (iii) the induced potential hazards on aquatic organisms; and (iv) the product fate at its end of life regarding management of treatment plant sludge and solid waste disposal, incineration or recycling (**Figure 1**). In addition, new experimental approaches are also proposed when specific questions are not yet, or not sufficiently, addressed in the scientific literature. Although there is extensive scientific literature on the nanosafety of TiO_2 and ZnO ENMs, only a minor part of it deals with the UV filter application. In this review, we primarily focused on this minor part, including original UV filters as well as aged UV filters, to be relevant to the lifecycle stages explored. However, when no or few references could be found at any of the above-mentioned stages, our review was extended more widely to the literature on sunscreens in general or on bare nano-TiO_2 and nano-ZnO. The resulting state of the art contributes to establish an objective cost/benefit evaluation regarding the use of nanoparticulate UV-filters in sunscreen cosmetic products. It aims at helping regulators, manufacturers and consumers to follow appropriate criteria in their respective choices, while some remaining knowledge gaps are also raised. By considering each development stage of the sunscreen, from the choice of the UV-filter(s) and its (their) integration into a cosmetic formulation, to the knowledge of the risk involved in this choice all along the product lifecycle, an eco-design approach can be achieved and risk can be minimized (**Figure 2**).

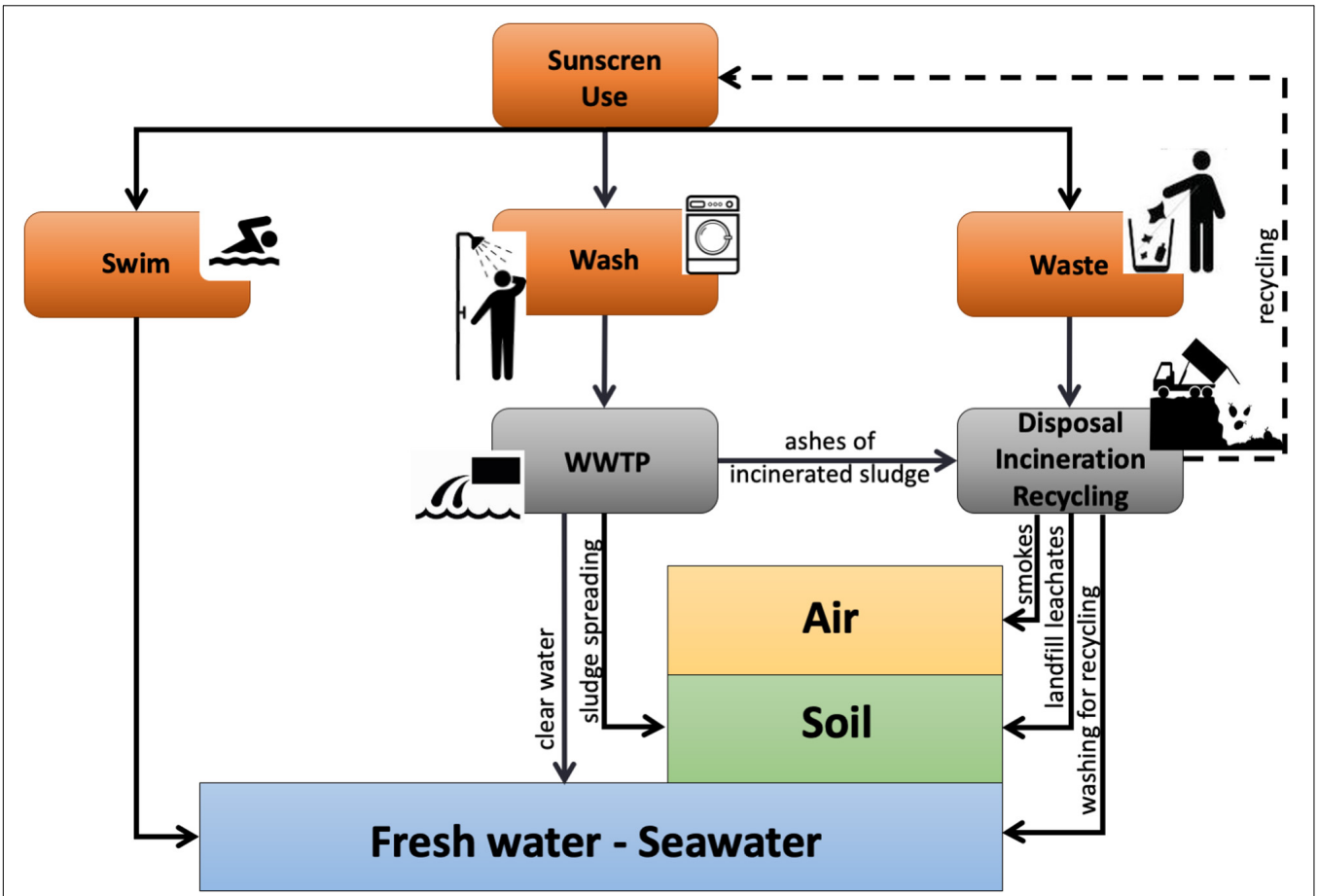

FIGURE 1 | Possible transport pathways from sunscreen use to air, water or soil, through bathing water, domestic wastewater, and solid waste disposal.

SUNSCREEN DESIGN

Environmental Life Cycle Assessment (LCA) quantifies the environmental impacts associated with a good or service throughout its lifecycle, from raw material extraction, manufacturing, distribution and use, to final recycling and waste disposal. In the cosmetics industry, LCA and other life cycle thinking approaches such as Environmental-, Carbon- and Water-footprinting have been used to identify and measure environmental impacts and prioritize adaptations to products, processes and packaging to develop cosmetics with improved environmental profiles (Cosmetics Europe TPCA, 2018). The development of formulations with a smaller carbon footprint or with a higher share of readily biodegradable raw materials is promoted so that the eco-design of formulas and packaging are encouraged via education and sharing of best practices. Sustainability can be accounted for during the design process by making the appropriate decisions in advance to minimize the environmental risk posed by the sunscreen ingredients (**Figure 2**). For example, reducing the potential release and/or (eco)toxicity of the nanoparticles contained in the cream during its entire lifecycle is a decisive criterion for its eco-design. Both the active UV-filter(s) and the emulsion type in which it (they) is (are) incorporated are to be considered. The surface properties of the former and the overall characteristics of the latter both control the potential ecological impact of the sunscreen along its lifecycle.

UV-Filter Selection

ZnO and TiO_2 are both used in sunscreens as mineral UV-filters as they are able to reflect and absorb UV-rays. ZnO has a broad UVA- UVB absorption curve, while TiO_2 provides better UVB absorption and a UVA protection depending on the particle size (Smijs and Pavel, 2011; Schneider and Lim, 2019). This is because in this range of 320–400 nm, UV-rays are rather scattered by nano-TiO_2 (Shao and Schlossman, 1999) and optimal scattering is thought to occur when the diameter of the particles is approximately half the wavelength of the light to be scattered (Fairhurst and Mitchnick, 1997; U.S. EPA, 2010). When used together, ZnO and TiO_2 provide a good broadband UV protection. These mineral UV-filters typically consist of a ZnO or TiO_2 nanoparticulate core with size varying from tens to hundreds of nm. Different combinations of coating obtained by different routes of surface functionalization aim at blocking the nanomaterial photoactivity and favor dispersion of the nanomaterial in the sunscreen formulation.

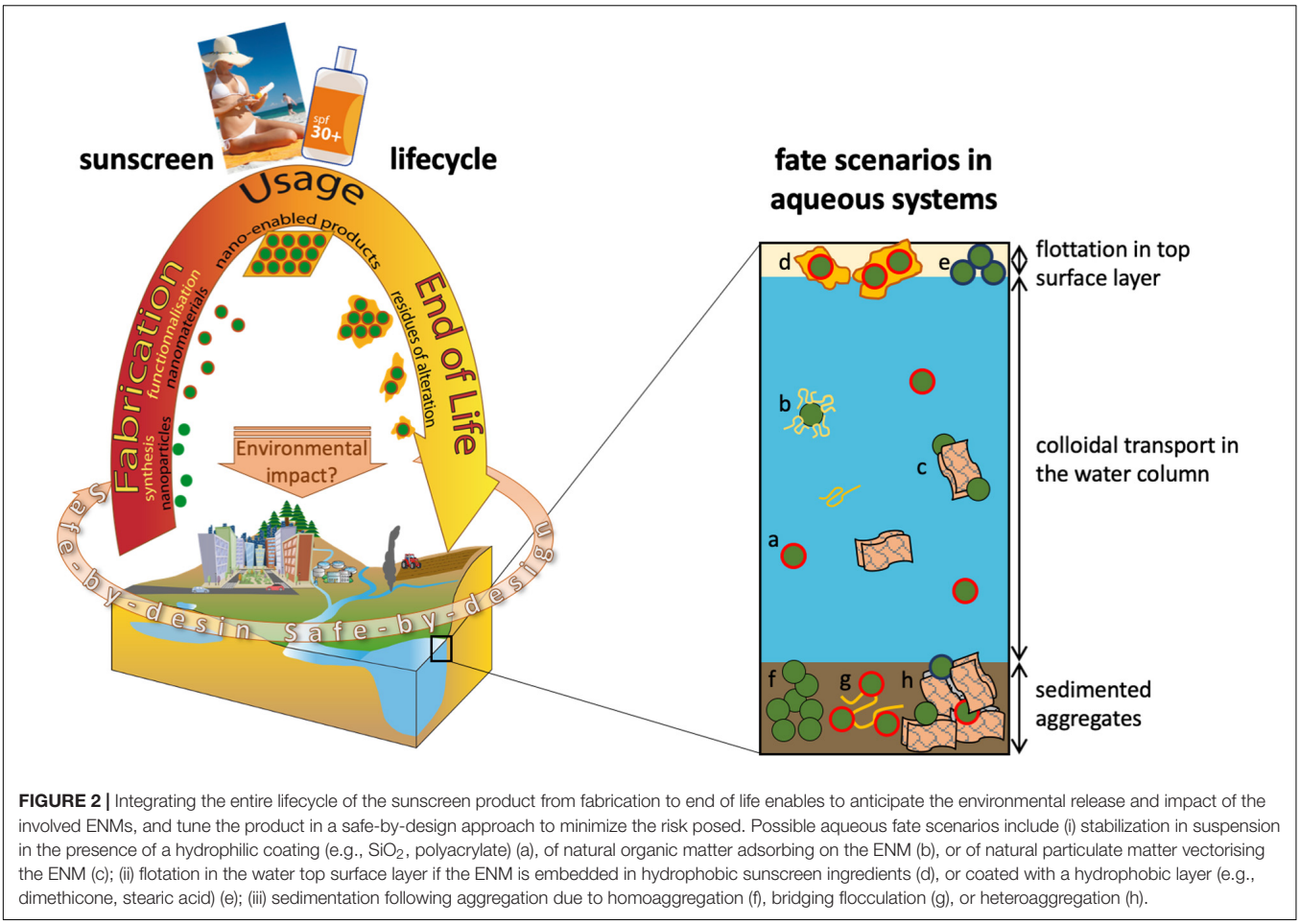

FIGURE 2 | Integrating the entire lifecycle of the sunscreen product from fabrication to end of life enables to anticipate the environmental release and impact of the involved ENMs, and tune the product in a safe-by-design approach to minimize the risk posed. Possible aqueous fate scenarios include (i) stabilization in suspension in the presence of a hydrophilic coating (e.g., SiO_2, polyacrylate) (a), of natural organic matter adsorbing on the ENM (b), or of natural particulate matter vectorising the ENM (c); (ii) flotation in the water top surface layer if the ENM is embedded in hydrophobic sunscreen ingredients (d), or coated with a hydrophobic layer (e.g., dimethicone, stearic acid) (e); (iii) sedimentation following aggregation due to homoaggregation (f), bridging flocculation (g), or heteroaggregation (h).

UV-Filter Photopassivation

The efficient absorption of UV wavelengths by ZnO or TiO_2 is enabled via the excitation of the outermost electrons of the constituting atoms. However, this comes with the generation of reactive oxygen species (ROS) when the electrons come back to a stable state. In particular, photo-induced reactions of TiO_2 have gained much attention and have proved to be useful in environmental applications like wastewater treatment processes (Herrera Melian et al., 2000). This so-called photocatalytic feature has to be eliminated in sunscreen products in order to prevent any induced oxidative stress on the skin or damage of the lotion (Wakefield et al., 2004; Sendra et al., 2017). For this reason, the less photocatalytic rutile form of TiO_2 is preferred to the anatase form in cosmetic applications (Fujishima et al., 2008). In addition to high material purity, photopassivation is a priority criterion to authorize any TiO_2 candidate to the role of UV-filter in cosmetic products. Of note, the European Scientific Committee on Consumer Safety (SCCS) adopted a threshold of photopassivation efficiency (no more than 10% of pure TiO_2 rutile) to accept any TiO_2 nanomaterial candidates for sunscreen use (SCCS, 2014). Generally, TiO_2 photopassivation is achieved by precipitating an inert mineral layer at the nanoparticle surface. The most common photopassivating coatings found in sunscreen are alumina and silica (Braun et al., 1992; King et al., 2008; Labille et al., 2010). Another approach proposed to increase TiO_2 nanoparticles photostability, consists in "doping" the particle with metals such as manganese, vanadium, chromium, and iron (Wakefield et al., 2004). Manganese for example, occupies some titanium sites in the nanoparticle lattice structure, where it creates a electron-hole de-excitation route, giving the sunscreen the advantages of increased UV-A absorption, reduced free radical generation, and increased free radical scavenging behavior.

UV-Filter Dispersion in the Formulation

The ability to prepare and handle concentrated and stable dispersions of nanoparticles is important for the performance of the final product since aggregation is a major cause of poor performance in UV ray absorption and of limited transparency. Efficient utilization of the broad absorption in the UV-B and UV-A regions of mineral UV-filters in transparent sunscreens requires not only that the particle size be reduced far below the wavelength of visible light but also that dispersion be maximized (Tyner et al., 2011; Faure et al., 2013). If such conditions are fulfilled, it takes a significantly lower concentration of finely dispersed nanoparticles in the formulated product than needed with large aggregates to attain the same functionality, i.e., a given solar protection factor. This reduced metal "load" in the final product is also an interesting point in lowering environmental

exposure. This is evidenced in **Figure 3A**, plotting the UV absorption of different commercial nanoparticulate TiO_2 UV-filters dispersed in a sunscreen oil, as a function of the aggregate size. This relation is due to the sunscreen homogeneity that is maximized when the UV-filter aggregate size is minimized, as highlighted by 2D X-ray nano-tomography (**Figure 3B**) for two contrasting formulations (Catalano, 2020). The lower sunscreen image evidences the existence of large aggregates forming over-concentrated patches of several μm size that caused a lower UV absorption efficacy. Meanwhile, no significant difference was observed between the respective UV-filters at the nm scale of the primary particle, because both consisted of ultrafine rutile nanoparticles (**Figure 3C**).

This determining role is given to the outermost nanoparticle coating. Organic additives are grafted to the inorganic surface to improve the compatibility with the dispersing medium and thus favor the nanoparticle dispersion in the cream (Catalano et al., 2020). A hydrophilic, amphiphilic or lipophilic feature is given to the nanoparticles via this coating process, in order to preferentially enhance their dispersion in the aqueous or the oil phase of the emulsion (Faure et al., 2013). For example, silane-type polymers such as poly-dimethyl-syloxane or stearic acid result in a lipophilic surface character (Labille et al., 2010), while polyacrylic acid or bare silica coating typically favor aqueous dispersion (Dzumedzey et al., 2017; Rowenczyk et al., 2017). Amphiphilic character can also be obtained with, e.g., simethicone coating, which enables nanoparticle dispersion in both oil and water phases (Schulz et al., 2002; Faure et al., 2013).

From an industrial point of view, an optimal UV filter formulation is generally sought indirectly by maximizing the SPF and shelf life while minimizing the dosage of the active ingredients. However, in a mechanistic approach, any attempt to optimize the ENM dispersion in the sunscreen formulation has to deal with the analytical challenge of the cream characterization. Generally, this involves ENM extraction based on dispersion of the material in a surfactant solution or a solvent phase, sonication, and ultracentrifugation or ultrafiltration (Contado and Pagnoni, 2010; Dan et al., 2015; Philippe et al., 2018). Philippe et al. (2018) have pointed out the challenge of this extraction process with respect to the agglomeration state of the ENMs. In their screening of 11 commercialized sunscreens, while cryo-TEM revealed that most of the particles were agglomerated in the creams/lotions, the "mild" extraction methods proposed resulted in dispersed primary particles, questioning the representativeness and relevancy of such extracted particles for environmental and toxicology studies. Some dense micro-aggregates most often exist with TiO_2 nanoparticles, which result from the synthesis process. They are due to secondary precipitation at the contact points between the primary particles, binding them together into a larger assembly. A key question regarding safety is whether such aggregates remain intact throughout the entire sunscreen

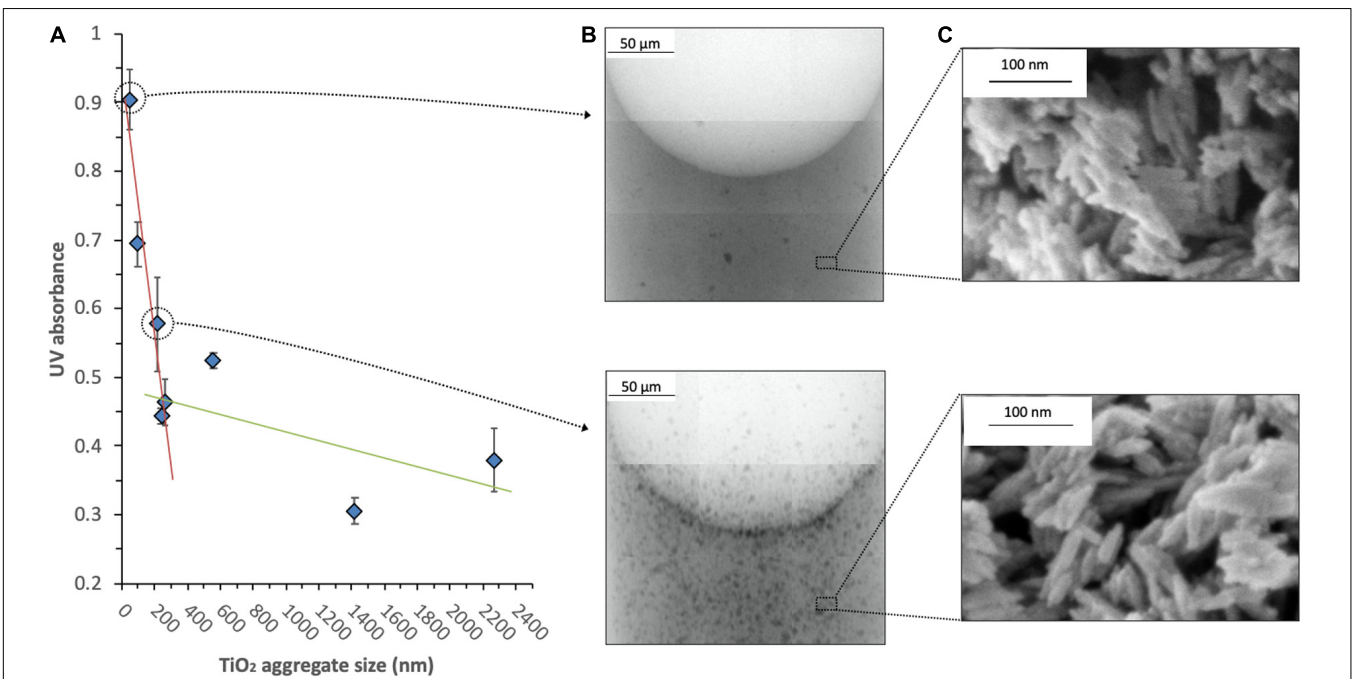

FIGURE 3 | Effect of TiO_2 nanoparticle aggregate size on the UV absorption efficacy. Different commercial nanoparticulate TiO_2 UV-filters were dispersed in a sunscreen oil phase. The UV absorption at the wavelength of 270 nm was measured by UV/vis spectrophotometer; it is plotted according to the aggregate size measured by dynamic light scattering **(A)**. The resulting homogeneity of the w/o sunscreen formulation was analyzed at the micrometric aggregate scale by 2D X-ray nano-tomography **(B)**. The top pictures show a finely dispersed UV-filter leading to homogeneous sunscreen and maximum UV absorption, while the bottom pictures correspond to an aggregated UV-filter leading to a heterogeneous sunscreen and lowered UV absorption (Catalano, 2020). However, both top and bottom UV-filters display similar primary nanoparticle structure at the nm scale, as observed by HR-scanning electron microscopy **(C)**.

lifecycle, because the size of the smallest dispersed units will certainly affect the environmental risk associated both in terms of exposure and hazard. Indeed, decreasing the size of nanoparticles down to that of primary particles around 20 nm may favor bioaccessibility and internalization by living organisms and transfer via the food chain. Nevertheless, it is worthwhile noting that for precautionary principle, the EU cosmetic regulation 1223/2009 considers the smallest existing units (Eur-Lex, 2009). According to this regulation, the definition of a nanomaterial below the size threshold of 100 nm is based either on the external dimensions or on the internal structure of that material. The internal structure of the material prevails on the outer size of some possibly existing aggregates because the fragmentation of such aggregates along the product lifecycle and the resulting dispersive potential of the ENMs are mostly unknown.

The chemical coating of the nanoparticle surface thus plays a determining role at many stages of the sunscreen lifecycle and should be optimized at the manufacturing stage in an eco-design concept. At the conception and production stages, it must both increase UV absorption efficiency by maximizing the particle dispersion in the formulation matrix and optimize the photopassivation of the functional nanoparticle core, while during further stages like usage and end of life of the sunscreen, this coating may determine both the nanomaterial fate and toxicity in the environment (see sections "Release, fate and exposure in aquatic systems" and "Effects on aquatic living organisms").

Effects of the Formulation Ingredients on the ENM Fate

Different types of formulations are used on sunscreen market, mostly constituted of either water-in-oil (w/o) or oil-in-water (o/w) emulsions, one or the other type being preferred to tailor the rheology and to obtain specific galenic properties. The nanoparticulate UV-filters can be dispersed in one or the other liquid phase of the emulsion (Semenzato et al., 1994; Turkoglu and Yener, 1997; Gamer et al., 2006; Monteiro-Riviere et al., 2011; Tyner et al., 2011; Faure et al., 2013). In addition, sunscreen formulations usually contain emulsifying, thickening and preservative agents all aimed at maximizing the stability of the final product. All these ingredients mixed together result in a complex system in which cross effects may take place. Some formulation ingredients can unintentionally interact with the nanoparticulate UV-filters and alter their properties (Rossano et al., 2014). For example, Catalano et al. (2020) found that an emulsifying agent containing a glucosidic moiety can adsorb onto the nanoparticulate UV-filter and alter its dispersion, finally affecting the UV absorption of the sunscreen (**Figure 3**). A mixture effect exists and must be considered and optimized in a safe-by-design approach, not only at the fabrication stage of product quality control, but also at further lifecycle stages because certain ingredient combinations affect weathering and environmental dispersion of the product (Botta et al., 2011; Tovar-Sanchez et al., 2019). In this context, the expected contrasted fates of the oily or aqueous by-products are of particular interest in future research.

RELEASE, FATE AND EXPOSURE IN AQUATIC SYSTEMS

Sunscreens can be washed off the skin either through bathing activity or via a domestic wastewater pathway. The formulations and their ingredients undergo a constant aging once released into aquatic media. The fate of nanoparticulate UV-filters depends on the extent and routes of the aging process and determines their potential effects on the environment. The propensity of the products to be dispersed in the aqueous phase as nanoparticles or colloids is a point that eco-design should seek to minimize.

Determining the environmental concentration of engineered nanoparticles is a challenging task that can be approached by field sampling at local scale or model estimation at varying scales. While the field approach was limited by ever evolving detection methods (see section "Environmental occurrence of UV-filters due to bathing activity") (Zhang et al., 2019), model estimations have been developed to estimate the environmental fate scenario and occurrence of ENMs in aqueous media. Even if many knowledge gaps (e.g., on ENM production, application and release) still affect the modeled values, an order of magnitude of the environmental concentrations was reached and agreed. Boxall et al. (2007) presented the first quantitative approach, predicting concentrations of various ENMs from cosmetic products in soil, sludge, and water. They obtained ranges of 24–245 μg/L and 76–760 μg/L for TiO_2 and ZnO in water, respectively. Gottschalk et al. (2010) developed a probabilistic method to compute the distributions of environmental concentrations (PEC) in nanomaterials based on flow modeling and Monte-Carlo simulation, in order to deal with the uncertainty in the model parameterization related to lack of knowledge on transfer, partitioning coefficients and emission factors. The modeled PEC values proposed in the literature are not always comparable due to the different scenarios considered and nanoparticle characteristics used. A dozen of those existing models was reviewed in 2013 in order to clarify those key parameters that determine the modeled values (Gottschalk et al., 2013).

Keller et al. (2014) estimated the ENM release from personal care products (PCP) into soils, water, air, and landfills in California and China. They accomplished this by surveying consumer's habits and analyzing container sizes and ENM concentration in each product. The total sunscreen consumption in the United States was estimated at 90,000 metric tons per year, involving 2,300–2,700 mt/yr of ENMs. Authors revealed that sunscreen is the most intensive ENM application among PCPs, with 81–82% of the total ENM mass flow, and that ZnO and TiO_2 are the most commonly used ENMs, representing together 94w% of the ENM use in PCPs. From the overall sunscreen usage, including everyday use and recreational activities, they predicted that the amount of sunscreen directly released from the skin to the bathing area water levels at 5%. The rest of the consumed products was mostly used out of recreational activity, giving about 60–90% washed off during showering and flowed to the wastewater treatment plant (WWTP). The efficiency of the WWTP for ENM removal from the wastewater controls the ENM partitioning between the downstream compartments soil

and surface water (**Figure 2**) (see also section "Risk related to indirect release at the product end of life").

Environmental Occurrence of UV-Filters Due to Bathing Activity

The scenario of direct release into rivers, lakes or seashores during recreational activity is of particular interest since UV-filters have been repeatedly blamed for harmful effects toward aquatic ecosystems, and particularly in coral reef areas (see section "Biological effects on marine organisms"). Indeed, as coastal tourism has reached its peak in recent decades, the use and consequently the emission of sunscreen products in the nearshore environment has increased (UNEP, 2009). A retention factor of the sunscreen on the consumer's skin needs to be determined to estimate how much of the sunscreen remains on the skin after bathing and will eventually end up in the shower outflow. This retention factor is expected to be related to the water resistance of the product, which is a point that manufacturers often try to maximize. A retention factor was measured using pig skin (*a proxy for human skin*) covered with five different commercial sunscreens (Jeon et al., 2016). The tested products contained TiO_2, ZnO, or both at various concentrations. After 30 min agitation in a synthetic swimming pool water, the release from the skin ranged from 2 to 30%, and it increased to 10–50% after 120 min. A similar value of 25% was obtained with organic UV-filters released from skin to seawater after 20 min of immersion (Danovaro et al., 2008). From this value the authors could determine that 4,000–6,000 t/y of sunscreen are released worldwide in reef areas. At a local scale, a social survey carried out on three beaches of the Mediterranean coast enabled to estimate that on a beach attended by 3,000 people during the summer peak of activity (from June to September), an average mass of 52 kg/day or 1.4 t/month of suncare products is consumed before bathing (Labille et al., 2020). From these products, a mass concentration of 3–10% was reasonably used to estimate the amount of each UV-filter indicated among the component list on the packaging, giving 15.7 kg of UV-filter per day in average. A retention factor remains to be applied to this value to estimate the UV-filter mass possibly released to bath water. Organic UV-filters were present in most of the products consumed. As for mineral UV-filters, they were used in only 20% of the products, with 65% being labeled [nano].

The detection of anthropogenic TiO_2 and ZnO minerals (nano or non-nano) in aquatic environments where both Ti and Zn elements naturally occur in varying background concentrations remains an analytical challenge. The available analytical methods are often not sensitive enough for current environmentally relevant concentrations and cannot distinguish natural materials in the nanoscale size range from manufactured nanomaterials (Englert, 2007; Domingos et al., 2009; Simonet and Valcarcel, 2009). Single particle (sp) ICP-MS is of particular interest in this context as it enables to detect and quantify Ti-containing particles of nanometric size at ppb/ppt levels in a complex liquid medium (Gondikas et al., 2014, 2018; Venkatesan et al., 2018). However, high resolution equipment may sometimes be required to solve isobaric interferences, such as ^{48}Ca with regard to ^{48}Ti, which can hamper the detection of titanium ENMs in waters containing high Ca concentrations, like river waters for instance (Tharaud et al., 2017). ^{47}Ti isotope may also be used but leads with a higher limit of detection due to its lower abundance. Some element ratios have been tested as proxies to distinguish the geogenic materials containing Ti or Zn elements from the ENMs in water. Indeed, any chemical element that is characteristic of geogenic materials only can be quantified relatively to the Ti or Zn element in order to distinguish Ti and Zn contributions due to geogenic materials from those related to ENM peak release. Al and Si are not good candidates for this purpose as they are abundant in both natural systems and in the coating of mineral UV-filters. Fe, V or rare earths elements (Ga, Y, Nb, Eu, Ho, Er, Tm, Yb, Ta) have been proposed as proxies for geogenic materials (Gondikas et al., 2014, 2018; Reed et al., 2017; Labille et al., 2020).

In seawater, a specific fate scenario has been observed, that facilitates the identification of mineral UV-filters: they appear concentrated in the water top surface layer (Tovar-Sanchez et al., 2013; Labille et al., 2020) (**Figures 2d,e**). This preferred localization minimizes possible confusion with any geogenic material containing Ti or Zn elements since these are rather found in the water column or in sediments. This is certainly related to the hydrophobic character of some sunscreen components. Meanwhile, such vertical differentiation has not been reported yet in freshwater systems. This may be due to the high salinity of seawater that decreases the solubility of the sunscreen components. A similar effect, so-called salting-out, is known for example on protein solubility in electrolyte with very high ionic strength (Duong-Ly and Gabelli, 2014). In beaches of the Mediterranean Coast, the enrichment in UV-filters in the water top 1-cm surface layer of the bathing zone was evidenced with regard to the water column below (Labille et al., 2020), giving respectively 100–900 and 20–50 μg/L of TiO_2, 10–15 and 1–3 μg/L of ZnO. Values corresponding to La Lave Beach are reported in **Figure 4**. They show similar patterns for TiO_2 and ZnO, both found in the bathing zone and preferentially concentrated in the top surface layer compared to the water column. Moreover, a tenfold concentration of TiO_2 was measured with regard to ZnO. This difference could be due to the prevalence of TiO_2 over ZnO as a UV filter in the sunscreens consumed in Europe (Euromonitor International, 2015). Moreover, ZnO has a higher solubility than TiO_2, which likely favors its rapid dissociation into dissolved zinc species, and thus its disappearance from the particulate fraction analyzed here. Of note, most of the UV-filters evidenced in suspension in the water column were found in a size fraction larger than 0.5 μm, meaning that the ENMs were not dispersed back to their initial size < 100 nm so far.

Both mineral and organic UV-filters can be released simultaneously in the bathing water since they are often associated in sunscreens or they originate from different products used at the same place. Consequently, they may be found together in the aquatic environment. The co-evolution of organic and mineral UV-filters has been measured in waters impacted by recreational areas with time-dependent concentrations (Tovar-Sanchez et al., 2013; Reed et al., 2017). For example, in nearshore waters of the Mediterranean coast, benzophenone

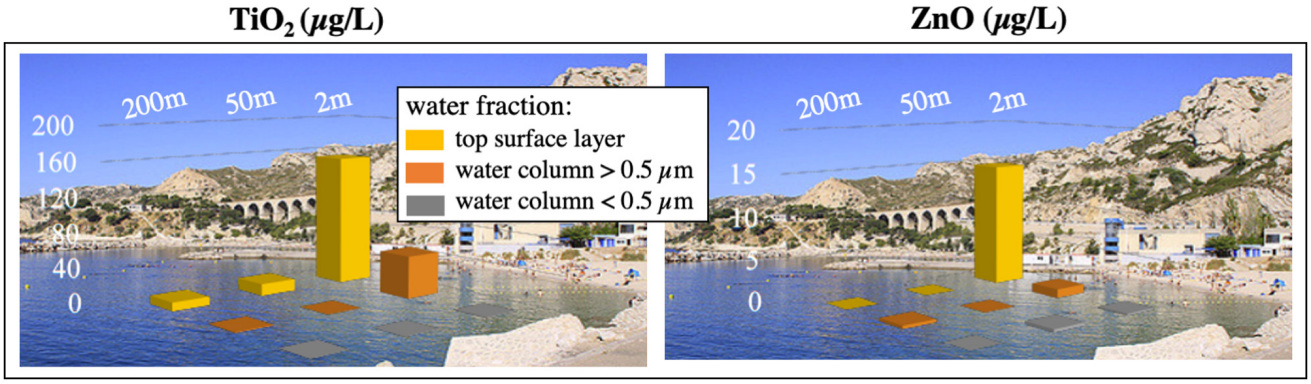

FIGURE 4 | TiO_2 and ZnO concentrations calculated from Ti and Zn elements measurements in marine beach water on the French Mediterranean Coast (La Lave Beach, Marseille), at different distances from the shore line, respectively 2 and 50 m in the bathing zone, and 200 m beyond the bathing zone. Top surface layer and water column were compared. Water column samples were further fractionated by tangential flow filtration in two size classes, >0.5 µm and 0.02–0.5 µm, in order to estimate the aggregation state of the UV-filters (Labille et al., 2020).

3 (53.6–577.5 ng/L), 4-methylbenzylidene camphor (51.4–113.4 ng/L), Ti (6.9–37.6 µg/L) (assumed related to TiO_2), and Zn (1.0–3.3 µg/L) (assumed related to ZnO) were detected with variable concentrations along the day and mainly concentrated in the surface microlayer (Tovar-Sanchez et al., 2013). In freshwater from Colorado, oxybenzone and TiO_2 were also detected together during recreation time (Reed et al., 2017). However, a lack of knowledge remains regarding the respective environmental fate and persistence of these two types of UV-filters, which may be contrasted. The hydrophilic or hydrophobic feature of the UV-filter will affect its propensity to remain individually in the water column, to float at the surface or to attach to the surface of naturally occurring suspended matter (Giokas et al., 2007) (**Figure 2**). In addition, the fate of particulate mineral UV-filters depends on both their solubility and their tendency to disperse or aggregate (Labille and Brant, 2010). A comparative co-evolution of both UV-filter types was proposed by Labille et al. (2020), estimating the respective fluxes from the beachgoer's skin to the bathing water. They showed that very contrasting fates exist, with 35–50% of the nanoparticulate UV-filters being recovered in water, while the organic filters were minimally recovered in the environment, most likely due to internalization through the skin barrier (Matta et al., 2019, 2020), or partial photodegradation. For this reason, it is not recommended that the organic molecules, being more easily analyzed because not present in natural background, are used as a proxy of the mineral UV-filters for environmental quantification.

Mechanisms Driving the Environmental Fate

The residence time and fate of the ENM residues in the water column is a key variable for estimating the level and duration of organism exposure in the different aqueous compartments. Strong experience was gained from past research on bare nanoparticles. The ever-existing balance between colloidal stability favoring transport in suspension and aggregation favoring rapid sedimentation and immobilization must be evaluated (Labille and Brant, 2010). Homoaggregation of ENMs may be determining when they are locally concentrated at the mg/L level, for example close to the point of release. However, in most cases, the released ENMs are below the µg/L level in surface or seawater. Then, heteroaggregation with natural inorganic or organic colloids suspended in the medium is expected to drive the ENM fate (**Figure 2**) (Praetorius et al., 2014; Labille et al., 2015; Sani-Kast et al., 2015).

The mechanisms driving the environmental fate of ENMs are largely determined by the nanoparticle surface properties and the medium characteristics. In the balance of forces acting at the solid/liquid interface, pH and ionic composition of the solution generally control the extent of particle surface charge, i.e., of electrostatic interactions with neighboring components. For example, a positive correlation was found between the aggregation rate of TiO_2 ENMs and the concentration of Ca^{2+} in natural surface waters (Topuz et al., 2015). Dissolved organic carbon, especially high molecular weight molecules, also plays a determining role in the stabilization or agglomeration of the ENMs, depending on both the natural organic matter (NOM) nature and concentration. While NOM stabilization is usually observed (Domingos et al., 2009), bridging flocculation can be favored at low natural macromolecule concentration (Labille et al., 2010).

In addition to these well-known mechanisms on bare ENMs, a particular attention must be paid to the more or less hydrophobic character of the sunscreen and its by-products which is expected to play a role in the localization and kinetics of dispersion. This hydrophobic/philic property depends on the type of emulsion used for the product formulation. O/W emulsions are expected to readily disperse in aqueous environment since water is already the dispersing phase in the original product, whereas W/O emulsions that display a more hydrophobic character may result in a higher water resistance of the product on the skin and a higher tendency to flotation once released (Leroy and Deschamps, 1986). Actually, both hydrophilic and hydrophobic

scenarios may not be very distinct for a given sunscreen, as the formulation ingredients can fractionate once released in the aqueous system, depending on their respective polarities and affinities (Tovar-Sanchez et al., 2019) (**Figure 2**).

In ENM UV-filters, this property is typically determined by the external coating, which can be either hydrophilic or hydrophobic (see section "Sunscreen design") and will accordingly control the overall fate of the ENM. This also depends on the lifetime of the coating, which undergoes constant aging likely or not to promote the dispersion of the ENMs (Labille et al., 2010; Rossano et al., 2014). For this reason, the nature and lifetime of a given UV-filter coating must be particularly studied as a function of the environmental system encountered in order to estimate the fate scenario. Water chemistry strongly influences the aging reaction and kinetics. For example, a nano-TiO_2 UV-filter coated with a first layer of $Al(OH)_3$ and a second layer of polydymethylsiloxane (PDMS) was studied. In swimming pool water, an increase in chlorine concentration was shown to significantly affect the integrity of the $Al(OH)_3$ protective layer, rendering the TiO_2 nanoparticles rather unstable in suspension due to the new surface charge (Virkutyte et al., 2012). A redistribution of the Al atoms at the ENM surface from ~4 to as high as 15.6% was achieved when the sunscreen was subjected to 3.5 and 7 ppm of chlorine. In a model pure water, no alteration of this $Al(OH)_3$ layer was evidenced, but the integrity of the PDMS layer was shown to be strongly affected, due to the oxidation and desorption of silane moieties (Auffan et al., 2010; Labille et al., 2010). This resulted in the loss of the hydrophobic character of the aged ENMs, which favored subsequent dispersion and transport in aqueous media (**Figure 5**). The aging of another nano-TiO_2 UV-filter coated with one single layer of SiO_2 was also studied in different water chemistries. The rapid dissolution of the silica in fresh water and in seawater was evidenced by the appearance of the underlying TiO_2 chemistry at the surface (Slomberg et al., 2020). This process not only decreased the colloidal stability of the aged ENMs in water, but it also implied new chemical reactivity and photoactivity. Indeed, the coating lifetime also determines how long the nanoparticles remain inert once released in the environment.

Nano-ZnO UV filters can also have surface coatings similar to those of nano-TiO_2. For example, PDMS-coated nano-ZnO displayed a hydrophobic nature while non-coated ZnO easily dispersed in water (Hanigan et al., 2018). In that work, little or no PDMS dissolution was assumed after product use. Aging of the nanoparticulate UV-filter coating may also be accelerated under solar radiation, which is particularly strong when sunscreen residues tend to float at the water surface. Few data exist in the literature regarding the effect of solar radiation on the aging of mineral sunscreens or UV-filters. The $Al(OH)_3$/PDMS-coated nano-TiO_2 mentioned here before was submitted to aging under simulated sunlight and showed an accelerated oxidation of the PDMS coating (Auffan et al., 2010). This reaction induced by sun radiation could be further controlled and studied using a climatic chamber to mimic sun radiation (1.44 W m^{-2} at 420 nm), relative humidity (50%) and temperature (40°C) typical of a hot summer day on the beach. A nanoparticulate UV-filter or a real sunscreen product can be deposited on an inert substrate (e.g., PTFE) and left to age under the conditions listed above during

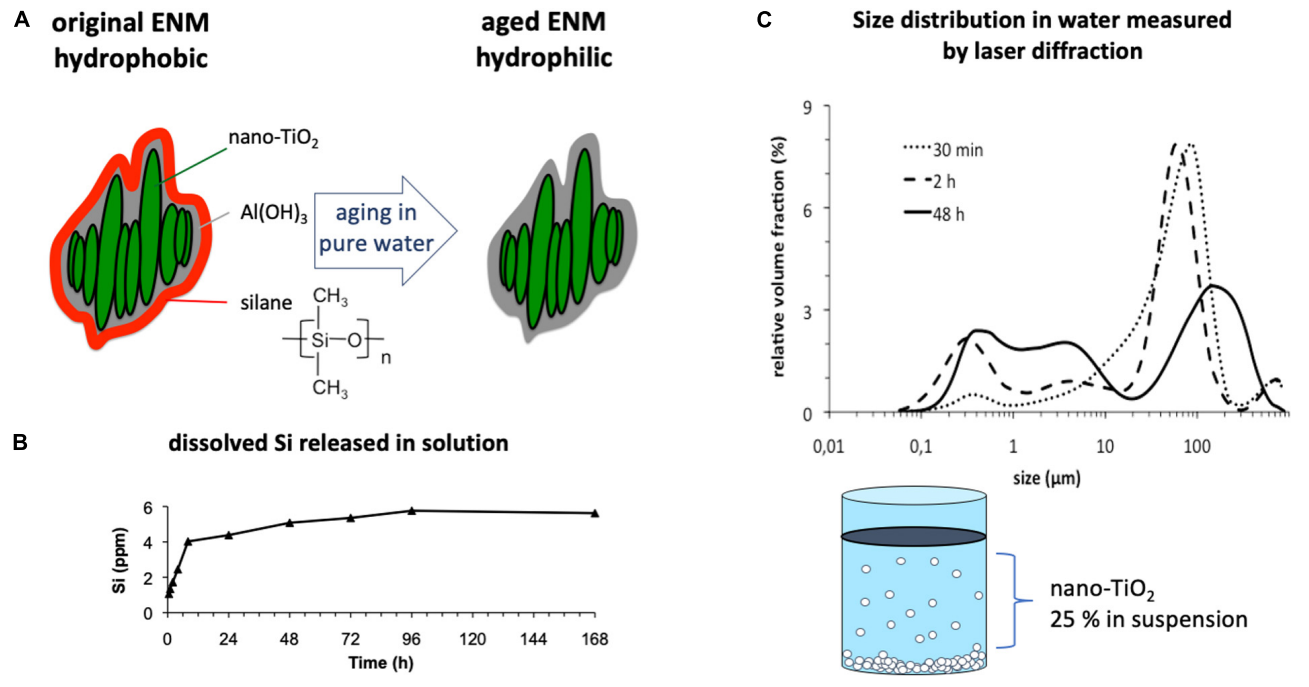

FIGURE 5 | Aging of a hydrophobic TiO_2 ENM coated with $Al(OH)_3$/PDMS in pure water **(A)**. The polydimethylsiloxane (PDMS) coating alteration is confirmed by dissolved Si release **(B)** and leads to aqueous dispersion and colloidal stabilization **(C)** due to new hydrophilic $Al(OH)_3$ surface (Labille et al., 2010).

a relevant time period, typically up to 8 h to mimic the duration of daylight. Any alteration of the nanoparticle coating induced by these conditions, could be evaluated by characterizing the physical-chemical properties of the ENM before and after aging, using spectroscopic analysis and surface charge measurement. While, such an aging scenario has not been explored for mineral UV filters to our knowledge, UV radiation is already known to alter the integrity of the polymer coating. For example, the photochemical modification of a PDMS polymer under UV irradiation was studied by Graubner et al. (2004). The authors were able to evidence the oxidation of the surface silane groups to the silanol form, such as found in the SiO_2 structure, which was responsible for an increased hydrophilicity. As for stearic acid, while its photocatalytic degradation is well-known, it is assumed to be very stable under UV illumination in the absence of a photocatalyst material. For this reason, it has been widely used as a degrading probe to assess the activity of self-cleaning titania photocatalysts (Mills and Wang, 2006).

EFFECTS ON AQUATIC LIVING ORGANISMS

Whether the aged ENMs end up suspended in the water column, sedimented, or floating at the surface determines the type of environmental media and living organisms most impacted by these substances. While transport in the colloidal form comes with a large dilution of the substances and a possible exposure to planktonic organisms, sedimentation and *in situ* accumulation of the UV-filters imply higher local concentration and exposure to benthic organisms. Last but not least, the floating tendency of the aged UV-filters that leads to an oily film at the water surface constitutes a way of exposure to aquatic organisms that has not been studied to date, and from which the possible ecological effects remain mostly unknown.

Biological Effects on Marine Organisms

Sunscreen products are a significant source of organic and inorganic chemicals that reach the sea with potential ecological consequences on the coastal marine ecosystem. The need to understand the ecotoxicological effects on marine ecosystems becomes increasingly important, as long-term effects on marine biota are largely unknown, encouraging studies on the hazards posed by their use through biological models (Corsi et al., 2014). Phytoplankton is a key component of the microbiota community. It forms the basis of the aquatic trophic networks, and any change in the natural population of phytoplankton can affect the structure of aquatic biota. The effects of 13 commercial sunscreens were studied on the growth rate of the marine phytoplankton *Chaetoceros gracilis* commonly found in Western Mediterranean Sea (Tovar-Sanchez et al., 2013). A relatively high average half maximal effective concentration (EC50) after 72 h incubation was obtained at 125 ± 71 mg L^{-1}, with no distinction of the sunscreen components or UV-filters involved in these products. While different studies highlighted the ecotoxicity of some organic UV-filters on marine systems like coral reef (bleaching) and particularly on marine organisms such as crustaceans, echinoderms and algae (Danovaro et al., 2008; Fent et al., 2010; Downs et al., 2016), the status of mineral and nanoparticulate UV-filters remains under consideration. Despite TiO_2 nanoparticles are among the most studied ENMs to evaluate the overall risk related to nanomaterials, the majority of these studies on marine systems deal with the anatase or P25 TiO_2 forms (Minetto et al., 2014), which are not relevant analogs of sunscreen UV-filters. Indeed, TiO_2 based UV-filters consist not only of the rutile form, they are also always functionalised in surface, all these characteristics certainly modifying the nanomaterial reactivity and toxicity (Labille and Brant, 2010; Gerloff et al., 2012). Large knowledge gaps thus remain regarding the marine eco-toxicity of relevant mineral UV-filters.

The hydrogen peroxide produced by three commercial sunscreens in marine system under solar radiation was studied with different UV-filter compositions and as a function of time (Sanchez-Quiles and Tovar-Sanchez, 2014; Sendra et al., 2017). It revealed that the sunscreens containing TiO_2 or ZnO-based UV-filters produced 797.7 and 424.8 nmol ROS/mg of nanoparticles respectively, while a sunscreen free of these two mineral UV-filters, but containing only organic UV-filters, generated 59- and 31-times lower ROS respectively. No information was provided on the nature of the ENM coatings found in these products. Such high ROS production was measured during maximum solar radiation and caused toxicity in the phytoplankton population. Differential sensitivity of microalgae to sunscreens and TiO_2 ENMs can produce a change in the dynamics of phytoplankton populations and provoke undesirable ecological effects, such as giving dinoflagellates more prominence (Sendra et al., 2017). Even if the authors note that many other components in the sunscreens, including additional organic UV-filters, may also contribute to ROS production, these results raise the question of the nanoparticulate UV-filters inertness once released in the environment, i.e., what is the lifetime of the photo-passivating layer originally present at the nanoparticle surface?

Among marine organisms, the sea urchin is globally distributed in almost all depths, latitudes, temperatures, and environments in the ocean and plays a dominant role in structuring and functioning of the rocky reef ecosystem (Pinsino and Matranga, 2015). It possesses an extraordinary adaptive capability for adjusting to environmental changes, which enables us to learn about the molecular signaling pathways involved in protection, robustness and plasticity (Smith et al., 2008). Moreover, a good understanding of gene functions and developmental Gene Regulatory Networks (GRN) and a close genetic relationship to humans all together make sea urchin an attractive and emerging probing model to monitor the state of marine environmental health and to study the ENM safety/toxicity both at the cellular and molecular levels. *Paracentrotus lividus* has been nominated for inclusion on the list of alternative animal models presented by the EPAA (European Partnership for Alternative Approaches to Animal Testing) committed to pooling knowledge and resources to accelerate the development, validation and acceptance of alternative approaches to promote the replacement, reduction, and refinement (3Rs) of animal use in regulatory testing. Pioneering eco-toxicological and immuno-toxicological experimental

studies were carried out with free-living *P. lividus* by Matranga et al. (2006); Pinsino et al. (2008), Pinsino and Matranga (2015), and Migliaccio et al. (2019). Nevertheless, most of the research on the ecotoxicity of ENMs on sea urchins thus far has been focused on the embryonic development and carried out according to classical toxicological criteria: dose- and time-dependent responses, analysis of the effects on development and analysis of the tissues accumulating nano/micromaterial such as metal-oxide, metal, carbon-based particles (Fairbairn et al., 2011; Buric et al., 2015; Mesaric et al., 2015; Alijagic and Pinsino, 2017). However, precise and predictive linkages between laboratory and natural exposures (unrealistic and realistic) have not yet been established, and future work on sunscreen residues should tackle these points, considering for example direct and indirect release into the sea and the possible transformations underwent before internalisation by living organisms.

The existence of a protein corona was detected at the ENM surface upon their entering in the biological medium (Marques-Santos et al., 2018), indicating that the ENMs interact with the components constituting the biological medium, which alters both their bioavailability and toxicity. Similar interaction was also observed with commercial TiO_2 UV-filters exposed to the *P. lividus* immune cells *in vitro* (Alijagic et al., 2019; Catalano, 2020). Cellular responses seem to depend on the composition of the corona *in vivo* and *in vitro*. For example, the main constituents of the protein corona on the surface of TiO_2 NP exposed to the supernatant of cultured sea urchin immune cells were identified as a subset of adhesion and cytoskeletal proteins (Alijagic et al., 2019). Primary sea urchin immune cell cultures show how simplified cell model can inform our understanding of complex networks in intact organism on focusing on the role of extracellular protein/peptide molecules/metabolites/other signals involved in cellular communication and potential particle functionalization (Pinsino and Alijagic, 2019). The potential immune-toxicity of a few metal oxide nanoparticles, including TiO_2 was investigated *in vivo*, pointing out the potential pathway that can be involved in the interaction with immune cell (Falugi et al., 2012; Pinsino et al., 2015). For example, the biological regulatory mechanism in signal transduction underlying the effects of TiO_2 nanoparticles on *P. lividus* immune cell behavior *in vivo*, demonstrated that phagocytes interact with these particles eliciting a receptor-mediated phagocytic mechanism involving Toll-like receptor 4 (TLR4)/p38 MAPK signaling pathway without eliciting an inflammatory response or other harmful effects on biological functions (Pinsino et al., 2015). In analogy, TiO_2 nanoparticle activates suppressive mechanisms by down-regulating the expression of genes encoding immune-related and apoptotic proteins, elicits metabolic rewiring by boosting the immune cell antioxidant activity and restores homeostasis by keeping at physiological levels some key immune-related proteins, *in vitro* (Alijagic et al., 2020).

Biological Effects on Freshwater Systems

Sunscreen usage may affect the quality of freshwater systems via multiple routes. Not only recreational areas near rivers and lakes constitute a major input during the summer season but, in addition, most of the effluents produced by domestic wastewater treatment, that may contain sunscreen residues, are released to surface water. In their review on ZnO and TiO_2 inorganic UV filters, Schneider and Lim (2019) included the environmental effects on fish, coral, and algae. Among the works cited therein, biological effects of ZnO nanoparticles were measured and discussed with regard to the Zn^{2+} ionic form. However, it is worthwhile noting that these studies referred to bare ZnO nanoparticles, which do not take into account the passivating role of the surface layer generally found on mineral UV filters. As mentioned earlier, this layer is likely to favor biocompatibility and to screen any chemical reactivity related to the TiO_2 or ZnO core. This point can explain some contradictory data in the literature. For instance, Corinaldesi et al. (2018) measured a lower impact (coral bleaching) of two commercial nano-TiO_2 UV filters than bare ZnO nanoparticles on tropical stony corals, certainly because the former was made more biocompatible thanks to the surface coating. Conversely, Hanigan et al. (2018) measured abnormal embryogenesis in zebrafish more pronounced with TiO_2 than with ZnO UV filters, both extracted from a commercial sunscreen. In this latter work, one can hypothesize that the ENM surface coatings were altered during the sunscreen treatment in the organic solvent used to extract the ENMs from the matrix, as revealed by the high photo-induced reactivity of the TiO_2 ENM measured by the authors.

The effect of the surface coating on ZnO nanoparticles was studied by Yung et al. on the ecotoxic response of exposed algaes (Yung et al., 2017). The authors prepared ZnO ENMs coated with a hydrophilic or a hydrophobic layer, using silane coatings similar to what could be used in UV filter synthesis. They also studied non-coated ZnO ENMs for comparison. After 96 h of exposure at varying ZnO concentrations from 0.1 to 100 mg/L, they found that the hydrophilic and the non-coated ZnO were more potent at inhibiting growth of algal cells than the hydrophobic ZnO. It remains in question to what extent this difference resulted from a reduced exposure of the algal cells to ZnO with the hydrophobic coating, since the hydrophobic ENM surface could favor aggregation, adsorption or flotation. The authors also pointed out that the uncoated ZnO ENM generally formed larger aggregates, but was more soluble than the two coated ZnO ENMs. This was certainly due to some steric repulsion induced by the organic coating between the coated nanoparticles, favoring their dispersion, while the additional surface layer hindered the dissolution of the ZnO core.

In order to assess the ecotoxicity and transfer of nanoparticulate UV filters through the food chain, an ENM consisting of a nano-TiO_2 core coated with $Al(OH)_3$ and PDMS was aged under simple aquatic conditions and exposed at three levels: algae, microcrustacean and fish (Fouqueray et al., 2012, 2013). The aging process resulted in the loss of the hydrophobic PDMS coating, and the subsequent aqueous dispersion of the ENM-residues (Labille et al., 2010) (see aging reaction in **Figure 5**). *Pseudokirchneriella subcapitata* cultures were contaminated with the ENM-residues and a significant association of algae and TiO_2 was evidenced

(**Figure 6A**). A *Daphnia magna* dietary chronic exposure of these contaminated algae was performed. It revealed that the TiO_2 brought by food was localized in the digestive tract of the daphnia (**Figure 6B**), in an extent that was correlated to the original algae contamination (**Figure 6D**). This induced low mortality but decreased growth and reproduction which can be partly related to the modification of the digestive physiology of daphnia. The toxicity of the aged ENMs was also studied on *Danio rerio* fish as a further step of the food chain (**Figure 6C**), *via* this indirect trophic route or by direct food contamination. Indirect and low exposure *via* the trophic route did not alter fish growth (weight). No modification of energy reserves, digestive and antioxidant enzymes was measured after the 7 days of exposure to contaminated Daphnia as food. However, direct exposure to contaminated food caused a low toxicity on juvenile zebrafish *Danio rerio*. At the early life stage, premature hatching was observed, possibly due to embryo hypoxia. Moreover, digestive physiology was altered after 14 days of exposure and seemed to be an indirect target of the ENM-residues when provided by food.

RISK RELATED TO INDIRECT RELEASE AT THE PRODUCT END OF LIFE

Two scenarios were investigated at the end of life of the sunscreen, through liquid and solid wastes: cosmetic products having been rinsed- or washed off, flow to WWTP while packaging waste is subject to various waste management techniques which depend on available infrastructures and consumer habits (**Figure 1**).

Fate of Sunscreens and Associated ENMs in Solid Waste

After usage, sunscreen packaging is disposed of primarily as municipal solid waste (MSW) and ends up in landfills or incinerators, or may be recycled. While some investments are made in modern collection, separation and processing systems, and in the packaging type and material(s) to minimize the environmental footprint (Cosmetics Europe TPCA, 2018), the fate through these waste management processes of the unused lotion/cream remaining in the trashed container, and of the involved ENMs, is another potential concern.

The recycling process of plastic packaging often involves cleaning, which generates large volumes of effluent. According to the requirements for emission of wastewater into the domestic sewage, these effluents must be treated before their discharge, so that various waste constituents are removed. The pollutant load in the effluent and its effect on the environment depend on the treatment used. To date, no data dealing with the contribution of cream/lotion residues remaining in sunscreen packaging exists. However, relationships between the effluent quality and the optimization of the washing step have been pointed out (Santos et al., 2005), suggesting that some ENMs contained in the discarded products may ultimately reach domestic sewage via this pathway. Therein, their fate is driven by the wastewater treatment

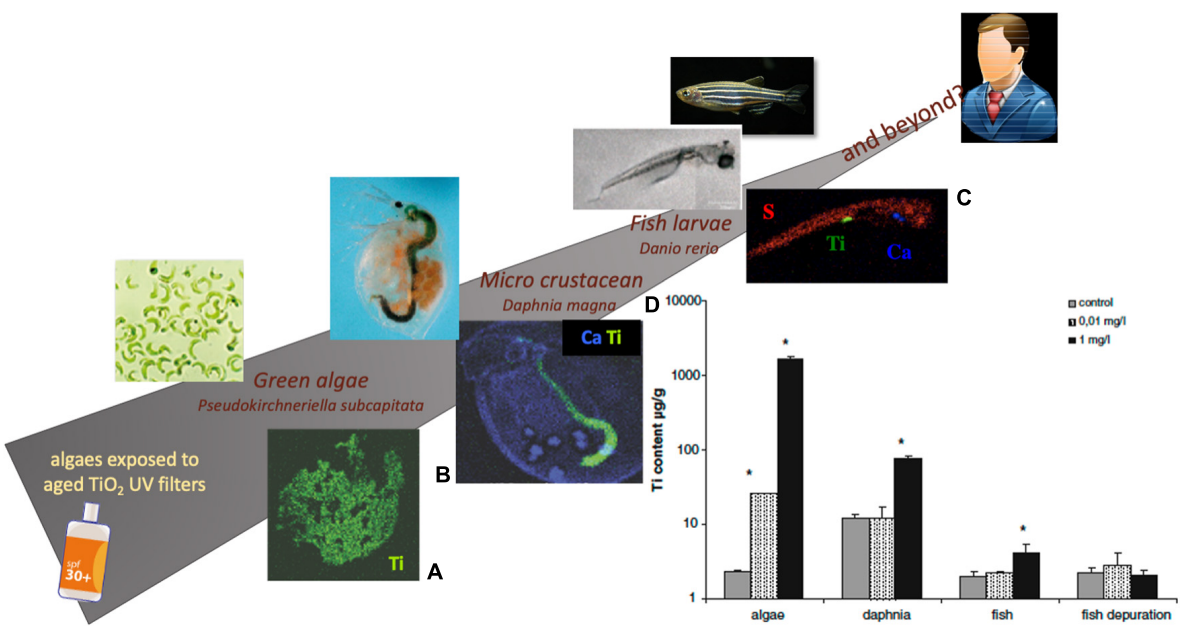

FIGURE 6 | Example of trophic transfer of an aged nano-TiO_2 UV-filter, from green algae to micro-crustacean and fish. Elemental mapping of the internalized Ti element after exposure was achieved on *P. subcapitata* **(A)**, the *D. magna* **(B)**, and the *D. rerio* larvae **(C)**, using X-ray microfluorescence. Ca and S maps were also superimposed in Daphnia and *D. rerio* in order to visualize the entire body. Ti quantification in these organisms as a function of the exposure concentration, was realized by ICP-MS analysis coupled to total digestion **(D)** (Fouqueray et al., 2012, 2013).

process as detailed in section "Fate of UV-filters in wastewater and sludge."

In a solid waste landfill, the unused lotion remaining in the trashed container may leach toward downstream reservoirs. The extent of this phenomenon depends on many factors, including the integrity of the liners and leachate collection systems, if present (Hennebert et al., 2013). Solid waste leachates typically result from rainwater that percolates through the solid wastes by gravity and mobilizes compounds, either particulate or soluble, that are able to detach/dissolve from the solid matrix. They are generally collected in settling ponds, where leachate sludge is formed by sedimentation. Further management of both the leachate and the formed sludge requires knowledge of the occurrence of pollutants in these reservoirs.

No field data is available regarding ENMs released from sunscreens in this context. The only field study which investigated nano-TiO_2 release was dedicated to a construction and demolition waste landfill (Kaegi et al., 2017). It showed that the total elemental Ti content of the leachate amounted to a few tens of μg/L and was strongly correlated with total suspended solids. The annual emission of TiO_2 particles was estimated to be 0.5 kg/y, and nanoscale TiO_2 particles to 0.5 g/y, with a predominance of spherically shaped TiO_2 particles, indicating their man-made origin from micro- and nanoscale white pigments.

The factors influencing the ENM stability in suspension in landfill leachates have complicated actions and interactions (Bolyard et al., 2013; Part et al., 2018). For example, colloidal organic matter acts mainly as a stabilizer of suspended ENMs, and salinity as an aggregating and precipitating agent. Bolyard et al. (2013) studied the fate of two hydrophobic TiO_2 and ZnO commercial UV-filters that were spiked into leachates obtained from conventional MSW landfills (Bolyard et al., 2013). The ENM coatings were triethoxycaprylylsilane on ZnO and dimethicone/methicone copolymer and aluminum hydroxide on TiO_2. They showed that both ENMs did not affect the biochemical oxidation of organic matter and did not inhibit either aerobic or anaerobic processes. Their findings support the dispersibility of hydrophobic UV-filters in leachates and revealed that the majority of them underwent aggregation, due to interaction with leachate components (such as humic acid) in which they were recovered. This suggests that nanoparticulate UV-filters would likely be recovered in the leachate sludge after sedimentation. A colloidal Ti content of 32 μg/L was detected in 2012 in a landfill leachate (Hennebert et al., 2013). In landfill leachate sludge, the total Ti concentration ranges from <5 to 35 mg/kg with a mean concentration of 23 mg/kg (n = 10) (Hennebert et al., 2017). This is up to 200 times less than representative concentration in soil, 4000 mg/kg (Lindsay, 1979) or 2400 mg/kg (Sposito, 2008), which suggests that the landfill probably acts as an ENM sink.

Regarding sunscreens, the retention of unused cream/lotion in a landfill compared to its transport by the percolating water is determined by the polarity of the formulation. Thus, one can expect that the type of emulsion, O/W or W/O, plays a determining role here, the former being preferably transported in the aqueous leachate. To our knowledge, this key point was not studied in the literature and no published experimental data is available. For this reason, an experimental approach is briefly proposed here (**Figure 7**), to investigate the effect of the formulation type on the ability of two different nano-TiO_2 UV-filters to be removed from the sunscreen container by a landfill leachate. O/W and W/O sunscreens are formulated in the laboratory with 5% nano-TiO_2, respectively hydrophilic (i.e., TiO_2/SiO_2) or hydrophobic (TiO_2/Al_2O_3/stearic acid). These UV filters were characterized elsewhere (Catalano et al., 2020; Slomberg et al., 2020). A real solid waste leachate is recovered from the settling pond of a municipal landfill. A 1L sample is added to a translucent high-density polyethylene (HDPE) container and 2 g of sunscreen is applied to the inside of the container lid. The container lid is gently placed on the bottle and the ensemble is agitated end-over-end for 1 day (**Figure 7B**). After this time, the lid is removed and the leachate is allowed to settle. Samples are taken from the liquid over time. Following this approach, contrasted scenarios could be revealed, depending on the type of sunscreen formulation used. The O/W emulsion with hydrophilic TiO_2 (i.e., TiO_2/SiO_2) would likely show complete leaching from the container lid and transport within the leachate, while most of the W/O emulsion and the hydrophobic TiO_2 (TiO_2/Al_2O_3/stearic acid) it contains, would remain in the container (**Figures 7C,D**). Hydrophilic nano-TiO_2 entering the leachate would likely be recovered in the leachate sludge after sedimentation since aggregation and settling are likely to occur in the leachate. The lipophilic formulation would be less mobile at the product end-of-life and thus hydrophobic TiO_2 UV-filters and W/O sunscreens should be preferred from a "landfilling" point of view.

Incineration is a common process that enables both reduction of the volume of waste and its conversion into energy at the same time. A recent review concluded that incineration of MSW and sewage sludge can concentrate metals from ENMs in the incineration slags or fly ashes. Depending on the incineration method or material (e.g., MSW, sewage sludge, etc.), the mineralogical phase of the solid residues, their associated metal content and the morphology of the inclusions can all be highly variable (Part et al., 2018). For example, the emission behavior of nano-$BaSO_4$ in a MSW incineration plant was studied (roller grate furnace, boiler, dry exhaust gas purification unit, fabric filter, and selective catalytic reduction). It revealed that almost 87% of the recovered ENMs were found in the bottom ash, 8.5% in boiler ash, and 4.5% in residue from fabric filter. The separation efficiency of the fabric filter for the barium sulfate particles was more than 99%. The authors also pointed out that the tested ENMs tended to sinter at temperatures lower than bulk $BaSO_4$ and exhibited a strong tendency to adhere to fly ash particles after combustion. Indeed, laboratory studies have shown that fusing and sintering usually makes the ENMs non separable from the solid matrix of the ashes (Le Bihan et al., 2017). The residues from waste incineration potentially containing concentrated ENMs will either be landfilled or used for recycling materials (e.g., construction materials). Although there is no data available regarding sunscreens specifically, we can assume that the same process of concentration will occur with the nanoparticulate

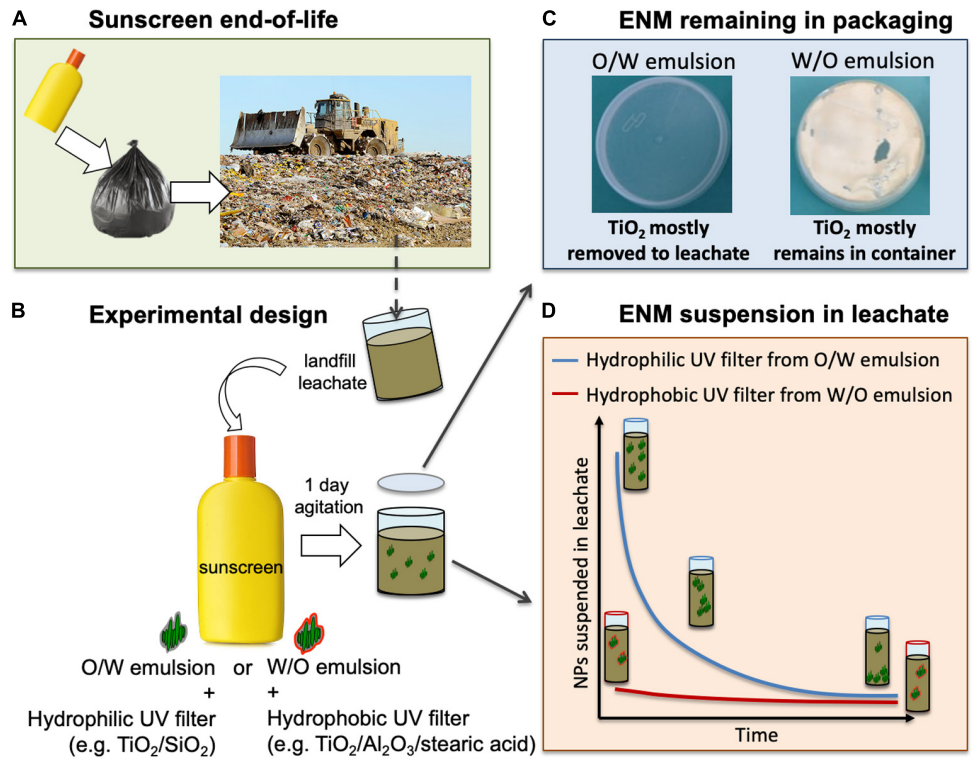

FIGURE 7 | Experimental approach proposed to mimic leaching in solid waste disposal at end of life **(A)**. A sunscreen product in packaging is agitated in a real landfill leachate over 1 day **(B)**. Then, the sunscreen remaining in the packaging is quantified **(C)** and the ENM suspended in the leachate are quantified over time **(D)**.

UV-filters left in the packaging. During incineration, wastes are oxidized at high operating temperatures of 850–1100°C (Part et al., 2018). While the organic components of sunscreens and UV-filters are totally calcined to the CO_2 form, the minerals constituting the UV-filters core (TiO_2, ZnO) or their coatings (e.g., SiO_2, Al_2O_3) may have different fates. Titanium dioxide occurs as two important polymorphs, the stable rutile and metastable anatase. Anatase transforms irreversibly to rutile at elevated temperatures, between 550 and about 1000°C (Hanaor and Sorrell, 2010), which suggests that the rutile form that is mainly used in UV-filters will not be altered by incineration (Mueller et al., 2013). Nevertheless, the other constituents of the matrix can play a role in determining the final form of the ENM after incineration. Massari et al. (2014) investigated in lab the behavior of TiO_2 ENMs during incineration at 950°C of solid paint waste containing these particles. They did not observe any release of TiO_2 ENM into the atmosphere, but the Ti underwent physicochemical transformation during the incineration that resulted in a calcium titanate product immobilized in a glass matrix and recovered in the ashes (Massari et al., 2014). Considering the fate of nano-ZnO during incineration, when under reducing conditions, elemental Zn starts to evaporate at a temperature of 905°C. It is assumed to recondensate in the flue gas stream as soon as it cools, but unlikely to return into its nanoscale form (Mueller et al., 2013). Under oxidizing conditions ZnO remains in a solid state at temperatures up to 1500°C. Thus, similarly to the fate of TiO_2, it is likely that this ENM will accumulate in the bottom ash as a fused-in component and will ultimately end up landfilled (Mueller et al., 2013; Part et al., 2018). Aluminum (hydr)oxides are used as a coating of TiO_2 or ZnO UV-filter. Aluminum hydroxides are the precursors of metastable aluminas. Several polymorphs exist that have a thermal stability increasing with decreasing degree of hydration (Digne et al., 2002). This means that alumina is the stable form recovered after incineration. Finally, under heat treatment, the amorphous silica used as a nanoparticle coating is expected to undergo densification to the glass form due to condensation of Si-OH groups into Si-O-Si network bridging units (Kamitsos et al., 1993). It should be noted that these expected respective fates based on the existing scientific literature are only considered individually and do not take into account any matrix effect or pre-existing associations with other phases. Nevertheless, no significant alteration of these mineral constituents of UV-filter is expected from the heat treatment underwent during incineration, so the nanoparticulate forms are expected to remain in the resulting ashes.

Significant knowledge gaps still remain on the fate of ENMs from solid waste disposal that limit our current ability to develop appropriate end-of-life management strategies. There is a need for continued research in this area. No work has been conducted to quantify ENMs present in discarded materials, and an understanding of ENM release from consumer products

under conditions representative of those found in relevant waste management process is needed (Part et al., 2018).

Fate of UV-Filters in Wastewater and Sludge

The everyday use of sunscreens results in draining the product with wash water toward sewage treatment plants. The fate of the nanomaterials determines the exposure of different downstream environmental compartments. Two complementary scenarios can be considered: nanomaterials ending up in the sewage sludge may be spread as fertilizing material in agriculture, while those remaining suspended in the treated water would be directly released to surface waters (**Figure 1**). The respective impacts on soil and river ecosystems thus depend on the WWTP efficiency for ENM removal. A partition coefficient of ENMs from water to the WWTP sludge or landfill can be used by quantifying the substance in the respective compartments in order to estimate the respective fates (Sun et al., 2014; Gottschalk et al., 2015).

An assessment of the fate, behavior and environmental risk associated with sunscreens containing TiO_2 ENMs was studied in a UK field scenario (Johnson et al., 2011). It revealed a decrease of concentration from 30 to 3.2 μg/L of TiO_2 particles below 0.45 μm in size from the influent to the effluent of a treatment plant, suggesting that the majority of the ENMs ends up in the activated sludge. Some topical sunscreen constituents were detected in untreated wastewater, treated wastewater, and biosolids (Balmer et al., 2005). The organic compounds detected in these studies were UV-filter compounds such as 4-MBC (4-methylbenzylidene camphor) and OC (octocrylene), which generally biodegrade slowly and can bioaccumulate. Although nano-TiO_2 is unlikely to behave exactly the same way as the other sunscreen components, its low solubility suggests a probable persistence of this substance in the receptacle compartments. However, no studies to date have documented the occurrence of nano-TiO_2 specifically from sunscreens in wastewater or natural water bodies receiving wastewater (U.S. EPA, 2010).

The total titanium concentration in WWTP sludge results from the sum of multiple possible sources. It was analyzed in 13 sludge samples from different regions of France. and was found to be present in half of the sludges studied (7 out of 13 raw sludges and 4 out of 9 digested sludges), revealing an order of magnitude of 50–400 mg/kg with a mean concentration of 170 mg/kg (Hennebert et al., 2017). The Ti speciation was investigated using electron microscope coupled to EDX. Distinct phases bearing Ti, such as areas corresponding to TiO_2 NP aggregates, could not be evidenced. In the raw sludge, Ti was mostly associated with major elements such as Al, Ca, Fe, K, Mg, Na, P, S, Si, and Cl. The Ti concentration ranged between 1 and 2% excluding C and O elements. Ti was thus part of the organo-mineral matrix constituting the sludge, but it was not homogenously distributed at this scale of observation as it was not identified in all the areas analyzed for a given sludge. Its origin could be anthropogenic, in relation with white paints, toothpastes, food additives, sunscreens and façade run-offs, or pedogenic. Both origins could not be discriminated, as well as the nano or non-nano forms (Hennebert et al., 2017). Distinguishing the different origins of TiO_2 in such complex matrix indeed remains an analytical challenge. However, by comparing nano-TiO_2 characteristics originating from a natural soil and from an anthropic sludge, it was shown that the anthropogenic TiO_2 form homo and heteroaggregates of simpler structure, richer in organic matter (Pradas del Real et al., 2018). Thus, studying the morphology of TiO_2 particles and their status in the mineral–organic assemblages may provide some insights into their natural or anthropic origin.

The accumulation of ENMs in activated sludge may also eventually affect the bacterial activity in the sludge, and in turn the epuratory effect carried by the local fauna in the water treatment plant. Only considering the effects of ENMs on cell viability and growth of microorganisms does not completely assess their potential environmental risks *via* the activated sludge. To comprehensively evaluate the potential effects of ENMs on the microorganism functionality, the effects on processes such as nitrogen removal ability and anaerobic digestion should be investigated. The effect of metal oxide nanoparticles, including nano-TiO_2, nano-Al_2O_3, nano-SiO_2 and nano-ZnO, on anaerobic digestion was investigated by fermentation experiments using waste activated sludge as the substrates (Mu et al., 2011). At doses up to 150 milligram per gram total suspended solids (mg/g-TSS), no inhibitory effect was observed, except with ZnO showing a dose – effect relation. The released Zn^{2+} from nano-ZnO was an important reason for its inhibitory effect on methane generation. Higher dosages of nano-ZnO even inhibited the steps of sludge hydrolysis, acidification and methanation. Biological nitrogen removal was also shown to be affected by TiO_2 NPs (Zheng et al., 2011). A denitrifier bacteria, isolated from the activated sludge was used to evaluate the influences of TiO_2 NPs on its nitrogen removal ability (Li et al., 2016). TiO_2 had antibacterial effects from 5 to 50 mg/L due to ROS production, and the microbial diversity of activated sludge was substantially reduced after 7 days of exposure at the highest TiO_2 NP concentration tested, of 50 mg/L. Such effects should be also considered in further lifecycle stages, notably in the context of sludge spreading on soils as fertilizer (see also section "Effects on terrestrial ecosystem").

Mobility of UV-Filters in Soil Porous Media

Nanoparticulate UV-filters in topical sunscreens could end up in the sludge produced from wastewater treatment plants via domestic sewage. The disposal of this sludge on land likely represents the primary pathway by which ENMs from sunscreens could enter the soil. The Ti occurrence in sludge was calculated at 305 mg/kg dry weight. Thus, using sludge as a fertilizer at the recommended maximal agricultural application rate would result in a predicted deposition of up to 250 mg/m^2 of Ti to soil surfaces (Johnson et al., 2011). The modeled predicted environmental concentration of nano-TiO_2 from cosmetics in sludge-treated soils is 0.1–3.1 mg kg^{-1}, while that for ZnO is close to zero (<0.03 μg/kg^{-1})

(Sun et al., 2014; Gottschalk et al., 2015). Besides, direct discharge into recreational waters accounts for a significant increase in TiO_2 ENMs suspended in water, which may end up in porous systems like sediments, soils or aquifers. The TiO_2 ENMs suspended in percolating water can undergo sedimentation (Gondikas et al., 2018) and/or filtration through these porous media, depending on the physico-chemical parameters of the medium.

Conventionally, the study of pollutant transfer through porous media, nanoparticulate or not, is based on experiments using a percolation column filled with the porous medium and connected to a quantitative monitoring of the pollutant in the outlet, using in-line analytical techniques (Spectrometry UV/fluorescence, conductivity) or offline after collection (atomic absorption spectrometry, ICP-MS). Mainly pure or mineral-coated quartz sand (Joo et al., 2009; Solovitch et al., 2010), and limestone (Esfandyari Bayat et al., 2015) are used as porous media, and most of the studies that address the transfer of TiO_2 or ZnO ENMs in porous media deal with bare NPs. Only a few of them consider the role of particle coating, although it obviously alters the particle surface properties, by screening or increasing the surface charge or changing the surface area for instance, and the interactions with the soil minerals accordingly. This point was clearly demonstrated by comparing the transfer of bare TiO_2 or ZnO ENMs and their coated counterparts, either with carboxymethyl cellulose (CMC) (Joo et al., 2009; Kanel and Al-Abed, 2011) or partially crosslinked polyacrylic acid (PAA) (Petosa et al., 2012), in a sand-packed column. The conclusions drawn from these studies were concordant: while rapid aggregation was observed with the uncoated ENMs, even at low ionic strength, the coated TiO_2 ENMs were significantly more stable in a large range of ionic strengths (up to 100–200 mM $NaNO_3$) (Petosa et al., 2012), which was assigned to the shift of the point of zero charge (PZC) toward lower pH values (which increased the negative charge at the pH of the experiments) as well as to the steric barrier in the case of the adsorbed CMC layer. Even if similar interfacial reactions exist in the case of CMC-coated ZnO ENMs, the Zn mobility in the column followed a more complex trend that was correlated to the ENM solubility, which was also dependent of pH (Kanel and Al-Abed, 2011). The zeta potential measurement of the particles and of the porous system in the various media tested can be considered as determining in the affinity and thus the retention of nanoparticles with respect to the porous medium collector, and should allow a better understanding. Subsequently, uncoated TiO_2 NPs showed high retention on the sand whereas their coated counterparts were much more mobile in the same conditions, thus highlighting the importance of considering not only the nature of the core of the ENMs but also the composition of their shell (if relevant) in contamination assessment.

TiO_2 ENMs used in sunscreens fall into this category of surface-modified particles that will certainly behave differently from bare TiO_2 NPs of the same crystallinity (rutile) and primary size (50–100 nm), particularly in terms of surface charge and surface hydro/lipophilicity (see section "Biological effects on marine organisms"). The question was raised by Englehart et al. (2016) who specifically investigated the influence of a polymer additive (TEGO carbomer) used in commercial sunscreens on the transport of a TiO_2 (78% anatase, 14% rutile, and 8% amorphous) suspension through a quartz sand column. TEGO is an acrylate/C10-C30 alkyl acrylate crosspolymer designed for emulsion thickening, close to the PAA investigated elsewhere (Petosa et al., 2012). The results show the same trends, with a net tendency to aggregation and retention in the porous medium for uncoated TiO_2, enhanced with increasing ionic strength (from deionized water to 3 mM NaCl) whereas the addition of TEGO carbomer decreased the PZC, stabilized the suspension, and resulted in greater recovery of the particles eluted from the column. Again, enhancement of TiO_2 mobility was demonstrated, with the risk of larger pollution dispersion in the environment with a hydrophilic stabilizing agent compared to uncoated TiO_2 ENMs which are usually considered in most studies.

Parameters of the porous medium such as the nature (Joo et al., 2009), grain size and heterogeneity (Lv et al., 2016) were also shown to play a significant role in the behavior of TiO_2 ENM transfer rate. Environmentally relevant Fe and Al hydroxide coated quartz sand resulted in delayed breakthrough curves compared with pure quartz sand for CMC-coated TiO_2 ENMs (Joo et al., 2009). These observations were assigned to an increased surface of the metal hydroxide coated collector, to the possible formation of chelates between CMC and the adsorbed metal hydroxides, and to the reduction of the net negative charge of the collector. Retention of TiO_2 ENMs was also increased with decreasing the sand grain size while heterogeneity introduced in the column by packing it with two types of sand (coarse and fine) revealed the occurrence of preferential (faster) flow pathways that induced faster and greater transport than expected in the homogeneous sand bed. The environmental significance of such finding is important, particularly in fracture-containing rocks, as confirmed by the study reported by Ollivier et al. (2018): contrary to the usual packed sand bed, the column was composed of a drill core of a fractured Schist rock containing quartz, feldspar, phyllosilicates and iron oxides with a low porosity (6% compared with 30–50% in the case of packed sand beds). With this configuration, and despite interaction energy profiles favorable to particle retention, which was observed to occur specifically on the minerals along the fractures, TiO_2 ENMs were partially transferred through the rock.

Other investigations related to the flow-through solutions (chemistry, pH, ionic strength, and velocity) were made for the fate of bare TiO_2 NPs. They basically show that poorer stability leading to greater deposition occurs with divalent cations [Ca^{2+} (Joo et al., 2009; Petosa et al., 2012) or Mg^{2+} (Esfandyari Bayat et al., 2015)] compared with monovalent Na^+ at identical ionic strength. The same conclusions can be drawn with a decrease in pH and/or an increase in ionic strength (Joo et al., 2009; Solovitch et al., 2010; Labille et al., 2012; Petosa et al., 2012; Esfandyari Bayat et al., 2015). Naturally occurring colloids have also a significant role in increasing the transport of TiO_2 through a porous medium when unfavorable attachment is obeyed (Cai et al., 2016).

Finally, Chowdhury et al. (2011) raised the mechanisms of straining and blocking to explain their unexpected results where they obtained the greatest retention of TiO_2 NPs under electrostatically unfavorable deposition and significant elution from the column under favorable conditions. They also hypothesized the possible break-up of the attached aggregates via hydrodynamic forces when high flow velocity is applied, supported by the fact that the size of the eluted particles was smaller than that in the influent (aggregated) suspension. Hence, partial release of the previously deposited particles is susceptible to happen under flow increase (Godinez and Darnault, 2011), or by reducing the electrolyte concentration (or ionic strength) as demonstrated by Godinez et al. (2013).

Field experiments of transfer can also be proposed via tracer test experiments. These experiments in real environmental conditions are usually more difficult to carry out and to interpret due to additional features of the solid/liquid system, such as complexity of the medium, fracturation or inhomogeneity of the rock that induce preferential pathways. However, these large-scale experiments are needed to confirm (or not) the labscale column experiments (Cary et al., 2015).

Effects on Terrestrial Ecosystem

The practice of activated sludge or "biosolid" spreading is a source of contamination of agricultural soils from which ENMs may enter the food webs or cause direct and indirect toxicity to plants, microbial communities, or other soil organisms. This was evidenced on bacterial communities of grassland soils exposed to different doses of TiO_2 or ZnO nanoparticles in microcosms over 60 days (Ge et al., 2011). Both nanoparticles reduced microbial biomass and diversity and altered the composition of the soil bacterial community, with a stronger effect with nano-ZnO than with nano-TiO_2 at the same exposure concentration (0.5 mg g^{-1} soil). The stronger impact of ZnO ENM on soil due to its higher solubility was also evidenced in a study where biosolids produced from a pilot wastewater treatment plant were used to amend a soil with controlled and relevant ENM loads (Chen et al., 2015). The effects of Ag, ZnO, and TiO_2 ENMs added to the soil via the biosolids were monitored via toxicogenomic responses over a 6 months of exposure. In response to ENM exposure, many of the identified biological pathways, gene ontologies, and individual genes were associated with nitrogen metabolism, nodulation, metal homeostasis, and stress responses. Results showed inhibition of nodulation with ENM treatment primarily due to phytotoxicity likely caused by enhanced bioavailability of Zn ions. Very few data are available regarding the effects of TiO_2 or ZnO ENMs on soil via biosolid amendment and none of the experiments thus far had been carried out with a real UV-filter. The potential role of the ENM coating remains mostly unknown in such a system. With this in mind, an experimental approach is proposed here to mimic in the lab a realistic scenario where a sunscreen containing nano-TiO_2 is released from a domestic wash water to the wastewater treatment plant, ending up in the biosolids that are then used for cultivated soil amendment (**Figure 8**). Briefly, a sunscreen containing a known amount of nano-TiO_2 (e.g., 5%) can be aged in synthetic shower water (mineral water, 20 mg/L solid soap, 40°C, 5 min.) at 314 mg/L (**Figure 8A**). This nano-TiO_2 concentration is calculated using the average amount of sunscreen product consumed when applied to an entire adult body (15.7 g, Ficheux et al., 2016) and the average volume of water consumed per shower. Chronic injections of this freshly prepared wash water should then be added into an aerobic bioreactor over 1 month to achieve a final nano-TiO_2 concentration of ∼70–360 mg nano-TiO_2/kg in the dried biosolids (**Figure 8B**). This concentration corresponds to that estimated in biosolids (Lazareva and Keller, 2014; Gottschalk et al., 2015). Finally, plants can be cultured in a real soil amended with these biosolids (1–10 mg nano-TiO_2/kg amended soil) (**Figure 8C**) (Sun et al., 2014). A fast-growing, agriculturally relevant plant is recommended (e.g., rapeseed *Brassica napus*), so that the experiment takes a reasonable time (e.g., 30 days). A control experiment is required in parallel using the same sunscreen formulated without the nano-TiO_2 UV-filter. Biological effects due to the presence of the nano-TiO_2 UV-filter can be investigated through direct phytotoxic effects on plant growth, as well as indirect effects on soil microbial communities and plant defense systems.

In an exhaustive literature review on the toxicity of manufactured ZnO nanoparticles to ecological receptors such as bacteria, plants, and terrestrial, invertebrates and vertebrates (Ma et al., 2013), Ma et al. (2013) commented that more than 50% of the studies reviewed suggest ZnO NP dissolution to ionic zinc contributes at least partially, if not completely, to the toxicity observed. A second key property raised by the authors is the photoreactivity of the ZnO ENM, which can cause photo-induced toxicity. In spite of an abundant literature existing on the ecotoxic effects of ZnO ENM, there is little available data regarding real nano-ZnO UV filters, and the effects of the ENM coating or formulation on these two key properties determining the ecotoxicity are mostly unknown. The effect of a nano-ZnO UV filter extracted from a sunscreen was studied on *E. coli* (Baek et al., 2017). The authors investigated the antibacterial and toxicity pathways and compared the sunscreen extract to an industrial ZnO ENM reference. At very high exposure dosage (80 – 1280 mg/L), they could observe a growth inhibition rate proportional to the ZnO concentration and less pronounced with the sunscreen extract as compared to the industrial ZnO ENM. However, we can not conclude here on a possible protective effect of the ENM coating used in sunscreen, because the authors hypothesized that the ENM size could be a determining parameter in the toxicity pathway, as the sunscreen-extracted ENM was larger in size (225 nm) than the industrial reference (110 nm).

A research consortium has also been devoted to studying the effects of a nano-TiO_2-based UV filter on different soil organism endpoints. The ENM case study consisted of a TiO_2 nanoparticulate core originally coated with $Al(OH)_3$ and polydimethylsiloxane (PDMS) layers and that was first aged under aqueous conditions. The resulting aged nano-TiO_2 had lost most of its PDMS coating and in the end displayed a hydrophilic $Al(OH)_3$ surface chemistry favoring aqueous dispersion and bio accessibility (**Figure 5**). To determine the mutagenic potential of the aged nano-TiO_2 on bacteria, the bacterial reverse mutation test (Ames test) was modified and

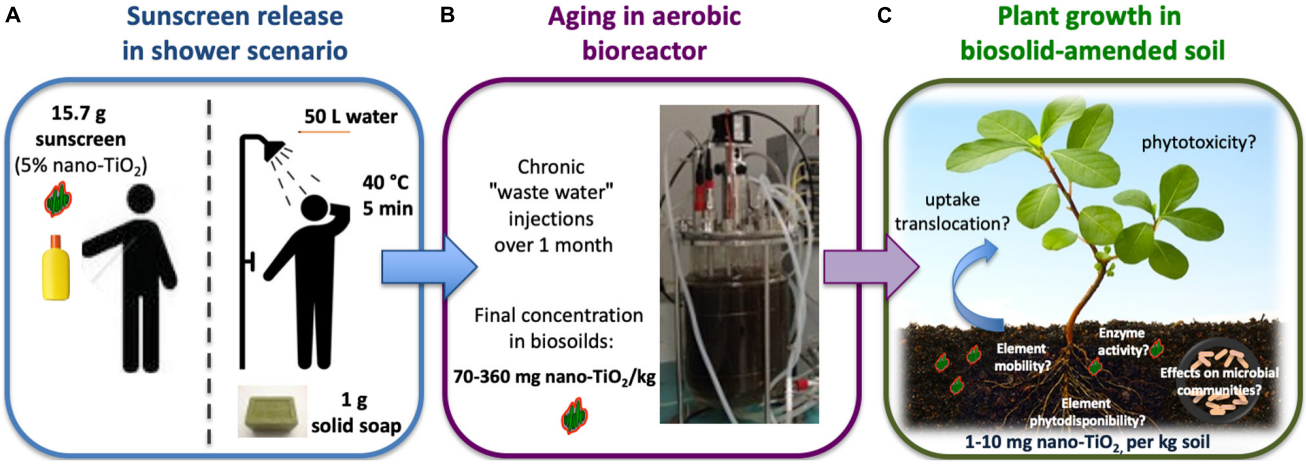

FIGURE 8 | Experimental approach to mimic **(A)** sunscreen and nano-TiO_2 release in a shower scenario, **(B)** subsequent aging in aerobic waste water treatment, and **(C)** end-of-life in biosolid-amended soil.

used with *Salmonella typhimurium* strains (Jomini et al., 2012). A relatively high exposure concentration from 1 to 100 mg/L was used. Mutagenicity was evidenced and more pronounced on a mutant strain, which suggested an oxidative stress-mediated mechanism. At lower exposure concentrations, *Escherichia coli* was used to study the effects on cell physiology (Santaella et al., 2014). The aged nano-TiO_2 first appeared safe, as it had no effect on the viability of *E. coli* nor on the mutant impaired in oxidative stress, did not induce mutagenesis and did not impair the integrity of membrane lipids. Nevertheless, when pre-exposed to the aged nano-TiO_2 under low intensity UV light, cells turned out to be more sensitive to cadmium, a priority pollutant widely disseminated in soils and surface waters. This behavior was not due to a Trojan Horse effect but was certainly related to the ROS production by the aged nano-TiO_2 under UV exposure. These results highlighted how the possible effects of UV-filters should be studied not only individually, but also in combination with other environmental pollutants, in order to deal with a possible cocktail effect.

In order to evaluate the behavior, uptake and ecotoxicity of the aged nano-TiO_2 on earthworms, *Eisenia fetida* worms were exposed to ENM suspensions at 0.1, 1, and 10 mg/L for 24 h (Bigorgne et al., 2011). This constituted a favored route of exposure to worms with regard to the more relevant soil pathway. Only worms exposed at the highest concentration showed detectable bioaccumulation of titanium, increasing expression of metallothionein and superoxide dismutase mRNA and induction of apoptotic activity. No cytotoxicity could be observed on coelomocytes, but a significant decrease of phagocytosis was observed starting from 0.1 mg/L. These results suggested that under such condition, bioaccumulation and ROS production could be responsible for the alteration of the antioxidant system in worms. The soil and food routes of exposure were also studied on the earthworm *Lumbricus terrestris* at concentrations ranging from 0 to 100 mg kg^{-1} (Lapied et al., 2011). Note that the modeled predicted concentration of nano-TiO_2 in sludge-treated soil ranges at lower level 0.1 to 3.1 mg kg^{-1} soil (Gottschalk et al., 2015). No mortality was observed, but an increased apoptotic frequency in cuticule, intestinal epithelium and chloragogenous tissue was measured. The aged nano-TiO_2 did not cross the intestinal epithelium/chloragogenous matrix barrier to enter the coelomic liquid, or the cuticule barrier to reach the muscular layers, so no bioaccumulation could be evidenced under these conditions of exposure.

Finally, the aged nano-TiO_2 was also tested on the plant model *Vicia faba*, exposed via a liquid medium during 48 h (Foltete et al., 2011). While, no change compared to controls could be observed on plant growth, photosystem II maximum quantum yield, genotoxicity or phytochelatins levels, the measurement of Ti and Al concentrations in roots revealed ENM internalization in superficial root tissues. This suggested that eventual long-term effects on plants may occur. Up-to-date analytical tools have been developed that enable to measure chemical mapping and speciation in complex samples in order to give insights on the internalization, localization/interactions of ENM in/with plants (Castillo-Michel et al., 2017).

REGULATIONS REGARDING NANOPARTICLES IN COSMETICS AND OTHER SUBSTANCES

Depending on countries, sun care products are regulated as cosmetics or as Over-The-Counter (OTC) drugs (Risk and Policy Analysts Limited, 2004). OTC means they are strictly regulated and require pre-market registration. Regardless of how they are regulated, all of these sunscreen regulations have analogies. Each country has a pre-approved list of permitted UV-filters, an accepted method of running efficacy by SPF determination, and regulated labels (Steinberg, 2007). United States, Europe, Australia, Canada, and South Korea have approved the use of TiO_2 as a UV-filter in sunscreens

with a maximum concentration of 25% (U.S. EPA, 2010). In the USA, the Food and Drug Administration regulation on sunscreens (FDA, 2000, 2014) does not distinguish between conventional and nanoscale TiO_2, between anatase and rutile, or between coated and uncoated particles. However it is important to note that some states have enforced additional requirements, such as California warning on TiO_2 of respirable size (OEHHA, 2020), or Hawaii and Florida banning oxybenzone and octinoxate (Hawaii State Legislature, 2018). Recently, in February 2019, the FDA rule was updated to address concerns regarding safety and efficacy of active ingredients, testing methods, dosage and labeling requirements (FDA, 2019). This rule describes the conditions under which the OTC sunscreen monograph products are generally recognized as safe and effective and not misbranded. An important point is the new status given to organic UV filters. Considering that current knowledge does not contain sufficient data to support the use of the UV filters cinoxate, dioxybenzone, ensulizole, homosalate, meradimate, octinoxate, octisalate, octocrylene, padimate O, sulisobenzone, oxybenzone, and avobenzone as safe and effective, they were listed as Category III. Additional information on these ingredients are requested so that FDA can evaluate their status. Indeed, both an increased sunscreen consumption and exposure and an evolving information about the potential risks associated with these products have led FDA to recommend such additional needs. The rapid internalization of some organic filters by the human body after sunscreen usage, that was recently evidenced (Matta et al., 2019, 2020), certainly constitutes a major basis for this recommendation. As for mineral UV filters, the FDA considers that sufficient safety data on both zinc oxide and titanium dioxide were produced to support the proposal that sunscreen products containing these ingredients (at concentrations up to 25%) would be safe and effective (Category I). There is no doubt that such new recommendation will soon increase the proportion of mineral-based products on the US sunscreen market.

In Europe, while the Cosmetics Regulation. 1223/2009 (Eur-Lex, 2009) allows 24 organic molecules and two mineral particles as UV filters, it also requires that manufacturers indicate the presence of nanomaterials in the list of cosmetics ingredients on the product packaging. Annexe VI of the present cosmetics regulation lists the four nanomaterials substances that are expressly authorized as UV-filters in cosmetics in 2018: nano-zinc oxide (ZnO), nano-titanium dioxide (TiO_2), nano-TBPT (tris-biphenyl triazine), and nano-MBBT (methylene bis-benzotriazolyl tetramethylbutylphenol). It should be noted that ZnO was approved late by the European Cosmetic Regulation, which only included it since 2016 in Annex VI, as some interrogations were remaining regarding the safety of its nano-form (SCCS, 2012). Moreover, since January 2020, the regulatory requirements under EU REACH regulation for substances in nanoform produced or imported over 1 t/y, have to be completed as a dossier that addresses new specific questions such hazard fate and exposure, in the aim of minimizing the associated risk (Eur-Lex, 2018).

CONCLUSION

In this review, we discussed the environmental risk associated with nanomaterials used as UV-filters in sunscreen. All stages of the product lifecycle, from its manufacture to its end of life, through the consumer use were considered in order to discuss the state of the art on both the exposure and hazard of these substances in the respective environmental receptacles. This included sunscreen design regarding both the safest UV-filter selection and the formulation optimization, the aquatic environment and living organisms directly exposed via bathing activity, or indirectly exposed via domestic wastewater pathways; and the product disposal at its end of life. From these considerations, some recommendations can be proposed for a safe-by-design approach that could be helpful not only to manufacturers and regulators, but also to consumers in their decision criteria to select a product.

Nanoparticulate UV-filters based on a TiO_2 core were the particular focus of this review as they constitute a main active ingredient of mineral sunscreens. However, ZnO was also considered here as an alternative mineral UV-filter when scientific literature exists. Despite an abundance of scientific literature on the risk associated with bare TiO_2 nanomaterials, a main output of this review is that such bare TiO_2 nanomaterials are not representative candidates for the risk evaluation of TiO_2-based UV-filters. Indeed, the external coating applied industrially on the UV-filters gives them specific surface properties that largely determine both fate, exposure and hazard of the nanomaterial, often independently of the TiO_2 core. The same recommendation stands with ZnO UV-filters that generally come with a man-made coating. The nature and lifetime within aging of the nanomaterial coating are thus key variables to account for in evaluating the associated risk. At present, knowledge gaps remain regarding the safety of nanomaterials used in sunscreen, as very few previous studies have been devoted to real sunscreen formulations. Moreover, systematic studies comparing different nanomaterials in one given formulation to highlight the effects of the nanoparticulate UV-filters in sunscreen safety are still lacking.

Guidelines in developing a safe-by-design sunscreen may differ according to the lifecycle stage considered, so that in a global consideration, each respective point should be integrated in order to minimize the overall risk by anticipation. Moreover, they should also be put in perspective with the respective knowledge about organic UV-filters safety in the same stages, since both mineral and organic UV-filter types are often balanced for selection criteria.

Consumer's Health

Even if the effect of the UV-filter on a consumer's health via topical application was not explored in this review, any recommendation for a safer product should certainly consider the propensity to penetrate through the skin barrier, as this feature may largely determine the eventual exposure to the substance. Here, nanoparticulate and organic UV-filters have very contrasted characteristics. While a safe skin is supposed to remain mostly impermeable to nanoparticles (Poland et al., 2013), it was

recently demonstrated that many organic UV-filters are able to rapidly reach the consumer's blood after passing the skin barrier (Matta et al., 2019, 2020). The UV-filter solubility is definitely a key characteristic here, as particulate substances of low solubility (e.g., TiO_2, MBBT nano) should be less likely to pass the skin barrier than dissolved molecules (e.g., avobenzone, octocrylene. . .). Meanwhile, particulate substances of high solubility such as ZnO nanoparticles are also prone to dissolve into ionic species that may easily pass the skin barrier (Gulson et al., 2010, 2012, 2015; Mohammed et al., 2019). Nevertheless, these are physiological ions that are not deemed to be dangerous and do not appear to cause any local toxicity at physiological concentration (Mohammed et al., 2019). Overall, any tendency to skin penetration should logically be inversely correlated to the environmental release, meaning that these two aspects should be weighed distinctly in a safe by design effort.

Environmental Release

The propensity of a sunscreen to be washed off the skin logically determines how much is being released directly into aquatic environment, particularly through recreational activities, vs. how much will end up in domestic wastewater treatment plant via daily cleansing. Although very few data are available regarding the retention factor of sunscreens on skin, the "water resistant" label found on some products obeys rules that indirectly suggest a high retention of the UV-filters on the skin (Cosmetics Europe TPCA, 2005). The ingredients of the sun care product can control the water resistance by creating a hydrophobic structure that is unfavorable to being washed off. Water in oil emulsions would be considered as the best choice in this aim (Leroy and Deschamps, 1986).

Environmental Impacts on Aquatic Systems

Whether the UV-filters released in aquatic environments end up suspended in the water column, sedimented, or floating at the surface determines the type of environmental media and living organisms most impacted by these substances. Colloidal transport implies a lower concentration due to dilution and a possible exposure to planktonic organisms. Sedimentation following aggregation favors *in situ* accumulation and implies a higher local concentration and exposure to benthic organisms. Finally, flotation of the most hydrophobic residues at the water surface may favor locally and temporary high UV-filter concentration, depending on weather and photodegradation. For nanoparticulate UV-filters, the preferential fate scenario and hazards are mostly determined by the nature and lifetime of the external coating. For example, aqueous dispersion can be limited with a hydrophobic feature on one hand, while hazards may be minimized with biocompatible and resistant coating features on the other hand. Moreover, the UV-filter photostability is an additional characteristic for which a compromise must be found. While we seek to maximize it on the skin for longer term sun protection, it also determines the substance recalcitrance in the environment. Organic molecules rapidly photodegraded and insoluble nanoparticles give antagonist features here.

Environmental Effects Through the Product End of Life

The fate and effects of UV-filters at the end of life of sunscreen products are probably the least documented points of their lifecycle. They may follow different routes, including, e.g., landfilling and activated sludge spreading on soil, beyond which the possible transfer to downstream environmental systems is mostly unknown. Nevertheless, similar key questions as in aquatic systems shall be considered here, dealing with the formulation aging and nanomaterial surface properties, that control both the dispersion tendency and chemical reactivity.

Sun damage is an ever-present danger that leads to myriads of deleterious effects on the exposed skin, including early skin aging and skin cancer. Since our modern lifestyle is not compatible with staying in the shadow, skin protection including anti-UV clothes and sunscreen must remain a priority to protect ourselves against these effects, and even to save lives. In many countries, regulations exist to control the composition, labeling and efficacy of sunscreens in blocking UV rays, so that consumers with no special knowledge can buy and use such products with confidence. Now, with the rising concern about environmental impacts of anthropic activities, sunscreen effects on the environment are also questioned. While their usage is not under debate and must remain a health priority, sunscreen composition can still be optimized with regard to the environment. By making, in advance, the appropriate choices that help minimize or prevent the environmental impact of the sunscreen UV-filters along with the product lifecycle, a sustainable design can be achieved. Whether it be industrial cosmetic formulators or policy makers in charge of safety and regulation, the provided risk knowledge can help lead to improvements in the assessment and management of cosmetics containing nanoparticulate UV-filters. Furthermore, the results of the present work will help provide better information for consumers and allow for easier decision-making for manufacturers and regulators.

AUTHOR CONTRIBUTIONS

JL: conceptualization, funding acquisition, project administration, resources, supervision, validation, and original draft writing. RC: data curation, formal analysis, and figure conceptualization. DS: conceptualization, original draft writing, data curation, and formal analysis. SM and AP: conceptualization, supervision, original draft writing, data curation, formal analysis, and validation. PH: original draft writing. CS: conceptualization. VB: data curation and formal analysis. All authors contributed to the article and approved the submitted version.

FUNDING

This work is a contribution to the Labex Serenade (no. ANR-11-LABX-0064) funded by the "Investissements d'Avenir" French Government program of the French National Research Agency (ANR) through the A*MIDEX project (no. ANR-11-IDEX-0001-02).

REFERENCES

Alijagic, A., Benada, O., Kofronova, O., Cigna, D., and Pinsino, A. (2019). Sea urchin extracellular proteins design a complex protein corona on titanium dioxide nanoparticle surface influencing immune cell behavior. *Front. Immunol.* 10:2261. doi: 10.3389/fimmu.2019.02261

Alijagic, A., Gaglio, D., Napodano, E., Russo, R., Costa, C., Benada, O., et al. (2020). Titanium dioxide nanoparticles temporarily influence the sea urchin immunological state suppressing inflammatory-relate gene transcription and boosting antioxidant metabolic activity. *J. Hazard Mater.* 384:121389. doi: 10.1016/j.jhazmat.2019.121389

Alijagic, A., and Pinsino, A. (2017). Probing safety of nanoparticles by outlining sea urchin sensing and signaling cascades. *Ecotoxicol. Environ. Saf.* 144, 416–421. doi: 10.1016/j.ecoenv.2017.06.060

Auffan, M., Pedeutour, M., Rose, J., Masion, A., Ziarelli, F., Borschneck, D., et al. (2010). Surface structural degradation of TiO2-based nanomaterial used in cosmetics. *Environ. Sci. Technol.* 44, 2689–2694. doi: 10.1021/es903757q

Baek, S., Joo, S. H., Kumar, N., and Toborek, M. (2017). Antibacterial effect and toxicity pathways of industrial and sunscreen ZnO nanoparticles on *Escherichia coli*. *J. Environ. Chem. Eng.* 5, 3024–3032. doi: 10.1016/j.jece.2017.06.009

Balmer, M. E., Buser, H. R., Muller, M. D., and Poiger, T. (2005). Occurrence of some organic UV filters in wastewater, in surface waters, and in fish from Swiss lakes. *Environ. Sci. Technol.* 39, 953–962. doi: 10.1021/es040055r

Bigorgne, E., Foucaud, L., Lapied, E., Labile, J., Botta, C., Sirguey, C., et al. (2011). Ecotoxicological assessment of TiO2 byproducts on the earthworm Eisenia fetida. *Environ. Pollut.* 159, 2698–2705. doi: 10.1016/j.envpol.2011.05.024

Bluthgen, N., Zucchi, S., and Fent, K. (2012). Effects of the UV filter benzophenone-3 (oxybenzone) at low concentrations in zebrafish (Danio rerio). *Toxicol. Appl. Pharmacol.* 263, 184–194. doi: 10.1016/j.taap.2012.06.008

Bolyard, S. C., Reinhart, D. R., and Santra, S. (2013). Behavior of engineered nanoparticles in landfill leachate. *Environ. Sci. Technol.* 47, 8114–8122.

Botta, C., Labille, J., Auffan, M., Borschneck, D., Miche, H., Cabie, M., et al. (2011). TiO2-based nanoparticles released in water from commercialized sunscreens in a life-cycle perspective: structures and quantities. *Environ. Pollut.* 159, 1543–1548.

Boxall, A., Chaudhry, Q., Sinclair, C., Jones, A., Aitken, R., Jefferson, B., et al. (2007). *Current and Future Predicted Environmental Exposure to Engineered Nanoparticles*. York: Central Science Laboratory.

Braun, J. H., Baidins, A., and Marganski, R. E. (1992). Tio2 pigment technology – a review. *Prog. Organ. Coat.* 20, 105–138.

Buric, P., Jaksic, Z., Stajner, L., Sikiric, M. D., Jurasin, D., Cascio, C., et al. (2015). Effect of silver nanoparticles on Mediterranean sea urchin embryonal development is species specific and depends on moment of first exposure. *Mar. Environ. Res.* 111, 50–59. doi: 10.1016/j.marenvres.2015.06.015

Cai, L., Peng, S., Wu, D., and Tong, M. (2016). Effect of different-sized colloids on the transport and deposition of titanium dioxide nanoparticles in quartz sand. *Environ. Pollut.* 208, 637–644. doi: 10.1016/j.envpol.2015.10.040

Calafat, A. M., Wong, L. Y., Ye, X. Y., Reidy, J. A., and Needham, L. L. (2008). Concentrations of the sunscreen agent benzophenone-3 in residents of the United States: national health and nutrition examination survey 2003-2004. *Environ. Health Perspect.* 116, 893–897. doi: 10.1289/ehp.11269

Cary, L., Pauwels, H., Ollivier, P., Picot, G., Leroy, P., Mougin, B., et al. (2015). Evidence for TiO2 nanoparticle transfer in a hard-rock aquifer. *J. Contaminant. Hydrol.* 179, 148–159. doi: 10.1016/j.jconhyd.2015.06.007

Castillo-Michel, H. A., Larue, C., Pradas del Real, A. E., Cotte, M., and Sarret, G. (2017). Practical review on the use of synchrotron based micro- and nano-X-ray fluorescence mapping and X-ray absorption spectroscopy to investigate the interactions between plants and engineered nanomaterials. *Plant Physiol. Biochem.* 110, 13–32. doi: 10.1016/j.plaphy.2016.07.018

Catalano, R. (2020). *Evaluation and Anticipation of the Risks Associated to Nanoparticulate UV Filters used in Sunscreens – A Lifecycle-Oriented Study, in Department of Environmental Sciences*. Ph.D. thesis of Aix-Marseille University, Aix-en-Provence.

Catalano, R., Masion, A., Ziarelli, F., Slomberg, D., Laisney, J., Unrine, J., et al. (2020). Optimizing the dispersion of nanoparticulate TiO2-based UV filters in a non-polar medium used in sunscreen formulations - the roles of surfactants and particle coatings. *Colloid. Surf. A* 599, 124792. doi: 10.1016/j.colsurfa.2020.124792

Chen, C., Unrine, J. M., Judy, J. D., Lewis, R. W., Guo, J., McNear, D. H. Jr., et al. (2015). Toxicogenomic responses of the model legume medicago truncatula to aged biosolids containing a mixture of nanomaterials (TiO(2), Ag, and ZnO) from a pilot wastewater treatment plant. *Environ. Sci. Technol.* 49, 8759–8768. doi: 10.1021/acs.est.5b01211

Chowdhury, I., Hong, Y., Honda, R. J., and Walker, S. L. (2011). Mechanisms of TiO2 nanoparticle transport in porous media: role of solution chemistry, nanoparticle concentration, and flowrate. *J. Colloid Interface Sci.* 360, 548–555. doi: 10.1016/j.jcis.2011.04.111

Contado, C., and Pagnoni, A. (2010). TiO2 nano- and micro-particles in commercial foundation creams: field flow-fractionation techniques together with ICP-AES and SQW Voltammetry for their characterization. *Anal. Methods* 2, 1112–1124.

Corinaldesi, C., Marcellini, F., Nepote, E., Damiani, E., and Danovaro, R. (2018). Impact of inorganic UV filters contained in sunscreen products on tropical stony corals (*Acropora* spp.). *Sci. Total Environ.* 637–638, 1279–1285. doi: 10.1016/j.scitotenv.2018.05.108

Corsi, G. N. I, Cherr, H. S., Lenihan, J., Labille, M., Hassellov, L., Canesi, F., et al. (2014). Common strategies and technologies for the ecosafety assessment and design of nanomaterials entering the marine environment. *ACS Nano* 8, 9694–9709. doi: 10.1021/nn504684k

Cosmetics Europe TPCA (2005). *Guidelines for Evaluating Sun Product Water Resistance*. Brussels: Cosmetics Europe TPCA, 13.

Cosmetics Europe TPCA (2018). *Environmental Sustainability: The European Cosmetics Industry's Contribution*. Brussels: Cosmetics Europe TPCA, 20.

Dan, Y., Shi, H., Stephan, C., and Liang, X. (2015). Rapid analysis of titanium dioxide nanoparticles in sunscreens using single particle inductively coupled plasma–mass spectrometry. *Microchem. J.* 122, 119–126. doi: 10.1016/j.microc.2015.04.018

Danovaro, R., Bongiorni, L., Corinaldesi, C., Giovannelli, D., Damiani, E., Astolfi, P., et al. (2008). Sunscreens cause coral bleaching by promoting viral infections. *Environ. Health Perspect.* 116, 441–447. doi: 10.1289/ehp.10966

Digne, M., Sautet, P., Raybaud, P., Toulhoat, H., and Artacho, E. (2002). Structure and stability of aluminum hydroxides: a theoretical study. *J. Phys. Chem. B* 106, 5155–5162. doi: 10.1021/jp014182a

Domingos, R. F., Tufenkji, N., and Wilkinson, K. J. (2009). Aggregation of titanium dioxide nanoparticles: role of a fulvic acid. *Environ. Sci. Technol.* 43, 1282–1286. doi: 10.1021/es8023594

Downs, C. A., Kramarsky-Winter, E., Segal, R., Fauth, J., Knutson, S., Bronstein, O., et al. (2016). Toxicopathological effects of the sunscreen UV filter, oxybenzone (Benzophenone-3), on coral planulae and cultured primary cells and its environmental contamination in hawaii and the US Virgin Islands. *Arch. Environ. Contaminat. Toxicol.* 70, 265–288. doi: 10.1007/s00244-015-0227-7

Duong-Ly, K., and Gabelli, S. (2014). Salting out of proteins usingammonium sulfate precipitation. *Methods Enzymol.* 541, 85–94. doi: 10.1016/b978-0-12-420119-4.00007-0

Dzumedzey, Y., Labille, J., Cathala, B., Moreau, C., and Santaella, C. (2017). Polysaccharide coating on environmental collectors affects the affinity and deposition of nanoparticles. *Nanoimpact* 5, 83–91. doi: 10.1016/j.impact.2016.12.004

Englehart, J., Lyon, B. A., Becker, M. D., Wang, Y., Abriola, L. M., and Pennell, K. D. (2016). Influence of a polymer sunscreen additive on the transport and retention of titanium dioxide nanoparticles in water-saturated porous media. *Environ. Sci. Nano* 3, 157–168. doi: 10.1039/c5en00174a

Englert, B. C. (2007). Nanomaterials and the environment: uses, methods and measurement. *J. Environ. Monitor.* 9, 1154–1161.

Esfandyari Bayat, A., Junin, R., Derahman, M. N., and Samad, A. A. (2015). TiO2 nanoparticle transport and retention through saturated limestone porous media under various ionic strength conditions. *Chemosphere* 134, 7–15. doi: 10.1016/j.chemosphere.2015.03.052

Eur-Lex (2009). Regulation (EC) No 1223/2009 of the European Parliament and of the Council of 30 November 2009 on cosmetic products. *OJL* 342, 59–209.

Eur-Lex (2018). COMMISSION REGULATION (EU) 2018/1881 of 3 December 2018 amending regulation (EC) No 1907/2006 of the European Parliament and

of the Council on the registration, evaluation, authorisation and restriction of chemicals (REACH) as regards Annexes I, III,VI, VII, VIII, IX, X, XI, and XII to address nanoforms of substances. *OJL* 308, 1–20.

Euromonitor International (2015). *Beauty and Personal Care*. London: Euromonitor International.

Fairbairn, E. A., Keller, A. A., Madler, L., Zhou, D. X., Pokhrel, S., and Cherr, G. N. (2011). Metal oxide nanomaterials in seawater: linking physicochemical characteristics with biological response in sea urchin development. *J. Hazard. Mater.* 192, 1565–1571. doi: 10.1016/j.jhazmat.2011.06.080

Fairhurst, D., and Mitchnick, M. A. (1997). "Particulate sun blocks: general principles," in *Sunscreens: Development, Evaluation, and Regulatory Aspects*, eds N. J. Lowe, N. A. Shaath, and M. A. Pathak (New York, NY: Marcel Dekker Inc).

Falugi, C., Aluigi, M. G., Chiantore, M. C., Privitera, D., Ramoino, P., Gatti, M. A., et al. (2012). Toxicity of metal oxide nanoparticles in immune cells of the sea urchin. *Mar. Environ. Res.* 76, 114–121. doi: 10.1016/j.marenvres.2011.10.003

Faure, B., Salazar-Alvarez, G., Ahniyaz, A., Villaluenga, I., Berriozabal, G., De Miguel, Y. R., et al. (2013). Dispersion and surface functionalization of oxide nanoparticles for transparent photocatalytic and UV-protecting coatings and sunscreens. *Sci. Technol. Adv. Mater.* 14:023001. doi: 10.1088/1468-6996/14/2/023001

FDA (2000). *Sunscreen Drug Products for Over-the-Counter Human Use; Final Monograph; Extension of Effective Date; Reopening of Administrative Record*. Silver Spring, MD: Food and Drug Administration.

FDA (2014). *Sunscreen Innovation Act (SIA)*. Silver Spring, MD: Food and Drug Administration.

FDA (2019). *Sunscreen Drug Products for Over-the-Counter Human Use, in 2019-03019*. Silver Spring, MD: Food and Drug Administration.

Fel, J. P., Lacherez, C., Bensetra, A., Mezzache, S., Beraud, E., Leonard, M., et al. (2019). Photochemical response of the scleractinian coral *Stylophora pistillata* to some sunscreen ingredients. *Coral Reefs* 38, 109–122. doi: 10.1007/s00338-018-01759-4

Fent, K., Kunz, P. Y., Zenker, A., and Rapp, M. (2010). A tentative environmental risk assessment of the UV-filters 3-(4-methylbenzylidene-camphor), 2-ethyl-hexyl-4-trimethoxycinnamate, benzophenone-3, benzophenone-4 and 3-benzylidene camphor. *Mar. Environ. Res.* 69, S4–S6.

Ficheux, A. S., Chevillotte, G., Wesolek, N., Morisset, T., Dornic, N., Bernard, A., et al. (2016). Consumption of cosmetic products by the French population second part: amount data. *Food Chem. Toxicol.* 90, 130–141. doi: 10.1016/j.fct.2016.02.008

Foltete, A.-S., Masfaraud, J.-F., Bigorgne, E., Nahmani, J., Chaurand, P., Botta, C., et al. (2011). Environmental impact of sunscreen nanomaterials: ecotoxicity and genotoxicity of altered TiO2 nanocomposites on *Vicia faba*. *Environ. Pollut.* 159, 2515–2522. doi: 10.1016/j.envpol.2011.06.020

Fouqueray, M., Dufils, B., Vollat, B., Chaurand, P., Botta, C., Abacci, K., et al. (2012). Effects of aged TiO2 nanomaterial from sunscreen on Daphnia magna exposed by dietary route. *Environ. Pollut.* 163:55. doi: 10.1016/j.envpol.2011.11.035

Fouqueray, M., Noury, P., Dherret, L., Chaurand, P., Abbaci, K., Labille, J., et al. (2013). Exposure of juvenile Danio rerio to aged TiO2 nanomaterial from sunscreen. *Environ. Sci. Pollut. Res.* 20, 3340–3350. doi: 10.1007/s11356-012-1256-7

Fujishima, A., Zhang, X. T., and Tryk, D. A. (2008). TiO2 photocatalysis and related surface phenomena. *Surf. Sci. Rep.* 63, 515–582. doi: 10.1016/j.surfrep.2008.10.001

Gamer, A. O., Leibold, E., and van Ravenzwaay, B. (2006). The in vitro absorption of microfine zinc oxide and titanium dioxide through porcine skin. *Toxicol. In Vitro* 20, 301–307. doi: 10.1016/j.tiv.2005.08.008

Ge, Y., Schimel, J. P., and Holden, P. A. (2011). Evidence for negative effects of TiO2 and ZnO nanoparticles on soil bacterial communities. *Environ. Sci. Technol.* 45, 1659–1664. doi: 10.1021/es103040t

Gerloff, K., Fenoglio, I., Carella, E., Kolling, J., Albrecht, C., Boots, A. W., et al. (2012). Distinctive toxicity of TiO2 rutile/anatase mixed phase nanoparticles on Caco-2 cells. *Chem. Res. Toxicol.* 25, 646–655. doi: 10.1021/tx200334k

Giokas, D. L., Salvador, A., and Chisvert, A. (2007). UV filters: from sunscreens to human body and the environment. *Trac Trends Anal. Chem.* 26, 360–374. doi: 10.1016/j.trac.2007.02.012

Godinez, I. G., and Darnault, C. J. G. (2011). Aggregation and transport of nano-TiO2 in saturated porous media: Effects of pH, surfactants and flow velocity. *Water Res.* 45, 839–851. doi: 10.1016/j.watres.2010.09.013

Godinez, I. G., Darnault, C. J. G., Khodadoust, A. P., and Bogdan, D. (2013). Deposition and release kinetics of nano-TiO2 in saturated porous media: effects of solution ionic strength and surfactants. *Environ. Pollut.* 174, 106–113. doi: 10.1016/j.envpol.2012.11.002

Gondikas, A., von der Kammer, F., Kaegi, R., Borovinskaya, O., Neubauer, E., Navratilova, J., et al. (2018). Where is the nano? Analytical approaches for the detection and quantification of TiO2 engineered nanoparticles in surface waters. *Environ. Sci. Nano* 5, 313–326. doi: 10.1039/c7en00952f

Gondikas, A. P., von der Kammer, F., Reed, R. B., Wagner, S., Ranville, J. F., and Hofmann, T. (2014). Release of TiO2 nanoparticles from sunscreens into surface waters: a one-year survey at the old danube recreational lake. *Environ. Sci. Technol.* 48, 5415–5422. doi: 10.1021/es405596y

Gottschalk, F., Lassen, C., Kjoelholt, J., Christensen, F., and Nowack, B. (2015). Modeling flows and concentrations of nine engineered nanomaterials in the Danish environment. *Int. J. Environ. Res. Public Health* 12, 5581–5602. doi: 10.3390/ijerph120505581

Gottschalk, F., Scholz, R. W., and Nowack, B. (2010). Probabilistic material flow modeling for assessing the environmental exposure to compounds: methodology and an application to engineered nano-TiO2 particles. *Environ. Modell. Softw.* 25, 320–332. doi: 10.1016/j.envsoft.2009.08.011

Gottschalk, F., Sun, T. Y., and Nowack, B. (2013). Environmental concentrations of engineered nanomaterials: review of modeling and analytical studies. *Environ. Pollut.* 181, 287–300. doi: 10.1016/j.envpol.2013.06.003

Graubner, V. M., Jordan, R., and Nuyken, O. (2004). Photochemical modification of cross-linked poly(dimethylsiloxane) by irradiation at 172 nm. *Macromolecules* 37, 5936–5953.

Gulson, B., McCall, M., Korsch, M., Gomez, L., Casey, P., Oytam, Y., et al. (2010). Small amounts of zinc from zinc oxide particles in sunscreens applied outdoors are absorbed through human skin. *Toxicol. Sci.* 118, 140–149. doi: 10.1093/toxsci/kfq243

Gulson, B., McCall, M. J., Bowman, D. M., and Pinheiro, T. (2015). A review of critical factors for assessing the dermal absorption of metal oxide nanoparticles from sunscreens applied to humans, and a research strategy to address current deficiencies. *Arch. Toxicol.* 89, 1909–1930. doi: 10.1007/s00204-015-1564-z

Gulson, B., Wong, H., Korsch, M., Gomez, L., Casey, P., McCall, M., et al. (2012). Comparison of dermal absorption of zinc from different sunscreen formulations and differing UV exposure based on stable isotope tracing. *Sci. Total Environ.* 420, 313–318. doi: 10.1016/j.scitotenv.2011.12.046

Hanaor, D., and Sorrell, C. (2010). Review of the anatase to rutile phase transformation. *J. Mater. Sci.* 46, 855–874.

Hanigan, D., Truong, L., Schoepf, J., Nosaka, T., Mulchandani, A., Tanguay, R. L., et al. (2018). Trade-offs in ecosystem impacts from nanomaterial versus organic chemical ultraviolet filters in sunscreens. *Water Res.* 139, 281–290. doi: 10.1016/j.watres.2018.03.062

Hawaii State Legislature (2018). *Environment; Water Pollution; Sunscreen; Oxybenzone; Octinoxate; Sale; Distribution; Prohibition, in SB2571, S.D.2, H.D.2, C.D.1*. Honolulu, HI: Hawaii State Legislature.

Hennebert, P., Anderson, A., and Merdy, P. (2017). Mineral nanoparticles in waste: potential sources, occurrence in some engineered nanomaterials leachates, municipal sewage sludges and municipal landfill sludges. *J. Biotechnol. Biomater.* 7:261.

Hennebert, P., Avellan, A., Yan, J. F., and Aguerre-Chariol, O. (2013). Experimental evidence of colloids and nanoparticles presence from 25 waste leachates. *Waste Manage.* 33, 1870–1881. doi: 10.1016/j.wasman.2013.04.014

Herrera Melian, J. A., Dona Rodriguez, J. M., Viera Suarez, A., Tello Rendon, E., Valdes do Campo, C., Arana, J., et al. (2000). The photocatalytic disinfection of urban waste waters. *Chemosphere* 41, 323–327. doi: 10.1016/s0045-6535(99)00502-0

Jeon, S.-k, Kim, E.-j, Lee, J., and Lee, S. (2016). Potential risks of TiO2 and ZnO nanoparticles released from sunscreens into outdoor swimming pools. *J. Hazard. Mater.* 317, 312–318. doi: 10.1016/j.jhazmat.2016.05.099

Johnson, A. C., Bowes, M. J., Crossley, A., Jarvie, H. P., Jurkschat, K., Jurgens, M. D., et al. (2011). An assessment of the fate, behaviour and environmental risk associated with sunscreen TiO2 nanoparticles in UK field

scenarios. *Sci. Total Environ.* 409, 2503–2510. doi: 10.1016/j.scitotenv.2011.03.040

Jomini, S., Labille, J., Bauda, P., and Pagnout, C. (2012). Modifications of the bacterial reverse mutation test reveals mutagenicity of TiO2 nanoparticles and byproducts from a sunscreen TiO2-based nanocomposite. *Toxicol. Lett.* 215, 54–61. doi: 10.1016/j.toxlet.2012.09.012

Joo, S. H., Al-Abed, S. R., and Luxton, T. (2009). Influence of carboxymethyl cellulose for the transport of titanium dioxide nanoparticles in clean silica and mineral-coated sands. *Environ. Sci. Technol.* 43, 4954–4959. doi: 10.1021/es900329d

Kaegi, R., Englert, A., Gondikas, A., Sinnet, B., von der Kammer, F., and Burkhardt, M. (2017). Release of TiO2 - (Nano) particles from construction and demolition landfills. *Nanoimpact* 8, 73–79. doi: 10.1016/j.impact.2017.07.004

Kamitsos, E. I., Patsis, A. P., and Kordas, G. (1993). Infrared-reflectance spectra of heat-treated sol-gel-derived silica. *Phys. Rev. B Condens. Matter.* 48, 12499–12505. doi: 10.1103/physrevb.48.12499

Kanel, S. K., and Al-Abed, S. R. (2011). Influence of pH on the transport of nanoscale zinc oxide in saturated porous media. *J. Nanopart. Res.* 13, 4035–4047. doi: 10.1007/s11051-011-0345-8

Keller, A. A., Vosti, W., Wang, H. T., and Lazareva, A. (2014). Release of engineered nanomaterials from personal care products throughout their life cycle. *J. Nanopart. Res.* 16:2489.

King, D. M., Liang, X. H., Burton, B. B., Akhtar, M. K., and Weimer, A. W. (2008). Passivation of pigment-grade TiO(2) particles by nanothick atomic layer deposited SiO(2) films. *Nanotechnology* 19:255604. doi: 10.1088/0957-4484/19/25/255604

Kunz, P. Y., and Fent, K. (2006). Multiple hormonal activities of UV filters and comparison of in vivo and in vitro estrogenic activity of ethyl-4-aminobenzoate in fish. *Aquat. Toxicol.* 79, 305–324. doi: 10.1016/j.aquatox.2006.06.016

Kunz, P. Y., and Fent, K. (2009). Estrogenic activity of ternary UV filter mixtures in fish (*Pimephales promelas*) – an analysis with nonlinear isobolograms. *Toxicol. Appl. Pharmacol.* 234, 77–88. doi: 10.1016/j.taap.2008.09.032

Labille, J., and Brant, J. (2010). Stability of nanoparticles in water. *Nanomedicine* 5, 985–998.

Labille, J., Feng, J. H., Botta, C., Borschneck, D., Sammut, M., Cabie, M., et al. (2010). Aging of TiO(2) nanocomposites used in sunscreen. Dispersion and fate of the degradation products in aqueous environment. *Environ. Pollut.* 158, 3482–3489. doi: 10.1016/j.envpol.2010.02.012

Labille, J., Harns, C., Bottero, J. Y., and Brant, J. (2015). Heteroaggregation of titanium dioxide nanoparticles with natural clay colloids under environmentally relevant conditions. *Environ. Sci. Technol.* 48, 10690–10698. doi: 10.1021/es501655v

Labille, J., Pelinovskaya, N., Botta, C., Bottero, J. Y., and Masion, A. (2012). "Fate of manufactured nanoparticles in aqueous environment," in *Encyclopedia of Nanotechnology*, ed. B. Bhushan (Dordrecht: Springer), 16.

Labille, J., Slomberg, D., Catalano, R., Robert, S., Apers-Tremelo, M. L., Boudenne, J. L., et al. (2020). Assessing UV filter inputs into beach waters during recreational activity: a field study of three French mediterranean beaches from consumer survey to water analysis. *Sci. Total Environ.* 706:136010. doi: 10.1016/j.scitotenv.2019.136010

Lapied, E., Nahmani, J. Y., Moudilou, E., Chaurand, P., Labille, J., Rose, J., et al. (2011). Ecotoxicological effects of an aged TiO2 nanocomposite measured as apoptosis in the anecic earthworm Lumbricus terrestris after exposure through water, food and soil. *Environ. Int.* 37:1105. doi: 10.1016/j.envint.2011.01.009

Lazareva, A., and Keller, A. (2014). Estimating potential life cycle releases of engineerednanomaterials from wastewater treatment plants. *ACS Sustain. Chem. Eng.* 2, 1656–1665. doi: 10.1021/sc500121w

Le Bihan, O., Ounoughene, G., Meunier, L., Debray, B., and Aguerre-Chariol, O. (2017). Incineration of a commercial coating with nano-CeO2. *J. Phys. Conf. Ser.* 838:012023. doi: 10.1088/1742-6596/838/1/012023

Leroy, D., and Deschamps, P. (1986). Influence of formulation on sunscreen water resistance. *Photodermatol.* 3, 52–53.

Li, D., Li, B., Wang, Q., Hou, N., Li, C., and Cheng, X. (2016). Toxicity of TiO2 nanoparticle to denitrifying strain CFY1 and the impact on microbial community structures in activated sludge. *Chemosphere* 144, 1334–1341. doi: 10.1016/j.chemosphere.2015.10.002

Lindsay, W. L. (1979). *The Chemical Equilibria in Soils*. Chuchester: Wiley, 449.

Lv, X., Gao, B., Sun, Y., Dong, S., Wu, J., Jiang, B., et al. (2016). Effects of grain size and structural heterogeneity on the transport and retention of nano-TiO2 in saturated porous media. *Sci. Total Environ.* 563–564, 987–995. doi: 10.1016/j.scitotenv.2015.12.128

Ma, H., Williams, P. L., and Diamond, S. A. (2013). Ecotoxicity of manufactured ZnO nanoparticles–a review. *Environ. Pollut.* 172, 76–85. doi: 10.1016/j.envpol.2012.08.011

Marques-Santos, L. F., Grassi, G., Bergami, E., Faleri, C., Balbi, T., Salis, A., et al. (2018). Cationic polystyrene nanoparticle and the sea urchin immune system: biocorona formation, cell toxicity, and multixenobiotic resistance phenotype. *Nanotoxicology* 12, 847–867. doi: 10.1080/17435390.2018.1482378

Massari, A., Beggio, M., Hreglich, S., Marin, R., and Zuin, S. (2014). Behavior of TiO(2) nanoparticles during incineration of solid paint waste: a lab-scale test. *Waste Manage.* 34, 1897–1907. doi: 10.1016/j.wasman.2014.05.015

Matranga, V., Pinsino, A., Celi, M., Di Bella, G., and Natoli, A. (2006). Impacts of UV-B radiation on short-term cultures of sea urchin coelomocytes. *Mar. Biol.* 149, 25–34. doi: 10.1007/s00227-005-0212-1

Matta, M. K., Florian, J., Zusterzeel, R., Pilli, N. R., Patel, V., Volpe, D.A., et al. (2020). Effect of sunscreen application on plasma concentration of sunscreen active ingredients a randomized clinical trial. JAMA 323, 256-267.

Matta, M. K., Zusterzeel, R., Pilli, N. R., Patel, V., Volpe, D. A., Florian, J., et al. (2019). Effect of sunscreen application under maximal use conditions on plasma concentration of sunscreen active ingredients: a randomized clinical trial. *JAMA* 321, 2082–2091.

Mesaric, T., Sepcic, K., Drobne, D., Makovec, D., Faimali, M., Morgana, S., et al. (2015). Sperm exposure to carbon-based nanomaterials causes abnormalities in early development of purple sea urchin (*Paracentrotus lividus*). *Aquat. Toxicol.* 163, 158–166. doi: 10.1016/j.aquatox.2015.04.012

Migliaccio, O., Pinsino, A., Maffioli, E., Smith, A. M., Agnisola, C., Matranga, V., et al. (2019). Living in future ocean acidification, physiological adaptive responses of the immune system of sea urchins resident at a CO2 vent system. *Sci. Total Environ.* 672, 938–950. doi: 10.1016/j.scitotenv.2019.04.005

Mills, A., and Wang, J. (2006). Simultaneous monitoring of the destruction of stearic acid and generation of carbon dioxide by self-cleaning semiconductor photocatalytic films. *J. Photochem. Photobiol. A Chem.* 182, 181–186. doi: 10.1016/j.jphotochem.2006.02.010

Minetto, D., Libralato, G., and Ghirardini, A. V. (2014). Ecotoxicity of engineered TiO2 nanoparticles to saltwater organisms: an overview. *Environ. Int.* 66, 18–27. doi: 10.1016/j.envint.2014.01.012

Mohammed, Y. H., Holmes, A. I, Haridass, N., Sanchez, W. Y., Studier, H., Grice, J. E., et al. (2019). Support for the safe use of zinc oxide nanoparticle sunscreens: lack of skin penetration or cellular toxicity after repeated application in volunteers. *J. Invest. Dermatol.* 139, 308–315. doi: 10.1016/j.jid.2018.08.024

Monteiro-Riviere, N. A., Wiench, K., Landsiedel, R., Schulte, S., Inman, A. O., and Riviere, J. E. (2011). Safety evaluation of sunscreen formulations containing titanium dioxide and zinc oxide nanoparticles in UVB sunburned skin: an in vitro and in vivo study. *Toxicol. Sci.* 123, 264–280. doi: 10.1093/toxsci/kfr148

Mu, H., Chen, Y., and Xiao, N. (2011). Effects of metal oxide nanoparticles (TiO2, Al2O3, SiO2 and ZnO) on waste activated sludge anaerobic digestion. *Bioresour. Technol.* 102, 10305–10311. doi: 10.1016/j.biortech.2011.08.100

Mueller, N. C., Buha, J., Wang, J., Ulrich, A., and Nowack, B. (2013). Modeling the flows of engineered nanomaterials during waste handling. *Environ. Sci. Process. Impacts* 15, 251–259. doi: 10.1039/c2em30761h

OEHHA (2020). *California's Proposition 65, in Safe Drinking Water and Toxic Enforcement Act of 1986*. Sacramento, CA: California office of environmental health hazard assessment.

Ollivier, P., Pauwels, H., Wille, G., Devau, N., Braibant, G., Cary, L., et al. (2018). Natural attenuation of TiO2 nanoparticles in a fractured hard-rock. *J. Hazard. Mater.* 359, 47–55. doi: 10.1016/j.jhazmat.2018.07.035

Osmond, M. J., and McCall, M. J. (2010). Zinc oxide nanoparticles in modern sunscreens: an analysis of potential exposure and hazard. *Nanotoxicology* 4, 15–41. doi: 10.3109/17435390903502028

Part, F., Berge, N., Baran, P., Stringfellow, A., Sun, W. J., Bartelt-Hunt, S., et al. (2018). A review of the fate of engineered nanomaterials in municipal solid waste streams. *Waste Manage.* 75, 427–449. doi: 10.1016/j.wasman.2018.02.012

Petosa, A. R., Brennan, S. J., Rajput, F., and Tufenkji, N. (2012). Transport of two metal oxide nanoparticles in saturated granular porous media: role of water chemistry and particle coating. *Water Res.* 46, 1273–1285. doi: 10.1016/j.watres.2011.12.033

Philippe, A., Košík, J., Welle, A., Guigner, J.-M., Clemens, O., and Schaumann, G. E. (2018). Extraction and characterization methods for titanium dioxide nanoparticles from commercialized sunscreens. *Environ. Sci. Nano* 5, 191–202. doi: 10.1039/c7en00677b

Pinsino, A., and Alijagic, A. (2019). Sea urchin *Paracentrotus lividus* immune cells in culture: formulation of the appropriate harvesting and culture media and maintenance conditions. *Biol. Open* 8:bio039289. doi: 10.1242/bio.039289

Pinsino, A., Della Torre, C., Sammarini, V., Bonaventura, R., Amato, E., and Matranga, V. (2008). Sea urchin coelomocytes as a novel cellular biosensor of environmental stress: a field study in the Tremiti Island Marine Protected Area, Southern Adriatic Sea, Italy. *Cell Biol. Toxicol.* 24, 541–552. doi: 10.1007/s10565-008-9055-0

Pinsino, A., and Matranga, V. (2015). Sea urchin immune cells as sentinels of environmental stress. *Dev. and Comp. Immunol.* 49, 198–205. doi: 10.1016/j.dci.2014.11.013

Pinsino, A., Russo, R., Bonaventura, R., Brunelli, A., Marcomini, A., and Matranga, V. (2015). Titanium dioxide nanoparticles stimulate sea urchin immune cell phagocytic activity involving TLR/p38 MAPK-mediated signalling pathway. *Sci. Rep.* 5:14492.

Poland, C. A., Read, S. A. K., Varet, J., Carse, G., Christensen, F. M., and JHankin, S. M. (2013). *Dermal Absorption of Nanomaterials, in Environmental* Project No. 1504, 2013. Copenhagen: Danish Ministry of the Environment.

Pradas del Real, A. E., Castillo-Michel, H., Kaegi, R., Larue, C., de Nolf, W., Reyes-Herrera, J., et al. (2018). Searching for relevant criteria to distinguish natural vs. anthropogenic TiO2 nanoparticles in soils. *Environ. Sci. Nano* 5, 2853–2863. doi: 10.1039/c8en00386f

Praetorius, A., Labille, J., Scheringer, M., Thill, A., Hungerbuhler, K., and Bottero, J. Y. (2014). Heteroaggregation of titanium dioxide nanoparticles with model natural colloids under environmentally relevant conditions. *Environ. Sci. Technol.* 48, 10690–10698. doi: 10.1021/es501655v

Reed, R. B., Martin, D. P., Bednar, A. J., Montano, M. D., Westerhoff, P., and Ranville, J. F. (2017). Multi-day diurnal measurements of Ti-containing nanoparticle and organic sunscreen chemical release during recreational use of a natural surface water. *Environ. Sci. Nano* 4, 69–77. doi: 10.1039/c6en00283h

Risk and Policy Analysts Limited (2004). *Comparative Study on Cosmetics Legislation in the EU and Other Principal Markets with Special Attention to So-Called Borderline Products*. Norfolk: Risk & Policy Analysts Limited.

Rodriguez-Romero, A., Ruiz-Gutierrez, G., Viguri, J., and Tovar-Sanchez, A. (2019). Sunscreens as a new source of metals and nutrients to coastal waters. *Environ. Sci. Technol.* 53, 10177–10187. doi: 10.1021/acs.est.9b02739

Rossano, M., Hucher, N., Picard, C., Colletta, D., Le Foll, F., and Grisel, M. (2014). Effects of aging on structure and stability of TiO2 nanoparticle-containing oil-in-water emulsions. *Int. J. Pharm.* 461, 89–96. doi: 10.1016/j.ijpharm.2013.11.039

Rowenczyk, L., Duclairoir-Poc, C., Barreau, M., Picard, C., Hucher, N., Orange, N., et al. (2017). Impact of coated TiO2-nanoparticles used in sunscreens on two representative strains of the human microbiota: effect of the particle surface nature and aging. *Colloid. Surf. B Biointerf.* 158, 339–348. doi: 10.1016/j.colsurfb.2017.07.013

Sanchez-Quiles, D., and Tovar-Sanchez, A. (2014). Sunscreens as a source of hydrogen peroxide production in coastal waters. *Environ. Sci. Technol.* 48, 9037–9042. doi: 10.1021/es5020696

Sani-Kast, N., Scheringer, M., Slomberg, D., Labille, J., Praetorius, A., Ollivier, P., et al. (2015). Addressing the complexity of water chemistry in environmental fate modeling for engineered nanoparticles. *Sci. Total Environ.* 535, 150–159. doi: 10.1016/j.scitotenv.2014.12.025

Santaella, C., Allainmat, B., Simonet, F., Chaneac, C., Labille, J., Auffan, M., et al. (2014). Aged TiO2-based nanocomposite used in sunscreens produces singlet oxygen under long-wave UV and sensitizes *Escherichia coli* to Cadmium. *Environ. Sci. Technol.* 48, 5245–5253. doi: 10.1021/es500216t

Santos, A. S. F., Teixeira, B. A. N., Agnelli, J. A. M., and Manrich, S. (2005). Characterization of effluents through a typical plastic recycling process: an evaluation of cleaning performance and environmental pollution. *Resour. Conserv. Recycl.* 45, 159–171. doi: 10.1016/j.resconrec.2005.01.011

SCCS (2012). *OPINION ON Zinc oxide (Nano Form) COLIPA S 76*. Brussels: Scientific Committee on Consumer Safety.

SCCS (2014). *OPINION ON Titanium Dioxide (Nano Form) COLIPA S75*. Brussels: Scientific Committee on Consumer Safety.

Schlumpf, M., Schmid, P., Durrer, S., Conscience, M., Maerkel, K., Henseler, M., et al. (2004). Endocrine activity and developmental toxicity of cosmetic UV filters – an update. *Toxicology* 205, 113–122. doi: 10.1016/j.tox.2004.06.043

Schneider, S. L., and Lim, H. W. (2019). A review of inorganic UV filters zinc oxide and titanium dioxide. *Photodermatol. Photoimmunol. Photomed.* 35, 442–446. doi: 10.1111/phpp.12439

Schulz, J., Hohenberg, H., Pflucker, F., Gartner, E., Will, T., Pfeiffer, S., et al. (2002). Distribution of sunscreens on skin. *Adv. Drug Deliv. Rev.* 54, S157–S163.

Semenzato, A., Dall'aglio, C., Boscarini, G. M., Ongaro, A., Bettero, A., Sangalli, M. E., et al. (1994). Chemico-physical and functional properties of inorganic sunscreens in cosmetic products. *Int. J. Cosmet. Sci.* 16, 247–255. doi: 10.1111/j.1467-2494.1994.tb00101.x

Sendra, M., Sanchez-Quiles, D., Blasco, J., Moreno-Garrido, I., Lubian, L. M., Perez-Garcia, S., et al. (2017). Effects of TiO2 nanoparticles and sunscreens on coastal marine microalgae: ultraviolet radiation is key variable for toxicity assessment. *Environ. Int.* 98, 62–68. doi: 10.1016/j.envint.2016.09.024

Shao, Y., and Schlossman, D. (1999). *Effect of Particle Size on Performance of Physical Sunscreen Formulas*. Shanghai: PCIA Conference.

Simonet, B. M., and Valcarcel, M. (2009). Monitoring nanoparticles in the environment. *Anal. Bioanal. Chem.* 393, 17–21. doi: 10.1007/s00216-008-2484-z

Slomberg, D., Catalano, R., Ziarelli, F., Viel, S., Bartolomei, V., Labille, J., et al. (2020). Aqueous aging of a silica coated TiO2 UV filter used in sunscreens: investigations at the molecular scale with dynamic nuclear polarization NMR. *RSC Adv.* 10, 8266–8274. doi: 10.1039/d0ra00595a

Smijs, T. G., and Pavel, S. (2011). Titanium dioxide and zinc oxide nanoparticles in sunscreens: focus on their safety and effectiveness. *Nanotechnol. Sci. Appl.* 4, 95–112.

Smith, L. C., Arizza, V., Hudgell, M. A. B., Barone, G., Bodnar, A. G., Buckley, K. M., et al. (2008). "Echinodermata: the complex immune system in echinoderms," in *Advances in Comparative Immunology*, ed. E. L. Cooper (Cham: Springer International Publishing), 409–501.

Solovitch, N., Labille, J., Rose, J., Chaurand, P., Borschneck, D., Wiesner, M. R., et al. (2010). Concurrent aggregation and deposition of TiO2 nanoparticles in a sandy porous media. *Environ. Sci. Technol.* 44, 4897–4902. doi: 10.1021/es1000819

Sposito, G. (2008). *The Chemistry of Soils*, 2nd Edn. Oxford: Oxford University Press, 329.

Steinberg, D. (2007). Global regulations of sunscreens. *Int. J. Cosmet. Sci.* 29, 409–411.

Sun, T. Y., Gottschalk, F., Hungerbuhler, K., and Nowack, B. (2014). Comprehensive probabilistic modelling of environmental emissions of engineered nanomaterials. *Environ. Pollut.* 185, 69–76. doi: 10.1016/j.envpol.2013.10.004

Tharaud, M., Gondikas, A. P., Benedetti, M. F., von der Kammer, F., Hofmann, T., and Cornelis, G. (2017). TiO2 nanomaterial detection in calcium rich matrices by spICPMS. A matter of resolution and treatment. *J. Anal. Atomic Spectr.* 32, 1400–1411. doi: 10.1039/c7ja00060j

Topuz, E., Traber, J., Sigg, L., and Talinli, I. (2015). Agglomeration of Ag and TiO2 nanoparticles in surface and wastewater: role of calcium ions and of organic carbon fractions. *Environ. Pollut.* 204, 313–323. doi: 10.1016/j.envpol.2015.05.034

Tovar-Sanchez, A., Sanchez-Quiles, D., Basterretxea, G., Benede, J. L., Chisvert, A., Salvador, A., et al. (2013). Sunscreen products as emerging pollutants to coastal waters. *PLoS One* 8:e65451. doi: 10.1371/journal.pone.0065451

Tovar-Sanchez, A., Sanchez-Quiles, D., and Rodriguez-Romero, A. (2019). Massive coastal tourism influx to the Mediterranean Sea: the environmental risk of sunscreens. *Sci. Total Environ.* 656, 316–321. doi: 10.1016/j.scitotenv.2018.11.399

Turkoglu, M., and Yener, S. (1997). Design and in vivo evaluation of ultrafine inorganic-oxide-containing-sunscreen formulations. *Int. J. Cosmet. Sci.* 19, 193–201. doi: 10.1046/j.1467-2494.1997.171714.x

Tyner, K. M., Wokovich, A. M., Godar, D. E., Doub, W. H., and Sadrieh, N. (2011). The state of nano-sized titanium dioxide (TiO2) may affect sunscreen

performance. *Int. J. Cosmet. Sci.* 33, 234–244. doi: 10.1111/j.1468-2494.2010.00622.x

U.S. EPA (2010). *Nanomaterial Case Studies: Nanoscale Titanium Dioxide in Water Treatment and in Topical Sunscreen*. Washington, DC: U.S. Environmental Protection Agency, 204.

UNEP (2009). *Sustainable Coastal Tourism: An Integrated Planning and Management Approach*. Nairobi: United Nations Environment Programme.

Venkatesan, A. K., Reed, R. B., Lee, S., Bi, X., Hanigan, D., Yang, Y., et al. (2018). Detection and sizing of Ti-containing particles in recreational waters using single particle ICP-MS. *Bull. Environ. Contaminat. Toxicol.* 100, 120–126. doi: 10.1007/s00128-017-0862216-1

Virkutyte, J., Al-Abed, S. R., and Dionysiou, D. D. (2012). Depletion of the protective aluminum hydroxide coating in TiO2-based sunscreens by swimming pool water ingredients. *Chem. Eng. J.* 191, 95–103. doi: 10.1016/j.cej.2012.02.074

Wakefield, G., Lipscomb, S., Holland, E., and Knowland, J. (2004). The effects of manganese doping on UVA absorption and free radical generation of micronised titanium dioxide and its consequences for the photostability of UVA absorbing organic sunscreen components. *Photochem. Photobiol. Sci.* 3, 648–652.

Yung, M. M. N., Fougeres, P. A., Leung, Y. H., Liu, F., Djurisic, A. B., Giesy, J. P., et al. (2017). Physicochemical characteristics and toxicity of surface-modified zinc oxide nanoparticles to freshwater and marine microalgae. *Sci. Rep.* 7:15909.

Zhang, M., Yang, J. H., Cai, Z. X., Feng, Y. D., Wang, Y. F., Zhang, D. Y., et al. (2019). Detection of engineered nanoparticles in aquatic environments: current status and challenges in enrichment, separation, and analysis. *Environ. Sci. Nano* 6, 709–735. doi: 10.1039/c8en01086b

Zheng, X., Chen, Y., and Wu, R. (2011). Long-term effects of titanium dioxide nanoparticles on nitrogen and phosphorus removal from wastewater and bacterial community shift in activated sludge. *Environ. Sci. Technol.* 45, 7284–7290. doi: 10.1021/es2008598

Conflict of Interest: The authors declare that the research was conducted in the absence of any commercial or financial relationships that could be construed as a potential conflict of interest.

frontiers in Environmental Science

ORIGINAL RESEARCH
published: 23 July 2020
doi: 10.3389/fenvs.2020.00125

Car Tire Crumb Rubber: Does Leaching Produce a Toxic Chemical Cocktail in Coastal Marine Systems?

Claudia Halsband[1], Lisbet Sørensen[2], Andy M. Booth[2] and Dorte Herzke[3]*

[1] Akvaplan-niva, Tromsø, Norway, [2] Department: Environment and New Resources, SINTEF Ocean, Trondheim, Norway, [3] NILU, Norwegian Institute for Air Research, Tromsø, Norway

Crumb rubber granulate (CRG) produced from end of life tires (ELTs) is commonly applied to synthetic turf pitches (STPs), playgrounds, safety surfaces and walkways. In addition to fillers, stabilizers, cross-linking agents and secondary components (e.g., pigments, oils, resins), ELTs contain a range of other organic compound and heavy metal additives. While previous environmental impact studies on CRG have focused on terrestrial soil and freshwater ecosystems, many sites applying CRG in Norway are coastal. The current study investigated the organic chemical and metal additive content of 'pristine' and 'weathered' CRG and their seawater leachates, as well as uptake and effects of leachate exposure using marine copepods (*Acartia* and *Calanus* sp.). A combination of pyrolysis gas chromatography mass spectrometry (py-GC-MS) and chemical extraction followed by GC-MS analysis revealed similar organic chemical profiles for pristine and weathered CRG, including additives such as benzothiazole, *N*-1,3-dimethylbutyl-*N*′-phenyl-*p*-phenylenediamine and a range of polycyclic aromatic hydrocarbons (PAHs) and phenolic compounds (e.g., bisphenols). ICP-MS analysis revealed g kg^{-1} quantities of Zn and mg kg^{-1} quantities of Fe, Mn, Cu, Co, Cr, Pb, and Ni in the CRG. A cocktail of organic additives and metals readily leached from the CRG into seawater, with the most abundant leachate components being benzothiazole and Zn, Fe, Co (metals), as well as detectable levels of PAHs and phenolic compounds. Concentrations of individual components varied with CRG source material and CRG to seawater ratio, but benzothiazole and Zn were typically the organic and metal components present at the highest concentrations in the leachates. While organic chemical concentrations in the leachates stabilized within days, metals continued to leach out over the 30-day period. Marine copepods exposed to high CRG leachate concentrations exhibited high mortalities within 48 h. The smaller lipid-poor *Acartia* had a higher sensitivity to leachates than the larger lipid-rich *Calanus*, indicating species-specific differences in vulnerability to leachates. The effect on survival was alleviated at lower leachate concentrations, indicating a dose-response relationship. Benzothiazole and its derivatives appear to be of concern owing to their proven toxicity, while bisphenols are also known to be toxic and were enriched in the leachates relative to the other compounds in the CRG.

Keywords: additives, organic compounds, metals, copepod, acute toxicity, zinc, benzothiazole, arctic

OPEN ACCESS

Edited by:
Antonia Praetorius, University of Amsterdam, Netherlands

Reviewed by:
Nadia Valentina Martínez-Villegas, Instituto Potosino de Investigación Científica y Tecnológica (IPICYT), Mexico
Amrika Deonarine, Texas Tech University, United States

****Correspondence:***
Claudia Halsband
claudia.halsband@akvaplan.niva.no

Specialty section:
This article was submitted to Biogeochemical Dynamics, a section of the journal Frontiers in Environmental Science

Received: *30 April 2020*
Accepted: *07 July 2020*
Published: *23 July 2020*

Citation:
Halsband C, Sørensen L, Booth AM and Herzke D (2020) Car Tire Crumb Rubber: Does Leaching Produce a Toxic Chemical Cocktail in Coastal Marine Systems? Front. Environ. Sci. 8:125. doi: 10.3389/fenvs.2020.00125

INTRODUCTION

In 2016, global production of natural and synthetic rubber reached 27.3 million tons (54% synthetic) (International Rubber Study Group, 2017), with ∼70% used in the manufacture of vehicle tires. It is estimated that there are 1 billion end-of-life tires (ELTs) generated globally each year (Wbscd, 2015). Despite the EU banning ELTs from landfill (European Community Directive 1999/31/EC and Waste Framework Directive 2006/12/EC) due to the risk of pollutant release, production of crumb rubber granulate (CRG) from ELTs has been considered an acceptable way of utilizing this waste material and is often considered recycling. Common CRG applications include outdoor artificial sports fields, playgrounds, general safety surfaces and on trails and walkways (Simon, 2010), where CRG is subject to weathering and transportation into the surrounding environment. It is estimated that 100–120 tons of CRG are used on a full-sized artificial football field (equivalent to ∼25000 ELTs) and that 1.5–2.5 tons is lost annually (Lassen et al., 2015). The European Chemicals Agency (ECHA) estimates there will be ∼21,000 full size and ∼72,000 mini-sized synthetic turf pitches in the EU by 2020, corresponding to 30% of all ELT usage (ECHA, 2017).

Car tire rubber and CRG from ELTs contains a broad range of additives including filler systems (carbon black, clays, silicas, calcium carbonate), stabilizer systems (antioxidants, antiozonants, waxes), cross-linking agents (sulfur, accelerators, activators) and secondary components such as pigments, oils, resins and short fibers. Chemical classes associated with car tires include polyaromatic hydrocarbons (PAHs), phthalates, sulfenamides, guanidines, thiazoles, thiuams, dithiocarbamates, sulfur donors, phenolics, phenylenediamines and heavy metals (Smolders and Degryse, 2002; ChemRisk Inc., 2008; Bocca et al., 2009; Llompart et al., 2013; Ruffino et al., 2013; Cheng et al., 2014; Canepari et al., 2017). Many of these chemicals can cause environmental impacts and pose risks to human health (Sadiktsis et al., 2012; Rodgers and Waddell, 2013; Ruffino et al., 2013; Cheng et al., 2014; Canepari et al., 2017; Halle et al., 2020).

In Europe, standards for Environmental Compatibility regulate the content of dissolved organic carbon (DOC), extractable organic halogens (EOX), Pb, Cd, Cr, Hg, Zn and Sn (DIN 18035-7:2002-06 and NF P90-112). Furthermore, EU REACH regulations (Annex XVII entry 28) require that carcinogens such as the EU-8 PAHs are not to be supplied to the general public above certain concentration limits (0.01–0.1% by weight; 100–1000 mg kg^{-1}), while the concentration of individual PAHs may not exceed 0.0001% (1 mg kg^{-1}) when present as PAH mixtures in consumer products (REACH Annex XVII entry 50). These concentrations are, however, regularly reached or exceeded for certain chemicals and metals in CRG derived from ELTs given the inhomogeneous nature of CRG sources (Diekmann et al., 2019). Identified compounds leaching from CRG into water include benzothiazoles, phthalates and phenols, where benzothiazole is typically observed in the highest quantities (Li et al., 2010; Llompart et al., 2013). In addition to being the largest contributor to the organic fraction of CRG leachates, benzothiazoles have also been identified as toxic to aquatic species including fish (He et al., 2011). Heavy metals leaching from CRG are also of concern, especially zinc (Zn) as it is present in quantities up to 1–2% (mass) and can leach in mg quantities over long periods of time, even after deposition in the environment (Rhodes et al., 2012).

Most environmental studies into the effects of CRG have focused on terrestrial soil and freshwater ecosystems, where leaching into rainwater and runoff via waterways occurs (Wik and Dave, 2009; Wagner et al., 2018; Halle et al., 2020). Regulated metals (As, Ag, Ba, Cd, Cr, Hg, Pb, and Se) and organic contaminants in freshwater leachates of tire rubber have been shown to have concentrations below their respective regulatory limits (Cheng et al., 2014). Laboratory studies with cladocerans (*Daphnia magna*) and algae (*Pseudokirchneriella subcapitata*) indicated the major toxic constituent in freshwater leachates is Zn, with minor contributions from organic compounds (Gualtieri et al., 2005; Wik et al., 2009). A recent study reported only small fractions of the heavy metals and PAHs present were bioavailable for freshwater benthic macroinvertebrates (Redondo-Hasselerharm et al., 2018). However, many urban areas are located on the coast, making the marine environment an additional likely sink for CRG as it is transported through the environment. For example, Norway has a number of artificial turfs using CRG as turf infill located near the coast or fjords, and also storage and production facilities for CRG adjacent to ports and the open sea (**Figure 1**; Møllhausen et al., 2017). There is very limited knowledge regarding the behavior and fate of CRG in the marine environment. Ecotoxicological metrics are often the starting point for environmental risk assessment. Risk assessment procedures include various metrics of species tolerance to chemicals (Forbes and Calow, 2002; Calow and Forbes, 2003).

FIGURE 1 | Example of CRG storage and production facilities located adjacent to port and open sea areas near Porsgrunn, Norway. Aerial image generated using Google Maps (2020).

TABLE 1 | Overview of tire-derived crumb rubber granulate (CRG) reference materials used in the studies.

Test material	CRG ID	Source/origin	Comments
Collected field sample of CRG	TRD	Sports field in Trondheim	Material had been in the environment for an unknown period of time. Represents material that has undergone weathering and leaching.
Collected field sample of CRG	TOS	Sports field in Tromsø	Material prior application on the field. Represents material before usage on turf.
Commercial CRG	RGS	Commercial supplier	'Pristine' consumer product ("Medium Infill") in size range 1.0–2.8 mm.
Commercial CRG cryo-milled fraction <1500 μm	RGS 1500 μm	CARAT	Cryo-milled and sieved to obtain the <1500 μm fraction
Commercial CRG cryo-milled fraction <1000 μm	RGS 1000 μm	CARAT	Cryo-milled and sieved to obtain the <1000 μm fraction
Commercial CRG cryo-milled fraction <250 μm	RGS 250 μm	CARAT	1000 μm fraction further sieved to obtain the <250 μm fraction

Survival, quantified through standardized laboratory toxicity tests, is a widely used expression of species tolerance to chemical exposures. The most common testing protocol is performed by exposing biota to several different concentrations of chemicals.

The current study aimed to investigate the organic chemical and metal profiles in CRG materials and their associated seawater leachates, as well as assessing the toxicity of CRG leachates to two coastal arctic species of copepod (*Acartia longiremis* and *Calanus* sp.). CRG test materials were sourced both directly from a commercial supplier ('pristine') and collected from outdoor sports fields in Trondheim and Tromsø ('weathered'). Additionally, the commercial material was cryomilled into small particle size fractions. The organic chemical content of the CRG materials was determined by a combination of non-target and target analysis using gas chromatography mass spectrometry (GC-MS) techniques, while metals were determined using inductive coupled plasma mass spectrometry (ICP-MS). Leachate studies were performed over a 30-day period and target organics and metals determined using the same techniques. CRG leachates were also produced and used to investigate their toxicity to marine copepods (*Acartia longiremis* and *Calanus* sp.).

MATERIALS AND METHODS

Chemicals and Materials

Pristine CRG (RGS) was supplied by RagnSells, Norway, pre-use CRG (TOS), produced by JOGRA, Steinindustri AS, Norway and weathered CRG (TRD) was collected directly from an outdoor sports field in Trondheim, Norway. All organic solvents and salts were of analytical grade and their purity verified in-house prior to use. Dichloromethane (DCM) was supplied by Rathburn (United Kingdom), ethyl acetate (EtOAc) was supplied by Fluka (Germany) and methanol was supplied by MERCK (Norway). Deionized water was produced from a MilliPore® MilliQ water system. Natural seawater was collected from 90 m depth in Trondhjemsfjorden and 60 m depth in Sandnessund (Tromsø), filtered to remove coarse particles and then sterile filtered (0.22 μm Sterivex®) prior to use in the experiments. Reference organic chemical standards were supplied by Chiron AS (Trondheim, Norway) and Sigma-Aldrich (Darmstadt, Germany). Reference inorganic chemical standards were supplied by Inorganic Ventures (Christiansburg, VA, United States). The suite of tire-derived CRG reference materials comprised a 'pristine' CRG procured from a commercial supplier (RGS) and two field collected samples representing 'pre-use' (TOS) and 'weathered' (TRD) CRG materials (**Table 1**). The pristine RGS CRG material (1.0–2.8 mm) was further cryomilled into <1500, <1000 and <250 μ m fractions.

Characterization of CRG Materials

Prior to use in leaching and toxicity studies, the metal and organic chemical content of the CRG samples was determined using a combination of non-target and target analytical chemical methods; conventional gas- and liquid chromatography mass spectrometry (GC- and LC-MS), pyrolysis-GC-MS and inductively coupled plasma mass spectrometry (ICP-MS). For conventional non-target GC-MS analysis, triplicate samples of CRG (∼100 mg) were solvent extracted with DCM and triplicate samples were extracted using EtOAc. For target analysis of phthalates, duplicates were extracted using DCM/hexane (1:1, *v/v*), where 4 mL solvent and a mixture of surrogate organic chemical internal standards (DEP-*d*4, DIBP-*d*4, DHXP-*d*4, DBzP-*d*4, DEHP-*d*4) was added to each sample prior to extraction. Extraction of all samples was conducted using bath sonication for 30 min (Bandelin Sonorex Super RK 510H, 640W, 35 kHz) at either room temperature (DCM and DCM/hexane) or 65°C (EtOAc) to bath sonication for 30 min. Solvent extracts were then filtered through a pipette packed with Bilson cotton and a small amount of anhydrous Na_2SO_4 to remove particulates and moisture. Extracts were then concentrated by solvent evaporation (40°C under a gentle flow of N_2) to approximately 500 μL and recovery internal standards (fluorene-*d*10, acenapthene-*d*10 or DOP-*d*4 depending on the target chemicals) added prior to analysis by GC- and LC-MS. Phenolic compounds in CRG were determined by extracting a sub sample (0.1 g) twice with 2 mL of distilled methanol under 15 min of ultrasonication (USC-THD, VWR, Norway). Internal standards (^{13}C-labeled BPA, BPB, BPE, 4,4′-BPF, BPP, 4,4′-BPS, 2,4′-BPS, BPZ, BPAF, TBBPA, nonylphenol, octylphenol and D-labeled 2,2′-BPF, and BPAP) were added prior to extraction. The extracts were combined and concentrated to 0.5 mL, followed by centrifugation to remove any suspended particulate material prior to analysis by LC-MS. For pyrolysis GC-MS, CRG samples were analyzed directly without any pre-treatment. The samples (a few mg of each) were placed in a 45 μL glass vial, which was subsequently heat-sealed. Samples were analyzed using both thermal desorption and pyrolysis approaches.

Leaching of Chemicals From CRG

The influence of CRG particle size, CRG concentration and natural weathering (both field-collected samples and samples placed in ocean for 12 months) on the metal and organic chemical profile of the resulting leachates was investigated. To generate leachates for chemical characterization, CRG samples were shaken (orbital shaker) at 250 rpm in sterile-filtered seawater at room temperature (approximately 20°C) in the dark. The leachate studies investigated the influence of CRG concentration (1, 10 and 100 g L^{-1}), exposure time (1–30 days), the influence of CRG origin (pristine, pre-use, weathered) and the influence of CRG particle size (medium infill particles (1.0–2.8 mm) and cryomilled particles: 250, 1000, and 1500 μm) on the resulting leachate composition. To generate leachates for toxicity testing, a standard exposure time (14 days), CRG concentration (100 and 10 g L^{-1}, respectively), and size (medium infill) was applied. Dilutions of filtered leachate were prepared directly in sterile filtered seawater (salinity 34–35 psu, pH 8.0–8.2).

On sampling, the leachates were isolated from the CRG material using a glass fiber filter (GF/F or GF/C, 0.7–1.2 μm nominal pore size) and then sub-sampled for metal and organics analysis. For GC-MS analysis, surrogate internal standards (same as above) were added to the aqueous leachates, which were then acidified (HCl, pH∼2). The samples were extracted three times with either DCM only or with a mixture of DCM and *n*-hexane (1:1, v/v) in appropriate volumes depending on the sample size. The combined extracts were gently evaporated to approximately 500 μL and a recovery internal standard (same as above) added immediately prior to analysis by GC-MS. For LC-MS analysis of the phenolic compounds, 20 μL of each leachate was mixed into 80 mL of HCl and an internal standard (^{13}C-labeled BPA, BPB, BPE, 4,4′-BPF, BPP, 4,4′-BPS, 2,4′-BPS, BPZ, BPAF, TBBPA, non-ylphenol, octylphenol and D-labeled 2,2′-BPF and BPAP) added. An equal amount of methanol was added to an aliquot of the acidified mixture and thoroughly mixed prior to analysis by LC-MS. Aliquots of the leachates were set aside for metal analysis by ICP-MS.

Analytical Methods

Both the thermal desorption and full pyrolysis methods used to analyses the CRG materials employed an Agilent 7890A GC coupled to an Agilent 5975C MS, fitted with a ZB5-MSplus column (60 m × 0.25 mm × 0.25 μm) and an EI source operated at 230°C and 70 eV. The CRG samples were introduced into the pyrolysis chamber at 230°C, and the chamber temperature rapidly increased to the final temperature (300°C or 600°C), before the vial was manually broken and the analytes released onto a cryogenic (liquid nitrogen) trap. The pyrolysis chamber was heated to 300°C (2 min hold) for thermal desorption analysis and heated to 600°C (2 min hold) for full pyrolysis. After the hold time, the analytes are released onto the analytical column with helium as the carrier gas. The GC temperature was held at 40°C (1 min), ramped to 320°C at 12°C min^{-1} (12 min hold). The MS was operated in full scan mode (*m/z* 50–500) and analytes identified based on >90% match to NIST 2017 library spectra.

Each CRG material and corresponding leachate extract was analyzed by three different GC-MS approaches: (i) a non-target full-scan analysis to identify all GC-amenable additive chemicals, (ii) a selected ion monitoring (SIM) method specifically targeted toward PAHs, and (iii) a SIM method targeted toward benzothiazole. All analyses were performed with a GC-MS system comprising an Agilent 7890A GC equipped with an Agilent 5975C Mass Selective Detector (MSD) fitted with an EI ion source. A detailed overview of the instrumental conditions is provided in the **Supplementary Information**. After initial inspection of chromatograms, peaks were deconvoluted using Unknowns algorithms and best hits from NIST 2017 library were extracted. Compounds were filtered based on observed presence in at least 3 of 6 replicates and >90% match to NIST 2017 library mass spectra. Biogenic compounds or compounds of possible biogenic origin were removed from the data set. All compounds found in control samples were removed from the data set. For target analyte quantification, a 6-level calibration curve was applied to calculate concentrations after normalizing response to internal standards.

Phenolic compounds were analyzed using the Agilent 1290 UHPLC coupled to Agilent 6550 HR-QTOF system operated in a negative electrospray ionization mode. Separation of bisphenols was achieved with the use of a Waters HSS T3 column (1.8 μm, 150 × 3.0 mm) with a gradient of water and methanol used as a mobile phase. The phthalate extract was measured directly without further pre-treatment by LC-MS (Vantage, Thermo Fisher Scientific, United States) using a Waters UPLC column with a BEH Phenyl 100 × 2.1 mm, 1.8 μm phase. A solvent gradient of A: 0.1% Formic acid in water and B: 0.1% formic acid in methanol was applied as the mobile phase. For quantification of bisphenols and phthalates, the isotopic dilution method was applied. Detection limits were calculated based on the instrumental sensitivity of control samples. All data are blank corrected.

Metal concentrations in the CRG extracts and leachate extracts were determined for different experiments at two laboratories using two slightly different, but comparable ICP-MS approaches. A detailed overview of the sample preparation approach and instrumental conditions are provided in the **Supplementary Information**. Briefly, the first approach involved digestion of the samples using HNO_3, HCl and H_2O_2 at 220°C for 20 min, followed by dilution in MilliQ and addition of ^{103}Rh and ^{115}In internal standards. Analysis was performed using an Agilent 8800 Triple Quadrupole ICP-MS (ICP-QQQ) fitted with a SPS 4 Autosampler. In the second approach, samples were digested in 5 mL HNO_3 and 3 mL deionized water at 250°C for 65 min, followed by dilution in MilliQ and addition of ^{115}In as an internal standard. Analysis was performed using an Agilent 7700x ICP-MS.

Exposure of Marine Copepods to Seawater CRG Leachates

Zooplankton was collected in Balsfjord and Håkøybotn near Tromsø (Norway, 69.67°N 18.79°E) with a WP2 net fitted with a 180 μm mesh and a non-filtering cod end. The organisms

were diluted in ambient seawater and brought to the laboratory for acclimation in 50 L tanks aerated with silicone tubes. Individual adult female copepods were sorted into small bowls and kept at ambient temperature (8°C) prior to use. For exposure experiments, a series of seawater CRG leachate stock solutions were produced using the method described above. The stock solutions represented leachates derived from (i) 100 g L^{-1} of TOS CRG, (ii) 10 g L^{-1} TOS CRG, (iii) 10 g L^{-1} TRD CRG, and (iv) 10 g L^{-1} RGS CRG. The leachates were isolated by passing the sample through a glass fiber filter (GF/C, 1.2 μm nominal pore size). For toxicity testing, the stock solutions were diluted with filtered seawater to the desired concentrations (0.01–100 g L^{-1}). The corresponding CRG mass concentrations for each leachate dilution are presented in **Supplementary Table S1**.

A pilot study (Experiment 1) to determine general concentration ranges leading to copepod mortality was conducted with 24 individuals of two coastal arctic species (*Acartia longiremis* females and *Calanus* sp. pre-adult copepodite stage 5 (C5) and adult females) sorted from the field samples collected at Håkøybotn. The organisms were exposed to seawater leachate solutions of CRG TOS (100 g L^{-1}) at 100 (i.e., undiluted) and 50 g L^{-1} dilution in 5 mL wells on two 12-multiwell plates ($n = 24$). Mortalities were recorded in 4 h intervals (*Acartia* only) and at the end of the 24 h exposure period. In a second study (Experiment 2), groups of copepods ($n = 10$) were incubated in 3 replicate 500 mL blue cap glass bottles (total volume 620 mL) containing filtered seawater, microalgae food (*Tetraselmis* sp. >5000 cells mL^{-1}) and a range of leachate concentrations corresponding to 5–35 g L^{-1} of CRG (TOS only). Control exposures contained only copepods, algae and filtered seawater (no leachate). The bottles were attached onto a plankton wheel (**Supplementary Figure S1**) and rotated slowly (0.26 rpm) for up to 17 days (or until all individuals in the exposure bottles had died) while submersed in seawater at 8°C. A third study (Experiment 3) used the same approach as Experiment 2, but with lower leachate concentrations (representing 0.01, 0.1 and 1 g L^{-1} of CRG) and for 3 different CRG types (TOS, TRD and RGS). Survival was monitored daily over a 2-week period.

To study the effect of the leachates on the survival of the copepods, effect sizes were calculated as mean differences, subtracting average mortality in the corresponding controls from the mortality recorded in the leachate dilutions:

$$x_{Diff} = \overline{x_{leach}} - \overline{x_{contr}}$$

The variance was estimated as the pooled standard deviation (Rosnow and Rosenthal, 1996):

$$var = \sqrt[2]{\frac{SD^2_{leach} + SD^2_{contr}}{2}}$$

The pooled standard deviation was then multiplied with 1.96, representing 95% of the area under a normal distribution curve, to plot vertical error bars of the mean differences. Error bars above (and not crossing) the zero line denote significantly higher mortality in the exposures than in the controls.

RESULTS AND DISCUSSION

CRG Characterization

Non-target Screening Analysis of CRG

An overview of the organic compounds detected in the CRG extracts by non-target analysis is presented in **Supplementary Table S2**. In total, 19 different compounds were identified with a ≥90% match to NIST 2017 library mass spectra. Compounds included PAHs (pyrene and phenanthrene), benzothiazoles (benzothiazole, 2-mercaptobenzothiazole), phenols (4-tert-octylphenol, 3-tert-butylphenol), methyl stearate, quinolines and amines (N-(1,3-dimethylbutyl)-N′-phenyl-1,4-benzenediamine, diphenylamine) amongst others. PAHs and benzothiazoles are well-known components of CRG, with many classified as environmental and human toxins (ChemRisk Inc., 2008; ECHA, 2017). However, some of the other compounds identified represent classes of chemicals that are less commonly reported and less is known about their potential risks (Rogge et al., 1993; Llompart et al., 2013; Wagner et al., 2018).

Quantitative Analysis of Target Organic Compounds in CRG

A summary of the concentrations of the target 16 EPA PAHs (presented as total PAHs), phenolics, benzothiazole and other selected compounds in the CRG extracts (TRD, TOS and RGS) is presented in **Table 2**. Concentrations of individual detectable compounds ranged from 0.0004 mg kg^{-1} (4,4′-bisphenol S in TRD) to 540 mg kg^{-1} (acetophenone in TOS) of CRG. Total PAH concentrations across the 3 different CRG materials were largely consistent and ranged from 47 mg kg^{-1} (TOS) to 58 mg kg^{-1} (TRD). The most prevalent PAH was pyrene at 24–25 mg kg^{-1}, followed by fluoranthene and phenanthrene at 8–7 mg kg^{-1} and 3.8–6.5 mg kg^{-1}, respectively. These findings are well within the range of concentrations reported in CRG by ECHA (9.12–58.2 mg kg^{-1}) and by the US EPA (mean of 41 mg kg^{-1}; $n = 27$) (ECHA, 2017; US EPA and CDC/ATSDR, 2019). Benzothiazole exhibited high concentrations in all CRG materials, but with greater variation than the PAHs, ranging from 37 mg kg^{-1} (TRD) to 110 mg kg^{-1} (TOS). These values are slightly higher to those reported previously by the US EPA of 11 mg kg^{-1} (US EPA and CDC/ATSDR, 2019). Acetophenone and phthalide were present in very low concentrations in the TRD and RGS materials (0.22–0.37 and 0.1–0.4 mg kg^{-1}, respectively), but were present in very high concentrations in the TOS material (78–540 mg kg^{-1}, respectively). In general, phenolic compounds were present in very low concentrations ranging from 0.0004 mg kg^{-1} to 4 mg kg^{-1}, with seven of the twelve target phenols not being found in any of the CRG materials. Only 2,4-bisphenol A, 2,4-bisphenol F, 4,4′-bisphenol F and trace amounts of 4,4′-bisphenol S and 4,4′-bisphenol A were detected. Sum Bisphenol concentrations ranged from at 2.26 mg kg^{-1} (TOS) to 6.33 mg kg^{-1} (TRD), with 2,4-bisphenol F as the major contributor at 0.61–1.21 mg kg^{-1}, followed by 4,4′-bisphenol F at 0.38–0.83 mg kg^{-1} and 2,4-bisphenol A with 0.16–0.18 mg kg^{-1}. Interestingly, there was quite a large degree of variation in the concentrations of some compounds between the different CRG samples. This may reflect

different source materials used in the preparation or, in the case of TRD samples which had been exposed in the environment, changes due to weathering. While there does not appear to be any studies comparing the chemical composition of a wide range of different tires, an ecotoxicological assessment of the leachates from 25 different tires indicated a range of EC50 values, suggesting varying chemical compositions (Wik and Dave, 2006).

Of the 14 analyzed phthalates, only 7 could be detected in CRG (**Table 2**). DEHP dominated with 17.7 mg/kg followed by DiNP, DiBP and DnBP (10.1, 2.94, 2.60, and 2.06 mg/kg). The total phthalate load in CRG is similar to the PAH load and benzothiazole (47–58 mg kg^{-1} and 37–110 mg/kg^{-1}, respectively). A previous study found lower average concentrations for all four of these phthalates in CRG sampled directly from artificial pitches, but the values from the current study are well within the variation of the data reported (RIVM, 2016). Four phthalates (DiBP, DBP, BBP and DEHP) are classified by ECHA as toxic to reproduction in category 1B (may damage the unborn child and are suspected of damaging fertility), with BBP and DBP also categorized as toxic to the aquatic environment. In addition, ECHA's Member State Committee (MSC) has unanimously confirmed that these four phthalates are endocrine disruptors related to human health (although they did not agree unanimously that they were of equivalent concern) and that DEHP is an endocrine disruptor in the environment. All four phthalates are registered as substances of very high concern (SVHC) (ECHA, 2017). Both phthalates and their metabolites were found in marine species such as turtles and porpoises, indicating existing exposure to these rubber and plastic additives. After being taken up by the organisms, they are metabolized relatively fast, forming stable metabolites with unknown toxicity (Savoca et al., 2018; Rian et al., 2020).

TABLE 2 | Concentrations of organic compounds in rubber granulates (mg kg^{-1}).

	Concentration of target compounds (mg kg^{-1})		
Target compound	**TRD**	**TOS**	**RGS**
Pyrene	24 ± 4	25 ± 8	24 ± 3
Fluoranthene	8 ± 2	8 ± 2	7 ± 1
Phenanthrene	6.5 ± 0.3	3.8 ± 0.3	5.9 ± 0.1
Σ PAH	**52 ± 6**	**47 ± 11**	**58 ± 7**
Benzothiazole	37 ± 1	110 ± 28	105 ± 15
n-Cyclohexylformamide	2 ± 2	9 ± 2	22 ± 5
Acetophenone	0.22 ± 0.03	540 ± 37	0.37 ± 0.06
Phthalide	0.40 ± 0.04	78 ± 15	0.10 ± 0.02
Σ Additives	**39.6**	**737**	**127.5**
Bisphenol A	4 ± 5	1.1 ± 0.3	3 ± 1
4,4′-bisphenol S	0.0004	0.001	N/A
2,4′-bisphenol S	n.d.	n.d.	N/A
4,4′-bisphenol F	0.83	0.38	N/A
2,4′-bisphenol F	1.21	0.61	N/A
2,2′-bisphenol F	0.11	0.005	N/A
4,4′-bisphenol A	0.18	0.16	N/A
2,4′-bisphenol A	0.003	n.d.	N/A
Bisphenol B	n.d.	n.d.	N/A
Bisphenol E	n.d.	n.d.	N/A
Σ Phenols	**6.33**	**2.26**	**–**
DMP	N/A	n.d.	N/A
DEP	N/A	0.25	N/A
BBP	N/A	0.62	N/A
DiBP	N/A	2.94	N/A
BnBP	N/A	n.d.	N/A
DnBP	N/A	2.60	N/A
DCHP	N/A	n.d.	N/A
DMPP	N/A	n.d.	N/A
DHxP	N/A	n.d.	N/A
DEHP	N/A	17.7	N/A
DOP	N/A	n.d.	N/A
DiNP	N/A	10.2	N/A
DNP	N/A	n.d.	N/A
DiDCP	N/A	2.04	N/A
Σ Phthalates	**–**	**36.3**	**–**

Data is presented for field collected CRG from a football field (TRD), pre-use CRG (TOS), and 'pristine' CRG (RGS). Standard deviation is given where replicates were measured (n = 3). n.d. = not detected. N/A = not analyzed.

CRG Characterization by Pyrolysis GC-MS

Thermal desorption chromatograms and pyrograms are presented in **Supplementary Table S3**. The pyrograms are complex but reveal similar "fingerprints" between pristine infill (RGS) and weathered CRG (TRD). This is not surprising, given that most of the compounds revealed by this type of analysis are large molecules and small fragments typically produced by the pyrolysis process. Additive-related compounds identified included benzothiazole and its methylated isomers, *N*-(1,3-dimethylbutyl)-*N*′-phenyl-1,4-benzenediamine, *d*-limonene, and quinolines. Other compounds identified included small aliphatic (alkanes, alkenes and cyclic compounds) and aromatic hydrocarbons (BTEX (benzene, toluene, ethylbenzene, xylenes), C4-C6 alkylbenzenes, styrene, indanes, PAHs) and small ketones. The smaller hydrocarbons are expected to be products of partial fragmentation of the styrene butadiene rubber (SBR) in the CRG, while the other compounds are mostly known rubber additives. A number of additional additives were identified by chemical extraction followed by fullscan GC-MS analysis of the CRG (**Supplementary Table S2**), with benzothiazole being the most pronounced additive peak, alongside *N*-(1,3-dimethylbutyl)-*N*′-phenyl-1,4-benzenediamine, which was also identified in the pyrograms.

Metals in CRG

The results of the metals analysis of pristine (RGS), pre-use (TOS) and weathered (TRD) CRG, as well as cryomilled CRG of different size fractions, are given in **Table 3**. Zinc was the most abundant metal in all samples, ranging from 22601 mg kg^{-1} (TOS) to 12544 mg kg^{-1} (TRD). Mg ranged from 1046 mg kg^{-1} (TRD) to 273 mg kg^{-1} (RGS), Al ranged from 1305 mg kg^{-1} (TRD) to 1066 mg kg^{-1} (RGS), Fe ranged from 1214 mg kg^{-1} (TRD) to 729 mg kg^{-1} (TOS), Co ranged from 84 mg kg^{-1} (RGS) to 36.5 mg kg^{-1} (TRD) and Cu ranged from 85 mg kg^{-1} (TOS) to 18 mg kg^{-1} (TRD). All other metals (Cr, Mn, Ni, Cd, Sb and Pb) were below 25 mg kg^{-1} in all CRG samples. The variation in individual metal concentrations between TRD, TOS

TABLE 3 | Concentrations of metals in CRG (mg kg^{-1}).

Element	TRD	TOS	RGS	RGS 1500 μm	RGS 1000 μm	RGS 250 μm
Cr	5.50 ± 0.09	1.9	2.11 ± 0.09	2.24 ± 0.09	2.93 ± 0.03	23.3 ± 0.9
Mn	15.6 ± 0.2	N/A	5.12 ± 0.05	4.4 ± 0.2	4.99 ± 0.08	11.5 ± 0.3
Fe	1214 ± 27	729	562 ± 0.9	349 ± 4	385 ± 10	1220 ± 22
Co	36.5 ± 0.5	200	84 ± 2	66 ± 2	70 ± 1	203 ± 4
Ni	4.3 ± 0.2	2.56	2.8 ± 0.1	3.4 ± 0.2	3.6 ± 0.3	11.4 ± 0.4
Cu	17.7 ± 0.2	85.1	22.6 ± 0.4	6.7 ± 0.2	10.3 ± 0.1	123.8 ± 0.8
Zn	12544 ± 150	22 601	14136 ± 89	14987 ± 200	15399 ± 226	19491 ± 295
Cd	0.83 ± 0.05	1.84	0.71 ± 0.02	0.93 ± 0.04	1.36 ± 0.06	1.1 ± 0.1
Sb	4.39 ± 0.06	0.24	6.7 ± 0.2	6.2 ± 0.2	4.88 ± 0.09	8.3 ± 0.3
Pb	17.8 ± 0.3	24.9	16.6 ± 0.3	18.1 ± 0.4	28.6 ± 0.6	25.3 ± 0.8

Data is presented for CRG collected from a football field (TRD), pre-use CRG (TOS), and 'pristine' CRG (RGS), as well as different sizes of RGS (1500, 1000, and 250 μm). Standard deviation is given where replicates were measured (n = 3). N/A = not analyzed.

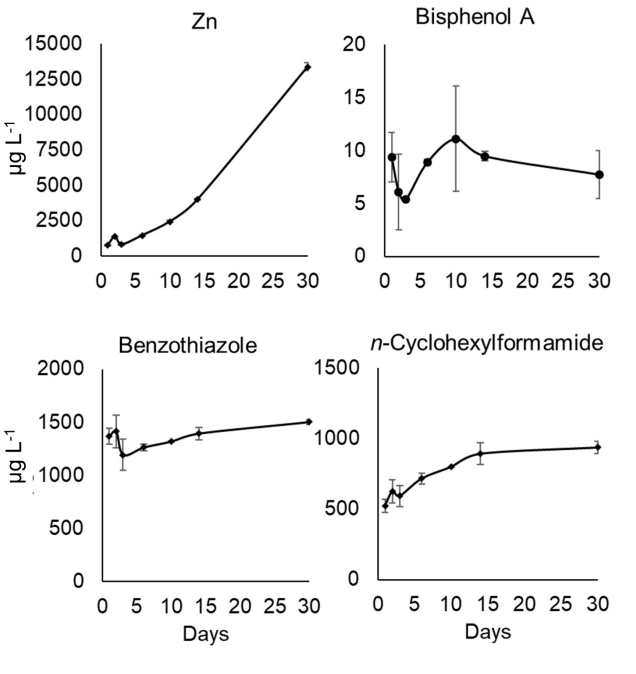

FIGURE 2 | Leaching of zinc, bisphenol A, benzothiazole and n-cyclohexylformamide from pristine crumb rubber granulate (RGS) into seawater over 30 days at a crumb rubber concentration of 100 g L^{-1}.

and RGS was typically less than an order of magnitude (**Table 3**). The observed variation appears to reflect differences in the source materials for the different CRG materials as the concentration of some metals was highest in the weathered TRD material (Mg, Al, Cr, Mn, Fe, Ni). However, Zn was lower in TRD than either TOS or RGS and may indicate loss of this metal through leaching in the environment.

Leaching of CRG Chemicals Into Seawater

The pilot study investigating the effect of exposure time (1–30 days) on metal and organic additive composition and concentration in seawater leachates indicated that an exposure time of 14 days was sufficient to generate stable leachate concentrations of organic chemicals in a static system (**Figure 2**). However, Zn concentrations in the seawater leachate continued to increase until the end of the experiment, which lasted for 30 days. This is in line with previous studies on Zn leaching from tire rubber, which showed that continued leaching in a flow-through system did not deplete the Zn reservoir in the granulate significantly (Rhodes et al., 2012). Based on these data, an exposure time of 14 days was used to generate leachates for the remaining leachate studies and toxicity studies.

After 14 days, a distinct coloration of the seawater was clearly visible, indicating leaching and dispersion of fine CRG particulates (**Supplementary Figure S2**). Target analysis of the leachates revealed that a number of organic (**Tables 4**, **5**) and metal (**Table 6**) additives leached from the CRG into the seawater. Benzothiazole was the organic compound with the highest concentration in all CRG leachates, irrespective of the

TABLE 4 | Concentration of benzothiazole and total PAHs in seawater leachates as a function of CRG concentration.

	Organic chemical concentrations (μg L^{-1})	
Test Material	**Σ PAH**	**BT**
TOS 100 g L^{-1}	2.5 ± 0.5	1415 ± 781
TOS 10 g L^{-1}	1.7 ± 0.1	690 ± 389
TOS 1 g L^{-1}	<2	68 ± 49
TRD 100 g L^{-1}	2.8 ± 0.6	126 ± 70
TRD 10 g L^{-1}	4 ± 2	48 ± 27
TRD 1 g L^{-1}	5 ± 5	27 ± 37
RGS 100 g L^{-1}	4.4 ± 0.7	1693 ± 930
RGS 10 g L^{-1}	2.3 ± 0.4	563 ± 308
RGS 1 g L^{-1}	3.3 ± 2.5	80 ± 46
RGS 1500 μm 10 g L^{-1}	2.2 ± 0.1	546 ± 302
RGS 1000 μm 10 g L^{-1}	2.4 ± 0.6	526 ± 289
RGS 250 μm 10 g L^{-1}	2.4 ± 0.1	512 ± 281
Seawater control	<2	<2

Data is presented for 'pristine' CRG (RGS), pre-use CRG (TOS) and field collected CRG from a football field (TRD), as well as different sizes of RGS (1500, 1000, and 250 μm). Standard deviation is given where replicates were measured (n = 3).

TABLE 5 | Concentration of phenols and total phthalates in the seawater leachate of TOS (100 g L^{-1}).

Organic chemical	Concentration in TOS 100 g L^{-1} (μg L^{-1})
BPA	n.d.
4,4′-BPS	0.98
2,4′-BPS	n.d.
4,4′-BPF	6.2
2,4′-BPF	11.9
2,2′-BPF	n.d.
4,4′-BPA	n.d.
2,4′-BPA	n.d.
BPB	n.d.
BPE	n.d.
ΣPhenols	19.1
ΣPhthalates	<LOD
Seawater control	<LOD

Only one replicate was measured. n.d = not detected.

CRG to water ratio used to generate the leachate, while Zn was the metal with the highest concentration in all leachates. The most abundant organic and metal components measured in the original CRGs materials were also most abundant in the corresponding leachates. Benzothiazole concentrations in leachates from the three different CRGs differed but were consistent with the distributions in the source CRG materials where the lowest concentrations were determined for TRD CRG and the corresponding leachate (**Table 4**). This may reflect inherent variability of the CRG composition or that this low molecular weight compound (MW 135) preferentially leaches out of CRG in the natural environment. However, benzothiazole concentrations in the leachates closely reflected those in the respective source CRGs. Previous studies have reported benzothiazole CRG leachate concentrations of 293–578 μg L^{-1} (Nilsson et al., 2008), 526 μg L^{-1} (Ly and Walker, 2009), 18 μg L^{-1} (Celeiro et al., 2014), which are comparable to the values determined in the current study (**Table 4**). The concentrations of benzothiazole and Zn in seawater leachates showed a linear relationship with the amount of CRG added to the seawater (**Figure 3**), supporting the suitability of direct dilution of stock leachates for the toxicity study.

The total PAH concentrations in the different seawater leachates were generally low, ranging between <LOD (for the leachate produced from TOS at 1 g L^{-1}) and 4.4 μg L^{-1} (for the leachate produced from RGS at 100 g L^{-1}) (**Table 4**). In contrast to benzothiazole and metals, there was no clear increase in the total PAH concentration relative to increasing CRG exposure concentration. Phenolic compounds were found in low abundance in the TOS leachate, dominated by 2,4-bisphenol F and 4,4′-bisphenol F (11.9 and 6.2 μg L^{-1}), while phthalates were not found in the TOS leachate at all (**Table 5**). After Zn, the metals present at the highest concentration in the different CRG leachates (from CRG at 100 g L^{-1}) were Fe (126–377 μg L^{-1}), Mn (25–79 μg L^{-1}), Cu (39–66 μg L^{-1}) and Co (13.57 μg L^{-1}) (**Table 6**). All other target metals (Cr, Ni, Cd, Sb and Pb) were present at concentrations of <10 μg L^{-1} in all leachates. The metal profiles in the leachates largely reflect those in the CRG materials (**Table 3**), with metals at higher concentrations in the parent CRG materials also being present at higher concentrations in the resulting leachates.

In the samples investigating the influence of particle size on leachate composition, the concentrations of individual organic chemicals and metals showed different patterns (**Tables 4**–**6**). In general, the concentrations of specific organic chemicals were similar for all three of the different particle sizes studied (250, 1000, 1500 μm) at CRG concentrations of 10 g L^{-1}. Total PAHs ranged from 2.2–2.4 μg L^{-1} and benzothiazole ranged from 512–546 μg L^{-1}, which was also comparable to the non-cryomilled material at the same exposure concentration (2.7 and 563 μg L^{-1}, respectively). A similar pattern was observed for the metals Cr (4.2–5.0 μg L^{-1}) and Pb (3.0–3.6 μg L^{-1}), which also compared to the non-cryo-milled material (4.0 and 2.7 μg L^{-1}, respectively). The other metals generally exhibited an increase in leachate concentration with a corresponding decrease in CRG particle size, although this was more pronounced for some metals than others. For example, metal concentrations more than doubled in leachates derived from 250 μm CRG particles compared those from 1500 μm CRG particles, where Zn increased from 1.7 mg L^{-1} to 4.1 mg L^{-1}, Cu increased from 23 to 33 μg L^{-1}, Mn increased from 4 μg L^{-1} to 20 μg L^{-1} and Co increased from 2.3 μg L^{-1} to 11.4 μg L^{-1}. Smaller particles have

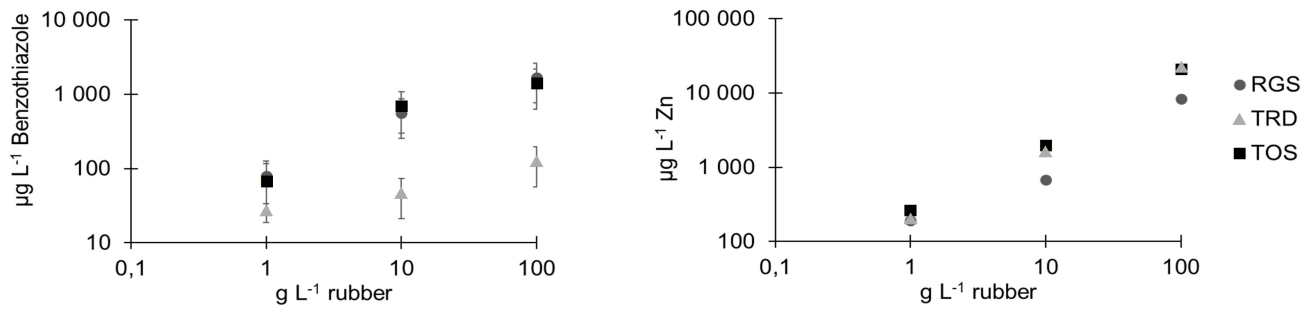

FIGURE 3 | Increasing concentrations of benzothiazole **(left)** and zinc **(right)** in seawater leachates (μg L^{-1}) as a function of CRG concentration. The graphs show averages and standard deviations for 3 replicates of leachate produced from 'pristine' CRG (RGS), pre-use CRG (TOS) and field collected CRG from a football field (TRD).

TABLE 6 | Content of target metals in seawater leachates as a function of CRG concentration.

	Metal concentrations (μg L^{-1})									
Test material	**Cr**	**Mn**	**Fe**	**Co**	**Ni**	**Cu**	**Zn***	**Cd**	**Sb**	**Pb**
TOS 100 g L^{-1}	10.6 ± 0.5	79 ± 4	377 ± 84	57 ± 2	4 ± 1	66 ± 4	20.9 ± 0.5	1.5 ± 0.3	1.0 ± 0.2	4.9 ± 0.2
TOS 10 g L^{-1}	4.8 ± 0.2	8.4 ± 0.3	53 ± 2	7.5 ± 0.3	<2	58 ± 2	2.0 ± 0.0	0.3 ± 0.1	0.3 ± 0.1	4.0 ± 0.1
TOS 1 g L^{-1}	4.0 ± 0.4	<2	21 ± 2	<2	<2	29 ± 1	0.26 ± 0.02	<0.2	<0.2	1.8 ± 0.1
TRD 100 g L^{-1}	5.8 ± 0.3	25 ± 1	176 ± 15	22 ± 1	3 ± 1	39 ± 3	22.4 ± 0.3	0.6 ± 0.1	0.5 ± 0.1	7.3 ± 0.3
TRD 10 g L^{-1}	4.0 ± 0.2	2.6 ± 0.1	28 ± 2	2.5 ± 0.1	<2	44 ± 3	1.7 ± 0.1	<0.2	0.2 ± 0.1	2.9 ± 0.2
TRD 1 g L^{-1}	4.0 ± 0.2	<2	20 ± 2	<2	<2	28 ± 2	0.21 ± 0.01	<0.2	<0.2	1.7 ± 0.1
RGS 100 g L^{-1}	4.5 ± 0.3	54 ± 1	126 ± 6	13.4 ± 0.5	3 ± 1	49 ± 2	8.4 ± 0.2	2.2 ± 0.3	1.8 ± 0.1	3.8 ± 0.2
RGS 10 g L^{-1}	4.0 ± 0.2	2.7 ± 0.3	29 ± 2	<2	<2	23 ± 2	0.67 ± 0.03	<0.2	0.3 ± 0.1	2.7 ± 0.1
RGS 1 g L^{-1}	3.7 ± 0.5	<2	38 ± 1	<2	<2	34 ± 2	0.19 ± 0.01	<0.2	0.25 ± 0.05	1.6 ± 0.1
RGS 1500 μm 10 g L^{-1}	4.2 ± 0.2	4 ± 1	28 ± 3	2.3 ± 0.5	<2	23 ± 2	1.74 ± 0.06	<0.2	0.3 ± 0.1	3.0 ± 0.2
RGS 1000 μm 10 g L^{-1}	5.0 ± 0.4	5 ± 1	60 ± 3	2.5 ± 0.4	<2	18 ± 2	2.20 ± 0.07	<0.2	0.3 ± 0.1	3.6 ± 0.2
RGS 250 μm 10 g L^{-1}	4.6 ± 0.2	20 ± 2	33 ± 3	11.4 ± 0.4	4 ± 1	34 ± 2	4.11 ± 0.07	0.3 ± 0.1	0.8 ± 0.1	3.4 ± 0.1
Seawater control (Agilent 8800 triple quadrupole ICP-MS)	4.0 ± 0.3	2.5 ± 0.2	23 ± 2	<2	<2	34 ± 2	0.13 ± 0.01	<0.2	0.3 ± 0.1	1.8 ± 0.1
Seawater control (Agilent 7700 single quadrupole ICP-MS)	0.43	n.d.	2.2	0.02	0.15	0.7	0.01	0.08	0.27	0.05

Data is presented for 'pristine' CRG (RGS), pre-use CRG (TOS) and field collected CRG from a football field (TRD), as well as different sizes of RGS (1500, 1000, and 250 μm). All concentrations are presented in μg L^{-1}, except for Zn which is presented in mg L^{-1}. Standard deviation is given where replicates were measured (n = 3); n.d. = not determined. *Zn concentrations presented in mg L^{-1}.*

a greater surface area to volume ratio, which is known to promote leaching to aqueous media. The increased leaching of Zn from CRG of decreasing particle size observed in the current study has previously been demonstrated (Rhodes et al., 2012). Very few studies have investigated the release of other metals from CRG or tire wear particles of different sizes, but the available literature indicates that the leaching of many metals is independent of particle size (Selbes et al., 2015). While it would have been interesting to normalize the leached metal concentration data by surface area to identify size effects, the size distribution of the test materials was actually quite broad and therefore the estimated surface area became a 'surface area range'. Furthermore, the particles in the current study were very irregular in shape with detailed surface morphologies, meaning that estimation of surface area based on the assumption of spherical particles is too far away from an accurate surface area estimation to be sufficiently robust. Dissolved organic carbon leaching from SBR particles has been shown to increase with smaller particle sizes (Selbes et al., 2015), which contrasts the observations for specific organic compounds in the current study. A comprehensive review of tire wear particles in the environment concluded that the influence of particle size on leaching is inconclusive (Wagner et al., 2018). The results of the current study suggest leaching of CRG components is influenced by particle size and the partitioning coefficient of individual organics and metals between the CRG and aqueous phase, as well as the background concentration of the compounds in the surrounding water (direction of concentration gradient to reach equilibrium).

The values recorded in leachates here were all above EU guideline thresholds for marine and freshwater (EU DIRECTIVE 2008/105/EC), where Environmental Quality Standards (EQS) of 0.28, 1.0 and 7.8 μg L^{-1} have been defined for cobalt, copper and zinc, respectively. Leached concentrations were exceeding these concentrations by up to three orders of magnitude (**Table 6**), with Zn over the recommended threshold by a factor of >2500.

Phthalic anhydride and *n*-cyclohexylformamide were observed in the CRG leachates but not in the original CRG materials by any of the extraction and analysis techniques (**Supplementary Table S2**). Compounds observed in CRG leachates and not in solvent extracts or pyrograms of the original CRG materials could reflect the differing water solubilities of organic chemicals present in car tire rubber. Both phthalic anhydride and *n*-cyclohexylformamide are highly polar, low molecular weight compounds (MW 148 and 127, respectively). Such compounds may be present in low levels in the CRG, but preferentially leach into aqueous solution. *n*-Cyclohexylformamide has previously been identified in fumes of ethylene propylene diene rubber, suggesting it could be a component of CRG (Forrest, 2019).

Toxicity of CRG Leachates to Marine Copepods

As relevant marine environmental concentrations are currently unknown, three exposure experiments using CRG TOS tested a wide selection of leachate concentrations, ranging from

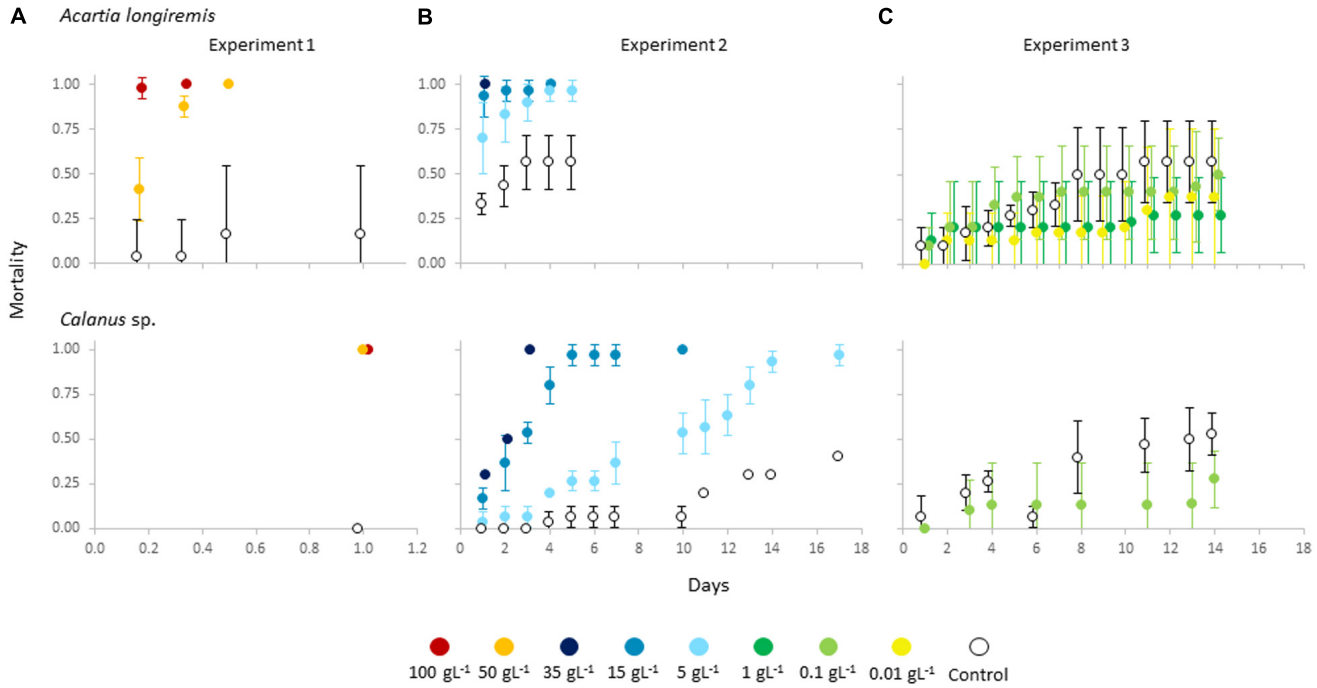

FIGURE 4 | Mortality of *Acartia longiremis* (upper panels) and *Calanus* sp. (lower panels) exposed to a range of TOS CRG leachate concentrations in three experiments; **(A)** Experiment 1 (50 and 100 g L^{-1}), **(B)** Experiment 2 (35, 15 and 5 g L^{-1}), **(C)** Experiment 3 (1, 0.1 and 0.01 g L^{-1}). Experiments 1, 2, and 3 ran for 1, 17, and 14 days, respectively.

high in Experiment 1 (100 and 50 g L^{-1}), via medium in Experiment 2 (5–35 g L^{-1}), to low in Experiment 3 (1-0.01 g L^{-1}). Mortality was chosen as the endpoint for the two copepods, the smaller *Acartia longiremis* and the larger *Calanus* sp. CRG TOS was selected as test material due to immediate availability of sufficient CRG amounts to produce the leachates. Mortality in control bottles was variable over time and between experiments, but did not mask the dose response in the treatments, except at the lowest concentrations where mortality in controls was higher than in the exposures in some instances. This may simply be due to stochastic variation in the data since we do not expect a beneficial effect of low leachate doses on the copepods. We cannot, however, rule out that non-lethal doses of one or several of the measured contaminants trigger a physiological defense response in the exposed copepods, which may increase their survival compared to non-exposed counterparts. This possibility would have to be investigated further and the nature of the defense mechanism studied with suitable methods (e.g., gene expression mapping). Cumulative mortality over time is presented in **Figure 4** for each experiment and both copepod species. At high leachate concentrations (Experiment 1), all copepods died within 24 h. This was studied in more detail for *A. longiremis*, showing a slower deterioration at 50 g L^{-1} than at 100 g L^{-1} after 4, 8 and 12 h of incubation (**Figure 4A**). Medium leachate concentrations (Experiment 2) induced a clear dose-response in both species, but also demonstrated higher sensitivity in *Acartia* than in *Calanus*, where *Acartia* reached 100% mortality much faster than *Calanus* at all three leachate concentrations (**Figure 4B**). The LC_{50} values at 48 h were 35 g L^{-1} for *Calanus* compared to <5 g L^{-1} for *Acartia*. At the lowest concentrations (Experiment 3), mortalities were higher in the controls than in the leachate exposures for both species and final mortalities after 2 weeks were ≤50% for exposed copepods (**Figure 4C**). For *Calanus*, only one low TOS concentration (0.1 g L^{-1}) was tested, where survival was 72% on day 14. The low leachate concentrations did therefore not induce negative effects in either species (**Figure 4C**). Experiment 3 (low concentrations; 1-0.01 g L^{-1}) was repeated with two more CRG types, the weathered TRD and the pristine RGS (**Supplementary Figure S3**). Again, copepod mortalities in leachate exposures were similar to those in the controls, except for TRD at 1 g L^{-1}, for which elevated mortalities were observed in both copepod species (**Supplementary Figure S3b**).

To test for significant differences in mortality between exposed and unexposed copepods, effect sizes were calculated for three selected time points: day 1, day 8 and day 14. Significant effect sizes were recorded for all exposure concentrations ≥5 g L^{-1} of CRG TOS (**Figure 5**). The lower exposure concentrations (0.01–1 g L^{-1}) were not different from controls, including for TRD at 1 g L^{-1}, despite the elevated mortalities mentioned above (**Supplementary Figure S3b**). Nonetheless, it can be hypothesized that the increased weathering state of this rubber appeared to contribute to the observed increase in toxicity. It is suggested that the partial weathering alters the rubber properties, for example making it more brittle and increasing the available

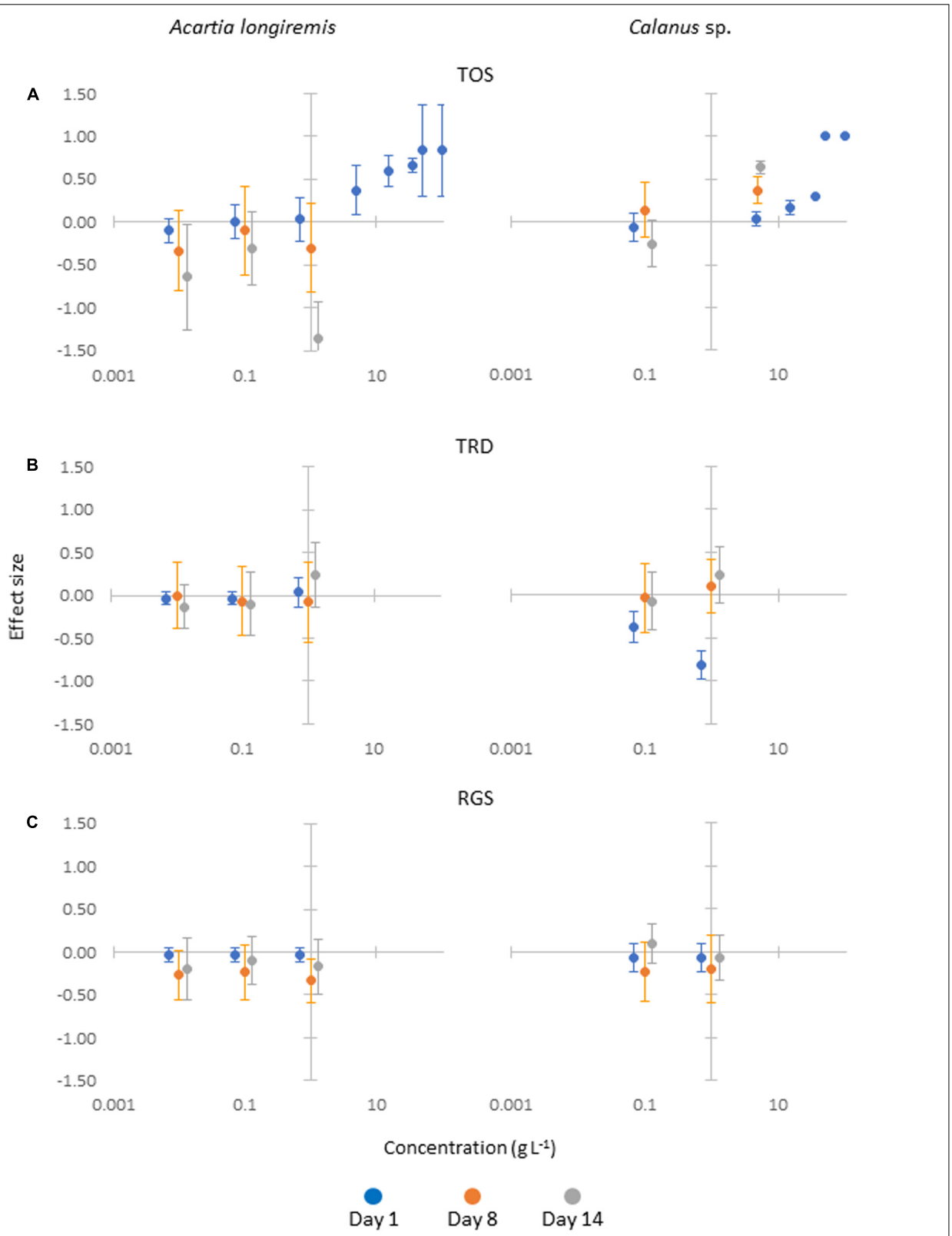

FIGURE 5 | Effect sizes of different CRG concentrations for *Acartia longiremis* (left) and *Calanus* sp. (right) for three CRG types: **(A)** TOS, **(B)** TRD, and **(C)** RGS. Positive values with error bars not crossing the zero line indicate significantly higher mortality in leachate treatments than in controls.

surface area, leading to a higher degree of contaminant release from the material.

Species-Specific Toxicity

The study demonstrates different sensitivities of the two copepods studied: *Acartia* responded with higher mortality more quickly than *Calanus* at a given CRG concentration. This may be explained by (a) the difference in body size (Neumann et al., 2005), where the smaller *Acartia* may receive higher doses via a larger surface to volume ratio than the larger *Calanus*, or (b) ingest more toxin due to higher clearance rates (volume of water filtered per time unit), or (c) due to differences in defense/repair mechanisms or internal toxin pathways. For example, *Calanus* C5 stages have lipid reserves that may help them to 'buffer' toxic molecules and remove them from their metabolism, while *Acartia* lacks this option and may be more exposed to oxidative stress (Hansen et al., 2018; Sørensen et al., 2020). The toxicity of CRG leachates on aquatic organisms has been reviewed in Wik and Dave (2009) and Halle et al. (2020). Effect concentrations ranged widely and depended on the type (e.g., abrasion method), origin (e.g., summer versus winter tires) and state (e.g., weathering, UV exposure) of the CRG applied. To our knowledge, no other studies on marine zooplankton have been performed to date, except for one study on the brackish *Eurytemora affinis* (Hall et al., 1993), where leachate exposure resulted in 100% mortality. Effect concentrations for freshwater cladocerans (daphnids), comparable to the pelagic marine copepods studied here, ranged widely but seemed to be generally lower than those recorded here. The reported 48 h EC_{50} values for *D. magna* ranged from 0.25 g L^{-1} to 10 g L^{-1} (Wik and Dave, 2005, 2006), while another study found an LC_{50} of 25 g L^{-1} after 72 h of incubation (Goudey and Barton, 1992), which is a relatively high value compared to the LC_{50} values (48 h) between 5 and 35 g L^{-1} determined in the current study. It has been proposed that tire-derived leachates exhibit reduced toxicity with increasing salinity (Hartwell et al., 2000) and the current study supports this. When leachates were eluted at pH values <7, toxicity increased in parallel with increasing Zn concentrations in the eluate (Gualtieri et al., 2005), indicating that the leachability of contaminants is variable and depends on the state of the leaching rubber (e.g., weathering state) and the prevailing leaching conditions. UV exposure of the rubber also seemed to play a role for the level of toxicity of the resulting leachate (Wik and Dave, 2006).

What Are the Drivers of CRG Leachate Toxicity?

Ingestion of CRG particles by marine organisms is known to occur (Redondo-Hasselerharm et al., 2018; Khan et al., 2019), leading to potential exposure through leaching during gut transit. However, exposure of marine organisms to additive chemicals in CRG is likely to be more widespread through leaching to the aqueous phase, especially as some of these additives exhibit persistency in the environment (Halle et al., 2020). The variety of organic additives present in CRG make it extremely challenging to determine which chemical groups are of most interest for assessing the potential environmental impacts and risks associated with CRG. Leachate toxicity studies with TWP and CRG material have been conducted in different aquatic environments with a variety of species, resulting in large variations in effects that have been attributed to differences in tire composition, leachate generation method and species sensitivity (Wik and Dave, 2009; Wagner et al., 2018). However, full elucidation of the components of TWP and CRG leachates driving toxicological responses in aquatic environments has yet to be achieved. Furthermore, comparison of CRG/TWP toxicity data is compromised by a lack of standard methods for generating leachates, for characterizing the additive chemical composition and for measuring their hazard potential, although adjustment of already existing guidelines on soluble contaminants could be fine-tuned to suit a leachate guideline (Khan et al., 2017). It will also be important going forward to established methods for distinguishing between particle effects and those deriving from additive chemicals reaching from CRG/TWP (Wik and Dave, 2009; Wagner et al., 2018; Halle et al., 2020).

In the current study, it was not possible to clearly establish which components of the CRG leachates were driving the observed toxicity and the complexity of the leachates meant that it was only possible to quantify a subset of the organic chemicals present. Benzothiazole and its derivatives appear to be strong candidates for contributing to the observed effects based on the high leachate concentrations and established toxicity. Acute and chronic toxicity of benzothiazole and its derivatives was shown for the daphnid *C. dubia* (Nawrocki et al., 2005). Benzothiazole produced EC_{50}s at 24.6 mg L^{-1} in acute (24 h) exposures and at 54.9 mg L^{-1} in chronic 1-week exposures, respectively, while several of the derivatives (including 2-mercaptobenzothiazole) had much higher toxicity. Although the concentrations of benzothiazole measured in our leachates remained below these values, with a range of 0.068 to 1.42 mg L^{-1} (**Table 4**), they may well have contributed to the overall toxicity observed in this study. The benzothiazole derivate 2-mercaptobenzothiazole was detected in CRG, but not in the leachates with the available method (**Supplementary Table S2**). Future studies should include this group of contaminants with higher resolution in the analytical chemistry to better pinpoint its contribution to CRG leachate toxicity.

In contrast to benzothiazole, PAHs in our CRG materials exceeded REACH Annex XVII entry 50 levels, but not EU REACH regulations (Annex XVII entry 28). Furthermore, PAHs only leached in limited quantities, suggesting they represent only a minor contribution to the observed toxicity. Similarly, phthalates did not leach significantly. While present in relatively small amounts in the original CRG material (3 mg kg^{-1}), a range of bisphenols leached from CRG into seawater at relatively high concentrations compared to other organics (seemingly reported for the first time herein). Bisphenols have well-documented endocrine disrupting properties, with BPS and BPF being more potent than BPA (Chen et al., 2016). While very little data is available on the aquatic toxicity of these chemicals, a field study has shown that marine copepods accumulate bisphenols, especially in earlier developmental stages (Staniszewska et al., 2016). Bisphenols from CRG may thus contribute not only to toxic effects in the copepods themselves, but in addition pose

a risk to secondary consumers in marine food webs. Zn was by far the most prevalent metal present in the CRG leachates and is often cited as the candidate most likely responsible for observed CRG/TWP leachate toxicity. For example, zinc toxicity was shown to relate to a disruption of calcium ion uptake in *Daphnia magna* (Muyssen et al., 2006) and similar mechanisms could apply for marine copepods.

Many other unidentified and unquantified organic compounds were also present in the leachates and may also be contributing to the overall toxicity. In general, the total concentrations of metals and organic pollutants are a limited means of assessing fate and transport. For example, metal toxicity depends not on total the concentration of a specific element, but on speciation, which is in turn controlled by environmental parameters such as redox, adsorption and interactions with dissolved organic matter. For organic pollutants, individual congeners of a group might exhibit a different toxic impact than others, as well as metabolization and bioaccumulation characteristics caused by variations in their molecular structure and the subsequent interactions with organisms and the environment. It is therefore important to consider that the most abundant compounds or metals in a leachate are not necessarily the most toxic and that additive toxicity may also occur. Depending on the mode(s) of action of single toxins and/or toxin mixtures, the effects may differ between marine habitats (e.g., sediment versus water column) and functional groups (e.g., feeding mode, foraging strategy, reproductive strategy, etc.). Although a previous study has indicated that leachates from car tire rubber materials are likely to be a greater threat to freshwater habitats than to estuarine or marine habitats (Hartwell et al., 2000), the current study suggests that impacts in the marine environment should also be considered, especially in regions with high emissions of TWP/CRG (e.g., urban runoff) and the Arctic, where some species may exhibit greater sensitivity than others. Beyond standardized laboratory-based effect concentrations, realistic environmental exposure scenarios are needed that study *in situ* CRG concentrations together with lethal and sublethal effects on individuals and populations in realistic concentration gradients from point sources (e.g., open-air storage facilities, coastal snow removal dumping sites). Long-term exposure of the daphnid *Cerodaphnia dubia* yielded EC_{50} values of 0.01–1.8 g L^{-1} (Wik et al., 2009), but any equivalent data for marine organisms is currently lacking. Finally, it will be important to pinpoint which leachate components are driving the observed toxicity and whether this varies across different marine species. This will provide the knowledge needed to develop risk assessments for ELTs and CRG, as well as providing industry with a priority list of additives that should be reduced or removed from rubber products.

CONCLUSION

The current work represents one of the first experimental studies to investigate the impacts of chemical additive leachates from CRG from ELTs on marine organisms. Detailed characterization of pristine and weathered CRG reference materials and their leachates indicated a complex mixture of organic chemical and metal additives were present in the materials and their corresponding leachates. Importantly, there were significant differences in additive profiles between CRG materials and their leachates, but pristine and weathered CRG materials had similar profiles, indicating that CRG particulates and the leaching chemicals will continue to pose a threat to wildlife long after their disposal. Marine copepods exhibited a dose-dependent response to CRG leachates, but species-specific differences were observed suggesting some organisms are more vulnerable to exposure than others. While benzothiazole and Zn were typically the organic and metal components identified at the highest concentrations in the leachates, further studies are necessary to elucidate which CRG leachate components are driving the observed toxicity. Furthermore, the long-term effects of CRG leachate exposure and sublethal endpoints should be studied in the future, also in combination with ingestion/exposure to the rubber particles.

DATA AVAILABILITY STATEMENT

The raw data supporting the conclusions of this article will be made available by the authors, without undue reservation.

AUTHOR CONTRIBUTIONS

CH, DH, AB, and LS contributed equally to the study. They all conceived and designed the study in collaboration. LS, DH, and AB conducted analysis of the samples. CH prepared samples and conducted the toxicity studies. All authors contributed equally to the preparation of the manuscript and approved its submission.

FUNDING

This work has been funded by the Fram Center Flagship Hazardous Substances (Framsenteret, Norway), project number 1002018.

ACKNOWLEDGMENTS

We are grateful to Itsasne Beitia Aguirre, Lisbet Støen, and Marianne Kjos at SINTEF and Mikael Harju, Pawel Rostkowski, and Marit Vadset at NILU for assistance with chemical analysis. We also acknowledge Kristine Hopland Sperre and Hector Andrade (Akvaplan-niva) for assistance with field sampling, exposure experiments, and plotting of toxicity data. We thank CARAT GmbH (Germany) for conducting cryomilling of the RGS CRG material.

SUPPLEMENTARY MATERIAL

The Supplementary Material for this article can be found online at: https://www.frontiersin.org/articles/10.3389/fenvs.2020.00125/full#supplementary-material

REFERENCES

Bocca, B., Forte, G., Petrucci, F., Costantini, S., and Izzo, P. (2009). Metals contained and leached from rubber granulates used in synthetic turf areas. *Sci. Total Environ.* 407, 2183–2190. doi: 10.1016/j.scitotenv.2008.12.026

Calow, P., and Forbes, V. E. (2003). Peer reviewed: does ecotoxicology inform ecological risk assessment? *Environ. Sci. Technol.* 37, 146A–151A. doi: 10.1021/es0324003

Canepari, S., Castellano, P., Astolfi, M. L., Materazzi, S., Ferrante, R., Fiorini, D., et al. (2017). Release of particles, organic compounds, and metals from crumb rubber used in synthetic turf under chemical and physical stress. *Environ. Sci. Pollut. Res.* 25, 1448–1459. doi: 10.1007/s11356-017-0377-4

Celeiro, M., Lamas, J. P., Garcia-Jares, C., Dagnac, T., Ramos, L., and Llompart, M. (2014). Investigation of PAH and other hazardous contaminant occurrence in recycled tyre rubber surfaces. Case-study: restaurant playground in an indoor shopping centre. *Int. J. Environ. Anal. Chem.* 94, 1264–1271. doi: 10.1080/03067319.2014.930847

ChemRisk Inc. (2008). *State of Knowledge Report for Tire Materials and Tire Wear Particles*. San Francisco, CA: ChemRisk Inc.

Chen, D., Kannan, K., Tan, H., Zheng, Z., Feng, Y.-L., Wu, Y., et al. (2016). Bisphenol analogues other than BPA: environmental occurrence, human exposure, and toxicity—a review. *Environ. Sci. Technol.* 50, 5438–5453. doi: 10.1021/acs.est.5b05387

Cheng, H., Hu, Y., and Reinhard, M. (2014). Environmental and health impacts of artificial turf: a review. *Environ. Sci. Technol.* 48, 2114–2129. doi: 10.1021/es4044193

Diekmann, A., Giese, U., and Schaumann, I. (2019). Polycyclic aromatic hydrocarbons in consumer goods made from recycled rubber material: a review. *Chemosphere* 220, 1163–1178. doi: 10.1016/j.chemosphere.2018.12.111

ECHA (2017). *An evaluation of the Possible Health Risks of Recycled Rubber Granules Used as Infill in Synthetic Turf Sports fields*. Helsinki: ECHA.

Forbes, V. E., and Calow, P. (2002). Species sensitivity distributions revisited: a critical appraisal. *Hum. Ecol. Risk Assess. Int. J.* 8, 473–492. doi: 10.1080/10807030290879781

Forrest, M. J. (2019). *Rubber Analysis: Characterisation, Failure Diagnosis and Reverse Engineering*. Berlin: De Gruyter.

Google Maps (2020). Available online at: https://www.google.com/maps/

Goudey, J. S., and Barton, B. A. (1992). "Toxicity of scrap tire materials to selected aquatic organisms," in *Report to Souris Basin Development Authority*, ed. R. Saskatchewan (Calgary, AB: Hydroqual Laboratories Limited and Environmental Management Associates).

Gualtieri, M., Andrioletti, M., Vismara, C., Milani, M., and Camatini, M. (2005). Toxicity of tire debris leachates. *Environ. Int.* 31, 723–730. doi: 10.1016/j.envint.2005.02.001

Hall, L. W., Ziegenfuss, M. C., and Anderson, R. D. (1993). *Toxicity of Tire Leachate to Eurytemora Affinis*. Queenstown, MD: University of Maryland.

Halle, L. L., Palmqvist, A., Kampmann, K., and Khan, F. R. (2020). Ecotoxicology of micronized tire rubber: past, present and future considerations. *Sci. Total Environ.* 706:135694. doi: 10.1016/j.scitotenv.2019.135694

Hansen, B. H., Olsen, A. J., Salaberria, I., Altin, D., Øverjordet, I. B., Gardinali, P., et al. (2018). Partitioning of PAHs between crude oil microdroplets, water, and copepod biomass in oil-in-seawater dispersions of different crude oils. *Environ. Sci. Technol.* 52, 14436–14444. doi: 10.1021/acs.est.8b04591

Hartwell, S. I., Jordahl, D. M., and Dawson, C. E. O. (2000). The effect of salinity on tire leachate toxicity. *Water Air Soil Pollut.* 121, 119–131.

He, G., Zhao, B., and Denison, M. S. (2011). Identification of benzothiazole derivatives and polycyclic aromatic hydrocarbons as aryl hydrocarbon receptor agonists present in tire extracts. *Environ. Toxicol. Chem.* 30, 1915–1925. doi: 10.1002/etc.581

International Rubber Study Group (2017). *Statistical Summary of World Rubber Situation. Rubber Statistical Bulletin*. Singapore: IRSG.

Khan, F. R., Halle, L. L., and Palmqvist, A. (2019). Acute and long-term toxicity of micronized car tire wear particles to Hyalella azteca. *Aqu. Toxicol.* 213:105216. doi: 10.1016/j.aquatox.2019.05.018

Khan, F. R., Syberg, K., and Palmqvist, A. (2017). Are standardized test guidelines adequate for assessing waterborne particulate contaminants? *Environ. Sci. Technol.* 51, 1948–1950. doi: 10.1021/acs.est.6b06456

Lassen, C., Hansen, S. F., Magnusson, K., Norén, F., Hartmann, N. B., Jensen, P. R., et al. (2015). *Microplastics. Occurrence, Effects and Sources of Releases to the Environment in Denmark*. Copenhagen: The Danish Environmental Protection Agency.

Li, X., Berger, W., Musante, C., and Mattina, M. I. (2010). Characterization of substances released from crumb rubber material used on artificial turf fields. *Chemosphere* 80, 279–285. doi: 10.1016/j.chemosphere.2010.04.021

Llompart, M., Sanchez-Prado, L., Pablo Lamas, J., Garcia-Jares, C., Roca, E., and Dagnac, T. (2013). Hazardous organic chemicals in rubber recycled tire playgrounds and pavers. *Chemosphere* 90, 423–431. doi: 10.1016/j.chemosphere.2012.07.053

Ly, L., and Walker, R. (2009). *An assessment of Chemical Leaching, Releases to Air and Temperature at Crumb Rubber Infilled Synthetic Turf Fields*. Albany, NY: New York State Department of Environmental Conservation.

Møllhausen, M., Thorsheim, F., and Herzke, D. (2017). "Rapport fra undersøkelser om svinn av gummigranulat fra kunstgressbaner, gjennomført av over 12 000 elever og spillere høsten 2017," in *Report for Forskningskampanjen*, (Stockholm: Swedish Environmental Protection Agency).

Muyssen, B. T. A., De Schamphelaere, K. A. C., and Janssen, C. R. (2006). Mechanisms of chronic waterborne Zn toxicity in *Daphnia magna*. *Aqu. Toxicol.* 77, 393–401. doi: 10.1016/j.aquatox.2006.01.006

Nawrocki, S. T., Drake, K. D., Watson, C. F., Foster, G. D., and Maier, K. J. (2005). Comparative aquatic toxicity evaluation of 2-(Thiocyanomethylthio)benzothiazole and selected degradation products using ceriodaphnia dubia. *Arch. Environ. Contaminat. Toxicol.* 48, 344–350. doi: 10.1007/s00244-004-0105-1

Neumann, G., Veeranagouda, Y., Karegoudar, T. B., Sahin, Ö, Mäusezahl, I., Kabelitz, N., et al. (2005). Cells of *Pseudomonas putida* and *Enterobacter* sp. adapt to toxic organic compounds by increasing their size. *Extremophiles* 9, 163–168. doi: 10.1007/s00792-005-0431-x

Nilsson, N. H., Malmgren-Hansen, B., and Sognstrup Thomsen, U. (2008). "Mapping, emissions and environmental and health assessment of chemical substances in artificial turf," in *Survey of Chemical Substances in Consumer Products*, (Taastrup: The Danish Technological Institute).

Redondo-Hasselerharm, P. E., De Ruijter, V. N., Mintenig, S. M., Verschoor, A., and Koelmans, A. A. (2018). Ingestion and chronic effects of car tire tread particles on freshwater benthic macroinvertebrates. *Environ. Sci. Technol.* 52, 13986–13994. doi: 10.1021/acs.est.8b05035

Rhodes, E. P., Ren, Z., and Mays, D. C. (2012). Zinc leaching from tire crumb rubber. *Environ. Sci. Technol.* 46, 12856–12863. doi: 10.1021/es3024379

Rian, M. B., Vike-Jonas, K., Gonzalez, S. V., Ciesielski, T. M., Venkatraman, V., Lindstrøm, U., et al. (2020). Phthalate metabolites in harbor porpoises (*Phocoena phocoena*) from Norwegian coastal waters. *Environ. Int.* 137:105525. doi: 10.1016/j.envint.2020.105525

RIVM (2016). *Beoordeling Gezondheidsrisico's Door Sporten op Kunstgrasvelden Met Rubbergranulaat*. Netherlands: Kenniscentrum Sport & Bewegen.

Rodgers, B., and Waddell, W. (2013). "The science of rubber compounding," in *The Science and Technology of Rubber*, 4th Edn, eds J. E. Mark, B. Herman, and C. M. Roland (Amsterdam: Elsevier), 417–470.

Rogge, W. F., Hildemann, L. M., Mazurek, M. A., Cass, G. R., and Simoneit, B. R. T. (1993). Sources of fine organic aerosol. 3. Road dust, tire debris, and organometallic brake lining dust: roads as sources and sinks. *Environ. Sci. Technol.* 27, 1892–1904. doi: 10.1021/es00046a019

Rosnow, R. L., and Rosenthal, R. (1996). Computing contrasts, effect sizes, and counternulls on other people's published data: general procedures for research consumers. *Pyschol. Methods* 1, 331–340. doi: 10.1037/1082-989x.1.4.331

Ruffino, B., Fiore, S., and Zanetti, M. C. (2013). Environmental–sanitary risk analysis procedure applied to artificial turf sports fields. *Environ. Sci. Pollut. Res.* 20, 4980–4992. doi: 10.1007/s11356-012-1390-2

Sadiktsis, I., Bergvall, C., Johansson, C., and Westerholm, R. (2012). Automobile Tires—A potential source of highly carcinogenic dibenzopyrenes to the environment. *Environ. Sci. Technol.* 46, 3326–3334. doi: 10.1021/es204257d

Savoca, D., Arculeo, M., Barreca, S., Buscemi, S., Caracappa, S., Gentile, A., et al. (2018). Chasing phthalates in tissues of marine turtles from the Mediterranean sea. *Mar. Pollut. Bull.* 127, 165–169. doi: 10.1016/j.marpolbul.2017.11.069

Selbes, M., Yilmaz, O., Khan, A. A., and Karanfil, T. (2015). Leaching of DOC, DN, and inorganic constituents from scrap tires. *Chemosphere* 139, 617–623. doi: 10.1016/j.chemosphere.2015.01.042

Simon, R. (2010). *Review of the Impacts of Crumb Rubber in Artificial Turf Applications*. Oakland, CA: University of California.

Smolders, E., and Degryse, F. (2002). Fate and effect of zinc from tire debris in soil. *Environ. Sci. Technol.* 36, 3706–3710. doi: 10.1021/es025567p

Sørensen, L., Rogers, E., Altin, D., Salaberria, I., and Booth, A. M. (2020). Sorption of PAHs to microplastic and their bioavailability and toxicity to marine copepods under co-exposure conditions. *Environ. Pollut.* 258:113844. doi: 10.1016/j.envpol.2019.113844

Staniszewska, M., Nehring, I., and Mudrak-Cegiołka, S. (2016). Changes of concentrations and possibility of accumulation of bisphenol A and alkylphenols, depending on biomass and composition, in zooplankton of the Southern Baltic (Gulf of Gdansk). *Environ. Pollut.* 213, 489–501. doi: 10.1016/j.envpol.2016.03.004

US EPA, and CDC/ATSDR (2019). *Synthetic Turf Field Tire Crumb Rubber Research Under the Federal Research Action Plan Final Report: Part 1 - Tire Crumb Characterization (Volumes 1 and 2)*. Washington, DC: U.S. Environmental Protection Agency.

Wagner, S., Hüffer, T., Klöckner, P., Wehrhahn, M., Hofmann, T., and Reemtsma, T. (2018). Tire wear particles in the aquatic environment - A review on generation, analysis, occurrence, fate and effects. *Water Res.* 139, 83–100. doi: 10.1016/j.watres.2018.03.051

Wbscd (2015). *Tire Industry Project 10-year Progress Report (2005–2015)*. Geneva: Wbscd.

Wik, A., and Dave, G. (2005). Environmental labeling of car tires—toxicity to Daphnia magna can be used as a screening method. *Chemosphere* 58, 645–651. doi: 10.1016/j.chemosphere.2004.08.103

Wik, A., and Dave, G. (2006). Acute toxicity of leachates of tire wear material to Daphnia magna—Variability and toxic components. *Chemosphere* 64, 1777–1784. doi: 10.1016/j.chemosphere.2005.12.045

Wik, A., and Dave, G. (2009). Occurrence and effects of tire wear particles in the environment – A critical review and an initial risk assessment. *Environ. Pollut.* 157, 1–11. doi: 10.1016/j.envpol.2008.09.028

Wik, A., Nilsson, E., Källqvist, T., Tobiesen, A., and Dave, G. (2009). Toxicity assessment of sequential leachates of tire powder using a battery of toxicity tests and toxicity identification evaluations. *Chemosphere* 77, 922–927. doi: 10.1016/j.chemosphere.2009.08.034

Conflict of Interest: CH was employed by the company Akvaplan-niva. LS and AB were employed by the company SINTEF Ocean. DH was employed by the research foundation NILU. All authors declare that any commercial or financial relationships that could be construed as a potential conflict of interest had no influence on the findings of this research.

frontiers in Environmental Science

ORIGINAL RESEARCH
published: 28 July 2020
doi: 10.3389/fenvs.2020.00100

Characterization of TiO_2 NPs in Radish (*Raphanus sativus* L.) by Single-Particle ICP-QQQ-MS

Justyna Wojcieszek[1], Javier Jiménez-Lamana[2], Lena Ruzik[1], Monika Asztemborska[3], Maciej Jarosz[1] and Joanna Szpunar[2]*

[1] Chair of Analytical Chemistry, Faculty of Chemistry, Warsaw University of Technology, Warsaw, Poland, [2] Universite de Pau et des Pays de l'Adour, E2S, UPPA, CNRS, IPREM UMR 5254, Pau, France, [3] Isotopic Laboratory, Faculty of Biology, University of Warsaw, Warsaw, Poland

Titanium dioxide nanoparticles (TiO_2 NPs) are increasingly used in a wide range of consumer products and industrial applications, causing their presence in the environment, where they can interact with plants including edible ones. In addition, the released TiO_2 NPs can undergo chemical and physical transformations, which may influence their potential toxicity. However, the study of TiO_2 NPs in environmental samples by the technique offering the highest sensitivity, ICP-MS, is hampered by the presence of some elements (such as, e.g., Ca abundant in plant tissues) that cause polyatomic and/or isobaric interferences. This study proposed, for the first time, the use of a triple-quadrupole ICP operating in tandem mass spectrometry and single-particle mode (SP-ICP-QQQ-MS) to study the uptake, translocation, and possible transformations of TiO_2 NPs with two different nominal sizes in a model plant (*Raphanus sativus* L.). A careful optimization of the reaction cell conditions (O_2 and H_2 gas flows) allowed the reduction in background level and resulted in a significant increase in the sensitivity of the analysis, bringing size detection limits for TiO_2 NPs down to 15 nm in ultrapure water and to 21 nm in a matrix containing 50 mg L^{-1} of Ca. In addition, an enzymatic digestion procedure was applied in order to extract intact nanoparticles from the tissues of plants treated with TiO_2 NPs, followed by size characterization by SP-ICP-MS. The size distributions obtained in roots treated with TiO_2 NPs suggested a preferential uptake of smaller nanoparticles. Results also revealed that the majority of TiO_2 NPs were retained in roots. Additionally, no significant dissolution was observed, as well as no differences for nanoparticles found in roots and leaves, proving that radish is able to translocate intact TiO_2 NPs up to aboveground organs.

Keywords: titanium dioxide nanoparticles, model plant, tandem mass spectrometry, single particle ICP-MS, uptake, translocation, size characterization

OPEN ACCESS

Edited by:
Denise M. Mitrano, Swiss Federal Institute of Aquatic Science and Technology, Switzerland

Reviewed by:
Nathaniel Clark, University of Plymouth, United Kingdom
Geert Cornelis, Swedish University of Agricultural Sciences, Sweden
Manuel David Montaño, Western Washington University, United States

****Correspondence:***
Javier Jiménez-Lamana
j.jimenez-lamana@univ-pau.fr

Specialty section:
This article was submitted to Biogeochemical Dynamics, a section of the journal Frontiers in Environmental Science

Received: *31 March 2020*
Accepted: *09 June 2020*
Published: *28 July 2020*

Citation:
Wojcieszek J, Jiménez-Lamana J, Ruzik L, Asztemborska M, Jarosz M and Szpunar J (2020) Characterization of TiO_2 NPs in Radish (Raphanus sativus L.) by Single-Particle ICP-QQQ-MS. Front. Environ. Sci. 8:100. doi: 10.3389/fenvs.2020.00100

INTRODUCTION

With the fast development of nanotechnology over the past decade, there are more and more applications of nanomaterials in daily life, e.g., in many commercial and industrial products, medicine, electronics, and energy sectors. Especially, metal and metal-oxide nanoparticles have been widely applied in different fields due to their unique physical and chemical properties. Among

them, titanium dioxide nanoparticles (TiO_2 NPs) are one of the most widely applied nanoparticles (Capaldi Arruda et al., 2015; Shah et al., 2017). TiO_2 NPs occur in three different crystallographic forms: anatase and rutile (tetragonal) and, more rarely, brookite (orthorhombic). Among those three major polymorphs, anatase is extensively applied in commercial products due to its higher activity comparing to other forms, although rutile is the more stable form (Chen and Mao, 2007; Zhang et al., 2015). Additionally, there are no commercial TiO_2 NPs products in the brookite phase (Tan et al., 2018). Titanium is a common metal in soil that occurs in naturally occurring nano-sized particles, such as clays. It is important to mention that TiO_2 found in soil is known to be rather non-toxic to most organisms. TiO_2 NPs are being used for many products such as plastics, paints, surface coatings, medical devices, cosmetics, and nanofertilizers (Hong et al., 2017). They are applied as food additives or in nutritional supplements, and therefore, oral exposure to TiO_2 NPs may happen through the consumption of such products (Shakeel et al., 2016). In the field of nanomedicine, an intravenous injection can deliver TiO_2 NP carriers directly into the human body (Shakeel et al., 2016). Because of their UV light-resistant properties, TiO_2 NPs are also commonly used in sunscreens or toothpaste (Vidmar et al., 2017). In general, TiO_2 NPs account for about 70% of the total production volume of pigments worldwide and are in the top five NPs used in consumer products (Jafarizadeh-Malmiri et al., 2019; Dar et al., 2020).

The wide applications of TiO_2 NPs have raised serious concerns regarding their potential threat to the environment, as during their whole life cycle, TiO_2 NPs may be released into the air, soil, and/or water, affecting all components of the environment, including plants, which are directly exposed to these emerging contaminants (Oliver et al., 2015; Tan et al., 2018). It has been reported that the emission of TiO_2 NPs represents more than one-fourth of the estimated mass flow of engineered nanoparticles (ENPs) in a worldwide range (Keller and Lazareva, 2013). By the year 2025, the estimated global production of TiO_2 NPs would be 1000 tons, and once they persist for a long time in the environment, the chances of exposure to plants will increase and therefore a better understanding of the possible toxicity of TiO_2 NPs is important in assessing environmental risks (Du et al., 2019). In addition, it has to be taken into account that the potential toxicity of released NPs may be influenced by the different transformations they can undergo, which are still not well understood. If TiO_2 NPs enter the environment, they become bioavailable to plants and hence their impact on edible plants and food safety needs to be further investigated (Capaldi Arruda et al., 2015; Dan et al., 2015; Reddy et al., 2016). However, it is important to remember that the presence of Ti-containing clays could disturb the investigation of plants exposed in real soil (i.e., not hydroponically) from the ecotoxicological point of view. During the studies, the clays should be removed from the plant, to avoid contamination of the sample since they would not be distinguishable from TiO_2 using single-element SP-ICP-MS.

The study of the interactions between TiO_2 NPs and plants has been addressed through different analytical techniques, such as microscopy (electron, optical, fluorescence, or confocal), mass spectrometry, UV-Vis, and FT-IR spectroscopy and ICP-based and μX-ray techniques (Tan et al., 2018). Electron microscopy (scanning – SEM and transmission – TEM) and ICP-OES/MS have been widely used due to their capability to determine the size and shape of NPs in plant cells and their high sensitivity, respectively (Kole et al., 2016). For instance, the accumulation of TiO_2 NPs in roots and leaves of rice (*Oryza sativa*) and their adsorption on the surface of the roots of lettuce were shown by using TEM, SEM, and ICP-OES/MS techniques (Cai et al., 2017; Deng et al., 2017). However, the low resolution of electron microscopy or the complicated sample preparation may bring some difficulties during the analysis (Larue et al., 2014; Tan et al., 2018). Synchrotron-based techniques can provide higher resolutions than microscopy, although they require high concentrations of NPs (Castillo-Michel et al., 2017). By using μX-ray fluorescence (μ-XRF) and μX-ray absorption near edge structure (μ-XANES), it has been shown that TiO_2 NPs can be translocated from roots to stems (in lettuce – *Lactuca sativa*) (Larue et al., 2016), leaves (Servin et al., 2012), and even fruits (in cucumber – *Cucumis sativus*) (Servin et al., 2013). TEM and μ-XRF have shown the presence of TiO_2 NPs in nuclei and vacuoles of *Arabidopsis thaliana* roots and leaf stomata (Kurepa et al., 2010). It should be also highlighted that plant cultivation with TiO_2 NPs influences accumulation of other elements. For example, the increasing content of P, Ca, Mg, and Zn was determined in roots, shoots, and grains of rice (Du et al., 2017; Zahra et al., 2017), whereas an enhanced accumulation of Fe in roots (Burke et al., 2015) was shown in the case of soybean. On the other hand, the differences in the physicochemical properties of TiO_2 NPs such as their size, aggregation, surface area, coating, and crystal structure have a huge influence on the interactions of NPs with living organisms like plants, inducing different toxicities (Du et al., 2019). In this context, size characterization and monitoring of different processes that nanoparticles may undergo (agglomeration, dissolution) have to be monitored throughout the whole interaction with plants: contact with the growth medium, uptake by roots, and translocation to aboveground organs. Additionally, the investigation and study at environmentally relevant concentrations require the use of the highest-sensitivity techniques.

Single-particle inductively coupled plasma mass spectrometry (SP-ICP-MS) is a well-established technique used for the detection, characterization, and quantification of engineered nanoparticles in environmental samples (Laborda et al., 2016). SP-ICP-MS is able to provide information about particle size, particle concentration, and dissolved element concentration as well as to monitor possible transformation processes like agglomeration or dissolution. These metrics cannot be routinely measured with the abovementioned techniques. However, the analysis of TiO_2 NPs in environmental samples using conventional single-quadrupole instruments (ICP-Q-MS) presents some challenges. In fact, the determination of Ti in plant tissues can be hindered by the presence of Ca, since the most abundant isotope of Ti, ^{48}Ti (73.7% abundance), suffers an isobaric interference from one of the isotopes of Ca (^{48}Ca). Therefore, studies using single-quadrupole ICP-MS are compelled to monitor less interfered Ti isotopes, such as ^{47}Ti and ^{49}Ti, with 7.4% and 5.4% abundances, respectively, rendering

the detection of smaller TiO_2 NPs more difficult due to a lower sensitivity of ICP-MS. These limitations can be overcome by using triple-quadrupole ICP-MS (ICP-QQQ-MS), allowing for controlled interference removal by introducing a reaction gas, which interacts with the interfering ions. It leads to higher sensitivity thanks to the monitoring of the most abundant ^{48}Ti isotope (73.7% abundance), which suffers an isobaric interference from ^{48}Ca, and gives a possibility of an effective characterization of low-size TiO_2 NPs in biological and environmental samples.

In the context of the widespread production and distribution of TiO_2 NPs in different fields and the possible risk regarding their release into the environment, the main purpose of this work was to study the uptake, translocation, and possible transformations of TiO_2 NPs in the model plant, radish (*Raphanus sativus L.*), a popular vegetable consumed all over the world whose edible part is in direct contact with the soil where contamination may take place. After a careful optimization of reaction cell conditions, the fate of two TiO_2 NPs suspensions with different nominal sizes in radish was studied by means of tandem ICP-MS in single-particle mode (SP-ICP-QQQ-MS). The use of tandem mass spectrometry allowed the monitoring of ^{48}Ti in plant tissues, hence improving the sensitivity and size detection limit. To the best of our knowledge, this is the first application of triple-quadrupole ICP in the study of the interactions of TiO_2 NPs with edible plants in single-particle ICP-MS mode.

MATERIALS AND METHODS

Samples and Reagents

Seeds of radish (*Raphanus sativus* L.) were purchased from Vilmorin Garden (Komorniki, Poland). Analytical- or biological reagent-grade chemicals and LC-MS-grade solvents were purchased from Sigma-Aldrich (St. Louis, MO, United States), unless stated otherwise. Ultrapure water (18 MΩ cm) obtained with a Milli-Q system (Millipore, Guyancourt, France) was used throughout this work. The nitric acid of purity for trace metal analysis was purchased from Fluka (Buchs, Switzerland). An ionic standard solution of 1000 mg L^{-1} titanium was purchased from Agilent Technologies (Tokyo, Japan). Macerozyme R-10 enzyme (pectinase from *Rhizopus* sp., Sigma-Aldrich), a multicomponent enzyme mixture containing cellulase (0.1 unit per mg), hemicellulase (0.25 unit per mg), and pectinase (0.5 unit per mg), was used to digest plant tissues for TiO_2 NP extraction.

Powder of TiO_2 NPs in rutile form with nominal sizes of 30 and 100 nm was purchased from US Research Nanomaterials, Inc. (Houston, TX, United States). Stock suspensions of TiO_2 NPs (500 mg L^{-1}) were prepared by dispersion of NP powder (25 mg) in ultrapure water (50 mL). These stock suspensions will be referred to as suspension A (nominal diameter: 30 nm) and suspension B (nominal diameter: 100 nm) throughout the rest of the manuscript. Diluted suspensions of TiO_2 NPs were prepared daily in ultrapure water by accurately weighing aliquots of the stock suspensions after 1-min sonication. Before each analysis, the suspensions were bath sonicated for approximately 1 min. A gold nanoparticle (AuNPs) standard with a nominal diameter of 50 nm (BBI Solutions, Cardiff, United Kingdom) was used for the determination of transport efficiency. All suspensions of nanoparticles were stored in darkness at 4°C and sonicated directly before SP-ICP-MS analysis.

Instrumentation

Homogenization of the plant tissues was performed by a KIMBLE Dounce tissue grinder set of 7 mL (Sigma-Aldrich). Incubation of samples was performed in a Memmert water bath (Memmert, Schwabach, Germany). A Bandelin DT 52 H ultrasonic bath (BANDELIN Electronic, Berlin, Germany) was used for sonication of nanoparticle suspensions and enzymatic extraction before SP-ICP-MS analysis.

Single-Particle ICP-MS Method

Characterization of TiO_2 NPs was carried out using an Agilent 8900 ICP-QQQ-MS equipped with a Single Nanoparticle Application Module. The default instrumental and data acquisition parameters are listed in **Table 1**. The position of the torch and nebulizer gas flow was adjusted each day of work with special emphasis to decrease the level of CeO/Ce below 0.2% with the aim to minimize the risk of polyatomic interferences caused by oxide formation. The working conditions of ICP-MS were optimized daily using a 1-μg L^{-1} solution of $^{7}Li^{+}$, $^{89}Y^{+}$, and $^{205}Tl^{+}$ in 2% (v/v) HNO_3. During analysis, ^{48}Ti with a natural abundance of about 73.7% was monitored. The reaction gas containing O_2 and H_2 was used in order to resolve the spectral interferences on ^{48}Ti. The use of O_2 as reaction cell gas allows the analysis of ^{48}Ti by monitoring the oxide ion at m/z + 16 u, which means that the ICP-QQQ-MS instrument worked in "mass-shift" mode during this study. Therefore, the first quadrupole was set to m/z 48 (the precursor ^{48}Ti ion) and the second quadrupole was set to m/z 64 (the target product ion $^{48}Ti^{16}O$). O_2 promoted the formation of the $^{48}Ti^{16}O^{+}$ product ion, and H_2 helped with the formation of $^{48}Ca^{16}O^{1}H^{+}$, avoiding interference on $^{48}Ti^{16}O^{+}$ by $^{48}Ca^{16}O^{+}$. In addition, working in mass-shifted mode allows one to avoid any potential isobaric interference at m/z 64 like ^{64}Zn, since these ions are filtered by the first quadrupole. SP-ICP-MS analyses

TABLE 1 | Default instrumental and data acquisition parameters for SP-ICP-MS.

Instrumental parameters	
RF power	1550 W
Plasma, auxiliary, and nebulizer gas flow	15.0, 0.9, and 1.15 L min^{-1}
H_2 gas flow	8 mL min^{-1}
O_2 gas flow	10%
Cones	Skimmer – Ni, sampler – Ni
Sample uptake rate	0.35 mL min^{-1}
Data acquisition parameters	
Dwell time	100 μs
Readings per replicate	600000
Total acquisition time	60 s
Analyte	Ti
Mass (amu)	48 (48 → 64)
Density	4.61 g cm^{-3}
Mass fraction	0.6

were performed in time-resolved analysis (TRA) mode using a dwell time of 100 μs, with a total time of data acquisition of 60 s. A AuNPs standard with a nominal diameter of 50 nm was used for the determination of transport efficiency, which was calculated by the particle size method described by Pace et al. (2011). The sample flow rate was calculated daily by measuring the mass of water taken up by the peristaltic pump for 2 min (this operation was repeated three times). Under the experimental conditions used in this work, the transport efficiency at a sample flow rate of 0.35 mL min^{-1} was 6%. After each sample analysis, the software automatically processed the raw data and generated the particle size, particle concentration, size distribution, and information about the concentration of dissolved metal. The dwell time is a critical parameter in single-particle detection mode. Working with microsecond dwell times allows the recording of particle events as resolved transient signals, improving hence the resolution and working range. In this work, the discrimination between dissolved signal and nanoparticle signal was done in the basis of threshold (I_{thresh}) determined as $I_{thresh} = I_b + 5\sigma_b$, where I_b is the intensity of the baseline and σ_b the standard deviation of the baseline of each sample. A criterion of $5\sigma b$ was recently considered as a good compromise (Laborda et al., 2019).

Scanning Electron Microscopy Analysis

Electron-microscopy images were taken with the use of a Hitachi SU8230 ultra-high-resolution field-emission scanning electron microscope (Hitachi High-Technologies Corporation) using secondary electron detectors (SE) at a 30.0-kV accelerating voltage. Images were taken with the use of gold TEM grids coated with a Lacey carbon film, which were immersed in samples in the form of DI water suspensions and dried prior to observation. Magnifications used were in the range of ×100 000–350 000.

Procedures

Plant Cultivation

Portions of radish seeds (ca. 1 g) were germinated in distilled water in darkness for 3 days, and then the seedlings were transferred to 350-mL containers with a Knop nutrient solution (the composition is shown in **Supplementary Table 1**) and placed in a growth chamber. After 4 days, the TiO_2 NP suspension of different sizes (30 and 100 nm) was added separately to three different containers with the medium at a titanium concentration of 5 mg L^{-1}. As a control variant, plants were left in the nutrient solution without the addition of titanium. Cultivation was carried out for the next 7 days in a growth chamber. Each variant of the cultivation was performed in three replicates. After cultivation, the plants were harvested and the roots were gently rinsed with deionized water. The plants were divided into roots and aboveground organs (leaves plus stems) and lyophilized. Dried plant material was ground in a mortar before further analysis.

Enzymatic Digestion Method

After the cultivation of radish, plant tissues were digested enzymatically as reported in previous works (Jiménez-Lamana et al., 2016; Wojcieszek et al., 2019), with small modifications, as it was necessary to change the way of sample homogenization. Therefore, grounded samples of leaves together with stems and roots (0.020 g) were homogenized for 15 min with 7 mL of 2 mM citrate buffer (pH 4.5; adjusted with citric acid) by using a tissue grinder set. The ultrasonic probe used in previous works could not be used due to the fact that its composition contains titanium and a significant amount of Ti was detected even in blanks. After the end of homogenization, 1.5 mL of Macerozyme R-10 solution (0.01 g of enzyme powder for roots and 0.04 g of enzyme powder for leaves plus stems, dissolved in 1.5 mL of ultrapure water) was added to samples, and the samples were next shaken at 37°C for 24 h in a water bath with continuous shaking. After digestion, the samples were settled down for approximately 60 min and the obtained supernatants were analyzed by SP-ICP-MS. Filtration studies were performed by using syringe filters of 0.45 and 1.0 μm pore size with PTFE and PES membrane purchased from VWR (Gdańsk, Poland).

RESULTS AND DISCUSSION

Development and Optimization of an Analytical Method Based on SP-ICP-QQQ-MS for the Characterization of TiO_2 NPs in Plant Tissues

Optimization of H_2 and O_2 Gas Flows

When working on SP-ICP-MS, special attention should be paid to the size limit of detection. This limit is dependent on the response of the instrument toward the isotope monitored and on the background signal, with the latter critically affected by isobaric and polyatomic interferences. The higher the background signal, the lower the capability of detecting small nanoparticles and hence the higher the size limit of detection. This is especially relevant for the determination of TiO_2 NPs in real samples like plant tissues, since the most abundant ^{48}Ti isotope (73.7% abundance) suffers an isobaric interference from one of the isotopes of Ca (^{48}Ca), which is an essential plant nutrient (White and Broadley, 2003). In order to overcome this problem, ^{48}Ti was measured in mass-shifted mode by using a mixed O_2/H_2 cell gas.

Prior to the analysis of the plant samples, the O_2/H_2 cell gas was optimized in terms of flow of both gases. To do that, three different matrices were analyzed: ultrapure water, 1 mg L^{-1} Ca, and 50 mg L^{-1} Ca. The three solutions were analyzed by means of single-particle ICP-MS according to the conditions shown in **Table 1** and with varying flows of H_2 and O_2. For each condition tested (i.e., different O_2 and H_2 flows), the response of the instrument toward Ti was obtained, in terms of per ppb of Ti, by analyzing a solution of 0.5 ppb. Subsequently, the three matrices were analyzed and the corresponding signal provided by the software was treated mathematically in order to obtain the associated noise (calculated as δ), and hence the signal-to-noise ratio was obtained.

Figure 1A shows the signal-to-noise ratios obtained by using different H_2 flows (from 5 to 9 mL min^{-1}) for the analysis of the three different matrices. The presence of Ca at relatively low concentrations (1 mg L^{-1}) did not have a significant effect since

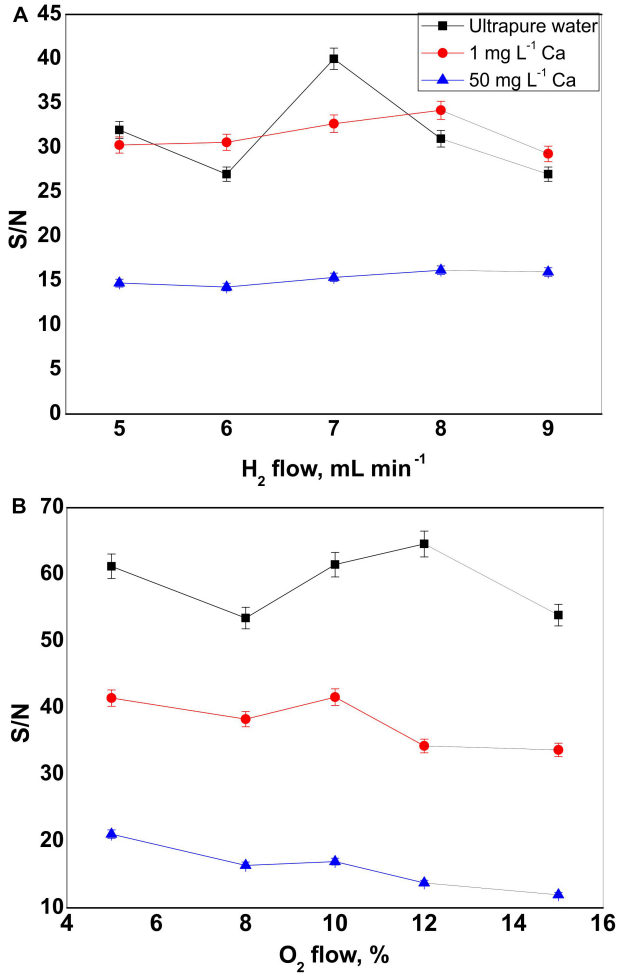

FIGURE 1 | Signal-to-noise ratio obtained for three different matrices: ultrapure water (black line, squares), 1 mg L^{-1} Ca (red line, circles), and 50 mg L^{-1} Ca (blue line, triangles) at different **(A)** hydrogen gas flows, and **(B)** oxygen gas percentages. Error bars represent the standard deviation of the measurement.

signal-to-noise ratios obtained were similar to those obtained for ultrapure water for the different flows studied. However, this ratio dropped dramatically (around 50%) when the Ca concentration increased up to 50 mg L^{-1}. The best ratios were obtained with H_2 flows of 7 and 8 mL min^{-1} for ultrapure water and calcium-containing matrices, respectively. Since a significant amount of Ca is expected in plant tissues [up to 0.1–5% of dry weight (Thor, 2019)], an H_2 flow of 8 mL min^{-1} was retained for the rest of the experiment.

The O_2 flow was optimized in a similar way. O_2 gas at percentages of 5, 8, 10, 12, and 15 was tested, and the corresponding signal-to-noise ratios were obtained for the three mentioned matrices. As it is shown in **Figure 1B**, the ratio decreased significantly when analyzing titanium in a matrix highly charged in calcium. On the other hand, the best results for both calcium-containing matrices were obtained when working at 5 and 10% of O_2. In order to promote a more significant formation of $^{48}Ti^{16}O^+$ from $^{48}Ti^+$ in the first quadrupole, the higher O_2 flow (10%) was chosen for the rest of the study.

Size Detection Limit

The attainable size detection limit (LOD_{size}) is directly affected by the standard deviation (σ_B) of the intensity corresponding to the background and/or to the dissolved species. By applying a 3σ criterion (Laborda et al., 2014), the size detection limit can be calculated through the following equation:

$$LOD_{size} = \left(\frac{18\sigma_B}{\pi \rho X_{NP} K_{ICPMS} K_M} \right)^{\frac{1}{3}} \quad (1)$$

where ρ is the density of the particles (g cm^{-3}), X_{NP} is the mass fraction of the element in the particle, K_{ICPMS} is the detection efficiency (ratio of the number of ions detected vs. the number of atoms of the isotope introduced into the ICP), and K_M (= AN_{Av}/M_M) is related with the contribution from the element measured (A is the atomic abundance of the isotope considered; N_{Av}, the Avogadro number; M_M, the atomic mass of the element). K_{ICPMS} can be deduced from the equation that relates the signal R (ions counted per time unit) and the mass concentration of a solution of the analyte, C^M (Laborda et al., 2014):

$$R = K_{intr} K_{ICPMS} K_M C^M \quad (2)$$

where K_{intr} (= η_{neb} Q_{sam}) can be estimated through the transport efficiency and the sample uptake rate (η_{neb} and Q_{sam}, respectively, whose values are detailed in "Materials and Methods"). Therefore, by knowing K_{intr} and K_M and by analyzing a dissolved titanium standard, K_{ICPMS} can be determined. σ_B is estimated as the experimental standard deviation of the baseline of the sample (Laborda et al., 2019). Since in this work the signal baseline in samples is mainly caused by the presence of Ca, σ_B was calculated from three different Ca background levels.

Size detection limits, calculated for ^{48}Ti, of 15, 16, and 20 nm, were obtained for ultrapure water, 1 mg L^{-1} Ca, and 50 mg L^{-1} Ca matrices, respectively. As it can be observed, an increase in the Ca concentration in the matrix implies an increase in the baseline and, inevitably, of its noise, which leads to an increase in σ_B and hence in the LOD_{size}. In any case, the use of a triple-quadruple ICP tandem mass spectrometry operating in mass-shift mode allowed the use of the most abundant isotope ^{48}Ti, through the monitoring of its oxide $^{48}Ti^{16}O^+$, achieving size detection limits of 15 nm in ultrapure water and 20 nm in a matrix highly charged in calcium. This LOD_{size} represents a gain of a factor of 5 with respect to those attainable by monitoring less abundant Ti isotopes by single-quadrupole ICP-MS (Lee et al., 2014). In addition, the use of an O_2/H_2 reaction cell resulted in better size detection limits than those reported by using other reaction gases: 64 nm in ultrapure water and 101 nm in 50 mg L^{-1} Ca were achieved with a mixture of ammonia and helium (Tharaud et al., 2017). In comparison with studies performed by high-resolution (HR) ICP-MS (Tharaud et al., 2017), the current study presented a slightly higher LOD_{size} in ultrapure water (15 nm vs. 10 nm by HR-ICP-MS) but a significant improvement when analyzing TiO_2 NPs in a matrix containing 50 mg L^{-1} of Ca (21 nm vs. 37 nm by HR-ICP-MS). Finally, the size

detection limits obtained here by single-particle QQQ-ICP-MS in MS/MS mode were at similar levels than those reported by using double-focusing magnetic sector field ICP-MS (ICP-SF-MS): 19.2 nm for samples injected as a wet aerosol (Hadioui et al., 2019) and 20 nm for TiO_2 NPs the snow and rain waters (Azimzada et al., 2020).

Characterization of TiO_2 NP Suspensions

TiO_2 NP commercial suspensions with two different nominal sizes were analyzed by SP-ICP-MS with the optimized cell gas conditions. The corresponding size distributions are shown in **Figures 2A,B**. For both suspensions, highly polydisperse distributions and nanoparticles of bigger diameters than the nominal ones provided by the manufacturer were obtained. Nanoparticles with sizes ranging from 100 to 400 nm were observed for both suspensions analyzed. In addition, median diameters of 180 ± 13 and 220 ± 10 nm were obtained for commercial suspensions A and B, with nominal sizes of 30 and 100 nm, respectively (**Table 2**). In order to discard any artifact during SP-ICP-MS measurements and/or calculations, both commercial suspensions were analyzed by SEM. The images (**Supplementary Figure 1**) reflected the high polydispersity of both suspensions, with sizes up to 400 nm and only a few with sizes below 100 nm, which is in good agreement with the results obtained by SP-ICP-MS. On the other hand, images show a certain degree of particle agglomeration. Even though nanoparticle suspensions are analyzed by SP-ICP-MS at a very low concentration and after bath sonication, the occurrence of some agglomerates is still likely to happen, as it will be discussed in detail below. Images obtained by SEM also showed several non-spherical nanoparticles. It is important to emphasize this information since SP-ICP-MS calculations that allow to get the size distribution of nanoparticles are based on the assumption that nanoparticles are spherical. Therefore, this may inevitably lead to a certain degree of inaccuracy on the size distributions obtained for both suspensions by SP-ICP-MS. However, the purpose of this study, i.e., the uptake of TiO_2 NPs by radish and the investigation of the possible transformation of nanoparticles, was not hampered by this fact.

Influence of Enzymatic Digestion

In order to check if the enzymatic procedure affects the size distribution of the TiO_2 NPs, suspensions of both commercial TiO_2 NPs were prepared at a concentration of titanium of 5 mg L^{-1}, without the presence of a plant matrix, and treated with the same conditions of enzymatic digestion as later applied for plant tissues. After incubation and analysis, the obtained results showed that the size distributions obtained for enzyme-treated TiO_2 NPs were in good agreement with the size distributions obtained for TiO_2 NPs stock suspension freshly prepared, regardless of the analyzed size of NPs (**Figures 2C,D**). It is worth mentioning that in the case of suspension B, the presence of nanoparticles with sizes around 20 nm and slightly above after the enzymatic digestion is more important than in the case of the size distribution obtained for the stock suspension. This fact would be explained by redispersion of smaller nanoparticles after enzymolysis corroborating the hypothesis of the presence of small agglomerates in the stock suspension. In any case, the integrity of TiO_2 NPs is not affected by the enzyme used in the digestion procedure. Therefore, it can be concluded that the Macerozyme R-10 enzyme used for enzymatic digestion was suitable for extracting intact TiO_2 NPs from plant tissues.

Influence of Filtration on the Size Characterization and Quantification of Extracted Nanoparticles

Filtration and ultrafiltration are membrane transport processes, widely used to separate solid particles, colloids, or macromolecules from fluids. Before analysis by ICP-MS, filtration is often used in order to prevent the introduction of particulate matter into the system, which may result in blocking of the nebulizer or in the contamination of the inner parts of the instrument. One of the advantages of membrane techniques is the possibility of separation of different species without using separating agents, decreasing then the probability of contamination. However, membrane filtration may be distorted by some physicochemical artifacts such as aggregation of compounds of any size at the membrane surface (Fedotov et al., 2011; Vidmar et al., 2017). In this sense, the influence of filtration on the number of nanoparticles detected during SP-ICP-MS analysis was investigated before analysis of plant samples. Both TiO_2 NP suspensions were filtered through 0.45-μm filters with PTFE membrane and analyzed by SP-ICP-MS. The time scans obtained (**Supplementary Figure 2**) showed that only a small part of nanoparticles was detected in the recovered filtrates: only 15% and 3% of nanoparticles were observed after filtration TiO_2 NP suspensions A and B, respectively (**Table 3**). These phenomena can be explained by agglomeration and/or adsorption of nanoparticles on the membrane surface and pore walls. Moreover, the size distributions of filtered nanoparticle suspensions were obtained and the corresponding median diameters determined and compared with stock suspension. As it is shown in **Table 3**, the nanoparticles subjected to filtration through 0.45-μm filters presented median diameters between 60 and 70 nm lower, suggesting that bigger nanoparticles are more prone to be retained in filters. These results are contradictory with a previous study showing that TiO_2 NPs were not adsorbed on 0.45-μm syringe filters, although the nature of the membrane used was not mentioned (Vidmar et al., 2017). In order to check whether the problem with low efficiency of TiO_2 NP filtration is caused by pore size or membrane type of the filter used, two additional filters (PTFE and PES membrane with pore size of 1.0 μm) were also checked in the same way as described above. However, no significant improvement of results was observed compared to those obtained after the use of 0.45-μm filters: most of NPs still retained on the membrane surface. It can lead to the conclusion that TiO_2 NPs are adsorbed on syringe filters regardless of pore size (at least up to 1.0 μm) or membrane used. As a result, no filtration of plant samples was performed. After incubation, samples were allowed to settle down by gravity for 1 h, and the upper part of the suspension was taken for further analysis, avoiding the pipetting of the solid plant matrix. Each sample was subjected to enzymatic digestion by triplicate and good

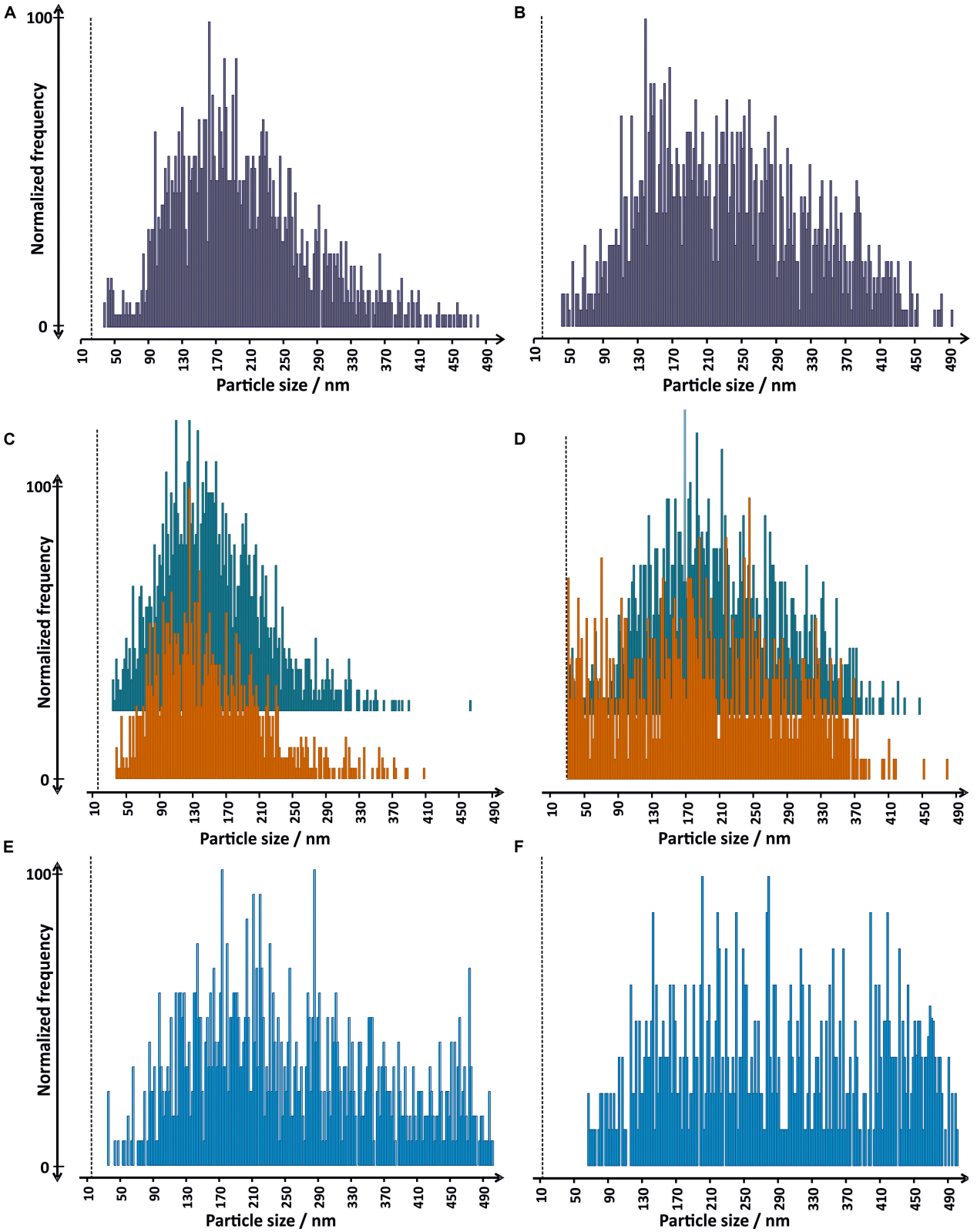

FIGURE 2 | Size distributions obtained by SP-ICP-MS for commercial TiO_2 NP suspensions in ultrapure water: **(A)** A and **(B)** B, used during plant cultivation; TiO_2 NP stock suspension **(C)** A, and **(D)** B, freshly prepared (blue) and after enzymatic digestion procedure (orange); and commercial suspensions **(E)** A and **(F)** B, after 7 days in contact with growth medium. Vertical lines represent the size limit of detection for each sample.

TABLE 2 | Median diameters, particle number concentrations, and mass concentrations obtained by SP-ICP-MS for the analysis of stock TiO_2 NP suspensions, the same nanoparticle suspensions after 7 days in contact with the growth medium, after enzymatic digestion procedure and extraction from plant tissues.

	Diameter/nm				
TiO_2 suspension	**Stock suspension**	**Enzymatic digestion**	**Growth medium**	**Leaves of treated plants**	**Roots of treated plants**
A	180 ± 13	188 ± 9	238 ± 13*	121 ± 1*	118 ± 5*
B	220 ± 10	215 ± 8	276 ± 12*	115 ± 2*	116 ± 2*
	Mass concentration/ng L^{-1}				
A	1745 ± 233	1241 ± 211	2419 ± 338	725 ± 49	751 ± 97
B	2556 ± 351	1507 ± 13	2671 ± 270	437 ± 12	539 ± 12
	Particle number concentration/NPs L^{-1}				
A	$6.51 \pm 0.61 \times 10^7$	$9.39 \pm 0.32 \times 10^7$	$3.40 \pm 0.53 \times 10^7$	$6.61 \pm 0.29 \times 10^7$	$7.50 \pm 0.32 \times 10^7$
B	$6.10 \pm 0.51 \times 10^7$	$4.84 \pm 0.45 \times 10^7$	$2.69 \pm 0.41 \times 10^7$	$4.15 \pm 0.10 \times 10^7$	$5.47 \pm 0.17 \times 10^7$

*All results are expressed as mean ± SD with n = 3. *Diameters presenting no significant differences with diameter obtained for stock suspension with a level of confidence >99% (one-way ANOVA).*

TABLE 3 | Comparison of median diameters, particle number concentrations, mass concentrations, and number of detected events obtained for two TiO_2 suspensions before and after filtration through a 0.45-μm pore size filter.

	Particle number concentration/NPs L^{-1}		Mass concentration/ng L^{-1}		Diameter/nm		Number or detected events	
TiO_2 suspension	**Before filtr.**	**After filtr.**	**Before filtr.**	**After filtr.**	**Before filtr.**	**After filtr.**	**Before filtr.**	**After filtr.**
A	$6.51 \pm 0.61 \times 10^7$	$9.97 \pm 0.42 \times 10^6$	1745 ± 233	80 ± 3	180 ± 13	129 ± 8	1445 ± 44	176 ± 35
B	$6.10 \pm 0.51 \times 10^7$	$2.08 \pm 0.30 \times 10^6$	2556 ± 351	20 ± 3	220 ± 10	157 ± 3	1299 ± 33	47 ± 11

All results are expressed as mean ± SD with n = 3.

reproducibility was observed, discarding any impact that this procedure may have on the determination of nanoparticle number concentration.

In conclusion, an analytical method based on monitoring ^{48}Ti by single-particle ICP-QQQ-MS followed by enzymatic digestion without filtration has been developed and optimized for the characterization and quantification of TiO_2 NPs in plant tissues.

Characterization of TiO_2 NPs in Radish

Investigation of TiO_2 NP Stability in the Growth Medium

First, the stability of TiO_2 NPs was tested in the growth media used for plant cultivation. TiO_2 NP suspensions of 5 mg L^{-1} were spiked into the nutrient solution, and the size distributions of the nanoparticles were determined by means of SP-ICP-MS after 7 days (**Figures 2E,F**). The results have shown the presence of several nanoparticles with bigger sizes (between 400 and 500 nm) than those obtained for the stock suspensions of both commercial TiO_2 NP suspensions. As a result, the median diameters obtained for both suspensions were shifted around 50 nm toward bigger sizes (**Table 2**) and hence presented significant differences with respect to stock solution (one-way ANOVA, level of confidence >99%). These results suggested that TiO_2 NPs undergo agglomeration to a small degree during the 7-day contact with the growth medium. On the other hand, no background signal corresponding to dissolved titanium was observed on the SP-ICP-MS time scans of both suspensions, showing that TiO_2 NPs did not undergo dissolution during the plant cultivation.

Single-Particle ICP-MS Analysis of Leaves Plus Stems and Roots of Radish

In order to study the uptake of TiO_2 NPs by radish, samples of roots and samples of leaves plus stems of plants treated with both nanoparticle suspensions were subjected to the enzymatic procedure followed by SP-ICP-MS analysis with the optimized conditions of H_2 and O_2 gas flows. Before the analysis of treated samples, roots and leaves plus stems of control plants were analyzed and the corresponding time scans obtained (**Figures 3A,B**). A few pulses above the background were observed for control plants. The occurrence of these pulses was not significant (less than 15 pulses out of 600,000 readings); in addition, a similar number of pulses (<15 particle events) were observed for the analysis of ultrapure water due to a carryover effect and did not have any effect on further analyses of treated plant tissues. On the other hand, low background signals were obtained for both tissues, and hence the possibility of having interference on titanium signal due to the plant matrix was discarded.

Afterward, radish tissues treated with both TiO_2 NP suspensions were analyzed by SP-ICP-MS, after enzymatic sample preparation procedure. Before SP-ICP-MS analysis, samples of leaves plus stems were diluted 100 times while samples of roots were diluted 5000 times, for TiO_2 NP suspension A. In the case of radish tissues treated with TiO_2 NP suspension B, samples were diluted 20 and 10000 times for leaves and roots, respectively. Time scans obtained showed a significant number of pulses in both plant tissues for both nanoparticle suspensions (**Figures 3C–F**), proving that radish is able to uptake TiO_2 NPs and transport them into the aerial part of the plant. Taking into

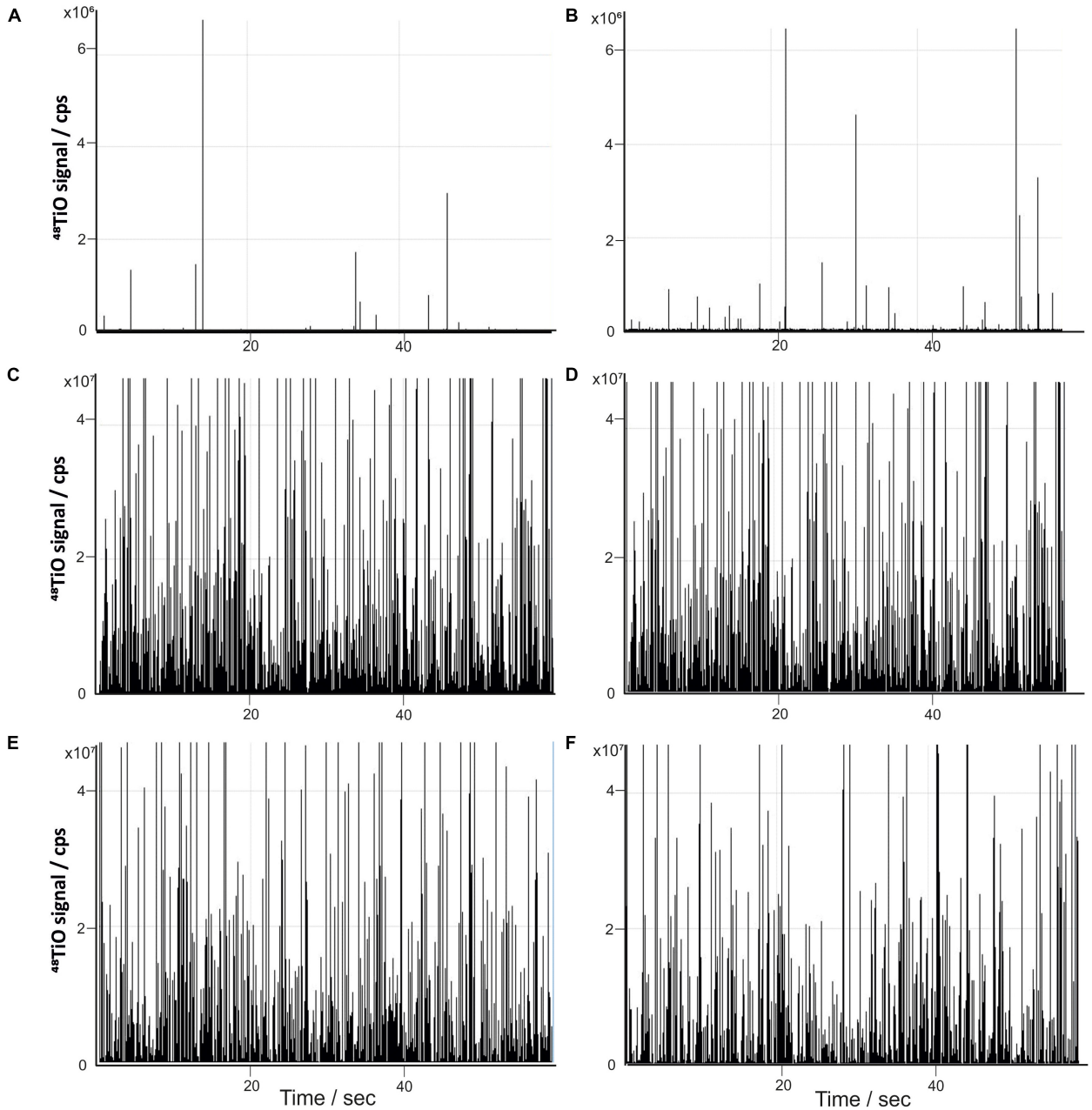

FIGURE 3 | Time scans obtained by SP-ICP-MS for **(A)** roots of control plants, **(B)** leaves plus stems of control plants, **(C)** roots of plants treated with TiO_2 NP suspension A, **(D)** leaves plus stems of plants treated with TiO_2 NP suspension A, **(E)** roots of plants treated with TiO_2 NP suspension B, and **(F)** leaves plus stems of plants treated with TiO_2 NP suspension B.

account the number of pulses detected, the nanoparticle number concentration in roots and in leaves together with stems was calculated as 3.7×10^{11} and 3.3×10^{9} NPs L^{-1}, respectively, for TiO_2 NP suspension A and as 5.5×10^{11} and 8.3×10^{8} NPs L^{-1} for suspension B.

Size distributions obtained from time scans for roots and leaves plus stems treated with both TiO_2 NP suspensions are shown on **Figure 4**. Although plant cells are surrounded by the cell wall that has pores with diameters ranging from 5 to 30 nm (Tan et al., 2018) and in theory only small TiO_2 NPs are likely to enter plants through cell wall pores, the presence of particles above 100 nm was detected in both radish tissues. It could indicate that TiO_2 NPs possibly enlarged cell pores or created new ones, as it has been suggested (Tan et al., 2018). Remarkably, the size distributions of nanoparticles from both suspensions extracted from roots did not show the presence of bigger nanoparticles and/or agglomerates (**Figures 4A,B**), presenting median diameters smaller than those

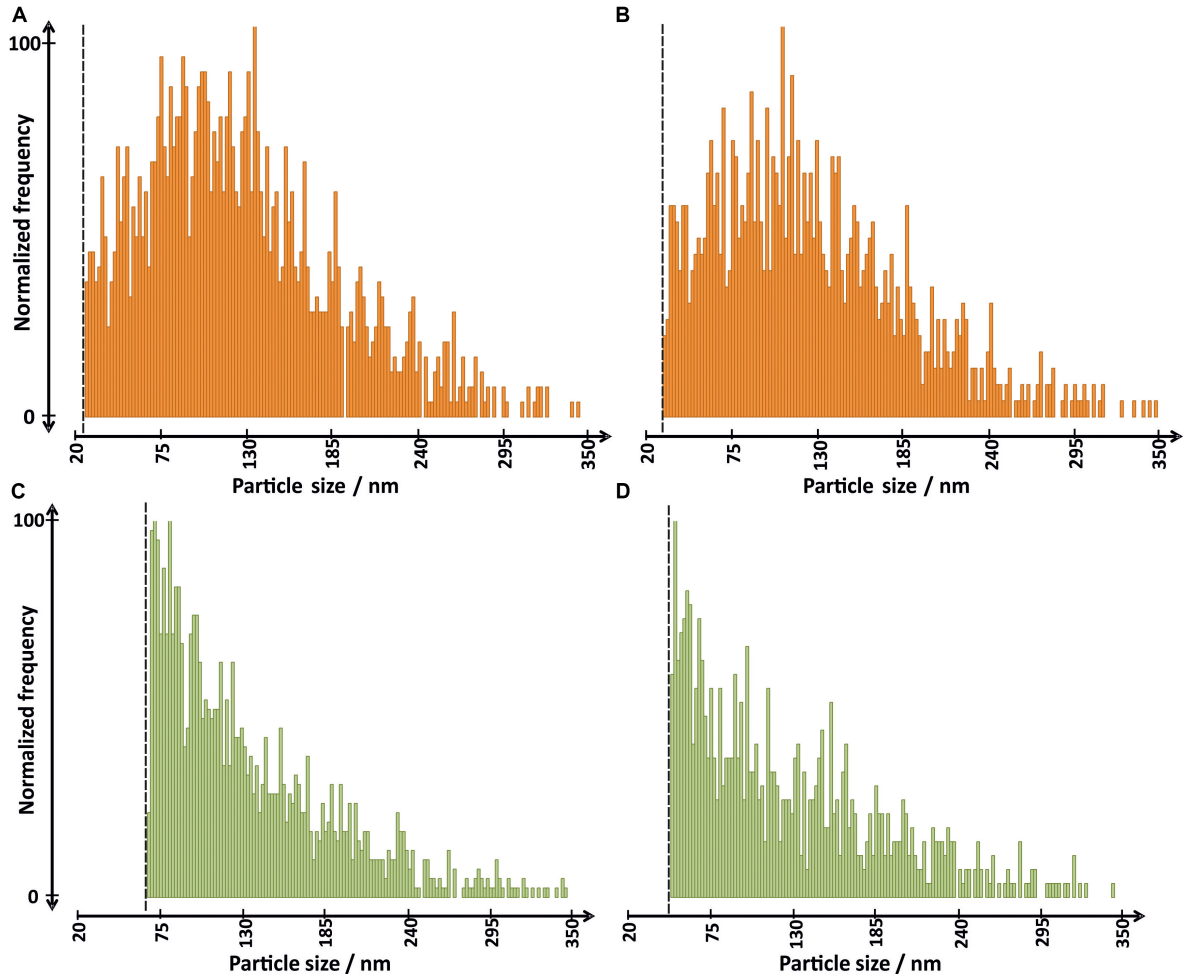

FIGURE 4 | Size distributions obtained by SP-ICP-MS for **(A)** roots of plants treated with TiO_2 NP suspension A, **(C)** leaves plus stems of plants treated with TiO_2 NP suspension A, **(B)** roots of plants treated with TiO_2 NP suspension B, and **(D)** leaves plus stems of plants treated with TiO_2 NP suspension B. Vertical lines represent the size limit of detection for each sample.

of the distributions obtained for fresh suspensions (**Table 2**), suggesting a preferential uptake of smaller nanoparticles and the occurrence of some redispersion. A similar behavior has been observed for other metal and metal-oxide nanoparticles (Kińska et al., 2018; Wojcieszek et al., 2019). On the other hand, one-way ANOVA revealed no significant differences, with a level of confidence of >99%, between nanoparticle diameters obtained for leaves and roots of plants treated with both TiO_2 NP suspensions (**Table 2**). From the results obtained, it can be concluded that nanoparticles did not undergo agglomeration during their translocation to aboveground tissues. It should also be highlighted that the use of a $5\sigma_b$ criterion to discriminate between nanoparticle events and dissolved signal may lead to the occurrence of false negatives, i.e., small nanoparticles below the size limit of detection are considered as background and hence not reflected in the corresponding size distribution. This fact is especially important for the size distribution obtained for nanoparticles in leaves (**Figures 4C,D**) where the presence of a higher background signal implied a higher size limit of detection (reported in **Figure 4** as a vertical line), which leads to the apparent loss of small nanoparticles in the histogram. Although smaller nanoparticles could not be detected, the occurrence of a redispersion process in leaf tissues should not be ignored, as it was shown for samples after enzymatic digestion and root samples.

Unlike other metal-oxide NPs, including CuO, ZnO, or even CeO_2 NPs, TiO_2 NPs have very high stability and low dissolution rate (Schmidt and Vogelsberger, 2006; Tan et al., 2018). Moreover, the root-to-shoot translocation factor was found to be low, although results have proved that TiO_2 NPs can be transported from roots to aboveground tissues. Previous studies by using various analytical techniques have already reported the presence of TiO_2 NPs in different plants such as barley, thale cress, or wheat, showing accumulation of NPs mainly in roots (Kurepa et al., 2010; Mattiello et al., 2015; Jiang et al., 2017). Finally, SP-ICP-MS (with a single-quadrupole instrument) and electron microscopy were used in order to study the translocation of TiO_2 NPs in rice (*Oryza sativa* L.), showing the presence of NPs in both roots and aboveground organs

(Deng et al., 2017). However, only the less abundant isotope of Ti (^{49}Ti) was monitored. In the case of the present study, the not engagement of a collision cell would have resulted in a significant number of nanoparticles missed in roots and leaf samples.

CONCLUSION

The using of a triple-quadrupole ICP operating in tandem mass spectrometry and single-particle mode (SP-ICP-QQQ-MS) allowed the reduction in the background signal in plant matrices for monitoring the most sensitive isotope of titanium. Under the optimal conditions of reaction cells, the uptake, translocation, and transformations of two TiO_2 NPs with different nominal sizes in radish were investigated by single-particle ICP-MS for the first time. The results demonstrated that both types of TiO_2 NPs underwent agglomeration in a small degree after 7 days in contact with the growth medium, but the enzymatic digestion procedure performed for their extraction from plant tissues did not affect the integrity of the studied nanoparticles. On the other hand, the use of filtration after the enzymatic treatment was discarded, due to the loss of the majority of nanoparticles because of membrane adsorption. The analysis of roots indicated that radish only takes up smaller nanoparticles since the presence of bigger nanoparticles was not observed for both TiO_2 NP suspensions studied. Additionally, the presence of nanoparticles without significant changes in diameter was observed in both leaves and roots, proving the plant's ability to translocate TiO_2 NPs up to aboveground organs without undergoing any transformation like dissolution or agglomeration. Finally, it should be noted that the uptake of TiO_2 NPs by plants may be favored by hydroponic cultivation, which may induce root damage allowing the nanoparticles to pass the Casparian strip and later be transported to leaves via the xylem. In this context, studies about the uptake of nanoparticles by plants in soil and at lower nanoparticle concentrations are needed.

DATA AVAILABILITY STATEMENT

The raw data supporting the conclusions of this article will be made available by the authors, without undue reservation.

AUTHOR CONTRIBUTIONS

JW and JJ-L wrote the manuscript. JW performed the single-particle ICP-MS analysis experiments. MA performed the plant cultivations. JW, JJ-L, LR, MJ, and JS conceived the project, designed the experiments, and interpreted the results. LR and JS corrected and improved the manuscript. MJ financed the research. All authors contributed to the article and approved the submitted version.

FUNDING

This work was financially supported by the National Science Centre, Poland (grant No. 2015/18/M/ST4/00257) and Warsaw University of Technology.

ACKNOWLEDGMENTS

The authors would like to thank Maciej Trzaskowski [Centre for Advanced Materials and Technologies (CEZAMAT), Warsaw University of Technology], for SEM analysis of TiO_2 NPs suspensions.

SUPPLEMENTARY MATERIAL

The Supplementary Material for this article can be found online at: https://www.frontiersin.org/articles/10.3389/fenvs.2020.00100/full#supplementary-material

REFERENCES

Azimzada, A., Farner, J. M., Hadioui, M., Liu-Kang, C., Jreije, I., Tufenkji, N., et al. (2020). Release of TiO2 nanoparticles from painted surfaces in cold climates: characterization using a high sensitivity single-particle ICP-MS. *Environ. Sci. Nano* 7, 139–148. doi: 10.1039/c9en00951e

Burke, D. J., Pietrasiak, N., Situ, S. F., Abenojar, E. C., Porche, M., Kraj, P., et al. (2015). Iron oxide and titanium dioxide nanoparticle effects on plant performance and root associated microbes. *Int. J. Mol. Sci.* 16, 23630–23650. doi: 10.3390/ijms161023630

Cai, F., Wu, X., Zhang, H., Shen, X., Zhang, M., Chen, W., et al. (2017). Impact of TiO2 nanoparticles on lead uptake and bioaccumulation in rice (*Oryza sativa* L.). *NanoImpact* 5, 101–108. doi: 10.1016/j.impact.2017.01.006

Capaldi Arruda, S. C., Diniz Silva, A. L., Moretto Galazzi, R., Antunes Azevedo, R., and Zezzi Arruda, M. A. (2015). Nanoparticles applied to plant science: a review. *Talanta* 131, 693–705. doi: 10.1016/j.talanta.2014.08.050

Castillo-Michel, H. A., Larue, C., Pradas del Real, A. E., Cotte, M., and Sarret, G. (2017). Practical review on the use of synchrotron based micro- and nano-X-ray fluorescence mapping and X-ray absorption spectroscopy to investigate the interactions between plants and engineered nanomaterials. *Plant Physiol. Biochem.* 110, 13–32. doi: 10.1016/j.plaphy.2016.07.018

Chen, X., and Mao, S. S. (2007). Titanium dioxide nanomaterials: synthesis, properties, modifications and applications. *Chem. Rev.* 107, 2891–2959. doi: 10.1021/cr0500535

Dan, Y., Zhang, W., Xue, R., Ma, X., Stephan, C., Shi, H. (2015). Characterization of gold nanoparticle uptake by tomato plants using enzymatic extraction followed by single-particle inductively coupled plasma-mass spectrometry analysis. *Environ. Sci. Technol.* 49, 3007–3014. doi: 10.1021/es506179e

Dar, G. I., Saeed, M., and Wu, A. (2020). "Toxicity of TiO_2 nanoparticles," in *TiO_2 Nanoparticles: Applications in Nanobiotechnology and Nanomedicine*. doi: 10.1002/9783527825431.ch2

Deng, Y., Petersen, E. J., Challis, K. E., Rabb, S. A., Holbrook, R. D., Ranville, J. F., et al. (2017). Multiple Method Analysis of TiO2 Nanoparticle Uptake in Rice (*Oryza sativa* L.) Plants. *Environ. Sci. Technol.* 51, 10615–10623. doi: 10.1021/acs.est.7b01364

Du, J., Xu, S., Zhou, Q., Li, H., Fu, L., Tang, J. H., et al. (2019). The ecotoxicology of titanium dioxide nanoparticles, an important engineering nanomaterial. *Toxicol. Environ. Chem.* 101, 165–189. doi: 10.1080/02772248.2019.1693572

Du, W., Gardea-Torresdey, J. L., Xie, Y., Yin, Y., Zhu, J., Zhang, X., et al. (2017). Elevated CO2 levels modify TiO2 nanoparticle effects on rice and soil microbial

communities. *Sci. Total Environ.* 578, 408–416. doi: 10.1016/j.scitotenv.2016.10.197

Fedotov, P. S., Vanifatova, N. G., Shkinev, V. M., and Spivakov, B. Y. (2011). Fractionation and characterization of nano- and microparticles in liquid media. *Anal. Bioanal. Chem.* 400, 1787–1804. doi: 10.1007/s00216-011-4704-1

Hadioui, M., Knapp, G., Azimzada, A., Jreije, I., Frechette-Viens, L., Wilkinson, K. J. (2019). Lowering the size detection limits of Ag and TiO2 nanoparticles by single particle ICP-MS. *Anal. Chem.* 91, 13275–13284. doi: 10.1021/acs.analchem.9b04007

Hong, F., Yu, X., Wu, N., and Zhang, Y. Q. (2017). Progress of: in vivo studies on the systemic toxicities induced by titanium dioxide nanoparticles. *Toxicol. Res.* 6, 115–133. doi: 10.1039/c6tx00338a

Jafarizadeh-Malmiri, H., Sayyar, Z., Anarjan, N., and Berenjian, A. (2019). *Nanobiotechnology in Food: Concepts, Applications and Perspectives*. 1–155. doi: 10.1007/978-3-030-05846-3

Jiang, F., Shen, Y., Ma, C., Zhang, X., Cao, W., Rui, Y. (2017). Effects of TiO2 nanoparticles on wheat (*Triticum aestivum* L.) seedlings cultivated under super-elevated and normal CO2 conditions. *PLoS One* 12:e178088. doi: 10.1371/journal.pone.0178088

Jiménez-Lamana, J., Wojcieszek, J., Jakubiak, M., Asztemborska, M., and Szpunar, J. (2016). Single particle ICP-MS characterization of platinum nanoparticles uptake and bioaccumulation by Lepidium sativum and Sinapis alba plants. *J. Anal. At. Spectrom.* 31, 2321–2329. doi: 10.1039/C6JA00201C

Keller, A. A., and Lazareva, A. (2013). Predicted releases of engineered nanomaterials: from global to regional to local. *Environ. Sci. Technol. Lett.* 1, 65–70. doi: 10.1021/ez400106t

Kińska, K., Jiménez-Lamana, J., Kowalska, J., Krasnodębska-Ostręga, B., and Szpunar, J. (2018). Study of the uptake and bioaccumulation of palladium nanoparticles by Sinapis alba using single particle ICP-MS. *Sci. Total Environ.* 615, 1078–1085. doi: 10.1016/j.scitotenv.2017.09.203

Kole, C., Kumar, D. S., and Khodakovskaya, M. V. (2016). Biophysical methods of detection and quantification of uptake, translocation, and accumulation of nanoparticles. *Plant Nanotechnol.* 29–63. doi: 10.1007/978-3-319-42154-4

Kurepa, J., Paunesku, T., Vogt, S., Arora, H., Rabatic, B. M., Lu, J., et al. (2010). Uptake and distribution of ultrasmall anatase TiO2 alizarin red s nanoconjugates in arabidopsis thaliana. *Nano Lett.* 10, 2296–2302. doi: 10.1021/nl903518f

Laborda, F., Bolea, E., and Jiménez-Lamana, J. (2014). Single particle inductively coupled plasma mass spectrometry: a powerful tool for nanoanalysis. *Anal. Chem.* 86, 2270–2278. doi: 10.1021/ac402980q

Laborda, F., Bolea, E., and Jiménez-Lamana, J. (2016). Single particle inductively coupled plasma mass spectrometry for the analysis of inorganic engineered nanoparticles in environmental samples. *Trends Environ. Anal. Chem.* 9, 15–23. doi: 10.1016/j.teac.2016.02.001

Laborda, F., Gimenez-Ingalaturre, A. C., Bolea, E., and Castillo, J. R. (2019). Single particle inductively coupled plasma mass spectrometry as screening tool for detection of particles. *Spectrochim. Acta Part B At. Spectrosc.* 159:105654. doi: 10.1016/j.sab.2019.105654

Larue, C., Castillo-Michel, H., Sobanska, S., Trcera, N., Sorieul, S., Cécillon, L., et al. (2014). Fate of pristine TiO2 nanoparticles and aged paint-containing TiO2 nanoparticles in lettuce crop after foliar exposure. *J. Hazard. Mater.* 273, 17–26. doi: 10.1016/j.jhazmat.2014.03.014

Larue, C., Castillo-Michel, H., Stein, R. J., Fayard, B., Pouyet, E., Villanova, J., et al. (2016). Innovative combination of spectroscopic techniques to reveal nanoparticle fate in a crop plant. *Spectrochim. Acta Part B At. Spectrosc.* 119, 17–24. doi: 10.1016/j.sab.2016.03.005

Lee, S., Bi, X., Reed, R. B., Ranville, J. F., Herckes, P., Westerhoff, P. (2014). Nanoparticle size detection limits by single particle ICP-MS for 40 elements. *Environ. Sci. Technol.* 48, 10291–10300. doi: 10.1021/es502422v

Mattiello, A., Filippi, A., Pošćić, F., Musetti, R., Salvatici, M. C., Giordano, C., et al. (2015). Evidence of phytotoxicity and genotoxicity in *Hordeum vulgare* L. Exposed to CeO2 and TiO2 Nanoparticles. *Front. Plant Sci.* 6:1043. doi: 10.3389/fpls.2015.01043

Oliver, A. L. S., Muñoz-Olivas, R., Sanz Landaluze, J., Rainieri, S., and Cámara, C. (2015). Bioaccumulation of ionic titanium and titanium dioxide nanoparticles in zebrafish eleutheroembryos. *Nanotoxicology* 9, 835–842. doi: 10.3109/17435390.2014.980758

Pace, H. E., Rogers, N. J., Jarolimek, C., Coleman, V. A., Higgins, C. P., Ranville, J. F., et al. (2011). Determining transport efficiency for the purpose of counting and sizing nanoparticles via single particle inductively coupled plasma mass spectrometry. *Anal. Chem.* 83, 9361–9369. doi: 10.1021/ac201952t

Reddy, P. V. L., Hernandez-Viezcas, J. A., Peralta-Videa, J. R., and Gardea-Torresdey, J. L. (2016). Lessons learned: are engineered nanomaterials toxic to terrestrial plants? *Sci. Total Environ.* 568, 470–479. doi: 10.1016/j.scitotenv.2016.06.042

Schmidt, J., and Vogelsberger, W. (2006). Dissolution kinetics of titanium dioxide nanoparticles: the observation of an unusual kinetic size effect. *J. Phys. Chem. B* 110, 3955–3963. doi: 10.1021/jp055361l

Servin, A. D., Castillo-Michel, H., Hernandez-Viezcas, J. A., Diaz, B. C., Peralta-Videa, J. R., Gardea-Torresdey, J. L., et al. (2012). Synchrotron micro-XRF and micro-XANES confirmation of the uptake and translocation of TiO2 nanoparticles in cucumber (*Cucumis sativus*) plants. *Environ. Sci. Technol.* 46, 7637–7643. doi: 10.1021/es300955b

Servin, A. D., Morales, M. I., Castillo-Michel, H., Hernandez-Viezcas, J. A., Munoz, B., Zhao, L., et al. (2013). Synchrotron verification of TiO2 accumulation in cucumber fruit: a possible pathway of TiO2 nanoparticle transfer from soil into the food chain. *Environ. Sci. Technol.* 47, 11592–11598. doi: 10.1021/es403368j

Shah, S. N. A., Shah, Z., Hussain, M., and Khan, M. (2017). Hazardous effects of titanium dioxide nanoparticles in ecosystem. *Bioinorg. Chem. Appl.* 2017:4101735. doi: 10.1155/2017/4101735

Shakeel, M., Jabeen, F., Shabbir, S., Asghar, M. S., Khan, M. S., Chaudhry, A. S., et al. (2016). Toxicity of Nano-Titanium Dioxide (TiO2-NP) through various routes of exposure: a review. *Biol. Trace Elem. Res.* 172, 1–36. doi: 10.1007/s12011-015-0550-x

Tan, W., Peralta-Videa, J. R., and Gardea-Torresdey, J. L. (2018). Interaction of titanium dioxide nanoparticles with soil components and plants: current knowledge and future research needs-a critical review. *Environ. Sci. Nano* 5, 257–278. doi: 10.1039/c7en00985b

Tharaud, M., Gondikas, A. P., Benedetti, M. F., von der Kammer, F., Hofmann, T., Cornelis, G., et al. (2017). TiO2 nanomaterial detection in calcium rich matrices matrices by spICPMS . A matter of resolution and treatment. *J. Anal. At. Spectrom.* 32, 1400–1411. doi: 10.1039/C7JA00060J

Thor, K. (2019). Calcium — nutrient and messenger. *Front. Plant Sci.* 10:440. doi: 10.3389/fpls.2019.00440

Vidmar, J., Milačič, R., and Ščančar, J. (2017). Sizing and simultaneous quantification of nanoscale titanium dioxide and a dissolved titanium form by single particle inductively coupled plasma mass spectrometry. *Microchem. J.* 132, 391–400. doi: 10.1016/j.microc.2017.02.030

White, P. J., and Broadley, M. R. (2003). Calcium in plants. *Ann. Bot.* 92, 487–511. doi: 10.1093/aob/mcg164

Wojcieszek, J., Jiménez-Lamana, J., Bierła, K., Ruzik, L., Asztemborska, M., Jarosz, M., et al. (2019). Uptake, translocation, size characterization and localization of cerium oxide nanoparticles in radish (*Raphanus sativus* L.). *Sci. Total Environ.* 683, 284–292. doi: 10.1016/j.scitotenv.2019.05.265

Zahra, Z., Waseem, N., Zahra, R., Lee, H., Badshah, M. A., Mehmood, A., et al. (2017). Growth and Metabolic Responses of Rice (*Oryza sativa* L.) Cultivated in Phosphorus-Deficient Soil Amended with TiO2 Nanoparticles. *J. Agric. Food Chem.* 65, 5598–5606. doi: 10.1021/acs.jafc.7b01843

Zhang, X., Li, W., and Yang, Z. (2015). Toxicology of nanosized titanium dioxide: an update. *Arch. Toxicol.* 89, 2207–2217. doi: 10.1007/s00204-015-1594-6

Conflict of Interest: The authors declare that the research was conducted in the absence of any commercial or financial relationships that could be construed as a potential conflict of interest.

frontiers in Environmental Science

ORIGINAL RESEARCH
published: 30 July 2020
doi: 10.3389/fenvs.2020.00114

Geochemistry of Engineered Nanoparticles (CdSe/ZnS Quantum Dots) in Surface Waters

*N. Izyan Supiandi, Rute F. Domingos, Marc F. Benedetti and Yann Sivry**

Institut de Physique du Globe de Paris, Université de Paris, CNRS UMR7154, Paris, France

The difficulties when studying the behavior of engineered nanoparticles (ENPs), and the subsequent metal speciation in aquatic ecosystems, at environmentally relevant concentrations (i.e., ppt level) are often related to the occurrence of ENP constitutive elements at high concentrations as a background in aquatic media. In this study, the physicochemical behavior of CdSe/ZnS quantum dots (QDs) when spread at very low concentrations in surface waters was investigated. The above-mentioned issues were overcome with the use of isotopically labeled QDs, separated by centrifugal ultrafiltration (CU) and measured by high-resolution inductively coupled plasma mass spectrometry (HR-ICP-MS), combined with the detection of free and labile metal ions by scanned stripping chronopotentiometry (SSCP). They firmly provided a thorough comprehension regarding the transformation of QDs in surface waters. The physicochemical conditions of the medium including the presence of an analog of natural organic matter and a mineral (i.e., fulvic acid and goethite), the manufactured coating of the QDs [here thioglycolic acid (TGA)], and the occurrence of added Zn in the medium were considered in the study. The overall results show that, in the absence of mineral/organic matter, the TGA ligands in solution that detached from the QD surface after dissolution control the metal speciation, especially for Cd. Conversely, in a more representative aquatic ecosystem condition (i.e., with Zn in the background media together with fulvic acid and goethite), almost no Zn or Cd dissolution from the QDs is detected. SSCP measurements reveal that the Zn complexes formed with the organic/mineral material in the system are inert, whereas the speciation model calculations indicated that Cd^{2+} is bound to TGA ligands in solution and organic/inorganic matter—therefore suggesting that, under the studied conditions, aquatic organisms will be exposed to a very low concentration of free and labile metal ions issued from the QDs.

Keywords: quantum dots, isotopic labeling, speciation, surface waters, dissolution, zinc, cadmium

OPEN ACCESS

Edited by:
Vera I. Slaveykova, Université de Genève, Switzerland

Reviewed by:
Claude Fortin, Institut National de la Recherche Scientifique (INRS), Canada
Huacheng Xu, Nanjing Institute of Geography and Limnology (CAS), China

***Correspondence:**
Yann Sivry
sivry@ipgp.fr

Specialty section:
This article was submitted to Biogeochemical Dynamics, a section of the journal Frontiers in Environmental Science

Received: *31 March 2020*
Accepted: *29 June 2020*
Published: *30 July 2020*

Citation:
Supiandi NI, Domingos RF, Benedetti MF and Sivry Y (2020) Geochemistry of Engineered Nanoparticles (CdSe/ZnS Quantum Dots) in Surface Waters. Front. Environ. Sci. 8:114. doi: 10.3389/fenvs.2020.00114

INTRODUCTION

The progress of nanotechnology led to numerous applications of engineered nanoparticles (ENPs), which results in the increase of studies concerning their fate and behavior in environmental compartments (e.g., wastewater treatment plants, surface water, sediments, and soils), as well as their potential toxic effects. However, most of these studies are often carried out at conditions far

from the ones expected in the environment, mostly for two main reasons. Firstly, the concentrations of ENPs used are generally higher than those predicted or measured for aquatic ecosystems, i.e., micromolar vs nanomolar (Gottschalk et al., 2009; Piccinno et al., 2012), mostly due to the analytical detection limits but also to the difficulty in detecting these ENPs in complex matrices with high natural concentrations of ENP constitutive elements. Secondly, the presence of other metal ions and organic/mineral matter, which are key players for metal ion speciation, is much neglected, especially during the investigations of ENP effects on living organisms.

Nevertheless, it is known that changes in ENP concentration and the occurrence of other metal ions and mineral/organic matters can affect their behavior, and the speciation of metal ions from ENP dissolution can change due to metal ions binding to the mineral and organic matters. For example, it has been shown that the dissolution of ZnO nanoparticles (NPs) decreases with its increasing concentration (Yung et al., 2015) or that the presence of humic substances in aquatic systems results in less ZnO and TiO_2 NP homoaggregation due to their heteroaggregation, suggesting that NP dispersion should be stable in a natural environment (Domingos et al., 2009, 2013b). On the other hand, Cd and Pb metal ions were shown to interact with CdTe/CdS NPs, influencing their dissolution and metal ion speciation (Cd and Pb) and thus their environmental fate (Domingos et al., 2015).

To this day, studies have not yet investigated the fate of ENPs under environmentally relevant conditions for aquatic ecosystems (i.e., at predicted or measured ENP concentrations) and in the presence of organic/mineral matter and other metal ions as well. In this study, we characterized the fate of ENPs at low and environmentally relevant concentrations and identified the geochemical processes at work. We have specifically focused on (i) ENP stability (i.e., dissolution and its rate) in aquatic media and (ii) the phases (e.g., organic/mineral matter and ENPs constitutive elements) susceptible to control the fate of ENPs. Some environmental implications of the findings on ENP behavior for the aquatic ecosystems are discussed in this article.

To answer those questions, we decided to use CdSe/ZnS quantum dot (QD) ENPs. CdSe/ZnS QDs are highly representative of core/shell-structured ENPs; they are exponentially used for light conversion purposes (e.g., in devices and materials intended for display, photovoltaic, lighting, and sensors) as well as in laboratory use for imaging (Piccinno et al., 2012; Pickering et al., 2012; Zhao et al., 2012; Dai et al., 2017). Moreover, one of their constituting elements (i.e., Zn) has high background concentration values in most of the aquatic ecosystems (ppb level), which contrasts with the estimated concentration of Zn-containing ENPs (ppt level) in surface water (Piccinno et al., 2012; Gottschalk et al., 2015).

Batch experiments were performed, using mixtures of QDs and water with different chemical compositions and analogs of suspended matter to follow, as a function of time, the changes in chemical composition of the model surface waters. The use of isotopically modified (or "spiked") ENPs (Supiandi et al., 2019, 2020) with centrifugal ultrafiltration (CU) separation and detection by high-resolution inductively coupled plasma mass spectrometry (HR-ICP-MS) overcame the analytical barriers (detection limits and geochemical background) to obtain the metal ion concentration and origins in the dissolved fraction. The speciation of QDs constituting metal ions (Cd and Zn) in the experimental systems (Domingos et al., 2008) was followed by scanned stripping chronopotentiometry (SSCP).

MATERIALS AND METHODS

We used concentrations of QDs approaching the ENP predicted concentrations in the environment (nanomolar/ppt level), in the absence and presence of one organic and mineral suspended matter constituent (a fulvic acid and an iron oxide, namely, goethite), while also considering the absence and presence of Zn from the geochemical background.

Multi-Isotopically Labeled $^{111}Cd^{77}Se/^{68}ZnS$ QDs

The CdSe/ZnS QDs used in this study were enriched in ^{111}Cd, ^{77}Se, and ^{68}Zn. The chemicals used including the synthesis protocol and the characterization methods of the multi-spiked QDs were described in previous works (Supiandi et al., 2019, 2020). Briefly, a stock solution of the QDs in an organic phase was synthesized and used to prepare water-soluble QDs, i.e., functionalized with thioglycolic acid (TGA). A solution of TGA-coated QDs was used in the experiments carried out in this study.

Synthetic River Water

The choice was made to work with a synthetic water instead of a real natural water. Being the first study targeting such low concentrations of ENPs, therefore, it is of major concern to have full control of the water constituents that can have an impact on the QD fate and speciation. A synthetic river water (SRW), analog of the Seine river flowing in Paris (Hammes et al., 2013; Sivry et al., 2014), was prepared. $Ca(NO_3)_2$, Na_2SO_4, and NaHEPES salts were added into a known quantity of ultrapure water from Milli-Q Millipore (resistivity > 18 MΩ.cm) to obtain a 2 mM Ca^{2+} solution, buffered at pH 8 (1 mM of NaHEPES) and 0.56 mM of Na^+ and 0.28 mM of SO_4^{2-}. HEPES is assumed to be noncomplexing; therefore, it would not have implications on the speciation studies (Soares and Conde, 2000). Carbonates in the systems come from the equilibration with the atmosphere, since no specific effort was made to prevent CO_2 dissolution during the experiments. The ionic strength of the prepared SRW was approximately 7 mM.

Different components were then added to the SRW, to obtain a total of five different water conditions: (A) SRW; (B) SRW-Zn, SRW in which $Zn(NO_3)_2$ was added to reach a concentration of 60 nM; (C) SRW-Zn-FA, corresponding to SRW-Zn with an addition of Suwannee river fulvic acid to a concentration of 5 ppm (SRFA; from the International Humic Substances Society, noted as FA hereafter); (D) SRW-Zn-G corresponding to SRW-Zn with an addition of goethite to reach 20 ppm of concentration. The goethite was prepared according to Hiemstra et al. (1989), and its characterization can be found in Zelano et al. (2016); and (E) SRW-Zn-FA-G, corresponding to SRW-Zn with an addition of FA (5 ppm) and goethite (20 ppm). The concentrations of these

components are relevant in most natural river systems (Hammes et al., 2013; Sivry et al., 2014).

Batch Experiments

The dissolution and speciation of the QD constituting elements (Zn and Cd) in synthetic waters A, B, C, D, and E were followed for 8 days, at different intervals of time (t = 0, 2, 6, 24, 48, 96, 144, and 192 h). The initial QD concentrations used were relevant to the estimated ENP concentrations found in the environment, i.e., ppt–ppb level (Gottschalk et al., 2009; Piccinno et al., 2012), and significantly higher than the limit of quantification (LOQ) previously determined for the isotopically labeled QDs spread in natural waters (i.e., QD-LOQ, Supiandi et al., 2019). For each time step and for both dissolution and speciation experiments, 20 ml of each water sample was prepared in a disposable polystyrene cup. The concentration of QDs added at t = 0 in each cup was to reach 7.6 nM of Zn (500 ppt), corresponding to 1.4 nM of Cd (160 ppt) and 0.8 nM of Se (63 ppt). For the latter, this concentration is too close to the HR-ICP-MS LOQ (60 ppt) to obtain reliable data. Therefore, only Zn and Cd results are discussed hereafter. To summarize the batch experiments, the dissolution of the QDs in each cup was followed by CU and HR-ICP-MS analysis; meanwhile, the speciation was studied using SSCP; both methods are detailed hereafter.

Besides, electrophoretic mobility (EPM) measurements of QDs and organic and mineral matter in waters A, B, C, D, and E were also carried out using a Malvern Zetasizer Nano-ZS (Malvern, DTS1061) at 20°C. Each sample value corresponds to the mean of at least five independent measurements. The standard DTS1235 for zeta potential was used after every ∼10 measurements to verify the performance of the system.

CU + HR-ICP-MS

Centrifugal filter units (Amicon® Ultra Centrifugal Filter Units, 3 kDa cutoff equivalent to 1–2 nm pore diameters) were used to separate QDs from free Zn and Cd ions as well as complexes resulting from QD dissolution with a smaller size than the cutoff. At different time intervals (t = 0, 2, 6, 24, 48, 96, 144, and 192 h), 4 ml of QD-containing solutions (from conditions A–E) was sampled and centrifuged for 35 min at 3,220 g. The filtrates were collected and acidified (2% of HNO_3 in solution) prior to analysis by HR-ICP-MS. The concentrations of spiked Zn and Cd in the CU dissolved fraction were calculated using the equations adapted from Dybowska et al. (2011) (see **Supplementary Material**), which allowed us to trace the dissolved metal released from the spiked ENPs, notwithstanding the high background concentrations, especially in Zn. The potential bias caused by CU on metal concentration due to the progressive and relative increase in large binding ligands while the volume of solution decreases over a 35 min period has been assessed in a previous study and found negligible in the experimental conditions fixed (Sivry et al., 2014). In addition, the information on the dissolution of isotopically labeled QDs is contained on the isotopic composition of the dissolved fraction, not on the concentration of the latter. Therefore, the use of isotopically labeled QDs allows us to get rid of a potential adsorption of dissolved metal on the membrane or on the walls of the CU cell.

External standard solutions containing 1, 5, 10, 100, 500, 1,000, and 5,000 ppt of total Cd and Zn were prepared in 2% HNO_3 and used for the HR-ICP-MS analyses. A solution containing 5 ppb of rhodium (^{103}Rh) prepared in 2% HNO_3 was used as an internal standard solution to correct from instrumental drift and mass bias. The isotopes of Cd (^{106}Cd, ^{108}Cd, ^{110}Cd, ^{111}Cd, ^{112}Cd, ^{113}Cd, ^{114}Cd, and ^{116}Cd) and Zn (^{64}Zn, ^{66}Zn, ^{67}Zn, ^{68}Zn, and ^{70}Zn) were analyzed with HR-ICP-MS. The isotopes ^{105}Pd, ^{115}In, ^{118}Sn, ^{60}Ni, and ^{72}Ge were also analyzed to correct for possible isobaric interferences. Each intensity used for data treatment corresponds to the average of 15 blocks of three replicates, allowing an internal reproducibility with a standard error better than 5%. Within each measurement sequence, reproducibility of the in-house multielement isotopic reference material (TM-23.4 Lake Ontario water from National Research Council Canada) was monitored at the beginning and the end of each analysis sequence, yielding less than 10% shift from the certified values. All results are presented as the mean and standard deviation of three replicates when available; meanwhile, results from single-replicated samples are presented as the mean and standard deviation of measurements of the 15 blocks of three replicates (standard error <5%).

Zn Speciation in Solution by SSCP

According to Merdzan et al. (2014), it is necessary to complement the CU data with other techniques to fully understand the behavior of the ENPs in complex waters, since each technique measures a slightly different fraction of the metal. SSCP was used here to obtain information on the lability degree of the complexes by following SSCP shift in the half-wave deposition potential (Pinheiro and van Leeuwen, 2004). A full description of SSCP can be found in Domingos et al. (2013a) (see **Supplementary Material**).

Scanned stripping chronopotentiometry was performed on all solutions from conditions A–E using an Eco Chemie potentiostat PGSTAT 128N in conjunction with a Metrohm 663 VA stand and the NOVA 1.11 software. Electrodes included an Ag/AgCl reference electrode with a 0.1 M $NaNO_3$ salt bridge, a platinum counter electrode, and a thin mercury film electrode plated onto a rotating glassy carbon disk (1.9 mm diameter, Metrohm). Calibration solutions ($C = 1 \times 10^{-7}$ M, pH = 4) were prepared daily. All solutions were purged with nitrogen for 20 min prior to the voltammetric experiments, and the measurements were carried out at room temperature (18–20°C). During an SSCP analysis, the potential was held at a deposition potential of Zn (E_d) for the duration of the deposition time (t_d = 45 or 90 s), during which Zn was accumulated on the working electrode, with E_d held at −1.3, −1.13, −1.075, −1.23, −1.19, −1.25, −1.09, −1.17, −1.15, −1.115, −1.16, −1.21, −1.1, −1.14, −1.125, −1.3, −1.065, and −1.055 V. After the accumulation step, an oxidizing strip current, $I_s = 1 \times 10^{-6}$ A, was applied in quiescent solution until the potential reached a value sufficiently beyond the transition plateau (−0.2 V). The raw signal is a measurement of the variation of potential with time that is automatically converted to the dt/dE-vs-E format. The

Zn concentrations calculated from the measurement data are representing the sum of Zn^{2+} ions in solution and Zn^{2+} coming from labile Zn complexes.

Scanned stripping chronopotentiometry results are presented as the mean and standard deviation or range of minimum and maximum values of at least three measurement replicates performed on different days with freshly prepared samples.

Model Calculations

Visual MINTEQ software (version 3.1) was used to evaluate the thermodynamic speciation of Zn and Cd in all water conditions, i.e., binding to inorganic ligands, TGA, FA, and goethite (Sivry et al., 2014), complementing the results obtained by CU/HR-ICP-MS and SSCP for Zn (see **Supplementary Material** for modeling details, parameters, and assumptions).

RESULTS

Characterization of CdSe/ZnS QDs

The multi-spiked QDs exhibit a green emission centered at 540 nm with an emission full width at half maximum (FWHM) of 40 nm. The synthesized QDs are round-shaped, and some are slightly oval, with an average of ∼7.6 nm in size. Figures and detailed characterization results are provided in the **Supplementary Material**.

General Observation on the CU/HR-ICP-MS Data

Figure 1 shows the CU/HR-ICP-MS filtrate concentrations of Zn and Cd, hereafter denoted Zn_{QDs} and Cd_{QDs}, respectively. The QD dissolution profiles are presented as a function of time for conditions A–E. The ratio between Zn_{QDs} and Cd_{QDs} dissolved fraction concentrations [$(Zn_{QDs})/(Cd_{QDs})$] compared to the initial Zn and Cd concentration (i.e., added as QDs) ratio is given in **Figure 2** to test congruent vs incongruent release of the two constituting elements under the studied conditions.

In simplified media, in the absence of mineral/organic matter (conditions A and B), the concentrations of Zn and Cd dissolved from the QD shell and core, (Zn_{QDs}) and (Cd_{QDs}), respectively, increase slowly within 24 h of exposure time, and total dissolution of Zn_{QDs} and Cd_{QDs} was observed after 48 h of exposure. The variation of $(Zn_{QDs})/(Cd_{QDs})$ ratios in the function of time seems similar in both cases, indicating that the addition of extra Zn in condition B does not seem to affect the dissolution of the QDs. At the beginning of the interaction, the ratios are much higher than the initial one (50 vs 5) showing that Zn_{QDs} is preferentially released compared to the Cd_{QDs} that dissolves slowly. At $t = 2$ and 6 h, this ratio is higher in condition A, indicating a higher release in Zn_{QDs} compared to that of condition B. But in both cases, the ratio toward the end of the experiment is equal the initial one [$(Zn_{QDs})/(Cd_{QDs}) = 5$].

In the presence of organic matter analog (FA), i.e., condition C, Zn_{QDs} and Cd_{QDs} dissolved slowly and did not reach total dissolution even after 8 days. This could be explained by the protection of the QDs by the FA (Domingos et al., 2009; Oriekhova and Stoll, 2016). The FA is most probably surrounding the QD surface, conferring a much more negative environment and thus stabilizing the particle and slowing down their dissolution, which is coherent with the EPM data (**Figure 3**). The $(Zn_{QDs})/(Cd_{QDs})$ ratios are slightly higher but almost similar to that of condition B, also indicating that the Zn_{QDs} release is more favored than that of Cd_{QDs}. However, the ratio has a different profile toward the end of the interaction (t = 96–144 h), showing that the concentration of dissolved Zn_{QDs} or its complexes in solution is higher than that of the Cd_{QDs} if

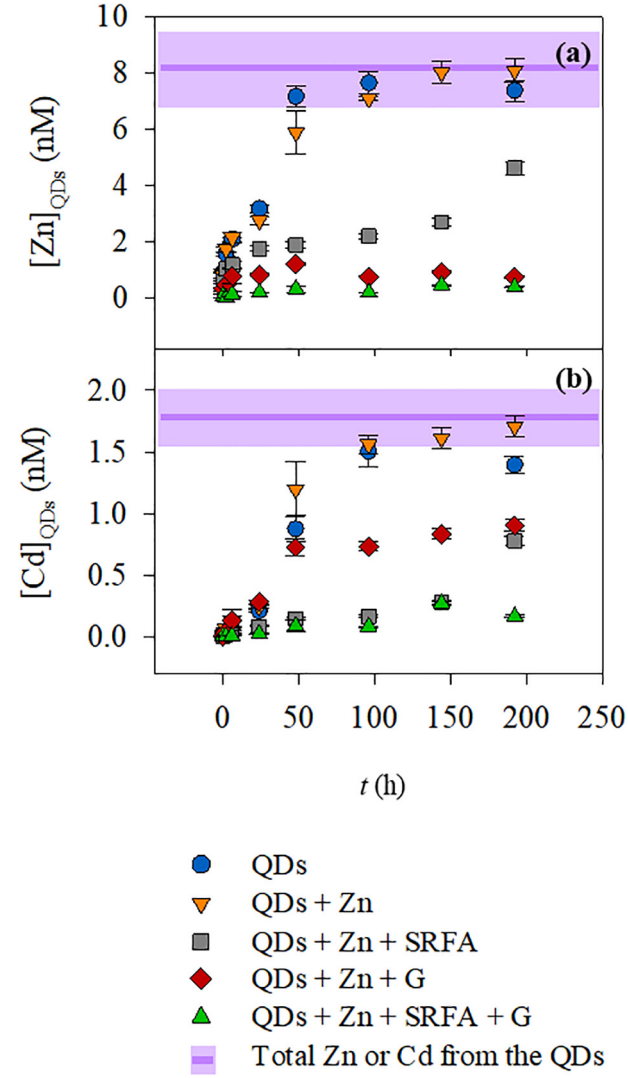

FIGURE 1 | Zn **(a)** and Cd **(b)** concentrations on the filtrates after CU as a function of time for the QDs dispersed in five different conditions: (●) QD dissolution in SRW; (▼) QD dissolution in SRW containing Zn (110 nM); (■) QD dissolution in SRW containing Zn and Suwannee river fulvic acid (FA, 5 ppm); (♦) QD dissolution in SRW containing Zn and goethite (G, 20 ppm); and (▲) QD dissolution in SRW containing Zn, FA, and G. The purple lines and shadowed areas represent the average and the standard deviation, respectively, of the total Zn or Cd of the QDs added at the beginning of the dissolution experiment.

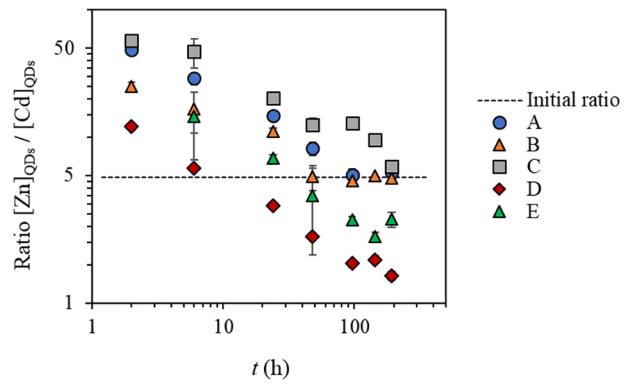

FIGURE 2 | The ratio between Zn_{QDs} and Cd_{QDs} dissolved fraction concentrations compared to the initial Zn_{QDs} and Cd_{QDs} concentration ratio in water conditions A–E. Conditions (A) SRW, (B) SRW-Zn, (C) SRW-Zn-FA, (D) SRW-Zn-G, and (E) SRW-Zn-FA-G.

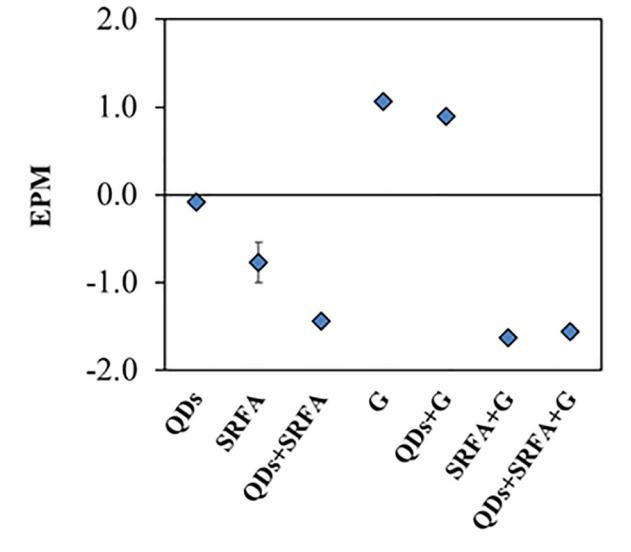

FIGURE 3 | EPM data obtained for the different samples containing only QDs, FA and goethite, and mixtures of them after 24 h of stabilization.

compared to conditions A and B. This can be explained by the speciation of Cd metal ions in the presence of FA, which are most probably forming complexes larger than the CU membrane cutoff. The ratio at 8 days (192 h) decreases to almost the initial one, indicating that the concentration of dissolved Cd_{QDs} in solution is identical to that of Zn_{QDs}.

In the presence of goethite mineral phase (condition D), almost no dissolved Zn_{QDs} shell was detected, but the release of the Cd_{QDs} core was observed. This indicates that the QD Zn shell should be totally dissolved, allowing the Cd core to dissolve unless the particles are highly porous. The absence of Zn in the CU filtrate indicates that Zn could be complexed by the goethite, which is much larger than the membrane pores. The presence of Cd in the filtrate suggests that goethite has a higher affinity for Zn compared to Cd, which was in fact previously shown (Spathariotis and Kallianou, 2007; Juillot et al., 2008). This can be seen from the dissolved $(Zn_{QDs})/(Cd_{QDs})$ ratios which are much lower compared to other conditions and especially lower than the initial ratio after 50 h of interaction, showing that dissolved Cd_{QDs} or its small complexes (<3 kDa) remain in solution after its release. However, the measured concentrations of dissolved Zn_{QDs} are lower than the LOQ of spiked QDs in surface waters found in our previous study, i.e., QD-LOQ_{Zn} = 1.4 nM = 95 ppt (Supiandi et al., 2019); therefore, the values of (Zn_{QDs}) in this condition are speculated to be unreliable.

In the presence of both FA and goethite (condition E), almost no dissolved Zn_{QDs} and Cd_{QDs} were observed, and the dissolved $(Zn_{QDs})/(Cd_{QDs})$ ratios are higher than those of conditions D, indicating that the release of Zn_{QDs} is more preferential. This can be explained by the speciation of Zn and Cd metal ions (forming complexes larger than the CU membrane cutoff) that will be verified later in this article.

Besides the information on the QD dissolution obtained from the CU/HR-ICP-MS, the overall data have shown in parallel the advantage of the ENP isotopic labeling technique when used with CU/HR-ICP-MS. The data of Zn particularly showed that the Zn dissolved from the QDs can be detected at nanomolar (ppt) level even in media with high-Zn background. The total concentration analysis by ICP-MS (not shown in the CU figures) indicated that the medium in condition A contains 51 nM of Zn in solution even without any initial addition of Zn as for the other waters, possibly due to the contamination coming from the various salts added for the preparation of the SRW. The media in conditions B–E contain about 110 nM of Zn resulting from the contamination plus the initial added Zn salt (60 nM). Even though these waters contain already almost 7–15 times higher Zn concentrations compared to the one coming from the QD [(Zn_{QDs}) = 7.4 nM], the dissolved Zn from the QDs was still quantified at such a low concentration.

DISCUSSION

Zn Lability

The SSCP data are presented separately for each condition (A–E) (**Figure 4**), showing the concentrations of labile Zn as a function of time. Overall, the labile Zn concentration (background + QDs) in all conditions decreases with time. However, in conditions D and E, the measured concentrations are much lower than those of conditions B and C, which have the same total Zn concentration initially added. This shows that the presence of goethite in the system influences the speciation of Zn, which most is probably forming strong complexes that are not easily dissociated, inducing much lower labile Zn concentrations.

The SSCP shift in the half-wave deposition potential ($\Delta E_{d,1/2}$) for all water conditions is presented altogether in **Figure 5**. Recall that $\Delta E_{d,1/2} = E_{d,1/2}$ (ML) $- E_{d,1/2}$ (M) is the difference of $E_{d,1/2}$ between the complexes (ML) and the free metals (M). For example, an increasing $|\Delta E_{d,1/2}|$ means formation of stronger labile complexes.

For conditions A and B, the values of $\Delta E_{d,1/2}$ are quite similar, indicating a formation of complexes with similar strength in both conditions, e.g., $ZnCO_3$, $ZnOH^+$, or ZnTGA. In the presence of

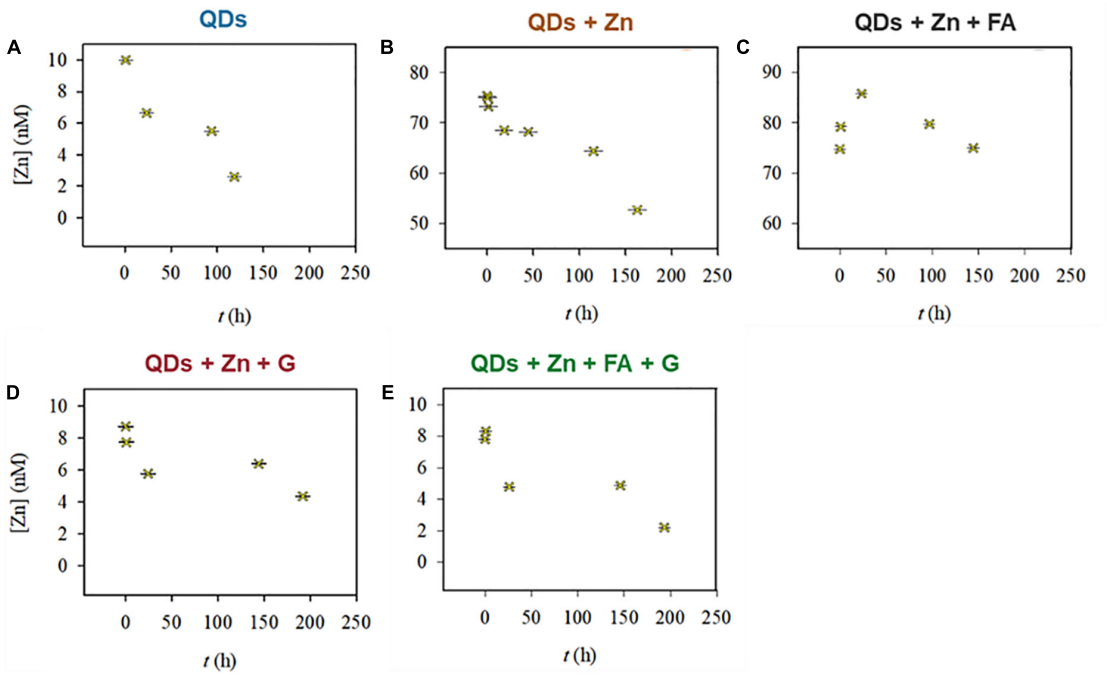

FIGURE 4 | Labile Zn concentrations in conditions **(A–E)**. Conditions **(A)** SRW, **(B)** SRW-Zn, **(C)** SRW-Zn-FA, **(D)** SRW-Zn-G, and **(E)** SRW-Zn-FA-G.

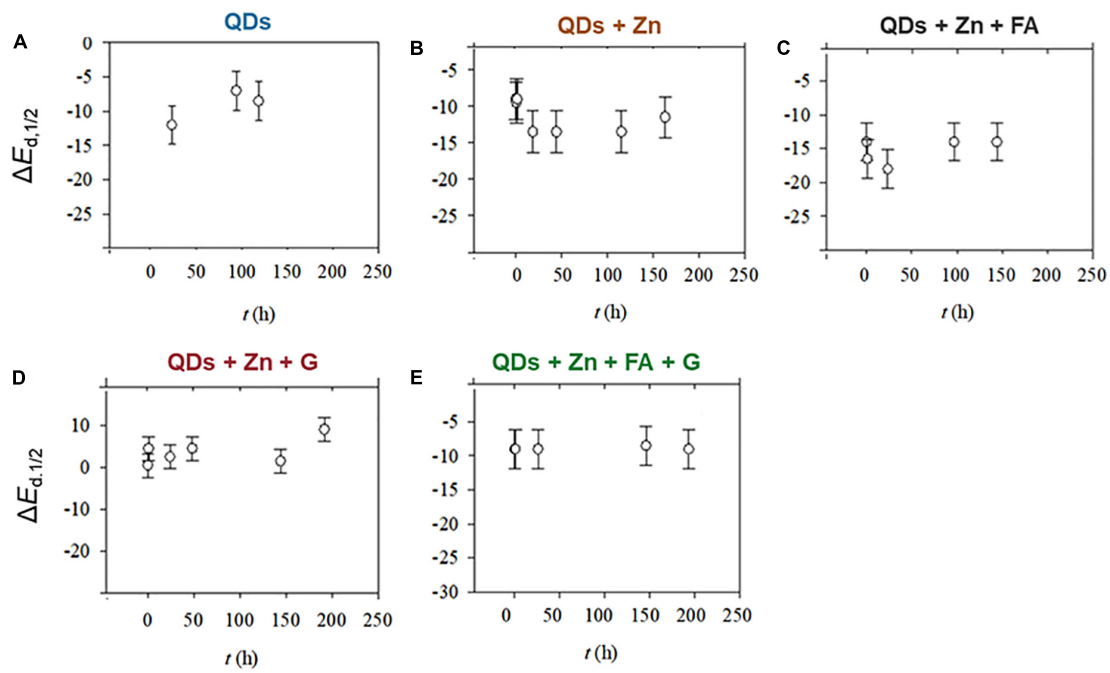

FIGURE 5 | Shift in the half-wave deposition potential, $\Delta E_{d,1/2}$, for conditions **(A–E)**. Conditions **(A)** SRW, **(B)** SRW-Zn, **(C)** SRW-Zn-FA, **(D)** SRW-Zn-G, and **(E)** SRW-Zn-FA-G.

FA (condition C), $|\Delta E_{d,1/2}|$ values are slightly higher than those of conditions A and B. This could be explained by the formation of slightly stronger complexes, e.g., ZnFA. In condition D (in the presence of goethite), the $\Delta E_{d,1/2}$ remained around 0, implying that the possible Zn complexes are inert, thus not possible to be measured. In fact, the SSCP wave (see **Supplementary Figure S3**) shows that the system is slightly heterogeneous (van Leeuwen and Town, 2003), indicating that Zn can be adsorbed

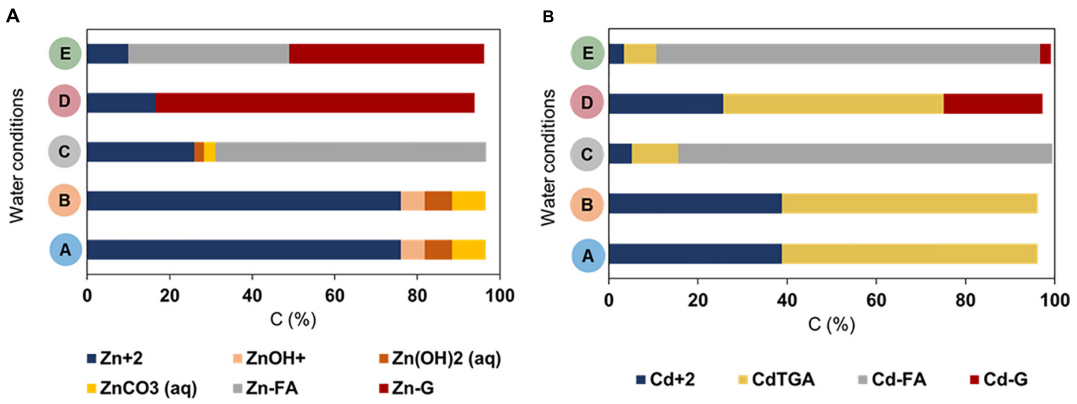

FIGURE 6 | Speciation of Zn **(A)** and Cd **(B)** by thermodynamic modeling. Conditions (A) SRW, (B) SRW-Zn, (C) SRW-Zn-FA, (D) SRW-Zn-G, and (E) SRW-Zn-FA-G.

by different binding sites of goethite particles. As for condition E (in the presence of both FA and goethite), the $\Delta E_{d,1/2}$ remained constant, but with a value around −10 mV compared to that of condition D (0 mV). Here, the FA impact can be seen with the formation of more labile complexes.

Zinc and Cadmium Speciation

The model calculations indicate that, under all studied conditions, the solid microsized CdSe, greenockite (CdS), and sphalerite (ZnS) are supposed to undergo total dissolution at equilibrium (see parameters in **Supplementary Table S8**). This is consistent with CU data of conditions A and B at the end of experiment, but not with the dissolution profile of conditions C–E from CU data that are not showing total dissolution. This can be explained by the speciation of Zn and Cd in each condition, presented in **Figure 6**. The concentrations of Zn^{2+} and Cd^{2+} decrease with the complexity of the water condition (A–E). In the absence of mineral and/or organic matter, Zn forms complexes with hydroxides and also few carbonates as shown previously by Sivry et al. (2014), in spite of the initial purge of the samples with nitrogen (see section "Zn Speciation in Solution by SSCP"), which highlights that the system is also equilibrating with atmospheric CO_2. TGA is known as a complexing agent for metal ions, e.g., Cd^{2+} and Hg^{2+} (Khatkar and Devi, 2006). However, there is less than 0.5% of ZnTGA complex formation according to the thermodynamic model. This is clearly related to the competition between Zn^{2+} and H^+ or Cd^{2+} to bind with TGA (log $K_{1,ZnTGA}$ = 7.8 vs log $K_{1,HTGA}$ = 10.3 and log $K_{1,CdTGA}$ = 11.5, see **Supplementary Table S1**). In addition, the complexes Cd forms with the TGA seem to be strong enough to not be detected during SCP. For all the conditions, the solutions were buffered at pH 8, in the range of pH with the largest binding capacity of TGA for the metal ions, in accordance with the first TGA dissociation constant (pKa_1 = 3.7, extrapolated to I = 0 M at 25°C; Domingos et al., 2015). The presence of Ca^{2+} in the medium does not induce any notable competition with Cd regarding its complexation with TGA (stability constants 1.5 vs 11.5, respectively, see **Supplementary Table S1**).

In a medium containing the organic matter analogue (FA, condition C, **Figure 6A**), Zn is shown to mostly complex with FA, but up to 30% remains free Zn^{2+}. On the contrary, 94% of Cd forms complex with organic matter (84% with FA and 10% with TGA, see **Supplementary Table S13**). However, in a medium with mineral matter (goethite, condition D, **Figure 6B**), Cd is mostly complexed with TGA rather than goethite (50% vs 22%), compared to Zn for which 77% is bound to goethite. These results are coherent with CU/HR-ICP-MS and SSCP data obtained previously: (i) the concentration of dissolved Cd_{QDs} in solution is higher than that of Zn_{QDs} in condition D since the CdTGA complexes are smaller than the CU membrane cutoff, and (ii) and Zn is not observed during SSCP, suggesting that its complexes with goethite are inert. Coherent with CU data, goethite has a higher affinity for Zn compared to Cd. When both mineral and organic matter are present in the medium, almost all Cd is bound to FA whereas Zn is complexed to both FA and goethite, which finally results in very low concentrations of Cd_{QDs} and Zn_{QDs} in solution since both are forming complexes bigger than 3 kDa. In addition, the model calculation (not shown here) indicates that FA surrounds the goethite surface forming very stable heteroaggregate, which is consistent with EPM data.

QD Fate in Surface Waters

The absence and the presence of mineral/organic matter in surface water analogs are shown to affect the speciation of Zn and Cd in solution, resulting in different QD core/shell dissolution profiles. CU data indicated a total dissolution of Zn shell and Cd core of the QDs after approximately 48 h when dispersed in simplified river water (in the absence of organic/inorganic phases but in the presence of natural Zn). However, the SSCP data showed a decrease in labile Zn concentrations with time. As for Cd, the presence of the TGA ligands in solution that detached from the QD surface after dissolution could potentially and strongly complex the Cd^{2+} metal ions, since no significant degradation of TGA itself is expected in these physicochemical conditions and timescale (De Villiers et al., 1997). No further SCP was applied for Cd due to the low concentration in Cd of the QDs used in this study, thus reaching the limit of detection of

the technique (0.05 nM, i.e., 5 ppt). However, model calculations showed that CdTGA complexes are the majority species of Cd in all studied water conditions, except when in the presence of organic matter analog FA since Cd^{2+} is mostly bound to FA binding sites.

Contrary to simplified systems, when the QDs were dispersed in a more representative aquatic system, i.e., in the presence of Zn, fulvic acids, and goethite, almost no Zn or Cd dissolution from the QDs was observed. The concentration of labile Zn measured was also very low compared to the one measured in simplified systems, yet still decreasing with time. In addition, the SSCP data reveal that the Zn complexes formed with the organic/inorganic matter in the system are strong/inert, whereas the CU/SCP/modeling data of Cd suggest its binding to the TGA ligands and FA (thus also FA–goethite heteroaggregates)—therefore suggesting that, under the conditions studied, aquatic organisms could be exposed to a lower concentration of free and labile metal ions coming from the QDs, therefore having less bioavailability and toxicity to water column organisms.

CONCLUSION

The difficulties when studying the fate of QDs in aquatic water systems at ppt-level concentrations and the subsequent metal speciation were surmounted by the combination of the two mentioned methods, isotopically labeled QDs/CU and SSCP. They firmly provided a thorough comprehension regarding the transformation of QDs in the environment, despite the low concentration used. The QD behavior in aquatic systems is affected by various factors: (i) the physicochemical conditions of the medium including the presence of natural organic and mineral matter, (ii) the presence of the manufactured coating of the QDs, and (iii) the interaction of the metal ions in the medium with the coating itself. For instance, the CU data indicated a total dissolution of Zn shell and Cd core of the QDs after approximately 48 h when dispersed in simplified river water (in the absence of organic/inorganic phases but in the presence of naturally occurring Zn). However, the SSCP data showed that these Zn and Cd are forming complexes with time, whose strength is stronger than the ones present in the system at the initial state, namely, the QD structure itself or some metal bound to the TGA present at the QD surface. In fact, the overall results seem to indicate that the presence of the TGA ligands in solution detached from the QD surface after dissolution could strongly complex the metal ions. Indeed, at pH 8, the largest binding capacity for the metal ions is expected, in accordance with the TGA dissociation constants: $pKa_1 = 3.7$ and $pKa_2 = 10.3$. As for Cd, no further SSCP was applied due to the low Cd concentration of the QDs used, thus reaching the limit of detection of the technique (5 ppt).

Contrary to when dispersed in a more representative aquatic system, i.e., in the presence of Zn, fulvic acids, and goethite, almost no Zn or Cd dissolution from the QDs was observed. The concentration of free and labile Zn measured was also very low compared to the one measured in the simplified system, yet still decreasing with time. In addition, the SSCP data reveal that the Zn complexes formed with the organic/inorganic matter in the system are inert, suggesting less concern regarding their bioavailability and toxicity to water column organisms, but the opposite for organisms in the sediment's top layer, such as filter feeds, due to the possible sedimentation of these inert complexes.

The unusual approach where two different yet complementary techniques were combined has surpassed the analytical limitations when studying the fate of ENPs at relevant concentrations, while simultaneously giving a detailed understanding regarding dynamic speciation. Precisely, without applying the isotopic labeling technique, dissolved ENPs would not be observed using the CU/HR-ICP-MS when working at very low concentrations in a complex system containing high background noise. The exact speciation of the ENPs under environmentally relevant conditions (i.e., with the presence of other metals and organic/inorganic matter) can be eventually determined with the coupling of isotopically labeled ENPs with CU/HR-ICP-MS and SSCP.

DATA AVAILABILITY STATEMENT

All datasets presented in this study are included in the article/**Supplementary Material**.

AUTHOR CONTRIBUTIONS

NS was in charge of all the experiments, analyses, and writing. NS was supervised and guided by RD for the SSCP experiments and data treatment. YS conceived the presented idea and coordinated and supervised the whole work. MB helped him supervise the project. All authors discussed and wrote the final manuscript.

FUNDING

This research project was co-financed by the French Agency for Food, Environmental and Occupational Health and Safety (ANSES) under the convention nos. EST-2013/1/264 and the ANR-18-IDEX-0001, IdEx Université de Paris. Part of this work was supported by the IPGP multidisciplinary program PARI and by Paris-IdF region SESAME grant no. 12015908.

ACKNOWLEDGMENTS

Our thanks go to Ms. Laure Cordier and M. Mickaël Tharaud for the assistance they provided during various multielemental analyses and to Dr. Gaëlle Charron for supervising the synthesis of this QD batch.

SUPPLEMENTARY MATERIAL

The Supplementary Material for this article can be found online at: https://www.frontiersin.org/articles/10.3389/fenvs.2020.00114/full#supplementary-material

REFERENCES

Dai, X., Deng, Y., Peng, X., and Jin, Y. (2017). Quantum-dot light-emitting diodes for large-area displays: towards the dawn of commercialization. *Adv. Mater. Weinheim* 29:1607022. doi: 10.1002/adma.201607022

De Villiers, M., Wurster, D. E., and Narsai, K. (1997). Stability of lactic acid and glycolic acid in aqueous systems subjected to acid hydrolysis and thermal decomposition. *J. Cosm. Sci.* 48, 165–174.

Domingos, R. F., Franco, C., and Pinheiro, J. P. (2013a). Stability of core/shell quantum dots—role of pH and small organic ligands. *Environ. Sci. Pollut. Res.* 20, 4872–4880. doi: 10.1007/s11356-012-1457-0

Domingos, R. F., Franco, C., and Pinheiro, J. P. (2015). The role of charged polymer coatings of nanoparticles on the speciation and fate of metal ions in the environment. *Environ. Sci. Pollut. Res. Int.* 22, 2900–2906. doi: 10.1007/s11356-014-3546-8

Domingos, R. F., Huidobro, C., Companys, E., Galceran, J., Puy, J., and Pinheiro, J. P. (2008). Comparison of AGNES (absence of gradients and Nernstian equilibrium stripping) and SSCP (scanned stripping chronopotentiometry) for trace metal speciation analysis. *J. Electroanal. Chem.* 617, 141–148. doi: 10.1016/j.jelechem.2008.02.002

Domingos, R. F., Rafiei, Z., Monteiro, C. E., Khan, M. A. K., and Wilkinson, K. J. (2013b). Agglomeration and dissolution of zinc oxide nanoparticles: role of pH, ionic strength and fulvic acid. *Environ. Chem.* 10, 306–312. doi: 10.1071/EN12202

Domingos, R. F., Tufenkji, N., and Wilkinson, K. J. (2009). Aggregation of titanium dioxide nanoparticles: role of a fulvic acid. *Environ. Sci. Technol.* 43, 1282–1286. doi: 10.1021/es8023594

Dybowska, A. D., Croteau, M.-N., Misra, S. K., Berhanu, D., Luoma, S. N., Christian, P., et al. (2011). Synthesis of isotopically modified ZnO nanoparticles and their potential as nanotoxicity tracers. *Environ. Pollut.* 159, 266–273. doi: 10.1016/j.envpol.2010.08.032

Gottschalk, F., Lassen, C., Kjoelholt, J., Christensen, F., and Nowack, B. (2015). Modeling flows and concentrations of nine engineered nanomaterials in the danish environment. *Int. J. Environ. Res. Public Health* 12, 5581–5602. doi: 10.3390/ijerph120505581

Gottschalk, F., Sonderer, T., Scholz, R. W., and Nowack, B. (2009). Modeled environmental concentrations of engineered nanomaterials (TiO2, ZnO, Ag, CNT, Fullerenes) for different regions. *Environ. Sci. Technol.* 43, 9216–9222. doi: 10.1021/es9015553

Hammes, J., Gallego-Urrea, J. A., and Hassellöv, M. (2013). Geographically distributed classification of surface water chemical parameters influencing fate and behavior of nanoparticles and colloid facilitated contaminant transport. *Water Res.* 47, 5350–5361. doi: 10.1016/j.watres.2013.06.015

Hiemstra, T., De Wit, J. C. M., and Van Riemsdijk, W. H. (1989). Multisite proton adsorption modeling at the solid/solution interface of (hydr)oxides: a new approach. *J. Coll. Interface Sci.* 133, 105–117. doi: 10.1016/0021-9797(89)90285-3

Juillot, F., Maréchal, C., Ponthieu, M., Cacaly, S., Morin, G., Benedetti, M., et al. (2008). Zn isotopic fractionation caused by sorption on goethite and 2-Lines ferrihydrite. *Geochim. Cosmochim. Acta* 72, 4886–4900. doi: 10.1016/j.gca.2008.07.007

Khatkar, S. P., and Devi, R. (2006). Thioglycolic acid as a reagent for trace determination of Zn(II), Cd(II) and Hg(II). *Asian J. Chem.* 18, 724–726.

Merdzan, V., Domingos, R. F., Monteiro, C. E., Hadioui, M., and Wilkinson, K. J. (2014). The effects of different coatings on zinc oxide nanoparticles and their influence on dissolution and bioaccumulation by the green alga, C. reinhardtii. *Sci. Total Environ.* 488, 316–324. doi: 10.1016/j.scitotenv.2014.04.094

Oriekhova, O., and Stoll, S. (2016). Stability of uncoated and fulvic acids coated manufactured CeO2 nanoparticles in various conditions: from ultrapure to natural Lake Geneva waters. *Sci. Total Environ.* 562, 327–334. doi: 10.1016/j.scitotenv.2016.03.184

Piccinno, F., Gottschalk, F., Seeger, S., and Nowack, B. (2012). Industrial production quantities and uses of ten engineered nanomaterials in Europe and the world. *J. Nanopart Res.* 14, 1–11. doi: 10.1007/s11051-012-1109-9

Pickering, S., Kshirsagar, A., Ruzyllo, J., and Xu, J. (2012). Patterned mist deposition of tri-colour CdSe/ZnS quantum dot films toward RGB LED devices. *Opto Electron. Rev.* 20, 148–152. doi: 10.2478/s11772-012-0019-9

Pinheiro, J. P., and van Leeuwen, H. P. (2004). Scanned stripping chronopotentiometry of metal complexes: lability diagnosis and stability computation. *J. Electroanal. Chem.* 570, 69–75. doi: 10.1016/j.jelechem.2004.03.016

Sivry, Y., Gelabert, A., Cordier, L., Ferrari, R., Lazar, H., Juillot, F., et al. (2014). Behavior and fate of industrial zinc oxide nanoparticles in a carbonate-rich river water. *Chemosphere* 95, 519–526. doi: 10.1016/j.chemosphere.2013.09.110

Soares, H. M. V. M., and Conde, P. C. F. L. (2000). Electrochemical investigations of the effect of N-substituted aminosulfonic acids with a piperazinic ring pH buffers on heavy metal processes which may have implications on speciation studies. *Anal. Chim. Acta* 421, 103–111. doi: 10.1016/S0003-2670(00)01028-X

Spathariotis, E., and Kallianou, C. (2007). Adsorption of copper, zinc, and cadmium on goethite, aluminum−substituted goethite, and a system of kaolinite–goethite: surface complexation modeling. *Commun. Soil Sci. Plant Anal.* 38, 611–635. doi: 10.1080/00103620701216005

Supiandi, I., Charron, G., Tharaud, M., Benedetti, M. F., and Sivry, Y. (2020). Tracing multi-isotopically labelled CdSe/ZnS quantum dots in biological media. *Sci. Rep.* 10:2866. doi: 10.1038/s41598-020-59206-w

Supiandi, N. I., Charron, G., Tharaud, M., Cordier, L., Guigner, J.-M., Benedetti, M. F., et al. (2019). Isotopically labeled nanoparticles at relevant concentrations: how low can we go? the case of CdSe/ZnS QDs in surface waters. *Environ. Sci. Technol.* 53, 2586–2594. doi: 10.1021/acs.est.8b04096

van Leeuwen, H. P., and Town, R. M. (2003). Electrochemical metal speciation analysis of chemically heterogeneous samples:? the outstanding features of stripping chronopotentiometry at scanned deposition potential. *Environ. Sci. Technol.* 37, 3945–3952. doi: 10.1021/es030033p

Yung, M. M. N., Wong, S. W. Y., Kwok, K. W. H., Liu, F. Z., Leung, Y. H., Chan, W. T., et al. (2015). Salinity-dependent toxicities of zinc oxide nanoparticles to the marine diatom *Thalassiosira pseudonana*. *Aquat. Toxicol.* 165, 31–40. doi: 10.1016/j.aquatox.2015.05.015

Zelano, I. O., Sivry, Y., Quantin, C., Gélabert, A., Maury, A., Phalyvong, K., et al. (2016). An isotopic exchange kinetic model to assess the speciation of metal available pool in soil: the case of nickel. *Environ. Sci. Technol.* 50, 12848–12856. doi: 10.1021/acs.est.6b02578

Zhao, L., Hu, L., and Fang, X. (2012). Growth and device application of CdSe nanostructures. *Adv. Funct. Mater.* 22, 1551–1566. doi: 10.1002/adfm.201103088

Conflict of Interest: The authors declare that the research was conducted in the absence of any commercial or financial relationships that could be construed as a potential conflict of interest.

frontiers in Environmental Science

ORIGINAL RESEARCH
published: 20 August 2020
doi: 10.3389/fenvs.2020.00139

Trace Metal Dynamics in a Tropical Mangrove Tidal Creek: Influence of Porewater Seepage (Can Gio, Vietnam)

Nguyen Thanh-Nho[1,2], Cyril Marchand[2,3], Emilie Strady[4,5], Truong Van Vinh[2,6], Pierre Taillardat[7], Nguyen Cong-Hau[1] and Tran-Thi Nhu-Trang[1]*

[1] Faculty of Environmental and Food Engineering, Nguyen Tat Thanh University, Ho Chi Minh City, Vietnam, [2] IMPMC, Institut de Recherche pour le Développement (IRD), UPMC, CNRS, MNHN, Noumea, France, [3] ISEA, Université de la Nouvelle-Calédonie (UNC), Noumea, France, [4] Aix-Marseille Univ., Mediterranean Institute of Oceanography (MIO), Marseille, Université de Toulon, CNRS/IRD, France, [5] CARE-HCMUT, Ho Chi Minh City, Vietnam, [6] Department of Forest Resources Management, Faculty of Forestry, Nong Lam University HCMC, Ho Chi Minh City, Vietnam, [7] GEOTOP, Université du Québec à Montréal, Montréal, QC, Canada

OPEN ACCESS

Edited by:
Gaetane Lespes, Université de Pau et des Pays de l'Adour, France

Reviewed by:
Xueyan Jiang, Ocean University of China, China
Nadia Valentina Martínez-Villegas, Instituto Potosino de Investigación Científica y Tecnológica (IPICYT), Mexico

***Correspondence:**
Cyril Marchand
cyril.marchand@unc.nc

Specialty section:
This article was submitted to Biogeochemical Dynamics, a section of the journal Frontiers in Environmental Science

Received: *20 February 2020*
Accepted: *23 July 2020*
Published: *20 August 2020*

Citation:
Thanh-Nho N, Marchand C, Strady E, Van Vinh T, Taillardat P, Cong-Hau N and Nhu-Trang T-T (2020) Trace Metal Dynamics in a Tropical Mangrove Tidal Creek: Influence of Porewater Seepage (Can Gio, Vietnam). Front. Environ. Sci. 8:139. doi: 10.3389/fenvs.2020.00139

Mangrove soils are considered as sinks for trace metals, protecting coastal waters from pollutions. However, the cycling of trace metals in mangroves is complex due to various biogeochemical processes across the intertidal zone, notably the dissolution of bearing phases resulting in high trace metal concentrations in porewaters. Previous studies demonstrated a decrease of trace metal stocks in mangrove soils seaward, possibly due to the export of dissolved metals through tidal pumping. Can Gio mangrove is the largest one in Vietnam, developing downstream Ho Chi Minh City (Viet Nam's biggest industrial city). The objectives of the present study were to characterize the dynamics of trace metals in a tidal creek of the Can Gio mangrove that does not receive any upstream inputs and to identify the role of porewater seepage on their dynamics. To reach our goals, surface water and suspended particulate matters were collected every 2 h during two different tidal cycles (spring and neap tides) and at the two different seasons, dry and wet. Mangroves porewaters were also collected. In addition to particulate and dissolved trace metals, physico-chemical parameters and a groundwater tracer (Radon – ^{222}Rn) were measured. The results showed that trace metal concentrations at flood tides, both in the dissolved and the particulate phases, were in the same range that those measured in the Can Gio Estuary. Then during ebb tides, we evidenced high inputs of dissolved Fe, Mn, Co, and Ni from mangrove soils. However, the dynamics of these inputs differed depending on the element considered. Mn was exported from the tidal creek in its dissolved form. However concerning Fe, and to a lesser extent Co and Ni, we suggest that, when delivered to the creek from the soils under dissolved forms, these trace metals precipitated because of different physicochemical characteristics between mangrove soils and tidal creek, notably higher

dissolved oxygen concentrations and higher pH. Consequently, these elements were exported to the estuary in particulate forms. We suggest that budget studies of trace metals in mangroves should be developed like the ones concerning carbon to efficiently determine their role as a barrier for pollutants between land and sea.

Keywords: mangrove, trace metals, tidal creek, partitioning, monsoon, Vietnam

INTRODUCTION

Mangrove forests can trap suspended solids, with their load of trace metals originating from upstream soils, rocks, or anthropogenic activities (Wolanski, 1995; Furukawa et al., 1997; Tam and Wong, 1999). Mangroves are, thus, considered as efficient barriers between land and sea, being sinks for trace metals and protecting coastal waters from pollutions. However, this ability may depend on soil characteristics and hydrology (Kaly et al., 1997). Trace metals dynamics in mangroves are complex due to various biogeochemical processes across the intertidal zone (McKee, 1993; Marchand et al., 2011; Noël et al., 2015). Numerous physicochemical parameters, such as redox, pH, sulfides, and salinity, can influence the distribution of trace metals between solid and liquid phases in mangrove soils, and thus their transfer at the soil-water interface (Patrick and Jugsujinda, 1992; Van Ryssen et al., 1998). Because of metal toxicities to mangrove biodiversity and also to human health, their cycling is a serious question addressed by many authors during the last few decades (Lacerda et al., 1988; Clark et al., 1998; Ferreira et al., 2007) and recently (Xiao et al., 2015; Marchand et al., 2016). In most of the published studies, authors focused on trace metal distributions and dynamics between soils, porewaters, and plants. Only a few and recent publications were interested in the transfer of trace metals from mangrove soils to tidal creeks through tidal pumping and porewaters seepage (Sanders et al., 2015; Holloway et al., 2016). Tidal pumping induces advective flushing of permeable soils and the transport of organic and inorganic products to the open water column (Maher et al., 2013). Other recent studies measured a decrease of the stocks of some trace metals in mangrove soils from the landside to the seaside of the studied forests due to a more reactive substrate that leads to the enhanced dissolution of metals bearing phases (Noël et al., 2014; Deborde et al., 2015; Marchand et al., 2016). In previous studies concerning trace metals distribution in Can Gio mangrove (Thanh-Nho et al., 2019a,b), we showed that trace metals dynamics in the soil as well as their transfer to mangrove plants were notably driven by the position of the stand and the soil organic matter content. We also demonstrated that trace metal stocks were lower in the mangrove soils than in the mudflat, and that concentrations in mangrove porewaters could be really high. Consequently, we suggested that the export of dissolved trace metals through tidal pumping may occur.

In the present study, we were interested in trace metal dynamics in a mangrove tidal creek of the Can Gio mangrove adjacent to the forest we previously studied. This tidal creek is 1,400 m long and do not receive any upstream inputs. Our objectives were to understand the variability of trace metals (Fe, Mn, Co, Ni) concentrations and distributions between the particulate and the dissolved phases with tides and seasons, and thus to confirm our hypothesis of export of trace metal from mangrove soils to tidal creeks. We were also interested in the relationships between physicochemical parameters [pH, salinity, dissolved oxygen (DO), dissolved organic carbon (DOC), particulate organic carbon (POC), total suspended solids (TSS)] and trace metals. Our main hypothesis was that dissolved metal concentrations in the tidal creek would increase during the ebb tide as a result of inputs from mangrove soils. To reach our goals, we collected waters and suspended matters every 2 h during 24 h at different tidal cycles and at distinct seasons (dry and rainy). Physico-chemical parameters of the water column were monitored continuously during the sampling. Groundwater tracer (Radon – ^{222}Rn) in the water column and dissolved metal concentrations in porewaters were also measured.

MATERIALS AND METHODS

Study Site

The studied tidal creek is situated in the core zone of the Can Gio mangrove (10°30.399N-106°52.943E), and has approximately 1,400 m of length (**Figure 1**). This tidal creek does not receive any direct freshwater inputs except for rainwater. The Can Gio mangrove (i.e., 35,000 ha) accounts for 20% of the total mangrove area in Vietnam and is located downstream Ho Chi Minh City (Vietnam's biggest industrial city). It is considered as one of the most beautiful mangroves of Southeast Asia, and is usually classified as "Mangrove afforestation and re-forestation area" (Blasco et al., 2001), and has been declared as a World's Biosphere Reserve by the UNESCO since 2000. The tidal regime is irregular semi-diurnal. The climate is typical of the monsoonal zone with two distinct seasons, in which the dry season starts in November and lasts until the end of May, the wet season starts from the end of May until the end of October. The annual mean precipitation is ∼1,400 mm, with ∼90% of the precipitation falling during the wet season. The annual mean temperature ranges from 26.5 to 30°C. The Can Gio mangrove has a high biodiversity with more than 200 species of fauna and 52 species of flora. The dominant mangrove species are *Rhizophora apiculata* and *Avicennia alba* (Luong et al., 2015). The main economic activities of the local people in the Can Gio mangrove are aquacultures, fishing, and salt production (Kuenzer and Tuan, 2013).

Field Sampling

For each sampling period, during the dry season (April 11th – 12th and 18th – 19th, 2015) and the wet season (October 19th – 20th and 26th – 27th, 2015), a boat was anchored in

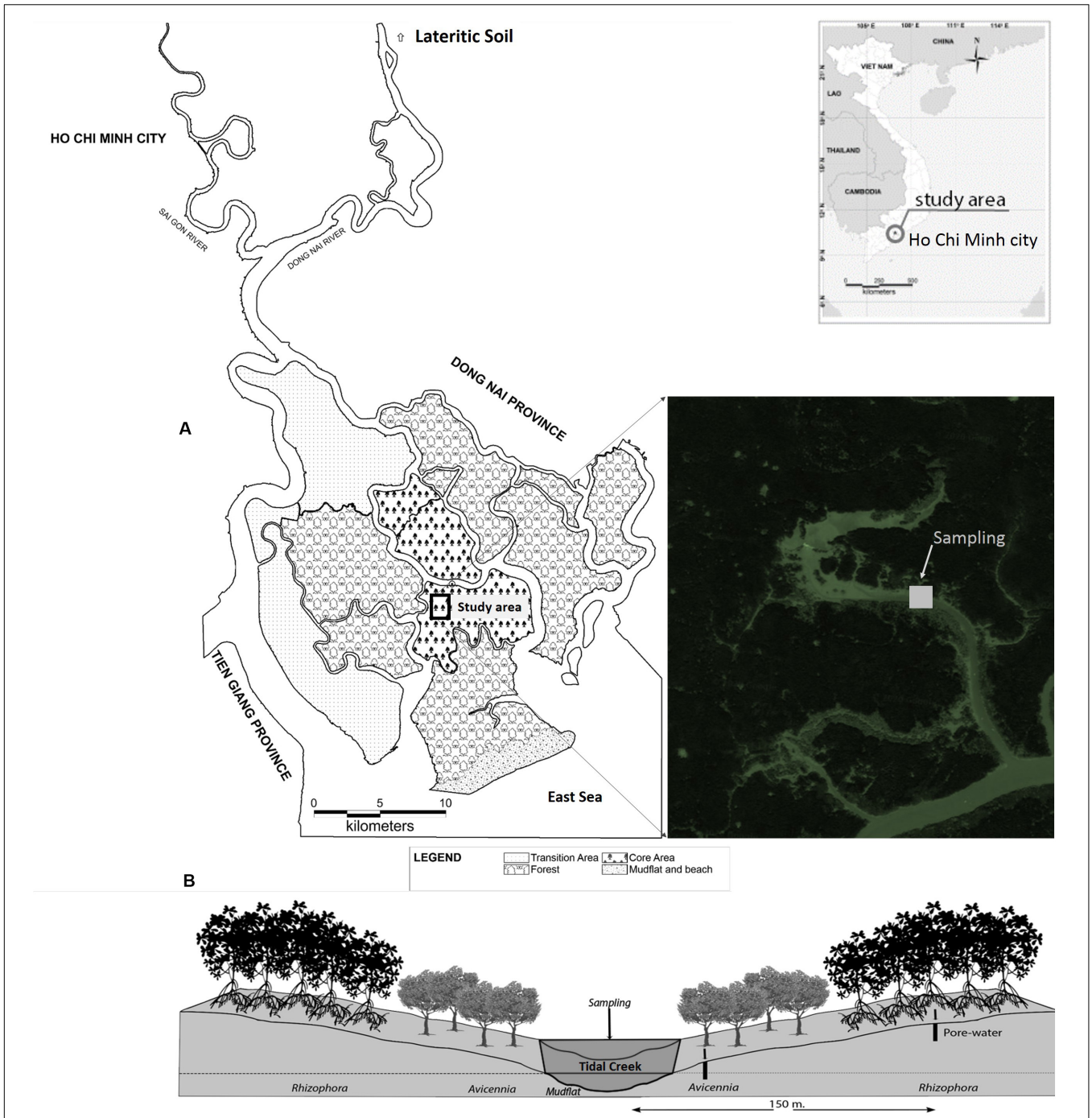

FIGURE 1 | Map of the study area showing: **(A)** the location of Can Gio mangrove in Vietnam and the location of the study site in Can Gio; and **(B)** the cross-section of the tidal creek without any direct fresh-water inputs except from rainwater.

the middle of the tidal creek (**Figure 1**). For each season, two series of the 24 h (24-h) were carried out during asymmetric and symmetric tidal cycles. During each sampling campaign, surface waters (50 cm below the water-air interface) were collected in duplicates every 2 h using a pre-decontaminated bucket. The water samples were immediately transferred into acid pre-cleaned polypropylene bottles (1 L) – previously rinsed with estuarine water. After that, these samples were filtered through 0.2 μm JG PTFE Omnipore^{TM} Membrane Filters: the filtrates were then transferred into pre-cleaned 50 mL polypropylene tubes, immediately acidified to pH <2 using concentrated suprapur® HNO_3 (HNO_3: sample = 1:1000 (v/v)) for sample preservation until trace metals analysis (Strady et al., 2009). The filters were stored in small plastic boxes with closed cover

for future analyses of trace metals concentrations in suspended particulate matters. Both types of samples were stored in a cooler box during the sampling campaign and then stored at 4°C at the laboratory until analysis. Filtration for the determination of TSS, POC, and DOC was also simultaneously carried out as follow: (i) water samples were filtered through pre-combusted and pre-weighted glass fiber filters (Whatman® GF/F 0.7 μm); (ii) the filters were stored at −20°C, and the filtrates were transferred into sterile 15 mL polypropylene tubes; (iii) these filtrates were then acidified using concentrated suprapur® HCl and stored at 4°C until DOC analysis (Thanh-Nho et al., 2018).

Mangrove porewaters were also collected along a transect from the tidal creek to the upper intertidal area. One hole beneath each mangrove stand (i.e., *R. apiculata*, *A. alba*) and in the mudflat were drilled to approximately 1 m depth at low tide, using an Eijkelkamp gouge auger. The holes were purged at least two times with a hand pump before sampling. All samples were filtered through 0.45 μm Sartorius® filter, stored in pre-cleaned 50 mL polypropylene, and were then acidified to pH <2 using concentrated suprapur® HNO_3 (Merck), and stored at 4°C until analysis.

In situ Measurements of Physicochemical Parameters

Surface water salinity and pH were logged continuously using a multi-probe (Yellow Spring Instrument® meters YSI 6920). The pH probe was calibrated using buffer solutions: 4, 7, and 10 (NIST scale). DO was monitored with a HOBO Dissolved Oxygen data logger (HOBO U26-001). These above probes were immerged 50 cm below the water-air interface. Data were recorded every 5 min. Water level profiles were measured using a Hondex PS-7.

Radon is considered as a natural groundwater tracer, widely used to quantify porewater exchange in a mangrove system (Maher et al., 2013; Tait et al., 2016; Taillardat et al., 2018a). ^{222}Rn measurements were performed only during the wet season because of a system failure during the dry one. ^{222}Rn concentrations in creek waters were measured using a showerhead equilibrator. The head-space gas was streamed into an automated ^{222}Rn-in-air analyzer with the Rad Aqua package installed (RAD 7, Durridge Co.) (Burnett et al., 2001). The ^{222}Rn monitor logged data at 30 min intervals, resulting in analytical uncertainty <10% for individual concentrations, except during the first 3 h when the analytical uncertainty was 30%.

Three soil cores (1 m depth) beneath *R. apiculata*, *A. alba*, and in the mudflat were collected using an Eijkelkamp gouge auger for *in situ* measurements of pH and salinity. For each parameter, the value was recorded every 10 cm. pH was measured using a glass electrode (pH 3110-WTW), which was calibrated using standard buffer solution of 4, 7, and 10 (NIST scale). Salinities were determined using an ATAGO refractometer (S-10, Japan) after extracting a drop of porewater from each soil layer.

Sample Analysis

Dissolved Metal (M_D) Concentrations

Mn_D, Co_D, and Ni_D concentrations in the filtrates were analyzed after matrix separation (notably dissolved solids and chloride ions) and pre-concentration by solid-liquid extraction, using 6 mL *DigiSEP* Blue® cartridges (SCP SCIENCE), with amino–diacetate as a functional group. The experimental steps are described in Strady et al. (2009). Fe_D concentrations in the filtrates were analyzed after two-folds dilution with deionized water. Dissolved trace metal concentrations were then, measured by ICP-MS (Agilent 7700×) using spike ^{103}Rh and ^{197}Au as internal standards. The analytical precision and accuracy were evaluated using certified reference material of estuarine water (SLEW-3, **Table 1a**). All reagents were suprapur grade (Merck).

Particulate Metal (M_P) Concentrations

Particulate Fe, Mn, Co, and Ni concentrations were quantified according to total extractable metal digestion adapted from the USEPA 3051a method (USEPA, 2007). The experimental steps and analytical evaluations are described in Thanh-Nho et al. (2018). In brief, a mixture of 6 mL concentrated HNO_3 and 2 mL of concentrated HCl was used for sample preparation. Co_P and Ni_P concentrations were analyzed by ICP-MS (Agilent 7700×) using ^{103}Rh and ^{197}Au as internal standards. Fe_P and Mn_P concentrations were measured using Flame Atomic Absorption Spectrophotometer (Shimadzu AA-6650). The analytical precision and accuracy were insured by analyzing certified reference material of estuarine sediments (BCR-277R), which were also intercalated in each batch of samples digestion (**Table 1b**).

Dissolved Organic Carbon (DOC) and Particulate Organic Carbon (POC)

Dissolved organic carbon was measured using a Shimadzu® TOC-L series analyzer employing a 680°C combustion catalytic oxidation method. The analyzer was coupled to a solid sample module (SSM-5000A) heated up to 900°C for the POC determinations (Leopold et al., 2013). A 40% glucose standard was used for calibrations. Repeated measurements of different standards concentrations indicated deviations <2%.

Data Calculations

The partitioning coefficient (K_D) was calculated to get a better understanding of the interaction of trace metals between dissolved and particulate phases during tidal cycles. K_D is defined as the ratio of particulate metal concentration (M_P) to dissolved metal concentration (M_D) in the water column (Turner et al., 1993).

$$K_D = M_P / M_D$$

where, M_P is a particulate metal concentration and M_D is a dissolved metal concentration.

Pearson correlation coefficients was determined using the statistical package for the social science software (SPSS: version 23) to identify major relationships between metal concentrations and the physicochemical parameters as well as interrelationships between metal concentrations together, which help to clarify the main factors controlling metal partitioning between particulate and dissolved phases.

TABLE 1 | Quality control of analytical methods applied for dissolved and particulate metal concentration analysis including accuracy, precision, and quantitation limit, using: (a) estuarine water SLEW-3; (b) sediment BCR-277R.

(a) Dissolved metal concentration analysis

Element	Quantitation limit ($\mu g\ L^{-1}$)	Certified values ($\mu g\ L^{-1}$)	Measured values ($\mu g\ L^{-1}$)	Recovery (%)	Relative standard deviation (%)
Fe	0.20	0.568 ± 0.059	0.682 ± 0.068	120	10
Mn	0.09	1.61 ± 0.22	1.48 ± 0.10	92	7
Co	0.05	0.042 ± 0.010	0.0464 ± 0.0025	116	15
Ni	0.11	1.23 ± 0.07	1.37 ± 0.11	112	8

(b) Particulate metal concentration analysis

Element	Certified values ($mg\ kg^{-1}$)	Measured values ($mg\ kg^{-1}$, n = 9)	Recovery (%)	Relative standard deviation (%)	Analytical method
Fe	NA	51855 ± 3146	–	6.1	FAAS
Mn	NA	835 ± 29	–	3.5	FAAS
Co	22.5 ± 1.4	22.9 ± 0.7	102	2.8	ICP-MS
Ni	130 ± 8	128.9 ± 3.2	99	2.5	ICP-MS

RESULTS

Physico-Chemical Parameter Variability

The temporal variations of water levels, salinity, pH, DO, TSS, POC, and DOC during the four tidal cycles are presented in **Figure 2**. Salinity presented different distribution patterns between seasons, ranging from 22 to 23 and 18.5 to 22 during the dry and wet seasons, respectively. The highest salinity values were measured at the lowest water levels during the dry season, while during the wet season, the opposite trend was observed. pH values varied from 7.0 to 7.5 during the dry season and from 6.7 to 7.2 during the wet season. DO was higher during the dry season than the wet one (4.6–6.4 $mgO_2\ L^{-1}$ vs. 2.1–4.2 $mgO_2\ L^{-1}$, respectively). TSS concentrations varied between the four tidal cycles (i.e., 36–119 mg L^{-1} in neap tide vs. 60–675 mg L^{-1} in spring tide during the dry season; 54–291 mg L^{-1} vs. 60–460 mg L^{-1} in neap and spring tides during the wet season, respectively). For each tidal cycle, the highest TSS concentrations were measured at the lowest water level. POC ranged from 0.9 to 2.4% for all tidal cycles. A higher POC amplitude was observed during spring tides (1.03–2.41 and 0.8–2.37% in the dry and the wet seasons, respectively) than neap ones (1.6–1.72 and 0.9–1.6% in the dry and wet seasons, respectively). The highest POC concentrations in each tidal cycle were measured at the lowest water level. DOC values were in the same range for all tidal cycles and varied from 129.5 to 192.1 $\mu molC\ L^{-1}$. The maximum DOC values were measured at the lowest water level, whatever the tidal cycle. ^{222}Rn concentrations in the surface waters increased during the ebb and reached maximum values at the lowest water level (**Figure 2**).

Dissolved Metal (M_D) Concentrations

Fluctuations of Mn_D, Fe_D, Co_D and Ni_D concentrations during 24-h tidal cycles are presented in **Figure 3**. All trace metals presented higher mean concentrations during the wet season than during the dry season. In addition, trace metals concentrations were higher at low tides than at high tides. Mn_D increased during ebb tides and reached maximum values at the lowest water level for all tidal cycles. During the dry season, Mn_D reached 1,530 and 510 $\mu g\ L^{-1}$, respectively, whereas during the wet season, they reached 1,779 and 1,274 $\mu g\ L^{-1}$ for neap and spring tides, respectively. The same pattern was observed for Fe_D with maximum values of 194, 17, 193, and 85 $\mu g\ L^{-1}$ at lowest water levels for neap and spring tidal cycles during the dry season and the wet season, respectively. Co_D concentrations varied from less than 0.1 $\mu g\ L^{-1}$ to approximately 2.0 $\mu g\ L^{-1}$. The highest Co_D was also observed during the periods of the lowest water levels. Ni_D was under the detection limit (i.e., $<0.11\ \mu g\ L^{-1}$) during the dry season, and varied from 0.78 to 3.48 $\mu g\ L^{-1}$ during the wet season, with high values also observed at low tides.

Particulate Metal (M_P) Concentrations

Variability of Mn_P, Fe_P, Co_P, and Ni_P concentrations during 24-h tidal cycles are shown in **Figure 4**. Mn_P and Fe_P mean concentrations did not differ between seasons, however and like the dissolved concentrations, they were strongly influenced by tides but differently. Mn_P concentrations ranged from 320 to 1,024 mg kg^{-1}, decreasing during the ebb. Fe_P concentrations ranged from 34,000 to 50,000 mg kg^{-1}, but conversely to Mn, the highest values were measured at the lowest water levels. Co_P concentrations varied with seasons, ranging from 5.7 to 11.7 mg kg^{-1} during the dry season, and from 9.1 to 19.8 mg kg^{-1} during the wet season. Ni_P concentrations were quite stable with tides, showing higher concentrations during the wet season than during the dry season, with mean concentrations of 42 and 30.7 mg kg^{-1}, respectively.

Porewater Characteristics

Salinity and pH values, as well as the average concentrations of trace metals (Fe, Mn, Co, and Ni) in mangrove porewaters during the two seasons, are presented in **Table 2**. We calculated mean values using all the samples collected in the three zones: mudflat, *A. alba*, *R. apiculata*. Salinity varied from 20 to 28 during the dry season and 14 to 22 during the rainy season. pH

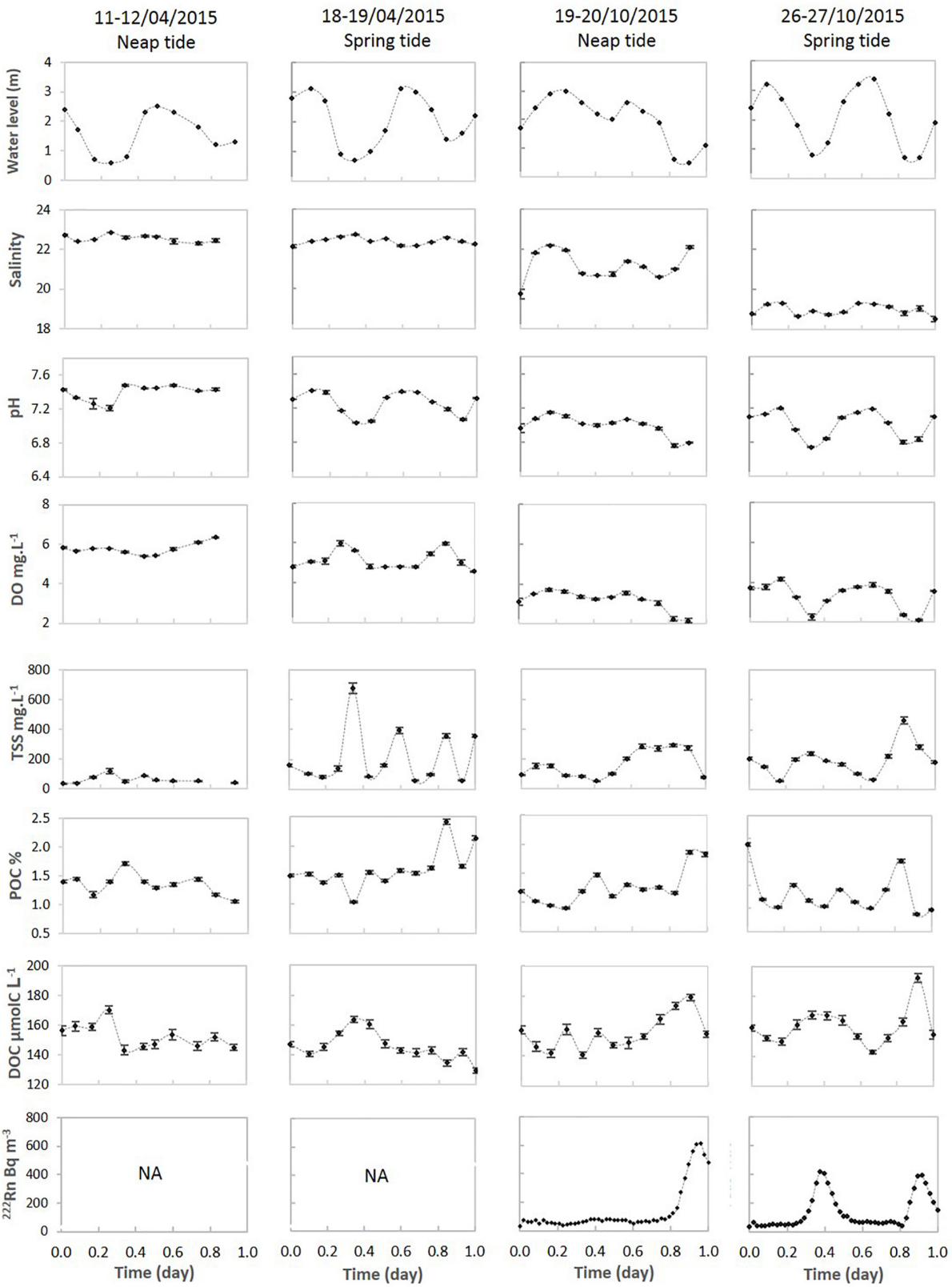

FIGURE 2 | Temporal variations of water level, salinity, pH, DO, TSS, POC, and DOC measured during neap and spring tidal cycles during the dry season (04/2015) and the wet season (10/2015). NA: not available.

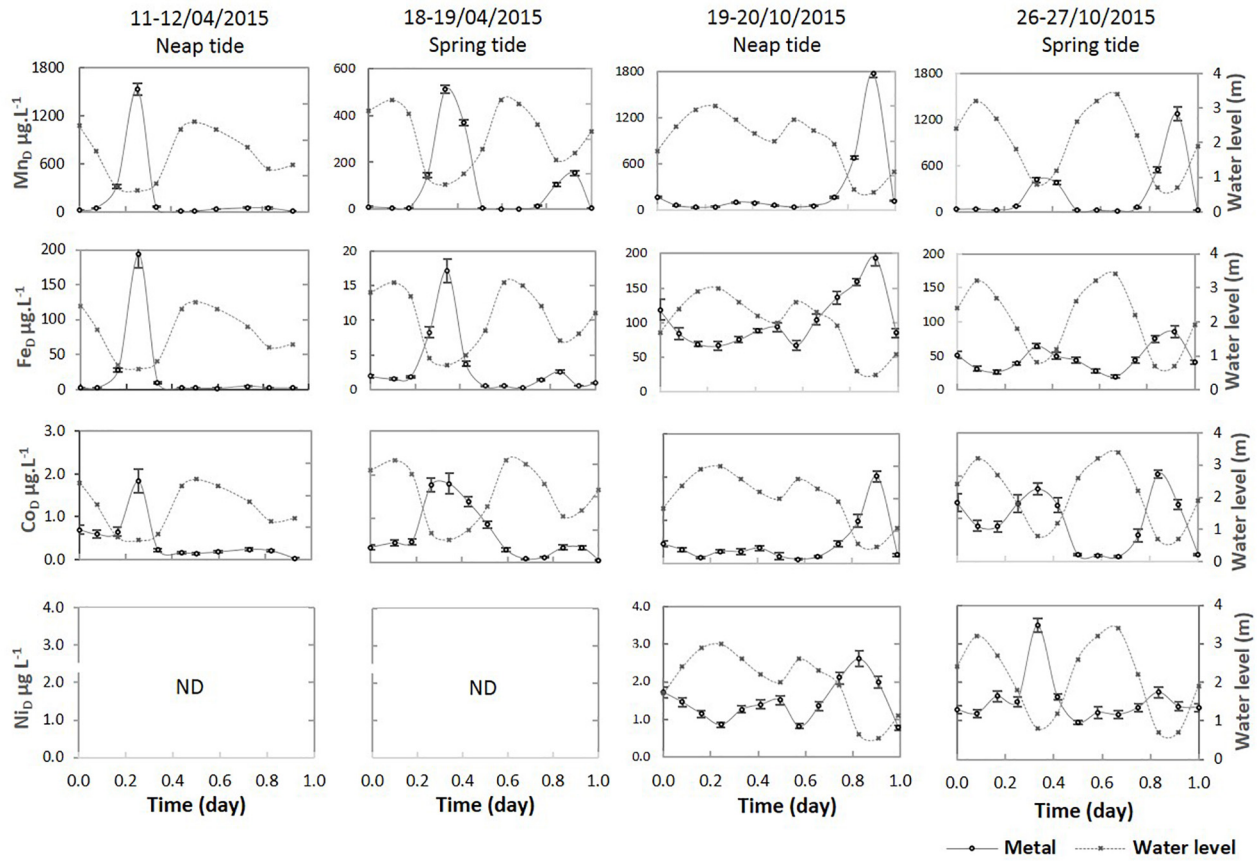

FIGURE 3 | Temporal fluctuations of dissolved metal concentrations (M_D) during the neap and the spring tidal cycles during the dry season (04/2015) and the wet season (10/2015). ND: not detection.

ranged from 4.6 to 6.7 during the dry season, and from 5.5 to 6.8 during the rainy season. Most dissolved metal concentrations presented higher amplitudes during the wet season than the dry season except for Co. Mean Fe concentrations were 1,203 ± 780 and 2,429 ± 2,744 µg L^{-1} during the dry and the wet season, respectively. Mean Mn concentrations were 1,523 ± 919 µg L^{-1} during the dry season and 2,891 ± 1,768 µg L^{-1} during the wet season. Co and Ni concentrations were far lower than Fe and Mn ones, being 9.4 ± 8.5 and 5.7 ± 0.9 µg L^{-1} for Co and 1.2 ± 0.8 and 9.0 ± 8.7 µg L^{-1} for Ni during the dry and the wet seasons, respectively.

DISCUSSION

Temporal Variability of Mangrove Tidal Creek Characteristics

In Can Gio, mangrove porewaters in the different stands studied were acidic and enriched in DOC, which is consistent with previous studies that showed that because of the high productivity of mangrove forests, DOC concentrations in porewaters could be really high (Marchand et al., 2006; Sadat-Noori and Glamore, 2019), and that because of organic matter decomposition (Taillardat et al., 2018b) and possible sulfide oxidation (Marchand et al., 2012), mangrove soils are usually acidic. The observed correlations between pH, DOC and water level in the tidal creek whatever the season (**Tables 3**, **4** and **Supplementary Figure S1**) provide evidences that porewater inputs partly controlled tidal creek characteristics. This was confirmed by the ^{222}Rn concentrations evolution with tides, even though other parameters such as estuarine waters inflow during the flood and *in situ* biogeochemical processes may be involved. The key role of mangrove porewater seepage on tidal creeks was recently evidenced in several studies (Bouillon et al., 2008; Call et al., 2015; Dittmar and Lara, 2001; Maher et al., 2013). In addition, at low tides, DOC concentrations were higher and pH values were more acidic during the rainy season than during the dry season (**Figure 2**). These results may suggest a greater contribution of mangrove porewaters to the tidal creek during the rainy season because of the larger volume of water exchanged between mangrove soils and mangrove creek, and because of a larger mangrove area immerged resulting from the higher water level. In addition, higher temperature during summer may also be involved, inducing enhanced processes of organic matter decomposition in mangrove soils as suggested in other studies (Taillardat et al., 2019; Vinh et al., 2020). Mangrove

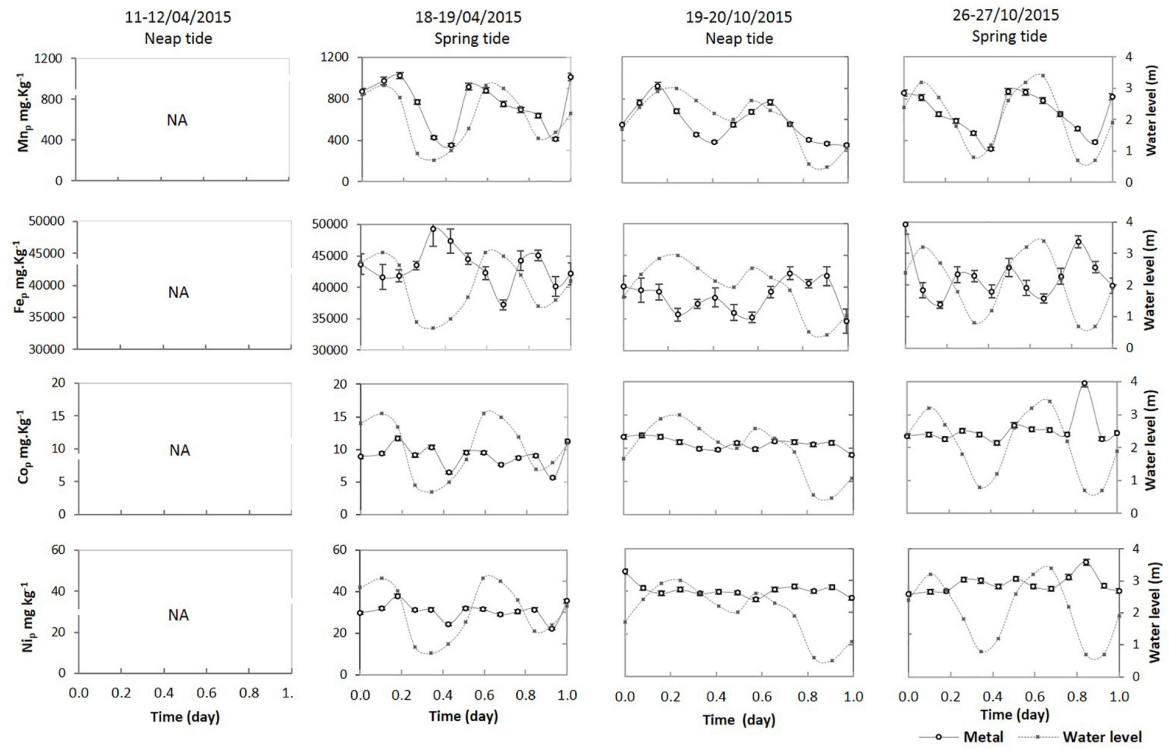

FIGURE 4 | Distributions of the particulate metal concentrations (M_P) during neap and spring tidal cycles during the dry season (04/2015) and the wet season (10/2015). NA: not available.

soils are most of the time anoxic (Kristensen et al., 2017), which is also the case for Can Gio (Thanh-Nho et al., 2019b; Vinh et al., 2019). The very low DO concentrations measured at low tide in the tidal creek, may also confirm porewater seepage. The even lower concentrations during the rainy season may also be consistent with our hypothesis of enhanced OM decomposition in mangrove soils during this season. However, the relationship with the water level in the creek was not always clear. In a previous study concerning the same tidal creek (David et al., 2018), it was suggested that algal cells could grow at low tide using nutrients and CO_2 provided by the tidal pumping of mangrove porewater, and thus resulting in increased DO content. In mangrove soils, salinity can be highly variable with depth and between mangrove stands, depending on the salinity of the incoming water (estuarine waters or rainfall) and evapotranspiration processes (Marchand et al., 2004). However in Can Gio, the low salinity differences between the estuarine waters and the porewaters, which was related to the humid tropical climate, prevent the use of salinity to trace porewater inputs to the tidal creek studied. Nevertheless, the intense rainfall occurring during the rainy season induced slightly lower salinity values during the rainy season both in the porewaters and in the tidal creek. Concerning TSS variability, we suggest that resuspension and bottom erosion can be the main drivers when the water level is low and the flow is rapid, either in the mangrove or in the creek. There were no significant differences in POC concentrations between seasons, and most of the time POC concentrations were higher at low tide. In mangrove tidal creeks, POC concentrations significantly increased due to particle resuspension, either from mangrove soils or creek bottom (Bouillon et al., 2008).

Tidal and Seasonal Dynamics of Trace Metals in the Mangrove Creek

Manganese Dynamic

The high Mn_P concentrations measured in the tidal creek during the flood periods, irrespective of the seasons, may be related to the high Mn_P concentrations measured at the mouth of the Can Gio mangrove estuary, reaching up to 800 mg kg^{-1} (Thanh-Nho et al., 2018). Consequently, in the tidal creek studied, the positive correlations between Mn_P and the water levels during the dry and the wet seasons (**Supplementary Figure S1**) suggest that Mn_P mainly originated from the estuary. However, the correlation between Mn_P and TSS was low (**Tables 3**, **4**). This result may be attributed to the fact that the fluctuation of TSS during the tidal cycles in the creek mainly depended on particle resuspension during the ebb, either from mangrove soils or creek bottom with Mn concentrations lower than those measured in the estuary (Thanh-Nho et al., 2018). Thanh-Nho et al. (2019b) showed that trace metals in the Can Gio mangrove soils have mainly a natural origin, being deposited in the mangrove as oxyhydroxides originating from the upstream lateritic soils with richness in hematite and goethite minerals (Egawa and Ooba, 1963). Therefore, we

TABLE 2 | Characteristics of mangrove sediments and porewaters.

Parameter	Dry season	Wet season	References
Fe (μg/L)	1,203 ± 780	2,429 ± 2,744	Present Study
Mn (μg/L)	1,523 ± 919	2,891 ± 1,768	
Co (μg/L)	9.4 ± 8.5	5.7 ± 0.9	
Ni (μg/L)	Na	9.0 ± 8.7	
pH	4.6–6.7	5.5–6.8	
Sal	20–28	14–22	
Eh (mV)	−107 to − 262		(Thanh-Nho et al., 2019b)
OC (%)	2.1–4.6		
Sand (%)	5.0 ± 6.7		(Taillardat et al., 2018a)
Silk (%)	87.8 ± 6.2		
Clay (%)	7.8 ± 2		
DIC (mmol m^{-3})	4,861 ± 2,398		
DOC (mmol m^{-3})	219 ± 78.6		
^{222}Rn (dpm m^{-3})	77,520 ± 41,660		

Mean concentrations (n = 3) ± SD; na: not available.

suggest that Mn_P mainly originates from the estuary and thus increases in the tidal creek when the contribution of the estuarine waters increases, and thus with the flood. Variations of Mn_D concentrations in the tidal creek were the opposite of Mn_P. In the Can Gio mangrove estuary, dissolved Mn concentrations were low, with a mean value of 1.3 μg L^{-1} (Thanh-Nho et al., 2018), which corresponds to what we measured in the creek at high tide. However, at low tide, Mn_D concentrations in the tidal creek reached up to 1,800 μg L^{-1} (**Figure 3**). Therefore, the contribution of Mn_D possibly originating from other sources is suggested. The enrichment of mangrove-derived organic matter from the mudflat to the *Rhizophora* stand was suggested to induce the reductive dissolution of Fe-Mn oxyhydroxides by bacteria for organic matter decay processes (Thanh-Nho et al., 2019b). Noël et al. (2014) showed that tidal fluctuations may be a major cause for continuous Fe reduction–oxidation cycles in mangrove wetlands. This process could release trace metals in porewaters, with Mn_D concentration reaching up to 2,891 ± 1,768 μg L^{-1} (**Table 2**). Considering the matrix of Pearson correlation coefficient between trace metals concentrations and physicochemical parameters in the creek water (**Tables 3**, **4**), we suggest that Mn_D originated from mangrove soils, and was exported through porewater seepage as observed in Australian mangroves (Holloway et al., 2016). This hypothesis is supported by positive correlations between Mn_D and ^{222}Rn. We also suggest that organomanganese complexes were possibly formed. Previous studies described the coupling between DOC and redox-sensitive elements, like Mn (Dang et al., 2015), and a positive correlation between DOC and Mn_D was measured (**Supplementary Figure S2**). In the tidal creek, Log $K_D{}^{Mn}$ varied in a larger range (i.e., from 2.32 to 5.72, **Figure 5A**) than in the Can Gio mangrove estuary [i.e., from 4.5 to 5.8 (Thanh-Nho et al., 2018)]. We suggest that the drop of Log $K_D{}^{Mn}$ observed at the low tides during both seasons in the tidal creek resulted from the increasing porewater Mn_D inputs. The positive correlation between Log $K_D{}^{Mn}$ and the water level may be related to the decrease of dissolved Mn by either the physical mixing between porewater and estuarine water containing lower Mn_D concentrations or the Mn_D adsorption onto particulate matter with pH increases during the flood. Along the salinity gradient of the estuary, Thanh-Nho et al. (2018) suggested that pH and DO increases resulted in Mn_D adsorption onto particle surface by the simultaneous oxidation and precipitation of dissolved Mn (II) to insoluble Mn (III) and Mn (IV) (hydr)oxides, as previously observed by Fang and Lin (2002). It is thus possible that pH also plays an important role in the fluctuation of Mn_D concentrations in the creek studied during the tidal cycles, supported by a negative correlation between Mn_D and pH (**Tables 3**, **4**). Additionally, we observed that the highest Mn_D concentrations were measured at the low tide of high amplitude cycle following a tidal cycle of low amplitude (**Figure 3**). We suggest that due to the low amplitude of the previous tidal cycle, Mn_D produced by Mn oxyhydroxide dissolution accumulated in mangrove soils, and was then exported during the tidal cycle of higher amplitude. Consequently, in the specific system of the Can Gio mangrove, the intensity of the export of dissolved Mn was not only related to the alternation between spring tides and neap tides, but also to the irregularity of the tidal cycles. Eventually, we measured higher Mn_D concentrations in the tidal creek during the rainy season. We suggest that these higher concentrations were related to higher Mn_D concentrations in porewaters (**Table 2**). Vinh et al. (2020) showed that during the rainy season, the elevated temperature and the high rainfall induced enhanced mineralization rates of leaf litter, which may have resulted in higher Mn_D production in mangrove soils. In addition, during the rainy season, the water level of the river and thus of the tidal creek was higher. Consequently, at high tide, mangrove immersion was more important during the rainy season, which may have induced increased exchanges between mangrove soils and tidal creek, also possibly partly explaining the higher Mn_D in the tidal creek during the rainy season. These results confirm those of Holloway et al. (2016), who showed that porewater exchange could release large amounts of dissolved Mn to mangrove creeks, and then to the nearby ocean surface water.

Iron Dynamic

In the mangrove tidal creek studied, Fe, which is a redox-sensitive element like Mn (Lacerda et al., 1999), presented the same variability than Mn in the dissolved phase but the opposite one in the particulate phase. In fact, the highest Fe_P concentrations were measured at low tide (**Figure 4**) irrespective of the season or the tidal range, reaching almost 50,000 mg kg^{-1} during the rainy season. Conversely, at high tide, Fe_P varied between ∼35,000 and 45,000 mg kg^{-1}, which was the same range as what was measured in the Can Gio mangrove estuary (Thanh-Nho et al., 2018) for a similar range of salinity than in the tidal creek. Consequently, we suggest that at high tide in the creek, Fe_P concentrations were related to the estuarine inputs and originated from the lateritic soils developing upstream like for Mn (Egawa and Ooba, 1963). In the Can Gio mangrove estuary, Fe_D concentrations were never higher than 30 μg L^{-1}, while at low tide in the tidal creek, they reached almost 200 μg L^{-1}. Consequently, like for Mn_D, another sources than the estuarine waters must be considered. In mangrove porewaters, mean Fe_D

TABLE 3 | Matrix of Pearson correlation coefficients between trace metal concentrations and different physicochemical parameters in the tidal creek during the dry season.

(a) Neap tide: 11-12/04/2015.

	MnD	FeD	CoD	NiD	Mnp	Fep	Cop	Nip	Water level	Sal	pH	DO	DOC	POC
MnD	1													
FeD	0.997**	1												
CoD	0.926**	0.918**	1											
NiD	.[b]	.[b]	.[b]	.[b]										
Mnp	.[b]	.[b]	.[b]	.[b]	.[b]									
Fep	.[b]	.[b]	.[b]	.[b]	.[b]	.[b]								
Cop	.[b]	.[b]	.[b]	.[b]	.[b]	.[b]	.[b]							
Nip	.[b]	.[b]	.[b]	.[b]	.[b]	.[b]	.[b]	.[b]						
Water level	−0.559	−0.534	−0.454	.[b]	.[b]	.[b]	.[b]	.[b]	1					
Sal	0.572	0.601	0.587	.[b]	.[b]	.[b]	.[b]	.[b]	−0.098	1				
pH	−0.786**	−0.750*	−0.848**	.[b]	.[b]	.[b]	.[b]	.[b]	0.624	−0.274	1			
DO	0.058	0.034	0.061	.[b]	.[b]	.[b]	.[b]	.[b]	−0.321	−0.439	−0.104	1		
DOC	0.766**	0.738**	0.895**	.[b]	.[b]	.[b]	.[b]	.[b]	−0.331	0.349	−0.848**	0.167	1	
POC	0.055	0.082	0.141	.[b]	.[b]	.[b]	.[b]	.[b]	0.019	0.133	0.269	−0.354	−0.073	1

(b) Spring tide: 18-19/04/2015.

	MnD	FeD	CoD	NiD	Mnp	Fep	Cop	Nip	Water level	Sal	pH	DO	DOC	POC	TSS
MnD	1														
FeD	0.821**	1													
CoD	0.779**	0.811**	1												
NiD	.[b]	.[b]	.[b]	.[b]											
Mnp	−0.804**	−0.445	−0.443	.[b]	1										
Fep	0.717**	0.671*	0.671*	.[b]	−0.432	1									
Cop	−0.228	0.201	−0.013	.[b]	0.697**	0.142	1								
Nip	−0.388	0.039	−0.133	.[b]	0.787**	−0.014	0.972**	1							
Water level	−0.791**	−0.662*	−0.781**	.[b]	0.679*	−0.680*	0.202	0.314	1						
Sal	0.571*	0.699**	0.718**	.[b]	−0.314	0.596*	0.205	0.139	−0.752**	1					
pH	−0.871**	−0.612*	−0.635*	.[b]	0.900**	−0.609*	0.469	0.599*	0.888**	−0.532	1				
DO	0.345	0.557*	0.453	.[b]	−0.311	0.375	0.052	0.053	−0.536	0.750**	−0.426	1			
DOC	0.768**	0.713**	0.870**	.[b]	−0.531	0.623*	−0.172	−0.291	−0.560*	0.460	−0.570*	0.230	1		
POC	−0.346	−0.464	−0.515	.[b]	0.102	−0.180	−0.039	0.047	0.038	−0.190	0.074	0.093	−0.756**	1	
TSS	0.474	0.650*	0.295	.[b]	−0.141	0.552	0.456	0.284	−0.321	0.346	−0.265	0.254	0.160	−0.005	1

***Correlation is significant at the 0.01 level (two-tailed). *Correlation is significant at the 0.05 level (two-tailed). b, Cannot be computed because at least one of the variables is not available.*

concentrations were 1,203 and 2,429 $\mu g\ L^{-1}$ during the dry and the rainy season, respectively (**Table 2**). As explained for Mn, Fe oxyhydroxide dissolution in suboxic conditions during organic matter (OM) diagenetic processes were responsible for these elevated concentrations (Thanh-Nho et al., 2019b), and the high temperature and intense rainfall, enhancing OM decomposition, induced the higher concentrations measured during the rainy season. Consequently, we suggest that porewater seepage was responsible for the high Fe_D concentrations measured in the tidal creek at low tide, which was even higher during the wet season because of possible increased geochemical processes in mangrove soils. This hypothesis was confirmed by the positive correlations between dissolved Fe_D concentrations and ^{222}Rn (r = 0.63, **Supplementary Figure S2**). However, the correlation was less strong than the one between Mn_D and ^{222}Rn (**Supplementary Figure S2**), which possibly suggests that Fe_D was subject to specific biogeochemical processes. In addition, Fe_D and Mn_D concentrations in mangrove soil porewaters were in the same range, but at low tide in the tidal creek, when porewater inputs were maximum, Fe_D concentrations were 10 times lower than Mn_D. However and conversely to Mn_P, Fe_P concentrations in the tidal creek were maximum at low tides, with higher values than those we measured in the estuary. Consequently, we suggest that, because of different physico-chemical properties between the tidal creek and mangrove soils, notable O_2 and pH, part of the dissolved iron that was exported from mangrove soil precipitated in the creek, explaining the high Fe_P concentrations measured at low tide and the fact that Fe_D concentrations were 10 times lower than Mn_D. In mangrove soils, pH ranged between 4.6 and 6.8 (**Table 2**), while in the tidal creek at low tide, pH was always higher than 6.5 (**Figure 2**), which can favor Fe_D precipitation even at low DO concentrations (Hatje et al., 2003).

TABLE 4 | Matrix of Pearson correlation coefficients between trace metal concentrations and different physicochemical parameters in the tidal creek during the wet season.

(a) Neap tide: 19-20/10/2015.

	MnD	FeD	CoD	NiD	Mnp	Fep	Cop	Nip	Water level	Sal	pH	DO	DOC	POC	TSS	^{222}Rn
MnD	1															
FeD	0.806**	1														
CoD	0.987**	0.846**	1													
NiD	0.537	0.830**	0.618*	1												
Mnp	−0.474	−0.480	−0.492	−0.342	1											
Fep	0.505	0.747**	0.584*	0.814**	−0.017	1										
Cop	0.014	0.198	0.074	0.301	0.653*	0.552	1									
Nip	0.150	0.540	0.249	0.449	0.021	0.594*	0.648*	1								
Water level	−0.743**	−0.829**	−0.743**	−0.638*	0.720**	−0.383	0.218	−0.152	1							
Sal	0.295	−0.201	0.239	−0.302	0.420	−0.091	0.185	−0.483	0.158	1						
pH	−0.781**	−0.900**	−0.815**	−0.868**	0.767**	−0.598*	0.195	−0.239	0.968**	0.211	1					
DO	−0.856**	−0.928**	−0.883**	−0.854**	0.707*	−0.651*	0.115	−0.244	0.976**	0.090	0.987**	1				
DOC	0.754**	0.812**	0.791**	0.608*	−0.402	0.486	0.085	0.309	−0.731**	0.118	−.778**	−0.813**	1			
POC	0.576*	0.428	0.520	0.040	−0.714**	0.026	−0.601*	−0.164	−0.682*	−0.032	−0.632*	−0.664*	0.354	1		
TSS	0.498	0.581*	0.486	0.588*	0.099	0.611*	0.229	0.022	−0.406	0.227	−0.553	−0.596*	0.612*	0.095	1	
^{222}Rn	0.732**	0.481	0.671*	0.095	−0.580*	0.062	−0.385	−0.179	−0.748**	0.383	−0.675*	−764**	0.543	0.868**	0.190	1

(b) Spring tide: 26-27/10/2015.

	MnD	FeD	CoD	NiD	Mnp	Fep	Cop	Nip	Water level	Sal	pH	DO	DOC	POC	TSS	^{222}Rn
MnD	1															
FeD	0.861**	1														
CoD	0.548	0.719**	1													
NiD	0.261	0.392	0.573*	1												
Mnp	−0.733**	−0.644*	−0.698**	−0.520	1											
Fep	0.241	0.605*	0.529	0.016	.020	1										
Cop	0.107	0.324	0.333	0.020	−0.006	0.459	1									
Nip	0.268	0.483	0.433	0.230	−0.356	0.355	0.805**	1								
Water level	−0.757**	−0.895**	−0.765**	−0.572*	0.822**	−0.384	−0.258	−0.512	1							
Sal	−0.089	−0.399	−0.327	−0.144	0.203	−0.456	−0.162	−0.208	0.563*	1						
pH	−0.716**	−0.844**	−0.791**	−0.649*	0.837**	−0.344	−0.269	−0.583*	0.938**	0.447	1					
DO	−0.852**	−0.917**	−0.717**	−0.573*	0.750**	−0.382	−0.323	−0.547	0.911**	0.353	0.944**	1				
DOC	0.819**	0.827**	0.487	0.201	−0.603*	0.438	0.001	0.239	−0.749**	−0.451	−0.753**	−.813**	1			
POC	−0.168	0.232	0.451	−0.052	0.205	0.874**	0.502	0.330	−0.090	−0.328	−0.091	−0.033	0.023	1		
TSS	0.531	0.797**	0.644*	0.254	−0.312	0.715**	0.726**	0.739**	−0.680*	−0.374	−0.643*	−0.727**	0.467	0.514	1	
^{222}Rn	0.655*	0.482	0.109	0.073	−0.618*	−0.138	−0.360	−0.127	−0.540	−0.302	−0.479	−0.486	0.710**	−0.490	−0.049	1

***Correlation is significant at the 0.01 level (two-tailed). *Correlation is significant at the 0.05 level (two-tailed).*

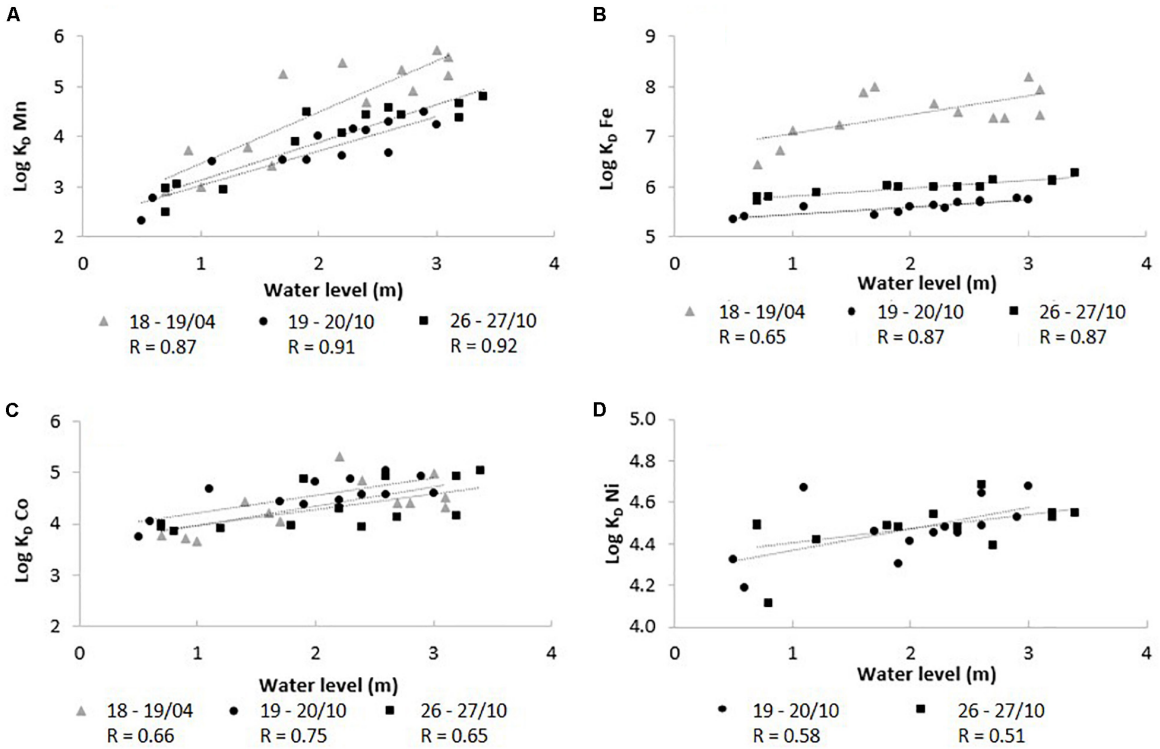

FIGURE 5 | Correlations between Log K_D of trace metals and water level for all tidal cycles in the creek during the dry (gray dots) and the wet seasons (black dots).

This hypothesis could be supported by the positive correlation between Log K_D^{Fe} and pH (r = 0.56 and 0.60 during the dry and the wet season, respectively, **Supplementary Figure S1**), and by the positive correlation between Log K_D^{Fe} and the water level confirming Fe precipitation with increasing pH. In addition, in the tidal creek, Log K_D^{Fe} ranged between 5.33 and 8.19 (**Figure 5B**), while in the Can Gio estuary, Log K_D^{Fe} varied between 6.39 and 7.6 (Thanh-Nho et al., 2018). Eventually, at low tide, TSS increase in the tidal creek, because of resuspension of bottom sediments due to the low water depth may also partly explain the higher Fe_P concentrations. However, the different dynamics between Fe and Mn in the creek evidenced that Fe_P distribution was not only related to physical processes, but that geochemical processes were involved, like Fe_D precipitation or colloidal flocculation. These results confirmed those obtained by Sanders et al. (2015), who suggested that small tidal estuaries may be important conduits for dissolved Fe to the ocean. However, we suggest that the great variability of pH and DO in mangrove ecosystems may limit this export under the dissolved form. Our results also confirm the hypothesis developed by Thanh-Nho et al. (2018) of Fe_P inputs from mangroves to the estuary, where they measured increased Fe_P concentrations at the "mangrove" station. In addition, like observed for different forms of carbon (Maher et al., 2013; Call et al., 2015), the type of tides and their ranges (i.e., neap and spring tides, respectively; **Figure 4**) influenced Fe concentrations in the tidal creek, being higher when a large tidal range (spring tides of 18-19/04/2015 and 26-27/10/2015, respectively) followed a small one (neap tide of 19-20/10/2015) because of elevated water residence time in the mangrove and larger mangrove area immerged.

Cobalt and Nickel Dynamics

Because of their similar distributions in dissolved and particulate phases in the mangrove tidal creek, Co and Ni are discussed together. Surprisingly, we did not observe any significant difference between Co_P and Ni_P concentrations at low tide and high tide. For similar salinity values in the estuary, Co_P concentrations ranged between 10 and 20 $\mu g\ L^{-1}$, and Ni_P between 40 and 50 $\mu g\ L^{-1}$ (Thanh-Nho et al., 2018), which was similar to what we measured in the tidal creek. We, thus, consider that estuarine waters were the main sources of Co_P and Ni_P in the tidal creek. However, the highest concentrations of Co_P and Ni_P were measured at the lowest water level of the spring tide during the wet season (**Figure 4**), which may suggest that these two elements were subject to the same geochemical processes than iron, being exported from mangrove soils under dissolved form and precipitating in the creek. This process may also explain the almost stable concentrations measured in the creek whatever the tidal period, without Co and Ni precipitations at low tide, a decrease of their concentrations would have been observed. In fact, Co_D and Ni_D presented higher concentrations in the creek water than the mouth of the Can Gio mangrove estuary irrespective of the season, with mean concentrations lower than 0.1 $\mu g\ L^{-1}$ for Co_D and lower than 1.0 $\mu g\ L^{-1}$ for Ni_D irrespective of the season (Thanh-Nho et al., 2018). We suggest that the increasing Co_D and Ni_D concentrations during

the ebb resulted from porewater inputs, being consistent with the negative correlations between Co_D, Ni_D and water levels during the tidal cycles ($r = -0.57$; -0.68 for Co_D during the dry and the wet season, **Supplementary Figure S1**; and $r = -0.59$ for Ni during the wet one, **Supplementary Figure S1**). However, we did not observe any good correlations between Co_D, Ni_D and ^{222}Rn (**Supplementary Figure S2**), most probably because, like we suggested, these elements were subject to geochemical processes during their transfer from the soil to the creek and also in the creek. Like for Mn_D, Co_D concentrations in the tidal creek were positively correlated to DOC ($r = 0.62$; 0.77 with DOC during the dry season and the wet season, respectively) (**Supplementary Figure S2**). Like Mn, in addition to a common origin, i.e., mangrove porewaters, we suggest the formation of organocobalt complexes, which may have increased the mobility of Co_D during its transfer from the porewater to the tidal creek (Noble et al., 2008). Log K_D^{Co} presented a large range of values, from 3.7 to 5.3, being positively correlated with the water level (**Figure 5C**). As a result of porewater inputs, Log K_D^{Co} decreased during the ebb. During the flood, Co_D may be adsorbed onto Fe-oxyhydroxide as they precipitate because of variable redox and pH conditions (Murray and Dillard, 1979). This hypothesis may be supported by the negative correlation between Co_D and pH ($r = -0.66$ and -0.72 during the dry and the wet season, respectively, **Supplementary Figure S1**) and by the negative correlation between Log K_D^{Co} and DOC ($r = -0.83$ during the dry season and $r = -0.58$ during the wet season, **Supplementary Figure S1**). Furthermore, the Co_D decrease during the flow can result from the physical mixing of the creek water with the estuarine water, containing lower Co_D concentrations.

Similarly to Co, Log K_D^{Ni} was positively correlated with the water level (**Figure 5D**), implying that physicochemical processes also played key roles in Ni partitioning in the tidal creek. During the flood, the decreasing Ni_D concentrations in the tidal creek most probably resulted from the dilution by the estuarine water, containing lower Ni_D, and/or from the adsorption onto TSS and the precipitation with Fe oxyhydroxide. The latter hypothesis may be supported by the negative correlation between Ni_D and pH ($r = -0.72$ during the wet season, **Supplementary Figure S1**). This result was consistent with the positive correlation between Log K_D^{Ni} and pH ($r = 0.65$, **Supplementary Figure S1**).

CONCLUSION

The present study evidences that trace metals dynamics in mangrove tidal creeks, that have no upstream inputs, depend both on the estuarine inputs during the flood, and mangrove soils inputs during the ebb. Mangrove soils can lose part of their trace metals stocks, exporting dissolved trace metals through process of porewater seepage. Additionally in the tidal creek, physical and geochemical processes during tidal cycles (i.e., physical dilution, precipitation, etc.) could modify trace metals partitioning between dissolved and particulate phases. Tidal ranges and irregularities of the tidal cycles influenced trace metal concentrations in the tidal creek, by controlling porewater seepage. When a larger area of mangrove is immerged and when there is an increased residence time of the water in the mangrove, like what happened when a strong tide followed a small one or during the rainy season, enhanced export of trace metals in the tidal creek during the ebb occurred. These processes resulted in large amount of dissolved Mn exported from the soils to the tidal creek and then possibly to the coastal ocean. Dissolved iron was also exported from mangrove soils, but conversely to Mn, we suggest that the different physico-chemical characteristics between the soils and the creek, notably higher dissolved oxygen concentrations and higher pH, resulted in its precipitation. Consequently, Fe was mainly exported from the creek to adjacent systems under particulate forms. Nickel and Cobalt dynamics were similar to the one of iron. Consequently, the mangrove ability to act as a sink for trace metals may be questioned and budget studies must be developed.

DATA AVAILABILITY STATEMENT

All datasets generated for this study are included in the article/**Supplementary Material**.

AUTHOR CONTRIBUTIONS

CM, NT-N, and T-TN-T performed the experimental design. NT-N, CM, TV, PT, and NC-H performed the data collection and statistical analyses. CM, NT-N, ES, and T-TN-T performed the data interpretation. All authors wrote the manuscript.

FUNDING

The research was funded by IRD (Institut de Recherche pour le Développement) through the BEST grant to NT-N. This research was supported by Vietnam National Foundation for Science and Technology Development (NAFOSTED) under grant number 05/2020/STS01.

ACKNOWLEDGMENTS

We would like to thank the authorities of Can Gio District People Committee and the CGMBR who facilitated the fieldwork.

SUPPLEMENTARY MATERIAL

The Supplementary Material for this article can be found online at: https://www.frontiersin.org/articles/10.3389/fenvs.2020.00139/full#supplementary-material

FIGURE S1 | Correlations between dissolved, particulate metal concentrations, physicochemical parameters, and water level over tidal cycles. The relationships between Log K_D of trace metals and physicochemical parameters are also presented.

FIGURE S2 | Correlations between trace metals and ^{222}Rn during the ebb in in the dry season (gray dots) and the wet season (black dots): **(a)** Mn_D, **(b)** Fe_D, **(c)** Co_D, **(d)** Ni_D and $_{222}Rn$; **(e)** DOC and ^{222}Rn, **(f)** Mn_D and DOC, **(g)** Co_D and Mn_D, **(h)** Co_D and DOC.

REFERENCES

Blasco, F., Aizpuru, M., and Gers, C. (2001). Depletion of the mangroves of Continental Asia. *Wetlands Ecol. Manag.* 9, 245–256.

Bouillon, S., Borges, A. V., Castañeda-Moya, E., Diele, K., Dittmar, T., Duke, N. C., et al. (2008). Mangrove production and carbon sinks: a revision of global budget estimates. *Glob. Biogeochem. Cycles* 22:GB2013.

Burnett, W., Kim, G., and Lane-Smith, D. (2001). A continuous monitor for assessment of 222Rn in the coastal ocean. *J. Radioanal. Nuclear Chem.* 249, 167–172.

Call, M., Maher, D. T., Santos, I. R., Ruiz-Halpern, S., Mangion, P., Sanders, C. J., et al. (2015). Spatial and temporal variability of carbon dioxide and methane fluxes over semi-diurnal and spring–neap–spring timescales in a mangrove creek. *Geochim. Cosmochim. Acta* 150, 211–225. doi: 10.1016/j.gca.2014.11.023

Clark, M. W., McConchie, D., Lewis, D. W., and Saenger, P. (1998). Redox stratification and heavy metal partitioning in Avicennia-dominated mangrove sediments: a geochemical model. *Chem. Geol.* 149, 147–171. doi: 10.1016/s0009-2541(98)00034-5

Dang, D. H., Lenoble, V., Durrieu, G., Omanovic, D., Mullot, J. U., Mounier, S., et al. (2015). Seasonal variations of coastal sedimentary trace metals cycling: insight on the effect of manganese and iron (oxy)hydroxides, sulphide and organic matter. *Mar. Pollut. Bull.* 92, 113–124. doi: 10.1016/j.marpolbul.2014.12.048

David, F., Marchand, C., Taillardat, P., Thành-Nho, N., and Meziane, T. (2018). Nutritional composition of suspended particulate matter in a tropical mangrove creek during a tidal cycle (Can Gio, Vietnam). *Estuar. Coast. Shelf Sci.* 200, 126–130. doi: 10.1016/j.ecss.2017.10.017

Deborde, J., Marchand, C., Molnar, N., Patrona, L., and Meziane, T. (2015). Concentrations and fractionation of carbon, iron, sulfur, nitrogen and phosphorus in mangrove sediments along an intertidal gradient (Semi-Arid Climate, New Caledonia). *J. Mar. Sci. Eng.* 3, 52–72. doi: 10.3390/jmse3010052

Dittmar, T., and Lara, R. J. (2001). Driving forces behind nutrient and organic matter dynamics in a mangrove tidal creek in North Brazil. *Estuar. Coast. Shelf Sci.* 52, 249–259. doi: 10.1006/ecss.2000.0743

Egawa, T., and Ooba, Y. (1963). Mineralogical studies of some soils in the central highland of Vietnam. *Soil Sci. Plant Nutr.* 9, 14–20. doi: 10.1080/00380768.1963.10431057

Fang, T. H., and Lin, C. L. (2002). Dissolved and particulate trace metals and their partitioning in a hypoxic estuary: the tanshui estuary in Northern Taiwan. *Estuaries* 25, 598–607. doi: 10.1007/bf02804893

Ferreira, T. O., Otero, X. L., Vidal-Torrado, P., and Macías, F. (2007). Effects of bioturbation by root and crab activity on iron and sulfur biogeochemistry in mangrove substrate. *Geoderma* 142, 36–46. doi: 10.1016/j.geoderma.2007.07.010

Furukawa, K., Wolanski, E., and Mueller, H. (1997). Currents and sediment transport in mangrove forests, estuarine, coastal and shelf. *Estuar. Coast. Shelf Sci.* 44, 301–310. doi: 10.1006/ecss.1996.0120

Hatje, V., Payne, T. E., Hill, D. M., McOrist, G., Birch, G. F., and Szymczak, R. (2003). Kinetics of trace element uptake and release by particles in estuarine waters: effects of pH, salinity, and particle loading. *Environ. Int.* 29, 619–629. doi: 10.1016/s0160-4120(03)00049-7

Holloway, C. J., Santos, I. R., Tait, D. R., Sanders, C. J., Rose, A. L., Schnetger, B., et al. (2016). Manganese and iron release from mangrove porewaters: a significant component of oceanic budgets? *Mar. Chem.* 184, 43–52. doi: 10.1016/j.marchem.2016.05.013

Kaly, U. L., Eugelink, G., and Robertson, A. I. (1997). Soil conditions in damaged North Queensland mangroves. *Estuaries* 20, 291–300.

Kristensen, E., Connolly, R. M., Otero, X. L., Marchand, C., Ferreira, T. O., and Rivera-Monroy, V. H. (2017). *Biogeochemical Cycles: Global Approaches and Perspectives. Mangrove Ecosystems: A Global Biogeographic Perspective*. Cham: Springer, 163–209.

Kuenzer, C., and Tuan, V. Q. (2013). Assessing the ecosystem services value of can gio mangrove biosphere reserve: combining earth-observation- and household-survey-based analyses. *Appl. Geogr.* 45, 167–184. doi: 10.1016/j.apgeog.2013.08.012

Lacerda, L. D., Martinelli, L. A., Rezende, C. A., Mozetto, A. A., Ovalle, A. R. C., Victoria, R. I., et al. (1988). The fate of heavy metals in suspended matter in a mangrove creek during a tidal cycle. *Sci. Tot. Environ.* 75, 249–259.

Lacerda, L. D., Ribeiro, M. G. Jr., and Gueiros, B. B. (1999). Manganese dynamics in a mangrove mud flat tidal creek in SE Brazil. *Mangroves Salt Marshes* 3, 105–115.

Leopold, A., Marchand, C., Deborde, J., Chaduteau, C., and Allenbach, M. (2013). Influence of mangrove zonation on CO2 fluxes at the sediment–air interface (New Caledonia). *Geoderma* 202-203, 62–70. doi: 10.1016/j.geoderma.2013.03.008

Luong, N. V., Tateishi, R., and Hoan, N. T. (2015). Analysis of an impact of succession in mangrove forest association using remote sensing and GIS technology. *J. Geogr. Geol.* 7:106.

Maher, D. T., Santos, I. R., Golsby-Smith, L., Gleeson, J., and Eyre, B. D. (2013). Groundwater-derived dissolved inorganic and organic carbon exports from a mangrove tidal creek: the missing mangrove carbon sink? *Limnol. Oceanogr.* 58, 475–488. doi: 10.4319/lo.2013.58.2.0475

Marchand, C., Albéric, P., Lallier-Vergès, E., and Baltzer, F. (2006). Distribution and characteristics of dissolved organic matter in mangrove sediment pore waters along the coastline of French Guiana. *Biogeochemistry* 81, 59–75. doi: 10.1007/s10533-006-9030-x

Marchand, C., Baltzer, F., Lallier-Vergès, E., and Albéric, P. (2004). Pore-water chemistry in mangrove sediments: relationship with species composition and developmental stages (French Guiana). *Mar. Geol.* 208, 361–381. doi: 10.1016/j.margeo.2004.04.015

Marchand, C., Fernandez, J. M., and Moreton, B. (2016). Trace metal geochemistry in mangrove sediments and their transfer to mangrove plants (New Caledonia). *Sci. Tot. Environ.* 562, 216–227. doi: 10.1016/j.scitotenv.2016.03.206

Marchand, C., Fernandez, J. M., Moreton, B., Landi, L., Lallier-Vergès, E., and Baltzer, F. (2012). The partitioning of transitional metals (Fe, Mn, Ni, Cr) in mangrove sediments downstream of a ferralitized ultramafic watershed (New Caledonia). *Chem. Geol.* 300-301, 70–80. doi: 10.1016/j.chemgeo.2012.01.018

Marchand, C., Lallier-Vergès, E., and Allenbach, M. (2011). Redox conditions and heavy metals distribution in mangrove forests receiving effluents from shrimp farms (Teremba Bay, New Caledonia). *J. Soils Sediments* 11, 529–541. doi: 10.1007/s11368-010-0330-3

McKee, K. L. (1993). Soil physicochemical patterns and mangrove species distribution-reciprocal effects. *J. Ecol.* 81, 477–487.

Murray, J. W., and Dillard, J. G. (1979). The oxidation of cobalt (II) adsorbed on manganese dioxide. *Geochim. Cosmochim. Acta* 43, 781–787. doi: 10.1016/0016-7037(79)90261-8

Noble, A. E., Saito, M. A., Maiti, K., and Benitez-Nelson, C. R. (2008). Cobalt, manganese, and iron near the Hawaiian Islands: a potential concentrating mechanism for cobalt within a cyclonic eddy and implications for the hybrid-type trace metals. *Deep Sea Res. Part II Top. Stud. Oceanogr.* 55, 1473–1490. doi: 10.1016/j.dsr2.2008.02.010

Noël, V., Marchand, C., Juillot, F., Ona-Nguema, G., Viollier, E., Marakovic, G., et al. (2014). EXAFS analysis of iron cycling in mangrove sediments downstream a lateritized ultramafic watershed (Vavouto Bay, New Caledonia). *Geochim. Cosmochim. Acta* 136, 211–228. doi: 10.1016/j.gca.2014.03.019

Noël, V., Morin, G., Juillot, F., Marchand, C., Brest, J., Bargar, J. R., et al. (2015). Ni cycling in mangrove sediments from New Caledonia. *Geochim. Cosmochim. Acta* 169, 82–98. doi: 10.1016/j.gca.2015.07.024

Patrick, W. H., and Jugsujinda, A. (1992). Sequential reduction and oxidation of inorganic nitrogen, manganese and iron in flooded soil. *Soil Sci. Soc. Am. J.* 56, 1071–1073. doi: 10.2136/sssaj1992.03615995005600040011x

Sadat-Noori, M., and Glamore, W. (2019). Porewater exchange drives trace metal, dissolved organic carbon and total dissolved nitrogen export from a temperate mangrove wetland. *J. Environ. Manag.* 248:109264. doi: 10.1016/j.jenvman.2019.109264

Sanders, C. J., Santos, I. R., Maher, D. T., Sadat-Noori, M., Schnetger, B., and Brumsack, H.-J. (2015). Dissolved iron exports from an estuary surrounded by coastal wetlands: can small estuaries be a significant source of Fe to the ocean? *Mar. Chem.* 176, 75–82. doi: 10.1016/j.marchem.2015.07.009

Strady, E., Blanc, G., Schäfer, J., Coynel, A., and Dabrin, A. (2009). Dissolved uranium, vanadium and molybdenum behaviours during contrasting freshwater discharges in the Gironde Estuary (SW France). *Estuar. Coast. Shelf Sci.* 83, 550–560. doi: 10.1016/j.ecss.2009.05.006

Taillardat, P., Pim, W., Marchand, C., Friess, D., Widory, D., Baudron, P., et al. (2018a). Porewater discharge and carbon fluxes in a mangrove tidal creek: the importance of in situ processes over tidal export. *J. Hydrol.* 563, 303–318. doi: 10.1016/j.jhydrol.2018.05.042

Taillardat, P., Ziegler, A. D., Friess, D. A., Widory, D., Truong Van, V., David, F., et al. (2018b). Carbon dynamics and inconstant porewater input in a mangrove tidal creek over contrasting seasons and tidal amplitudes. *Geochim. Cosmochim. Acta* 237, 32–48. doi: 10.1016/j.gca.2018.06.012

Taillardat, P., Ziegler Alan, D., Friess Daniel, A., Widory, D., David, F., Nobuhito, O., et al. (2019). Assessing nutrient dynamics in mangrove porewater and adjacent tidal creek using nitrate dual-stable isotopes: a new approach to challenge the outwelling hypothesis? *Mar. Chem.* 214:103662. doi: 10.1016/j.marchem.2019.103662

Tait, D. R., Maher, D. T., Macklin, P. A., and Santos, I. R. (2016). Mangrove pore water exchange across a latitudinal gradient. *Geophys. Res. Lett.* 43, 3334–3341. doi: 10.1002/2016gl068289

Tam, N. F. Y., and Wong, Y. S. (1999). Mangrove soils in removing pollutants from municipal wastewater of different salinities. *J. Environ. Qual.* 28, 556–564. doi: 10.2134/jeq1999.00472425002800020021x

Thanh-Nho, N., Marchand, C., Strady, E., Huu-Phat, N., and Nhu-Trang, T.-T. (2019a). Bioaccumulation of some trace elements in tropical mangrove plants and snails (Can Gio, Vietnam). *Environ. Pollut.* 248, 635–645. doi: 10.1016/j.envpol.2019.02.041

Thanh-Nho, N., Marchand, C., Strady, E., Vinh, T.-V., and Nhu-Trang, T.-T. (2019b). Metals geochemistry and ecological risk assessment in a tropical mangrove (Can Gio, Vietnam). *Chemosphere* 219, 365–382. doi: 10.1016/j.chemosphere.2018.11.163

Thanh-Nho, N., Strady, E., Nhu-Trang, T. T., David, F., and Marchand, C. (2018). Trace metals partitioning between particulate and dissolved phases along a tropical mangrove estuary (Can Gio, Vietnam). *Chemosphere* 196, 311–322. doi: 10.1016/j.chemosphere.2017.12.189

Turner, A., Millward, G., Bale, A., and Morris, A. (1993). Application of the KD concept to the study of trace metal removal and desorption during estuarine mixing. *Estuar. Coast. Shelf Sci.* 36, 1–13. doi: 10.1006/ecss.1993.1001

USEPA (2007). *US Environmental Protection Agency, Method 3051A: Microwave Assisted Acid Digestion of Sediments, Sludges, Soils, and Oils, part of Test Methods for Evaluating Solid Waste*. Washington, DC: USEPA.

Van Ryssen, R., Alam, M., Goeyens, L., and Baeyens, W. (1998). The use of flux-corer experiments in the determination of heavy metal re-distribution in and of potential leaching from the sediments. *Water Sci. Technol.* 37, 283–290. doi: 10.2166/wst.1998.0763

Vinh, T. V., Allenbach, M., Aimée, J., and Marchand, C. (2019). Seasonal variability of CO2 fluxes at different interfaces and vertical CO2 concentrations profiles in a *Rhizophora* mangrove stand (Can Gio, Viet Nam). *Atmos. Environ.* 201, 301–309. doi: 10.1016/j.atmosenv.2018.12.049

Vinh, T. V., Allenbach, M., Linh, K. T. V., and Marchand, C. (2020). Changes in leaf litter quality during its decomposition in a tropical planted mangrove forest (Can Gio, Vietnam). *Front. Environ. Sci.* 8:10. doi: 10.3389/fenvs.2020.00010

Wolanski, E. (1995). Transport of sediment in mangrove swamps. *Hydrobiologia* 295, 31–42. doi: 10.1007/978-94-011-0289-6_5

Xiao, R., Bai, J., Lu, Q., Zhao, Q., Gao, Z., Wen, X., et al. (2015). Fractionation, transfer, and ecological risks of heavy metals in riparian and ditch wetlands across a 100-year chronosequence of reclamation in an estuary of China. *Sci. Total Environ.* 517, 66–75. doi: 10.1016/j.scitotenv.2015.02.052

Conflict of Interest: The authors declare that the research was conducted in the absence of any commercial or financial relationships that could be construed as a potential conflict of interest.

frontiers in Environmental Science

ORIGINAL RESEARCH
published: 22 September 2020
doi: 10.3389/fenvs.2020.00141

Occurrence and Origins of Cerium Dioxide and Titanium Dioxide Nanoparticles in the Loire River (France) by Single Particle ICP-MS and FEG-SEM Imaging

Karine Phalyvong[1,2], Yann Sivry[1], Hélène Pauwels[2], Alexandre Gélabert[1], Mickaël Tharaud[1], Guillaume Wille[2], Xavier Bourrat[2] and Marc F. Benedetti[1]*

[1] CNRS, Institut de Physique du Globe de Paris, Sorbonne Paris Cité, Paris Diderot University, Paris, France, [2] BRGM, Orleans, France

OPEN ACCESS

Edited by:
Gaetane Lespes, Université de Pau et des Pays de l'Adour, France

Reviewed by:
Wenzhi Liu, Wuhan Botanical Garden (CAS), China
Huacheng Xu, Nanjing Institute of Geography and Limnology (CAS), China

***Correspondence:**
Yann Sivry
sivry@ipgp.fr

Specialty section:
This article was submitted to Biogeochemical Dynamics, a section of the journal Frontiers in Environmental Science

Received: *06 April 2020*
Accepted: *23 July 2020*
Published: *22 September 2020*

Citation:
Phalyvong K, Sivry Y, Pauwels H, Gélabert A, Tharaud M, Wille G, Bourrat X and Benedetti MF (2020) Occurrence and Origins of Cerium Dioxide and Titanium Dioxide Nanoparticles in the Loire River (France) by Single Particle ICP-MS and FEG-SEM Imaging. Front. Environ. Sci. 8:141. doi: 10.3389/fenvs.2020.00141

The need to quantify engineered nanoparticles (ENPs) in the environment is due to the increasing incorporation of these particles in the daily products, which threatens human health and can possibly impact natural systems. Ceria NPs (CeO_2NPs) and titanium dioxide NPs (TiO_2NPs) are two of the most used ENPs in the world. In this study their occurrence was determined in river waters with accurate and relevant techniques such as single particle ICP-MS (spICPMS). In the Loire River (France), the variation of both CeO_2NPs and TiO_2NPs could be assessed locally, with an increase of the concentrations near a wastewater treatment plant (WWTP) outlet as well as in a lake connected to the river and dedicated to outdoor activities. In the upstream river water, supposedly less impacted by NPs, $6.4 \pm 1.2 \times 10^4$ part mL^{-1} Ce-bearing and $13.4 \pm 1.8 \times 10^4$ part mL^{-1} Ti-bearing particles were measured. These values increased to $33.9 \pm 3.4 \times 10^4$ part mL^{-1} Ce-bearing and $80.3 \pm 3.4 \times 10^4$ part mL^{-1} Ti-bearing particles near the WWTP outlet. Equivalent size for sphere distributions ranged from 24 nm to 70 nm for CeO_2 and from 80 nm to 500 nm for TiO_2 in the river water. In the lake, a raise of the concentrations has been observed with $38.3 \pm 2.0 \times 10^4$ part mL^{-1} and $71.6 \pm 2.1 \times 10^4$ part mL^{-1} containing Ce and Ti, respectively, with similar size distributions. FEG-SEM imaging confirms the occurrence of Ce- and Ti-bearing particles in the water samples. On the contrary, NPs seem to undergo strong heteroaggregation in the Loire river water. The Ce/La elemental ratios does not evolve from upstream to downstream the WWTP outlet, suggesting that a natural origin cannot be excluded to explain the increase observed in NPs number concentration. On the contrary, the Ce/La ratio increases in the outdoor activities center, which suggests the contribution of NPs potentially related to the cars parked nearby. Besides, elemental ratios Ti/V and Ti/Y have been assessed to highlight an anthropogenic source of Ti in both sampling sites, possibly to the sunscreens used during the summer.

Keywords: detection of nanoparticles, spICPMS, natural river water, anthropogenic source, TiO_2, CeO_2, FEG-SEM

INTRODUCTION

Engineered nanoparticles (ENPs) are of great importance thanks to their small size which gives them specific properties, especially valuable in different areas such as medicine (Zhang et al., 2008), biology (De et al., 2008), or industry (Piccinno et al., 2012). Ceria (CeO_2NPs) and titanium dioxide NPs (TiO_2NPs) are among the most used NPs in the world (Keller and Lazareva, 2014, Hochella et al., 2019). CeO_2NPs are mostly selected for their high oxygen storage capacity (Zhang et al., 2011), their ability to absorb UV (Lima et al., 2009) and their low redox potential (Ce^{3+}/Ce^{4+}; Van Hoecke et al., 2009). They have several applications, especially in the automobile industry as a diesel fuel additive and as part of catalytic converters. Because of their anti-inflammatory properties (Hirst et al., 2009), these ENPs are also useful in medicine. Regarding TiO_2NPs, their UV blocking properties and their white color make them very interesting to be incorporated in daily products such as sunscreens, toothpaste, food (as an additive) and paints (Weir et al., 2012). In addition, TiO_2NPs are usually coated with a protective layer of alumina or silica. This layer is used to complex hydroxyl radicals (Serpone et al., 2007) and superoxide anion radicals (Virkutyte et al., 2012) produced by TiO_2NPs, which are harmful for human health. It is also known to decrease the photocatalytic activity of TiO_2NPs. In addition, TiO_2NPs constitute the largest release of nanomaterials into the environment (water, air and soil; Sun et al., 2016). The increasing use of ENPs, notably by their incorporation in daily products, raises questions about their release into the environment (Keller and Lazareva, 2014), about their fate and behavior in such complex media (Nowack and Bucheli, 2007; Wagner et al., 2014; Lead et al., 2018), but also about their toxicity (Navarro et al., 2008; Kahru and Dubourguier, 2010). The mobility of NPs (Cary et al., 2015) is difficult to assess, especially as modeled concentrations have been estimated at ng L^{-1} to µg L^{-1} (Gottschalk et al., 2013; Nowack et al., 2015). In addition, the very low concentrations make ENPs difficult to be quantified among natural NPs geochemical background. That is why the use of trustworthy analytical tools allowing the detection and quantification of ENPs in the environment, at relevant concentrations, is required.

Single particle Inductively Coupled Plasma-Mass Spectrometry (spICPMS) is an innovative technique that can determine particle size distribution and particle number concentration. In the early 2000s, this method was firstly applied to colloids (Degueldre and Favarger, 2003, 2004; Degueldre et al., 2004, 2006a,b) and more recently to ENPs (Laborda et al., 2011; Mitrano et al., 2012). Lately, a study underlined that spICPMS presented limitations in terms of minimum size detection (Lee et al., 2014). Few applications of spICPMS in environmental matrix have been assessed, especially in aquatic media. Most studies are about silver ENPs detected (Mitrano et al., 2012; Tuoriniemi et al., 2012; Wang et al., 2020) or spiked (Telgmann et al., 2014) in wastewater samples (Polesel et al., 2018) and in natural waters (Mitrano et al., 2014; Yang et al., 2016). One study deals with the detection of ZnONPs in water by using both a binding resin and spICPMS (Hadioui et al., 2015). The fate of several ENPs was also studied during the drinking water treatment process, showing that ENPs were detected and quickly removed after the first water treatment step (Donovan et al., 2016a,b). To our knowledge, the studies conducted by Gondikas et al. (2014) revealing the release of TiO_2NPs from sunscreens in the Old Danube Lake during 1 year of sampling, in the Meuse and Ijssel rivers (Peters et al., 2018) and the one conducted by Reed et al. (2017), revealing elevated Ti-containing particles during bathing hours in a stream used for recreation are the only ones applying the spICPMS technique for TiO_2NPs evidences in a natural matrix at relevant environmental concentrations. While this study efficiently assessed the temporal variation of TiO_2NPs concentration at one single point, no spatial investigation of the ENPs dynamics was performed.

The aim of the present study was to assess the occurrence of NPs potentially resulting from anthropogenic activities in a complex environmental system, the Loire River. Particularly, some potential ENPs inflows were investigated: a direct water release considering sunscreen use in a recreational area (TiO_2NPs for instance), an indirect airborne contamination involving fuel burning (automobile use with CeO_2NPs), and NPs released from a wastewater treatment plant (WWTP). The occurrence of TiO_2NPs and CeO_2NPs at different locations in the Loire River watershed were determined with two powerful analytical tools: spICPMS and FEG-SEM imaging, specifically dedicated to the NPs detection in complex environmental matrices. These tools were combined with a geochemical approach involving the use of elemental ratios for the determination of the NPs origins and sources.

MATERIALS AND METHODS

Field Settings

The site study is located around the city of Orléans (France), along the Loire Rive which is 1,012 km long and is one of the largest river in Europe. Indeed, the Loire River drains an area of 117,000 km^2 (Camenen et al., 2016) and constitutes one of the major input of water discharge in the Atlantic Ocean with 26 km^3 per year (Figueres et al., 1985; Grosbois et al., 2000). The Loire River basin (20% of France territory) can be divided into three smaller basins: the Upper Loire, the Middle Loire, and the Lower Loire which correspond to 18, 24, and 65% of the basin area, respectively (Minaudo et al., 2015). In its upper basin, the Loire River drains old plutonic and volcanic rocks such as granites, gneisses, and mica schists (Grosbois et al., 2000; Dhivert et al., 2015), whereas in its middle basin, where Orleans is seated, 200 to 6 million years old carbonate deposits from Paris basin dominate (Négrel et al., 2000). For this study, seven sampling sites were chosen from upstream to downstream the Orléans city (**Figure 1**).

The sampling campaign took place during two sunny days of September 2014: 15th and 16th, where the water level was low. A first sampling site, called LS1, has been chosen upstream from Orléans city, at Jargeau city. Given its location, this site was postulated to be the one the least affected by anthropogenic activities of Orléans. In Orleans city, LS2 site is located before the WWTP outlet where two sampling points were selected (LS3 and LS4). At the downstream of these points, water sample has been

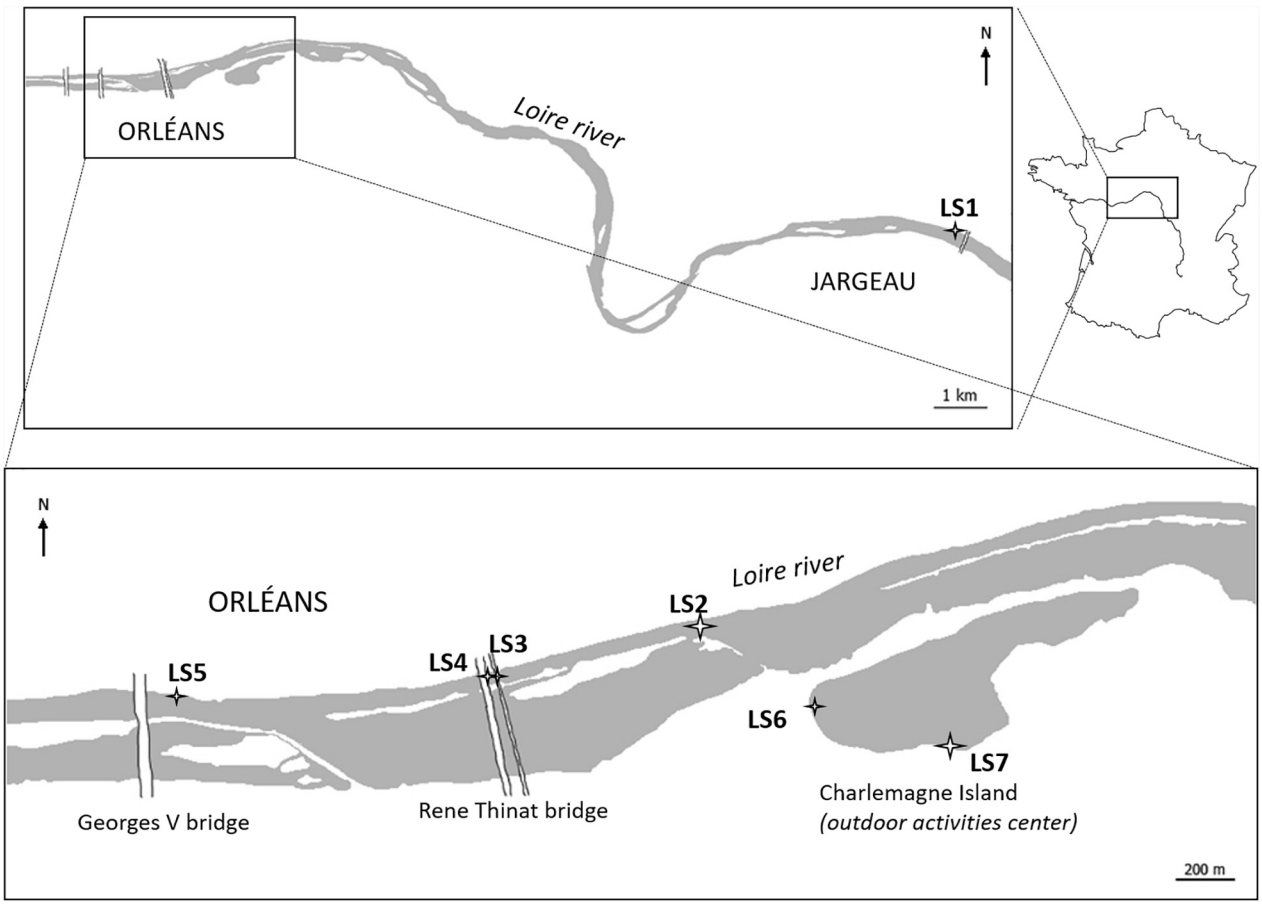

FIGURE 1 | Loire River sampling sites from LS1 (in Jargeau city) to LS7, in Orleans city.

taken up on LS5, at the very end of the Orleans city. LS6 and LS7 are located close to an outdoor activities center where people can swim into a lake which water has underground connections with the Loire River.

Water Chemistry

On site measurements on surface waters were performed including pH, dissolved oxygen, conductivity, and temperature. Water samples were filtered through 0.22 μm acetate cellulose syringe filters and stored in Falcon tubes (PP). An aliquot of the water sample was acidified with distilled 16N HNO3 for dissolved trace and major cations analysis. Another one was kept unacidified for the anions and the alkalinity analyses. Concentrations of major anions and cations were determined by ionic chromatography (Thermo Fisher Scientific ICS 1100) and Inductively Coupled Plasma Atomic Emission Spectroscopy (ICP-AES, Thermo Fisher Scientific iCAP 6200), respectively. Alkalinity was measured by automatic titration with 10^{-2} mol L^{-1} HCl with a Titrando 809 from Metrohm. Moreover, Loire River water was also filtered through 0.7 μm glass microfiber filters to measure the non-purgeable organic carbon (NPOC) in the filtrate after acidification with 85% H_3PO_4, using a Shimadzu Total Organic Carbon Analyzer (TOC V CSH). For each sampling site, around one liter of Loire surface water (bulk water) was collected in view of spICPMS analysis. Suspended matters were also collected on 0.2 μm polyethersulfone filters, picked up, and freeze-dried prior to FEG-SEM analyses. Total concentrations in bulk water samples of Al, Sc, Ti, V, Cr, Mn, Fe, Co, Cu, Zn, Sr, Y, Ag, Cd, and Pb as well as REE except Pm) in water were obtained by performing evaporation of the bulk water followed by acid digestion with distilled 27N HF/16N HNO_3 at 1:1 ratio at 95°C overnight. Samples were then diluted with 2% HNO_3 before ICP-AES and ICP-MS analyses. Total and dissolved trace element concentrations were measured with a High Resolution-ICP-MS (Thermo Fisher Scientific ELEMENT II). If the measured concentrations were too high (especially, in total fractions, superior to 10 ppb), samples were analyzed by ICP-AES (Thermo Fisher Scientific iCAP 6200).

Single Particle ICP-MS (spICPMS)

A High Resolution Thermo Fisher Scientific ELEMENT II ICP-MS was used in single counting mode for spICPMS measurements. The number of measurements was fixed at 10,000 data with a dwell time of 1 ms and a settling time of 1 ms. Besides, the flow rate was measured manually in triplicate, during the analysis day, at 0.2 mL min^{-1}. Calibration curves were made in

the same matrix as the samples: the sample LS1 was ultrafiltered at 500 Da then used for dilution (from 50 to 1,000 ppt) of gold (Au), cerium (Ce) and titanium (Ti) SCP Science with 10 ppm stock solutions. Furthermore, using the second method called "particle size" and described by Pace et al. (2011), 5 ppt of gold NPs with a 15 nm size (BBInternational) were used to determine the transport efficiency (12% in low resolution and 6.4% in medium resolution). ^{140}Ce and ^{47}Ti were measured in low and medium resolutions, respectively. spICPMS technique requires diluted samples to have single particle events. Similarly to standards, each bulk water samples as well as AuNPs suspension were diluted with LS1 500 Da ultrafiltered water, with the objective to disturb as less as possible the chemical equilibriums of samples while diluting as well as to eliminate any matrix effect. Ultrafiltered LS1 sample also served as a blank during analyses. Several dilutions were assessed (2, 5, 10, 100, and 1,000), and the 5-fold dilution was chosen as the best compromise between a minimum number of particles and an accurate peak resolution. Samples were measured in triplicate (3 times 10000 data) which allows calculating averages and standard deviations.

Data treatment procedure was provided by Colorado School of Mines coming from Pace et al. (2011) and could be sum up as following: at first, count intensities were classified as a function of their frequency. The lowest intensities represented the dissolved ions and higher intensities accounted for NPs. Different methods exist to determine the threshold between dissolved and NPs such as iterative algorithms with 3σ (Mitrano et al., 2012) or 5σ (Tuoriniemi et al., 2012), a K-mean clustering algorithm (Bi et al., 2014), a deconvolution method (Cornelis and Hassellöv, 2014), or simply by using the first minimum as the limit between dissolved and NPs (Mitrano et al., 2014). In our study, the threshold between dissolved and NPs species was determined experimentally by measuring LS1 500 Da ultrafiltered water in single counting mode. LS1 water sample was chosen as the least impacted with NPs. Actually, below this threshold, all measured species are considered in a non-particulate form referred here as a "true dissolved state." Then, the frequency *versus* count intensity of LS1 500 Da ultrafiltered water was simultaneously drawn with the unknown sample to determine the cut-off between dissolved and NPs. Consequently, if the distribution for the dissolved ions can be measured and drawn, the threshold between dissolved and NPs can be determined, experimentally.

In spICPMS, the detection limit in size depends on several factors such as the instrument sensitivity or the background noise level. Indeed, a chart proposed by Lee et al. (2014) summarizes the detection size limit for 40 elements including Ce and Ti where the minimum size for ^{140}Ce is around 10 nm, and for ^{49}Ti, around 80 nm. Among the several approaches tested by Tharaud et al. (2017) to reduce the Ca interference while measuring TiO_2 in solutions, we decided to use with a High-Resolution ICPMS). Furthermore, in the Loire River, a high concentration of calcium was measured (∼600 nmol L^{-1}) and this element has an isobaric interference with ^{48}Ti, the most abundant isotope of titanium (73.8%). Hence, the third most abundant isotope ^{47}Ti was chosen (7.3%) as suggested by Gondikas et al. (2014) who faced the same issue. This has a direct consequence on the smallest detected size which will be high for Ti (>80 nm).

FEG-SEM

A TESCAN MIRA 3 XMU Field Emission Gun – Scanning Electron Microscopy (FEG-SEM) was used for imaging particles collected on 0.2 μm filters using a secondary electron detector (Everhart-Thornley detector) and a YAG-doped scintillator backscattered electrons detector (Autrata type detector). Only pictures obtained with the backscattered electrons detector are shown in this study, as this detector highlights the compounds with an important averaged atomic number. Elemental analyses were performed by Energy Dispersive X-ray Spectroscopy (EDS) on the targeted particles in samples using an EDAX team system [ApolloXPP silicon drift detector (SDD)]. Samples were prepared as followed: freeze-dried suspended matters were dispersed in absolute ethanol, and ultrasonicated in a bath during 10 min. Samples were dispersed onto aluminum stubs and dried at 45°C in an oven for approximately 4 h. Afterward, samples were cleaned with an argon plasma cleaner (GAMBETTI Colibri) to remove traces of impurities. Then, samples were coated with a 1.5 nm layer of platinium-paladium using a CRESSINGTON 208HR sputter coater prior to SEM-EDS analyses. In each sample, between 5 and 10 particles containing the NPs of interest (Ti- or Ce-containing NPs) were identified by this technique, among over approximately 40 particles scanned per sample.

RESULTS

Evolution of the Water Chemistry Around Orleans City

Along the Loire River, the pH value remained relatively constant (8.07 ± 0.22), with a light increase in LS3 and LS4 (8.24) close to the WWTP outlet, with respect to LS1 measurement (7.71; **Supplementary Table S1**) whereas dissolved O_2 (8.82 mg L^{-1}), alkalinity (2.83 meq L^{-1}) and the NPOC concentration (4.43 ± 0.08 mg L^{-1}) remain constant. Besides, the conductivity was lower at LS3 (230 μS cm^{-1}) than at LS1 (248 μS cm^{-1}). Close to the outdoor activities center, in the lake connected to the Loire River (LS6 and LS7 sites), the chemical composition of the water presented significant contrasts with respect to the Loire River, particularly regarding the pH values (8.84 and 8.76 for LS6 and LS7, respectively), dissolved O_2 concentrations (13.76 mg L^{-1} and 11.81 mg L^{-1}), and NPOC concentrations (3.91 ± 0.05 mg L^{-1} and 3.79 ± 0.03 mg L^{-1}). The alkalinity and conductivity were also higher in LS7 where the values were found at 3.50 meq L^{-1} and at 261 μS cm^{-1}, respectively.

NPs Profile Along the Loire River

Figure 2 shows the particle number concentrations of Ce and Ti as well as the Ti/Ce ratio of particle number concentrations in Orleans city (**Figure 2A**) and in the lake dedicated to the outdoor activities center (**Figure 2B**), both compared with the upstream water (LS1) taken as site of reference.

The particle number concentration for Ce was measured at 6.4 ± 1.2 × 10^4 part mL^{-1} containing Ce at LS1, upstream Orleans city (**Figure 2A**). It rose up to 33.9 ± 3.4 × 10^4 part mL^{-1}, at LS3, before decreasing down

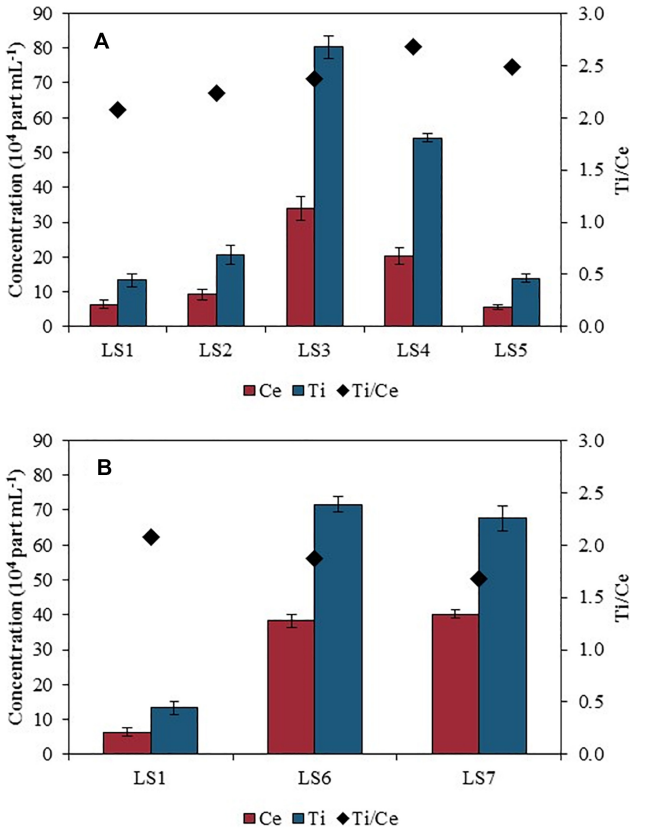

FIGURE 2 | Ce and Ti particle number concentration (PNC, left-hand side axis) and Ti/Ce PNC ratio (right-hand side axis) in the river water measured by spICPMS along **(A)** Orleans city (LS1 to LS5) and **(B)** in the outdoor activities center (LS6 and LS7 compared with LS1).

to 5.6 ± 0.7 × 10^4 part mL^{-1}, downstream the WWTP outlet (LS5). At LS6 and LS7 (**Figure 2B**), the particle number concentrations were high, similar to the concentration measured in LS3, with 38.3 ± 2.0 × 10^4 part mL^{-1} in LS6 and 40.3 ± 1.0 × 10^4 part mL^{-1} containing Ce in LS7.

A similar trend was obtained for Ti-bearing NPs with 13.4 ± 1.8 × 10^4 part mL^{-1} measured at LS1, and an increased concentration at LS3 with 80.3 ± 3.4 × 10^4 part mL^{-1}. Downstream, the concentration decreased with 14.0 ± 1.1 × 10^4 Ti-bearing part mL^{-1} detected, at LS5 (**Figure 2A**). Water samples collected at LS6 and LS7 contained 71.6 ± 2.1 × 10^4 part mL^{-1} and 67.7 ± 3.6 × 10^4 part mL^{-1} containing Ti, respectively (**Figure 2B**), which were significantly higher than the concentration found in the Loire River upstream section. The ratio of the particle number concentrations of Ti over Ce was also represented in **Figure 2**. The Ti/Ce ratio increased gradually downstream LS1, especially near LS4, but is lower in LS6 and LS7.

Making the assumption that particles were spherical and in oxidized states, spICPMS analysis for all sampling sites gave a CeO_2NPs equivalent size for sphere distributions ranging from 24 nm to 70 nm (**Figure 3**). For TiO_2NPs, the equivalent size for sphere distributions (**Figure 4**) ranged between 80 nm and 500 nm for all sampling sites.

Variation of Trace Elements Total Concentrations

Figure 5 shows the total concentrations (dissolved + particulate) of Ce and La measured in bulk samples after the acid digestion, at the different sampling sites from LS2 to LS5 in the Loire River (**Figure 5A**) and in the lake at LS6 and LS7 sampling sites, both compared to LS1 (**Figure 5B**).

Ce concentration increased from LS1 (2.29 ± 0.04 nmol L^{-1}) up to LS3 (7.48 ± 0.14 nmol L^{-1}), and then decreased at LS5 (1.99 ± 0.01 nmol L^{-1}). In the same way, La concentration rose up from LS1 (1.09 ± 0.02 nmol L^{-1}) to LS3 (3.52 ± 0.02 nmol L^{-1}). Then, the concentration decreased when reaching the downstream part of the studied area (0.92 ± 0.01 nmol L^{-1}). Regarding LS6 and LS7 sampling sites (**Figure 5B**), Ce concentration also increased (∼3.00 ± 0.05 nmol L^{-1}). On the contrary, La concentration measured in LS6 and LS7 remained approximately constant (∼1.30 ± 0.01 nmol L^{-1}).

The variations of Al and Ti total concentrations along the Loire River are displayed in **Figure 6**. Similarly to Ce concentration, Ti concentration increased from LS1 to LS3 (0.10 ± 0.01 and 0.68 ± 0.01 μmol L^{-1}, respectively) and then decreased downstream the Orléans city at LS5 (0.14 ± 0.00 μmol L^{-1}). In the water samples, concentrations in Al were higher than Ti concentrations, but the trend observed along the river was similar: a lower value at LS1 site with 2.10 ± 0.05 μmol L^{-1}, an increase in LS3 up to 18.05 ± 0.49 μmol L^{-1} and a decrease at LS5 site to 3.51 ± 0.06 μmol L^{-1}. In LS6 and LS7 (**Figure 6B**), both Ti and Al display concentrations higher than in LS1, with 0.15 ± 0.01 μmol L^{-1} and 0.34 ± 0.01 μmol L^{-1} for Ti in LS6 and LS7, respectively, and with 3.36 ± 0.05 μmol L^{-1} and 10.36 ± 0.22 μmol L^{-1} for Al in LS6 and LS7, respectively.

FEG-SEM Characterization

Figure 7 shows the particles observed with FEG-SEM imaging and analyzed by EDS for chemical composition.

At LS6 and LS7 sampling points, Ce-bearing particles were observed in the suspended matter. These particles displayed different sizes, typically ranging from 155 × 240 nm up to 850 × 1000 nm, as shown in **Figures 7A,B** for LS6 and LS7, respectively. It must be emphasized that these Ce-containing particles also contained some La, according to the EDS spectra. For all FEG-SEM observations (n = 56), sizes of the detected particles were bigger than the equivalent size for sphere distribution calculated by spICPMS.

Ti-bearing particles were observed in suspended matter of all the samples, as shown for the two sampling sites LS2 and LS3 in **Figures 7C,D**. In LS2, for example, an aggregate of NPs can be observed stick, or deposited, on the surface of a diatom. Actually, the aggregate was 560 nm large and 670 nm long and contained primary particles with sizes smaller than 100 nm. In **Figure 7D** (LS3), the Ti-bearing particles were usually larger (400 ± 50 nm) and longer (880 ± 50 nm). In addition to titanium, elements such as sodium, silicon, and iron were detected in the particles,

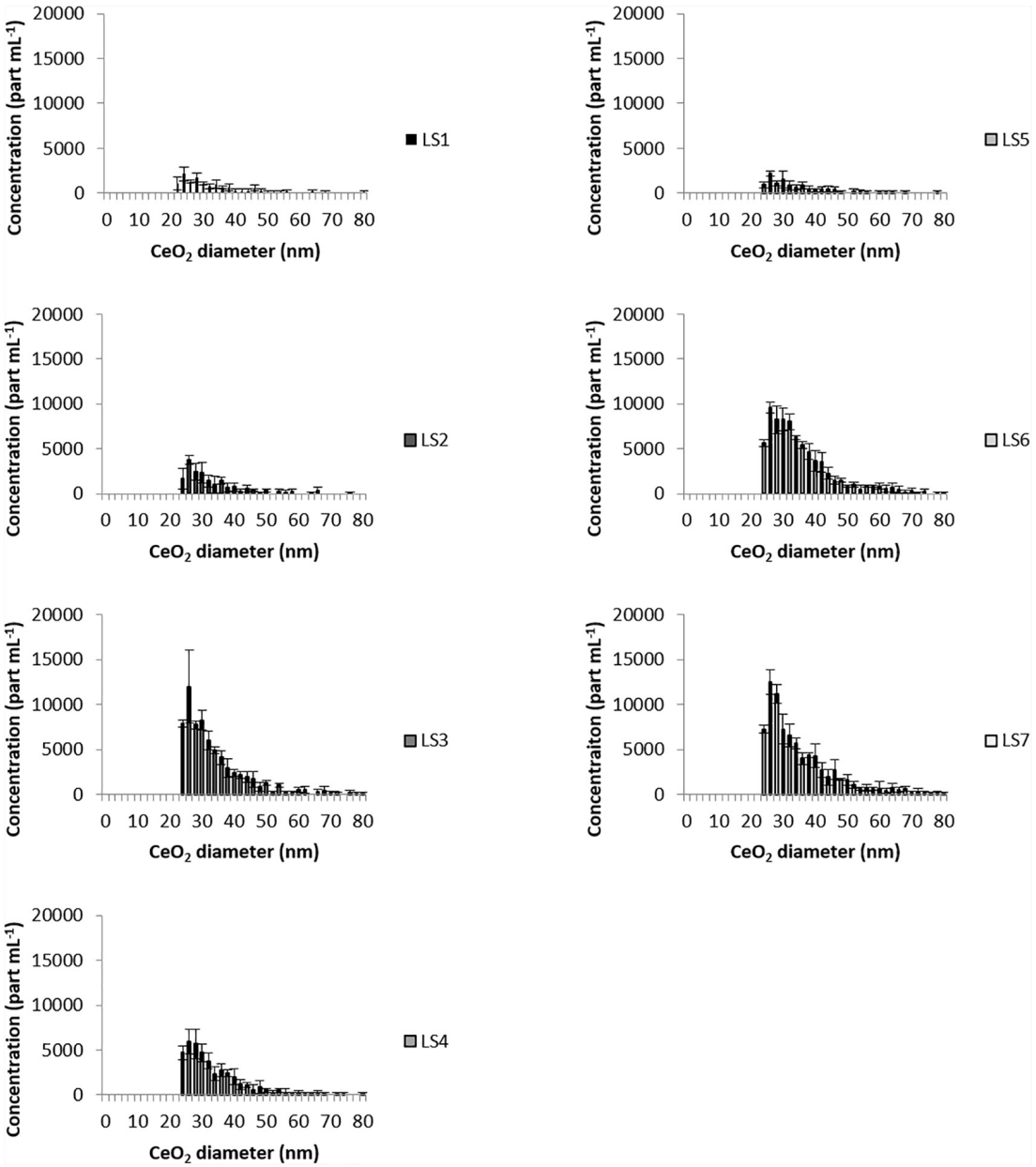

FIGURE 3 | Size distribution of CeO_2NPs in Loire River water samples.

as displayed in the EDS spectra. One has to notice that in each sample the detected NPs were aggregated or deposited onto larger structures such as mineral phases, and no individual NPs were observed in these samples.

DISCUSSION

Detection of CeO_2NPs and TiO_2NPs in the Loire River

Ce and Ti-bearing particles were truly observed by SEM-EDS in the Loire River waters and the associated particle number concentrations (PNC) determined by single counting ICPMS. The spICPMS measurements show an increase of the PNC for both Ce and Ti in the LS3 sampling point area, downtown Orleans city, which is close to the WWTP outlet (**Figure 2A**). Besides, an increase of the particle number concentrations is also measured for both elements at LS6 and LS7 (**Figure 2B**), as compared with the lower values at the upstream point (LS1). However, in spite of these high PNC, particles were rarely observed by SEM-EDS at the nanoscale size and more frequently at the microscale. This is partly explained by the occurrence of large mineral phases in SPM that can hide the NPs dispersed on the sample. In addition, the particles seem to undergo

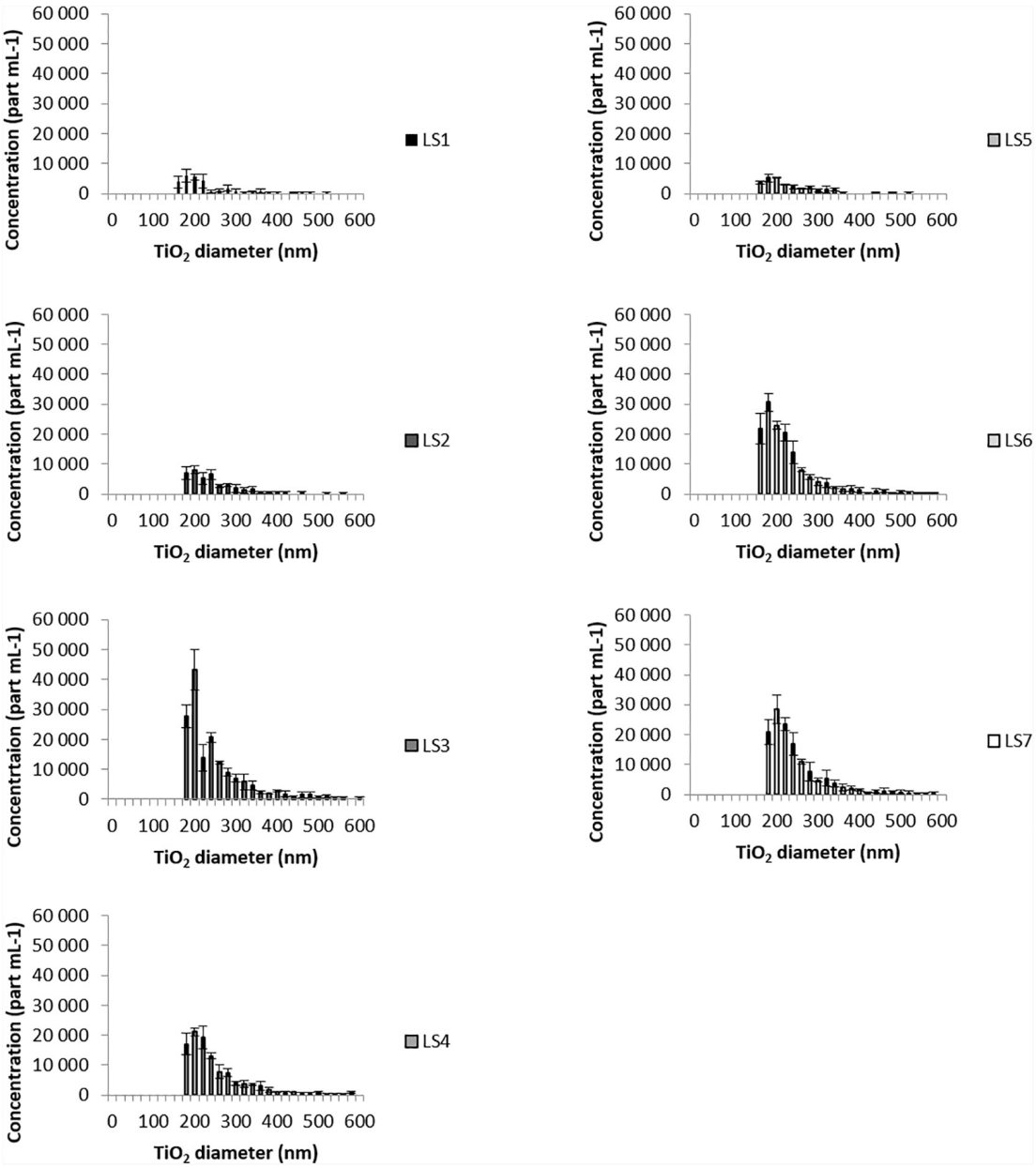

FIGURE 4 | Size distribution of TiO_2NPs in Loire River water samples.

heteroaggregation with these mineral phases. This can either happen naturally in the environment or be an artifact caused by the ethanol dispersion and drying process used for sample preparation. Additional tries were performed by direct deposition of bulk river water onto the stub (data not shown), in order to get rid of this potential artifact, but the formation of carbonates during the drying process makes the NPs detection even harder. Yet, more "nano" TiO_2 particles should be observed by SEM-EDS, since the equivalent size for sphere distributions (**Figure 4**) measured by spICPMS ranged between 80 nm and 500 nm for all sampling sites. This suggests that the PNC of TiO_2NPs in the river water is too low regarding the SPM content in river water, and thus inadequate for SEM-EDS. The spICPMS results display a CeO_2NPs equivalent size for sphere distributions ranging from 24 nm to 70 nm (**Figure 3**) and could not provide information about particles bigger than 100 nm, as those observed in the samples by SEM-EDS.

The size distributions of CeO_2NPs and TiO_2NPs (**Figures 3**, **4**) assessed with spICPMS are not Gaussian, as observed in most of the spICPMS studies where standards of monodispersed NPs are used (Laborda et al., 2011; Mitrano et al., 2012). In the present study, all the sampling sites display the same long tailed NPs size distribution. At least two populations of size can be observed for Ti in some samples (notably, LS3

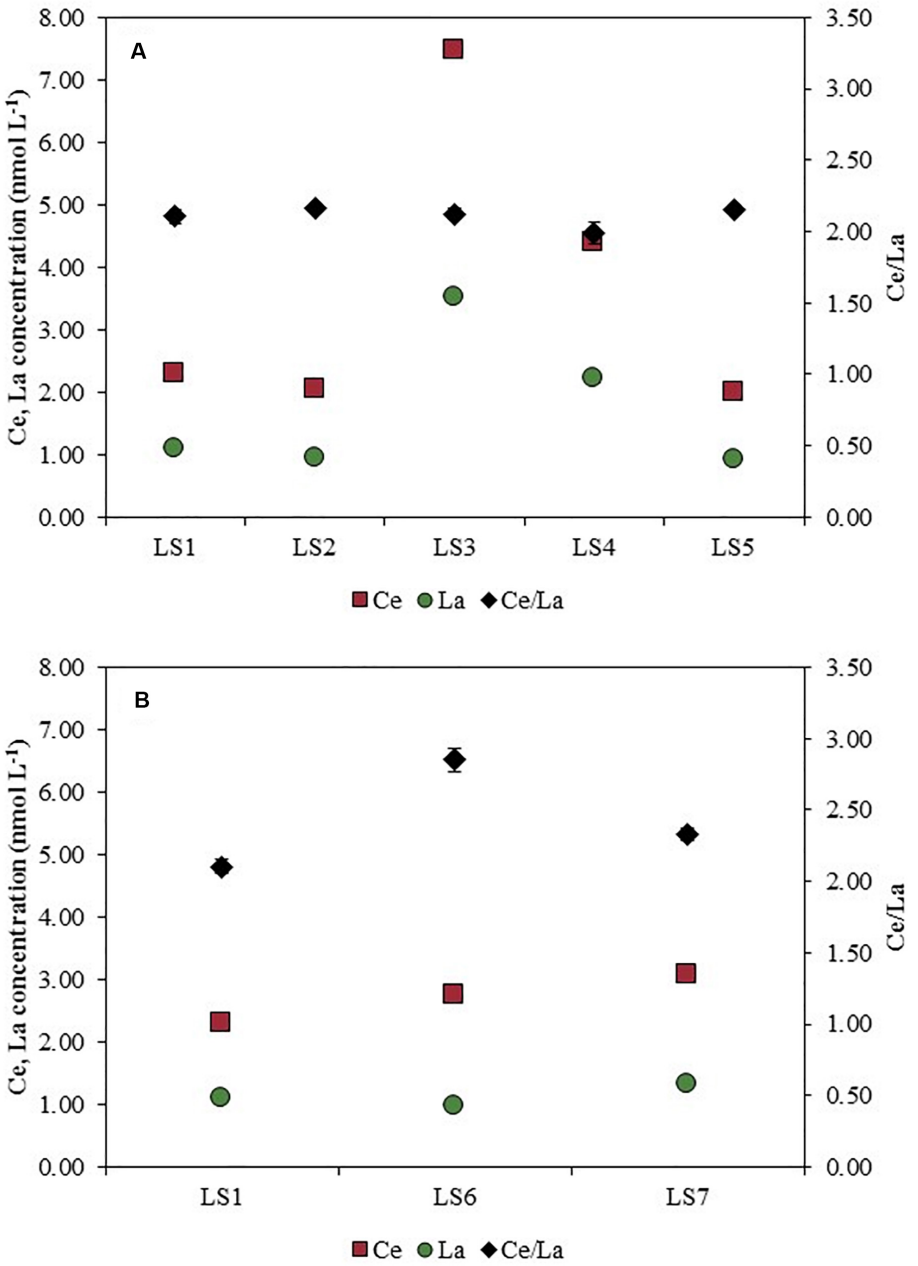

FIGURE 5 | Total Ce and La concentrations (left-hand side axis) and Ce/La ratios (right-hand side axis) along **(A)** Orleans city (LS1 to LS5) and in **(B)** the outdoor activities center (LS6 and LS7 compared with LS1) after an acid digestion.

sampling site), with equivalent size for spherical distributions from 80 nm to 200 nm and from 200 nm to 500 nm. These values are in the same order of magnitude than the ones determined by Lee et al. (2014) where the minimum equivalent sizes for sphere detected in a river water sample were estimated at 33 nm and at 186 nm, for CeO_2 and TiO_2, respectively. The instrument settings and ^{48}Ca-^{48}Ti interference, that prevent using the most abundant Ti isotope, are responsible for the high minimum equivalent size for sphere values and also for the shape of the diagram determined by spICPMS (Gondikas et al., 2014; Lee et al., 2014; Reed et al., 2017). The long tail observed for size distributions is also due to the occurrence of larger particles in the samples, as seen in the study of Reed et al. (2012) where the authors analyzed polydispersed samples by spICPMS. The hypotheses made during spICPMS data treatment (spherical NPs and in oxidized state) imply the indirect assumption that particles analyzed are anthropogenic. However, this latter hypothesis is weakened by SEM-EDS analyses that mostly displayed particles containing impurities and rather mixed with other natural phases: EDS analysis

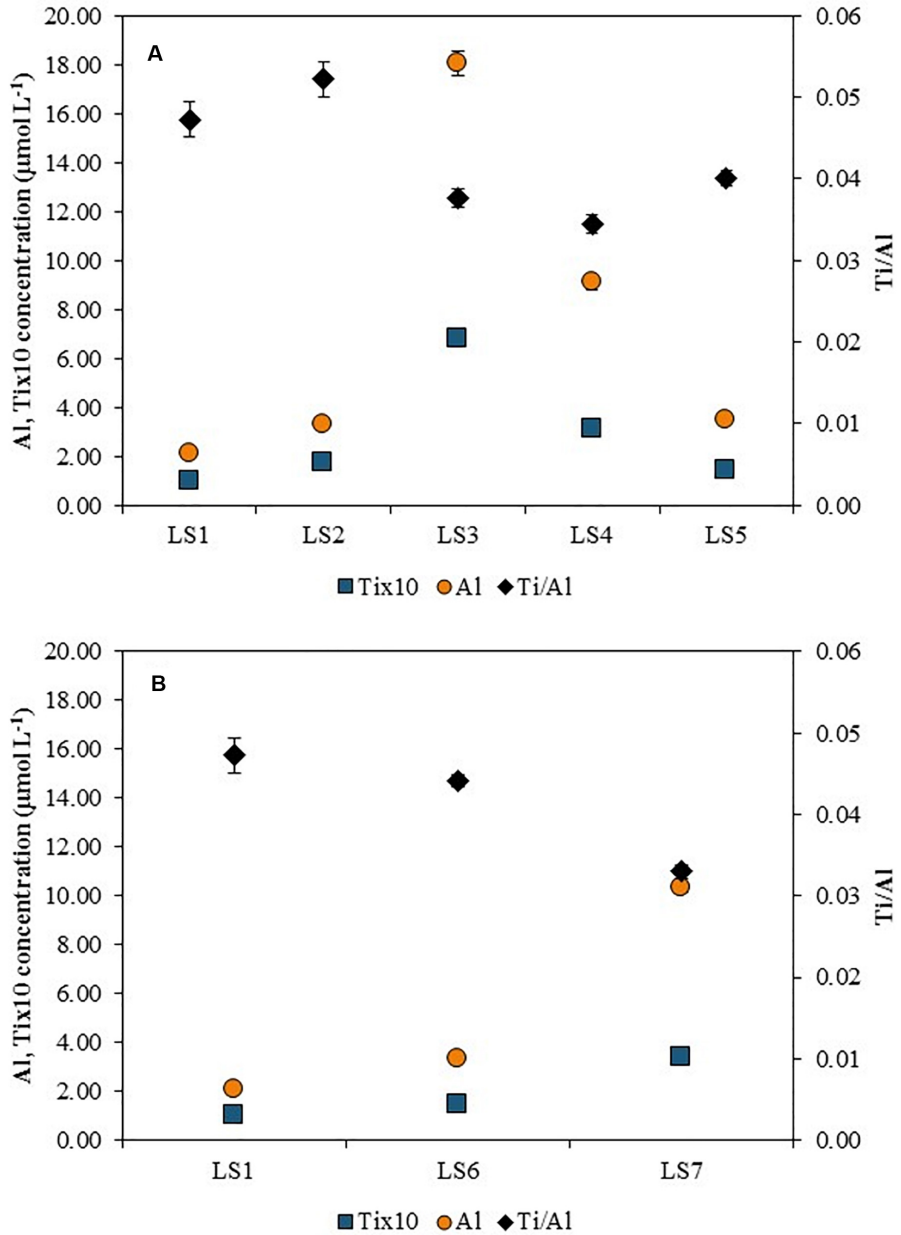

FIGURE 6 | Total Al and Ti concentrations (left-hand side axis) and Ti/Al elemental ratios (right-hand side axis) along **(A)** Orleans city (LS1 to LS5) and in **(B)** the outdoor activities center (LS6 and LS7 compared with LS1) after an acid digestion.

volume is typically larger than the particles size, and could have interacted with the surrounding substrate during measurements, thus showing additional elements that are not truly present in the analyzed NPs.

One question is the relative stability of the two types of NPs, which can be afforded through the Ti/Ce particle number concentration ratio and compared with LS1 upstream point. At LS1, the ratio is equal to 2. Then, Ti/Ce ratio rises up to 2.5 near LS3 showing an important contribution of Ti rather than Ce from the WWTP outlet. Conversely, as comparison with LS1 value, Ti/Ce ratio decreases at LS6 and LS7 (1.5) which indicates a major contribution of Ce from the outdoor activities center.

Influence of the Water Chemistry on the NPs Stability

Both the natural organic matter (NOM) and the ionic strength can play an important role on the stability of the NPs. Indeed, the NPOC concentrations were quantified at 4 mg L^{-1} showing the occurrence of NOM in the river waters. Besides, the NOM in the river can stabilize the ENPs released in the environment.

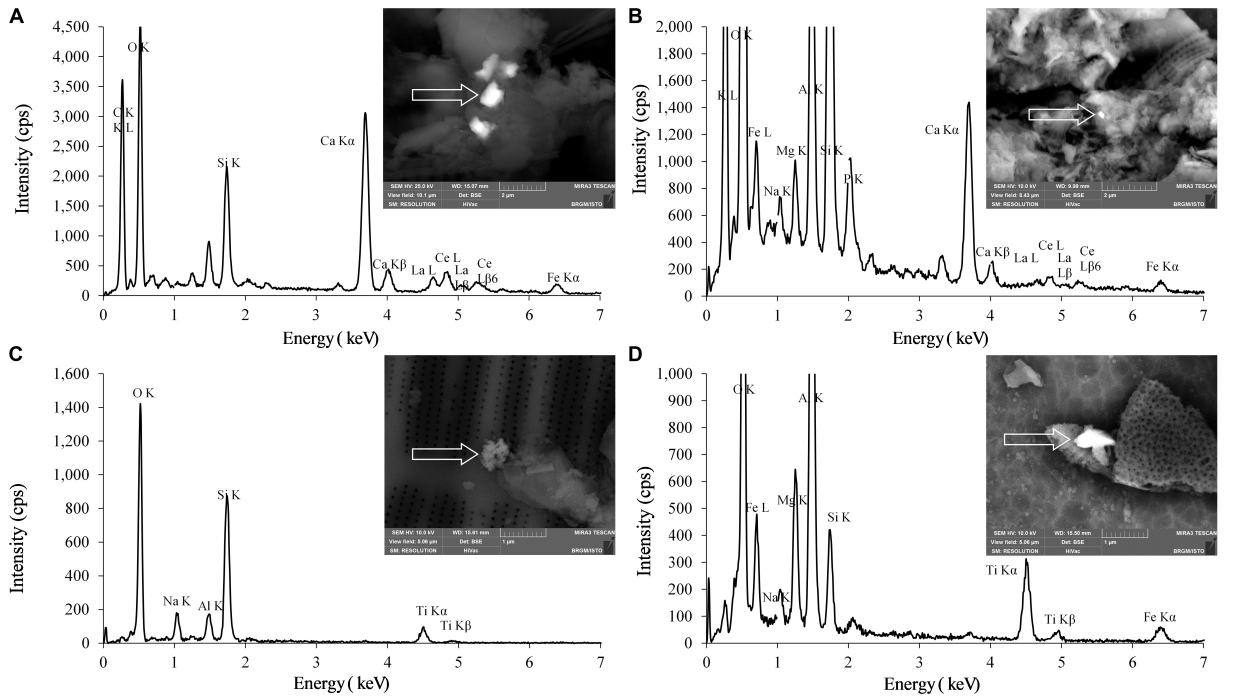

FIGURE 7 | FEG-SEM pictures of particles containing Ce and Ti and the associated EDS spectra on different sampling sites **(A)** LS6, **(B)** LS7, **(C)** LS2, and **(D)** LS3.

This is the case of TiO_2, ZnO, and CeO_2NPs which aggregates are stabilized at 300 nm with the occurrence of NOM in mesocosm freshwater (Keller et al., 2010). This heteroaggregation NPs-NOM can explain the high size value found in spICPMS and in SEM-EDS, especially for Ti-bearing particles. In another study, NOM stabilizes CeO_2NPs (from 2.2 mgC L^{-1} in an algal medium) and prevents the formation of larger aggregation of the NPs (>1 μm; Van Hoecke et al., 2011). Moreover, CeO_2NPs are supposed to be insoluble at pH higher than 7 (Dahle et al., 2015). In the case of the Loire River, the studied CeO_2NPs are supposed to be insoluble and are probably aggregated with sizes higher than 100 nm. They could not be detected by spICPMS but some particles with micrometer sizes were measured by SEM-EDS.

Contrary to LS3 water chemistry, the results show that in the Loire River, a particular chemistry is observed at LS6 and LS7 sampling points (**Supplementary Table S1**). For instance, ionic strength is determined at 2.50 mmol L^{-1} in LS3 water sample, which is similar to LS1 sampling point (2.65 mmol L^{-1}) but the values are higher for LS6 and LS7 (2.84 mmol L^{-1} and 2.97 mmol L^{-1}, respectively). The same observation can be done for the pH and the dissolved oxygen values. So, even if the outdoor activities center water comes from the Loire River, the water chemistry is particular at these sampling points. The ionic strength plays an important part in the stabilization state of the ENPs. Indeed, fast aggregation of TiO_2NPs can happen with an increase of the ionic strength (variation of the concentration of $CaCl_2$ from 0.01 to 0.1 mM; Thio et al., 2011). This could suggest that in the Loire River, TiO_2NPs are mostly aggregated in homoaggregation process. In a more realistic case, Gondikas et al. (2014) measured the hydrodynamic sizes of a TiO_2 cosmetic grade at mg L^{-1} level in MilliQ water, filtered lake water and unfiltered lake water as a function of time. They also suggested that TiO_2NPs undergo fast aggregation in the Danube water. However, for all the cited studies, the concentrations used in the experiment are higher than the one found in the environment (mg L^{-1} instead of μg L^{-1} or ng L^{-1}) which can have an importance on the behavior of the NPs studied in aquatic systems. Yet, homoaggregation is unlikely to happen in the Loire River and it was not observed in the SEM-EDS analyses but a heteroaggregation with mineral phases or NOM could occur more often. So, TiO_2NPs are expected to be aggregated with mineral phases since the aquatic system is relatively close to the Danube water.

Attempt for the CeO_2NPs and TiO_2NPs Origin Determination

The use of elemental ratios is the key for understanding the potential origins of these NPs (**Figures 5**, **6**). Indeed, Ce and La are often associated in the environment (Montaño et al., 2014; Dahle and Arai, 2015). For instance, Ce and La are present in natural minerals such as monazite [(Ce, La, Nd, Th, PO_4)] and natural NPs can originate from the weathering of such minerals. This association could be seen with the EDS spectra (**Figure 7**) where two particles among several analyzed were measured at different sizes but suggested that the particles are mainly from a natural origin. In **Figure 5A**, when compared to LS1 (Ce: 2.29 ± 0.04 nmol L^{-1} and La: 1.09 ± 0.02 nmol L^{-1}), the total concentrations of both Ce (7.48 ± 0.14 nmol L^{-1}) and La (3.52 ± 0.02 nmol L^{-1}) increased at LS3. The elemental ratio of Ce/La is also estimated at 2.10 ± 0.05 for LS1. From LS1

TABLE 1 | Elemental ratios of Ti over Al, V, and Y in the digested bulk samples.

	LS1	LS2	LS3	LS4	LS5	LS6	LS7
TI/AL	0.047 ± 0.002	0.052 ± 0.002	0.0380 ± .001	0.034 ± 0.001	0.040 ± 0.001	0.044 ± 0.001	0.033 ± 0.001
TI/V	4.28 ± 0.17	6.32 ± 0.26	17.39 ± 0.27	9.95 ± 0.24	5.52 ± 0.21	3.50 ± 0.04	6.39 ± 0.13
TI/Y	87.35 ± 3.60	117.10 ± 4.89	168.48 ± 4.34	110.34 ± 1.73	97.85 ± 1.91	145.43 ± 3.90	241.65 ± 4.23

to LS5, the elemental ratios are constant: an averaged value of 2.11 is found for these sampling sites. Consequently, along the Loire River, in Orleans city, several origins of Ce-bearing particles can't be distinguished and only a natural origin for CeO_2NPs is not excluded.

For LS6 and LS7 sampling sites, only the total concentration of Ce increased (2.76 ± 0.02 nmol L^{-1}), whereas the La total concentration decreased (0.97 ± 0.03 nmol L^{-1}). Moreover, the dissolved concentrations of Ce (0.03 ± 0.00 nmol L^{-1}) and of La (0.02 ± 0.00 nmol L^{-1}) are insignificant as comparison with the total concentrations of these elements showing that an important contribution originates from the particles (**Supplementary Table S2**). Besides, the elemental ratio of Ce/La rises up to 2.85 ± 0.08 in LS6 and reaches 2.33 ± 0.04 in LS7. At these sampling points, the high Ce concentration and the high Ce/La elemental ratio show the occurrence of anthropogenic Ce-bearing particles such as CeO_2NPs. This anthropogenic source can be explained by the cars present in the free access parking lot at the outdoor activities center where the NPs can originate from the catalytic converters, and from fuel additive (Piccinno et al., 2012) by indirect airborne contamination.

In **Figure 6**, for titanium, Ti/Al elemental ratio is studied because TiO_2 ENPs are often coated with an alumina layer to prevent TiO_2 ENPs to become harmful for our health, when incorporated into sunscreens (Serpone et al., 2007; Virkutyte et al., 2012). Actually, an acid digestion was also performed on three different TiO_2 ENPs and the Ti/Al elemental ratios were found equal to 4.1 ± 0.1, 5.3 ± 0.1, and 8.0 ± 0.1, consistently with the higher Ti content in the core relatively to the Al content in the coating.

Al total concentrations are higher than Ti total concentrations because of the important background of Al in the Loire River waters. An important increase of Al concentration is observed near LS3 (18.05 ± 0.49 μmol L^{-1}) which leads to a decrease of the Ti/Al elemental ratio (0.038 ± 0.001). The LS3 elemental ratio value is lower than the one calculated at LS1 (0.047 ± 0.002), which indicates an important release of Al at this sampling point, probably due to the WWTP outlet, where Al could be used as a flocculent in the WWTP process. Besides, the dissolved concentrations of Al and of Ti are negligible for all sampling points (**Supplementary Table S2**). For instance, at LS3, 0.30 ± 0.00 μmol L^{-1} are measured for Al dissolved concentration and 5.79 ± 0.05 nmol L^{-1} for Ti dissolved concentration. Since Al concentration is very high in LS3 sample water, the occurrence of Ti NPs is hidden while using these elemental ratios. Indeed, the spICPMS results show, at this sampling point, the highest Ti-bearing nanoparticles concentration in the Loire River (80.3 ± 3.4 × 10^4 part mL^{-1}).

The measured Ti/Al elemental ratios are very low in LS6 (0.044 ± 0.001) and LS7 (0.033 ± 0.001) sampling sites even if an increase of the particle number concentrations is measured (LS6: 71.6 ± 2.1 × 10^4 part mL^{-1} and LS7: 67.7 ± 3.6 × 10^4 part mL^{-1}). Here again, the occurrence of Ti-bearing nanoparticles is not excluded due to the high Al concentrations and the low Ti/Al ratios. However, the same order of magnitude has been observed in the Danube recreational lake with Ti/Al elemental ratios ranging from 0.04 to 0.055, during the bathing season (Gondikas et al., 2014) which is close to the results observed in the Loire River. Besides, as suggested by Gondikas et al., other elemental ratios can be used to assess the sources of the studied NPs such as Ti/V or Ti/Y because they can be associated with Ti in geogenic sample. In Gondikas et al. study, in the summer, 14.0 ± 4.8 and 182 ± 20 were calculated for Ti/V and Ti/Y ratios, respectively. By using these elemental ratios in the Loire River (**Table 1**), Ti/V ratio is the highest of all sampling points for LS3 sampling point, with 17.39 ± 0.27 value which is in the same order of magnitude than the ratio found in the Danube recreational lake (14.0 ± 4.8).

For Ti/Y, the ratios are also in the same order of magnitude than the one found in the Danube recreational lake. In the Loire River, two major increases of the elemental ratio were seen in LS3 (168.48 ± 4.34) and LS7 (241.65 ± 4.23), suggesting an anthropogenic origin of the NPs in these two sampling points, probably due to the use of sunscreens during this summer but also probably due to the whitening process near the WWTP outlet.

CONCLUSION

The occurrence of CeO_2NPs and TiO_2NPs was determined with the use of spICPMS and FEG-SEM imaging at relevant environmental concentrations, displaying the NPs in the Loire River with different equivalent size for sphere distributions (CeO_2: 24 nm to 70 nm; TiO_2: 80 nm to 500 nm). The use of elemental ratios (Ce/La) gave indications on the origins of the NPs, whether the NPs originated from natural process or from anthropogenic activities but it was not source-specific: only assumptions on the NPs origins could be made. Indeed, near the WWTP outlet, the occurrence of natural CeO_2NPs was determined (Ce/La elemental ratio stayed constant) whereas in the outdoor activities center, CeO_2NPs sources seemed to be anthropogenic since Ce/La elemental ratios increased, due to the cars in the parking lot. For TiO_2NPs, the origins could not be assessed with the use of Ti/Al ratios, due to the high concentration of Al in the Loire River, hiding the occurrence of TiO_2NPs in the river. Instead, Ti/V and Ti/Y

were assessed to complete the study showing an anthropogenic impact coming from TiO_2NPs (potentially related to the use of sunscreens during the summer and to the whitening process for the WWTP outlet). NPs containing Ce and Ti may also undergo heteroaggregation with larger mineral phases, which could also hide the occurrence of individual NPs in FEG-SEM analyses. Further investigations still need to be done on the other compartments of Earth such as the soils or the sediments to better characterize and understand the NPs cycle at relevant environmental concentrations. Moreover, other techniques should be used such as the single-counting Inductively-Coupled Plasma Time-of-Flight Mass Spectrometer (spICP-ToF-MS) method that allows detecting several elements in the same particle to better differentiate the natural NPs from the ENPs and determine their origins without much assumption.

DATA AVAILABILITY STATEMENT

The datasets presented in this study can be found in online repositories. The names of the repository/repositories and accession number(s) can be found in the article/ **Supplementary Material**. The remaining data will be made available on request to the authors.

AUTHOR CONTRIBUTIONS

KP was in charge of the sampling, analyses, and writing, and supervised and guided by MT and GW for spICPMS and MEB-FEG, respectively. YS conceived the presented idea, coordinated, and supervised the whole work with the help of MB and HP. XB and AG helped them supervising the project on the MEB-FEG and natural systems, respectively. All the authors discussed and wrote the final manuscript.

FUNDING

This research project "QUANTINANO" was fully supported by the Bureau de Recherche Géologique et Minière (BRGM) and Institut de Physique du Globe de Paris (IPGP) under the convention No. DAF/JAC/JUR/AS/no. 2013/422. Part of this work was supported by the IPGP multidisciplinary program PARI and by ParisŰIdF region SESAME Grant no. 12015908 and the ANR-18-IDEX-0001, IdEx Université de Paris.

ACKNOWLEDGMENTS

Our thanks go to Ms. Laure Cordier for the assistance she provided during various multi-elemental analyses.

SUPPLEMENTARY MATERIAL

The Supplementary Material for this article can be found online at: https://www.frontiersin.org/articles/10.3389/fenvs.2020.00141/full#supplementary-material

REFERENCES

Bi, X., Lee, S., Ranville, J. F., Sattigeri, P., Spanias, A., Herckes, P., et al. (2014). Quantitative resolution of nanoparticle sizes using single particle inductively coupled plasma mass spectrometry with the K-means clustering algorithm. *J. Anal. At. Spectrom.* 29, 1630–1639.

Camenen, B., Grabowski, R. C., Latapie, A., Paquier, A., Solari, L., and Rodrigues, S. (2016). On the estimation of the bed-material transport and budget along a river segment: application to the middle loire river. France. *Aquat. Sci.* 78, 71–81. doi: 10.1007/s00027-015-0442-3

Cary, L., Pauwels, H., Ollivier, P., Picot, G., Leroy, P., Mougin, B., et al. (2015). Evidence for TiO2 nanoparticle transfer in a hard-rock aquifer. *J. Contam. Hydrol.* 179, 148–159. doi: 10.1016/j.jconhyd.2015.06.007

Cornelis, G., and Hassellöv, M. (2014). A signal deconvolution method to discriminate smaller nanoparticles in single particle ICP-MS. *J. Anal. At. Spectrom.* 29, 134–144. doi: 10.1039/c3ja50160d

Dahle, J., and Arai, Y. (2015). Environmental geochemistry of cerium: applications and toxicology of cerium oxide nanoparticles. *Int. J. Environ. Res. Public Health* 12, 1253–1278. doi: 10.3390/ijerph120201253

Dahle, J. T., Livi, K., and Arai, Y. (2015). Effects of pH and phosphate on CeO2 nanoparticle dissolution. *Chemosphere* 119, 1365–1371. doi: 10.1016/j.chemosphere.2014.02.027

De, M., Ghosh, P. S., and Rotello, V. M. (2008). Applications of nanoparticles in biology. *Adv. Mater.* 20, 4225–4241.

Degueldre, C., and Favarger, P. Y. (2003). Colloid analysis by single particle inductively coupled plasma-mass spectroscopy: a feasibility study. *Colloids Surf. APhysicochem. Eng. Asp.* 217, 137–142. doi: 10.1016/s0927-7757(02)00568-x

Degueldre, C., and Favarger, P. Y. (2004). Thorium colloid analysis by single particle inductively coupled plasma-mass spectrometry. *Talanta* 62, 1051–1054. doi: 10.1016/j.talanta.2003.10.016

Degueldre, C., Favarger, P. Y., and Bitea, C. (2004). Zirconia colloid analysis by single particle inductively coupled plasma–mass spectrometry. *Anal. Chim. Acta* 518, 137–142. doi: 10.1016/j.aca.2004.04.015

Degueldre, C., Favarger, P. Y., Rosse, R., and Wold, S. (2006a). Uranium colloid analysis by single particle inductively coupled plasma-mass spectrometry. *Talanta* 68, 623–628. doi: 10.1016/j.talanta.2005.05.006

Degueldre, C., Favarger, P. Y., and Wold, S. (2006b). Gold colloid analysis by inductively coupled plasma-mass spectrometry in a single particle mode. *Anal. Chim. Acta* 555, 263–268. doi: 10.1016/j.aca.2005.09.021

Dhivert, E., Grosbois, C., Rodrigues, S., and Desmet, M. (2015). Influence of fluvial environments on sediment archiving processes and temporal pollutant dynamics (Upper Loire River, France). *Scie. Total Environ.* 505, 121–136. doi: 10.1016/j.scitotenv.2014.09.082

Donovan, A. R., Adams, C. D., Ma, Y., Stephan, C., Eichholz, T., and Shi, H. (2016a). Detection of zinc oxide and cerium dioxide nanoparticles during drinking water treatment by rapid single particle ICP-MS methods. *Anal. Bioana. Chem.* 408, 5137–5145. doi: 10.1007/s00216-016-9432-0

Donovan, A. R., Adams, C. D., Ma, Y., Stephan, C., Eichholz, T., and Shi, H. (2016b). Single particle ICP-MS characterization of titanium dioxide, silver, and gold nanoparticles during drinking water treatment. *Chemosphere* 144, 148–153. doi: 10.1016/j.chemosphere.2015.07.081

Figueres, G., Martin, J. M., Meybeck, M., and Seyler, P. (1985). A comparative study of mercury contamination in the Tagus estuary (Portugal) and major French estuaries (Gironde. Loire, Rhône). *Estuar. Coast. Shelf Sci.* 20, 183–203. doi: 10.1016/0272-7714(85)90037-x

Gondikas, A. P., von der Kammer, F., Reed, R. B., Wagner, S., Ranville, J. F., and Hofmann, T. (2014). Release of TiO2 nanoparticles from sunscreens into surface waters: a one-year survey at the Old Danube recreational lake. *Environ. Sci. Technol.* 48, 5415–5422. doi: 10.1021/es405596y

Gottschalk, F., Sun, T., and Nowack, B. (2013). Environmental concentrations of engineered nanomaterials: review of modeling and analytical studies. *Environ. Pollut.* 181, 287–300. doi: 10.1016/j.envpol.2013.06.003

Grosbois, C., Négrel, P., Fouillac, C., and Grimaud, D. (2000). Dissolved load of the loire river: chemical and isotopic characterization. *Chem. Geol.* 170, 179–201. doi: 10.1016/s0009-2541(99)00247-8

Hadioui, M., Merdzan, V., and Wilkinson, K. J. (2015). Detection and characterization of ZnO nanoparticles in surface and waste waters using single particle ICPMS. *Environ. Sci. Technol.* 49, 6141–6148. doi: 10.1021/acs.est.5b00681

Hirst, S. M., Karakoti, A. S., Tyler, R. D., Sriranganathan, N., Seal, S., and Reilly, C. M. (2009). Anti-inflammatory properties of cerium oxide nanoparticles. *Small* 5, 2848–2856. doi: 10.1002/smll.200901048

Hochella, M. F. Jr., Mogk, D. W., Ranville, J., Allen, I. C., Luther, G. W., and Marr, L. C. (2019). Natural, incidental, and engineered nanomaterials and their impacts on the Earth system. *Science* 363:eaau8299. doi: 10.1126/science.aau8299

Kahru, A., and Dubourguier, H.-C. (2010). From ecotoxicology to nanoecotoxicology. *Toxicology* 269, 105–119. doi: 10.1016/j.tox.2009.08.016

Keller, A. A., and Lazareva, A. (2014). Predicted releases of engineered nanomaterials: from global to regional to local. *Environ. Sci. Technol. Lett.* 1, 65–70. doi: 10.1021/ez400106t

Keller, A. A., Wang, H., Zhou, D., Lenihan, H. S., Cherr, G., Cardinale, B. J., et al. (2010). Stability and aggregation of metal oxide nanoparticles in natural aqueous matrices. *Environ. sci. Technol.* 44, 1962–1967. doi: 10.1021/es902987d

Laborda, F., Jiménez-Lamana, J., Bolea, E., and Castillo, J. R. (2011). Selective identification, characterization and determination of dissolved silver(I) and silver nanoparticles based on single particle detection by inductively coupled plasma mass spectrometry. *J. Anal. At. Spectrom.* 26, 1362–1371.

Lead, J. R., Batley, G. E., Alvarez, P. J. J., Croteau, M.-N., Handy, R. D., McLaughlin, M. J., et al. (2018). Nanomaterials in the environment: behavior, fate, bioavailability, and effects an updated review. *Environ. Toxicol. Chem.* 37, 2029–2063. doi: 10.1002/etc.4147

Lee, S., Bi, X., Reed, R. B., Ranville, J. F., Herckes, P., and Westerhoff, P. (2014). Nanoparticle size detection limits by single particle ICP-MS for 40 elements. *Environ. Sci. Technol.* 48, 10291–10300. doi: 10.1021/es502422v

Lima, J. F. D., Martins, R. F., Neri, C. R., and Serra, O. A. (2009). ZnO:CeO2-based nanopowders with low catalytic activity as UV absorbers. *Appl. Surf. Sci.* 255, 9006–9009. doi: 10.1016/j.apsusc.2009.06.071

Minaudo, C., Meybeck, M., Moatar, F., Gassama, N., and Curie, F. (2015). Eutrophication mitigation in rivers: 30 years of trends in spatial and seasonal patterns of biogeochemistry of the Loire River (1980–2012). *Biogeosciences* 2015, 2549–2563. doi: 10.5194/bg-12-2549-2015

Mitrano, D. M., Lesher, E. K., Bednar, A., Monserud, J., Higgins, C. P., and Ranville, J. F. (2012). Detecting nanoparticulate silver using single-particle inductively coupled plasma-mass spectrometry. *Environ. Toxicol. Chem.* 31, 115–121. doi: 10.1002/etc.719

Mitrano, D. M., Ranville, J. F., Bednar, A., Kazor, K., Hering, A. S., and Higgins, C. P. (2014). Tracking dissolution of silver nanoparticles at environmentally relevant concentrations in laboratory, natural, and processed waters using single particle ICP-MS (spICP-MS). *Environ. Sci.* 1, 248–259. doi: 10.1039/c3en00108c

Montaño, M. D., Badiei, H. R., Bazargan, S., and Ranville, J. F. (2014). Improvements in the detection and characterization of engineered nanoparticles using spICP-MS with microsecond dwell times. *Environ. Sci.* 1, 338–346. doi: 10.1039/c4en00058g

Navarro, E., Baun, A., Behra, R., Hartmann, N. B., Filser, J., Miao, A.-J., et al. (2008). Environmental behavior and ecotoxicity of engineered nanoparticles to algae, plants, and fungi. *Ecotoxicology* 17, 372–386. doi: 10.1007/s10646-008-0214-0

Négrel, P., Grosbois, C., and Kloppmann, W. (2000). The labile fraction of suspended matter in the Loire River (France): multi-element chemistry and isotopic (Rb–Sr and C–O) systematics. *Chem. Geol.* 166, 271–285. doi: 10.1016/s0009-2541(99)00225-9

Nowack, B., Baalousha, M., Bornhoft, N., Chaudhry, Q., Cornelis, G., Cotterill, J., et al. (2015). Progress towards the validation of modeled environmental concentrations of engineered nanomaterials by analytical measurements. *Environ. Sci. Nano* 2, 421–428. doi: 10.1039/c5en00100e

Nowack, B., and Bucheli, T. D. (2007). Occurrence, behavior and effects of nanoparticles in the environment. *Environ. Pollut.* 150, 5–22. doi: 10.1016/j.envpol.2007.06.006

Pace, H. E., Rogers, N. J., Jarolimek, C., Coleman, V. A., Higgins, C. P., and Ranville, J. F. (2011). Determining transport efficiency for the purpose of counting and sizing nanoparticles via single particle inductively coupled plasma mass spectrometry. *Anal. Chem.* 83, 9361–9369. doi: 10.1021/ac201952t

Peters, R. J. B., van Bemmel, G., Milani, N. B. L., den Hertog, G. C. T., Undas, A. K., van der Lee, M., et al. (2018). Detection of nanoparticles in Dutch surface waters. *Sci. Total Environ.* 621, 210–218. doi: 10.1016/j.scitotenv.2017.11.238

Piccinno, F., Gottschalk, F., Seeger, S., and Nowack, B. (2012). Industrial production quantities and uses of ten engineered nanomaterials in Europe and the world. *J. Nanopart. Res.* 14, 1109–1119.

Polesel, F., Farkas, J., Kjos, M., Almeida Carvalho, P., Flores-Alsina, X., Gernaey, K. V., et al. (2018). Occurrence, characterisation and fate of (nano)particulate Ti and Ag in two Norwegian wastewater treatment plants. *Water Res.* 141, 19–31. doi: 10.1016/j.watres.2018.04.065

Reed, R. B., Higgins, C. P., Westerhoff, P., Tadjiki, S., and Ranville, J. F. (2012). Overcoming challenges in analysis of polydisperse metal-containing nanoparticles by single particle inductively coupled plasma mass spectrometry. *J. Anal. At. Spectrom.* 27, 1093–1100.

Reed, R. B., Martin, D. P., Bednar, A. J., Montaño, M. D., Westerhoff, P., and Ranville, J. F. (2017). Multi-day diurnal measurements of Ti-containing nanoparticle and organic sunscreen chemical release during recreational use of a natural surface water. *Environ. Sci.* 4, 69–77. doi: 10.1039/c6en00283h

Serpone, N., Dondi, D., and Albini, A. (2007). Inorganic and organic UV filters: their role and efficacy in sunscreens and suncare products. *Inorganica Chim. Acta* 360, 794–802. doi: 10.1016/j.ica.2005.12.057

Sun, T. Y., Bornhoft, N. A., Hungerbuhler, K., and Nowack, B. (2016). Dynamic probabilistic modeling of environmental emissions of engineered nanomaterials. *Environ. Sci. Technol.* 50, 4701–4711. doi: 10.1021/acs.est.5b05828

Telgmann, L., Metcalfe, C. D., and Hintelmann, H. (2014). Rapid size characterization of silver nanoparticles by single particle ICP-MS and isotope dilution. *J. Anal. At. Spectrom.* 29, 1265–1272. doi: 10.1039/c4ja00115j

Tharaud, M., Gondikas, A. P., Benedetti, M. F., von der Kammer, F., Hofmann, T., and Cornelis, G. (2017). TiO2 nanomaterials detection in calcium rich matrices by spICPMS. A matter of resolution and treatment. *J. Anal. At. Spectrom.* 32, 1400–1411. doi: 10.1039/c7ja00060j

Thio, B. J., Zhou, D., and Keller, A. A. (2011). Influence of natural organic matter on the aggregation and deposition of titanium dioxide nanoparticles. *J. Hazard. Mater.* 189, 556–563. doi: 10.1016/j.jhazmat.2011.02.072

Tuoriniemi, J., Cornelis, G., and Hassellöv, M. (2012). Size discrimination and detection capabilities of single-particle ICPMS for environmental analysis of silver nanoparticles. *Anal. Chem.* 84, 3965–3972. doi: 10.1021/ac203005r

Van Hoecke, K., De Schamphelaere, K. A. C., Van der Meeren, P., Smagghe, G., and Janssen, C. R. (2011). Aggregation and ecotoxicity of CeO2 nanoparticles in synthetic and natural waters with variable pH, organic matter concentration and ionic strength. *Environ. Pollut.* 159, 970–976. doi: 10.1016/j.envpol.2010.12.010

Van Hoecke, K., Quik, J. T. K., Mankiewicz-Boczek, J., De Schamphelaere, K. A., Elsaesser, A., Van der Meeren, P., et al. (2009). Fate and effects of CeO2 nanoparticles in aquatic ecotoxicity tests. *Environ. Sci. Technol.* 43, 4537–4546.

Virkutyte, J., Al-Abed, S. R., and Dionysiou, D. D. (2012). Depletion of the protective aluminum hydroxide coating in TiO2-based sunscreens by swimming pool water ingredients. *Chemi. Eng. J.* 191, 95–103. doi: 10.1016/j.cej.2012.02.074

Wagner, S., Gondikas, A., Neubauer, E., Hofmann, T., and Von Der Kammer, F. (2014). Spot the difference: engineered and natural nanoparticles in the environment-release, behavior, and fate. *Angew. Chemie Int. Ed.* 53, 12398–12419.

Wang, J. L., Alasonati, E., Tharaud, M., Gelabert, A., Fisicaro, P., and Benedetti, M. F. (2020). Flow and fate of silver nanoparticles in small French catchments under different land-uses: the first one-year study. *Water Res.* 176:115722. doi: 10.1016/j.watres.2020.115722

Weir, A., Westerhoff, P., Fabricius, L., Hristovski, K., and von Goetz, N. (2012). Titanium dioxide nanoparticles in food and personal care products. *Environ. Sci. Technol.* 46, 2242–2250. doi: 10.1021/es204168d

Yang, Y., Long, C.-L., Li, H.-P., Wang, Q., and Yang, Z.-G. (2016). Analysis of silver and gold nanoparticles in environmental water using single particle-inductively coupled plasma-mass spectrometry. *Sci. Total Environ.* 563–564, 996–1007. doi: 10.1016/j.scitotenv.2015.12.150

Zhang, J., Kumagai, H., Yamamura, K., Ohara, S., Takami, S., Morikawa, A., et al. (2011). Extra-low-temperature oxygen storage capacity of CeO2 nanocrystals with cubic facets. *Nano Lett.* 11, 361–364. doi: 10.1021/nl102738n

Zhang, L., Gu, F., Chan, J., Wang, A., Langer, R., and Farokhzad, O. (2008). Nanoparticles in medicine: therapeutic applications and developments. *Clin. Pharmacol. Ther.* 83, 761–769. doi: 10.1038/sj.clpt.6100400

Conflict of Interest: The authors declare that the research was conducted in the absence of any commercial or financial relationships that could be construed as a potential conflict of interest.

frontiers in Environmental Science

ORIGINAL RESEARCH
published: 29 September 2020
doi: 10.3389/fenvs.2020.00151

Nanomaterial Fate in Seawater: A Rapid Sink or Intermittent Stabilization?

*Andreas Gondikas†, Julian Gallego-Urrea, Maurits Halbach†, Nicolas Derrien† and Martin Hassellöv**

Department of Marine Sciences, Kristineberg Marine Research Station, University of Gothenburg, Fiskebäckskil, Sweden

OPEN ACCESS

Edited by:
Vera I. Slaveykova, Université de Genève, Switzerland

Reviewed by:
Enrica Alasonati, Laboratoire National De Metrologie Et D'Essais, France
Peter H. Santschi, Texas A&M University, United States

***Correspondence:**
Martin Hassellöv
martin.hassellov@gu.se

†Present address:
Andreas Gondikas, Department of Geology and Geoenvironment, National and Kapodistrian University of Athens, Athens, Greece
Maurits Halbach, Carl von Ossietzky University of Oldenburg, Oldenburg, Germany
Nicolas Derrien, Université de Bordeaux, Talence, France

Specialty section:
This article was submitted to Biogeochemical Dynamics, a section of the journal Frontiers in Environmental Science

Received: *12 May 2020*
Accepted: *07 August 2020*
Published: *29 September 2020*

Citation:
Gondikas A, Gallego-Urrea J, Halbach M, Derrien N and Hassellöv M (2020) Nanomaterial Fate in Seawater: A Rapid Sink or Intermittent Stabilization? Front. Environ. Sci. 8:151. doi: 10.3389/fenvs.2020.00151

Coastal seas and oceans receive engineered nanoparticles that are released from nano-enabled consumer and industrial products and incidental nanoparticles that are formed as byproducts of combustion and friction. The marine environment is often perceived as a rapid sink for particles, because of the high salinity promoting the attachment between particles producing heavy agglomerates that sediment on the seafloor. In this work the effect of seasonal production of extracellular polymeric substances (EPS) on particle stability is tested using seawater collected from the Gullmarn fjord in the winter, spring, and summer. A novel approach is used that is based on light scattering of the bulk particle population for tracking agglomerates and of single particles for tracking particles smaller than approximately 300 nm. Results show that organic particles formed from EPS during algal blooms are capable of stabilizing nanoparticles in marine waters for at least 48 h. In contrast, particles agglomerate rapidly in the same seawater that has previously been filtered through 0.02 μm pore size membranes. Furthermore, particles with fibrillar shape have been detected using atomic force microscopy, supporting the argument that organic particles from EPS are responsible for the stabilization effect. These results suggest that seasonal biological activity can act as an intermittent stabilization factor for nanoparticles in marine waters.

Keywords: nanomaterials, fate, particle stability, marine water, extracellular polymeric substances

INTRODUCTION

Nanotechnology has enabled novel solutions in several sectors, from consumer products to high-tech industries and transportation. While these nano-enabled solutions are increasingly introduced in everyday life, there are more than 3,000 nano-enabled consumer products in the market[1] and numerous industrial and commercial products and parts currently in use[2]. The use and disposal of nano-enabled products and the incidental production of nanomaterials (e.g., through combustion or friction) will inevitably lead to their release in the environment and may pose a risk to human health and the ecosystem (Wiesner et al., 2006). Risk is a factor of the hazard assessment of a material to a certain organism and the level of exposure of the organism to the material. The former is an inherent parameter of the material, while the latter is largely dependent on the surrounding

[1]http://nanodb.dk/en/
[2]www.nanowerk.com

environment. For example, photocatalytic titania nanoparticles produce reactive oxygen species (ROS) when exposed to sunlight, which can be hazardous, but the amounts of ROS produced will depend on the factors determining the efficiency of photoexcitation (e.g., surface exposed or quenching effects) of particles exposed to sunlight (Sharma, 2009). In natural aquatic systems, such as seas and oceans, adsorption of organics and aggregation may drastically suppress the production of ROS (Carp et al., 2004). In addition, aggregation with suspended particulate matter will produce large aggregates that sink toward the seabed, thus reducing exposure to sunlight (Praetorius et al., 2020). It is therefore important to determine the fate of nanomaterials in the aquatic environment in order to assess their risk.

Engineered nanoparticles (ENPs) from nano-enabled consumer and industrial products may enter coastal seas and oceans through indirect routes after their use and disposal, e.g., effluent discharge from wastewater treatment plants and long-range atmospheric deposition (Linders et al., 2018). In this case, ENPs are likely to be significantly altered prior to entering the aquatic environment (Kaegi et al., 2011). Direct routes, such as emissions from shipping, water-based leisure activities, release of untreated wastewater, and other anthropogenic activities are more likely to release ENPs closer to their engineered form (Kaegi et al., 2017). When ENPs enter the environment, their fate will eventually determine their potential toxicity, a factor that has been ignored by many toxicological studies (Baalousha and Lead, 2013). It is therefore necessary to develop a clear understanding of those processes that regulate the fate of ENPs in the environment (Frimmel et al., 2007; Wiesner and Bottero, 2007). Several studies have been conducted on the fate and impact of ENPs in natural waters, such as rivers (Reed et al., 2017), lakes (Gondikas et al., 2014), and estuaries (Stolpe and Hassellöv, 2007). Fewer studies have focused on marine waters, because it is expected that ENPs would quickly aggregate and settle on the sediments.

Due to the high ionic strength of seawater, which suppresses the electrostatic repulsive forces between particles, it is often perceived that nanomaterials are likely to rapidly aggregate in marine waters. Aggregates are heavier than single nanoparticles and tend to sediment faster, and therefore sediments in seas and oceans are often perceived as sinks for the fate of ENPs. However, particle aggregation is strongly regulated by dissolved organic matter (Aiken et al., 2011) and marine waters host large scale biogeochemical processes in the earth's carbon cycle (Hedges, 1992), which involve massive amounts of organic compounds. Nutrient availability combined with increased sunlight and temperature in the spring trigger a rapid growth of phytoplankton and microorganisms (algal bloom), which in turn triggers zoo plankton grazing and viral activity, leading to dissolved organic matter release through exudates, sloppy feeding, and cell lysis (Tiselius and Kuylenstierna, 1996; Calliari and Tiselius, 2009). A fraction of the excreted organic matter forms extracellular polymeric substances (EPS) and may form larger entities that are operationally defined as transparent exopolymer particles (TEP), which is known to be correlated with the export of carbon when large structures are formed and sediment, sometimes called marine snow (Stolpe and Hassellöv, 2010). Such seasonal production and transformations of dissolved and colloidal organic matter has been shown to influence particle stability in the studied fjord (Waite et al., 2005) and may impact the fate of ENPs, as shown in lake water, where ionic strength is significantly lower than marine water (Ellis et al., 2018).

Another factor that is critical for the stability of particles in suspension is that the aggregation rate is proportional to the number concentration of the particles in the aqueous medium (Elimelech et al., 1995; Mylon et al., 2004). Marine waters contain significantly less suspended particles than river and estuary waters and aggregation may not be the primary process regulating the fate of ENPs. For example, Toncelli et al. (2017) found that it is dissolution and not aggregation that governs the fate of silver nanoparticles in seawater, at environmentally relevant particle concentrations. Terrestrial sources of ENPs in the sea include effluents of wastewater treatment plants, transport and deposition through wind, etc., while marine sources include cargo, leisure, and transportation ships. Maritime transport, in particular, is responsible for 90% of the world trade and release of ENPs from shipping (e.g., from antifouling paints) is likely to be gradual and in small amounts but impacting very large areas.

In this work, the hypothesis is tested that organic matter produced during the algal bloom may act as steric stabilizers for nanomaterials and overcome the suppression of electrostatic repulsion caused by the high ionic strength of seawater. Combined with the low concentration of natural suspended particles, the result is an extended stability of ENPs in the water column. In order to test this hypothesis, seawater was sampled and filtered sequentially through membranes with decreasing pore size to remove larger and smaller particles and organic matter that are naturally present in the seawater. Gold ENPs were then spiked in the different water fractions and the aggregation behavior of the particles over long periods, up to 2.5 days was monitored. Although sedimentation is an important process for the fate of ENPs in aquatic systems, in this work focus is given to aggregation processes.

MATERIALS AND METHODS

Seawater Sampling and Treatment

Seawater samples were collected from the Gullmarn Fjord in Sweden (approximate coordinates: 58°15′19.8″N 11°25′44.0″E) using a 2 L Ruttner water sampler (KC Denmark A/S). The sampler was filled sequentially with seawater at 1 m depth and decanted in pre-cleaned Nalgene barrel until 10 L were collected. The barrel was rinsed twice with seawater prior starting sample collection. Historical monitoring data from the sampling location have shown that there are elevated values of Chlorophyll-a during the spring bloom (typically late February to mid March), and summer blooms (more spread out in time, typically from July to September). Sampling took place during three separate seasons: (i) spring (March 21, 2016) representing the end of the spring bloom, (ii) winter (February 17, 2017) representing the beginning of the spring bloom following winter inactivity, and (iii) summer

(June 27, 2017) representing the more spread out summer blooms. No later than 1 h after sampling, the seawater was transferred to the lab and 5 L were gravity filtered through 5 μm mixed cellulose membrane (SMWP Millipore) to remove most microorganisms that may alter the composition of the organic matter in the seawater during storage. Prior to this first filtration step, the filters were rinsed by flowing 1 L of MQ water across the membrane. The seawater filtrate (labeled "micro-seawater," μSW) was stored at 5°C until further use. From the μSW, 2 L were filtered through 0.45 μm hydrophilic polyvinylidene fluoride (PVDF) membrane (HVLP Millipore) and this filtrate was labeled "submicron seawater" (sμSW) and was collected in polycarbonate containers (Nalgene). Subsequently, 0.5 L from the sμSW were filtered through a 0.02 μm alumina based (Anopore) membrane in a polypropylene housing (Whatman) and the filtrate was labeled "nano seawater" (nSW) and was collected in polycarbonate bottles.

ENP Aggregation Studies

The three seawater fractions (μSW, sμSW, and nSW) were spiked and thoroughly mixed with 30 nm Au ENPs to reach a total Au concentration in the test suspensions of 56 μg/L. This concentration was chosen to represent the higher end of the expected concentrations of nanomaterials in surface waters (Gottschalk et al., 2009). Detailed characterization of the Au ENPs used are given in Gallego-Urrea et al. (2016). Artificial seawater (ASW) was synthesized in the laboratory and spiked with Au ENPs, under the same conditions as for the filtered seawater fractions. Preliminary tests conducted under continuous stirring in a jar test apparatus showed no effect of stirring on aggregation, thus experiments were conducted in idle 50 ml polypropylene centrifuge tubes. Two replicates were prepared for each type of water matrix. Aggregation in the spiked waters was monitored by measuring the intensity-based hydrodynamic diameter with dynamic light scattering (DLS), (Zetasizer S, beam wavelength 532 nm, Malvern instruments) and the number concentration and hydrodynamic diameter of particles (including individual scattering intensity) in suspension using nanoparticle-tracking analysis (NTA), (NanoSight LM10, Malvern instruments; software NanoSight 2.3, threshold 18, gain 7). Prior to each measurement, the ENP suspension was gently mixed end over end and 1 mL was removed for DLS and NTA analysis, each.

The diffusion tracks recorded by the NanoSight software were analyzed and 2D histograms of particle size distribution and particle intensity distribution were obtained and normalized by the number of recordings (Gallego-Urrea et al., 2016) in order to allow comparison (Figure S1 in the SI). From **Figure 3**, the intensity-size signal from AuNP is distinguishable from the signal coming from other natural particles or aggregates, although there is not such a strong difference in intensity as observed in other works (Gallego-Urrea et al., 2016); this is probably due a combination of two factors: (i) the settings chosen during measurements to maximize the number of particles tracked and (ii) the presence of particles with relatively high scattering efficiency in the natural waters used here as compared to model particles used in Gallego-Urrea et al. (2016). Nevertheless, after visual identification of areas in the 2D histogram, it was possible to divide the histograms in three zones: the sum of all tracks encompassed by an ellipse between 10 and 60 nm hydrodynamic diameter and 0–4 intensity units (called "original"), a bigger ellipsoid covering the area not overlapping with the "original" ellipsoid between 10 and 300 nm and 2–9 intensity units ("Aggregates") and a third one summing the rest of particles called "Large" (**Figure 3**).

Atomic force microscopy (AFM) (Nanoscope IIIA, Digital Instruments) was used to image the physicochemical structure of the aquatic colloids and especially applied to investigate the presence of fibrillary biopolymers. Prior to analysis, 50 mL of the seawater fraction were placed in a polypropylene tube and a thin sheet of mica glass (approximate area 5 mm × 5 mm) was inserted for 2 h, allowing organics and particles to attach on the mica surface. The mica sheet was then removed and dipped in MQ water three times to rinse off the salts. Excess water was removed by touching a fiber-free paper (Kimwipe) and the mica sheet was stored in pre-cleaned polypropylene container. During analysis with AFM, random areas of the mica sheet were scanned.

RESULTS AND DISCUSSION

The intensity of scattered light measured with DLS (counts per second) on the collected seawater indicates that filtration with decreasing membrane pore size resulted in the removal of natural particles and organic matter that are larger than the membrane pore size. The largest difference was observed in seawater collected during the summer. Seawater filtered through 5 μm membranes (μSW) gave the highest background signal intensity in DLS (represented by the mean count rate in **Figure 1**, left) compared to seawater filtered through 0.45 μm (sμSW) and 0.02 μm (nSW). Background signal from nSW was at the same level as the instrument noise, indicating the absence of natural particles smaller than 20 nm that may scatter light. The same was observed for nSW, sμSW, and μSW of winter and spring water. The background signals from sμSW and μSW indicate the presence of natural particles from the algal bloom, most likely TEP precursors and other organic matter that are results of the seasonal biological activity. Spiking with Au ENPs more than doubled the scattering intensity of the suspension and, independently of the seawater fraction, the size of Au ENPs rapidly increased immediately after spiking. The intensity-based hydrodynamic diameter increased from 40 nm (ENPs in MQ water) up to 120 nm as soon as the particles got in contact with the seawater medium, likely caused by homoaggregation of the Au ENPs and attachment of natural particles and organic compounds on their surface. In summer nSW, the hydrodynamic diameter of the Au ENPs is gradually increasing over the time-span of 5 h (**Figure 1**, right), indicating a slow homoaggregation process that is the result of the high ionic content of the water and the low number of particles present. On the contrary, the hydrodynamic diameter of the Au ENPs in sμSW and μSW increase to approximately 120 nm within the first 10 min (not captured by the DLS measurements) and then increase with a slower rate compared to nSW. This behavior is indicative of

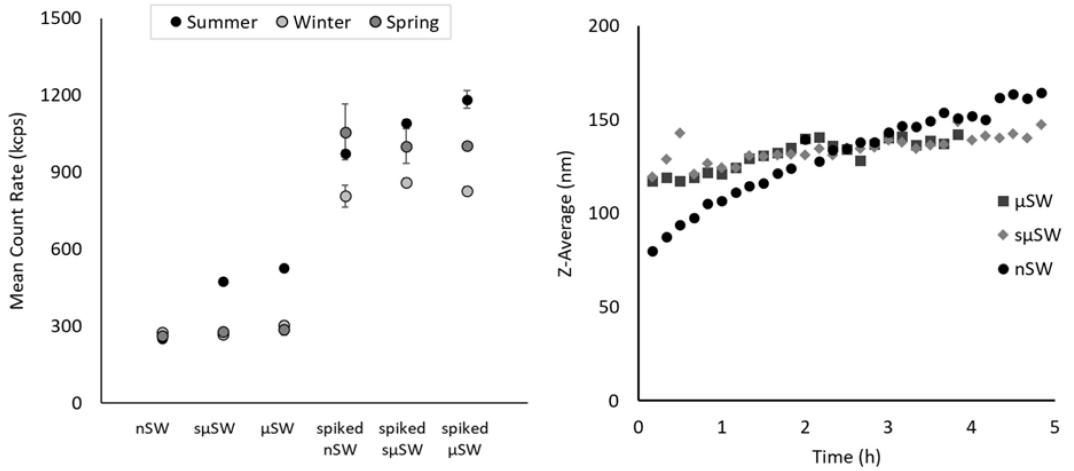

FIGURE 1 | Intensity of scattered light (measured with DLS) for nSW, sμSW, and μSW before and after spiking with Au ENPs in seawater collected during the summer, winter, and spring season **(left)**. Marker and error bars for non-spiked samples represent the average and standard deviation of three measurements, while marker and error bars for spiked samples represent the average and deviation between duplicate measurements. Intensity-based hydrodynamic diameter (Z-average) of summer seawater spiked with Au ENPs within 5 h from the time of spiking **(right)**.

a heteroaggregation process resulting in particles coated with organic compounds (corona formation) that are more stable than the bare particles (Liu et al., 2013).

Prolonged aggregation studies (up to 58 h after spiking with Au ENPs) showed that the hydrodynamic diameter of the suspensions continues to increase (**Figure 2**). Due to the absence of stabilizing factors, aggregation rates observed in nSW from all seasons were higher than those observed for the other fractions and similar to ASW. DLS is a technique measuring the size distribution of the bulk suspension and is highly sensitive to the presence of larger particles, since the intensity of scattered light is dependent on the particle diameter to the power of six (Schurtenberger and Meredith, 1993; Hassellov et al., 2008; Gallego-Urrea et al., 2014; Gondikas et al., 2019). As aggregation proceeds, the formation of larger aggregates will dominate the Z-Average values reported by DLS, overshadowing the original monomer particles and smaller aggregates. The aggregation process that was observed with DLS (**Figure 2**) is therefore indicative of the rate of formation of large aggregates (up to 1 μm). On the other hand, NTA is a single particle technique and is thus sensitive to the number concentration of the suspended particles. The larger aggregates reported by DLS are few in number and are thus rarely detected by NTA. Therefore, this technique was used to follow the particle population of smaller particles (10–300 nm), i.e., the monomer Au ENPs that were spiked in the seawater and small aggregates. In addition to the particle size and number concentration that is typically reported from NTA measurements, the intensity of scattered light and particle size was used (**Figure 3**) to differentiate between the Au NP monomers smaller than 60 nm (original), small aggregates of Au ENPs and natural particles less than 300 nm (aggregates), and larger particles and aggregates (large), as shown in **Figure 3**. Since the intensity and size are reported on a single particle basis, the bias toward larger particles posed by DLS is overcome.

A higher number of background particles (prior to spiking) was found in the summer samples, compared to the spring and winter (**Figure 4**, background), which is in agreement with DLS measurements. These particles are for the most part removed in the nSW. In ASW (**Figure 4**, left column) there is an increase of particle size with time, which plateaus after 7 h. The simultaneous decrease of the number concentration of particles (original, aggregates, and large) indicates that particles continue to aggregate into large particles, not captured by NTA.

In μSW and sμSW of the summer water (**Figure 4**, right column) populations of original, aggregate, and large particles were observed that are fluctuating around higher values, both in terms of number and size. Only in nSW a similar behavior to ASW was observed, where the number concentration decreases with time, indicating the formation of larger aggregates. This was observed in nSW from all seasons. In the μSW and sμSW of spring and winter water a similar behavior as in nSW and ASW was observed, with the number concentrations of all groups of particles decreased with time.

Overall, the NTA data shows that particles in the size range of 10–300 nm tend to disappear with a faster rate in the winter than in spring and they may remain suspended for periods of time longer than 2 days in the summer. The experiments were conducted in three aquatic colloid size fractions (μSW, sμSW, and nSW) show that background particles are responsible for the slower aggregation rates of Au ENPs. In order to elucidate the shape and size of these particles, AFM analysis was conducted on spiked and non-spiked waters. Several fibrils with lengths of 200–500 nm and width of 1.5–2.5 nm were detected in sμSW samples, along with some longer fibrils with lengths of more than 2 μm (**Figure 5**). These particles are likely products of the algal bloom, such as TEP and its precursors. Fibrillar shaped biopolymers have been reported with AFM previously (Santschi et al., 1998; Verdugo et al., 2004), and also from the

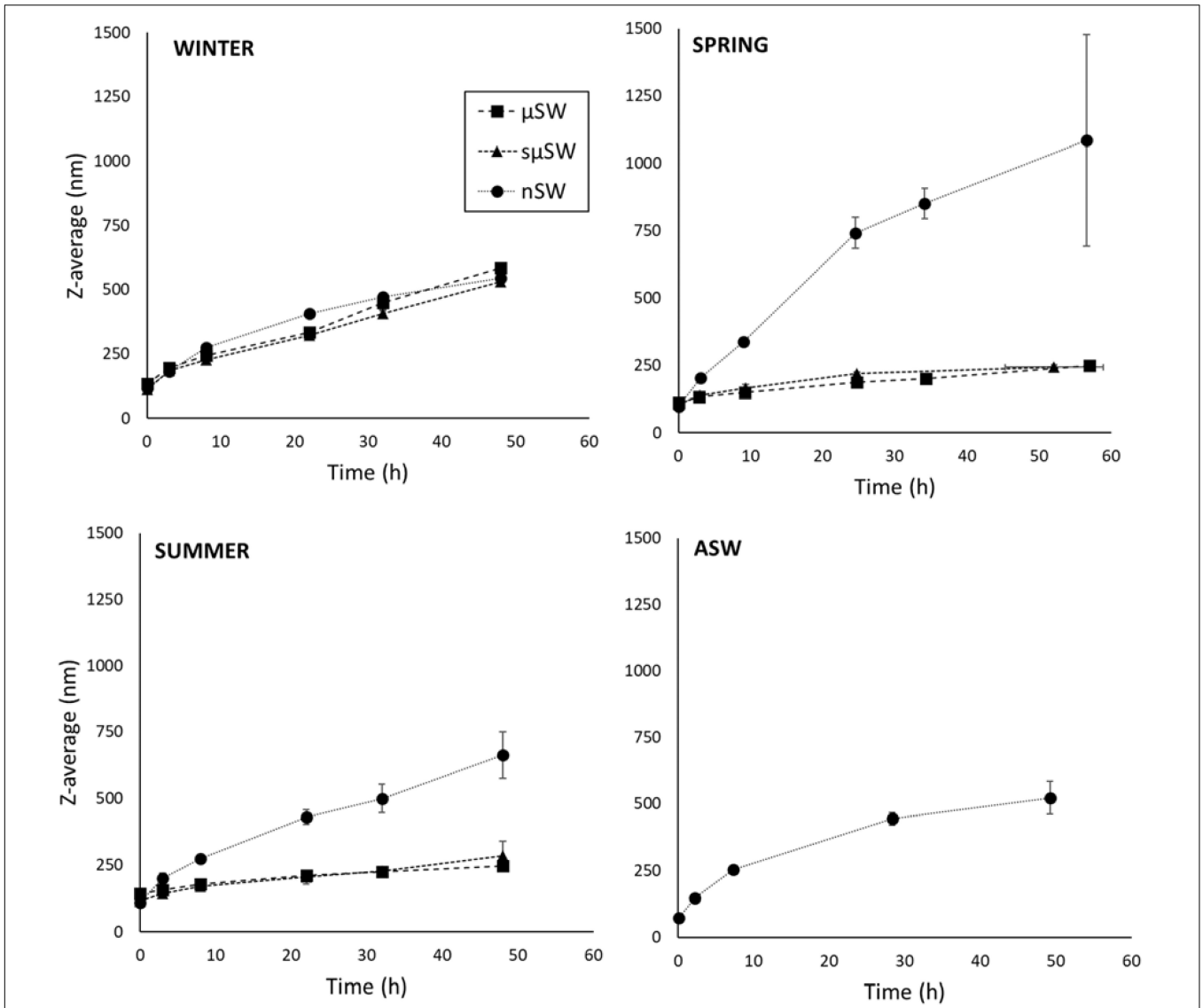

FIGURE 2 | Z-average measured with DLS over time for Au ENPs in seawater collected during the winter, spring, and summer and filtered through 5 μm (μSW), 0.45 μm (sμSW), and 0.02 μm (nSW) pore size membrane. Identical experiments in artificial seawater (ASW) are also shown.

same location (Stolpe and Hassellöv, 2010). The physicochemical structure and dynamics of such biopolymers from marine algae and bacteria has been proposed to conform to the dynamics of a gel system (Chin et al., 1998). Nanoparticle aggregates attached to fibrils were also observed due to their spherical shape and size. Physicochemical conditions regulate how free nanoparticles and homoagglomerates can adhere to microgels and large gel structures leading to the sedimentation process known as TEP or marine snow (Passow, 2002). The observations here provide plausible explanations that depending on season in any given marine biogeochemical domain, the rate of homoagglomeration for specific nanomaterials in the high ionic strength conditions is not only driving the ENP fate but as important is the interplay of free and agglomerated ENP with the marine biopolymers and its dynamics.

CONCLUSION

Here, a novel approach was used to study the aggregation process of ENPs in surface water collected from the field, combining DLS to detect the formation of large aggregates and NTA to track the number concentration and size distribution of particles, while distinguishing between ENPs, natural particles, and their aggregates based on their scattering intensity. The occurrence, shape and size of organic fibrils that has been reported in the literature was verified in our samples with AFM. The chemical composition of seawater induces rapid aggregation in nano-filtered and ASWs, due to the high ionic strength and suppression of the electric double layer (EDL) on the particles surface. It is therefore often perceived that ENPs will rapidly aggregate and sediment to the seafloor.

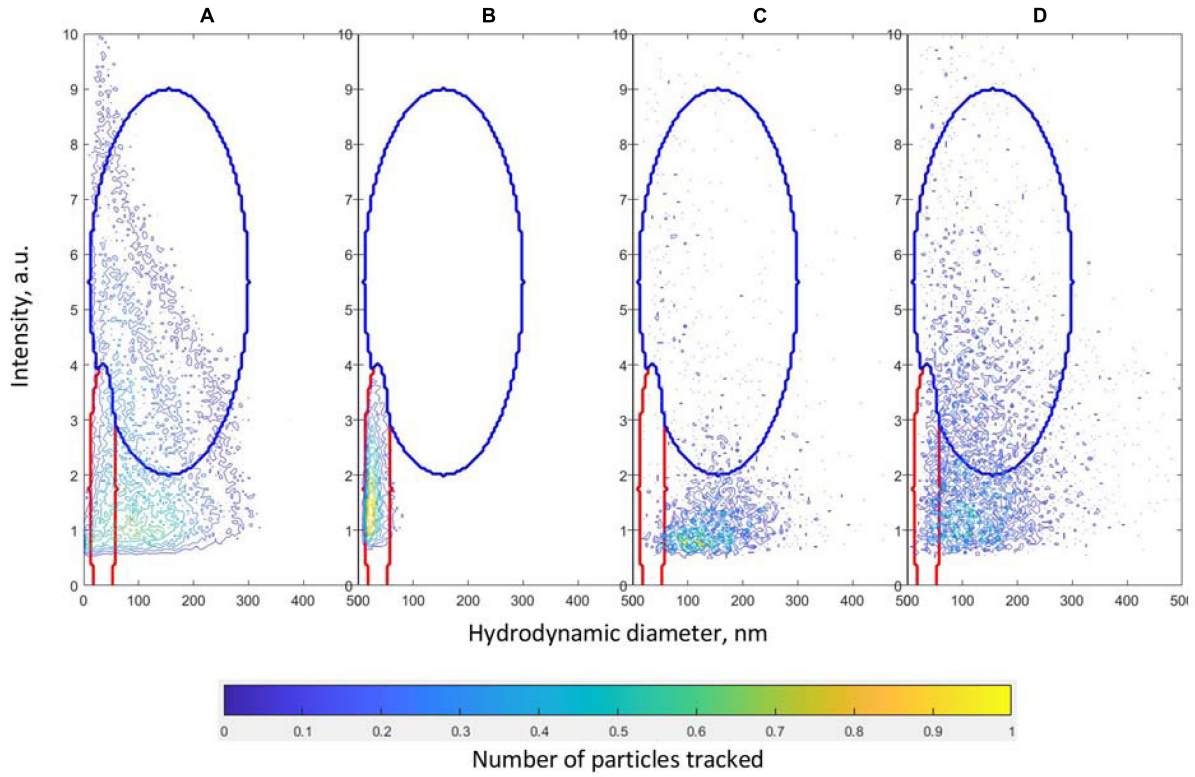

FIGURE 3 | Areas selected for estimating the concentration of particles from NTA measurements according to size and intensity. The inner red ellipse corresponds to "original" particles; the outer purple ellipse corresponds to "aggregates" particles, as described in the text. The contour plots correspond to the following samples, discriminated by size and intensity: **(A)** the average of all particles measured in the experiments (154 samples), **(B)** one replicate from the AuNP spiked in milli-Q water (number of particles tracked scaled by 10 to facilitate comparison), **(C)** one replicate of the summer sample μSW (background signal) and **(D)** one replicate for the spiked summer sample μSW taken at time 0.

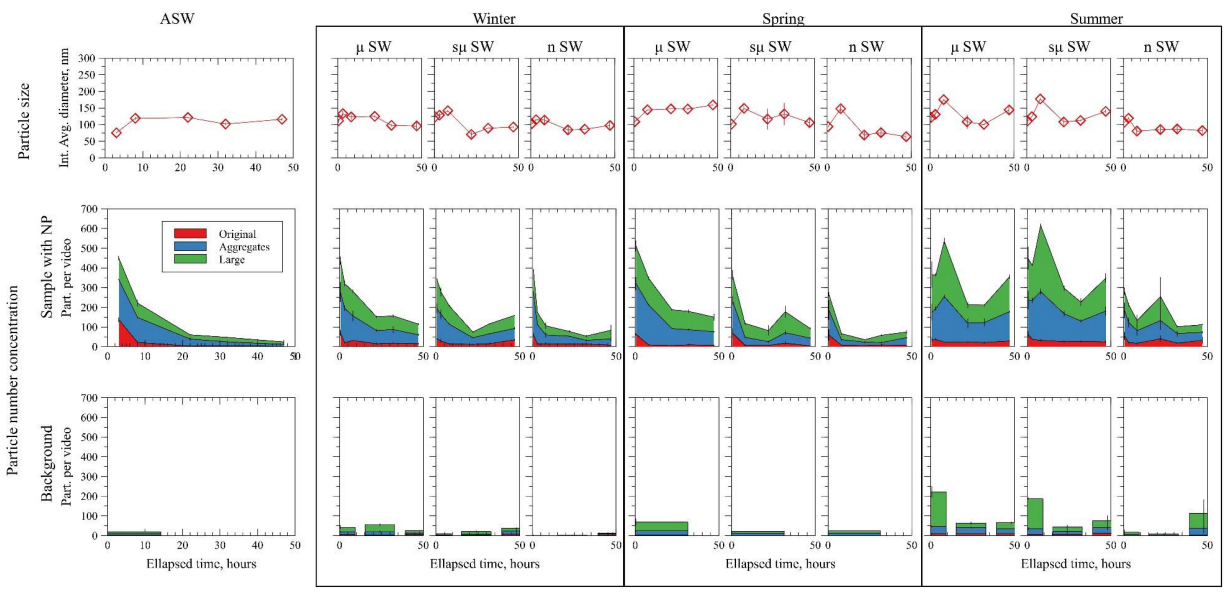

FIGURE 4 | Evolution in time of the intensity averaged diameter from NTA, concentration of particles from NTA in samples with AuNP and in the background. Original, aggregates and large particles are described in the text and **Figure 3**. Two replicates of the fractionated samples (nSW, suSW, and uSW as explained in text) are presented. Background samples (without AuNP spike) are presented when available.

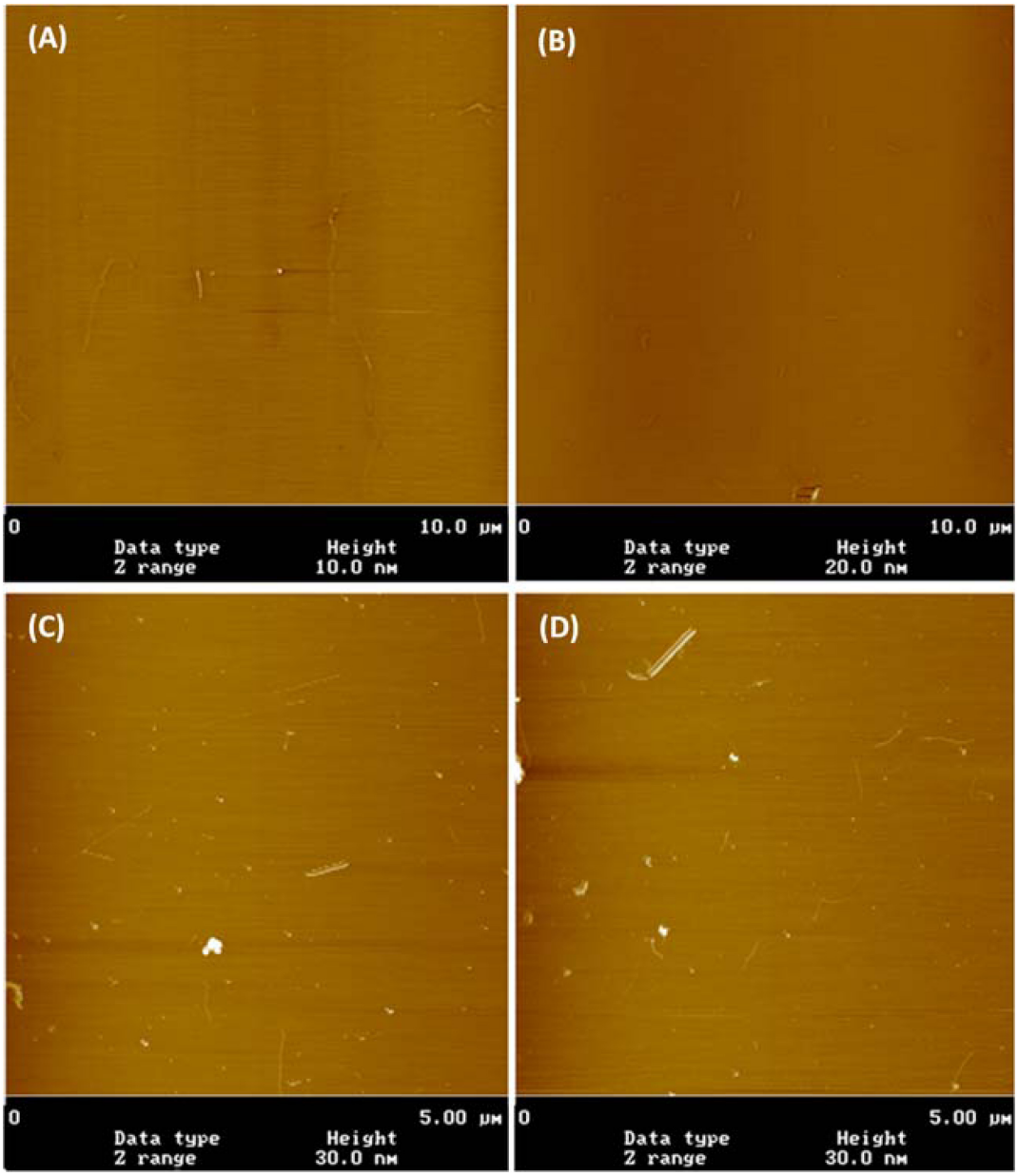

FIGURE 5 | Atomic force microscopy pictures of TEP molecules in unspiked summer sμSW **(A,B)** and TEP molecules with Au ENPs in spiked summer sμSW **(C,D)**.

Our work shows that this may be true when biological activity is suppressed by seasonal conditions, but when algal blooms occur seawaters are enriched with a variety of organic compounds that may stabilize ENPs for several days. It is therefore likely that organic matter, mostly TEP and precursors induce a steric stabilization mechanism that is counteracting the suppression of the EDL and the suspended particles maintain their numbers and particle size. A similar finding has been reported by Ellis et al., for seasonal variations of river water chemistry and its effect on nanoparticle stability (Ellis et al., 2018).

Our study shows that organic fibrils present in the fraction passing through the 5 μm filter and between 0.02 and 0.45 μm were able to stabilize Au ENPs for several days. Since this effect was only observed in the larger fractions (>0.02 μm), it is likely that these substances are responsible for the stabilization of AuNP in SW observed in this work. This material is present during spring and summer primarily due to biological activity. Biochemical properties of the seawater at the sampling location show that the biological activity may be significantly variable both temporally and spatially (Table S1 in SI). For example,

Chlorophyll-a values in the spring were higher than winter and summer, indicating a spring bloom event; however, elevated values were also reported in the winter and spring in the upper water layer (0–1 m depth), which is where our sampling took place. The winter sampling time co-occurred with an unusual early start of the spring bloom, so it corresponds to the early stage of the spring bloom that followed the winter inactivity, rather than truly winter conditions with no biological activity. A potential solution to the temporal and spatial variability has been recently proposed by Santschi et al., suggesting that the protein/carbohydrate ratio of EPS may be used as a proxy for their aggregation propensity (Santschi et al., 2020). Although not currently measured in routine monitoring, this approach may simplify predictions for the fate of ENPs in seawater.

Exopolymeric substances, dominated by acidic polysaccharides are exudated from phytoplankton during algal blooms (Alldredge et al., 1993). EPS form biotically in marine waters and have high affinity toward solids surfaces and are thus influenced by the presence of particles (Chen et al., 2011; Chiu et al., 2017). EPS are forming a gel network that may act as a stabilizing factor for nanomaterials in seawater, but in high concentrations can become the glue to form marine snow aggregates that lead to scavenging of suspended particles and depositing them on the sediments, a process that is critical for the biogeochemical cycling of elements (Zetsche and Ploug, 2015). Algal blooms are therefore acting as an intermittent stabilizing factor for ENPs in marine waters. This study calls for more studies on the fate of ENP under realistic conditions (*in situ* field studies or mesocosms) with complementary advanced minimum perturbing analytical techniques. For example, the settling fate of nanoparticles and intermediate buoyancy in the nepheloid benthic boundary layers of coastal seas under seasonal variations and the consequence on ecological exposure should be investigated.

DATA AVAILABILITY STATEMENT

The raw data supporting the conclusions of this article will be made available by the authors, without undue reservation.

AUTHOR CONTRIBUTIONS

MHas conceived the idea, developed the experimental plan, and contributed to writing of the manuscript. AG co-developed the experimental plan, carried out the sampling, sample analysis, data analysis, and wrote the manuscript. JG-U helped with the sampling, carried out data analysis, and contributed to writing of the manuscript. MHal and ND helped with the sampling, carried out sample analysis, and data analysis. All authors contributed to the article and approved the submitted version.

FUNDING

AG, JG-U, and MHas were partially supported by the Mistra Environmental Nanosafety Program, phases 1 and 2, financed by the Swedish Foundation for Strategic Environmental Research (grant no. DIA 2013/48) and the NANOFASE project funded under the European Union Horizon 2020 framework (grant no. 646002). AG has also received funding from the NanoIsland project, financed by the Hellenic Foundation for Research and Innovation (HFRI) and the General Secretariat for Research and Technology (GSRT), under grant agreement No. 1317. JG-U was also financed by the Centre for Future Chemical Risk Assessment and Management Strategies (FRAM), University of Gothenburg, Sweden.

ACKNOWLEDGMENTS

The authors would like to thank Anders Mårtensson for assisting with the AFM measurements and the reviewers for their insightful comments.

SUPPLEMENTARY MATERIAL

The Supplementary Material for this article can be found online at: https://www.frontiersin.org/articles/10.3389/fenvs.2020.00151/full#supplementary-material

REFERENCES

Aiken, G. R., Hsu-Kim, H., and Ryan, J. N. (2011). Influence of dissolved organic matter on the environmental fate of metals, nanoparticles, and colloids. *Environ. Sci. Technol.* 45, 3196–3201. doi: 10.1021/es103992s

Alldredge, A. L., Passow, U., and Logan, B. E. (1993). The abundance and significance of a class of large, transparent organic particles in the ocean. *Deep. Res. Part I.* 40, 1131–1140. doi: 10.1016/0967-0637(93)90129-Q

Baalousha, M., and Lead, J. R. (2013). Nanoparticle dispersity in toxicology. *Nat. Nanotechnol.* 8, 308–309. doi: 10.1038/nnano.2013.78

Calliari, D., and Tiselius, P. (2009). Organic carbon fluxes through the mesozooplankton and their variability at different time-scales in the Gullmarsfjord. *Sweden. Estuar. Coast. Shelf Sci.* 85, 107–117. doi: 10.1016/j.ecss.2009.06.016

Carp, O., Huisman, C. L., and Reller, A. (2004). Photoinduced reactivity of titanium dioxide. *Prog. Solid State Chem.* 32, 33–177. doi: 10.1016/j.progsolidstchem.2004.08.001

Chen, C. S., Anaya, J. M., Zhang, S., Spurgin, J., Chuang, C. Y., Xu, C., et al. (2011). Effects of engineered nanoparticles on the assembly of exopolymeric substances from phytoplankton. *PLoS One* 6:e21865. doi: 10.1371/journal.pone.0021865

Chin, W. C., Orellana, M. V., and Verdugo, P. (1998). Spontaneous assembly of marine dissolved organic matter into polymer gels. *Nature* 391, 568–572. doi: 10.1038/35345

Chiu, M. H., Khan, Z. A., Garcia, S. G., Le, A. D., Kagiri, A., Ramos, J., et al. (2017). Effect of engineered nanoparticles on exopolymeric substances release from marine phytoplankton. *Nanoscale Res. Lett.* 12:620. doi: 10.1186/s11671-017-2397-x

Elimelech, M., Gregory, J., Jia, X., and Williams, R. (1995). *Particle Deposition and Aggregation*. Woburn, MA: Butterworth-Heinemann.

Ellis, L. J. A., Baalousha, M., Valsami-Jones, E., and Lead, J. R. (2018). Seasonal variability of natural water chemistry affects the fate and behaviour of silver nanoparticles. *Chemosphere* 191, 616–625. doi: 10.1016/j.chemosphere.2017.10.006

Frimmel, F. H., von der Kammer, F., and Flemming, H.-C. (2007). *Colloidal Transport in Porous Media*. Berlin: Springer-Verlag.

Gallego-Urrea, J. A., Hammes, J., Cornelis, G., and Hassellöv, M. (2014). Multimethod 3D characterization of natural plate-like nanoparticles: Shape effects on equivalent size measurements. *J. Nanoparticle Res.* 16:2383. doi: 10.1007/s11051-014-2383-5

Gallego-Urrea, J. A., Hammes, J., Cornelis, G., and Hassellov, M. (2016). Coagulation and sedimentation of gold nanoparticles and illite in model natural waters: influence of initial particle concentration. *NanoImpact* 3–4, 67–74. doi: 10.1016/j.impact.2016.10.004

Gondikas, A., Von Der Kammer, F., Reed, R. B., Wagner, S., Ranville, J. F., and Hofmann, T. (2014). Release of TiO2 nanoparticles from sunscreens into surface waters: a one-year survey at the old danube recreational lake. *Environ. Sci. Technol.* 48, 5415–5422. doi: 10.1021/es405596y

Gondikas, A., Wagner, S., and Navratilova, J. (2019). "Nanomaterials in water: detection and characterization," in *Encyclopedia of Water: Science, Technology, and Society*, ed. P. A. Maurice (Hoboken, NJ: JohnWiley & Sons, Inc), doi: 10.1002/9781119300762.wsts0078

Gottschalk, F., Sonderer, T., Scholz, R. W., and Nowack, B. (2009).). Modeled environmental concentrations of engineered nanomaterials (TiO2, ZnO, Ag, CNT, fullerenes) for different regions. *Environ. Sci. Technol.* 43, 9216–9222. doi: 10.1021/es9015553

Hassellov, M., Readman, J. W., Ranville, J. F., and Tiede, K. (2008). Nanoparticle analysis and characterization methodologies in environmental risk assessment of engineered nanoparticles. *Ecotoxicology* 17, 344–361. doi: 10.1007/s10646-008-0225-x

Hedges, J. I. (1992). Global biogeochemical cycles: progress and problems. *Mar. Chem.* 39, 67–93. doi: 10.1016/0304-4203(92)90096-S

Kaegi, R., Englert, A., Gondikas, A., Sinnet, B., von der Kammer, F., and Burkhardt, M. (2017). Release of TiO2 – (Nano) particles from construction and demolition landfills. *NanoImpact* 8, 73–79. doi: 10.1016/j.impact.2017.07.004

Kaegi, R., Voegelin, A., Sinnet, B., Zuleeg, S., Hagendorfer, H., Burkhardt, M., et al. (2011). Behavior of metallic silver nanoparticles in a pilot wastewater treatment plant. *Environ. Sci. Technol.* 45, 3902–3908. doi: 10.1021/es1041892

Linders, T., Infantes, E., Joyce, A., Karlsson, T., Ploug, H., Hassellöv, M., et al. (2018). Particle sources and transport in stratified Nordic coastal seas in the Anthropocene. *Elem Sci Anth* 6:29. doi: 10.1525/elementa.149

Liu, W., Rose, J., Plantevin, S., Auffan, M., Bottero, J.-Y., and Vidaud, C. (2013). Protein corona formation for nanomaterials and proteins of a similar size: hard or soft corona? *Nanoscale* 5, 1658–1668. doi: 10.1039/c2nr33611a

Mylon, S. E., Chen, K. L., and Elimelech, M. (2004). Influence of natural organic matter and ionic composition on the kinetics and structure of hematite colloid aggregation: implications to iron depletion in estuaries. *Langmuir* 20, 9000–9006. doi: 10.1021/la049153g

Passow, U. (2002). Transparent exopolymer particles (TEP) in aquatic environments. *Prog. Oceanogr.* 55, 287–333. doi: 10.1016/S0079-6611(02)00138-6

Praetorius, A., Badetti, E., Brunelli, A., Clavier, A., Gallego-Urrea, J. A., Gondikas, A., et al. (2020). Strategies for determining heteroaggregation attachment efficiencies of engineered nanoparticles in aquatic environments. *Environ. Sci. Nano* 7, 351–367. doi: 10.1039/c9en01016e

Reed, R. B., Martin, D. P., Bednar, A. J., Montaño, M. D., Westerhoffd, P., and Ranville, J. F. (2017). Multi-day diurnal measurements of Ti-containing nanoparticle and organic sunscreen chemical release during recreational use of a natural surface water. *Environ. Sci. Nano* 4, 69–77. doi: 10.1039/c6en00283h

Santschi, P. H., Balnois, E., Wilkinson, K. J., Zhang, J., Buffle, J., and Guo, L. (1998). Fibrillar polysaccharides in marine macromolecular organic matter as imaged by atomic force microscopy and transmission electron microscopy. *Limnol. Oceanogr.* 43, 896–908. doi: 10.4319/lo.1998.43.5.0896

Santschi, P. H., Xu, C., Schwehr, K. A., Lin, P., Sun, L., Chin, W. C., et al. (2020). Can the protein/carbohydrate (P/C) ratio of exopolymeric substances (EPS) be used as a proxy for their 'stickiness' and aggregation propensity? *Mar. Chem.* 218:103734. doi: 10.1016/j.marchem.2019.103734

Schurtenberger, P., and Meredith, N. (1993). "Characterization of biological and environmental particles using static and dynamic light scattering," in *Environmental Particles*, Vol. 2, eds J. Buffle and H. van Leeuwen (Boca Raton, FL: Lewis), 37–115. doi: 10.1201/9781351270809-2

Sharma, V. K. (2009). Aggregation and toxicity of titanium dioxide nanoparticles in aquatic environment–a review. *J. Environ. Sci. Health. A Tox. Hazard. Subst. Environ. Eng.* 44, 1485–1495. doi: 10.1080/10934520903263231

Stolpe, B., and Hassellöv, M. (2007). Changes in size distribution of fresh water nanoscale colloidal matter and associated elements on mixing with seawater. *Geochim. Cosmochim. Acta* 71, 3292–3301. doi: 10.1016/j.gca.2007.04.025

Stolpe, B., and Hassellöv, M. (2010). Nanofibrils and other colloidal biopolymers binding trace elements in coastal seawater: significance for variations in element size distributions. *Limnol. Oceanogr.* 55, 187–202. doi: 10.4319/lo.2010.55.1.0187

Tiselius, P., and Kuylenstierna, M. (1996). Growth and decline of a diatom spring bloom: phytoplankton species composition, formation of marine snow and the role of heterotrophic dinoflagellates. *J. Plankton Res.* 18, 133–155. doi: 10.1093/plankt/18.2.133

Toncelli, C., Mylona, K., Kalantzi, I., Tsiola, A., Pitta, P., Tsapakis, M., et al. (2017). Silver nanoparticles in seawater: a dynamic mass balance at part per trillion silver concentrations. *Sci. Total Environ.* 601–602, 15–21. doi: 10.1016/j.scitotenv.2017.05.148

Verdugo, P., Alldredge, A. L., Azam, F., Kirchman, D. L., Passow, U., and Santschi, P. H. (2004). The oceanic gel phase: a bridge in the DOM-POM continuum. *Mar. Chem.* 92, 67–85. doi: 10.1016/j.marchem.2004.06.017

Waite, A. M., Gustafsson, Ö, Lindahl, O., and Tiselius, P. (2005). Linking ecosystem dynamics and biogeochemistry: sinking fractionation of organic carbon in a Swedish fjord. *Limnol. Oceanogr.* 50, 658–671. doi: 10.4319/lo.2005.50.2.0658

Wiesner, M., and Bottero, J.-Y. (2007). *Environmental Nanotechnology - Applications and Impacts of Nanomaterials*, 1st Edn. New York, NY: McGraw-Hill Education, doi: 10.1036/0071477500

Wiesner, M., Lowry, G., Alvarez, P., Dionysiou, D., and Biswas, P. (2006). Assessing the risks of manufactured nanomaterials. *Environ. Sci. Technol.* 40, 4336–4345. doi: 10.1021/es062726m

Zetsche, E. M., and Ploug, H. (2015). Marine chemistry special issue: particles in aquatic environments: from invisible exopolymers to sinking aggregates. *Mar. Chem.* 175, 1–82. doi: 10.1016/j.marchem.2015.04.008

Conflict of Interest: The authors declare that the research was conducted in the absence of any commercial or financial relationships that could be construed as a potential conflict of interest.

frontiers in Environmental Science

ORIGINAL RESEARCH
published: 19 November 2020
doi: 10.3389/fenvs.2020.551075

Algal Growth at Environmentally Relevant Concentrations of Suspended Solids: Implications for Microplastic Hazard Assessment

Elena Gorokhova, Karin Ek and Sophia Reichelt*

Department of Environmental Science (ACES), Stockholm University, Stockholm, Sweden

Hazard assessment of microplastic is challenging because standard toxicity testing is targeting soluble (at least partially) chemicals. Adverse effects can occur when test organisms are exposed to turbid environments in the presence of various particulate matter (PM), both natural, such as clay and cellulose, and anthropogenic, such as microplastic. It is, therefore, relevant to compare responses to PM exposure between the microplastic and other suspended solids present at ecologically relevant concentrations. This comparison is possible when reference materials are included in the testing of microplastic hazard potential. Here, we evaluated growth inhibition in unicellular alga *Raphidocelis subcapitata* exposed to different PM (microplastic, kaolin, and cellulose; 10, 100, and 1,000 mg/L); algae without added solids were used as a control. Also, aggregate formation in the exposure systems was analyzed using particle size distribution (PSD) data. At 10–100 mg/L, no adverse growth effects were observed in any treatments; moreover, algal growth was significantly stimulated in kaolin and cellulose treatments compared to the control. However, at 1,000 mg/L, all tested materials exerted growth inhibition, with no significant differences among the materials. Comparing PSD s across the treatments showed that both PM concentration and size of the particle aggregates were significant growth predictors for all materials tested. Therefore, at high concentrations, both natural and anthropogenic materials have a similar capacity to cause growth inhibition. Linking effects in unicellular organisms to microplastic fragments remains a challenge since plastics incorporate chemicals that may leach and elicit specific effects relative to the particulates. The use of reference materials in hazard assessment of plastic litter is needed to delineate these effects.

Keywords: algal growth inhibition test, plastic litter, suspended solids, particle size distribution, plastic weathering, aged plastic, hazard assessment, microplastic

OPEN ACCESS

Edited by:
Antonia Praetorius,
University of Amsterdam, Netherlands

Reviewed by:
Garth Aidan Covernton,
University of Victoria, Canada
Jesse Patrick Harrison,
CSC-IT Center for Science, Finland

****Correspondence:***
Elena Gorokhova
elena.gorokhova@aces.su.se

Specialty section:
This article was submitted to Biogeochemical Dynamics, a section of the journal Frontiers in Environmental Science

Received: *11 April 2020*
Accepted: *20 October 2020*
Published: *19 November 2020*

Citation:
Gorokhova E, Ek K and Reichelt S (2020) Algal Growth at Environmentally Relevant Concentrations of Suspended Solids: Implications for Microplastic Hazard Assessment. Front. Environ. Sci. 8:551075. doi: 10.3389/fenvs.2020.551075

INTRODUCTION

Plastics have become a global concern as a suite of emerging pollutants, and potential environmental impacts have been highlighted (Andrady and Neal, 2009; Rochman et al., 2019). However, plastic litter, including microplastic, is a new field in environmental pollution research with much-unsettled methodology, and standard methods for hazard assessment are not yet

available (Adam et al., 2019). Current test methods in ecotoxicology are intended for soluble (at least partially) chemicals, whereas testing particle suspensions, such as microplastic, requires different approaches (Paul-Pont et al., 2018; Gerdes et al., 2019). Moreover, plastics are diverse: they represent different polymers and materials that include a broad array of chemical additives and come in many sizes, colors, and shapes (Rochman et al., 2019), which complicates comparisons between the effect studies (Reichelt and Gorokhova, 2020). It is also essential to keep in mind that plastic is only a kind of persistent solid waste pollution, and common approaches for the risk assessment are needed (Coe et al., 2019). Therefore, the development of adequate microplastic hazard assessment methods under reproducible settings is the key challenge for the plastic litter toxicology and the toxicology of anthropogenic solids at large.

Despite environmental health concerns, only a few studies have shown consistent adverse effects of microplastics (Foley et al., 2018; Reichelt and Gorokhova, 2020), usually observed at very high microplastic concentrations. As a rule, these concentrations exceed levels that are recognized as environmentally relevant (Lenz et al., 2016; Phuong et al., 2016). For such studies, a valid critique is a high probability that these effects are not necessarily specific to the microplastic but arise from the exposure to any suspended solids that have no nutrition value for animals and—in the case of photosynthetic microorganisms—a capacity to cause shading effects and sorb nutrients and microelements, thus decreasing their availability for the test algae (Ogonowski et al., 2018b). Hence, the existing protocols for hazard assessment do not explicitly address the effects of microplastic but those of particulate matter (PM) that change light and nutrient availability for the test organisms, such as algae and periphyton, during the exposure, with possible downstream effects on nutrient acquisition pathways, photosynthesis efficiency, and, ultimately, growth (Reichelt and Gorokhova, 2020).

So far, most efforts have focused on animal responses to microplastic exposure (Foley et al., 2018; Ogonowski et al., 2018b), whereas far less research has addressed possible effects of microplastic on primary producers (Yokota et al., 2017). The reported consequences of the interactions between primary producers and particles of fossil-based polymers in nano- and microparticle size range include alterations in algal photosynthesis (Bhattacharya et al., 2010), growth (Sjollema et al., 2016; Bergami et al., 2017), and colony morphology (Yokota et al., 2017). These changes can propagate in the food web, affecting consumers and, ultimately, system productivity. However, the reported effects are not consistent across the studies, and no-effect reports are also published (Prata et al., 2019). As shown in the recent meta-analysis of the growth inhibition effects in algae exposed to nano-and microplastic, the lack of proper controls and methodological variability between the studies make it difficult to understand the driving forces, such as particle size, concentration, polymer type, behind the observed effects (Reichelt and Gorokhova, 2020). What is also essential is that similar effects on the same endpoints can be induced by natural suspended solids, such as clay and sand (Bilotta and Brazier, 2008; Chapman et al., 2017). These solids are ubiquitous in natural waters, commonly reaching gram per liter concentrations (Cahoon et al., 1999; Bilotta and Brazier, 2008), i.e., levels far exceeding those of microplastic. The adverse effects of fine sediments on algae are well-known from ecological studies (Cahoon et al., 1999; Ogonowski et al., 2018b), and it is, therefore, relevant to compare the algal responses to particle exposure between the microplastic and other suspended solids present in the fresh- and marine surface waters at ecologically relevant concentrations (mg L^{-1} to g L^{-1}).

Microalgae have a long history of use as test organisms in ecological and ecotoxicological assessments because of their high sensitivity toward various stressors, including environmental pollutants. In ecotoxicology, the standard algal growth inhibition test (Oecd., 2006) validated for several freshwater and marine species is widely used for hazard evaluation. When conducting this test with various effluents, it is recommended to measure total suspended solids and total settled solids because removing these fractions could influence the growth and, thus, toxicity estimates. The mechanisms of the growth inhibition in the presence of suspended solids, including microplastic, may vary, including shading effects and trapping of microalgae in the aggregates and subsequent inhibition of photosynthesis (He et al., 2017; Mao et al., 2018). Recently, such effects have been suggested to occur in the algae exposed to microplastic; moreover, increased production of organic carbon and its aggregation into gel particulates have been demonstrated in mesocosms amended with polystyrene microbeads (Galgani et al., 2019). Therefore, it is crucial to understand whether algae-microplastic aggregates have a higher capacity to inhibit growth compared to the aggregates with natural solids.

As a consequence of degradation processes, the plastic particles in the environment undergo weathering that changes their physicochemical properties, aggregation properties, and, possibly, hazard potential. Various forces, such as physical stress, UV-radiation, shifting temperatures, salinity, and oxidation, contribute to weathering resulting in changes in the surface properties and morphology (Jahnke et al., 2017). Moreover, microbial biofilms also contribute to these physicochemical alterations, affecting aggregation capacity (McGivney et al., 2020; Rogers et al., 2020). Considering the abundance of various non-plastic particulates in the pelagia, the occurrence of non-aggregated sphaerical particles in the water column is highly unlikely. Moreover, given that microbeads are a minor contributor to microplastic contamination globally, it is questionable whether the broad use of uniform spherical MP in experiments, including algal growth inhibition tests (Reichelt and Gorokhova, 2020), is justifiable from ecological and ecotoxicological viewpoints. Hence, using aged polymer fragments to mimic the environmentally realistic exposure scenario has been advocated (Ogonowski et al., 2018b). However, only a very few studies have evaluated the weathering effect in MP toxicity tests (Bråte et al., 2018; Fu et al., 2019), and found that aging of MP (e.g., PVC) would pose more substantial inhibitory effects on microalgae (Fu et al., 2019). The exact mechanisms of the elevated adverse effects remain, however, unclear.

The objectives of this study were to (1) compare effects of a fossil-based polymer and natural (kaolin and cellulose) particles on the growth performance in the standard algal growth inhibition test (Oecd., 2006); (2) compare algal growth response to weathered and virgin microplastic; and (3) evaluate relationships between particle aggregation in the experimental system and algal growth. The present study does not aim to generate a robust test design for suspended solids in general or microplastic specifically but rather is intended to create debate on the methodology of microplastic hazard assessment and possibly influence further research efforts toward this goal.

MATERIALS AND METHODS

Test Organism

The freshwater unicellular green alga *Raphidocelis subcapitata* (Korshikov) Nygaard, Komárek, J. Kristiansen and O. M. Skulberg, 1987, formerly *Pseudokirchneriella subcapitata* and *Selenastrum capricornutum*, is a standard test organism in ecotoxicology (Oecd., 2006). It is a fast-growing species, sensitive to light and nutrients, and thus particularly well suited to evaluate stress effects on algal growth and production (Gonçalves et al., 2016). *Raphidocelis subcapitata* is one of the most commonly used algal species for testing microplastic effects (Reichelt and Gorokhova, 2020), and has also been used to evaluate plastic leachate toxicity (Capolupo et al., 2020). The algal culture for inoculation was grown for 1 week in Z8 media, at room temperature, with shaking (100–125 rpm) and the illumination of ∼40 μ $E{\cdot}m^{-2}{\cdot}s^{-1}$. Algal concentrations were determined by *in vivo* fluorescence using a 10 AU^{TM} Field Fluorometer (Turner Designs, Sunnyvale, California, and United States).

Chemicals, Reference, and Test Materials

Kaolin (Sigma-Aldrich, K7375) and native fibrous cellulose (Macherey-Nagel, MN 301) were used as the reference materials. Kaolin contains mainly the clay mineral kaolinite, a hydrous aluminosilicate, whereas cellulose is the primary substance in plant cell walls. Both materials occur globally in suspended particulates and have been used as reference material when assessing microplastic effects (Gerdes et al., 2019) and as a test material when assessing the effects of exposure to total suspended solids (Robinson et al., 2009; Ogonowski et al., 2018a,b).

As a test microplastic, we used polyethylene terephthalate (PET, Goodfellow GmbH, product number ES306312) mixed with Milli-Q water passed through a 40-μm sieve to produce a size fraction similar to that of kaolin and cellulose. According to the manufacturer, the material contains 1 ppm acetaldehyde, translating to a maximum of 0.001 mg/L in the test system. This concentration is about three orders of magnitude lower than EC_{50} for growth inhibition in green algae (Tsai and Chen, 2007). To investigate whether microplastic aging affects particle aggregation and algal response, we used both virgin and weathered PET particles, denoted as PET and PET_w, respectively. The stock of PET_w was prepared by UV exposure of the milled PET for 28 days (Oelschlägel et al., 2018) and size-fractionated in the same way as PET (**Supplementary Text S1** and **Supplementary Material**). Stocks of both reference and test materials contained 0.01% v/v of a non-ionic surfactant (Tween-80, Sigma-Aldrich), which was also added to the control media at the final concentration of 0.0001%. In the experimental treatments, the concentration of Tween-80 never exceeded 0.0001%, which is well below the levels regarded as non-toxic for green algae (Ma et al., 2004). In the stock suspensions, both PET materials (median size ∼11 and 12 μm for virgin and weathered PET, respectively) and kaolin (∼9 μm) showed unimodal size distributions, whereas cellulose (∼16 μm) had polymodal distribution and broader size range. See **Supplementary Text S1**, **Supplementary Table S1**, and **Supplementary Figure S1** for the description of the particle preparation and size distributions of the stock suspensions used to prepared exposure media at different nominal concentrations of suspended solids.

Standard growth media (Z8) contained all nutrients at surplus for the entire growth period of the algae in the incubation system: $NaNO_3$ (6 mM), $CaCl_2{\cdot}2H_2O$ (73 mg L^{-1}), $MgSO_3{\cdot}7H_2O$ (25 mg L^{-1}), K_2HPO_4 (31 mg L^{-1}), Na_2CO_3 (21 mg L^{-1}), $FeCl_3{\cdot}6H_2O$ (28 mg/L) 0.001 M HCl, ZnSO4·$7H_2O$ (5 μ g/L), $MnCl_2{\cdot}4H_2O$ (10 μ g/L), H_3BO_3 (5 μg L^{-1}), $CuSO_4{\cdot}5H_2O$ (0.5 μg L^{-1}), $CoCl_2{\cdot}6H_2O$ (2 μg L^{-1}), $NaMoO_4{\cdot}2H_2O$ (1.5 μg L^{-1}), $VOSO_4{\cdot}2H_2O$ (0.5 μg L^{-1}), $Na_2SeO_4{\cdot}10H_2O$ (0.5 μg L^{-1}), pH adjusted to 6.6–7.0. The chemicals were purchased from Sigma-Aldrich (Germany).

Experimental Setup

Five experimental media with different suspended solids were prepared by mixing stock suspensions of the test material and used as treatments with nominal concentrations of suspended solids (SS) 10, 100, and 1,000 mg L^{-1} (**Table 1**). The particle number concentrations for the lowest concentration treatment were 1.14, 0.93, and 0.94 particles × 10^7 L^{-1} for kaolin (specific gravity 2.36), cellulose (0.50), and PET materials (1.34), respectively. This design resulted in 12 different combinations

TABLE 1 | Experimental setup for growth inhibition assay with *R. subcapitata*

Treatment	Experimental media	Algae	SS concentration, mg L^{-1}
Algal control	Z8	yes	0
Kaolin	Z8 + Kaolin	yes	10, 100, 1,000
Kaolin blank	Z8 + Kaolin	no	10, 100, 1,000
Cellulose	Z8 + Cellulose	yes	10, 100, 1,000
Cellulose blank	Z8 + Cellulose	no	10, 100, 1,000
PET	Z8 + PET	yes	10, 100, 1,000
PET blank	Z8 + PET	no	10, 100, 1,000
PET_w	Z8 + PET_w	yes	10, 100, 1,000
PET_w blank	Z8 + PET_w	no	10, 100, 1,000

*Algae were exposed to test microplastics, virgin and weathered polyethylene terephthalate (PET and PET_w, respectively), and reference materials (kaolin and cellulose) at concentrations 10, 100, and 1,000 mg L^{-1}; algal control (no added suspended solids) and particle blanks (no added algae) were included. Each treatment included five replicates. Standard growth media (Z8) contained all nutrients at a surplus (**Supplementary Text S1**).*

of *material* × *concentration* factors for algal exposure and a single control with no added solids; five replicates were used for each of these incubations. Also, particle blanks were used for each *material* × *concentration* combination (**Table 1**) to control for contamination with microorganisms (algae and bacteria) and any background fluorescence induced by the test and reference materials under experimental conditions. When measuring fluorescence in the treatment tubes, the mean value of the particle blanks was subtracted from each replicate for the respective *material* × *concentration* combination.

A standard growth inhibition assay with *R. subcapitata* was conducted (Oecd., 2006) with some modifications. The assay is based on *in vivo* chlorophyll *a* (Chl *a*) measurement that exhibits endogenous red fluorescence (autofluorescence). The quantification of Chl *a* is useful for monitoring photosynthetic capacity and detection of stimulating or inhibiting effects. The algae were harvested from the culture and diluted with Z8 media to 10^5 cell mL^{-1} and then mixed with the experimental media (**Table 1**) to the final cell density of 5×10^3 cells mL^{-1}. These suspensions were transferred to 10 mL glass tubes filled to the top and sealed to avoid air bubbles. All tubes were mounted on a plankton wheel rotating at 0.5 rpm and incubated at room temperature and fluorescent light at 140 ± 10 μ $E{\cdot}m^{-2}$ s^{-1}. Light intensity was measured in the exposure area using photosynthetically active radiation sensor Quantum (Skye, United Kingdom). The algae were allowed to grow throughout the lag phase and exponential growth for 72 h, and fluorescence was measured at time points 0, 24, 48, and 72 h. Over the range of cell densities used in this experiment, the fluorescence was linearly related to the cell number as established by comparing the fluorescence measurements and cell counts with a hemocytometer. Upon the experiment termination, samples of the suspended matter were collected from each replicate and used for particle size distribution (PSD) analysis to establish relationships between the growth parameters and particle aggregation.

Growth Analysis

The algal growth response was inferred from the change in the Chl *a* fluorescence. Growth kinetics of the algae was examined using time-specific measurements fitted to an exponential growth curve with lag phase (Baranyi and Roberts, 1994); see **Supplementary Text S2** for the calculation details and explanations for algal growth kinetics. With DMFit software[1], the growth curves were constructed to estimate lag phase duration (λ, h) and maximal growth during the exponential phase (μ, d^{-1}). The lag phase duration reveals how fast test organisms acclimate to experimental conditions, while the growth rate in the exponential phase indicates proliferation in the adapted population. Model fit was evaluated by the coefficient of determination (R^2) and performance by the root mean square error (RMSE). An additional parameter, the change in fluorescence intensity between the observation points, was used to calculate the area under the curve (AUC), representing algal production during the observation period. This endpoint is commonly used in algal growth inhibition assay as it integrates the change in photosynthetically active biomass during both the lag and growth phases being an approximation of cumulative biomass at each time point (Vaas et al., 2012).

[1]www.combase.cc

Particle Distribution Analysis

The particle size distribution (PSD) was measured with a Spectrex laser particle counter (Spectrex, model PC-2000, Redwood City, United States). The size spectra were determined for 1—100 μm range (**Supplementary Text S1**), and processed with GRADISTAT program, version 8.0 (Blott and Pye, 2001) according to the method by Folk and Ward (Folk and Ward, 1957) to obtain mean particle size, sample sorting (variance), skewness, kurtosis, median particle size (D_{50}), and two points which describe the coarsest and the finest parts of the distribution (D_{90} and D_{10}, respectively), and D_{90}—D_{10} range. These parameters are commonly used in concert for characterization of PSD in powders and heterogeneous granular materials, such as soil and sediment (Blott and Pye, 2001).

Data Analysis and Statistics

If not stated otherwise, the results are expressed as mean value ± standard deviation (SD), the alpha level was set to 5%, and the data analysis was conducted with JMP,® Version 14.0 (SAS Institute Inc., Cary, NC, 1989–2019). The outline of the research questions addressed in the data analysis and the methods used is shown in **Figure 1**.

First, we used two-way ANOVA to evaluate the effects of suspended solids concentration (SS, mg/L) and test material on the algal growth parameters (λ, μ, and AUC) in different treatments. When the *material* × *concentration* interaction was significant, the main effects were not interpreted. In the follow-up analysis, the effect of *material* was evaluated for each concentration level using a two-stage Benjamini, Krieger, and Yekutieli (Benjamini et al., 2006) procedure for controlling the false discovery rate (FDR) in the multiple comparisons. The data were not transformed as the model residuals were normally distributed. Within-treatment variability was accessed using the coefficient of variation (CV%).

The PSD parameters estimated by GRADISTAT for all treatments were first examined by Principal Components Analysis (PCA) using PAST software, version 3.22 (Hammer et al., 2001), to explore the overall differences between the treatments with and without algae and examine the relationships between the PSD characteristics. Then, for each material, we used Generalized Linear Model (GLM, log-link, normal error structure) analysis to test the effects of algae in the system (present/absent) and SS concentration (10–1,000 mg L^{-1}) as predictors of the PSD characteristics (mean particle size, variance, skewness, kurtosis, D_{50}, D_{90}, D_{10}, and D_{10}—D_{90}); the interaction term *algae* × *SS* was included in each model. The data used in GLMs were Box-Cox transformed and centered. The model residuals were examined using QQ plots.

Finally, Partial Least Square Regression (PLSR) was used to study the relationships between the exposure variables (PSD metrics and SS concentration; X variables) and the growth parameters (λ, μ, and AUC; Y variables); see

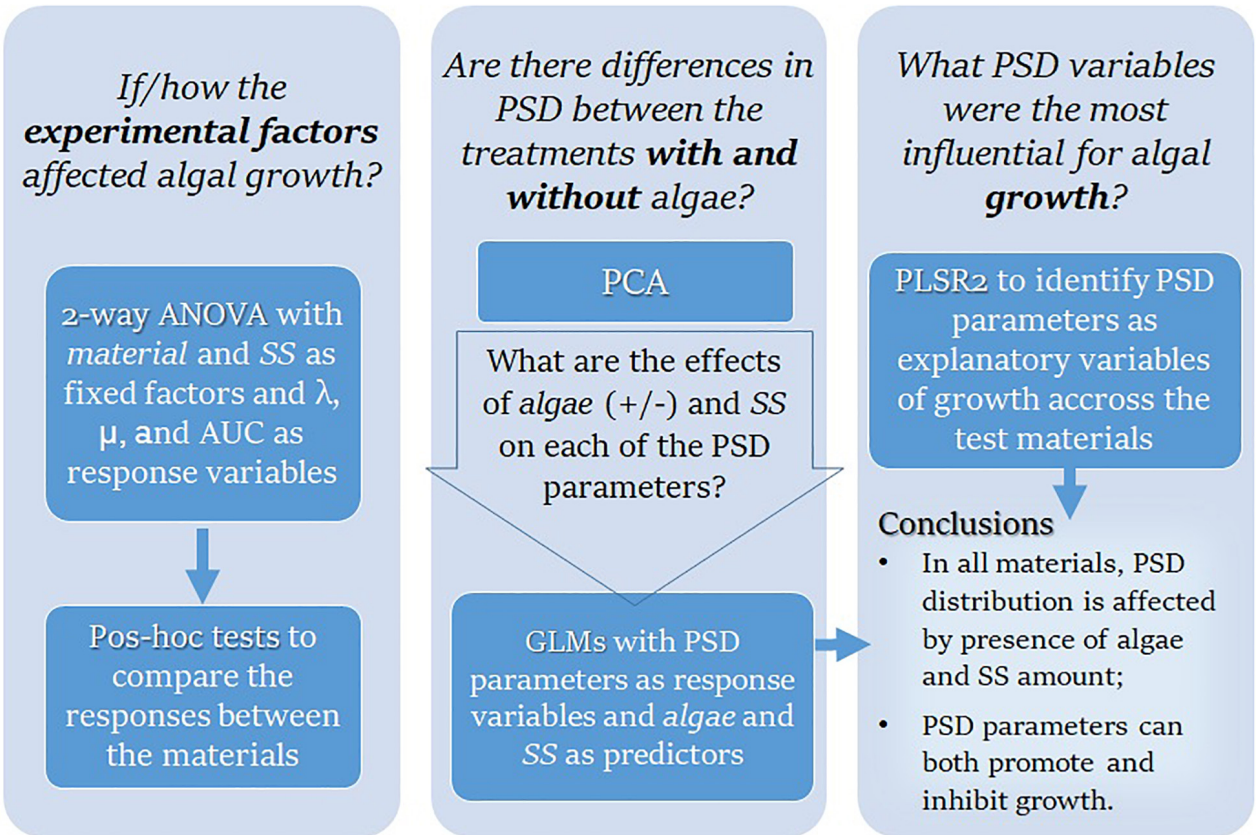

FIGURE 1 | Alignment of the research questions and statistical methods used in the data analysis.

Supplementary Text S3 for the details on PLSR design. The analysis was carried out for each material as well as for the pooled data set using the non-linear iterative partial least squares (NIPALS) algorithm; the data were centered and scaled. For cross-validation and determination of the optimal number of latent variables, we applied the leave-one-out method and predicted residual error sum of squares (PRESS) statistic as implemented in the PLS platform of the software to separate terms that do not make an important contribution to the dimensionality reduction involved in PLSR (Variable Importance in Projection; VIP < 0.8) and those that might (VIP ≥ 0.8). For each X variable, VIP value was used to assess its importance in determining the PLSR projection model (Wold et al., 2001).

RESULTS

Growth Response to Suspended Solids

Positive growth and growth models with high R^2-values (>0.97 in all cases) were observed in all treatments during the exposure, albeit with different growth trajectories (**Figure 2**). There were significant effects of exposure on all growth parameters (λ, μ, and AUC; **Table 2**); however, the significant interaction effects for μ and AUC indicated that the differences between the test materials as well as between the exposed and non-exposed algae, were concentration-specific. In the follow-up pairwise comparisons, both positive and negative effects of *material* were observed compared to the particle-free control (**Supplementary Table S2**); moreover, these effects occurred in both microplastic and reference material treatments (**Figure 2**).

Both λ and μ values varied among the treatments, with significant deviations observed only at the highest concentration (1,000 mg L^{-1}; **Figures 2A,B**). The lag phase was significantly longer in the algae exposed to 1,000 mg L^{-1} for all materials tested, except cellulose, compared to that in control (**Figure 2A** and **Supplementary Table S2A**). The major deviations from the control were observed for the maximal growth rate in the algae exposed to cellulose, with a significant decrease at 1,000 mg L^{-1}, whereas there were no significant effects for the other materials (**Figure 2B** and **Supplementary Table S2B**). Similarly, the most pronounced changes were found for the AUC values indicating a significant decrease in all tested materials at 1,000 mg L^{-1} (**Figure 2C** and **Supplementary Table S2C**). Notably, the within-treatment variability for AUC decreased significantly with time and increased with concentration (**Figure 3**).

There was an overall positive relationship between the maximal growth rate and lag phase duration across the treatments at concentrations of 10 and 100 mg L^{-1} (**Figure 4**). However, the algae exposed to 1,000 mg L^{-1} were deviating significantly from this relationship because of the lower μ

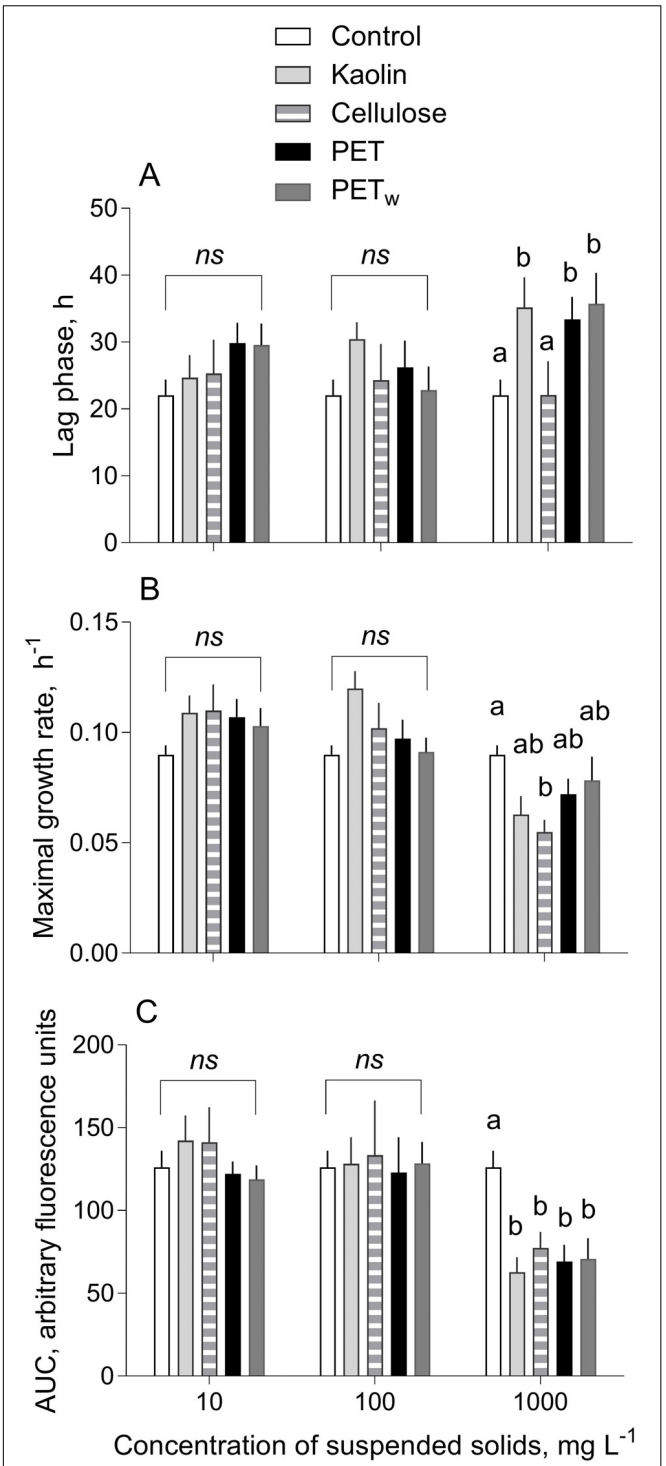

FIGURE 2 | Kinetic parameters (mean and SD; $n = 5$) of growth responses in *R. subcapitata* exposed to microplastics and reference materials **(A)** Lag phase (λ, h) preceding the active growth, **(B)** maximal growth rate (μ, d^{-1}) estimated for the exponential period, and **(C)** area under the curve (AUC) representing algal production during the observation period. Non-matching letters indicate a significant treatment difference evaluated by the multiple comparisons test with FDR correction; *ns* denotes a lack of significant differences between the materials within the test concentration of suspended solids; see **Supplementary Table S2** for the pairwise comparisons.

TABLE 2 | Two-way ANOVA models testing effects of suspended solids concentration (SS, mg/L) and test material (Control, Kaolin, Cellulose, PET, and PET_w) on the algal growth parameters (λ, μ, and AUC). Significant effects are in bold face.

	SS	DF	MS	F	*p*-value
Lag phase, λ					
Interaction	573.0	8	71.62	0.9955	0.4489
SS	277.3	2	138.6	1.927	0.1545
Material	856.7	4	214.2	2.977	**0.0261**
Residual	4317	60	71.94		
Max growth rate, μ					
Interaction	0.007348	8	0.0009185	2.877	**0.0089**
SS	0.01549	2	0.007747	24.27	<0.0001
Material	0.0006326	4	0.0001581	0.4953	0.7392
Residual	0.01916	60	0.0003193		
Area under curve, AUC					
Interaction	11150	8	1394	5.976	**<0.0001**
SS	37995	2	18998	81.46	<0.0001
Material	4636	4	1159	4.970	0.0016
Residual	13992	60	233.2		

*When the Material × SS interaction was significant, the main effects were not interpreted. The material effect was evaluated for each level of concentration using multiple comparison tests; the results are presented (**Supplementary Table S2**, **Supplementary Material**, and summarized in **Figure 2**).*

values in the algae exposed to all test materials at this concentration (**Figure 2B**).

Particle Aggregation in the System

All test materials were found to aggregate during the exposure compared to their respective stocks (**Supplementary Figure S3**). Moreover, the aggregation was significantly more substantial in the treatments with algae than in the particle controls (**Table 3** and **Supplementary Figure S4**). Principal component analysis (PCA) using the PSD characteristics determined for each material and treatment indicated that two principal components exceeded 5% of the total explained variance. Moreover, 83–94% and 6–15% of the accumulated dispersion were represented by PC1 and PC2, respectively, while only PC1 passed the broken-stick test (**Supplementary Figure S5**). The PCA biplot demonstrated separation between the treatments with and without algae for all four materials, with more apparent separation observed for cellulose and PET_w, whereas some overlap was found in the biplots for kaolin and PET treatments (**Figure 5**). The loadings on PC1 indicate the importance of the particle size metrics (mean and median particle sizes, D_{10}, D_{90}, and D_{90}–D_{10}), whereas variance, skewness, and kurtosis were not influential for the discrimination between the treatments with and without algae (**Supplementary Figure S6**).

Effect of Aggregation on Algal Growth

Significant PLSR models for growth parameters (Y variables) on PSD and SS concentration in the exposure systems (X variables) were obtained for all materials tested (**Table 4**

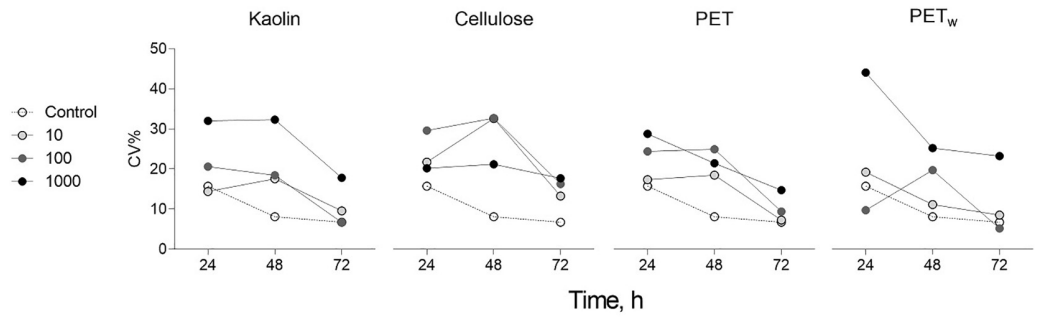

FIGURE 3 | Change in the coefficient of variation (CV%) of AUC values for growth curves of *R. subcapitata* exposed to microplastics and reference materials over the course of the experiment (72 h). The AUC values were grouped by test material (kaolin, cellulose, PET, and PET_w) and test concentration (10, 100, and 1,000 mg L^{-1}; $n = 5$); control values are shown on each plot for comparison.

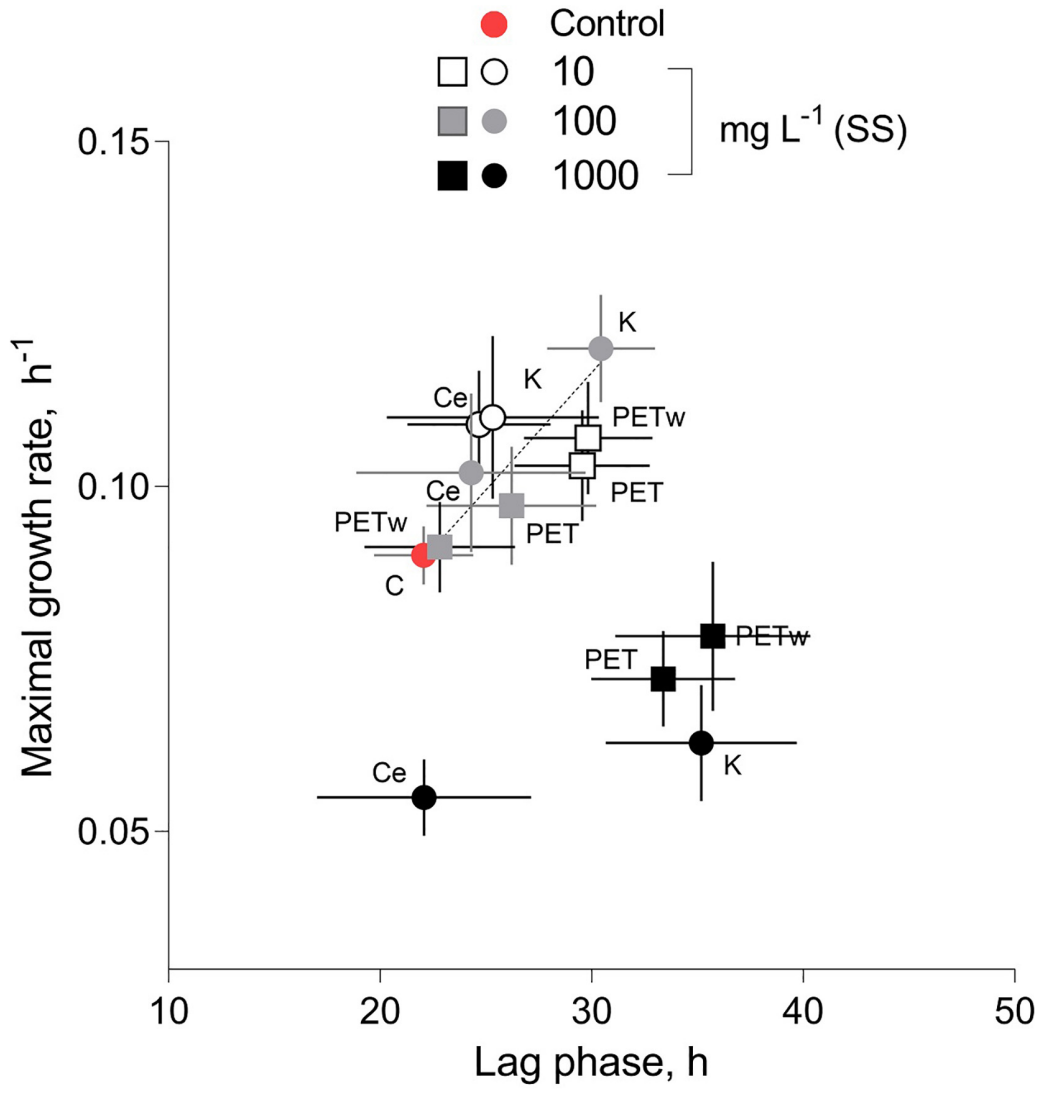

FIGURE 4 | Relationship between the maximal growth rate (μ, d^{-1}) and duration of the lag phase (λ, h) in *R. subcapitata* exposed to microplastic (virgin and weathered PET) and reference materials (kaolin, K, and cellulose, Ce) at concentrations of suspended solids (SS) 10, 100, and 1,000 mg L^{-1}. No suspended matter was added to the medium in control. Data are shown as means and SD ($n = 5$).

TABLE 3 | Outcome of Generalized Linear Models (GLMs) testing effects of the algae (*Algae*; present/absent) and suspended solids concentration (*SS*, mg L^{-1}) on the PSD characteristics for each reference (kaolin and cellulose) and test (PET and PET_w) material.

Material	PSD characteristic	Wald Stat. for		
		Main effects		Interaction
		Algae	SS	*Algae* × *SS*
Cellulose	Mean size	257.65***	461.64***	2.38
	Variance	10.18**	2.78	0.17
	Skewness	7.96**	4.30*	0.70
	Kurtosis	10.12**	6.02*	26.59***
	D_{10}	33.06***	103.71***	0.04
	D_{50}	217.46***	213.02***	9.04**
	D_{90}	52.87***	343.19***	11.84**
	D_{90} –D_{10}	1.64	24.61***	7.30*
Kaolin	Mean size	7.54*	0.39	0.57
	Variance	4.20*	20.18***	5.38*
	Skewness	3.64	22.85***	7.66*
	Kurtosis	5.71*	13.57***	23.98***
	D_{10}	11.79***	1.42	1.78
	D_{50}	8.05**	0.07	0.82
PET	Mean size	13.72**	0.40	3.49
	Variance	5.38*	1.44	2.02
	Skewness	5.02*	1.42	2.72
	D_{10}	0.01	0.55	11.77**
	D_{50}	10.95**	0.01	3.20
	D_{90}	9.02**	3.63	5.69*
	D_{90} –D_{10}	7.55*	3.64	1.97
PET_w	Mean size	360.68***	265.31***	56.20***
	Variance	1.41	4.16*	13.91**
	Skewness	0.50	1.20	10.86**
	Kurtosis	0.67	2.73	5.89*
	D_{10}	266.60***	59.24***	41.71***
	D_{50}	195.99***	99.81***	28.67***
	D_{90}	68.08***	103.95***	0.15
	D_{90} –D_{10}	16.08***	56.64***	1.06

*See **Figure 4** for the direction of the effects; *p < 0.05; **p < 0.01; ***p < 0.001. Not significant models were omitted.*

and **Supplementary Figure S7**). The predictive capacity for all models was high, with Q^2 varying from 74 to 96% (**Table 4**). In these models, 90–99% of the X-parameters variance explained 66–71% of the variance of the Y-variables (**Table 4**). Compared to the lag phase, the maximal growth rate and the AUC were better predicted by the X-variables, particularly in the algae exposed to kaolin and PET (**Supplementary Figure S7**). In all models, SS concentration, mean, and median particle sizes were identified as significant growth predictors (**Table 4**); other PSD characteristics in different combinations for different materials were also significant (**Supplementary Figure S7**).

For all materials, the overall growth performance was negatively related to particle size (mean size and D_{50}; **Supplementary Figure S7**). For kaolin, the SS concentration effects on the maximal growth and AUC values were weakly positive, whereas, for all other materials, it was negative, with the most substantial effects observed in the algae exposed to virgin PET. Other significant variables in the PLSR models were Variance and Skewness that were positive predictors in cellulose and PET_w models, whereas the particle range interval D_{90}–D_{10} was a significant negative predictor in kaolin and PET_w models (**Supplementary Figure S7**).

DISCUSSION

A step toward hazard assessment of plastic litter is to move it beyond its current exploratory state to experimental designs that provide delineation of microplastic effects from those of any suspended solids. Parallels can be drawn across particles and materials, regardless of whether they are natural solids, engineered nanomaterials, or plastics. On the other hand, it is essential to understand where the similarities end to avoid redundant testing and inappropriate methods and endpoints.

Using a combination of the standard growth inhibition test and PSD analysis, we found that both reference (kaolin and cellulose) and PET (virgin and weathered) materials with similar PSD s inhibited growth at the highest concentration (1,000 mg/L) but not at the lower concentrations. Similar results concerning the effect concentration were obtained for a green alga *Scenedesmus obliquus* exposed to polystyrene (PS; 0.07 μm particle size) by Besseling et al. (2014), who reported ∼3% inhibition rate at 1,000 mg/L and non-significant effects at lower concentrations. However, for another green alga *Dunaliella tertiolecta*, even lower concentrations of the same polymer (PS; particle size 0.05 μm, 250 mg/L) caused 57% growth inhibition (Sjollema et al., 2016). However, the effect mechanisms for nanoparticles are likely to be different from the micrometer-sized particles, as shown for nanoparticle-cell interactions that involve extracellular proteins in the algal cell membrane, with downstream effects on nutrient acquisition (Yue et al., 2017) or changes in colloidal stability affecting bio-physical interactions with cell walls (Gonzalo et al., 2014). In line with this, Nolte et al. (2017) using *Raphidocelis subcapitata*, i.e., the same green alga as in the present study, exposed to functionalized PS (0.11 μm) found 20–50% growth inhibition at concentrations 10–100 mg L^{-1}. Therefore, it is most likely the particle size, physicochemical properties, and chemical additives that leach out during the exposure, and not the polymer itself, govern algal responses in growth inhibition assays.

The responses may also vary during the exposure and depending on the growth phases, thus setting test duration requirements. For instance, in a green alga *Chlorella pyrenoidosa*, a reduction in growth was observed during the lag phase, with some inhibition in the exponential phase, but during the stationary phase, this trend was reversed due to a compensatory growth that exceeded the values observed in control (Mao et al., 2018). Such biphasic responses indicate that even when growth inhibition occurs, the algal populations are able to adapt and sustain productivity. In line with this, we found that at 10–100 mg L^{-1}, there was a significant positive correlation between the lag phase and the maximal growth

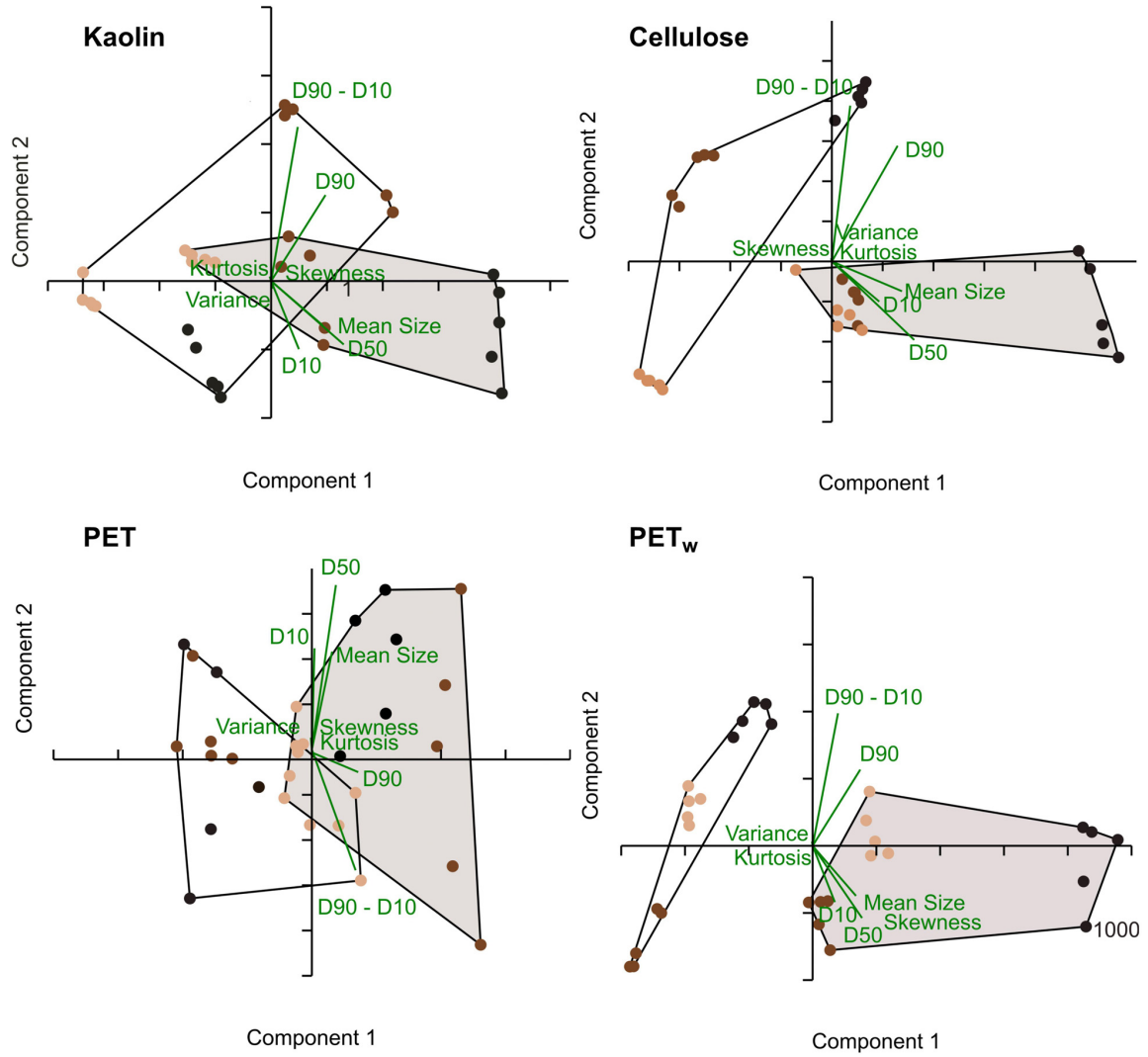

FIGURE 5 | PCA biplot for the PSD characteristics for the reference (kaolin and cellulose) and test (PET and PET_w) materials in the treatments with algae (shaded convex hulls) and without algae (open convex hulls). The color code for the test concentrations: light brown: 10 mg L^{-1}, dark brown: 100 mg L^{-1}, and black: 1,000 mg L^{-1}; $n = 5$ in all cases. The PCA loadings are shown in green.

rate during the exponential phase suggesting a compensatory growth due to adaptation during the exposure. A similar correlation between the growth parameters has been reported for algae exposed to other stressors (Andriukonis and Gorokhova, 2017). We also observed differential responses in the growth parameters, with the lag phase being the least affected by the test material (**Figure 2A**) and the total productivity represented by AUC values showing the most deviations from the controls (**Figure 2C**). Notably, while the lag phase in the lowest concentration was prolonged (albeit not significantly), the compensatory growth in 10–100 mg L^{-1} treatments was manifested as higher maximal growth during the exponential growth phase and the resulting total production that tended to be higher in the treatments with reference materials at 10 mg L^{-1} but not the polymers (**Figure 2**). At 100 mg L^{-1}, although a compensatory growth (33% higher than in control) was observed in kaolin treatment (**Figure 2B**), it was neither significant when corrected for multiple comparisons (**Supplementary Table S2**) nor sufficient to support the same production as in control (**Figure 1C**). At 1,000 mg L^{-1}, the significantly prolonged lag phase and lowered maximal growth rate resulted in significant production loss in all tested materials. Overall, the trends and the relationships between the growth parameters (**Figure 4**) were similar for all materials tested, suggesting the similarity of the adaptation mechanisms across all materials tested.

Low concentrations of suspended particles might also stimulate algal growth when the particles are both smaller (Zhao et al., 2019) and bigger (Chae et al., 2019) than the cell size. In line with that, some field studies suggested that, under certain conditions and at concentrations $<$ 100 mg L^{-1}, particulate matter may stimulate algal growth (Birkett et al., 2007). At

TABLE 4 | Significant PLSR models ($p < 0.05$) with growth parameters as dependent variables (all models) and PSD characteristics of the suspended solids and their concentration (SS) as explanatory variables for algae exposed to each reference and test material.

Response variables	Explanatory variables	Number of factors	R^2X	R^2X_{cum}	R^2Y	R^2Y_{cum}	Q^2	Q^2_{cum}	Root mean PRESS
Max growth rate, Lag phase, AUC					Kaolin				
	D_{90}–D_{10}, Mean size, SS, D_{50}, Skewness, D_{90}, D_{10}	1	0.755	0.755	0.512	0.512	0.627	0.627	0.817
		2	0.126	0.881	0.127	0.639	0.618	0.857	0.817
		3	0.108	0.989	0.055	0.696	0.638	0.948	0.780
	Cellulose								
	Variance, Mean size, D_{50}, D_{90}–D_{10}, Kurtosis, SS, D_{90}, D_{10}	1	0.762	0.762	0.486	0.487	0.512	0.513	0.823
		2	0.134	0.897	0.221	0.709	0.467	0.740	0.706
	PET								
	SS, D_{50}, Mean size	1	0.603	0.603	0.572	0.572	0.556	0.556	0.764
		2	0.375	0.979	0.083	0.655	0.782	0.903	0.714
	PET_w								
	Variance, D_{50}, Mean size, Skewness, D_{90}–D_{10}, D_{90}, D_{10}, SS	1	0.780	0.780	0.557	0.557	0.808	0.808	0.779
		2	0.141	0.920	0.136	0.694	0.789	0.960	0.727

The explanatory variables are listed in the order of importance based on their VIP score in the final model. All models comply with the quality criteria of Lundstedt et al. (1998). The Actual by Predicted plot for each model are shown in ***Supplementary Figure S8****.*

10–100 mg L^{-1}, the growth tended to be promoted in kaolin and cellulose exposures but not in the microplastic exposures. Moreover, the observed differences in AUC between the reference materials and PET_w were mainly due to this stimulatory effect in the kaolin and cellulose treatments. The growth stimulation decreased in the 100 mg L^{-1} treatments and became significantly inhibitory at 1,000 mg L^{-1} in all treatments. It is unlikely that kaolin and cellulose powder provided any additional nutrients to the algae; instead, the algal growth was most probably promoted by the topography of the heteroaggregates formed by algae and kaolin/cellulose at relatively low concentrations of suspended solids.

During the incubation, the aggregation occurred in both particle blanks (no algae) and all treatments with algae (**Supplementary Figure S3**). Moreover, the aggregation was significantly facilitated by the presence of algae compared to the blanks, indicating that heteroaggregates, i.e., aggregates formed by test particles and algal cells, had different PSD characteristics compared to homoaggregates, i.e., those formed by test particles only in the blank treatment for each material (**Supplementary Figure S4**). The production of extracellular polymeric substances (EPS) by algae was a likely driver facilitating heteroaggregate formation (Costa et al., 2018) and morphology (**Figure 5**). It has been suggested that EPS production is enhanced in algal cells exposed to foreign matter, such as polymer particles, facilitating aggregation (Bergami et al., 2017). Similarly, Lagarde et al. (2016) explained the observed variability in heteroaggregate formation as a result of different composition of EPS produced by algae in response to polymer material. Moreover, certain algal species produce more hydrophobic EPS resulting in bigger aggregates (Chen et al., 2011; Long et al., 2015). In time series, dose-response aggregation kinetics has been reported with a positive relationship between the aggregate size and mass concentration of particulate matter (Chen et al., 2011). *In situ*, however, the interactions between microorganisms, natural particulates, and microplastics may change the pollutant characteristics over time and define how and why cells attach to plastic particles. The attachment patterns can also vary depending on the microbial communities present in the system as well as other particulates (Rogers et al., 2020), which can be addressed in the test designs by using treatments with ambient water with natural bacterioplankton in addition to the treatments with sterile exposure media. Thus, the aggregate formation is species-, media-, and polymer-material-dependent (Long et al., 2015), making it challenging to incorporate it in microplastic hazard assessment and evaluate the effects of exposure to mixed particulates (including microplastic) in bioassays. However, in the effect studies, these dependencies can be evaluated.

We used a plankton wheel to prevent sedimentation that kept the test particles and the algae in suspension during the exposure. Clearly, control of sedimentation and aggregation should be an essential methodological requirement in effect studies with

particulate materials if we are to provide reliable data for the hazard assessment. During the toxicity testing, the aggregation can effectively remove particles from the system, thus decreasing particle number concentrations and adverse effects. For example, Fu et al. (2019) observed higher toxicity of PVC for algae at low levels (10 mg L^{-1}) compared to higher concentrations (1,000 mg L^{-1}). They explained this phenomenon as a result of particle aggregation and sedimentation in the experimental system (Fu et al., 2019), thus, efficiently decreasing the exposure. Moreover, homoaggregate formation implies a lower collision/encounter rate between the test particles and algal cells and thus a lower probability of direct interactions. Heteroaggregates, on the other hand, provide a different habitat for algae that are embedded in the aggregates, where the nutrient and light regimes may differ from that experienced by solitary cells, with concomitant effects on algal growth. Notably, these growth effects induced by aggregation with, for example, mineral particles, can be both positive and negative (Cuadros, 2017). We found that algal growth was affected primarily by the aggregate size and its variability, and to a lesser extent by the concentration of the suspended solids in the system (**Table 4**). In line with the nitrient/light limitation reasoning, smaller aggregates supported higher growth, whereas a higher concentration of the suspended solids had inhibitory effects in all but the kaolin treatments (**Supplementary Figure S7**).

No differences in any of the growth parameters were observed between the treatments with PET and PET_w (**Figure 2**). However, there was a significantly higher within-treatment variability in the PET_w treatment at the highest concentration (**Figure 3**). Moreover, there were significant differences in the PSD parameters between the weathered and virgin PET treatments following the exposure, with higher aggregation in the presence of algae for PET_w compared to PET. Also, the PSD-predictors driving algal growth in PET_w treatment were more diverse and included Variance and Skewness as positive drivers, suggesting that morphological variability of the aggregates (1) has increased following the weathering treatment, (2) facilitated cell-particles interactions, and (3) may become decisive in governing growth of algae and, perhaps, other microorganisms when present. Due to the changes in functional groups and an increase in the particle surface area, weathered PVC has been reported to induce more substantial growth inhibition in freshwater alga *Chlorella vulgaris* (Fu et al., 2019). This, however, can also be related to the increased leaching of chemicals associated with the weathered material. For our experiment, we selected PET as a test material having no measurable leachate toxicity on our test alga (Capolupo et al., 2020) in order to focus on the particle-alga interactions and the potential differences between the weathered and virgin particles of the same material as well as between the polymer and the reference materials. Our findings suggest that significant growth predictors in the PET_w exposure were more similar to the cellulose treatment than to the PET treatment (**Supplementary Figure S7**). Thus, plastic-microorganism interactions change with the plastic aging, but these changes may lead to convergence of the physicochemical properties in different materials, and they do not necessarily lead to more severe impacts on biota.

In conclusion, we need to be able to generate high-quality data on the plastic litter effects in biota, which is particularly challenging for the smaller size fractions of the plastic litter because of the inavoidable interactions with other particulate materials present in the environment but also interactions with microorganisms resulting in aggregation and secondary effects. We found no indication that PET particles, regardless of the weathering status, induced higher growth inhibition in unicellular algae than the naturally occurring particles represented by kaolin and cellulose. The comparison among PSD s across the treatments showed that both particulate matter concentration and topography of the particle aggregates were significant growth predictors for algae exposed to any test material, which must be taken into account when developing protocols for hazard assessment of plastic litter and other solid waste.

DATA AVAILABILITY STATEMENT

The datasets presented in this study can be found in online repositories. The names of the repository/repositories and accession number(s) can be found below: GitHub, https://github.com/elenagoro/MP_algae.

AUTHOR CONTRIBUTIONS

EG and KE designed the experiment. KE performed the experiment and collected data. EG and SR wrote the manuscript and conducted statistical analysis. All authors contributed to the data interpretation and writing.

FUNDING

This research was supported by the Joint Programming Initiative Healthy and Productive Seas and Oceans (JPI Oceans, WEATHER-MIC project, grant no. 942-2015-1866 to EG); The Swedish Innovation Agency (VINNOVA) and the joint Baltic Sea research and development program (BONUS, Blue Baltic) for MICROPOLL project (grant No. 2017-00979 to EG); The Swedish Environmental Protection Agency (Naturvårdsverket) for MIxT project (grant No. 802-0160-18 to EG).

ACKNOWLEDGMENTS

Zandra Gerdes and Birgitta Liewenborg (ACES, Stockholm University) are thanked for suggestions on the experimental design and technical assistance.

SUPPLEMENTARY MATERIAL

The Supplementary Material for this article can be found online at: https://www.frontiersin.org/articles/10.3389/fenvs.2020.551075/full#supplementary-material

REFERENCES

Adam, V., Yang, T., and Nowack, B. (2019). Toward an ecotoxicological risk assessment of microplastics: Comparison of available hazard and exposure data in freshwaters: Environmental risk assessment of microplastics. *Environ. Toxicol. Chem.* 38, 436–447. doi: 10.1002/etc.4323

Andrady, A. L., and Neal, M. A. (2009). Applications and societal benefits of plastics. *Philos. Trans. R. Soc. Lond. B Biol. Sci.* 364, 1977–1984. doi: 10.1098/rstb.2008.0304

Andriukonis, E., and Gorokhova, E. (2017). Kinetic 15N-isotope effects on algal growth. *Sci. Rep.* 7:44181. doi: 10.1038/srep44181

Baranyi, J., and Roberts, T. A. (1994). A dynamic approach to predicting bacterial growth in food. *Int. J. Food Microbiol.* 23, 277–294. doi: 10.1016/0168-1605(94)90157-90150

Benjamini, Y., Krieger, A. M., and Yekutieli, D. (2006). Adaptive linear step-up procedures that control the false discovery rate. *Biometrika* 93, 491–507. doi: 10.1093/biomet/93.3.491

Bergami, E., Pugnalini, S., Vannuccini, M. L., Manfra, L., Faleri, C., Savorelli, F., et al. (2017). Long-term toxicity of surface-charged polystyrene nanoplastics to marine planktonic species Dunaliella tertiolecta and Artemia franciscana. *Aquat. Toxicol.* 189, 159–169. doi: 10.1016/j.aquatox.2017.06.008

Besseling, E., Wang, B., Lürling, M., and Koelmans, A. A. (2014). Nanoplastic Affects Growth of S. *obliquus and Reproduction of D. magna*. *Environ. Sci. Technol.* 48, 12336–12343. doi: 10.1021/es503001d

Bhattacharya, P., Lin, S., Turner, J. P., and Ke, P. C. (2010). Physical Adsorption of Charged Plastic Nanoparticles Affects Algal Photosynthesis. *J. Phys. Chem. C* 114, 16556–16561. doi: 10.1021/jp1054759

Bilotta, G. S., and Brazier, R. E. (2008). Understanding the influence of suspended solids on water quality and aquatic biota. *Water Res.* 42, 2849–2861. doi: 10.1016/j.watres.2008.03.018

Birkett, C., Tollner, E. W., and Gattie, D. K. (2007). Total Suspended Solids and Flow Regime Effects on Periphyton Development in a Laboratory Channel. *Trans. ASABE* 50, 1095–1104. doi: 10.13031/2013.23118

Blott, S. J., and Pye, K. (2001). GRADISTAT: a grain size distribution and statistics package for the analysis of unconsolidated sediments. *Earth Surf. Process. Landforms* 26, 1237–1248. doi: 10.1002/esp.261

Bråte, I. L. N., Blázquez, M., Brooks, S. J., and Thomas, K. V. (2018). Weathering impacts the uptake of polyethylene microparticles from toothpaste in Mediterranean mussels (M . *galloprovincialis)*. *Sci. Total Environ.* 626, 1310–1318. doi: 10.1016/j.scitotenv.2018.01.141

Cahoon, L. B., Nearhoof, J. E., and Tilton, C. L. (1999). Sediment Grain Size Effect on Benthic Microalgal Biomass in Shallow Aquatic Ecosystems. *Estuaries* 22, 735. doi: 10.2307/1353106

Capolupo, M., Sørensen, L., Jayasena, K. D. R., Booth, A. M., and Fabbri, E. (2020). Chemical composition and ecotoxicity of plastic and car tire rubber leachates to aquatic organisms. *Water Res.* 169:115270. doi: 10.1016/j.watres.2019.115270

Chae, Y., Kim, D., and An, Y.-J. (2019). Effects of micro-sized polyethylene spheres on the marine microalga Dunaliella salina: focusing on the algal cell to plastic particle size ratio. *Aquat. Toxicol.* 216:105296. doi: 10.1016/j.aquatox.2019.105296

Chapman, P. M., Hayward, A., and Faithful, J. (2017). Total Suspended Solids Effects on Freshwater Lake Biota Other than Fish. *Bull. Environ. Contam. Toxicol.* 99, 423–427. doi: 10.1007/s00128-017-2154-y

Chen, C.-S., Anaya, J. M., Zhang, S., Spurgin, J., Chuang, C.-Y., Xu, C., et al. (2011). Effects of Engineered Nanoparticles on the Assembly of Exopolymeric Substances from Phytoplankton. *PLoS One* 6:21865. doi: 10.1371/journal.pone.0021865

Coe, J. M., Bud Antonelis, G., and Moy, K. (2019). Taking control of persistent solid waste pollution. *Mar. Pollut. Bull.* 139, 105–110. doi: 10.1016/j.marpolbul.2018.12.004

Costa, O. Y. A., Raaijmakers, J. M., and Kuramae, E. E. (2018). Microbial Extracellular Polymeric Substances: Ecological Function and Impact on Soil Aggregation. *Front. Microbiol.* 9:1636. doi: 10.3389/fmicb.2018.01636

Cuadros, J. (2017). Clay minerals interaction with microorganisms: a review. *Clay Miner.* 52, 235–261. doi: 10.1180/claymin.2017.052.2.05

Foley, C. J., Feiner, Z. S., Malinich, T. D., and Höök, T. O. (2018). A meta-analysis of the effects of exposure to microplastics on fish and aquatic invertebrates. *Sci. Total Environ.* 63, 550–559. doi: 10.1016/j.scitotenv.2018.03.046

Folk, R. L., and Ward, W. C. (1957). Brazos River Bar: A Study in the Significance of Grain Size Parameters. *J. Sediment. Petrol.* 27, 3–26. doi: 10.1306/74d70646-2b21-11d7-8648000102c1865d

Fu, D., Zhang, Q., Fan, Z., Qi, H., Wang, Z., and Peng, L. (2019). Aged microplastics polyvinyl chloride interact with copper and cause oxidative stress towards microalgae Chlorella vulgaris. *Aquat. Toxicol.* 216:105319. doi: 10.1016/j.aquatox.2019.105319

Galgani, L., Tsapakis, M., Pitta, P., Tsiola, A., Tzempelikou, E., Kalantzi, I., et al. (2019). Microplastics increase the marine production of particulate forms of organic matter. *Environ. Res. Lett.* 14:124085. doi: 10.1088/1748-9326/ab59ca

Gerdes, Z., Hermann, M., Ogonowski, M., and Gorokhova, E. (2019). A novel method for assessing microplastic effect in suspension through mixing test and reference materials. *Sci. Rep.* 9:10695. doi: 10.1038/s41598-019-47160-47161

Gonçalves, A. L., Pires, J. C. M., and Simões, M. (2016). The effects of light and temperature on microalgal growth and nutrient removal: an experimental and mathematical approach. *RSC Adv.* 6, 22896–22907. doi: 10.1039/C5RA26117A

Gonzalo, S., Llaneza, V., Pulido-Reyes, G., Fernández-Piñas, F., Bonzongo, J. C., Leganes, F., et al. (2014). A Colloidal Singularity Reveals the Crucial Role of Colloidal Stability for Nanomaterials In-Vitro Toxicity Testing: nZVI-Microalgae Colloidal System as a Case Study. *PLoS One* 9:109645. doi: 10.1371/journal.pone.0109645

Hammer, Ø, Harper, D. A. T., and Ryan, P. D. (2001). PAST: Paleontological statistics software package for education and data analysis. *Palaeontol. Electronic.* 4:9.

He, Q., Qiu, Y., Liu, H., Sun, X., Kang, L., Cao, L., et al. (2017). New insights into the impacts of suspended particulate matter on phytoplankton density in a tributary of the Three Gorges Reservoir, China. *Sci. Rep.* 7, 1–11. doi: 10.1038/s41598-017-13235-13230

Jahnke, A., Arp, H. P. H., Escher, B. I., Gewert, B., Gorokhova, E., Kühnel, D., et al. (2017). Reducing Uncertainty and Confronting Ignorance about the Possible Impacts of Weathering Plastic in the Marine Environment. *Environ. Sci. Technol. Lett.* 4, 85–90. doi: 10.1021/acs.estlett.7b00008

Lagarde, F., Olivier, O., Zanella, M., Daniel, P., Hiard, S., and Caruso, A. (2016). Microplastic interactions with freshwater microalgae: Hetero-aggregation and changes in plastic density appear strongly dependent on polymer type. *Environ. Pollut.* 215, 331–339. doi: 10.1016/j.envpol.2016.05.006

Lenz, R., Enders, K., and Nielsen, T. G. (2016). Microplastic exposure studies should be environmentally realistic. *PNAS* 113, E4121–E4122. doi: 10.1073/pnas.1606615113

Long, M., Moriceau, B., Gallinari, M., Lambert, C., Huvet, A., Raffray, J., et al. (2015). Interactions between microplastics and phytoplankton aggregates?: Impact on their respective fates. *Mar. Chem.* 175, 39–46. doi: 10.1016/j.marchem.2015.04.003

Lundstedt, T., Seifert, E., Abramo, L., and Thelin, B. (1998). Experimental design and optimization. *Chemom. Intell. Lab. Syst.* 42, 3–40.

Ma, J., Lin, F., Zhang, R., Yu, W., and Lu, N. (2004). Differential sensitivity of two green algae. *Scenedesmus quadricauda and Chlorella vulgaris, to 14 pesticide adjuvants. Ecotoxicol. Environ. Saf.* 58, 61–67. doi: 10.1016/j.ecoenv.2003.08.023

Mao, Y., Ai, H., Chen, Y., Zhang, Z., Zeng, P., Kang, L., et al. (2018). Phytoplankton response to polystyrene microplastics: Perspective from an entire growth period. *Chemosphere* 208, 59–68. doi: 10.1016/j.chemosphere.2018.05.170

McGivney, E., Cederholm, L., Barth, A., Hakkarainen, M., Hamacher-Barth, E., Ogonowski, M., et al. (2020). Rapid Physicochemical Changes in Microplastic Induced by Biofilm Formation. *Front. Bioeng. Biotechnol.* 8:205. doi: 10.3389/fbioe.2020.00205

Nolte, T. M., Hartmann, N. B., Kleijn, J. M., Garnæs, J., van de Meent, D., Jan Hendriks, A., et al. (2017). The toxicity of plastic nanoparticles to green algae as influenced by surface modification, medium hardness and cellular adsorption. *Aquat. Toxicol.* 183, 11–20. doi: 10.1016/j.aquatox.2016.12.005

Oecd. (2006). *Test No. 201: Alga, Growth Inhibition Test, OECD Guidelines for the Testing of Chemicals, Section 2: Effects on Biotic Systems*. Paris: OECD. Available online at: https://doi.org/10.1787/9789264069923-en (accessed February 2, 2020).

Oelschlägel, K., Pfeiffer, J., and Potthoff, A. (2018). "Imitating the Weathering of Microplastics in the Marine Environment," in *Proceedings of the International Conference on Microplastic Pollution in the Mediterranean Sea*, eds M. Cocca,

E. Di Pace, M. E. Errico, G. Gentile, A. Montarsolo, and R. Mossotti (New York, NY: Springer), 171–179. doi: 10.1007/978-3-319-71279-6_23

Ogonowski, M., Edlund, U., Gorokhova, E., Linde, M., Ek, K., Liewenborg, B., et al. (2018a). Multi-level toxicity assessment of engineered cellulose nanofibrils in Daphnia magna. *Nanotoxicology* 12, 509–521. doi: 10.1080/17435390.2018.1464229

Ogonowski, M., Gerdes, Z., and Gorokhova, E. (2018b). What we know and what we think we know about microplastic effects – A critical perspective. *Curr. Opin. Environ. Sci. Health* 1, 41–46. doi: 10.1016/j.coesh.2017.09.001

Paul-Pont, I., Tallec, K., Gonzalez-Fernandez, C., Lambert, C., Vincent, D., Mazurais, D., et al. (2018). Constraints and Priorities for Conducting Experimental Exposures of Marine Organisms to Microplastics. *Front. Mar. Sci.* 5:252. doi: 10.3389/fmars.2018.00252

Phuong, N. N., Zalouk-Vergnoux, A., Poirier, L., Kamari, A., Châtel, A., Mouneyrac, C., et al. (2016). Is there any consistency between the microplastics found in the field and those used in laboratory experiments? *Environ. Pollut.* 211, 111–123. doi: 10.1016/j.envpol.2015.12.035

Prata, J. C., da Costa, J. P., Lopes, I., Duarte, A. C., and Rocha-Santos, T. (2019). Effects of microplastics on microalgae populations: A critical review. *Sci. Total Environ.* 665, 400–405. doi: 10.1016/j.scitotenv.2019.02.132

Reichelt, S., and Gorokhova, E. (2020). Micro- and Nanoplastic Exposure Effects in Microalgae: A Meta-Analysis of Standard Growth Inhibition Tests. *Front. Environ. Sci.* 8:131. doi: 10.3389/fenvs.2020.00131

Robinson, S. E., Capper, N. A., and Klaine, S. J. (2009). The effects of continuous and pulsed exposures of suspended clay on the survival, growth, and reproduction of Daphnia magna. *Environ. Toxicol. Chem.* 29, 168–175. doi: 10.1002/etc.4

Rochman, C. M., Brookson, C., Bikker, J., Djuric, N., Earn, A., Bucci, K., et al. (2019). Rethinking microplastics as a diverse contaminant suite. *Environ. Toxicol. Chem.* 38, 703–711. doi: 10.1002/etc.4371

Rogers, K. L., Carreres−Calabuig, J. A., Gorokhova, E., and Posth, N. R. (2020). Micro-by-micro interactions: How microorganisms influence the fate of marine microplastics. *Limnol. Oceanogr. Lett.* 5, 18–36. doi: 10.1002/lol2.10136

Sjollema, S. B., Redondo-Hasselerharm, P., Leslie, H. A., Kraak, M. H. S., and Vethaak, A. D. (2016). Do plastic particles affect microalgal photosynthesis and growth? *Aquatic Toxicol.* 170, 259–261. doi: 10.1016/j.aquatox.2015.12.002

Tsai, K.-P., and Chen, C.-Y. (2007). An algal toxicity database of organic toxicants derived by a closed-system technique. *Environ. Toxicol. Chem.* 26:1931. doi: 10.1897/06-612R.1

Vaas, L. A. I., Sikorski, J., Michael, V., Göker, M., and Klenk, H.-P. (2012). Visualization and Curve-Parameter Estimation Strategies for Efficient Exploration of Phenotype Microarray Kinetics. *PLoS One* 7:e34846. doi: 10.1371/journal.pone.0034846

Wold, S., Sjöström, M., and Eriksson, L. (2001). PLS-regression: a basic tool of chemometrics. *Chemom. Intell. Lab. Syst.* 58, 109–130. doi: 10.1016/S0169-7439(01)00155-151

Yokota, K., Waterfield, H., Hastings, C., Davidson, E., Kwietniewski, E., and Wells, B. (2017). Finding the missing piece of the aquatic plastic pollution puzzle: Interaction between primary producers and microplastics: Aquatic plastic pollution puzzle. *Limnol. Oceanogr. Lett.* 2, 91–104. doi: 10.1002/lol2.10040

Yue, Y., Li, X., Sigg, L., Suter, M. J.-F., Pillai, S., Behra, R., et al. (2017). Interaction of silver nanoparticles with algae and fish cells: a side by side comparison. *J. Nanobiotechnol.* 15:16. doi: 10.1186/s12951-017-0254-259

Zhao, T., Tan, L., Huang, W., and Wang, J. (2019). The interactions between micro polyvinyl chloride (mPVC) and marine dinoflagellate Karenia mikimotoi: The inhibition of growth, chlorophyll and photosynthetic efficiency. *Environ. Pollut.* 247, 883–889. doi: 10.1016/j.envpol.2019.01.114

Conflict of Interest: The authors declare that the research was conducted in the absence of any commercial or financial relationships that could be construed as a potential conflict of interest.

frontiers in Environmental Science

ORIGINAL RESEARCH
published: 11 February 2021
doi: 10.3389/fenvs.2020.549896

Assessing CeO_2 and TiO_2 Nanoparticle Concentrations in the Seine River and Its Tributaries Near Paris

Karine Phalyvong[1,2], *Yann Sivry*[1]*, *Hélène Pauwels*[2], *Alexandre Gélabert*[1], *Mickaël Tharaud*[1], *Guillaume Wille*[2], *Xavier Bourrat*[2], *James F. Ranville*[3] and *Marc F. Benedetti*[1]

[1] Université de Paris, Institut de physique du globe de Paris, CNRS, Paris, France, [2] BRGM, Orleans, France, [3] Colorado School of Mines, Golden, CO, United States

OPEN ACCESS

Edited by:
Denise M. Mitrano,
ETH Zürich, Switzerland

Reviewed by:
Danielle Slomberg,
UMR7330 Center Européen de Recherche et d'enseignement de Géosciences de l'environnement (CEREGE), France
Jerome Labille,
Aix-Marseille Université, France

***Correspondence:**
Yann Sivry
sivry@ipgp.fr

Specialty section:
This article was submitted to Biogeochemical Dynamics, a section of the journal Frontiers in Environmental Science

Received: 07 April 2020
Accepted: 02 December 2020
Published: 11 February 2021

Citation:
Phalyvong K, Sivry Y, Pauwels H, Gélabert A, Tharaud M, Wille G, Bourrat X, Ranville JF and Benedetti MF (2021) Assessing CeO_2 and TiO_2 Nanoparticle Concentrations in the Seine River and Its Tributaries Near Paris.
Front. Environ. Sci. 8:549896.
doi: 10.3389/fenvs.2020.549896

Motivation for detecting engineered nanoparticles (ENPs) in the environment comes from a need to understand fate and behavior of these materials in natural matrices. The difficulty lies in the low expected ENP particle number concentration (PNC) and the presence of a large and variable background concentration of natural NPs. We report the PNCs and characteristics of cerium-bearing nanoparticles (Ce-NPs) and titanium-bearing nanoparticles (Ti-NPs) in an aquatic matrix (the Seine River and three of its tributaries) with the use of single particle ICP-MS (spICPMS) and electron microscopy (FEG-SEM). Ce-bearing and Ti-bearing particles were observed in suspended particulate matter collected onto 0.2 μm and 1 kDa filters, using FEG-SEM imaging. At Marnay-sur-Seine, the upstream point, PNCs for Ce-NPs and Ti-NPs were $0.47 \pm 0.07 \times 10^6$ and $1.35 \pm 0.17 \times 10^6$ particles as measured by spICPMS. The maximum PNC for both Ce-NPs and Ti-NPs, $1.59 \pm 0.10 \times 10^6$ particles mL^{-1} and $5.89 \pm 0.10 \times 10^6$ particles mL^{-1}, respectively, were found in the Marne River, a major tributary to the Seine. It was shown that downstream of each confluence, an increase in the PNC of the Seine is observed, suggesting a significant contribution of the different tributaries. Mass balance of particles flows and elemental ratios of Ce/La showed that in the Marne and the Oise River, a contribution of natural CeO_2 NPs exists. The anthropogenic contribution in TiO_2 ENPs for the Marne River was further assessed with Ti/Al, Ti/V, and Ti/Y elemental ratios. Near constant element ratios in the Seine below the Orge River and Paris city suggest neither contribute significantly to Ce or Ti NP concentrations. The study provides further investigation of the strengths and limitations of the application of spICPMS to natural samples and contributes data to the currently highly-limited dataset on natural NP backgrounds in rivers, information that is key to assessing the potential for quantifying the input of ENPs to surface waters. Of the total mass of Ce and Ti, 83 and 90%, respectively, could be detected as particles by spICPMS.

Keywords: engineered (nano)-particles, suspended particulate matter (SPM), TiO_2, CeO_2, FEG-SEM, elemental ratio, single-particle ICPMS, natural river water

INTRODUCTION

Quantifying engineered nanoparticles (ENPs) at relevant analytical concentrations is the key step to assess the fate and behavior of these particles in the environment. Numerous nanotoxicological studies have shown that ENPs can be acutely toxic (Navarro et al., 2008; Kahru and Dubourguier, 2010). However, nearly all toxicological studies utilize concentrations higher than that expected in the environment. Predicted environmental concentrations (PECs), obtained by materials flow analysis, are at ppb or ppt levels (Gottschalk et al., 2013). Even though PECs for most ENPs are low, the flows in the environment are significant (tons per year). For instance, titanium dioxide NPs (TiO_2NPs) have been modeled to have a flow from the production, manufacturing and consumption sector to sewage treatment plants of 1,586 tons per year in the United States (Gottschalk et al., 2009). These high flows are mostly due to the important production of ENPs, which keeps increasing over the years because of the industries that incorporate NPs to enhance their products' properties.

While assessing ENP concentrations is the primary driver of research in this area, natural NPs are an important component of earth systems (Hochella et al., 2019). Method development that advances our ability to examine these materials are also useful for better understanding biogeochemical cycles that involve NPs. Quantifying ENPs that exist among natural phases, especially natural NPs, requires analytical tools suitable to the quantification and characterization of NPs in these samples. The use of ICP-MS in single particle counting mode (spICPMS) is one of the most useful and powerful tools for the detection and the characterization of NPs in complex matrices. The theory of spICPMS has been widely described for size analysis of colloids (Degueldre and Favarger, 2003; Degueldre et al., 2006) and more recently for NPs (Laborda et al., 2011; Pace et al., 2011; Mitrano et al., 2012). This technique provides the mass of NP-associated elements, from which a size distribution can be computed, given assumptions about NP shape, composition, and density. Additionally, spICP-MS provides the particle number concentration (PNC) (Pace et al., 2011, 2012; Mitrano et al., 2012; Laborda et al., 2013). These two parameters (i.e., size distribution and PNC) are useful to characterize NPs in environmental matrices. While we report the spICPMS method as providing data on ceria nanoparticles (CeO_2NPs) and titanium dioxide nanoparticles (TiO_2NPs), the authors recognize that spICPMS does not give direct information on form. Individual NPs, heteroaggregates of NPs with suspended sediments, and suspended sediments containing minor amounts of Ce or Ti cannot be differentiated by the spICPMS method alone. Thus, the reporting of size is in order to follow convention and does not necessarily represent the size of the overall particle with which the Ce or Ti is associated.

The spICPMS technique has been recently applied to environmental samples such as surface waters for the detection of TiO_2NPs potentially released from sunscreens (Gondikas et al., 2014; Reed et al., 2017), or to decipher the AgNPs flow according to the land use (Wang et al., 2020). In drinking waters, spICPMS was successfully used to examine the removal of ENPs such as ceria NPs (CeO_2NPs) or AgNPs (Donovan et al., 2016a,b; Peters et al., 2018). Biological tissues have been examined by spICP-MS including foods like chicken and beef (Gray et al., 2013; Loeschner et al., 2013; Peters et al., 2014) as well as rice and tomato plants (Dan et al., 2015; Deng et al., 2017) for the study of TiO_2 NPs, AgNPs, and AuNPs.

The complexity of these matrices makes the characterization of NPs very challenging, which is why appropriate methods are required.

Ceria nanoparticles (CeO_2NPs) and titanium dioxide nanoparticles (TiO_2NPs) have beneficial properties (Serpone et al., 2007; Lima et al., 2009; Virkutyte et al., 2012). CeO_2 NPs are used as a fuel additive in cars and as an automobile catalyzer (Gómez-Rivera et al., 2012) because they possess a low redox potential (Van Hoecke et al., 2009) and a high oxygen storage capacity (Imagawa et al., 2011; Zhang et al., 2011). Regarding TiO_2NPs, they can be anticorrosive, stable in solution and photocatalytic (Hashimoto et al., 2005) so they are incorporated into paints, sunscreens and cosmetics. Engineered TiO_2NPs are often coated with a layer of alumina, with the aim of inhibiting their photocatalytic properties (Serpone et al., 2007; Virkutyte et al., 2012). They are some of the most studied NPs because they are wide-spread in the world (Keller and Lazareva, 2014). For example, mass flow modeling (using the highest estimate) predicts that 89 and 4,055 tons per year CeO_2NPs and TiO_2NPs are released into European River waters.

Relatively few studies have examined TiO_2NPs in aquatic systems. TiO_2NPs in a Danube recreational lake was examined over a year period and elevated summer levels (1.7×10^4 particles mL^{-1}) may indicate release of these NPs from sunscreens (Gondikas et al., 2014). In a similar study by Reed et al. (2017) Ti-containing particles were elevated during bathing hours in a stream that is used for recreation, with sediment resuspension by bathers being a likely cause. Additionally, Westerhoff et al. (2011) have indicated the presence of TiO_2 NPs between 4 and 30 nm in diameter in WWTP effluents that are particularly released into lakes, rivers, and streams. Particle characterization of surface waters by spICP-MS was recently performed in our group for samples of the Loire River around two sites of interest (wastewater treatment plant outlet and an outdoor activity center) (Phalyvong et al., 2020).

In this previous work, the studied CeO_2NPs in river water were shown to be potentially insoluble and probably aggregated with sizes higher than 100 nm. In addition to TiO_2, ZnO, and CeO_2NPs aggregates were also shown to be stabilized at 300 nm with the occurrence of NOM in mesocosm freshwater (Keller et al., 2010) and natural surface waters (Peters et al., 2018). In another study, NOM stabilized CeO_2NPs (from 2.2 mgC L^{-1} in an algal medium) and prevented the formation of larger aggregation of the NPs (>1 mm; Van Hoecke et al., 2011; Oriekhova and Stoll, 2019). Moreover, CeO_2NPs are supposed to be insoluble at pH higher than 7 (Dahle et al., 2015).

The objective of the study presented herein is three-fold. First the results of the study will contribute to the very few studies conducted on NP concentrations in surface waters. Specifically, the study applies the spICPMS technique to the detection and quantification of CeO_2NPs and TiO_2NPs in the Seine River,

France, one of the major rivers of Europe that is impacted by both agricultural and industrial activities. Secondly, the study investigates the spatial variability around a major capital (Paris) by assessing the possible contribution of both the city and three different tributaries. Finally, it evaluates the ability of some tools such as the elemental ratios of Ce/La and of Ti/Al, to discriminate the origin (natural or anthropogenic) of these NPs. Both Ce and La are known to exist in a relatively fixed ratio in suspended sediments and changes to this ratio may indicate anthropogenic contributions of Ce. Similarly, release of engineered TiO_2 could perturb its ratio to naturally-occuring elements such as Al.

MATERIALS AND METHODS

Field Settings

The study area is the Seine River in the vicinity of Paris, France, and includes the confluence with one minor (Orge River) and two major (Marne River, Oise Rivers) tributaries. The Seine is one of the longest rivers in Europe (780 km) flowing from the "Plateau de Langres" in the east of France to the English Channel. The Seine basin mainly drains sedimentary rocks, with the predominant rock types being 78% and 15% carbonates and silicates, respectively (Roy et al., 1999). Extensive farming and natural vegetation (forest) dominate most of the Seine River basin except near Paris city, where industrial and urban activities provide an important contribution to land use.

Sampling of the Seine River and three of its tributaries (**Figure 1**) was carried out on May 11th, 2015 during a high water level in order to optimize the chances to observe particles leached from surface runoff. Seven sampling sites on the Seine River (from SR1 to SR7) and three tributaries (TR1 for the Orge River, TR2 for the Marne River and TR3 for the Oise River) were selected for this field investigation. Several moderate water inputs to the Seine River exist between SR1 and TR1 but were not sampled in this study. Approximately one liter of water was collected per site for analysis by spICPMS and the FEG-SEM. Water sampled at Marnay-sur-Seine (SR1), 96 km upstream Paris, represents the Seine with the least influence of industrial, and urban activities. Thus, SR1 should have low ENP contributions to the total suspended particulate matter. Water samples collected at Alfortville city (SR2), Paris city (SR3), Argenteuil city (SR4), Bougival city (SR5), and at Conflans-Sainte-Honorine city (SR6) have greater potential for ENP inputs. A wastewater treatment plant (WWTP), discharges to the Seine River near Achères city (not sampled), between the SR5 and SR6 sampling locations. The most downstream sampling location is at Triel-sur-Seine (SR7). The first (TR1), second (TR2), and third tributary (TR3) are located between SR1 and SR2, SR2 and SR3, and SR6 and SR7 sampling points, respectively.

Water Chemistry, Major, and Trace Elements

Measurements of pH, dissolved oxygen, conductivity, and temperature were performed on site immediately after sampling, using a WTW 3410 Set 2 multiparameter field probe. To separate the conventional dissolved fraction from the Suspended Particulate Matter (SPM), filtration of 1 L of water sample was also performed on site with an Amicon filtration cell and 0.2 µm polyethersulfone (PES) filters, previously cleaned in the lab with MilliQ water and dried in an oven at 105°C. Laboratory measurements of non-acidified, filtered samples for anions and alkalinity utilized a ThermoScientific ICS 1100 and a Metrohm Titrando 809, respectively. The filtered waters were acidified with 16 N HNO_3 and dissolved major cations and trace elements were measured with an ICP-OES (ThermoScientific iCAP 6200) and a HR-ICP-MS (ThermoScientific ELEMENT II), respectively. Suspended particulate matter (SPM) on the 0.2 µm filters were collected for analysis by Field Emission Gun Scanning Electron Microscopy (FEG-SEM) analyses. Filtration at 0.7 µm with glass microfiber filters, followed by acidification with 85% H_3PO_4 was also done for non-purgeable carbon (NPOC) analysis using a Shimadzu Total Organic Carbon Analyzer.

For the total metal concentrations, non-filtered water samples were evaporated in a Savillex Teflon bomb using an oven operated at 80°C, before being acid digested with 1:1 ratio of distilled 27 N HF and distilled 16 N HNO_3 at 90°C. The samples were re-dried and 1 mL of distilled 16 N HNO_3 added. Sample was heated at 90°C for 15 min before dilution with MilliQ water. Element concentrations were determined in the digested samples with a ThermoScientific ELEMENT II and the data were processed with the uFreasi software (Tharaud et al., 2015). If the solution's concentration was expected to exceed 10 ppb, analysis used a ThermoScientific iCAP 6200.

Principal Component Analysis (PCA) were performed on the data set with the XLSTAT free software (https://www.xlstat.com/fr/). The overall objective of the method was to reduce the dimensionality of the data set, by its transformation into a smaller one that still contains most of the initial information and helps highlighting the correlation between the parameters. The specific aim was here to assess the link between Ti and Ce concentrations and the water chemistry (including the alkalinity, the ionic strength, the dissolved oxygen, the NPOC, the pH, and the Temperature), of Ce concentrations and the Rare Earth Elements (REEs) concentrations and of Ti concentrations and the others trace elements.

spICPMS

A sector-field ICP-MS (ThermoScientific ELEMENT II) was operated in single particle counting mode using a 1 ms dwell time, a 1 ms settling time, and a measured flow rate of 0.2 mL min^{-1}. Over 10,000 readings were collected for each of the triplicate analyses. Because of the occurrence of calcium in the rivers samples (^{48}Ca), ^{47}Ti was used to avoid the isobaric interference. ^{140}Ce was measured in low resolution and ^{47}Ti, in medium resolution. To determine particle number concentration and particle size, ^{197}Au was measured in both low and medium resolutions and the mass-based method for computing transport efficiency was used (Pace et al., 2011). We used 15 nm AuNPs from BBInternational at 10 ppt and dissolved Au standards (SCP science) to measure the transport efficiency at each resolution. Transport efficiency of 2.5% was estimated. Dissolved gold (Au), cerium (Ce), and titanium (Ti) (from SCP Science) were used for the calibration curves (from 50 to 1,000 ppt). To take into account matrix effects on instrument sensitivity, dissolved

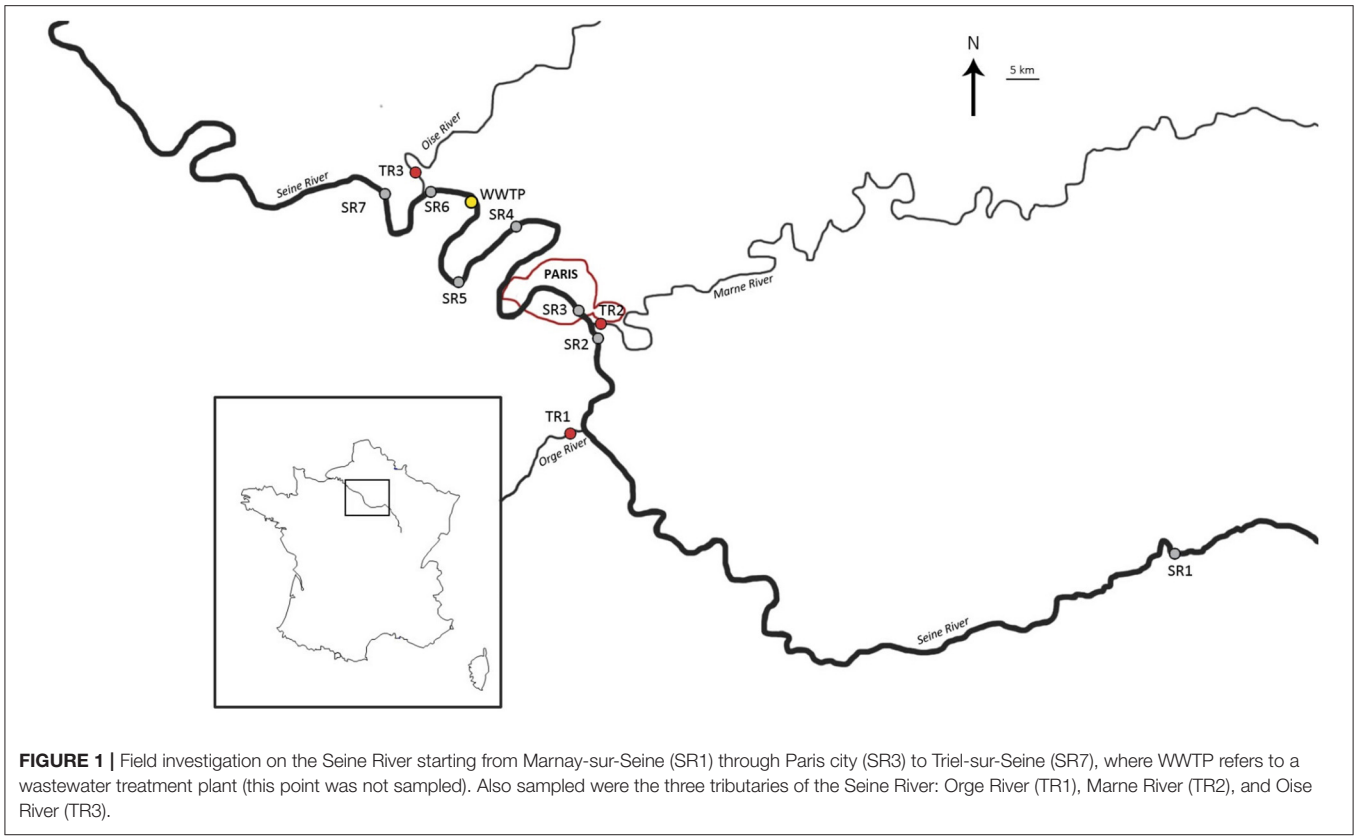

FIGURE 1 | Field investigation on the Seine River starting from Marnay-sur-Seine (SR1) through Paris city (SR3) to Triel-sur-Seine (SR7), where WWTP refers to a wastewater treatment plant (this point was not sampled). Also sampled were the three tributaries of the Seine River: Orge River (TR1), Marne River (TR2), and Oise River (TR3).

standards were freshly-prepared in ultrafiltered Seine River water to which dilutions from a 10 ppm stock solutions were made. A few days before the field investigation, Seine River water from Paris city near the "quai Saint Bernard," was collected and ultrafiltered at 1 kDa with a regenerated cellulose (RC) membrane filter, which was cleaned with DI water prior to use. The water chemistry, including major elements concentrations, of this sample was found to be consistent to the one of the Seine River samples collected on 11th May (**Supplementary Tables S1, S2**). This water sample was used for both the dissolved calibration curves and for a 10-fold dilution of the Seine River bulk samples. This approach presumably maintained the chemical equilibrium of the solutions so as not to change the aggregation state and NPs distribution. In addition, SR1 and each tributary (TR1, TR2, and TR3) were also ultrafiltered at 1 kDa for standard ICP-MS analysis of dissolved constituents. The surface of the 1 kDa filters were also analyzed by FEG-SEM to examine the particle morphology.

Results of time-resolved spICPMS analysis are particle-generated pulses of ions over a constant background level of counts, which is a result of both the dissolved element concentration and the inherent instrumental noise. The count intensity that differentiated between the dissolved elements and the NPs was determined by comparing the spICPMS results of the diluted ultrafiltered water to that of the associated diluted non-filtered samples. The mass concentrations of Ti and Ce were also determined from spICPMS data by integrating the signal over the entire sample analysis and comparing to the dissolved Ti and Ce calibration data.

FEG-SEM

Field Emission Gun—Scanning Electron Microscopy (FEG-SEM) imaging was applied with a MIRA 3 XMU from TESCAN. A secondary electron detector (Everhart–Thornley detector) and a YAG-doped scintillator backscattered electron detector (Autrata type detector) were used to highlight the occurrence of the particles in the samples. Particles bearing a higher averaged atomic number appear brighter with the backscattered electrons detector, allowing distinguishing Ce-bearing particles and Ti-bearing particles from other particles. For the investigation, at first, the backscattered electrons detector was applied on the samples to detect Ce and Ti-bearing particles. An Energy Dispersive X-ray Spectroscopy using an EDAX team system (ApolloXPP silicon drift detector) was then applied to the targeted particles for the elemental analyses to confirm the occurrence of Ce or of Ti. A secondary electron detector was applied to image the shape of the analyzed particles. The sample preparation was to filter ∼1 L of river water to collect suspended particulate matter (SPM). Parallel filtrations were performed using 0.2 μm PES membrane filters and 1 kDa RC membrane filters: assuming that the sickness of SPM deposited on the 0.22 μm pore size membrane will provide a significant chance to

retain, simultaneously with coarser particles, and some particles on the nanosize range. Meanwhile, it appeared necessary to also look for single NPs deposited onto 1 kDa filters, in case the first hypothesis was wrong. The filters were dried at room temperature. Each Al stub was covered with a double-faced adhesive made of carbon. The carbon adhesives were then tapped gently onto the surface of the filters to retrieve a sufficient quantity of particles to analyze. This technique prevents having any drying artifacts after the particle dispersion. A 1.5 nm layer of platinum-palladium was coated onto the surface of the samples using a Cressington 208 HR sputter coater, to avoid a charge accumulation during the analyses. The stubs were put into the FEG-SEM for particle analysis with an accelerating voltage set at 25 kV and with a working distance of 15 mm. Between 4 and 10 particles containing Ce or Ti were detected over 20–30 particles analyzed in each sample. All the 0.2 μm filters and one of the five 1 kDa filters were analyzed by FEG-SEM.

RESULTS

Water Chemistry of the Seine River and Its Tributaries

The water chemistry along the Seine River varied little from locations SR1 to SR7 (**Supplementary Table 1**). The average pH value, conductivity, and dissolved oxygen are measured to be 8.11 ± 0.2, at 522 ± 9 μS cm^{-1}, and at 9.4 ± 0.4 mg L^{-1}, respectively. The major cations and anions were calcium and hydrogenocarbonates, with 2,240 ± 123 μmol L^{-1} for Ca and 8.54 ± 0.54 meq L^{-1} for alkalinity, in average (**Supplementary Tables S1, S2**). The ionic strength was calculated at 5.8 ± 0.2 mmol L^{-1}, based on cations and anions concentrations. NPOC concentration was measured at 3.65 ± 0.51 mg L^{-1}.

TR1 and TR3 samples, collected from two Seine River tributaries, present higher conductivity and ionic strength. Conductivity values are 724 and at 610 μS cm^{-1} for TR1 and TR3 points, respectively. Ionic strength is calculated at 9.1 mmol L^{-1} for TR1 and at 7.1 mmol L^{-1} for TR3. Alkalinity is also higher in the TR3 sample (9.10 meq L^{-1}), as well as Ca concentrations, with 2,585 and 2,433 μmol L^{-1}, respectively, in TR1 and TR3 samples. The NPOC concentration was also higher in TR1 (5.20 mg L^{-1}) compared to the Seine River water. The other tributary, TR2, is characterized by a higher alkalinity value (9.14 meq L^{-1}), but a lower NPOC concentration (2.61 mg L^{-1}) compared to the Seine river.

NP Number Concentrations Quantified by spICPMS

Due to the isobaric interference of ^{48}Ca on ^{48}Ti and the subsequent use of ^{47}Ti for spICPMS detection, only Ti-NPs having a mass larger than an equivalent of a 60 nm TiO_2 particle could be observed as a pulse, and thus be counted. In the case of Ce-NPs, the smallest equivalent CeO_2NP that can be counted were on the order of 5 nm. Making the assumption that particles were spherical and in oxidized states, spICPMS analysis for all sampling sites gave a CeO_2NPs equivalent size for sphere distributions ranging from 5 to 80 nm, with an average of 24 nm. For TiO_2NPs, the equivalent size for sphere distributions ranged between 60 and 300 nm with an average of 160 nm for all sampling sites. As explained above, individual NPs cannot be differentiated, with spICPMS, from NPs heteroaggregates and SPM containing minor amounts of Ce or Ti. Thus, the reporting of "equivalent size for sphere distribution" is not the most relevant parameter for environmental studies. Therefore, the choice was made to display the Ti-bearing- and Ce-bearing PNCs (Particle Number Concentrations) as well as the Ti/Ce ratio of PNCs measured at the different sampling sites (**Figure 2**). It shows that in all samples, both Ce-bearing and Ti-bearing particles were detected, at concentrations of millions of particles per mL. Along the Seine River, a slight increase in the Ce-bearing PNC, and a significant Ti-bearing PNC variability are observed. The upstream SR1 sampling point exhibits 0.47 ± 0.07 × 10^6 of Ce-bearing particles per mL and 1.35 ± 0.17 × 10^6 of Ti-bearing particles per mL, the lowest PNCs over the studied area. The highest concentrations are measured at the SR3 sampling point, downtown Paris, for both Ce and Ti, with PNCs of 1.36 ± 0.13 × 10^6 and of 4.68 ± 0.25 × 10^6 part mL^{-1}, respectively. Finally, at the downstream location SR7, a decrease in PNCs is observed with 0.86 ± 0.08 × 10^6 part mL^{-1} and 3.14 ± 0.34 × 10^6 part mL^{-1} for Ce and Ti, respectively.

At the first tributary point (TR1), the PNC is high compared to the upstream location SR1, with 0.98 ± 0.04 × 10^6 Ce-containing and 3.15 ± 0.35 × 10^6 Ti-containing part mL^{-1}.

Similarly, the second tributary (TR2) exhibits high particles concentrations compared to the Seine River location at SR2, with 1.59 ± 0.10 × 10^6 Ce-bearing part mL^{-1} and 5.89 ± 0.10 × 10^6 Ti-bearing part mL^{-1} for TR2, and 0.77 ± 0.07 × 10^6 particles per mL containing Ce and 2.91 ± 0.22 × 10^6 particles per mL containing Ti for SR2.

Upstream of the confluence with the third tributary, the Seine river (SR6) exhibits PNCs of 1.16 ± 0.16 × 10^6 part mL^{-1} and at 4.04 ± 0.44 × 10^6 part mL^{-1} for Ce and Ti, respectively. These values are higher than the concentrations measured in the last tributary (TR3), with 0.49 ± 0.09 × 10^6 Ce-bearing part mL^{-1} and at 1.82 ± 0.13 × 10^6 Ti-bearing part mL^{-1}. As a comparison, these values are 2 orders of magnitude higher than those measured in the Danube recreational lake for Ti (Gondikas et al., 2014), and in the Loire River for both Ce and Ti (Phalyvong et al., 2020).

Total Mass Concentrations From spICPMS and From Acid Digestion

Unlike the Ce PNC, which had a maximum Seine River value at SR3, Ce mass concentration (nmol L^{-1}) shows a monotonic, nearly 10-fold increase in mass concentration proceeding downstream (**Figure 3**). This increase is also seen in La, resulting in a nearly constant Ce/La ratio.

The total Ce and La mass concentrations at SR-1 were 1.40 ± 0.07 nmol L^{-1} for Ce, and 0.76 ± 0.03 nmol L^{-1} for La, representing the lowest Ce and La total concentrations of the Seine River. The highest Ce and La concentrations in the Seine River are measured at SR7 with 13.61 ± 0.17 nmol L^{-1} for Ce

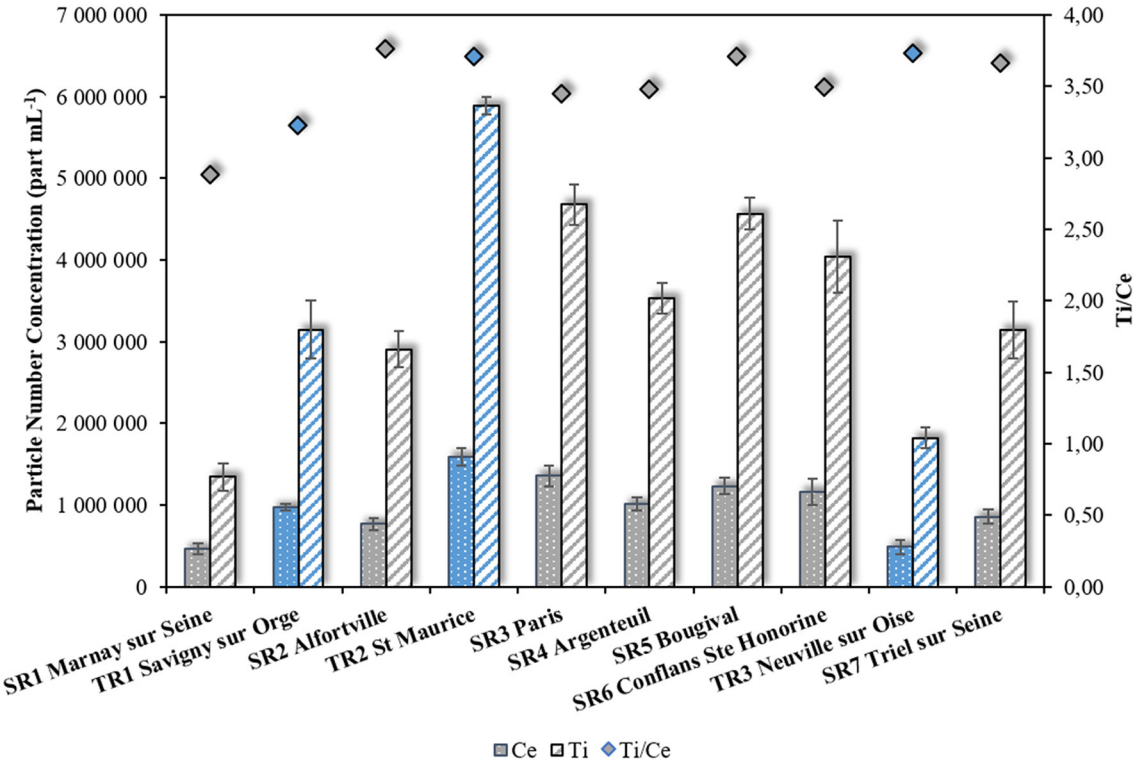

FIGURE 2 | Particle number concentration (left-hand side axis) determined by spICPMS for Ce- and Ti-bearing particles along the Seine River. In gray are the sampling points located in the Seine River and in red, in the tributaries. Also shown is the Ti/Ce particle number on the secondary *y*-axis.

and 6.71 ± 0.12 nmol L^{-1} for La. Compared to the Seine river upstream of the confluences, the first tributary contains Ce and La at a similar concentration range (TR1: 3.35 ± 0.01 nmol L^{-1} in Ce and 1.78 ± 0.02 nmol L^{-1} in La). The second tributary had substantially higher levels of both elements (TR2: 17.27 ± 0.25 nmol L^{-1} for Ce and 8.37 ± 0.07 nmol L^{-1}, for La), representing the highest found in the study area for both Ce and La. The third tributary is largely depleted (TR3: 4.30 ± 0.02 nmol L^{-1} for Ce and 2.06 ± 0.04 nmol L^{-1} for La) relative to all sites downstream of SR-2.

Compared to the upstream sampling point (SR1), the three concentrations of Ce (total, spICPMS, and dissolved) increase along the Seine River (**Supplementary Figure 1**). After SR3 sampling point, the dissolved Ce concentration stayed constant in the Seine River with an average of 0.14 ± 0.01 nmol L^{-1}. The dissolved concentrations in TR2 and TR3 were slightly lower than the one found in the Seine River with 0.07 ± 0.01 nmol L^{-1} and 0.10 ± 0.01 nmol L^{-1} for TR2 and TR3, respectively. The mass concentrations obtained by spICPMS show Ce considerably above the dissolved value, demonstrating a significant contribution of Ce by particles. However, the spICPMS value remains smaller than the total obtained by acid digestion/ICPMS analysis, which is consistent. This result suggests that although spICPMS gives mass concentration data for some particles, not all were measured by spICPMS. According to the sampling points, only 6–34% of the total Ce concentration was detected as "nano" with spICPMS, with an averaged value of 16%.

Figure 4 displays the total mass concentrations of Ti and Al in the bulk water samples. Previous works on TiO_2 released by sunscreens into surface waters plotted the Ti/Al elemental ratio to attempt differentiation of anthropogenic Ti from geogenic Ti (Gondikas et al., 2014; Reed et al., 2017; Phalyvong et al., 2020), as most of engineered TiO_2NPs are alumina coated (Serpone et al., 2007; Virkutyte et al., 2012). Using this approach in the present study, the Ti/Al elemental ratios have also been plotted on **Figure 4**. In SR1 sample, the total concentrations of 0.15 ± 0.01 μmol L^{-1} and of 5.69 ± 0.06 μmol L^{-1} were measured for Ti and Al, respectively. From that point, the concentrations increase and reach 1.78 ± 0.04 μmol L^{-1} for Ti and 58.29 ± 0.66 μmol L^{-1} for Al at the last sampling point. The concentration in TR2 sample from the second tributary (2.28 ± 0.03 μmol L^{-1} and 72.14 ± 0.32 μmol L^{-1} for Ti and Al, respectively) greatly exceeds the concentration in the Seine River but the third tributary appears to be largely depleted in both Ti and Al (0.49 ± 0.01 μmol L^{-1} and of 15.40 ± 0.26 μmol L^{-1}, for Ti and Al, respectively).

The three concentrations of Ti (total, derived from spICPMS and dissolved) in the first sampling point (SR1) were low but the concentrations increased along the Seine River (**Supplementary Figure 2**). The dissolved concentration of

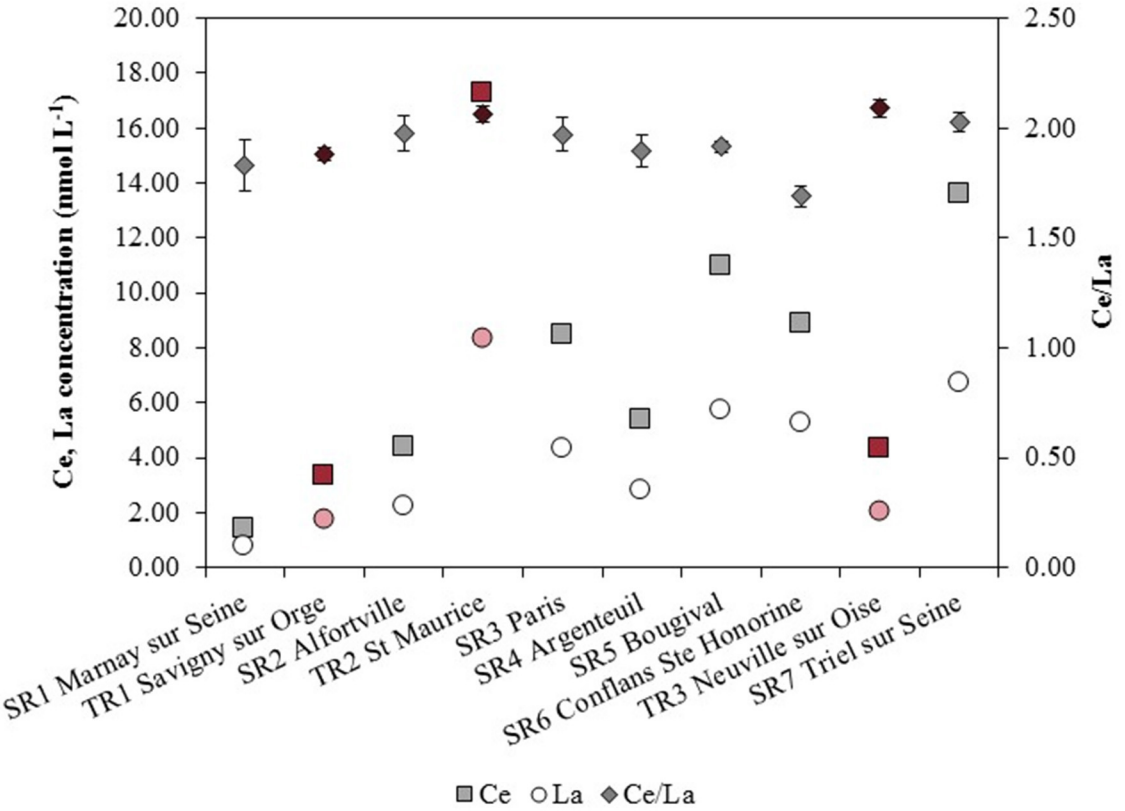

FIGURE 3 | Ce and La total concentrations (left-hand side axis) and Ce/La elemental ratios (right-hand side axis) as a function of the different sampling sites from SR1 to SR7 (in gray), with the three different tributaries (in red).

Ti was one hundred times lower than that from the spICPMS and the total concentrations. The lowest dissolved concentrations is measured in SR1 water sample (1.00 ± 0.10 nmol L^{-1}), and it increases along the Seine River to reach the maximum value at SR6 sampling point where 3.37 ± 0.40 nmol L^{-1} were quantified. The first tributary (TR1) had also a higher dissolved concentration than the SR1 sample with 2.33 ± 0.18 nmol L^{-1}. TR2 and TR3 water samples had lower dissolved concentrations than TR1, with 1.12 ± 0.06 nmol L^{-1} and 1.66 ± 0.17 nmol L^{-1}, respectively. As for Ce, the spICPMS concentration of Ti were lower than the total concentrations measured after acid digestion. However, the balance is reduced for Ti comparatively to Ce, as 25–100% of the total Ti concentration was detected as "nano" with spICPMS according to the sampling points, with an average of 67% in the present field study.

Imaging of NPs

Among all the observations made, the **Figure 5** illustrates a selection of 10 observations from FEG-SEM and subsequent analyses performed on SPM collected on 0.2 µm and on 1 kDa filters. The elements detected by EDS include those from the particle itself but also those from the matrix around the particle, since the volume of material analyzed by the EDS is larger than the particles bearing Ce and La, as well as those bearing Ti, that were found in all samples. These particles had a range of different sizes and shapes. **Figure 5** illustrates Ce and La bearing particles observed in TR1, SR2, SR5, SR6, and SR7 suspended matter having a dimensions in the range 0.2–4 µm, larger than the nano-size. Ti-containing particles are also shown in **Figure 5** from SR1, SR3, SR4, TR2, and TR3 sampling points where particles ranging from 100 nm to 1 µm could be found. The SR1 sample retentate filtered at 1 kDa (**Figure 5**) shows three different sized particles: the size of these particles vary from (150 nm × 190 nm) in the upper-right corner to (280 nm × 190 nm) in the center and even (620 nm × 680 nm) at the bottom-left of the picture. No individual particles were detected: they were all embedded in a matrix made of larger structures (e.g., mineral phases) suggesting that particles are heteroaggregated, the best example being the TR3 sample (**Figure 5**).

DISCUSSION

Quantifying NPs in the Seine River

The spICPMS method quantified the occurrence of CeO_2NPs and TiO_2NPs in the Seine River and its tributaries (**Figure 2**). When compared to the Loire River results (Phalyvong et al., 2020), the quantity of particles detected in the Seine River is two order of magnitude higher, which may be either related

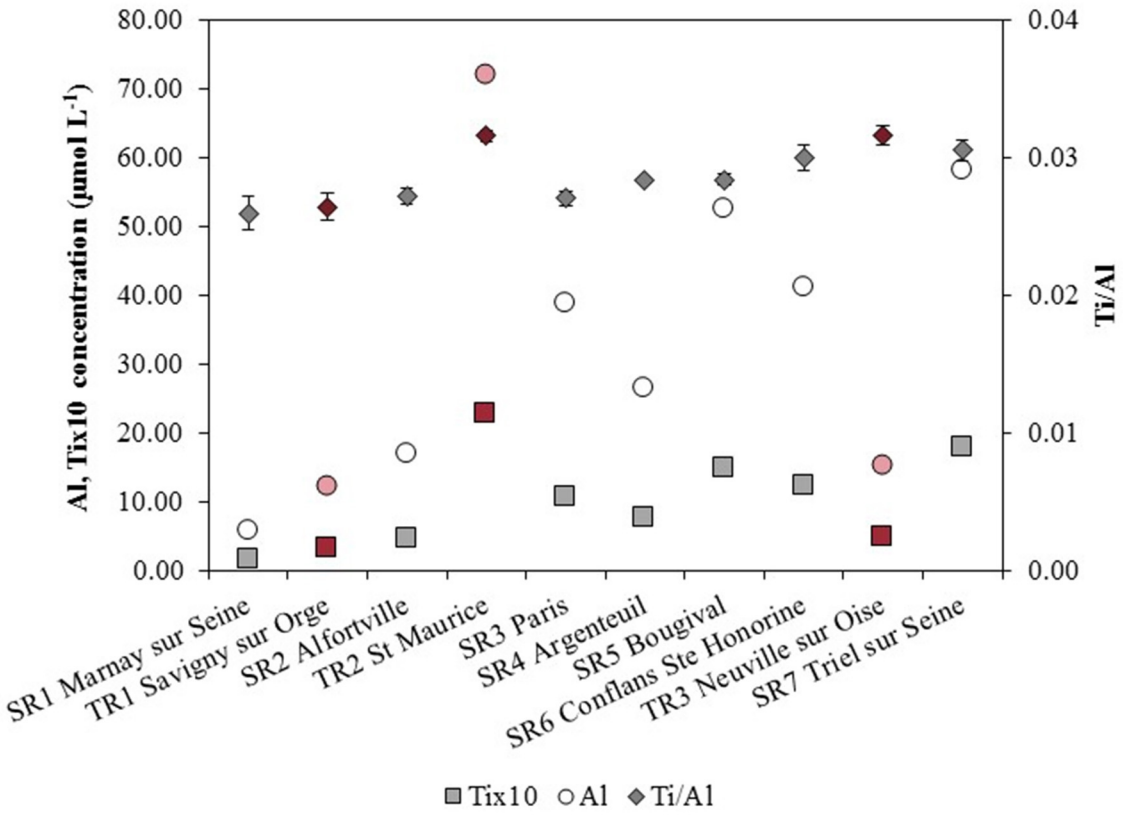

FIGURE 4 | Ti and Al total concentrations (left-hand side axis) and Ti/Al elemental ratios (right-hand side axis) for the different sampling sites from SR1 to SR7 (in gray), with the three different tributaries (in red).

to (i) the different substratum of both watersheds; (ii) the different climatic conditions of the sampling; or (iii) the different anthropic contributions.

In spite of these relatively high PNCs, one has to notice that these values are probably underestimated due to the isobaric interference of ^{48}Ca on ^{48}Ti and the subsequent use of ^{47}Ti for spICPMS detection, that prevent the detection of the Ti-NPs smaller than 60 nm. The detection limit in size of spICPMS (Dmin) depends on several factors such as the instrument sensitivity or the background noise level. Indeed, a chart proposed by Lee et al. (2014) summarizes the detection size limit of quadrupolar ICPMS for 40 elements including Ce and Ti where the minimum size for ^{140}Ce is around 10 nm, and for ^{49}Ti, around 80 nm. Among the several approaches tested by Tharaud et al. (2017) to reduce the Ca interference while measuring TiO_2 in solutions, we decided to use a High-Resolution ICPMS). FEG-SEM analyses detected particles containing both Ce and Ti only in particles larger than 100 nm (**Figure 5**), and thus by definition, not NPs. The lack of observations of NPs is mostly due to the complexity of the SPM and to the abundance of natural phases that could hide the Ce-bearing and Ti-bearing particles. NP can also be embedded in heteroaggregates that would hide their presence.

The lack of correspondence in the relationship between particle number and mass also suggests changes in NP size or Ce and Ti content that could be related to heteroaggregation: an increase in mass concentration along the river flow, yet a decrease in PNC, is consistent with two analytical competing particle size effects. In one case the Ce (respectively, Ti) content of the particles may be becoming too low to separate them from the background signal. Conversely, an input of suspended sediment particles >5–10 micron could also explain this observation, as these particles are likely too large to be transported and ionized by the ICP-MS. The increase in Ce and La mass concentration is also in contrast to the constant values of conductivity and ionic strength seen at nearly all Seine River locations (**Supplementary Table 1**, **Supplementary Figure 1**). The processes that introduce NPs into the river system do not seem to increase or decrease the concentration of dissolved constituents in the river water. The lack of correlation of PNC or mass concentration with stream discharge (**Supplementary Table 3**) suggests that simple velocity-driven suspension and transport does not explain NP abundance, but rather other factors within the watersheds are important.

When compared with the total concentrations, only 6–25% of the total Ce that were in a particulate state could be detected by

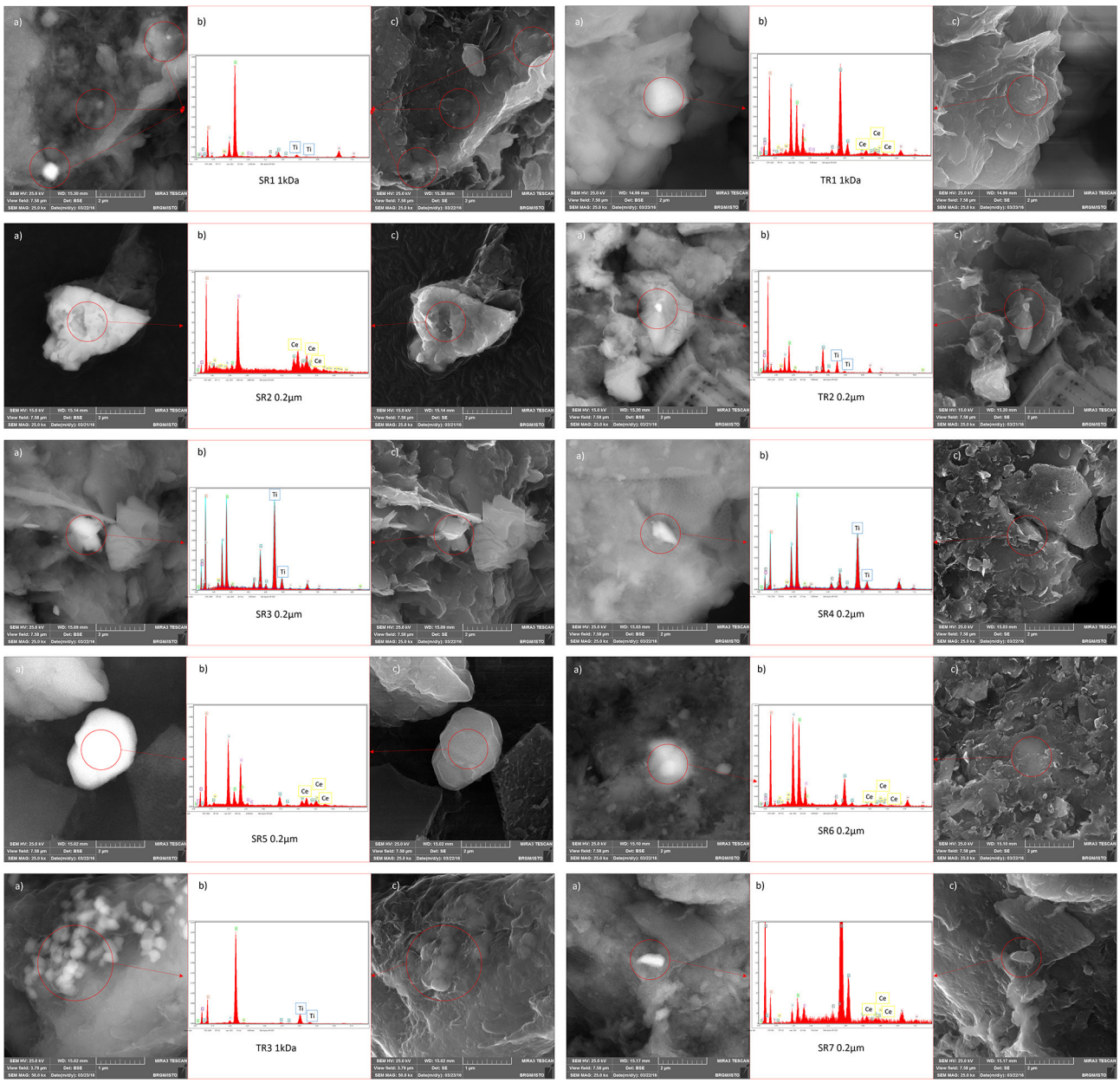

FIGURE 5 | FEG-SEM analyses on either 0.2 micron filter or 1 kDa filter for each of the 10 SPM samples collected; **(a)** are pictures obtained with BSE detector, **(b)** represent the corresponding EDS analysis of the target particle(s), and **(c)** the corresponding SE picture.

spICPMS. For Ti-containing particles, the discrepancy is smaller (from 25 to 100% of total Ti) and both dissolved values for Ce and for Ti were at least one hundred times lower than the total concentrations. Larger Ce bearing particles that are not likely to be fully transported and ablated by the ICP could explain the difference between the total and the spICPMS concentrations. For instance, natural Ce particles can be found in the form of monazites [(Ce, La, Nd, and Th) (PO_4)] (Dahle and Arai, 2015) which are natural particles with a typical range of size from 150 nm to >1 µm. The good correlations observed between the SPM concentrations and the Ti and Ce total concentrations (R^2 = 0.88 and 0.84, respectively, **Supplementary Table 3**) highlight the fact that the biggest loss of particles would induce the biggest Ti and Ce loss if these particles are not fully ionized in the plasma.

Our findings demonstrated that the observations made with the water chemistry was in good agreement with the principal component analyses (PCA) made with XLSTAT (**Supplementary Figures 3**, **4**). CeO_2NPs are insoluble in water when the pH is superior to 7 (Dahle et al., 2015), which is the case of the Seine River and of the studied tributaries. Moreover,

the occurrence of Natural Organic Matter (NOM) as well as the ionic strength are parameters that will partly control the aggregation state of TiO_2NPs and CeO_2NPs (Van Hoecke et al., 2011; Oriekhova and Stoll, 2019). The aggregation of the NPs are dependent of the ionic strength with a commonly observed increase of aggregation when the ionic strength increases (Thio et al., 2011). In the Seine River field investigation, the ionic strength is calculated, in average, at 5.8 ± 0.2 mmol L^{-1}. For the Orge River (TR1), the ionic strength is calculated at 9.1 mmol L^{-1} while natural organic matter concentration is higher (5.20 vs. 2.72 mg L^{-1}), suggesting that the aggregation state would be strongly different than in the Seine River. Therefore, the water chemistry suggests that the Orge River may not significantly contribute in TiO_2NPs in the Seine River (PCA, **Supplementary Figure 4**). On the contrary, the ionic strength and NPOC concentration of TR2 water sample are closer to the ones found in the Seine River (**Supplementary Table 1**), indicating that in both the Marne and the Seine rivers, the aggregation rate may be similar.

In the studied rivers, the particles could undergo heteroaggregation with mineral phases (Topuz et al., 2014; Labille et al., 2015; Topuz and Talinli, 2015). This was directly seen with the FEG-SEM results and also indirectly with the spICPMS results, for which the occurrence of poorly ionized (and detected) particles >5 µm is consistent with heteroaggregation. Besides, in the FEG-SEM analyses, no individual particle nor aggregate are detected, and only particles embedded in mineral matrix were observed. This embedment of NPs in mineral matrix which can occur either in the environment or during the filtration and drying of SPM deposited on the 0.2 µm pore size filter, at least indicates that heteroaggregation is predominant over homoaggregation of TiO_2NPs in the river waters studied here. Contrary to the Danube River water study (Gondikas et al., 2014) where the authors suggest that TiO_2NPs from the sunscreen underwent fast homoaggregation favored by the hydrochemistry, this specific behavior does not seem to happen in river waters of the present study, probably because of the different hydrochemical parameters (pH, ionic strength, NOM quality, and quantity) that here favors heteroaggregation.

Mass Balance of PNC

After the confluence between SR1 and TR1 sampling points, an increase of the PNC is observed for Ce and Ti. The Ti/Ce ratio also significantly increases from 3 to 3.75 in SR1 and SR2, respectively (**Figure 2**), suggesting a relative contribution in Ti bearing particles. Then, the Ti/Ce ratios remains constant at 3.62 ± 0.12 up to SR7, including the Marne and Oise rivers tributaries. Therefore, a good way to assess the contribution at each tributary is the study of the mass balance of particle flows.

Multiplying the PNC of Ce and of Ti with the water flow (**Supplementary Table 3**), conservative or non-conservative mixing can be checked at each confluence between the Seine River and its tributaries (**Figure 6**). The theoretical mix corresponds to the sum (conservative behavior) of the flow of particles of the Seine River with the associated tributary. Given the uncertainties in the replicate PNC, the mass balance was conservative at the confluence between the Seine and the Marne

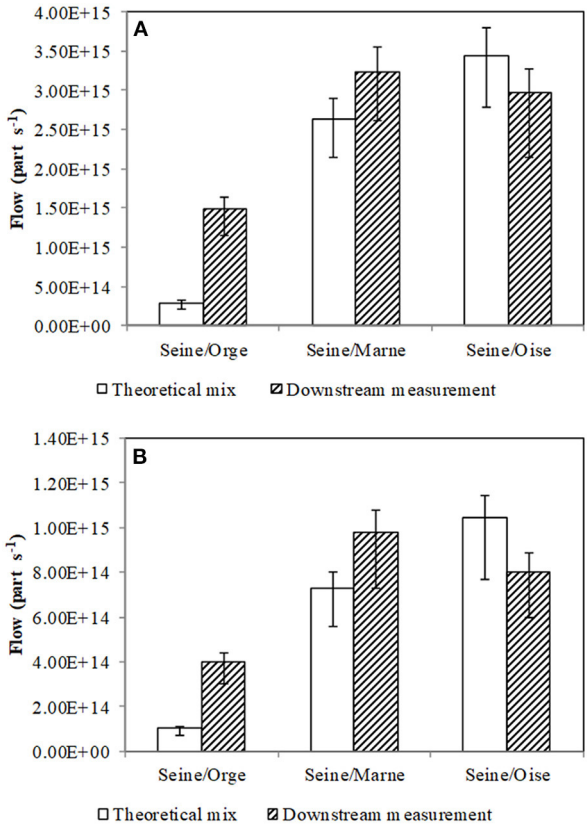

FIGURE 6 | Mass balance for the PNC of Ce **(A)** and of Ti **(B)**.

(TR2) Rivers, and also at the confluence between the Seine and the Oise (TR3) Rivers. However, for the mass balance at the confluence between the Seine and the Orge (TR1) Rivers, the downstream measurement value was higher than the theoretical mix. The difference in the water flow between the Orge River (2.87 m^3/s) and the Seine River (184 m^3 s^{-1}) also make the mixing calculation unreliable. More importantly, at the site downstream of the confluence between the Orge and the Seine Rivers, the water flow was equal to 474 m^3 s^{-1}, showing significant sources of water to the Seine that were not measured for discharge or PNC.

Paris city does not seem to have a contribution in CeO_2NPs since its Ce/La elemental ratio (**Figure 3**) was equal to the one found in the upstream point of the field investigated (SR3: 1.97 ± 0.08 vs. SR1: 1.83 ± 0.12). At the Paris city sampling point, the Ti/Al elemental ratio was also equal to the ratio calculated in SR1 water sample (0.027 ± 0.001) (**Figure 4**), consistent with the assumption made for CeO_2NPs of a non-significant contribution to TiO_2NPs in the Seine River from Paris city at the time of the sampling campaign.

However, a drop in Ce total concentration profile (**Figure 3**) was observed in SR6 water sample, which had a consequence on the Ce/La elemental ratio. The Ce/La ratio was estimated

at 1.69 ± 0.05 in SR6 water sample, which was lower than the elemental ratio measured in SR1 sampling point. This low ratio could be explained by the occurrence of the WWTP between the sampling points SR5 and SR6 that potentially act as an artificial tributary that plays a role: the average WWTP flow is 60 m^3/s vs. a Seine River flow of 400–500 m^3/s on the day of sampling and Ce/La elemental ratio in SPM from this WWTP effluent has been previously reported to 1.65 by Chen et al. (2014). Besides, contrary to CeO_2NPs, the WWTP effluent measured at Ti/Al = 0.078 by the these authors did not seemed to significantly impact the TiO_2NPs removal (**Figure 4**) since both Ti and Al diminished before SR6 sampling point and Ti/Al stayed constant.

Attempt to Discriminate the Origins of CeO_2NPs

The relative abundance of the Rare Earth Elements (REEs), and particularly their fractionation during geochemical processes make them powerful tracers of weathering and a means of examining the origin of elements in waters (Braun et al., 1990, 1993; Elderfield et al., 1990). Any significant contribution of CeO_2 ENPs in waters should result in a Ce anomaly in the REE patterns. Thus, the ratio of concentration of Ce with respect to that of another REE appears to be a potential tracer of CeO_2 ENPs occurrence. In the Seine River, Ce/La values vary from 1.72 to 2.12, very close to the natural background determined for stream waters over France at 1.96 (Salminen et al., 2005). Only the last point on the Seine River (SR7 with Ce/La = 2.12), and the Marne and the Oise Rivers present Ce/La ratios significantly above 2.00, with 2.06 ± 0.03 and 2.09 ± 0.04 for TR2 and TR3 respectively, suggesting a potential contribution of CeO_2NPS. The constant elemental ratios suggest a contribution in natural NPs of the Marne and of the Oise Rivers. In both samples, results of elemental ratios and of FEG-SEM show a contribution in Ce-bearing particles, coming from natural phases, since the elemental ratios are not significantly different in the tributaries with regard to the Seine river. In general, REE are correlated and it is the case of this study (**Supplementary Figure 5**). The PCA results show also that the REE are correlated with an important relation of Ce with La, Nd, and Sc for TR2 sampling point, in the upper-right corner of the PCA (which corresponds to the Marne River).

Attempt of Determination of TiO_2NPs Sources

The Ti/Al elemental ratio measured on engineered NPs varies from 4.08 ± 0.11 to 8.01 ± 0.11 (acid digestion realized on different TiO_2 ENPs, see **Supplementary Table 4**). This contrasts with the ratios measured in river waters in the present study, ranging from 0.026 to 0.032 (**Figure 4**). The typical Ti/Al elemental ratio measured in SPM from the Seine river over a 3-year period by Chen et al. (2014) corroborates these results (Ti/Al = 0.033 ± 0.003, $n = 50$, Chen et al., 2014). The most upstream point sampled on the Seine river in the present study displays the lowest Ti/Al elemental ratio (0.026 ± 0.001, SR1, **Figure 4**) as well as the lowest concentrations for both elements. Therefore, one could assume this point being relevant of the local background, in adequacy to the value of 0.02 proposed by Salminen et al. (2005) for the natural background of French streams. Both elements were correlated in several samples (especially, TR2, SR5, and SR6 sampling points) which was shown with the PCA (**Supplementary Figure 6**). The Ti/Al ratio in TR1 sample was close to the one found previously in SR1 water meaning that the Orge River did not had, during the field campaign, a significant contribution in TiO_2NPs coming from anthropogenic activities. Besides, in TR2 sampling point, an increase of Ti/Al elemental ratio was observed (0.032 ± 0.000). This indicates an addition in NPs from a different origin than SR1 point, probably from anthropogenic activities before the confluence between the Marne and the Seine Rivers. The Ti/Al value was high in TR3 sampling point with 0.032 ± 0.001, suggesting here again an anthropogenic origin of NPs in the tributary (the Oise River); but due to the low PNC in TR3 the contribution to the Seine river remains insignificant, lower than TR2 contribution. The low elemental ratio, in this study, was due to the high proportion of Al in the water samples. This low elemental ratio has been observed in the Danube recreational lake (Gondikas et al., 2014) and also in the Loire River (Phalyvong et al., 2020) and complicates the use of Ti/Al to determine the speciation of Ti particularly to highlight the presence of TiO_2NPs.

Therefore, other elements like V or Y were also used, as suggested by Gondikas et al. (2014), in order to distinguish the signal of engineered TiO_2NPs from natural Ti-containing particles that may also contain these elements, as a good correlation was also obtained between these elements and the SPM concentration (**Supplementary Table 3**). As for Ti/Al, a significant increase of the Ti/V and Ti/Y elemental ratios (**Figure 7**) was observed in the Marne River, with values of 30.99 ± 0.44 and 236.98 ± 3.39 for Ti/V and Ti/Y, respectively. After the confluence between the Seine and the Marne rivers, the mass balance is checked for these elements. Hence, this increase suggests a contribution of an enriched TiO_2 phase, potentially anthropogenic, from this tributary in the Seine River. The other tributaries do not display similar trends for Ti/V and Ti/Y compared to Ti/Al. Whereas, the latter was slightly higher in the Orge River and the Oise River before their respective confluences with the Seine river, Ti/V and Ti/Y are significantly lower in these tributaries compared to the Seine river. One can assume that the chemical signature of particles from these catchments are controlled by anthropogenic and geogenic contributions significantly different than in the Seine River watershed. The study of smaller area should be done to assess the local contribution of NPs coming from natural or anthropogenic process, as it was recently proposed for AgNPs by our group (Wang et al., 2020).

CONCLUSION

The occurrence of CeO_2NPs and TiO_2NPs were assessed with the use of spICPMS showing that millions of particles per milliliter containing Ce and Ti could be measured with this technique with the adequate dilution. In all suspended particulate matters,

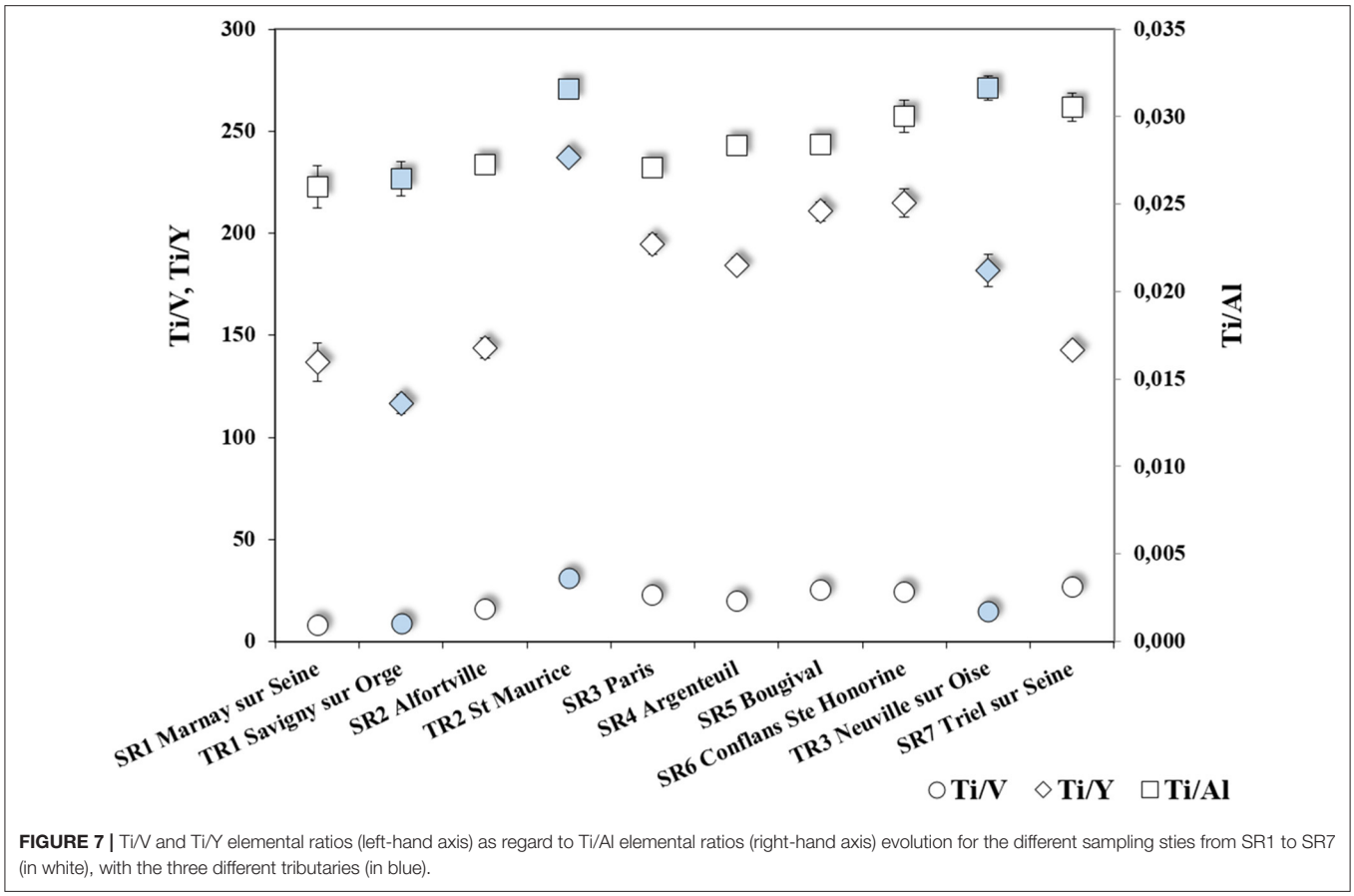

FIGURE 7 | Ti/V and Ti/Y elemental ratios (left-hand axis) as regard to Ti/Al elemental ratios (right-hand axis) evolution for the different sampling sties from SR1 to SR7 (in white), with the three different tributaries (in blue).

Ce-bearing and Ti-bearing particles were also detected with FEG-SEM imaging. After the confluence between the Seine River and its tributaries, an increase in the particle number concentration was determined, suggesting a contribution in NPs from all tributaries. However, the results of the elemental ratios and of the mass balance showed that only the Marne River and the Oise River had a significant contribution in natural CeO_2NPs. For TiO_2NPs, an anthropogenic origin was determined for the Marne River but the use of Ti/Al elemental ratios brings uncertainties since the concentration of Al in the rivers is very important and other elemental ratios (as Ti/V and Ti/Y) should be used to estimate the NPs origins. Besides, the contribution in NPs of the Orge River and the Paris city were not highlighted in this study, since the relative elemental ratios were constant. Hence, we conclude that this one-shot sampling campaign did not allowed to provide evidence of any significant contribution of the Paris city and the Orge River to the release of TiO_2NPs and CeO_2NPs in the Seine River. This emphasizes the need for more local and highly time-resolved studies that would allow to address the question of the potential impacts of diurnal (Reed et al., 2017) or seasonal changes in hydrological conditions and land use, as recently proposed by Wang et al. (2020) and Peters et al. (2018). spICPMS technique is a powerful tool but it also needs to be completed with other ones such as imaging with FEG-SEM and/or the use of elemental ratios to have a full investigation of the NPs origins in the river water. The detection of ENPs in environmental samples remains one of the biggest challenges for their monitoring and the assessment of the related risk. In order to distinguish the engineered from the natural NPs, groundbreaking analytical effort must be performed. The most promising solution to meet this challenge is probably the one recently developed by Praetorius et al. (2017) to distinguish engineered from natural CeO_2NPs in soils: the use of an inductively-coupled plasma time-of-flight mass spectrometer (ICP-TOFMS) in single-particle mode allows to simultaneously analyze all the elements in a given particle and thus to establish intrinsic elemental ratios.

DATA AVAILABILITY STATEMENT

The raw data supporting the conclusions of this article will be made available by the authors, without undue reservation.

AUTHOR CONTRIBUTIONS

KP was in charge of the sampling, analyses and writing. She was supervised and guided by MT and GW for spICPMS and MEB-FEG, respectively. YS conceived the presented idea, coordinated, and supervised the whole work with the help of MB, HP, and JR.

XB and AG helped them supervising the project on the MEB-FEG and natural systems, respectively. All authors discussed and wrote the final manuscript.

FUNDING

This research project QUANTINANO was fully supported by the Bureau de Recherche Géologique et Minière (BRGM) and Institut de Physique du Globe de Paris (IPGP) under the convention No. DAF/JAC/JUR/AS/no. 2013/422. Part of this work was supported by the IPGP multidisciplinary program PARI and by Paris-IdF Region SESAME Grant No. 12015908, the ANR-18-IDEX-0001, IdEx Université de Paris, and the PIREN Seine program.

ACKNOWLEDGMENTS

Our thanks go to Ms. Laure Cordier for the assistance she provided during various multi-elemental analyses. Two reviewers as well as the associate editor are thanks for their critical comments.

SUPPLEMENTARY MATERIAL

The Supplementary Material for this article can be found online at: https://www.frontiersin.org/articles/10.3389/fenvs.2020.549896/full#supplementary-material

REFERENCES

Braun, J.-J., Pagel, M., Muller, J.-P., Bilong, P., Michard, A., and Guillet, B. (1990). Cerium anomalies in lateritic profiles. *Geochim. Cosmochim. Acta* 54, 781–795. doi: 10.1016/0016-7037(90)90373-S

Braun, J. J., Pagel, M., Herbillon, A., and Rosen, C. (1993). Mobilization and redistribution of REEs and thorium in a syenitic lateritic profile: a mass balance study Geochim. *Cosmochim. Acta* 57, 4419–4434. doi: 10.1016/0016-7037(93)90492-F

Chen, J.-B, Gaillardet, J., Bouchez, J., Louvat, P., and Wang, Y. N. (2014). Anthropophile elements in river sediments: overview from the seine river, France. *G Cube* 15, 4526–4546. doi: 10.1002/2014GC005516

Dahle, J., and Arai, Y. (2015). Environmental geochemistry of cerium: applications and toxicology of cerium oxide nanoparticles. *Int. J. Environ. Res. Public Health* 12, 1253–1278. doi: 10.3390/ijerph120201253

Dahle, J. T., Livi, K., and Arai, Y. (2015). Effects of pH and phosphate on CeO_2 nanoparticle dissolution. *Chemosphere* 119, 1365–1371. doi: 10.1016/j.chemosphere.2014.02.027

Dan, Y., Zhang, W., Xue, R., Ma, X., Stephan, C., and Shi, H. (2015). Characterization of gold nanoparticle uptake by tomato plants using enzymatic extraction followed by single-particle inductively coupled plasma-mass spectrometry analysis. *Environ. Sci. Technol.* 49, 3007–3014. doi: 10.1021/es506179e

Degueldre, C., and Favarger, P. Y. (2003). Colloid analysis by single particle inductively coupled plasma-mass spectroscopy: a feasibility study. *Colloids Surf. A Physicochem. Eng. Aspects* 217, 137–142. doi: 10.1016/S0927-7757(02)00568-X

Degueldre, C., Favarger, P. Y., and Wold, S. (2006). Gold colloid analysis by inductively coupled plasma-mass spectrometry in a single particle mode. *Anal. Chim. Acta* 555, 263–268. doi: 10.1016/j.aca.2005.09.021

Deng, Y., Petersen, E. J., Challis, K. E., Rabb, S. A., Holbrook, R. D., Ranville, J. F., et al. (2017). Multiple method analysis of TiO_2 nanoparticle uptake in rice (*Oryza sativa* L.) plants. *Environ. Sci. Technol.* 51, 10615–10623. doi: 10.1021/acs.est.7b01364

Donovan, A. R., Adams, C. D., Ma, Y., Stephan, C., Eichholz, T., and Shi, H. (2016a). Detection of zinc oxide and cerium dioxide nanoparticles during drinking water treatment by rapid single particle ICP-MS methods. *Anal. Bioanal. Chem.* 408, 5137–5145. doi: 10.1007/s00216-016-9432-0

Donovan, A. R., Adams, C. D., Ma, Y., Stephan, C., Eichholz, T., and Shi, H. (2016b). Single particle ICP-MS characterization of titanium dioxide, silver, and gold nanoparticles during drinking water treatment. *Chemosphere* 144, 148–153. doi: 10.1016/j.chemosphere.2015.07.081

Elderfield, H., and Upstill-Goddard, R., E. R., Sholkovitz. (1990). The rare earth elements in rivers, estuaries, and coastal seas and their significance to the composition of ocean waters. *Geochim. Cosmochim. Acta* 54, 971–991 doi: 10.1016/0016-7037(90)90432-K

Gómez-Rivera, F., Field, J. A., Brown, D., and Sierra-Alvarez, R. (2012). Fate of cerium dioxide (CeO_2) nanoparticles in municipal wastewater during activated sludge treatment. *Bioresour. Technol.* 108, 300–304. doi: 10.1016/j.biortech.2011.12.113

Gondikas, A. P., von der Kammer, F., Reed, R. B., Wagner, S., Ranville, J. F., and Hofmann, T. (2014). Release of TiO_2 nanoparticles from sunscreens into surface waters: a one-year survey at the Old Danube recreational lake. *Environ. Sci. Technol.* 48, 5415–5422. doi: 10.1021/es405596y

Gottschalk, F., Sonderer, T., Scholz, R. W., and Nowack, B. (2009). Modeled environmental concentrations of engineered nanomaterials (TiO_2, ZnO, Ag, CNT, Fullerenes) for different regions. *Environ. Sci. Technol.* 43, 9216–9222. doi: 10.1021/es9015553

Gottschalk, F., Sun, T., and Nowack, B. (2013). Environmental concentrations of engineered nanomaterials: review of modeling and analytical studies. *Environ. Pollut.* 181, 287–300. doi: 10.1016/j.envpol.2013.06.003

Gray, E. P., Coleman, J. G., Bednar, A. J., Kennedy, A. J., Ranville, J. F., and Higgins, C. P. (2013). Extraction and analysis of silver and gold nanoparticles from biological tissues using single particle inductively coupled plasma mass spectrometry. *Environ. Sci. Technol.* 47, 14315–14323. doi: 10.1021/es403558c

Hashimoto, K., Irie, H., and Fujishima, A. (2005). TiO_2 photocatalysis: a historical overview and future prospects. *Jpn. J. Appl. Phys.* 44, 8269–8285. doi: 10.1143/JJAP.44.8269

Hochella, M. F. Jr., Mogk, D. W., Ranville, J., Allen, I. C., Luther, G. W., Marr, L. C., et al. (2019). Natural, incidental, and engineered nanomaterials and their impacts on the Earth system. *Science* 363:eaau8299. doi: 10.1126/science.aau8299

Imagawa, H., Suda, A., Yamamura, K., and Sun, S. (2011). Monodisperse CeO_2 nanoparticles and their oxygen storage and release properties. *J. Phys. Chem. C.* 115, 1740–1745. doi: 10.1021/jp109878j

Kahru, A., and Dubourguier, H.-C. (2010). From ecotoxicology to nanoecotoxicology. *Toxicology*. 269, 105–119. doi: 10.1016/j.tox.2009.08.016

Keller, A. A., and Lazareva, A. (2014). Predicted releases of engineered nanomaterials: from global to regional to local. *Environ. Sci. Technol. Lett.* 1, 65–70. doi: 10.1021/ez400106t

Keller, A. A., Wang, H., Zhou, D., Lenihan, H. S., Cherr, G., Cardinale, B. J., et al. (2010). Stability and aggregation of metal oxide nanoparticles in natural aqueous matrices. *Environ. Sci. Technol.* 44, 1962–1967. doi: 10.1021/es902987d

Labille, J., Harns, C., Bottero, J.-Y., and Brant, J. (2015). Heteroaggregation of titanium dioxide nanoparticles with natural clay colloids. *Environ. Sci. Technol.* 49, 6608–6616. doi: 10.1021/acs.est.5b00357

Laborda, F., Jiménez-Lamana, J., Bolea, E., and Castillo, J. R. (2011). Selective identification, characterization and determination of dissolved silver(I) and silver nanoparticles based on single particle detection by inductively coupled plasma mass spectrometry. *J. Anal. At. Spectrom.* 26, 1362–1371. doi: 10.1039/c0ja00098a

Laborda, F., Jiménez-Lamana, J., Bolea, E., and Castillo, J. R. (2013). Critical considerations for the determination of nanoparticle number concentrations, size and number size distributions by single particle ICP-MS. *J. Anal. At. Spectrom.* 28, 1220–1232. doi: 10.1039/c3ja50100k

Lee, B. X., Reed, R. B., Ranville, J. F., Herckes, P., and Westerhoff, P. (2014). Nanoparticle size detection limits by single particle ICP-MS for 40 elements sungyun. *Environ. Sci. Technol.* 48, 10291–10300. doi: 10.1021/es502422v

Lima, J. F.d, Martins, R. F., Neri, C. R., and Serra, O. A. (2009). ZnO:CeO_2-based nanopowders with low catalytic activity as UV absorbers. *Appl. Surf. Sci.* 255, 9006–9009. doi: 10.1016/j.apsusc.2009.06.071

Loeschner, K., Navratilova, J., Kobler, C., Molhave, K., Wagner, S., von der Kammer, F., et al. (2013). Detection and characterization of silver nanoparticles in chicken meat by asymmetric flow field flow fractionation with detection by conventional or single particle ICP-MS. *Anal. Bioanal. Chem.* 405, 8185–8195. doi: 10.1007/s00216-013-7228-z

Mitrano, D. M., Lesher, E. K., Bednar, A., Monserud, J., Higgins, C. P., and Ranville, J. F. (2012). Detecting nanoparticulate silver using single-particle inductively coupled plasma-mass spectrometry. *Environ. Toxicol. Chem.* 31, 115–121. doi: 10.1002/etc.719

Navarro, E., Baun, A., Behra, R., Hartmann, N. B., Filser, J., Miao, A.-J., et al. (2008). Environmental behavior and ecotoxicity of engineered nanoparticles to algae, plants, and fungi. *Ecotoxicology* 17, 372–386. doi: 10.1007/s10646-008-0214-0

Oriekhova, O., and Stoll, S. (2019). Heteroaggregation of CeO_2 nanoparticles in presence of alginate and iron(III) oxide. *Sci. Total Environ.* 648, 1171–1178. doi: 10.1016/j.scitotenv.2018.08.176

Pace, H. E., Rogers, N. J., Jarolimek, C., Coleman, V. A., Gray, E. P., Higgins, C. P., et al. (2012). Single particle inductively coupled plasma-mass spectrometry: a performance evaluation and method comparison in the determination of nanoparticle size. *Environ. Sci. Technol.* 46, 12272–12280. doi: 10.1021/es301787d

Pace, H. E., Rogers, N. J., Jarolimek, C., Coleman, V. A., Higgins, C. P., and Ranville, J. F. (2011). Determining transport efficiency for the purpose of counting and sizing nanoparticles via single particle inductively coupled plasma mass spectrometry. *Anal. Chem.* 83, 9361–9369. doi: 10.1021/ac201952t

Peters, R. J. B., Rivera, Z. H., van Bemmel, G., Marvin, H. J. P., Weigel, S., and Bouwmeester, H. (2014). Development and validation of single particle ICP-MS for sizing and quantitative determination of nano-silver in chicken meat. *Anal. Bioanal. Chem.* 406, 3875–3885. doi: 10.1007/s00216-013-7571-0

Peters, R. J. B., van Bemmel, G., Milani, N. B. L., den Hertog, G. C. T., Undas, A. K., van der Lee, M., et al. (2018). Detection of nanoparticles in Dutch surface waters. *Sci. Total Environ.* 621, 210-218. doi: 10.1016/j.scitotenv.2017.11.238

Phalyvong, K., Sivry, Y., Pauwels, H., Gélabert, A., Tharaud, M., Wille, G., et al. (2020). Occurrence and origins of cerium dioxide and titanium dioxide nanoparticles in the Loire River (France) by single particle ICP-MS and FEG-SEM imaging. *Front. Environ. Sci.* 8:141. doi: 10.3389/fenvs.2020.00141

Praetorius, A., Gundlach-Graham, A., Goldberg, E., Fabienke, W., Navratilova, J., Gondikas, A., et al. (2017). Single-particle multi-element fingerprinting (spMEF) using inductively-coupled plasma time-of-flight mass spectrometry (ICP-TOFMS) to identify engineered nanoparticles against the elevated natural background in soils. *Environ. Sci. Nano* 4, 307. doi: 10.1039/C6EN00455E

Reed, R. B., Martin, D. P., Bednar, A. J., Montaño, M. D., Westerhoff, P., and Ranville, J. F. (2017). Multi-day diurnal measurements of Ti-containing nanoparticle and organic sunscreen chemical release during recreational use of a natural surface water. *Environ. Sci. Nano* 4, 69. doi: 10.1039/C6EN00283H

Roy, S., Gaillardet, J., and Allègre, C. J. (1999). Geochemistry of dissolved and suspended loads of the Seine River, France: anthropogenic impact, carbonate and silicate weathering. *Geochim. Cosmochim. Acta* 63, 1277–1292. doi: 10.1016/S0016-7037(99)00099-X

Salminen, R., Batista, M. J., Bidovec, M., Demetriades, A., De Vivo, B., De Vos, W., et al. (2005). *Geochemical Atlas of Europe. Part 1: Background Information, Methodology and Maps*. Espoo: Geological Survey of Finland.

Serpone, N., Dondi, D., and Albini, A. (2007). Inorganic and organic UV filters: their role and efficacy in sunscreens and suncare products. *Inorganica Chim. Acta* 360, 794–802. doi: 10.1016/j.ica.2005.12.057

Tharaud, M., Gardoll, S., Khelifi, O., Benedetti, M. F., and Sivry, Y. (2015). UFREASI: user friendly elemental data processing. A free and easy-to-use tool for elemental data treatment. *Microchem. J.* 121, 32–40. doi: 10.1016/j.microc.2015.01.011

Tharaud, M., Gondikas, A. P., Benedetti, M. F., von der Kammer, F., Hofmann, T., and Cornelis, G. (2017). TiO_2 nanomaterials detection in calcium rich matrices by spICPMS. A matter of resolution and treatment. *J. Anal. At. Spectrom.* 32, 1400–1411. doi: 10.1039/C7JA00060J

Thio, B. J., Zhou, D., and Keller, A. A. (2011). Influence of natural organic matter on the aggregation and deposition of titanium dioxide nanoparticles. *J. Hazard. Mater.* 189, 556–563. doi: 10.1016/j.jhazmat.2011.02.072

Topuz, E., Sigg, L., and Talinli, I. (2014). A systematic evaluation of agglomeration of Ag and TiO_2 nanoparticles under freshwater relevant conditions. *Environ. Pollut.* 193, 37–44. doi: 10.1016/j.envpol.2014.05.029

Topuz, E., and Talinli, I. (2015). Agglomeration of Ag and TiO_2 nanoparticles in surface and wastewater: role of calcium ions and of organic carbon fractions. *Environ. Pollut.* 204, 313–323. doi: 10.1016/j.envpol.2015.05.034

Van Hoecke, K., De Schamphelaere, K. A. C., Van der Meeren, P., Smagghe, G., and Janssen, C. R. (2011). Aggregation and ecotoxicity of CeO_2 nanoparticles in synthetic and natural waters with variable pH, organic matter concentration and ionic strength. *Environ. Pollut.* 159, 970–976. doi: 10.1016/j.envpol.2010.12.010

Van Hoecke, K., Quik, J. T. K., Mankiewicz-Boczek, J., De Schamphelaere, K. A., Elsaesser, A., Van der Meeren, P., et al. (2009). Fate and effects of CeO_2 nanoparticles in aquatic ecotoxicity tests. *Environ. Sci. Technol.* 43, 4537–4546. doi: 10.1021/es9002444

Virkutyte, J., Al-Abed, S. R., and Dionysiou, D. D. (2012). Depletion of the protective aluminum hydroxide coating in TiO_2-based sunscreens by swimming pool water ingredients. *Chem. Eng. J.* 191, 95–103. doi: 10.1016/j.cej.2012.02.074

Wang, J.-L., Alasonati, E., Tharaud, M., Gelabert, A., Fisicaro, P., and Benedetti, M. F. (2020). Flow and fate of silver nanoparticles in small French catchments under different land-uses: the first one-year study. *Water Res.* 176, 115722. doi: 10.1016/j.watres.2020.115722

Westerhoff, P., Song, G., Hristovski, K., and Kiser, M. A. (2011). Occurrence and removal of titanium at full scale wastewater treatment plants: implications for TiO_2 nanomaterials. *J. Environ. Monit.* 13, 1195–1203. doi: 10.1039/c1em10017c

Zhang, J., Kumagai, H., Yamamura, K., Ohara, S., Takami, S., Morikawa, A., et al. (2011). Extra-low-temperature oxygen storage capacity of CeO_2 nanocrystals with cubic facets. *Nano Lett.* 11, 361–364. doi: 10.1021/nl102738n

Conflict of Interest: The authors declare that the research was conducted in the absence of any commercial or financial relationships that could be construed as a potential conflict of interest.

Advantages of publishing in Frontiers

OPEN ACCESS
Articles are free to read for greatest visibility and readership

FAST PUBLICATION
Around 90 days from submission to decision

HIGH QUALITY PEER-REVIEW
Rigorous, collaborative, and constructive peer-review

TRANSPARENT PEER-REVIEW
Editors and reviewers acknowledged by name on published articles

Frontiers
Avenue du Tribunal-Fédéral 34
1005 Lausanne | Switzerland

Visit us: www.frontiersin.org
Contact us: frontiersin.org/about/contact

REPRODUCIBILITY OF RESEARCH
Support open data and methods to enhance research reproducibility

DIGITAL PUBLISHING
Articles designed for optimal readership across devices

FOLLOW US
@frontiersin

IMPACT METRICS
Advanced article metrics track visibility across digital media

EXTENSIVE PROMOTION
Marketing and promotion of impactful research

LOOP RESEARCH NETWORK
Our network increases your article's readership